Integrin-mediated regulation of apicobasal polarity, cell states and cancer progression

Nicolas Pasquier

THÈSE DE DOCTORAT

NNT : 2024UPASL048

Integrin-mediated regulation of apicobasal polarity, cell states and cancer progression

Rôle des intégrines dans la régulation de la polarité apicobasale, l'architecture cellulaire et la progression cancéreuse

Thèse de doctorat de l'université Paris-Saclay et de l'université de Turku

École doctorale n° 582, Cancérologie : biologie – médecine – santé (CBMS)
Spécialité de doctorat : Sciences du Cancer
Graduate School : Sciences de la vie et santé. Référent : Faculté de Médecine

Doctoral Programme in Technology (DPT)
Biochemistry
Department of Life Technologies. Faculty of Technology

Thèse préparée dans les unités de recherche **Dynamique des cellules tumorales** (Université Paris-Saclay, INSERM, Institut Gustave Roussy) et **Cell Adhesion and Cancer** (Turku Bioscience, Université de Turku), en cotutelle sous la direction de **Fanny JAULIN**, directrice de recherche à l'Institut Gustave Roussy, et la direction de **Johanna IVASKA**, directrice de recherche à l'Université de Turku.

Thèse soutenue à Paris-Saclay, le 23 septembre 2024, par

Nicolas PASQUIER

Composition du Jury

Membres du jury avec voix délibérative

David BRYANT Directeur de recherche, CRUK-Beatson Institute (Glasgow, R.-U.)	Président
Jean-Léon MAÎTRE Directeur de recherche, Institut Curie (Paris)	Rapporteur & Examinateur
Julie PANNEQUIN Directrice de recherche, Institut de Génomique Fonctionnelle (Montpellier)	Rapportrice & Examinatrice
Patrick CASWELL Directeur de recherche, Université de Manchester (R.-U.)	Examinateur
Guillaume MONTAGNAC Directeur de recherche, Institut Gustave Roussy (Villejuif)	Examinateur
Emilia PEUHU Directrice de recherche, Université de Turku (Finlande)	Examinatrice

université PARIS-SACLAY

ÉCOLE DOCTORALE
Cancérologie : biologie - médecine - santé (CBMS)

Titre : Rôle des intégrines dans la régulation de la polarité apicobasale, l'architecture cellulaire et la progression cancéreuse

Mots clés : Intégrine-β1, Polarité apicobasale, Migration, Cancer colorectal, cellules souches pluripotentes induites humaines, capacitation, matrice, rigidité

Résumé : Les intégrines sont des protéines régulant l'adhésion, la migration et l'architecture cellulaires, jouant un rôle tant dans le développement des tissus sains que dans la progression cancéreuse. Bien que les intégrines aient été largement étudiées dans divers modèles biologiques, la manière dont leur disponibilité agit sur la polarité apicobasale, la migration et la capacitation cellulaires n'est pas entièrement connue à ce jour.
Ici, nous étudions le rôle des intégrines, et principalement de l'intégrine-β1, sur l'établissement de la polarité apicobasale ainsi que sur la migration cellulaire dans des modèles cancéreux. Nous décryptons également leur action sur l'établissement de l'identité cellulaire en étudiant leur rôle dans la capacitation des cellules souches pluripotentes induites humaines (hiPSCs).
Les résultats de cette thèse permettent d'identifier une nouvelle une boucle de recyclage de l'intégrine-β1, dépendante de SorLA, HER2 et HER3, permettant aux cellules de cancer du côlon de percevoir la matrice et d'orienter leur polarité apicobasale.
Nous approfondissons également la compréhension de la migration de cellules cancéreuses sur la matrice extra-cellulaire en identifiant deux compositions matricielles (collagène + laminine et laminine + ténascine C) permettant aux cellules cancéreuses d'ostéosarcome et aux fibroblastes de migrer indépendamment de la rigidité du substrat grâce à une augmentation du nombre de points d'ancrage moléculaires impliquant l'intégrine-β1. Nous investiguons également le rôle de l'intégrine-β1 dans le processus de capacitation des cellules souches et montrons que l'inhibition de l'intégrine-β1 maintient un phénotype similaire à l'état naïf chez les hiPSCs.
Ensemble, ces données soulignent l'importance des intégrines, et principalement de l'intégrine-β1, dans de nombreux processus cellulaires parmi les modèles, expliquant ainsi son importance dans l'adhésion cellulaire, l'architecture des cellules cancéreuses ainsi que dans l'établissement de l'identité cellulaire.

Title : Integrin mediated regulation of apicobasal polarity, cell states and cancer progression

Keywords : Integrin-β1, Apicobasal polarity, Spreading, Colorectal Cancer, hiPSC, Capacitation, Matrix, Stiffness

Abstract : Integrins regulate cell adhesion, migration and architecture which play a role both in development of healthy tissues and disease. While integrins have been widely studied amongst models, the way their availability acts on polarity, spreading and cell capacitation is not fully understood.
Here we investigate the role of integrins, and mainly integrin-β1, on polarity establishment as well as cell spreading in cancer models. We also decipher their action on cell states by studying their role in human induced pluripotent stem cells (hiPSCs) capacitation.
This thesis reveals a newly described SorLA, HER2 and HER3-dependent Integrin-β1 recycling loop, allowing colon cancer cells to sense the matrix and orient their polarity accordingly.
We also go deeper in cancer cell spreading on matrix, by identifying two matrix compositions (collagen + laminin and laminin + tenascin C) allowing osteosarcoma cancer cells and fibroblasts to spread in a stiffness-independent fashion through an increased amount of integrin-β1-positive molecular clutches. We also investigate the role of Integrin-β1 on the capacitation process of stem cells and show that inhibition of integrin-β1 maintains a naïve-like phenotype in hiPSCs.
Taken together, these data highlight the importance of integrins, and mainly integrin-β1, in many cell processes amongst models, thus explaining its key role in cell adhesion, cancer cell architecture and cell state establishment.

Synthèse en français

Les intégrines sont des protéines membranaires essentielles à la régulation de l'adhésion cellulaire, de la migration et de l'architecture des cellules, jouant un rôle crucial dans le développement des tissus sains ainsi que dans la progression de maladies telles que le cancer. Parmi elles, l'intégrine-β1 est particulièrement étudiée en raison de son implication dans plusieurs processus biologiques. Les intégrines forment des hétérodimères qui permettent aux cellules de s'ancrer dans la matrice extracellulaire (ECM) et d'intégrer les signaux mécaniques et biochimiques de leur environnement. Elles sont impliquées dans des processus variés tels que l'adhésion, la migration, la prolifération et la différenciation cellulaire. Les intégrines sont activées par des mécanismes bidirectionnels (inside-out et outside-in), et leur recyclage est finement régulé pour contrôler leur disponibilité à la membrane cellulaire. Ce recyclage est modulé par des protéines GTPases telles que Rab4 et Rab11, responsables de boucles courtes et longues de recyclage respectivement. Un aspect crucial des intégrines est leur rôle dans la polarité apicobasale, notamment dans les cellules épithéliales. L'établissement et le maintien de cette polarité sont déterminés par l'interaction des intégrines avec la matrice extracellulaire. De plus, les intégrines sont impliquées dans le remodelage de la matrice par les cellules cancéreuses, leur permettant d'envahir les tissus sains et de contribuer à la formation de métastases, ainsi que dans la capacitation de cellules souches humaines pluripotentes induites (hiPSCs).

Le principal objectif de cette thèse est d'explorer le rôle des intégrines, et plus spécifiquement de l'intégrine-β1, dans plusieurs processus biologiques essentiels, notamment :

1. **L'établissement de la polarité apicobasale** dans les modèles de cancer colorectal (CRC) mucineux, en analysant les voies d'interaction entre la cellule tumorale et la matrice extracellulaire, ainsi que les mécanismes de recyclage des intégrines.
2. **La migration et l'étalement des cellules cancéreuses** dans différentes conditions de rigidité et de composition de la matrice extracellulaire, afin de

comprendre les mécanismes de migration indépendants de la rigidité. Pour ce faire, nous utilisons des modèles d'ostéosarcomes et de fibroblastes.

3. **La capacitation des hiPSCs** et le rôle de l'intégrine-β1 dans la transition entre les états naïf et primé, essentiels pour le développement cellulaire et la différenciation.

Cette thèse permet de mettre en lumière les découvertes suivantes :

1. **Rôle des intégrines dans la polarité apicobasale** : Il a été découvert que dans les modèles de cancer colorectal mucineux, l'intégrine-β1 joue un rôle clé dans l'orientation de la polarité apicobasale. Cette orientation est régulée par une boucle de recyclage dépendante des récepteurs HER2/HER3 et de la protéine SorLA, permettant aux cellules cancéreuses de s'orienter en fonction des signaux de la matrice extracellulaire. Ce mécanisme est crucial pour maintenir une interaction adéquate entre la cellule tumorale et son environnement, influençant directement la progression métastatique.
2. **Migration cellulaire et composition de la matrice** : En explorant la migration des cellules d'ostéosarcome et de fibroblastes sur différentes compositions de matrice, il a été montré que certaines combinaisons, telles que le collagène associé à la laminine, ou la laminine associée à la ténascine C, permettent une migration indépendante de la rigidité de la matrice. Ces observations révèlent que l'engagement de différents hétérodimères d'intégrine, incluant l'intégrine-β1, permet aux cellules de s'adapter à diverses compositions de matrice, facilitant leur propagation dans des environnements de rigidité variable.
3. **Capacitation des cellules souches pluripotentes** : L'étude a révélé que l'inhibition de l'intégrine-β1 retarde le processus de capacitation des cellules souches pluripotentes induites (hiPSCs), maintenant ces cellules dans un état naïf. L'intégrine-β1 est essentielle pour la réorganisation des adhésions et de la morphologie des colonies au cours de la transition vers l'état primé, ce qui est nécessaire pour leur différenciation efficace.

Cette thèse met en lumière l'importance cruciale des intégrines, et notamment de l'intégrine-β1, dans des processus biologiques variés, allant du développement normal

des tissus à la progression du cancer. L'intégrine-β1 influence non seulement l'adhésion et la migration cellulaires, mais aussi l'établissement de la polarité cellulaire et l'état des cellules souches. En décryptant les mécanismes sous-jacents au recyclage des intégrines et à leur rôle dans la migration indépendante de la rigidité, ces travaux ouvrent de nouvelles perspectives pour le développement de thérapies ciblées, notamment dans le contexte de la progression métastatique des cancers.

Acknowledgements

I would first like to thank Riitta Lahesmaa, director of Turku Bioscience, and Fabrice Barlesi, director of the Gustave Roussy Institute, where I carried my PhD project as a cotutelle. Both these places have been incredible research environments, fostering interactions with brilliant scientists who taught me a lot.

I am also addressing my gratitude to Léa Poisot and Nina Lehtimäki, the coordinators of both my doctoral schools (namely CBMS and DPT), who have always been here to answer my numerous questions and made this cotutelle peaceful on an administrative point of view. I am also grateful to Eevi Rintamäki and Eric Deutsch, both directors of my doctoral schools, for having me in your exciting and stimulating research programs. Additionally, I am addressing special thanks to Sanna Ranto and Jyrki Heino, respectively Chief Academic Officer and Research Director at the University of Turku.

My research project was co-supervised by Johanna Ivaska (University of Turku) and Fanny Jaulin (Institut Gustave Roussy). To Johanna, I would like to address my deepest gratitude for the huge opportunity you gave me when hiring me as an intern in your lab in 2020, and for accepting to supervise my PhD project after that. You've been a true inspiration as a scientist, and I have always been impressed and honored by your endless involvement and excitement in my project. I need to put an emphasis on the time you give to each of your PhD students, including me. You actively assisted me in the progress of my project, and I owe you my gratitude. To Fanny, I am grateful for letting me work on this exciting CRC metastasis polarity project, for trusting me along my research path and for giving relevant feedback on my work. Your lab is a very inspirational environment for every scientist and gave me the opportunity to gain insight on a more clinical side of research, which taught me a lot. I am inspired by your scientific career, which made you a true mentor to me.

I could not write this section without mentioning Charlotte Canet-Jourdan, who supervised me during the first months of my PhD and whose project I decided to carry on. You taught me a lot on a technical point of view and I've always valued your feedback and advice so much! This period of time was short, but I deeply enjoyed working by your side.

I would like to address special thanks to Hellyeh Hamidi and Jacques Mathieu, research coordinators in the Ivaska Lab and the Jaulin lab respectively. Thank you both for your involvement in my project, your always relevant feedback and your patience.

I have had the privilege to be followed by Jacques Mathieu and David Bryant as part of my annual follow-up committee. Thank you both for your precious advice and scientific mentoring during these sessions. I would also like to thank Julie Pannequin and Jean-Léon Maître for accepting to be the reviewers of this thesis, as well as Patrick Caswell for agreeing to be my opponent with regard to the University of Turku during the defense. My jury will also be composed of David Bryant, Guillaume Montagnac and Emilia Peuhu, which I truly feel grateful for.

During my PhD project, I have had the honor to work with talented collaborators and co-authors, namely Hussein Al-Akhrass, James Conway, Aleksi Isomursu, Gautier Follain, Ville Härmä, Eva Jou-Ollé, Eetu Välimäki, Juha Rantala, Florent Péglion, Jacques Mathieu, Hellyeh Hamidi, Jouni Härkönen, Christophe Desterke, Valeria Barresi, Zoé Fusilier, Aki Stubb, Paula Rasila, Sonja Vahlman, Joonas Sokka and Ras Trokovic. I truly enjoyed working with you.

Both my labs were very exciting and fruitful environments to work in. Every single member has helped me in completing this PhD work, and for this I am deeply grateful. From the Ivaska Lab, I would like to address my gratitude to Martina, Johanna L., Mitro, Siiri, Gautier, Michal, James, Jenni, Petra, Hellyeh, Mathilde, Megan, Niklas, Omkar, Paulina, Meri, Veli-Matti, Eva, Michalis and Huayi. It was always fun and exciting to work by your side. I would also like to address special thoughts, gratitude and appreciation to Jasmin and Maria who have been an incredible emotional support, and I thank you for your friendship. From the Jaulin Lab, I would like to thank Jérôme, Raphaël, Emilie, Sabrina, Charlotte, Jean-Baptiste, Jacques, Joël, Emmanuel, Elise, Grégoire, Diane-Laure, Léa, Clémence, Ali, Alice, Anaïs, Florent, Ioanna, Ryme, Oliviano, Maximiliano and Xihong. I am also addressing special thanks to Aurore for being such a kind and supporting co-PhD student, often from afar! I also thank the whole Montagnac team, I had a lot of fun working by your side.

I would like to address my gratitude to all the technical staff for your help during these projects: thank you Petra and Jenni for your precious help, your patience and your kindness! I also could not have succeeded without the amazing help from Heli, Katri and Nina from the Turku Center for Disease Modelling, and from Mélanie from the Gustave Roussy Institute. Your help with all the mouse work was precious and I could not have done it without you.

To my family, I address my deepest gratitude. Thank you for always being by my side and for always supporting me, bringing me all the strength I needed in the hardest times of my PhD. I thank you for putting up with the distance during my time in Finland. I feel so grateful to have such a loving and understanding family. I am therefore sending lots of love to my mum Martine, my sister Charlotte, my brother Olivier and my stepdad Jean-Pierre. My dad Michel is always in my thoughts and in my heart. I also want to mention my friends, both in France and Finland, who being far away from at different times wasn't always easy. Thank you for the laughs, for your support and for your love; and to the Turku squad, thank you for introducing me to the best Finland has to offer and for being patient with my weak Finnish and Swedish skills. This has truly been the experience of a lifetime!

Lastly, I want to thank the Fondation Philantropia, the Turku University Foundation and the Pentti and Tyyni Ekbom Fund for funding my PhD work.

Table of Contents

1 Abbreviations 11

2 List of Publications 16

3 Introduction 17

4 Review of the literature 19

4.1 Integrins: Adhesion and Trafficking 19

4.1.1 Integrin structure and ligands 19

4.1.1.1 Integrin structure 19

4.1.1.2 Integrin ligands 21

4.1.2 Integrin activation and recycling 24

4.1.2.1 Integrin activation 24

4.1.2.2 Integrin trafficking to the membrane and recycling loops 25

4.1.2.3 Integrin trafficking regulation 27

4.1.2.4 Integrin trafficking functional consequences 29

4.1.2.4.1 Apicobasal polarity 29

4.1.2.4.2 Cell migration and invasion 29

4.1.2.5 Integrin glycosylation and its consequences 30

4.1.3 Integrin adhesion complexes (IACs) 32

4.1.3.1 Types of IACs 32

4.1.3.2 Structure of IACs 33

4.1.3.3 IAC signaling 34

4.1.4 Integrins in cancer 35

4.1.4.1 Integrins in tumor initiation 35

4.1.4.2 Integrins in cancer invasion and metastasis 36

4.1.4.3 Targeting integrins for anticancer treatments 37

4.2 Apicobasal polarity of epithelial cells 38

4.2.1 Polarity establishment 38

4.2.1.1 Molecular actors 38

4.2.1.1.1 Polarity complexes 38

4.2.1.1.2 Phosphoinositides (PIs) 40

4.2.1.1.3 Rho-GTPases 41

4.2.1.2 Sequence of events and interactions during polarity establishment 42

4.2.2 Polarity orientation and maintenance 44

4.2.2.1 ECM contact and subsequent orientation of polarity markers 44

4.2.2.2 Trafficking of polarity proteins in the polarity orientation process 46

4.2.2.3 Polarity maintenance 47
4.2.3 Inverted polarity 48
4.2.3.1 Inverted polarity in cancer 48
4.2.3.1.1 Consequences of inverted polarity on cancer invasion 50
4.2.3.1.2 Consequences of inverted polarity on drug resistance 50
4.2.3.1.3 Consequences of inverted polarity on immune escape 50
4.2.3.1.4 Plasticity of inverted polarity in cancer 51
4.2.3.2 Inverted polarity in genetic diseases 51
4.2.3.3 Inverted polarity in pathogen defense 52
4.2.3.4 Inverted polarity in development 52
4.3 Biological systems to study polarity and integrin-mediated adhesions 55
4.3.1 Colorectal adenocarcinomas (CRCs) 55
4.3.1.1 Healthy gut architecture 55
4.3.1.2 Characterization of CRCs 58
4.3.1.2.1 Histopathology 59
4.3.1.2.2 Consensus Molecular Subtypes (CMS) 60
4.3.1.2.3 Developmental pathways 61
4.3.1.3 Metastasis and invasion of CRCs 61
4.3.1.4 Models of CRCs 62
4.3.1.4.1 Cell lines: the example of LS513 62
4.3.1.4.2 Patient-derived xenografts (PDXs) 63
4.3.1.4.3 Patient-derived organoids (PDOs) 63
4.3.2 Human induced pluripotent stem cells (hiPSCs) 65
4.3.2.1 What are hiPSCs? 65
4.3.2.2 Naïve and primed states 65
4.3.2.3 Adhesion and polarity status of the blastocyst 66
4.3.3 Stiffness-insensitive spreading of cancer: the use of TIFs and U2OS 67
4.3.3.1 The role of matrix stiffness in cancer invasion 67
4.3.3.2 The role of matrix composition in cancer invasion 67
4.3.3.3 TIFs and U2OS 68
5 Aims of the PhD 69
6 Material and Methods 70
6.1 Cell culture and organoid formation 70
6.1.1 MUC CRC (II) 70
6.1.1.1 Culture and passaging of patient-derived xenografts (PDXs) 70
6.1.1.2 Generation of tumor spheres 71
6.1.1.3 Collagen embedding and culture of tumor spheres 71
6.1.1.4 Generation of a 14P-derived PDO line 72

6.1.1.5 Culture of LS513 and generation of TSIPs 72
6.1.2 hiPSC (IV) 72
6.1.2.1 Culture of naïve and primed stem cells 72
6.1.2.2 Capacitation 73
6.1.2.3 Colony formation assay 74
6.2 Protein and gene expressions 74
6.2.1 Western blotting (II) 74
6.2.2 PNGase digestion of lysates (II) 75
6.2.3 Mass cytometry (II) 75
6.2.4 Whole exome sequencing (II) 76
6.2.5 Analysis of SORLA and ITGB1 gene expression in human tumors (II) 76
6.2.6 Single cell RNA sequencing (scRNAseq) (IV) 76
6.3 Quantification of cell-matrix interactions 77
6.3.1 Generation of fluorescent collagen (II & III) 77
6.3.2 Generation of CNA35 and cloning (II) 78
6.3.3 Peritoneum *ex vivo* assay (II) 78
6.3.4 Collagen orientation analysis (II) 78
6.3.5 Collagen displacement fields (II) 80
6.4 Infections and polarity/trafficking analysis (II) 81
6.4.1 SorLA silencing using shRNA lentiviral transduction 81
6.4.2 SorLA KO using siRNA transient transfection 81
6.4.3 Integrin recycling assay 82
6.5 Stainings and microscopy (II) 83
6.5.1 Immunofluorescence staining 83
6.5.2 Confocal imaging 83
6.5.3 Immunohistochemistry staining 84
6.6 Statistical analysis and polarity quantification 84
6.6.1 Statistical analysis (II, III & IV) 84
6.6.2 Polarity score (II) 84
6.7 Annexes 85
Table 1 - Antibodies 85
Table 2 - siRNA and shRNA 88
7 Results 89
7.1 Implication of Integrin-β1 trafficking in the apicobasal polarity orientation of CRC metastasis (II) 89
7.1.1 MUC CRC polarity is regulated by ECM interactions and Focal Adhesion Pathway 89
7.1.2 Collagen-binding integrins regulate polarity establishment in MUC CRC 90

7.1.3 Inverted polarity is linked to altered expression of integrin trafficking regulators ..91
7.1.4 The SorLA-dependent integrin trafficking loop is induced by HER2 and HER3 93
7.1.5 The apicobasal polarity orientation allows proper interaction with the matrix 94
7.1.6 Higher HER2/HER3/SorLA expression correlates with a apical-in polarity 94
7.2 Uncoupling stiffness and matrix composition to determine ideal conditions for integrin-dependent cancer cell spreading (III) 96
7.3 Integrin-β1: a cornerstone in hiPSC capacitation (IV) 99
7.3.1 Blocking Integrin-β1 delays the capacitation process 99
7.3.2 Integrin-β1 is central to a fully primed feature acquisition during capacitation ... 100
8 Discussion 102
8.1 Understanding inverted polarity in health and disease (I) 102
8.2 A HER2/HER3/SorLA-dependent integrin-β1 reycling loop as a polarity regulator in CRC metastasis (II) 103
8.3 Ligand availability and integrin repertoire engagement determine cell behavior and stiffness-independent spreading (III) 105
8.4 Integrin-β1 blocking promotes naïve-like features and prevents effective capacitation of hiPSCs (IV) 107
9 Conclusion 109
9.1 Original Publication I 109
9.2 Original Publication II 109
9.3 Original Publication III 110
9.4 Original Publication IV 110
10 References 112
11 Original publications 145

1 Abbreviations

AB	Apicobasal
AGAP1	Arf-GAP with GTPase, ANK repeat and PH domain-containing protein 1
AJ	Adherent Junction
AMIS	Apical Membrane Initiation Site
AMOTL2	Angiomotin-like protein 2
Anx2	Annexin-2
AP2-μ	μ subunit of AP2 adaptor complex
APC	Adenomatous polyposis coli
aPKC	Atypical protein kinase C
APP	Amyloid precursor protein
ARE	Apical recycling endosome
ARH	Low Density Lipoprotein Receptor Adaptor Protein 1
ARHGAP15	Rho GTPase Activating Protein 15
AsC	Adenosquamous carcinoma
ASE	Apical sorting endosome
Atoh1	Protein atonal homolog 1
BRAF	v-raf murine sarcoma viral oncogene homolog B1
BRE	Basal recycling endosome
BSE	Basal sorting endosome
βTD	β tail domain
C-ERMAD	C-terminal ERM-association domain
CA	Classic adenocarcinoma
CAF	Cancer-associated fibroblast
CD	Cluster of Differentiation
Cdc42	Cell division control protein 42 homolog
CG	CLIC/GEEC
CGA	Glycoprotein Hormones, Alpha Polypeptide
CIMP	CpG island methylator phenotype
CIN	Chromosomal instability
CLIC	Clathrin-independent carrier
CMS	Consensus Molecular Subtype
Coll.	Collagen
Crb	Crumbs
CRC	Colorectal adenocarcinoma
CRE	Common recycling endosome
CTC	Circulating tumor cell
Dab2	Disabled homolog 2
Dlg	Discs large
DOK1	Docking protein 1

DPPA3	Developmental Pluripotency Associated 3
DSC	Deep secretory cell
ECM	Extracellular matrix
EE	Early endosome
EEC	Enteroendocrine cell
EGF	Epidermal Growth factor
EMT	Epithelial-to-mesenchymal transition
EpCAM	Epithelial cellular adhesion molecule
Eps15	Epidermal growth factor receptor substrate 15
ER	Endoplasmic reticulum
ERM	Ezrin, radixin, moesin
FA	Focal Adhesion
FAK	Focal Adhesion kinase
FB	Fibrillar adhesion
FC	Focal contact
FERM	4.1 protein, ezrin, radixin, moesin
FFPE	Formalin-fixed paraffin-embedded
FILIP1	Filamin-A-interacting protein 1
FMNL2	Formin-like protein 2
Fuc	Fucose
Gal	Galactose
Gal-1	Galectin-1
Gal-3	Galectin-3
GAP	GTPase activating protein
GDP	Guanosine diphosphate
GEEC	GPI-anchored protein-enriched early endosomal compartment
GEF	Guanine nucleotide exchange factor
GlcNac	N-Acetylglucosamine
GTP	Guanosine triphosphate
HAX-1	HS-1-associated protein X-1
HER2/ERBB2	Receptor tyrosine-protein kinase ErbB-2
HER3/ERBB3	Receptor tyrosine-protein kinase ErbB-3
Hes1	Hairy and enhancer of Split-1
hiPSC	Human induced pluripotent stem cells
HLA-DM	Human leukocyte antigen – DM isotype
HLA-DR	Human Leukocyte Antigen – DR isotype
I-EGF	4 integrin-EGF
IAC	Integrin Adhesion Complex
ICAM-1	Intercellular adhesion protein 1
ICAM-4	Intercellular Cell Adhesion Molecule 4
ICM	Inner Cell Mass
IF	Immunofluorescence
IHC	Immunohistochemistry

ILK	Integrin-linked kinase
ITGB1	Integrin-β1
JAM	Junctional Adhesion Molecule
KLF17	Krüppel-like factor 17
KLF4	Krüppel-like factor 4
KRAS	Kristen rat sarcoma viral oncogene homolog
L1TD1	LINE1 Type Transposase Domain Containing 1
Lam	Laminin
LDV	L/I-D/E-V/S/T-P/S consensus aminoacid sequence
Lgl	Lethal Giant Larvae
Lgr5	Leucine-rich repeat-containing receptor 5
LIF	Leukemia inhibitory factor
LIMD1	LIM domain Containing protein 1
LLPS	Liquid-liquid phase separation
MDCK	Madin-Darby canine kidney
MeC	Medullary carcinoma
MHC	Major histocompatibility complex
MIA-CID	Multiple intestinal atresia associated with combined immunodeficiency
MIDAS	Metal ion-dependent adhesion site
MiP	Micropapillary carcinoma
MMP	Metalloproteinase
MSI	Microsatellite instable
MT1G	Metallothionein 1G
MT1H	Metallothionein 1H
MUC	Mucinous
MUC1	Mucin 1
MUC2	Mucin 2
MVID	Microvillus inclusion disease
MYO5B	Myosin-Vb
N-WASP	Wiskott-Aldrich syndrome protein
NeC	Neuroendocrine carcinoma
NHERF1	Sodium/Hydrogen exchanger regulatory cofactor 1
OCT4	Octamer-binding transcription factor 4
PALS1	Protein associated with LIN7 1 / MAGUK p55 subfamily member 5
Par3	Partition Defective 3
Par6	Partition Defective 6
PATJ	InaD-like protein
PC	Peritoneal carcinomatosis
Pcx	Podocalyxin
PDO	Patient-derived organoid
PDX	Patient-derived xenograft
PHACTR-1	Phosphatase and actin regulator 1
PI	Phosphoinositide

PI(3,4,5)P3	Phosphatidylinositol 3,4,5-triphosphate
PI(4,5)P2	Phosphatidylinositol 4,5-diphosphate
PI3K	Phosphoinositide 3-kinase
PINCH	Particularly interesting new cysteine-histidine-rich protein
PIP5K	Phosphatidylinositol-4-phosphate 5-kinase
PKD	Polycystic kidney disease
PM	Plasma membrane
PNGase	Peptide-N-Glycosidase
PNRE	Perinuclear recycling endosome
PP2A	Protein Phosphatase 2
PRNRP	Papillary renal neoplasm with reverse polarity
PS	Polarity score
PSI	Plexin-semaphorin-integrin
PTB	F3 phospho-tyrosine binding domain
PtdIns	Phosphatidylinositol
PTEN	Phosphatase and tensin homolog
Rac1	Ras-related C3 botulinum toxin substrate 1
Ras	Rat sarcoma virus
RCP/Rab11fip1	Rab-coupling protein/Rab11 family-interacting protein 1
RGD	Argynyl-glycyl-aspartic acid
RhoGDI	RhoGTPase dissociation inhibitor
ROCK1	Rho-associated, coiled-coil-containing protein kinase 1
RTK	Receptor tyrosine kinase
SA	Sialic acid
Scrib	Scribble
scRNAseq	Single cell RNA sequencing
SeC	Serrated carcinoma
SFK	Src family of kinases
SFRP2	Secreted frizzled related protein 2
SORL1/SorLA	Sortilin-related receptor with A-type repeats
SOX2	SRY-box Transcription factor 2
SPCRP	Solid papillary carcinoma with reverse polarity
SRCC	Signet ring cell carcinoma
STX3	Syntaxin 3
STXBP2	Syntaxin-binding protein 2
Susp.	Suspension
t-SNARE	Target membrane SNAP receptor
TAZ	Transcriptional coactivator with PDZ-binding motif
TBX3	T-box transcription factor 3
TE	Trophectoderm
TEAD	TEA domain family member 1
TFM	Traction Force Microscopy
TGF-β	Transforming growth factor β

TGN	Trans-Golgi network
Tiam1	T-cell lymphoma invasion and metastasis-inducing protein 1
TIF	Telomerase immortalized fibroblasts
TJ	Tight junction
TLR	Toll-like receptor
TME	Tumor microenvironment
TNC	Tenascin C
TNF-α	Tumor necrosis factor α
TNM	Tumor, Node, Metastasis
TSIP	Tumor sphere with inverted polarity
TTC7A	Tetratricopeptide repeat domain 7A
uPA	Urokinase
v-SNARE	Vesicle membrane SNAP receptor
VASP	Vasodilator-stimulated phosphoprotein
VAV2	Vav guanine nucleotide exchange factor 2
VCAM-1	Vascular Cell Adhesion Molecule 1
vWA	Von Willebrand A domain
vWF	Von Willebrand factor
WAVE	WASP-family verprolin-homologous protein
WB	Western Blot
YAP	Yes-associated protein
ZIC2	Zinc finger protein 2
ZO	Zonula occludens

2 List of publications

This dissertation is based on the following publications, that will be referred to by their roman number in the text and enclosed at the end of the thesis.

I- **Pasquier, N.**, Jaulin, F., & Peglion, F. (2024). **Inverted apicobasal polarity in health and disease.** *Journal of Cell Science*, *137*(5).

II- **Pasquier N.**, Isomursu A., Mathieu J., Hamidi H., Härkönen J., Follain G., Desterke C., Barresi V., Fusilier Z., Jaulin F. & Ivaska J., **Signaling downstream of tumor-stroma interactions regulates mucinous CRC apicobasal polarity**, *manuscript submitted*

III- Conway, J. R., Isomursu, A., Follain, G., Härmä, V., Jou-Ollé, E., **Pasquier, N**., Välimäki E., Rantala J. & Ivaska, J. (2023). **Defined extracellular matrix compositions support stiffness-insensitive cell spreading and adhesion signaling**. *Proceedings of the National Academy of Sciences*, *120*(43)

IV- Taskinen, M., **Pasquier N**.*, Stubb A.*, Joshi S., Rasila P., Vahlman S., Sokka J., Trokovic R., Lönnberg T., Mikkola L. & Ivaska J., **Inhibition of integrin-β1 activity and contractility support naïve-like state in human induced pluripotent stem cells**, *manuscript submitted*

* equal contribution

3 Introduction

Integrins are membrane proteins that link the cell to its direct environment. They act as an adhesion and signaling platform, linking the cytoskeleton (actin and intermediate filaments) to matrix components. They are implicated in many cell processes, such as adhesion, migration and polarity, and they determine the cell state and architecture. Integrins are a wide family of adhesion molecules, and the most common subunit, shared by many distinct ECM-binding heterodimers is integrin-β1 which this thesis focuses on.

When carcinogenesis occurs, cancer cells go through a series of changes that leads to their reprogramming and modifications in their phenotype, such as changes in their architecture and invasiveness. Cancer clusters can indeed move within different types of extracellular matrix (ECM), adopting a different apicobasal polarity (I) or invade and spread differently to healthy tissues. In both these processes, integrins are involved, but the mechanistic cascade by which they control polarity and spreading in different cancer models is not fully understood.

Integrin-β1-dependent cell polarity establishment and maintenance during cancer progression remains incompletely understood. Indeed, some carcinomas are composed of cells that maintain a predominantly epithelial signature with a conserved apicobasal polarity. However, this polarity can be misoriented, and the mechanisms underlying the reprogramming of polarity orientation in cancer have not been elucidated yet. Because the polarity status of cancer cells can directly be linked to prognosis and outcome, we investigated the intricacies of polarity orientation in cancer, using a colorectal cancer patient-derived model. We studied the focal-adhesion dependent pathway by which cancer cells orient their polarity and discovered a new integrin-recycling loop, involving SorLA, HER2 and HER3 (II).

Integrins are involved in the architecture of cancer cells and tumors, but also in the way cells migrate throughout the body and invade. This is the main motor of metastasis formation which accounts for most cancer deaths. Because cancer cells efficiently remodel the matrix they migrate on, they have a direct impact on its physical and

chemical properties. However, while these parameters have been studied separately, few models comprehensively addressing the joint effects of the matrix stiffness and composition have been developed across literature. Here we describe a matrix array platform and employ it to test different combinations of stiffnesses and composition, allowing the discovery of matrix compositions supporting integrin-dependent cancer cell spreading independently of ECM stiffness. We found that the collagen/laminin and laminin/tenascin C combinations allow an engagement of a broader repertoire of integrin-β1 heterodimers facilitating efficient cell-ECM engagement and even on low rigidity (III).

Finally, integrins are not only involved in pathological processes as we have investigated above, but also efficiently participate in the organization and proper architecture and development of tissues. From the very first step of development, integrins play a role in cell-ECM interactions. In this thesis we studied the role of integrins in the maintenance of different stem cell states: the naïve pre-implantation and the primed post-implantation state. This process is key in the development, as it allows the adhesion of the blastocyst to the endometrium. Working with human induced pluripotent stem cells (hiPSCs), we found that the engagement of Integrin-β1 is necessary for stem cells to exit their naïve state and become primed for differentiation into different lineages (capacitation) and for the reorganization of hiPSC colony morphology and adhesions upon this transition (IV).

Altogether this thesis provides a wide overview of the actions of integrins across different biological process, from development to carcinogenesis and cancer development.

4 Review of the literature

4.1 Integrins: adhesion and trafficking

4.1.1 Integrin structure and ligands

Integrins are a family of heterodimeric receptors that interact with extracellular ligands sensing both their chemical and physical nature. In return, they induce a whole range of biochemical responses through different signaling pathways (Kechagia et al., 2019). Integrins both adhere to the extracellular matrix (ECM) and to other cells and integrate these signals through their connection to the actin cytoskeleton via a set of so-called Integrin adhesion complexes (IACs). Not only are integrins implicated in cell adhesion, but they also regulate crucial parameters such as cell shape, migration and motility (Conway and Jacquemet, 2019). While their role at the plasma membrane is well documented, integrins also play a role in the activation of signaling pathways when endocytosed (Moreno-Layseca et al., 2019).

4.1.1.1 Integrin structure

While integrins are present in all multicellular animals, they display an important diversity amongst species. In mammals, integrins are composed of 18 α and 8 β subunits. These monomers combine to form 24 functional heterodimeric integrin receptors (Humphries, 2000; Hynes, 2002). Since the discovery of the integrin receptor family (Hynes, 1987), the knowledge span has increased, further characterizing the bidirectionality of integrin signaling, both outside-in and inside-out (detailed in **4.1.2.1**). This signaling is mediated by conformational changes both in the extracellular and cytoplasmic regions of the integrin subunit (Hynes, 2002).

Both subunits are composed of a cytoplasmic tail, a single α helix inserted within the plasma membrane, and an extracellular or ectoplasmic domain. The latter is composed of a “head” where the binding sites of the ligands are found, as well as a “leg”, which conformation changes upon binding of the ligands (Campbell and Humphries, 2011). The

~1000 amino acid-long α subunit extracellular domain is composed of Calf-1, Calf-2, Thigh and β-propeller domains. Additionally, about half of α subunits contain an inserted αI domain, which contains a metal ion-dependent adhesion site (MIDAS) with the following gradual affinity for cations: Mn^{2+} > Mg^{2+} > Ca^{2+} and is responsible for ligand binding in these integrins. The ~750 amino acid-long β subunit extracellular domain is composed of β tail (βTD), 4 integrin-EGF (I-EGF), plexin-semaphorin-integrin (PSI), Hybrid and βI domains. MIDAS sites can also be found on the β subunit (Zhang and Chen, 2012) (see Figure 1).

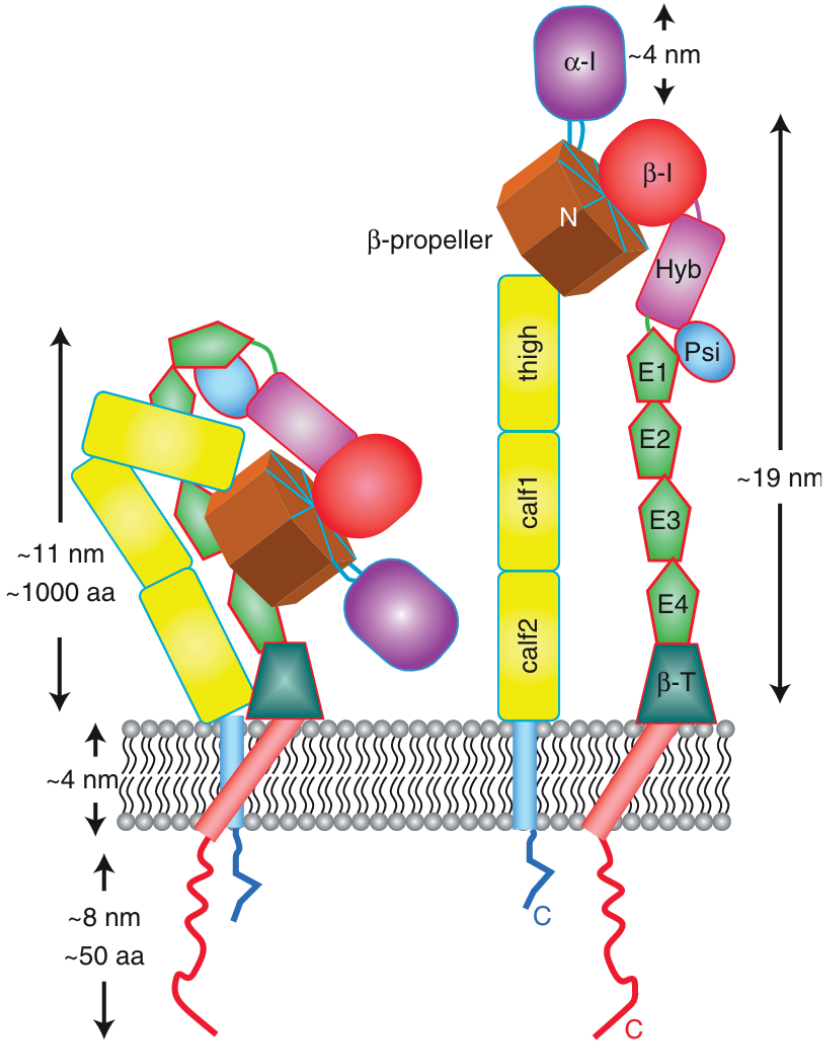

Figure 1- Integrin structure (from Campbell and Humphries, 2011).

Hyb=Hybrid dromain; β-T= βTD

4.1.1.2 Integrin ligands

Integrins have multiple ligands that can bind to their ectoplasmic domain (Chastney et al., 2021) and they can be divided into 5 categories depending on the ligands they bind to (Humphries et al., 2006) (see Figure 2):

→ **RGD-binding integrins** are composed of all five heterodimers of the αV subunit, two heterodimers of the β1 subunit (α5 and α8) as well as the αIIbβ3 heterodimer. Multiple ligands contain an RGD residue (argynyl-glycyl-aspartic acid) including fibrinogen, fibronectin, tenascin, thrombospondin, vitronectin and von Willebrand factor (vWF) (Plow et al., 2000). The RGD-motif interacts at the interface of the α and β subunits, the arginine binding to the β-propeller domain on the α subunit, and the aspartic acid binding to a von Willebrand A domain (vWA) on the β subunit (Whittaker and Hynes, 2002).

→ **LDV-binding integrins** are composed of α4β1, α4β7, α9β1, αEβ7 and the four heterodimers of the β2 subunit. The LDV sequence is functionally close to RGD, can be described by the consensus sequence L/I-D/E-V/S/T-P/S and can be found on several ligands such as fibronectin, osteopontin, tenascin and fibrinogen. Other LDV-containing ligands, such as VCAM-1 (Vascular Cell Adhesion Molecule 1), allow intercellular integrin-dependent interactions. Although structural information is lacking, it is also believed that the LDV residue interacts similarly to RGD, at the interface of the α and β subunits.

→ **I-domain-containing β1 integrins** are composed of integrin heterodimers which α subunit harbours the αI domain described earlier (Lee et al., 1995). These are α1β1, α2β1, α10β1 and α11β1. These form a collagen-binding subgroup, with some receptors reported to bind also laminin. In the case of collagen, a glutamate in a triple-helical GFOGER motif binds to a MIDAS in the αI domain of the α2 subunit (Emsley et al., 2000). The most ubiquitously expressed collagen-binding integrin for fibrillar type I collagen is the α2β1.

→ **Non-I-domain-containing integrins** form a subfamily composed of $\alpha 3\beta 1$, $\alpha 6\beta 1$, $\alpha 7\beta 1$ and $\alpha 6\beta 4$ that selectively bind to laminin, through a different site than that of the I-domain containing $\beta 1$ integrins.

→ **Other integrins** include integrin-ligand interactions with no-ECM ligands. This category also includes integrins mediating intercellular interactions, binding to cell adhesion molecules such as ICAM-4 (Intercellular Cell Adhesion Molecule 4) or E-cadherin (in the case of $\alpha_E\beta 7$) (U Kroneld, 1998).

Amongst all heterodimers, $\beta 1$ is the most common subunit. It can dimerize with 12 different α subunits, each with specific ligand binding specificity and signaling activity.

Figure 2- Integrin ligands (from Humphries et al., 2006) – see next page

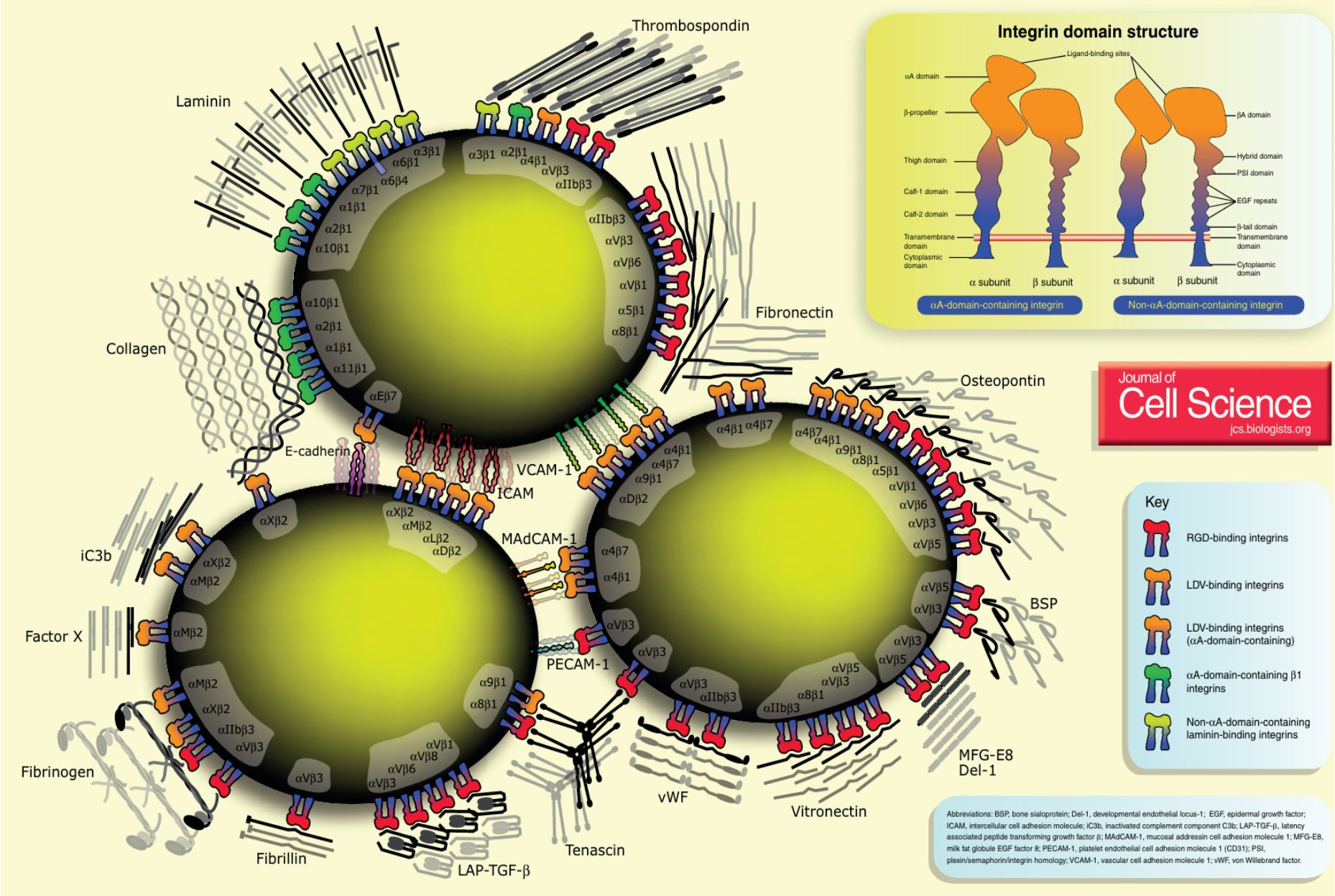
Thrombospondin
Laminin
Fibronectin
Collagen
Osteopontin
E-cadherin
VCAM-1
ICAM
MAdCAM-1
PECAM-1
iC3b
Factor X
BSP
Fibrinogen
Fibrillin
LAP-TGF-β
Tenascin
vWF
Vitronectin
MFG-E8
Del-1
Integrin domain structure
Ligand-binding sites
αA domain
β-propeller
Thigh domain
Calf-1 domain
Calf-2 domain
Transmembrane domain
Cytoplasmic domain
βA domain
Hybrid domain
PSI domain
EGF repeats
β-tail domain
Transmembrane domain
Cytoplasmic domain
α subunit
β subunit
α subunit
β subunit
αA-domain-containing integrin
Non-αA-domain-containing integrin
Journal of Cell Science
jcs.biologists.org
Key
RGD-binding integrins
LDV-binding integrins
LDV-binding integrins (αA-domain-containing)
αA-domain-containing β1 integrins
Non-αA-domain-containing laminin-binding integrins
Abbreviations: BSP, bone sialoprotein; Del-1, developmental endothelial locus-1; EGF, epidermal growth factor; ICAM, intercellular cell adhesion molecule; iC3b, inactivated complement component C3b; LAP-TGF-β, latency associated peptide transforming growth factor β; MAdCAM-1, mucosal addressin cell adhesion molecule 1; MFG-E8, milk fat globule EGF factor 8; PECAM-1, platelet endothelial cell adhesion molecule 1 (CD31); PSI, plexin/semaphorin/integrin homology; VCAM-1, vascular cell adhesion molecule 1; vWF, von Willebrand factor.

4.1.2 Integrin activation and recycling

4.1.2.1 Integrin activation

On the plasma membrane, integrins can be either in an inactive or an active state. When inactive, integrins are in a bent shape, not engaging with their ligands (Campbell and Humphries, 2011). This bent conformation is stabilized by integrin inactivators that bind to the integrin cytoplasmic tails and therefore prevent the binding of integrin-binding activating proteins, such as talin or kindlin. For instance, filamin or docking protein 1 (DOK1) are both inactivators that bind to the β subunit cytoplasmic tail and sharpin binds to both tails, stabilizing the inactive conformation (Bachmann et al., 2019; Gao et al., 2019).

Upon activation however, integrins can bind to extracellular ligands. There are two ways these integrins can be activated:

→ **The activation via inside-out signals**. Other cell-surface receptors receive extracellular signals, thus causing the binding of integrin activators such as talin and kindlin to the cytoplasmic tail of β subunits (Watanabe et al., 2008). The binding site of talin is precisely situated at the F3 phospho-tyrosine binding domain (PTB) (Calderwood et al., 2002) and is recruited to focal adhesions (FA – further detailed in **4.1.3**) from the cytosol (Rossier et al., 2012) which allows separation of the α/β "inter-legs" (disruption of hydrophobic and electrostatic interactions) and integrin activation through the unfolding of the ligand binding site followed by the "legs" moving apart from each other (Anthis et al., 2009). Kindlin is an important coactivator of integrins and binds to a membrane distal NxxY motif on the β subunit (Harburger et al., 2009). It is not known to activate integrins on its own (Karaköse et al., 2010) and talin-vinculin and talin-actin interactions also influence activation (Banno et al., 2012). Kindlin does not have a binding site to actin and Focal Adhesion Kinase (FAK) acts as an intermediate.

Whereas talin and kindlin have long been established as essential activators of integrins, this idea has been recently challenged, some findings qualifying talin as more of a stabilizer of an active state and suggesting that ligand binding to the bent integrin conformer is a key trigger for rapid activation and extension (Li et al., 2024).

→ **The activation via outside-in signals.** Ligand binding to integrins induces conformation changes that further increases ligand affinity of integrins, leading to increased integrin signaling (Arnaout et al., 2005). Ligand binding leads to clustering of integrins, consequently activating the autophosphorylation of the Src family of kinases (SFK) (Arias-Salgado et al., 2003). SFK then phosphorylates many components of the IACs triggering signaling. It has also been reported to phosphorylate a tyrosine within the integrin cytoplasmic domain (Law et al., 1999), which changes the strength of the affinity of the bond of integrins with its ligands, but also with other signaling molecules such as kinases, GTPases and adaptors constitutive of focal adhesions (Gahmberg et al., 2009).

The outside-in activation can be regulated internally, either through regulators of talin recruitment, the phosphorylation of integrin cytoplasmic domains or the binding of talin competitors.

4.1.2.2 Integrin trafficking to the membrane and recycling loops

Just like integrin activation, talin is an essential element in the trafficking of integrins to the plasma membrane (PM) after their synthesis (Margadant et al., 2011). Indeed, the binding of talin to integrins in the endoplasmic reticulum (ER) regulates the delivery of newly synthesized integrin heterodimers to the PM through transport along actin filaments (Martel et al., 2000). More precisely, talin binding to integrin exposes the GFFKR sequence that acts as an ER export signal. α subunits associate with the β subunits in the ER and stay dimerized during their whole travel to the plasma membrane through the Golgi (Tiwari et al., 2011).

Once at the PM, integrin trafficking controls the availability of integrin heterodimers via both clathrin-dependent and independent endocytosis pathways (Paul et al., 2015). It has been shown that most integrins are recycled back to the PM, and that only a small proportion is degraded in the lysosomal compartment (Böttcher et al., 2012). Differential trafficking of integrin heterodimers effectively leads to different responses to different

ECM cues such as formation of adhesions upon cell spreading (Shafaq-Zadah et al., 2016).

Integrins have been described to traffic through four recycling routes (Powelka et al., 2004; Caswell and Norman, 2006; Pellinen and Ivaska, 2006). The most studied recycling loops are (Mohrmann and Sluijs, 1999) (see Figure 3):

→ A Rab4-dependent **short loop** where integrins are endocytosed through a clathrin/dynamin-dependent mechanism and traffic through a Rab4-positive early endosome (EE) before being recycled to the membrane. The recycling half-time in this loop is of 3 minutes.

→ A Rab11-dependent **long loop** where, after being endocytosed in early endosomes, integrins traffic through a Rab11-positive perinuclear recycling endosome (PNRE) before being recycled to the membrane. The recycling half-time in this loop is of 10 minutes.

Additionally, other recycling routes have been described, including for example:

→ An **Arf6-dependent pathway** that is activated by the addition of serum or specific stimulants such as epidermal growth factor (EGF) (Powelka et al., 2004).

→An **actin-dependent pathway** characterized by its enhancement by supervillin, an actin-binding and myosin-II binding protein (Puthenveedu et al., 2010).

Both active and inactive integrins are recycled through different compartments at different rates. This has been especially documented for Integrin-β1 (Arjonen et al., 2012). Inactive β1 integrins can be endocytosed through a dynamin and clathrin-dependent endocytosis to early endosomes (EE) in a Rab5- and Rab21-dependent manner. This endocytosis is then quickly balanced by the Rab4-dependant recycling to Arf6-positive protrusions. Thus, inactive β1 integrins predominantly traffic through the previously described short loop.

Active β1 integrin is endocytosed predominantly via clathrin-independent Rab21 and Swip-1 regulated CLIC/GEEC (CG) – endocytosis (with a minor fraction endocytosed via a clathrin-dependent route) to a Rab5- and Rab21-positive EE (Arjonen et al., 2012; Moreno-Layseca et al., 2019). Recycling via this route is slower and involves Integrin-β1

being present in Rab11-positive endosomes, therefore predominantly using the long recycling loop (Arjonen et al., 2012), but also involving a step of Eplin α- and actin-dependent endosomal tubulation (Jäntti et al., 2024).

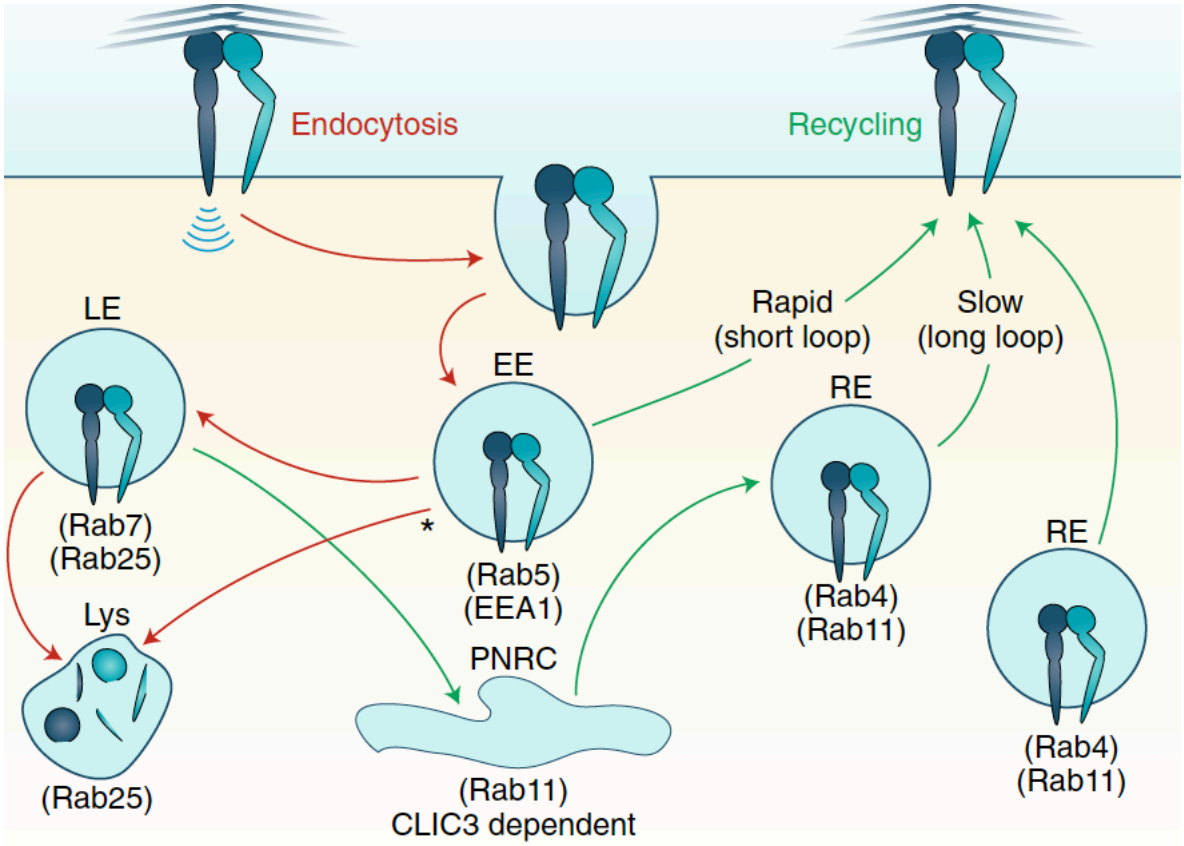

Figure 3- Integrin recycling loops (from Moreno-Layseca et al., 2019)

LE= late endosome; Lys=lysosome, PNRC=perinuclear recycling compartment

4.1.2.3 Integrin trafficking regulation

Integrin internalization is a continuous process in adherent cell types and the exact triggers of receptor uptake remain poorly understood. Integrin uptake has been linked to focal adhesion turnover. Integrin-ECM interactions induce the formation of focal contacts (FC) leading to the interaction of integrins with F-actin. When the connection to actin is disrupted through the disassembly of FCs, microtubules are targeted to the disassembling adhesions and clathrin adaptors have been implicated in the process (Ezratty et al., 2009, 2005). However, strong evidence for direct integrin uptake from

adhesions in lacking. The prevailing view is that unengaged integrins are taken up by endocytosis. These can be, for example, in their active conformation, adhering to ligand fragments still in the endosomes (Alanko et al., 2015; Moreno-Layseca et al., 2019; Nader et al., 2016) or inactive receptors clustered by extracellular glycans at the PM (Lakshminarayan et al., 2014; Shafaq-Zadah et al., 2016). However, more work is needed to determine exactly what regulates integrin endocytosis in different contexts.

Through their action within recycling loops, Rab and Arf GTPases are both regulators of integrin trafficking. Whereas Rab mostly control the fusion of membrane vesicles, as well as their transportation and that of cargo proteins (Zerial and McBride, 2001), Arf preferentially promotes the recruitment of coating proteins such as clathrin from the cytosol to the membrane (D'Souza-Schorey and Chavrier, 2006). As an example, Rab21 locked in a GDP-bound state causes β1-integrin accumulation at the PM at FAs. However, when locked in a GTP-bound state, this causes its accumulation in endocytic vesicles (Pellinen et al., 2006; Simpson and Jones, 2005).

GTP-locked Arf6 results in β1 accumulation in PI(4,5)P2 (phosphatidylinositol diphosphate)-containing macropinocytic vesicles (Brown et al., 2001). Conversely, AGAP1, an Arf6 GAP, promotes the recycling of active integrins to protrusions and drives invasion. This shows that the activation and inactivation of Arf6 is important for integrin trafficking, respectively its endocytosis and its recycling to the membrane (Nacke et al., 2021; Nikolatou et al., 2023).

Several studies have focused on the cytoplasmic domains of β subunits for trafficking regulation. Sequences have been identified on β1, β2 and β3 cytoplasmic tails (Caswell and Norman, 2006). In addition, the cytoplasmic domains of integrin α subunits contain key elements mediating signaling and playing a role in integrin internalization. For instance, the aforementioned Rab21 binds to a conserved sequence found in all integrin α tails to induce endocytosis (Pellinen et al., 2006; Pellinen and Ivaska, 2006). Additionally, AP2-μ has been shown to interact with a specific subset of integrin α tails harboring a classical AP2-binding motif, while Dab2 and ARH interact with integrin β cytoplasmic tails and regulate endocytosis (Caswell et al., 2007; De Franceschi et al., 2016).

4.1.2.4 Integrin trafficking functional consequences

Differential regulation of integrin recycling evidently plays a role on the integrin availability at the PM. This impacts different cell processes, such as polarity and cell migration and invasion.

4.1.2.4.1 Apicobasal polarity

Apicobasal polarity will be further discussed in section **4.2**. As seen previously, Rab5 and Arf6 are present in multiple integrin recycling loops and respectively activate PI3K and PIP5K. PIP5K's product PI(4,5)P_2 regulates actin remodeling as well as other actin-binding FA proteins such as ezrin, which is a specific apical marker and an apicobasal polarity stabilizer (Shin et al., 2005). Another protein of the Rab family, Rab10, has also been shown to mediate integrin recycling (Jin et al., 2021) and, simultaneously, has been identified around the Trans-Golgi Network (TGN) and involved in the polarized trafficking from basolateral regions (Larocque and Royle, 2022). As such, integrin trafficking plays an important role in apicobasal polarity maintenance.

4.1.2.4.2 Cell migration and invasion

Integrin availability modulated by recycling controls cell migration and invasion (Paul et al., 2015). In pancreatic and ovarian carcinoma, preferential recycling of $\alpha5\beta1$ over $\alpha V\beta3$ promotes a switch from mesenchymal to pseudopodial cell migration and cell invasion (Muller et al., 2009). It is important to mention that the impact of integrin endocytosis and recycling is context-dependent and varies between different cancer types. In ovarian cancer, Rab25 associates with $\beta1$ integrin and increases the recycling of the $\alpha5\beta1$ towards the cell surface, thus promoting an invasive phenotype (Caswell et al., 2007). However, in head and neck cancer, cells lacking Rab25 will present an invasive phenotype and detach from the primary tumor (Amornphimoltham et al., 2013). In bladder cancer, a Rab11-coupling protein (RCP or Rab11fip1) enhances the recycling of $\alpha5\beta1$ and promotes invasive cell migration (Rainero et al., 2012). Interestingly, $\alpha v\beta3$ can

inhibit the RCP-dependent recycling of α5β1, showing a competitive relationship between integrin heterodimers (Caswell et al., 2008; Christoforides et al., 2012).

Interestingly, the cell's glycocalyx can also play a role on cell invasion via integrin endocytosis. Indeed, the glycocalyx can facilitate integrin clustering (Paszek et al., 2014, 2009) which, through a recycling activation, can cause progression and invasion in cancers such as glioblastoma (Barnes et al., 2018). Cell migration and adhesion in normal epithelial cells and during development has been shown to be regulated by the transport of Integrin-β1 from the PM to the TGN to be recycled at the leading edge (Shafaq-Zadah et al., 2016).

Integrin trafficking influences invasion by regulating integrin recycling. For instance, HS1-associated protein X-1 (HAX-1) regulates clathrin-dependent endocytosis of αvβ6 integrin and facilitates invasion (Ramsay et al., 2007). Integrin internalization through the PKCα- and RhoC-dependent FMNL2 activation promotes integrin internalization and invasion of melanoma cells (Wang et al., 2015).

4.1.2.5 Integrin glycosylation and its consequences

Integrins have multiple N-glycosylation and O-glycosylation sites. The glycosylation profile of integrins change along their journey from the ER to the PM. In the ER, integrins are in a high-mannose state, characterized by a majority of mannose residues on the integrin glycosylation sites. Their glycosylation profile gets more complex when processed in the Golgi and brought to the PM, leading to so-called *hybrid* or *bisected* glycosylations, with sialic acid (SA), N-Acetylglucosamine (GlcNAc), galactose (Gal), and fucose (Fuc) residues.

The glycosylation sites of the α5β1 have been particularly well documented. It contains 26 N-glycosylation sites, amongst which 14 on the α subunit and 12 on the β subunit. The differential glycosylation on these sites has been shown to modulate the interaction with the ECM as well as integrin activation (Janik et al., 2010) and conformational changes (Isaji et al., 2004; Zhao et al., 2008). For instance, hyposialilation (ie. a low proportion of

SA residues) of β1-integrin enhances its binding to fibronectin (Passaniti and Hart, 1988; Reddy and Kalraiya, 2006).

Glycosylation of integrins has various functional consequences. One of the most studied examples is the β1 subunit. For instance, the removal of N-glycosylations on the βI domain decreases the formation of heterodimers, thus inhibiting cell spreading (Isaji et al., 2009). Direct consequences of glycosylation on endocytosis are a bit more unclear and indirect. Galectin-1 (Gal1) and Galectin-3 (Gal3) both interact with the glycosylated extracellular domain of the β1 subunit and control its endocytosis and recycling. For instance, Gal3 promotes mechanical deformation of the plasma membrane and a subsequent clathrin-independent endocytosis. Additionally, Gal1 knockdown leads to intracellular accumulation of β1-integrin (De Franceschi et al., 2016; Fortin et al., 2010; Furtak et al., 2001; Lakshminarayan et al., 2014). This link between glycosylation and recycling goes further, as it has been shown that an integrin-β1 cytoplasmic-tail mutant, which is not recognized and recycled by sorting nexin 17, is predominantly degraded in lysosomes resulting in low levels of glycosylated or "mature" forms of Integrin-β1 on the plasma membrane. Therefore, the level of mature, fully glycosylated integrin would correlate with active recycling of endocytosed Integrin-β1 back to the plasma membrane (Böttcher et al., 2012).

Other documented examples can be found in α subunits, such as α5. α5 lacking N-glycosylation sites showed increased cell surface localization and delayed internalization of the active form of the α5β1 heterodimer (Hang et al., 2017). It has also been shown that N-glycans on the α5β1 heterodimer allow the clustering of Gal3, which in return clamps it in its bent shape and primes it for endocytosis (Shafaq-Zadah et al., 2023).

4.1.3 Integrin adhesion complexes (IACs)

4.1.3.1 Types of IACs

Integrins are transmembrane proteins, with a short cytoplasmic tail, linking the cell to the ECM, intracellular proteins and the cytoskeleton. This link is permitted by a repertoire of proteins interacting with this cytoplasmic tail and/or each other, as well as with the actin microfilaments. The resulting protein complex, or adhesome, is composed of 147 proteins developing 361 different interactions, and giving rise to structures called Integrin Adhesion Complexes (IAC) (Chastney et al., 2021, 2020; Conway and Jacquemet, 2019). This adhesome is composed of integrins, cargo adaptors, scaffolding proteins, signaling molecules and components of the cytoskeleton. 60 of these proteins are part of a "consensus adhesome" sequence, centered around three axis: ILK-PINCH-kindlin, FAK-paxilin, talin-vinculin and α-actinin-zyxin-VASP (Horton et al., 2016, 2015).

IACs all involve integrins but are of different nature depending on their structure and the other proteins involved in the adhesion. Amongst them, we can find hemidesmosomes (Jones et al., 2017), podosomes (Veillat et al., 2015), invadopodia (Eddy et al., 2017), immunological synapses (Dieckmann et al., 2016) as well as Focal Adhesion (FA)-like structures.

FA-like structures constitute a link between the ECM and actin filaments and can be divided depending on their levels of maturations. From early filopodial adhesions, these IACs mature into nascent adhesions, proper FAs, and finally fibrillar adhesions (FBs). While early adhesions mostly function as a constant sensor of the cell environment, late adhesions are more specialized into other functions such as traction and ECM remodeling (Jacquemet et al., 2019; Zaidel-Bar et al., 2004, 2003). This maturation of FA-like structures is molecularly characterized, with a loss of talin and a recruitment of tensin along the maturation (Rainero et al., 2015).

Maturation and strengthening are also largely mediated by vinculin. Indeed, talin and vinculin are both recruited in early adhesion and the unfolding of the talin rod domain exposes vinculin binding sites. This allows a strengthening of the adhesion by increasing the talin/actin interaction (Atherton et al., 2015; Gingras et al., 2009; Han et al., 2021;

Himmel et al., 2009) and via vinculin binding to actin. Vinculin's activity for actin increases with mechanical load, therefore stabilizing the adhesion throughout maturation (Baumann et al., 2023).

4.1.3.2 Structure of IACs

IACs are layered vertically (see Figure 4). Most proximal to the ECM, on the plasma membare is first a layer of integrins, then a layer of adaptors such as paxillin and Focal Adhesion Kinase (FAK), higher up a layer of force transmitters such as talin, tensin and vinculin, and an actin regulatory layer (Case et al., 2015; Liu et al., 2015). The layering has been shown to change upon adhesion maturation with the position of vinculin moving higher with adhesion maturation in mesenchymal cells (Case et al., 2015) and N to C-terminus orientation of vinculin being distinctly "up-side down" in stem cells (Xia et al., 2019; Stubb et al., 2019). While the significance of the altered orientation remains to be fully elucidated, these studies imply that the vertical orientation may be a key determinant of IAC function in specific contexts such as during differentiation. Finally, actin interacting proteins, tropomyosins and α-actinin localize to different layers of IACs and regulate IAC turnover and integrin-mediated cell migration (Kumari et al., 2024).

The structure of IACs are affected by different parameters, such as the integrin heterodimers involved (Schiller et al., 2013) and their activation state (Byron et al., 2015), the ECM ligands (Humphries et al., 2009) and the previously mentioned maturation state (Horton et al., 2015).

The maturation of nascent adhesions into FAs are driven by actomyosin contractility, which generates the necessary forces for adhesion strengthening and signaling (Han et al., 2015; Roca-Cusachs et al., 2013). *In vitro*, liquid-liquid phase separation (LLPS) experiments have shown that p130Cas and FAK are involved in the clustering stage, while LIMD1 is implicated in the recruitment of proteins to IACs during this actomyosin-dependent maturation (Case et al., 2022; Y. Wang et al., 2021)

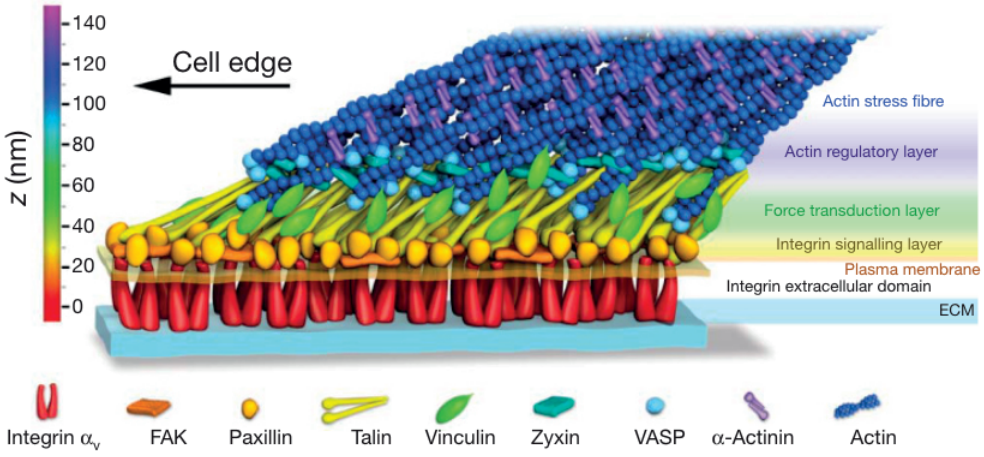

Figure 4- FA structure (from Kanchanawong et al., 2010)

Amongst several studies, FA-mediated adhesion was described using the molecular clutch model. It features a ligand-binding protein (clutch) composed of an ECM-receptor, such as an integrin heterodimer, and its adaptors linking it to the cytoskeleton (Bangasser et al., 2013; Chan and Odde, 2008; Elosegui-Artola et al., 2016; Isomursu et al., 2022). In this model, another unit, called motor, is composed of the actomyosin contractile force. This force is transmitted to the substrate through the clutches, thus enhancing cell spreading.

4.1.3.3 IAC signaling

Through integrins, IAC integrate biochemical and mechanical signals from the environment and mediate durotaxis (cells migrating in response to an ECM stiffness gradient towards increasing rigidity) and haptotaxis (cells migrating in response to an

ECM component gradient). Mechanical stimulations sensed by IACs cause YAP and TAZ to translocate to the nucleus where they bind to transcription factors of the TEAD family to regulate gene expression (Charras and Sahai, 2014; Cho et al., 2017; Kechagia et al., 2019).

FAs are phosphorylation platforms, with important roles of kinases and phosphatases like Src and the aforementioned FAK and paxillin (Humphries et al., 2019). The small GTPases signaling downstream of IACs regulate protrusion, cell contractility and cytoskeleton dynamics in general. This dynamic is finely controlled by the well described RhoA/Rac1 balance and mutual exclusion which controls integrin adhesion, with RhoA promoting cell contraction and Rac1 cell spreading (Bass et al., 2007; Jacquemet et al., 2013). Cells can switch between these two modes and therefore contribute to IAC formation (Lawson et al., 2014). This is discussed in further detail in section **4.2.1.1.3**.

IACs are also characterized by their spatiotemporal regulation. They constantly assemble and disassemble, and this process is mediated by several mechanisms including phosphorylation of different integrins and their adaptors, or endocytosis (Ezratty et al., 2009; Wilhelmsen et al., 2007; Zaidel-Bar et al., 2007). This causes a constant regulation in the adhesion strength. For instance, integrins are very motile within FAs and stay immobilized for less than 80 seconds, but this dynamic varies amongst integrin heterodimers (Rossier et al., 2012; Tsunoyama et al., 2018).

4.1.4 Integrins in cancer

Integrins can have an important role in cancer, namely in its initiation and progression. They have also been considered as targets for anti-cancer treatments (Hamidi and Ivaska, 2018).

4.1.4.1 Integrins in tumor initiation

Integrin-mediated interactions influence different cell functions, such as survival and proliferation by modulating signaling pathways such as the PI3K/Akt, Erk/MAPK, and Rho

GTPase pathways. In addition, some integrins such as α6β4 enhance oncogenic signals of receptor tyrosine kinases (RTK). Indeed, it amplifies HER2 signaling and promotes mammary tumorigenesis (Rubashkin et al., 2014). It also potentiates the oncogenic activity of the MET receptor (or HGFR, hepatocyte growth factor receptor) by engaging β4-integrin and the integrin associated tetraspanin CD151 (Bertotti et al., 2006, 2005).

Conversely, some integrins can act as tumor suppressors. In some occurrences, the αvβ3 heterodimer has been reported to suppress tumor growth by inducing cell differentiation and apoptosis (Ramovs et al., 2017). Loss of integrin αvβ3 expression has been associated with increased tumor progression and metastasis. In this way, the role of integrins in tumorigenesis is ambiguous, as integrin-mediated adhesion to the ECM regulates the cellular response to growth factors, which can either inhibit or promote tumor initiation depending on the cellular context and the involved heterodimers (Alanko et al., 2015).

4.1.4.2 Integrins in cancer invasion and metastasis

Integrins are implicated in cancer cell invasion and metastasis. Indeed, they facilitate ECM degradation, cell motility and invasion by upregulating metalloproteinases (MMPs) and interacting with other proteases (Macedo et al., 2015). For instance, integrin αvβ6 promotes invasion in carcinoma cells by upregulating MMP-9, which degrades the ECM and facilitates cancer cell migration (Nardone et al., 2017). Additionally, integrin α6β1 has been implicated in the invasion of breast cancer cells by activating urokinase (uPA), a protease involved in ECM degradation.

Integrins also contribute significantly to ECM remodeling by cancer-associated fibroblasts (CAFs), which generates a stiffer ECM, enhancing cancer cell migration and invasion (Winograd-Katz et al., 2014). Further details will be given in section **4.3.3.1**. For example, integrin α11β1 expression in CAFs has been shown to increase ECM stiffness, which promotes an invasive behavior of cancer cells (Cox et al., 2013). Furthermore, integrins play a crucial role during metastasis, supporting various steps such as

intravasation, survival of circulating tumor cells (CTCs), extravasation into secondary sites, and colonization of new tissues (Labernadie et al., 2017). Integrin β1, for instance, helps the survival of circulating tumor cells by maintaining cell-ECM interactions and activating survival pathways that prevent anoikis (a programmed cell death that occurs when cells detach from the ECM) (Desgrosellier et al., 2009).

During extravasation, heterodimers such as α3β1 facilitate the adhesion of cancer cells to the endothelial cells lining blood vessels, thus increasing their escape rate into surrounding tissues (Labernadie et al., 2017). Integrins also guide the formation of invasive structures such as invadopodia, which are protrusions that degrade the ECM and allow cancer cells to invade surrounding tissues.

4.1.4.3 Targeting integrins for anticancer treatments

Given their significant roles in tumor progression and metastasis, integrins are attractive targets for anti-cancer therapies. Therapeutic strategies include the use of monoclonal antibodies to block integrin function, integrin-directed delivery of therapeutics, and the inhibition of integrin-mediated signaling pathways. For example, the monoclonal antibody etaracizumab targets integrin αvβ3 and has shown promise in inhibiting angiogenesis and tumor growth in preclinical models (Canel et al., 2013).

Another strategy involves the use of integrin antagonists, such as cilengitide, which targets integrins αvβ3 and αvβ5 and has demonstrated anti-angiogenic and anti-tumor effects in glioblastoma (Borghi et al., 2010). However, so far, directly targeting integrins in cancer has failed, mostly because of cell plasticity, integrin redundancies and difficulty in patient stratification. Additionally, novel approaches such as integrin-targeted nanoparticles for drug delivery are being developed to improve the specificity and effectiveness of cancer treatments. For instance, integrin-targeted liposomes loaded with chemotherapeutic agents have shown improved delivery to tumor cells, reducing systemic toxicity and enhancing anti-tumor.

4.2 Apicobasal polarity of epithelial cells

A crucial feature of epithelial cells is to present an apicobasal polarity. This can be defined as an asymmetric segregation and distribution of membrane components such as proteins and lipids to distinct membrane sectors. Epithelial cells have an apical membrane facing the outside of the body or internal cavities named lumen, as well as a basolateral membrane on the opposite side featuring cell/ECM-interaction proteins, such as integrins.

This asymmetry allows the emergence of specialized cell functions (Nelson, 2003). The first polarized cells in mammals appear as soon as the 8-to-16 cells division at the blastocyst stage, further leading to a polarized trophectoderm (TE) and an apolar Inner Cell Mass (ICM) (Gerri et al., 2020; Nikas et al., 1996).

4.2.1 Polarity establishment

4.2.1.1 Molecular actors

The polarization process in cells is first initiated by cell-cell contacts (Bryant and Mostov, 2008). The process that polarizes the epithelium following this cue is called polarity establishment. During the formation of nascent cell-cell adhesions, a dimerization of E-cadherins will occur, thus triggering the recruitment of AJ and Tight Junction (TJ) proteins that will act as anchors for polarity proteins.

Three family of molecules have been reported to be a part of this polarity establishment process: polarity complexes, phosphoinositides (PIs) and Rho-GTPases.

4.2.1.1.1 Polarity complexes

Three protein polarity complexes have been well characterized across the literature. This molecular machinery is highly conserved in vertebrates.

→ **The Par3/Par6/aPKC complex** defines the apical domain. It is composed of Partition Defective 3 and Partition Defective 6 (Par3 and Par6) as well as atypical protein kinase C (aPKC) (Kemphues et al., 1988). There are three different Par6 proteins that can be found together as complexes or alone depending on the cell type: Par6A/C, Par6B and Par6D/G. Par6D/G is mostly found at TJs, Par6B in the cytosol, and Par6A/C in both. Par6 proteins help the accurate localization of other adhesion proteins and act as a mediator for the interaction between aPKC, Par3 and Lgl (Lethal Giant Larvae). For instance, downregulation of Par6 impairs TJs (Hurd et al., 2003; Joberty et al., 2000).

Two Par3 proteins have been identified: Par3A and Par3B. However, only Par3A binds atypical PKC (aPKC) and plays a role in the polarity complex (Lin et al., 2000). Indeed, after its association with Junctional Adhesion Molecules (JAMs) at nascent junctions, it recruits Par6 and aPKC therefore causing the junction's maturation. Indeed, it has been shown that a dysregulation in Par3 expression causes an incorrect localization of Par6, aPKC and defective TJs maturation (Itoh et al., 2001; Mizuno et al., 2003).

Interestingly, aPKC has been named "atypical" since it features an N-terminal PB1 domain that cannot be found in conventional PKCs. There are two isoforms of aPKC (aPKCλ/ι and aPKCζ), found to be colocalizing with Par proteins at TJs (Suzuki et al., 2001).

→ **The Crb/PALS1/PATJ complex** also defines the apical domain. First characterized in *Drosophila Melanogaster*, it is composed of Crumbs (or Crb), which interacts with PALS1 and PATJ (Tepass et al., 1990).

Three Crb proteins have been described: Crb1, Crb2 and Crb3. While they present varied localization within tissues, Crb3 is mostly found at the apical domain in epithelial cells. Its FERM domain allows it to interact with the cytoskeleton (Roh and Margolis, 2003) and even with Par6, thus showing an inter-complex interaction profile (Lemmers et al., 2004).

Crb3, PALS1 and PATJ are found at the apical pole and around TJs. PATJ interacts with TJ proteins such as ZO-1, ZO-3 and Claudin-1. While downregulation of PALS1 causes mislocalization of E-cadherin (Wang et al., 2007), dysregulation of PATJ prevents ZO-1,

ZO-3 and Claudin-1 from correctly localizing at TJs (Lemmers et al., 2004; Michel et al., 2005; K. Shin et al., 2005), therefore showing the role of this complex as a scaffold for TJ establishment during cell-cell contacts.

→ The **Scrib/Lgl/Dlg complex** defines the basolateral domain. The SCRIB (Scribble planar cell polarity protein), LGL (Lethal giant larvae) and DLG (Disc large) genes have first been discovered in *Drosophila Melanogaster*. Scribble plays a role in excluding apical proteins from the basolateral domain (Bilder and Perrimon, 2000a). While 5 Dlg-family proteins exist in mammals, Dlg1 has been the most extensively studied. It binds to APC, β-catenin and PI3K and is localized at the basolateral domain (Laprise et al., 2004; Matsumine et al., 1996).

The Lgl family presents two proteins: Lgl1 and Lgl2. They bind to the Par6/aPKC complex, after which aPKC phosphorylates Lgl causing its exclusion from the apical domain and its localization to the basolateral domain. This plays a key role in the apicobasal polarity establishment process (Suzuki et al., 2001).

4.2.1.1.2 Phosphoinositides (PIs)

PIs are a subtype of phospholipids that arise from a single precursor named phosphatidylinositol (PtdIns). This precursor can be phosphorylated at three different sites, therefore creating seven different PIs that have a different cellular localization (Di Paolo and De Camilli, 2006). These differentially phosphorylated PIs act as structural and signaling mediators. For instance, phosphatidylinositol-(4,5)-diphosphate ($PI(4,5)P_2$) controls the activity of the actin cytoskeleton by regulating the activity of actin-binding proteins (Yin and Janmey, 2003). The distribution of PIs is one of the main apicobasal polarity markers, with $PI(4,5)P_2$ being enriched at the apical membrane and phosphatidylinositol-(3,4,5)-triphosphate ($PI(3,4,5)P_3$) being enriched at the basolateral domain (Buckley and St Johnston, 2022; Gassama-Diagne et al., 2006; Martin-Belmonte et al., 2007).

→ **PI(4,5)P_2** is situated at the apical domain. A mechanism has been proposed (Martin-Belmonte and Mostov, 2007), in which PTEN (Phosphatase and tensin homolog deleted on chromosome ten), a phosphatase, converts PI(3,4,5)P_3 to PI(4,5)P_2. PTEN is targeted to the apical pole through a β1-integrin/ECM contact, activating the GTPase Rac1 (see section **4.2.1.1.3**). Because PTEN is targeted to the apical domain, it results in a polarization of PIs. PI(4,5)P_2 at the apical site recruits Annexin-2 (Anx2), which in turn recruits the GTPase Cdc42 (see section **4.2.1.1.3**), which acts as a binding platform for proteins of the Par6/aPKC complex, thus further characterizing an apical domain. PI(4,5)P_2 also interacts with other apical markers, such as ezrin, radixin and moesin (Di Paolo et al., 2002) which are polarity stabilizers, linking the apical membrane to the actin cytoskeleton.

→ **PI(3,4,5)P_3** is situated at the basolateral domain. The PI(4,5)P_2/PI(3,4,5)P_3 balance is finely regulated by the previously mentioned PTEN, but also by PI3K (phosphatidylinositol-3 kinase), which phosphorylates PI(4,5)P_2 into PI(3,4,5)P_3. PTEN and PI3K are therefore potent polarity drivers, and have been found to be regulated by localized Ras signaling (see section **4.2.1.1.3**) (Sasaki et al., 2004). Insertion of PI(3,4,5)P_3 within the apical domain of MDCK (Madin-Darby canine kidney) cyst is sufficient to localize basolateral molecular markers and inverting polarity (Gassama-Diagne et al., 2006).

4.2.1.1.3 Rho-GTPases

GTPases are enzymes that can be described as GTP-dependent molecular switches. They can take two different conformations: one is bound to GTP (Guanosine triphosphate), which is often called “active” or “on” state, while the other is bound to GDP (Guanosine diphosphate), the “inactive” or “off” state. Active GTPases can interact with effector molecules up until they go back to an off state. These GTPases can be divided in five categories: Ras, Rho, Ran and the aforementioned Rab and Arf. Rho-GTPases have been described to play a major role in polarity establishment, which are the ones we will be describing here (Etienne-Manneville and Hall, 2002).

The switch between the active and inactivate states of Rho-GTPases are regulated by activators (GEFs – Guanine nucleotide exchange factors) and inactivators (GAPs – GTPase-activating proteins) (Bos et al., 2007). They can also associate with dissociation inhibitors (RhoGDIs) that keep them in an inactive state (Boulter and Garcia-Mata, 2012). Amongst the twenty identified Rho-GTPases, three are playing an important role in polarity establishment: **RhoA**, **Rac1** and **Cdc42**. Mutations in one of these GTPases is sufficient to trigger loss or misorientation of the apicobasal polarity (O'Brien et al., 2001).

While RhoA, Rac1 and Cdc42 all regulate the actin cytoskeleton and are implicated in apicobasal cell polarity, they each have specific roles (Mack and Georgiou, 2014):

→ **RhoA** is implicated in stress fiber formation, actomyosin contractility and activation of myosin-II. RhoA supports the formation and assembly of actin filaments and generates contractile forces. Linking it to polarity, RhoA regulates AJs and TJs which are crucial to the stability of the epithelium (Ridley and Hall, 1992).

RhoA is recruited by the Crb/PALS1/PATJ complex in the first steps of cell-cell contacts and therefore increases cell contractility thanks to its effector ROCK. ROCK activity generates an actin belt in mature AJs. RhoA is therefore mostly localized at the apical domain, and recruits Rac1 GAPs which effectively disable Rac1 activity at the apical domain (Ratheesh et al., 2012). Therefore, the mutual RhoA/Rac1 exclusion is a founding characteristic of the apicobasal polarity establishment.

It should be kept in mind that the RhoA/Rac1 gradients can vary amongst the stages of apicobasal establishment and the maturation stages of cell-cell junctions. While RhoA plays a role in the maturation of the actomyosin belt on the AJs, it is then deactivated at the apical pole by its GAP, p190RhoGAP, but can later on be recruited once again for further maturation of AJs through E-cadherin recycling and activation of Myosin-II (Gomez et al., 2011).

→ **Rac1** is implicated in lamellipodia and membrane protrusion formation. It supports actin polymerization and allows cell migration. Through the establishment of a front-rear

polarity, it allows cells to move in a mesenchymal cell migration mode (Ridley and Hall, 1992). Rac1 impacts apicobasal polarity by signaling downstream of Integrin-β1 and assembling laminins at the basal membrane (O'Brien et al., 2001). It also plays a role at nascent AJs, just like RhoA. Indeed, Rac1 activation causes actin polymerization and membrane protrusions though its effector WAVE (Yamazaki et al., 2007), which causes cell-cell contacts and the formation of AJs. Once AJs are established, Rac1 is activated there by its GEFs: VAV2 and Tiam1 (Fukuyama et al., 2006; Hordijk et al., 1997; Malliri et al., 2004) which have been recruited by the E-cadherins of AJs. Rac1 inhibition has been shown to prevent clathrin-dependent cell-cell adhesion and proper epithelium polarization (Ehrlich et al., 2002).

→ **Cdc42**'s role is a key regulator of polarity as it regulates the localization of polarity complexes such as Par3/Par6/aPKC, and, consequently, the formation of TJs. Cdc42 is crucial in the formation of filopodia and plays a role in the formation of polarized structures in epithelial cells such as microvilli (Ngok et al., 2014).

Cdc42 acts by first binding to Anx2 and accurately localizes the Par3/Par6/aPKC (Martin-Belmonte et al., 2007). Cdc42 also localizes the Crb/Pals1/Patj complex through a Rab11-dependant mechanism (Schlüter et al., 2009).

Cdc42 forms filopodia through its activation of Arp2/3, which promotes branching of actin cytoskeleton in an N-WASP-dependent mechanism (Ngok et al., 2014). Just like other Rho-GTPases, Cdc42 activity is temporally and spatially controlled. Indeed, it plays an important role in the early stages of cell-cell junction, but the presence of Cdc42 GAPs such as ARHGAP17 at the apical pole and GEFs such as Tuba at the basal pole indicates that Cdc42 inactivation is necessary for junctional maturation (Elbediwy et al., 2012). The localized concentration and activation of Cdc42 is needed for apical growth, and it has been shown that Cdc42 inhibition prevents the proper growth and polarization of MDCK cysts (Jaffe et al., 2008; Salat-Canela et al., 2023).

4.2.1.2 Sequence of events and interactions during polarity establishment

During polarity establishment, Crb recruits PALS1 through its PDZ domain, which then recruits Par6. These components of the Crb/PALS1/PATJ complex, through Cdc42 and aPKC, mediate the phosphorylation of Par3, Par1 and Lgl. This causes exclusion of Lgl (along with other basolateral proteins such as Dlg and Scrib) from the apical domain. The phosphorylation of Par1 prevents the basal recruitment of apical markers such as Par3. This signaling cascade explains the segregation between Crb and Par complexes at the apical pole, and Scribble complex at the basolateral domain (see Figure 5).

As mentioned before, PIs are also responsible for membrane asymmetries. PTEN is recruited to cell-cell junctions through its interaction with Par3, which causes a higher concentration of $PI(4,5)P_2$ at the apical domain which in return causes the recruitment of Cdc42 through Anx2. Cdc42 activates aPKC, which closes a signaling loop as it can in return, phosphorylate Par3, Par1 and Lgl.

PI3K is recruited by E-cadherin to basolateral junctions which recruits basal markers such as Dlg, and causes a higher concentration of $PI(3,4,5)P_3$ (Rodriguez-Boulan and Macara, 2014). In this process, E-cadherin plays a central role as it mediates junction maturation by reducing the surface tension at cell-cell interactions (Slováková et al., 2022; Stachowiak et al., 2012; Winklbauer, 2015). Upon E-cadherin binding, there is a RhoA inactivation and a Rac1 activation, therefore better characterizing the basal domain (Anastasiadis et al., 2000; Yamada and Nelson, 2007).

4.2.2 Polarity orientation and maintenance

4.2.2.1 ECM contact and subsequent orientation of polarity markers

As discussed above, many key steps of the polarity establishment process have been described. Another important aspect is the polarity orientation process, i.e. the correct localization of both basal and apical poles. To detail the timeline of polarity orientation,

it is necessary to focus on a specific example. MDCK (Madin-Darby canine kidney) cells can generate polarized cysts and for this model, the sequence of events has been largely elucidated. Early on, through first MDCK cell contacts, podocalyxin (Pcx) (a glycoprotein, member of sialomucins and an apical marker) is distributed at the outer membrane of cysts. It is then endocytosed in a Rab8- and Rab11-dependant manner and delivered to a zone named AMIS (apical membrane initiation site). This is the first step of polarity orientation, as the AMIS is the precursor of what will become the apical membrane (Bryant et al., 2010). Anx2 and Cdc42 associate with the Rab8/Rab11-positive Pcx-transporting vesicles which, upon Cdc42 activation through its GEF, Tuba, initiates the luminogenesis process. Par6 bridges Cdc42 to the aPKC-Par3 complex, which allows the docking of the apical vesicle to the AMIS. This AMIS evolves to a Pcx-enriched pre-apical patch (PAP) which is where the lumen starts forming. The lumen expansion is allowed by kinase-dependent activation of apical chloride channels (Bryant et al., 2010; Li et al., 2004) (see Figure 5).

Several supplementary polarity actors have been described more recently (Bryant et al., 2014). Pcx forms a complex with NHERF1 (Na^+/H^+ Exchanger Regulatory Factor) and Ezrin (which stabilizes Pcx at the apical membrane). In cysts cultured in suspension, the inverted localization (ie. to the outer side) of this Pcx/NHERF1/ezrin complex is stabilized by the phosphorylation of ezrin through ROCK1 (a RhoA effector, member of the aforementioned ROCK family) activity. However, upon ECM sensing via $\beta1$ integrin (likely as $\alpha2\beta1$ and $\alpha3\beta1$ heterodimers), integrin heterodimers recruit FAK that leads to an activation of p190-RhoGAP which in return inactivates RhoA and causes a decrease in ezrin phosphorylation (Bryant et al., 2014). This, combined with the phosphorylation of Pcx by PKCβII induces a destabilization of the complex and a subsequent endocytosis of Pcx to the AMIS. This is followed by the action of phosphatase PP2A which dephosphorylates Pcx and causes a reassociation of the Pcx/NERF1/ezrin complex, at the AMIS this time, showing here a sequential timeline of the polarity orientation process.

This ECM-integrin contact also initiates the formation of a basal membrane with the assembly of laminin at the basal pole (O'Brien et al., 2001). This process is IRSp53-dependent, which also activates factors like WAVE leading to actin polymerization from the basal pole. Blocking Integrin-$\beta1$ forces an inverted-polarity phenotype. Conversely,

inhibiting RhoA will support a normal polarity phenotype, and this will be further described in **4.2.3** (Adams et al., 2004; O'Brien et al., 2001; Yu et al., 2008, 2004) and in **7.1**.

4.2.2.2 Trafficking of polarity proteins in the polarity orientation process

Polarity orientation goes hand in hand with redistribution of polarity-related molecules. In the case of Crb and Pcx, they are brought from the outer membrane to the AMIS by first being endocytosed in a clathrin-dependent manner. The heterotetramere Adaptor Protein Complex 2 (AP-2) is central here, playing a crucial role for the recognition and selection of polarity proteins that are destined for endocytosis (Bonifacino, 2014). This recognition is simultaneous to the formation of a clathrin triskelion-coated pit. Indeed, proteins such as Eps15 and Epsin interact with both clathrin and AP-2 to stabilize this budding endosome (Rodriguez-Boulan and Macara, 2014). Once in the early endosome (EE), Crb is brought to the AMIS through an Apical recycling endosome (ARE).

Once apically localized, Crb is constantly endocytosed and recycled back to the plasma membrane to maintain its localization. Endocytosis of Crb through ASE (Apical Sorting endosome) is then followed by a retrograde transport to the trans-Golgi network (TGN) through a Common Recycling endosome (CRE). From the TGN, it is recycled back to the apical membrane. In the TGN, the sorting of polarity proteins is helped by the heterotetramer Adaptor Protein Complex 1 (AP-1). However, some studies have shown that the localization of polarity proteins can be AP-independent (Schuck and Simons, 2004).

In a similar fashion, basolateral components traffic through BREs (Basal recycling endosomes) and BSEs (basal sorting endosomes) (Apodaca et al., 2012; Zhang et al., 2023).

After their recruitment via AP-1 and AP-2, the polarity protein-containing vesicles need to be fused at the proper membrane. This is controlled mainly by Anx2 which binds to vesicles containing apical proteins. The fusion is dependent on v-SNARE (on the vesicular

side) and t-SNARE (on the target side) proteins, the specific SNAREs involved differs between the apical and basal domains (Gerke et al., 2005; Pocard et al., 2007).

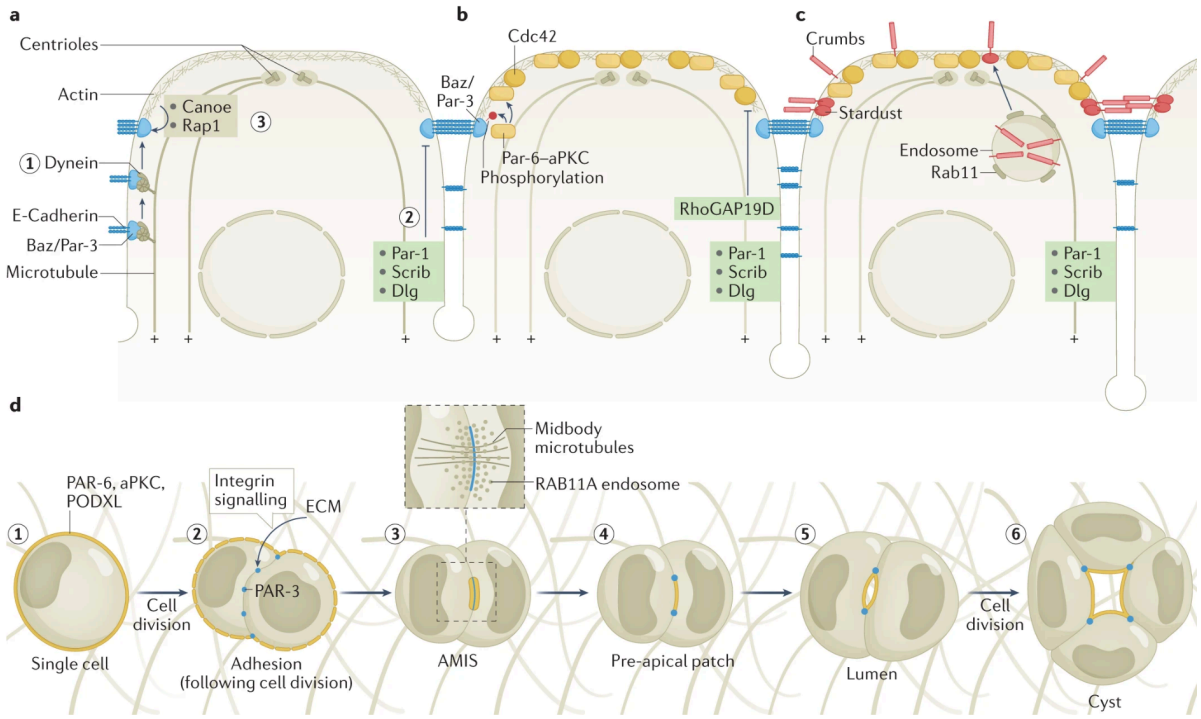

Figure 5- Polarity establishment and orientation (from Buckley and St Johnston, 2022)

a,b,c: Steps of polarity establishment. d: Polarity orientation. Stardust=PALS1, PODXL=podocalyxin

4.2.2.3 Polarity maintenance

Apicobasal polarity is maintained through the action of ERM proteins (for ezrin, moesin, radixin). Indeed, during the polarity orientation, a decrease in the phosphorylation of ezrin causes a destabilization of the Pcx/ezrin/NHERF1 complex and causes a relocalization of polarity markers (Bryant et al., 2014). ERM proteins all contain a plasma membrane-binding domain called the FERM domain (4.1,ezrin,radixin,moesin) and an actin-binding domain called C-ERMAD (C-terminal ERM-association domain). ERM proteins are found in various cells in the mammalian body, but ezrin is exclusively present in epithelial cells. When inactive in the cytoplasm, ERM's FERM and C-ERMAD domain interact and this intramolecular bond mediates the autoinhibition of the protein. Once recruited to the plasma membrane, phosphorylated by RhoA's effector ROCK1 and

bound to $PI(4,5)P_2$, the autoinhibitory interaction is disrupted, the two domains dissociate and the C-ERMAD domain become available for actin binding (Fehon et al., 2010; Saotome et al., 2004).

In intestinal epithelial cells mostly, ezrin is the only ERM protein expressed and acts as a polarity maintenance key regulator. Being a well polarized molecule, it is often used as a polarity marker (Saotome et al., 2004).

4.2.3 Inverted polarity

Inverted polarity englobes any non-conventional distribution of polarity molecules. It is always described as opposed to what a "normal polarity" would be. The normal polarity, also named "apical-in", is conventionally defined by an apical domain facing a lumen-like structure and a basolateral domain facing other cells or the ECM. However, inverted polarity sometimes called "reverse polarity" or "apical-out", is characterized by a reversion of the apical and basolateral domain while the overall polarity axis of the cell/cell cluster remains. In mammals, this inverted polarity occurs in pathological situations, an exception to this being the blastocyst development. More instances of inverted polarity can be found in other animals, such as within the *Drosophila Melanogaste*r embryo (Ebnet, 2015). All of these processes are well described in Pasquier et al., 2024 (see Figure 6). The study of inverted polarity has been the focus of **I**, which can be found enclosed at the end of this thesis.

4.2.3.1 Inverted polarity in cancer

For a long time, the loss of apicobasal polarity commonly referred to as EMT (epithelial-to-mesenchymal transition) was thought to be one of the main drivers in carcinoma progression and dissemination. It has been shown that nonpolarized epithelia were more likely to invade (Lee and Vasioukhin, 2008; Macara and McCaffrey, 2013; Peglion and Etienne-Manneville, 2023; Wodarz and Näthke, 2007). However, it has been found through histopathological analysis that some cancers such as colorectal

adenocarcinoma present structures with highly conserved AB polarity axis, with epithelial structures surrounding an inner lumen (Libanje et al., 2019).

A subtype of highly invasive carcinoma named micropapillary carcinoma show structures that have a fully inverted AB polarity (Verras et al., 2023). In these tumors, apical markers such as the membrane-bound glycoprotein MUC1 are found at the outer bound, whereas basolateral markers such as the cell adhesion molecule EpCAM is inside.

These inverted polarized structures can be found in multiple different cancers, such as breast or lung carcinomas (Adams et al., 2004; Hirakawa et al., 2022; Luna-Moré et al., 1994; Nassar et al., 2004; Siriaunkgul and Tavassoli, 1993), colorectal carcinoma (Verdú et al., 2011), cervical carcinoma (Stewart et al., 2018) and thyroid carcinoma (Asioli et al., 2013). Some cancers are even characterized by this inverted polarity, such as breast solid papillary carcinoma with reverse polarity (SPCRP) (Chiang et al., 2016) and papillary renal neoplasm with reverse polarity (PRNRP) (Al-Obaidy et al., 2020, 2019).

Inverted polarity cancer cell clusters have also been found in peritoneal effusions or pleural effusions (Ritch and Telleria, 2022; Zajac et al., 2018), in the lumen of lymphatic vessels or lymph nodes (de Boer et al., 2010; Mohammed et al., 2019) and in pools of mucins within tumors (Sun et al., 2020). These structures have been named TSIPs (Tumor spheres with inverted polarity) and can be described as tumor cell clusters that present an apical domain on their outer membrane. These structures have an apical-out polarity in suspension as expected, since there is no ECM to trigger any polarity establishment. However, in some instances TSIPs placed in matrix maintained an apical-out polarity, therefore demonstrating inverted polarity as a distinct malignant phenotype for some cancer subtypes (Canet-Jourdan et al., 2022; Okuyama et al., 2016; Onuma et al., 2021; Zajac et al., 2018).

4.2.3.1.1 Consequences of inverted polarity on cancer invasion

The presence of TSIP-like structures in cancer has a direct impact on cancer prognosis and invasion. Indeed, micropapillary carcinomas with inverted polarity structures show a high proportion of lymph node metastasis (Kuroda et al., 2004).

Because of their inverted polarity, TSIPs lack surface integrins that would allow them to form IACs with the ECM and form actin-based protrusions (Zajac et al., 2018). They propagate from a metastasis or another TSIP, budding from their structure. It has been shown that TSIPs adopt a collective amoeboid mode of migration, moving in a fashion that is similar to immune cells, which depends on friction forces and the contractility of the actomyosin ring at the rear of the cluster (Pagès et al., 2022). A partial inversion of polarity is enough to trigger invasion in a collective amoeboid manner in MDCK spheroids (Bryant et al., 2014).

4.2.3.1.2 Consequences of inverted polarity on drug resistance

In colorectal cancer organoids, TSIPs have a better resistance to chemotherapy than apical-in structures which is due to a lower proliferation of apical-out structures, therefore coffering resistance against some chemotherapies such as anti-mitotic drugs (Canet-Jourdan et al., 2022). This can also be linked to a protection that is inherently linked to inverted polarity. Indeed, transporters such as ABCB1 are localized at the outer membrane in TSIPs, causing drug exclusion (Ashley et al., 2019).

4.2.3.1.3 Consequences of inverted polarity on immune escape

Proteins necessary for the immune response such as Major histocompatibility complex (MHC) or toll-like receptors (TLRs) are polarized. Indeed, in healthy gut or lung epithelia, MHC-II proteins such as HLA-DR and HLA-DM are polarized at the basolateral domain. This polarization is essential for the regulation of CD4+ T-cells which have a well-

established anti-tumor role (Hershberg et al., 1998; Speiser et al., 2023; Wosen et al., 2018). In TSIPs with inverted polarity, MHC-II is not localized to the outward membrane. This may be linked to TSIPs escaping immune surveillance and to immunotherapy failure in cancer types with inverted polarity (Axelrod, 2019; Guo et al., 2008).

TLR-3 is also polarized in healthy tissue, as it is basolaterally localized in the intestinal epithelium (Stanifer et al., 2020). Because of this, TSIPs might lack TLR-3 on their outer membrane, therefore causing, once more, an immune escape.

4.2.3.1.4 Plasticity of inverted polarity in cancer

While the aforementioned TSIPs show an apical-out polarity in suspension, they can adopt two polarity phenotypes once embedded in an ECM. After culturing them in a collagen matrix, some of them revert to an apical-in polarity. This shift in polarity is not fully understood and has been the main object of this thesis, although an implication of the TGF-β pathway as the main driver of polarity in this system has been described (Canet-Jourdan et al., 2022). Blocking Integrin-β1 has been shown to prevent the establishment of a normal apical-in polarity in ECM-embedded TSIPs, which shows an implication of the Focal Adhesion Pathway in the polarity establishment process (Canet-Jourdan et al., 2022 and **7.1**).

4.2.3.2 Inverted polarity in genetic diseases

Some genetic diseases can cause pathological inverted polarity:

→ **Microvillus inclusion disease (MVID)** is a disease that affects absorption of nutrients through the intestinal epithelium, causing diarrhea. This disease can be cause by several mutations, including MYO5B, STX3 or STXBP2. This results in a loss of apical microvilli and mispolarization of key proteins (Schneeberger et al., 2015).

→ **Multiple intestinal atresia associated with combined immunodeficiency (MIA-CID)** is linked to a mutation in the TTC7A gene. This disease causes complete inversion of polarity in intestinal organoids (Bigorgne et al., 2014).

→ **Polycystic kidney disease (PKD)** is caused by mutations in PKD1 and PKD2 genes. This results in mispolarization of proteins leading to an abnormal cell proliferation and cyst formation (Menezes and Germino, 2019; Wilson Patricia D., 2004) in the kidney. This polarity inversion causes an alteration in fluid absorptions, therefore causing an expansion of these cysts (Li et al., 2022).

4.2.3.3 Inverted polarity in pathogen defense

Inverted polarity in epithelia caused by pathogen infection leads to a signaling to immune system. In chronic liver diseases for instance, damage caused to healthy cells causes a relocalization of ICAM-1, normally localized at the apical domain, to the basal pole. Indeed, TNF-α treatment of healthy hepatocytes is sufficient to invert ICAM-1 localization to the basal domain enhancing T-lymphocyte recruitment (Reglero-Real et al., 2014).

Some examples show that pathogen infection cause a local polarity inversion. Upon *Pseudomonas aeruginosa* infection, the intestinal epithelium cells form protrusions surprisingly enriched in basolateral markers such as PI3K, PI(3,4,5)P_3 and E-cadherin. This causes both a more favorable environment for bacterial colonization, but also triggers immune response signaling, so the effect is dual (Gassama-Diagne et al., 2006; Kierbel et al., 2007; Tran et al., 2014).

Similarly, *Neisseria meningitidis*, the cause of cerebrospinal meningitis, invades thanks to polarity disrupting. At infection sites, its membrane extensions containing basolateral and apical components destabilizes the endothelium which creates gaps allowing bacterial crossing (Coureuil et al., 2009).

4.2.3.4 Inverted polarity in development

Inverted polarity can also occur in a physiological situation, and more precisely during the early stages of embryonic development. From the 8-cell stage, blastomeres start compacting and develop an apical-out polarity. This inverted polarity is characterized by an increased localization of actin, actin-binding proteins and the Par3/Par6/aPKC polarity

complex at the outer membrane (Ducibella et al., 1977; Lehtonen and Badley, 1980; Nikas et al., 1996; Plusa et al., 2005; Reeve and Ziomek, 1981), when basolateral proteins such as the Scrib/Lgl1/Dlg1 are localized at cell/cell contacts (Hirate et al., 2013). Through asymmetrical and symmetrical divisions, polar cells differentiate into a polarized trophectoderm (TE) and an apolar Inner cell mass (ICM). ; Maître, 2017; Maître et al., 2016). The formation of the blastocoele (a lumen-like structure within the blastocyst) is interesting, because the lumen initiation at the basolateral domain obeys different laws than to the apical domain. While the apical domain does not harbor adhesion molecules and therefore makes it a favorable site for fluid accumulation, the blastocoele forming at the basolateral domain is due to the accumulation of fluid-filled microlumens, fusing to each other by Ostwald ripening, therefore creating and increasing the size of the cavity (Dumortier et al., 2019).

There is a marked plasticity in the polarity status of the blastocyst pre- and post-implantation. While the apical-out polarity has been well described pre-implantation, the polarity status adjusts during implantation. TE cells adhere to the endometrium, which requires a polarity adjustment of the blastocyst in order to avoid apical/apical repulsion. It has been shown that the mural blastocyst maintains its apical domain externally, but invert the localization of some integrins to promote the adhesion to the endometrium (Sutherland et al., 1993).

During the menstrual cycle, the polarity of luminal endometrial cells is changed, with the loss of the apical enrichment of the Par complex, the Crb complex and mucins (Whitby et al., 2020). The formation of pinopodes at the surface of the endometrium makes it receptive to implantation (Quinn et al., 2020), via different integrin heterodimers such as $\alpha v\beta 3$. No obvious link has been found between the implantation process and the involvement of integrin-$\beta 1$. Interestingly however, overexpression of Integrin-$\beta 1$ subsequent to a pathological situation, such as infection by *C. trachomatis*, enhances adhesion of the blastocyst within the Fallopian tubes and promotes ectopic pregnancies.

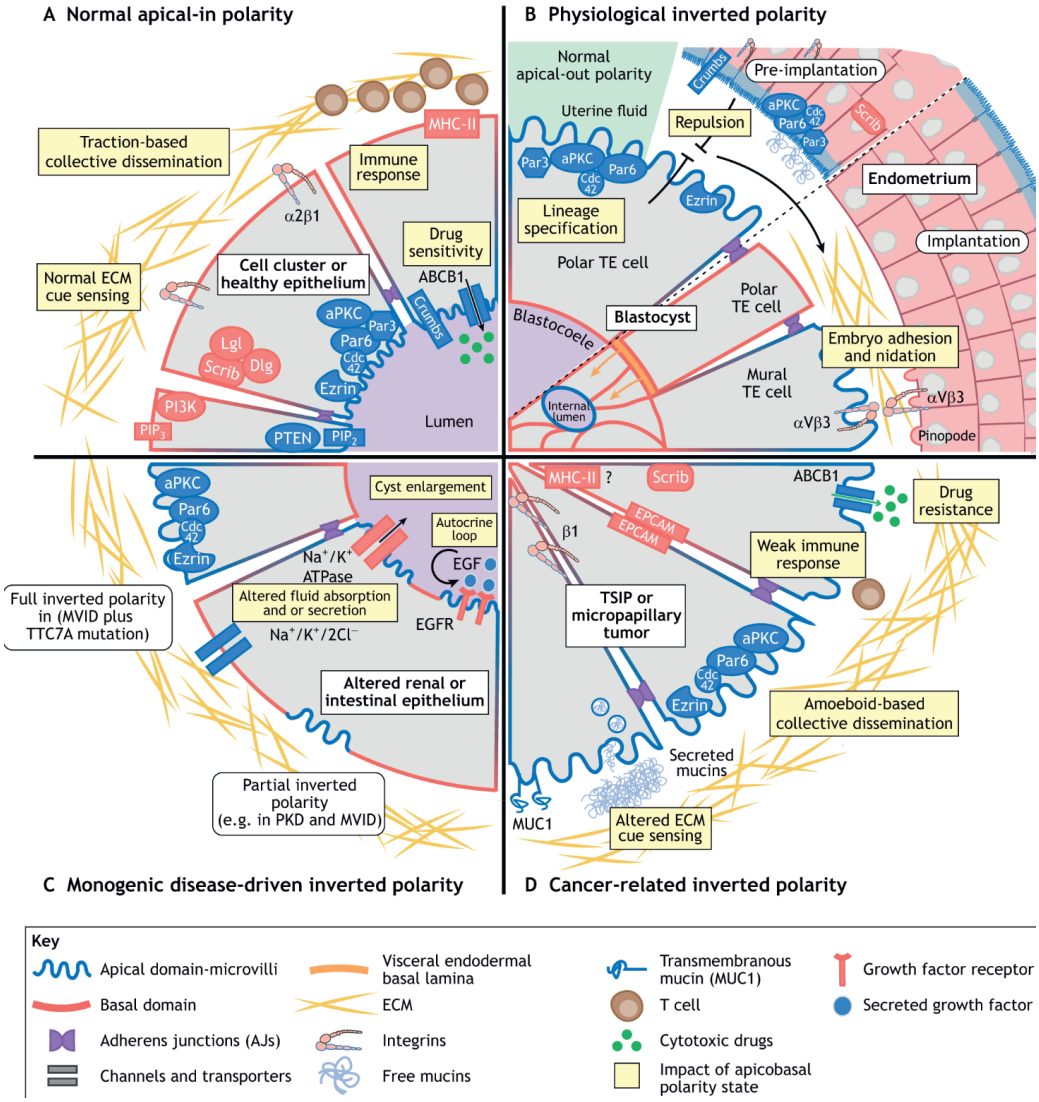

Figure 6- Inverted apicobasal polarity (from Pasquier et al., 2024)

(A) Normal epithelial polarity is regulated by the asymmetric localization of mutually antagonistic complexes. The Par and the Crumbs complexes define the apical pole which is enriched in PIP_2, PTEN and ezrin (proteins marked in blue). Below AJs, the Scribble complex defines the basolateral domain, which is enriched in PIP_3 and PI3K (proteins marked in red). ECM sensing through integrins controls the orientation of apicobasal polarity and ensures traction-based collective migration. Basal localization of MHC-II is thought to promote immune clearance of damaged cells by permitting T cell recruitment. Apical localization of the multidrug resistance transporter ABCB1 allows drugs to persist in lumens of epithelia. PIP_3, phosphatidylinositol 3,4,5-phosphate. (B) The pre-implantation blastula displays apical-out polarity, which prevents adhesion to the uterine wall due to apical–apical repulsion. During the menstrual cycle, to permit successful embryo nidation, apical determinants in the endometrium disappear from the lumen-facing membranes while integrins and pinopodes appear. In parallel, polar trophectoderm (TE) cells invert their polarity in response to emergence of the endodermal basal lamina and mural TE cells express integrins at the periphery of the blastula to promote implantation. (C) MVID enterocytes show partial inverted polarity of microvilli structures. MVID with an additional mutation in *TTC7A* results in fully inverted polarity in these cells. In PKD renal tubules, inverted polarity of ion channels and EGFR contribute to the growth of cysts via altered fluid absorption and secretion. (D) TSIPs arise from micropapillary and mucinous carcinoma. The absence of integrins and presence of mucins at the TSIP periphery prevent cell–ECM interactions resulting in tissue invasion via the collective amoeboid mode of migration. The inverted polarity of ABCB1 enhances cytotoxic drug resistance whereas basolateral localization of MHC-II could limit T cell infiltration and increase immune escape.

4.3 Biological systems to study polarity and integrin-mediated adhesions

4.3.1 Colorectal adenocarcinoma (CRC)

4.3.1.1 Healthy gut architecture

The colon is an organ which function is to uptake nutrients and water from the alimentary bolus. The role is dual, being both a structure of absorption and secretion. It is also an important epithelial barrier against pathogens. Because of all these combined functions, the colon displays a wide variety of cells with different architectures, thus creating a multifunctional epithelium.

Through histological analysis, the colon can be divided in four distinct zones from the lumen to the peritoneum (Maqbool, 2013):

→ **The mucosa** is the outermost layer (on the apical side, at the border with the lumen). This sheet is composed of the cells composing the Lieberkühn crypts, as well as the lamina propria, ie. the connective tissue and inflammatory cells joining the mucosal cells.

→ **The muscularis mucosa**, a thin muscular layer.

→ **The submucosa** is composed of nerves, blood and lymphatic vessels. It is a connective tissue surrounding the muscularis mucosa.

→ **The muscularis externa**, a thin sheet of smooth muscles.

In addition to these layers, **the serosa**, a monolayer of mesothelial cells, is one of the composing sheets of the peritoneum (the visceral layer) surrounding the gut as well most of the organs situated within the abdomen.

As mentioned above, the mucosa is composed of Lieberkühn crypts containing a set of different cells named colonic cells. These crypts increase the surface area of the gut,

therefore enhancing secretion and absorption. Different cell types are found in the crypt with specific localization and function (see Figure 7):

→ **Colonic stem cells** are situated at the base of the Lieberkühn crypt. These cells are nonmigratory, undifferentiated and maintain a pluripotent identity. They are characterized by the expression of stem cell marker Lgr5 (leucine-rich-repeat-containing G-protein-coupled receptor 5) (Barker et al., 2007). Lgr5 acts as a Wnt pathway amplifier by binding to its agonist, R-spondin. Colonic stem cells give rise to other mucosa cells, such as Paneth cells, goblet cells, enteroendocrine cells and tuft cells. This differentiation is finely tuned by a regulator called Notch. Indeed, Notch influences cell fate by activating Hes1, which represses Atoh1 to prevent secretory lineage entry. Hes1 deletion increases secretory cells production, while Atoh1 deletion eliminates them, indicating their crucial regulatory roles (Jensen et al., 2000; Shroyer et al., 2005).

→ **Deep secretory cells (DSCs)** have a similar structure and function to that of Paneth cells in the small intestine. They are issued from the first differentiation stage of colonic stem cells. They act as a protector against pathogens by secreting antimicrobial peptides such as α-defensins. These cells are also nonmigratory. They have a growth factor secretion activity and produce digestive enzymes (Bevins and Salzman, 2011).

→ **Goblet cells** have a protective function through the production of mucins. Mucins in the gut can be of two natures: membrane-bound mucins (mostly MUC1) compose the first layer, which acts as a filter protecting the epithelial cells against pathogens. The second layer is composed of free mucins (mostly MUC2), which acts as a protective layer and allows transport of secreted gut content (Birchenough et al., 2015). These cells progressively migrate from the bottom of the crypt towards the villi (Yang and Yu, 2021).

→ **Enteroendocrine cells (EECs)** mostly play a role in the synthesis of digestive enzymes and present ion transporters and channels allowing fluids and electrolyte transports. EECs also produces hormones that are stored within cytoplasmic granules. Upon signaling reception, these vesicles are released at the basolateral membrane, which triggers nerve endings at the basal membrane or reaches other distant cells through the bloodstream (Gribble and Reimann, 2016; Latorre et al., 2016).

→ **Tuft cells** have been less studied, but their structure is known to be close to that of taste buds on the tongue. Indeed, many molecular markers of the taste transduction pathway were found on tuft cells such as α-gutducin, β-endomorphin, metenkephalin and uroguanylin (Höfer et al., 1996; Luciano and Reale, 1990).

→ **Enterocytes** are the most common cells within the gastrointestinal (GI) tract and compose more than 80% of the gut epithelium. They present structures called microvilli at their apical pole (facing the lumen). Measuring around 1-3 μm long, these structures increase the absorption surface of the gut. These cells also present transporters and channels allowing the absorption of water and nutrients. Akin to goblet cells with mucins, enterocytes produce a membrane-bound mucin-type glycoprotein (Maury et al., 1995).

Enterocytes are mainly responsible for nutrients and water absorption and do so through two different transport pathways:

→ **The transcellular transport** is ensured by channel proteins or carrier proteins. Nutrient uptake can also be performed through endocytosis or pinocytosis (Conner and Schmid, 2003). In this pathway, nutrients travel within the cell.

→ **The intercellular or paracellular transport** relies on the plasticity of TJs which allows the diffusion of small nutrients (Pappenheimer, 2001) in between the cells.

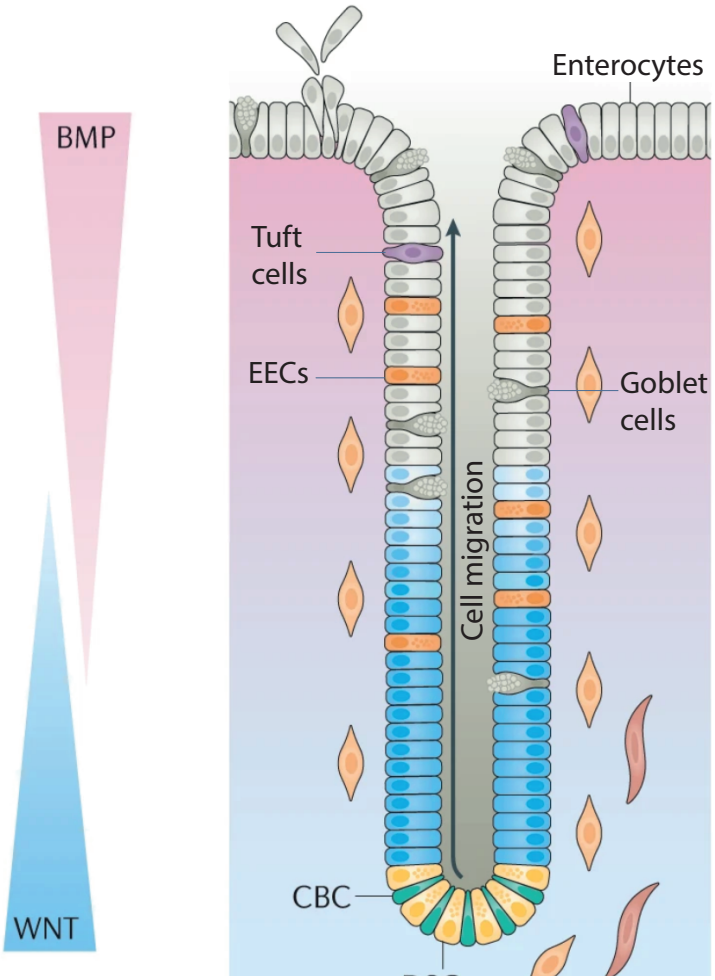

Figure 7- Structure of a crypt (adapted from Beumer and Clevers, 2021)

4.3.1.2 Characterization of CRCs

Colorectal adenocarcinoma (CRC) is the third most common cancer type worldwide as well as the second most common cause of cancer death (Siegel et al., 2023). In more than a half of cases, carcinogenesis can be attributed to specific risk factors, such as smoking, diet, alcohol consumption, physical inactivity or body weight (Islami et al., 2018). Some forms are hereditary, with Lynch syndrome being one of the best documented instances (Lynch et al., 2008).

4.3.1.2.1 Histopathology

Beyond conventional scoring such as TNM (Tumor, Node, Metastasis) score and the immune infiltration of tumor microenvironment, CRCs can be analyzed by anatomopathologists subsequently to a biopsy. Therefore, several histological CRC subtypes have been identified:

→ **Classic adenocarcinoma (CA)** is the most common histological subtype of CRC. It accounts for 80-90% of patients (Li et al., 2019; Bagante et al., 2018). They can be further characterized by their glandular status:

→Well differentiated CA-CRCs have more than 95% of the tumor that is gland-forming.

→Moderately differentiated CA-CRCs have 50-95% gland formation.

→Poorly differentiated CA-CRCs have less than 50% gland formation.

→ **Mucinous adenocarcinoma (MUC)** is characterized by more than 50% of the analyzed surface being composed of mucins. Although this has been challenged, MUC-CRC subtypes are correlated with a higher metastatic burden, a higher proportion of peritoneal carcinomatosis (PC) and is linked to a poorer outcome (Hugen et al., 2016; Mekenkamp et al., 2012).

→ **Micropapillary carcinoma (MiP)** is characterized by the presence of tumor clusters within the cancer stroma. They are more invasive than CAs and are associated with a poorer prognosis. Some of these MiP-CRCs keep a highly differentiated profile with the presence of polarized structures (Barresi et al., 2014; Nagtegaal et al., 2020).

→ **Serrated carcinoma (SeC)** is characterized by serrated lesions within the glandular sections of the tumor. It is thought that MUC-CRC actually arise from serrated lesions, therefore relegating these subtypes as two evolution stages of CRCs (Laiho et al., 2007).

→ **Medullary carcinoma (MeC)** are characterized by poorly differentiated clusters showing an eosinophilic cytoplasm, but this subtype can often be confused with the poorly differentiated grade of CA-CRCs (Wick et al., 2005).

→ **Signet ring cell carcinoma (SRCC)** are characterized by the presence of signet ring cells, which are big cells with a large vacuole. They have a high invasiveness towards lymph nodes and have a poor prognosis (Hugen et al., 2015).

→ **Neuroendocrine carcinoma (NeC)** arise from neuroendocrine (which enteroendocrine cells constitute a section of) cells within the gut. A tumor is classified NeC if it contains more than 30% of neuroendocrine cells (Bernick et al., 2004; Nagtegaal et al., 2020).

→ **Adenosquamous carcinoma (AsC)** is the least documented of these subtypes, and presents a very similar phenotype than CAs, with a poorer prognosis (Nagtegaal and Hugen, 2015).

4.3.1.2.2 Consensus Molecular Subtypes (CMS)

In addition to histological profiling, a molecular profiling called "Consensus Molecular subtypes" allows to classify different CRCs in 4 different categories (CMS1, 2, 3 and 4). This classification discriminates between different cancer subtypes using multiple criteria detailed below (Fessler and Medema, 2016):

→ **CMS1, or MSI (Microsatellite instable) immune group**, among which tumors are generally associated with a high MSI status, hypermethylation (CpG island methylator phenotype or CIMP) and $BRAF^{V600E}$ mutation. MSI tumors have a dysfunctional mismatch repair (MMR) machinery, causing an accumulation of mutations in the DNA. CIMP phenotype causes many cytosine- and guanine-enriched promoters to be methylated, thus causing a silencing of genes, and most importantly tumor suppressor genes.

→ **CMS2, or canonical subtype**, presents high levels of chromosomal instability (CIN) and an activation of Wnt signaling pathway. CIN phenotype causes an abnormal karyotype, with some chromosomes being aneuploid and showing structural defaults.

→ **CMS3, or metabolic subgroup**, displays KRAS mutations, increase in metabolic pathways, and present a hypomethylated phenotype.

→ **CMS4, or mesenchymal type**, presents an activation of EMT-associated genes, angiogenesis, TGF-β signaling and matrix remodeling.

CMS classification and histopathology do not necessarily coincide. For instance, MUC-CRCs can be found in CMS1, CMS3 and CMS4, but are practically absent from CMS2. Furthermore, 13% of CRCs cannot be stratified using this classification due to mixed phenotypes.

4.3.1.2.3 Developmental Pathways

Most CRCs arise from polyps, which are precursor lesions arising from colorectal cancer stem cells at the very base of intestinal crypts. A polyp evolves to CRCs in about 10-15 years. CRCs evolve along two distinct developmental pathways ("Comprehensive molecular characterization of human colon and rectal cancer," 2012; Dekker et al., 2019):

→ **The adenoma-carcinoma pathway** accounts for 70-90% of CRCs. These evolve by the accumulation of CIN and genetic mutations. This sequence is generated by an APC (Adenomatous polyposis coli) mutation, causing its loss of function. This is followed by RAS activation and loss of the anti-cancer TP53. This pathway leads to a tubular adenoma.

→ **The serrated neoplasia pathway** accounts for 10-20% of CRCs. This pathway is often started by genetic mutations of BRAF or KRAS and is characterized by a high CIMP status. This pathway leads to serrated lesions.

4.3.1.3 Metastasis and invasion of CRCs

CRCs invade following three main metastatic routes:

→ **The circulatory route** occurs using blood and lymphatic vessels. This cascade starts with the invasion of tumor cells within the surrounding matrix, followed by the intravasation of the tumor cells inside the circulatory system (where they are called circulating tumor cells - CTCs), the circulation of tumor cells, the extravasation from the

vessels to the parenchyma and the colonization of distant organs and formation of metastasis (Pretzsch et al., 2019). These CTCs have been shown to be tumorigenic and are able to colonize the liver *in vivo* (Grillet et al., 2017). The main metastatic site of CRCs is the liver, as the cancer cells easily migrate from the gut through the portal system.

→ **The transcoelomic route** is described when tumor cells invade through the digestive wall and through the serosa to reach the peritoneal cavity (in between the two sheets of the peritoneum). The peritoneum surrounds most organs within the abdomen, and this makes it an important route for the transport of fluid and cells within the abdomen. CRC cells easily migrate through the peritoneum and, once they adhere, form metastasis called peritoneal carcinomatosis (PC). It is generally believed that patients harboring PC have a lower prognosis and are in a terminal stage of CRC, although almost half the patients with metastasis present PC without liver metastasis (Aoyagi et al., 2014; Lemoine et al., 2016; Pretzsch et al., 2019).

→ **The perineural route** is the migration of cancer cells along the nerves from the primary tumor site. This dissemination route is associated with a poor prognosis (Krasna et al., 1988; Liebig et al., 2009).

4.3.1.4 Models of CRCs

CRCs can be studied using different models (Rizzo et al., 2021). Although multiple cell lines have been generated, thus representing a large phenotypical diversity (more than 100 CRC cell lines in different cell banks) and present the advantage of consistency and practicality, they do not model the intratumoral cell diversity, and the cell lines easily diverge from the original tumors. To solve these problems, other models can be used, such as Patient-derived xenografts (PDXs) and patient-derived organoids (PDOs).

4.3.1.4.1 Cell lines: the example of LS513

LS513 is a colorectal adenocarcinoma cell line which has been used for this project. It comes from a primary tumor in the caecum of a 64 year old male and presents a $KRAS^{G12D}$ mutation (Suardet et al., 1992). Because of its serrated origins and its CIMP-high, MSS

(microsatellite stable) statuses, it recapitulates the MUC-CRC phenotypes well and is classified in the CMS3 category. When cultured on plastic and reaching confluency, the LS513 monolayer starts to bud and releases TSIP-like structures in the medium that present an inverted polarity, which was particularly relevant for our study. Using a cell line allows an easier manipulation for basic biochemistry techniques and a higher throughput (Lopez, 2022). Genetic drift amongst passaging, the immortalization process as well as a culture exclusively *in vitro* are amongst the main limitations to the relevance of the use of such cell lines.

4.3.1.4.2 Patient-derived xenografts (PDXs)

Patient-derived xenografts have been used since their first successful report in 1953 (Toolan, 1953). This technique relies on grafting patient tumor tissue in an immunodeficient mouse. PDX are a very relevant technique to reproduce the tumor phenotype, as they correspond to the histopathological features of the original patient tumor (Blomme et al., 2018), as well as its CMS status (Sveen et al., 2018). However, there might still be a genetic divergence along with the increasing number of passages that should be taken into account (Rizzo et al., 2021). The subcutaneous engrafting of patient tumoral material allows to develop a full-grown tumor in vivo, and such tumor fragments can be passaged in immunocompromised mice. It must be noted that maintaining PDXs is expensive, slow and technically challenging, especially when it comes to genetic manipulation of the tumoral material ex vivo. For this research work, three CRC PDX models have been retrieved from the CReMEC (Center of Resource for Experimental Models of Cancer) consortium, all presenting mucinous characteristics and KRAS mutations (Julien et al., 2012).

4.3.1.4.3 Patient-derived organoids (PDOs)

The production of PDOs (Patient-derived organoids) is a good alternative to PDXs' limitations. It is easier to expand the tumoral material and requires a 3D ECM as well as a serum-free medium supplemented with stem cell growth factors. PDOs start with

patient tumoral material and follows three main steps: fragmentation and digestion of the tissues, embedment in the ECM and culture in the medium (Cartry et al., 2023; Date and Sato, 2015) (see Figure 8). At every passage, PDOs are digested into small fragments and seeded into fresh ECM and can be expanded this way. Having this small fragment/single cell stage at each passage step makes genetic manipulation of PDOs easier than that of PDXs but might compromise the cell diversity, although this has not been fully investigated.

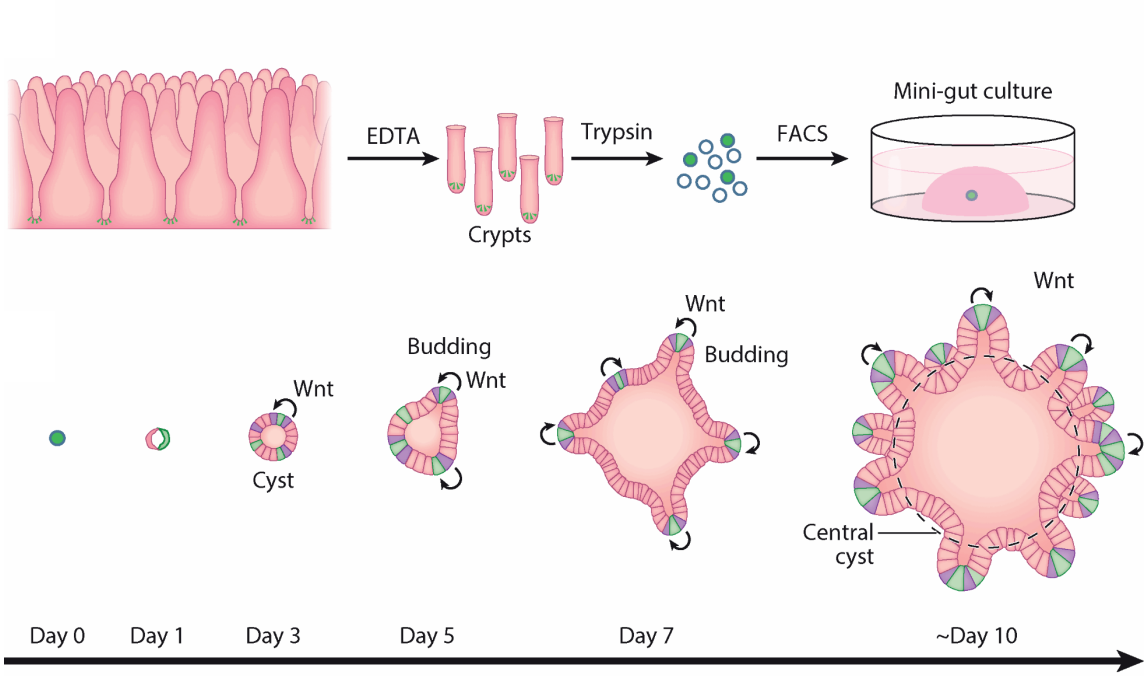

Figure 8- Generation of PDOs (from Date and Sato, 2015). After digestion, digested cells are embedded in Matrigel. From Lgr5+ cells, different cell types differentiate to form a full-grown organoid

4.3.2 Human induced pluripotent stem cells (hiPSCs)

4.3.2.1 What are hiPSCs?

hiPSCs are a type of pluripotent stem cells, which means they have the ability to renew and differentiate into multiple cell types. To avoid the use of embryonic stem cell, it is possible to reprogram human somatic cells for them to revert to pluripotency. These reprogrammed cells are hiPSCs (Takahashi et al., 2007; Takahashi and Yamanaka, 2006), and they overexpress pluripotency and stemness-related genes: OCT3/4, SOX2, KLF4, NANOG and c-Myc.

4.3.2.2 Naïve and primed states

hiPSCs can be described in two different states:

→ Naïve hiPSCs mimic the pre-implantation state of the Inner Cell Mass (ICM). They can give rise to both embryonic and extraembryonic cell lineages, and therefore can be qualified of pluripotent. These cells can be maintained in a naïve state *in vitro* by the addition of leukemia inhibitory factor (LIF).

→Primed hiPSCs however, have a state which is similar to that of post-implantation of ICM cells. These cells can give rise to the three documented germ layers: the ectoderm, the mesoderm and the endoderm (X. Wang et al., 2021). *In vivo*, primed stem cells surround the amniotic cavity which will contain the growing embryo.

While the transition mechanisms between the naïve and primed states are not fully understood to this day, several protocols are available to revert primed hiPSCs into naïve hiPSCs and to capacitate naïve hiPSCs into primed hiPSCs (Collier et al., 2022; Rostovskaya et al., 2019; Taei et al., 2020). Capacitation can be defined as the process during which naïve hiPSCs gain competence for lineage induction, turning them into primed hiPSCs, which does not require exogeneous growth factors but is facilitated by the inhibition of Wnt, which is what was performed in vitro (see **6.1.2.2**).

Some cell-state markers help discriminate between the naïve and primed states, namely the naïve markers Krüpel-like factor 17 (KLF17) and T-Box Transcription factor 3 (TBX3), and the primed markers Zix family member 2 (ZIC2) and secreted frizzled related protein 2 (SFRP2).

4.3.2.3 Adhesion and polarity status of the blastocyst

Integrins are crucial to the growth of hiPSCs. Indeed, they grow in colony-like structures, and their colony architecture is dependent on the attachment to the ECM through integrins. When cultured on Matrigel, naïve colonies tend to adopt a dome-shaped structure, while primed colonies tend to have a flatter phenotype. This flattened shape is accompanied by a contractile actin fence at the edge of the colony. These fibers present a specific type of focal adhesions at both ends, named cornerstone focal adhesions, which are enriched in integrin-β5 (Närvä et al., 2017; Stubb et al., 2019).

During the implantation of the embryo to the endometrium (and therefore during capacitation), it has been shown that the mouse blastocyst started its polarity orientation process (Bedzhov and Zernicka-Goetz, 2014). Indeed, the tissue epithelialization, and especially the lumen formation is concomitant with the naïve-to-primed transition (Cesare et al., 2022). This polarity establishment has been linked to the subsequent exit of pluripotency, with cells in contact at the basal membrane responding to survival signals, which triggers their differentiation into polarized columnar epithelium (Coucouvanis and Martin, 1995). To further understand this process, we have investigated the role of Integrin-β1 in the capacitation and reversion cascades, and how it translates into the architecture of stem cell colonies (see **7.3**).

4.3.3 Stiffness-insensitive spreading of cancer: the use of TIFs and U2OS

4.3.3.1 The role of matrix stiffness in cancer invasion

In solid tumors, the increased tissue stiffness is often seen as a hallmark of cancer and is a direct prognosis factor in different carcinomas such as breast, pancreas and colon (Paszek 2005, Lee 2019, Rice 2017, Baker 2013). Stiffness can also be used as a diagnosis tool, for example during palpation (Boyd et al 2007).

The increase in stiffness is due to the remodeling of the ECM within the tumor microenvironment (TME) which is mainly produced by cancer-associated fibroblasts (CAFs). Increased matrix protein deposition, altered collagen crosslinking and a change in the expression of metalloproteinases (MMP) that degrade ECM components cause dramatic remodeling altering matrix density and its visco-elastic properties. While a stiff ECM can cause the transformation of healthy epithelial cells into cancer cells, it can also influence and support cancer cell invasiveness (Bonnans et al., 2014; Fu et al., 2018; Katara et al., 2018; Najafi et al., 2019). Historically, cancer cells are often cultured on plastic, ie. on a substrate which stiffness is higher than physiological ones. However, it is more and more common to culture cells in more physiological stiffness regimes, where soft matrix is often mimicked with 0.5 kPa ECM coated hydrogels and stiff matrix with hydrogels with a Young Modulus of around 50 kPa (James R. W. Conway et al., 2023).

4.3.3.2 The role of matrix composition in cancer invasion

Matrix remodeling by CAFs is not characterized by a sole change in the physical visco-elastic properties of the ECM, but also in its biochemical composition. Carcinogenesis can be accompanied by altered expression or mutations in collagens, laminin and fibrillin (Bateman et al., 2009; Mao and Bristow, 2001). In addition, just like it is possible to correlate stiffness with prognosis, the matrix composition can also act as a prognostic

marker. For instance, higher proportions of collagen VI, tenascin C and fibronectin are correlated with a poorer prognosis (Fernandez-Garcia et al., 2014; Ishihara et al., 1995; Wishart et al., 2020). The mutations and overexpression of MMPs in cancer cells also implicate a change in the TME matrix through selective degradation of some components (Liao et al., 2021). By testing different stiffness and matrix compositions, it has been possible to find conditions that uncouple composition and stiffness in the cancer cell spreading process (James R. W. Conway et al., 2023).

4.3.3.3 TIFs and U2OS

Across our study, we have looked into the impact of the TME ECM composition and physical properties using two cell lines, namely telomerase immortalized fibroblasts (TIFs) and U2OS osteosarcoma cells (from a moderately differentiated sarcoma in a 15-year-old girl). Using these, it was possible to study the effect of the matrix both on the invasiveness of cancer cells and their associated fibroblasts.

5 Aims of the PhD

Integrins are crucial in the establishment of cell states. In the literature review, I have discussed their importance in cell spreading, apicobasal polarity establishment and in the architecture of stem cell colonies during the capacitation process. Therefore, this PhD work is a pan-model study (CRC PDXs and cell lines, osteosarcoma cell lines and hiPSCs) to further investigate a wide panel of the influence of integrin availability, trafficking and signaling in regulation of these three processes. While Integrin-β1 is the best-studied integrin monomer, owing to its involvement many integrin heterodimers, mechanisms by which it regulates these processes in a context and cell-type specific manner remain unclear. Consequently, the aims of this PhD are:

1. To better understand the underlying events in polarity orientation of inverted polarity structures, both in health and disease (Publication I).

2. To investigate the underlying reasons of the focal-adhesion pathway-dependent polarity reversion in CRC metastasis and the possible role integrin-mediated control of polarity on cancer invasiveness (Publication II).

3. To investigate the role of matrix stiffness and ECM composition on cell spreading using a matrix spot-array screening system (Publication III).

4. To investigate the role of Integrin-β1 on the architecture of hiPSC stem cell colonies and in the regulation of naïve and primed cell states (Publication IV).

6 Material and methods

6.1 Cell culture and organoid formation

6.1.1 MUC CRC (II)

6.1.1.1 Culture and passaging of PDXs

Animal experiments performed in France were compliant with French legislation and EU Directive 2010/63. The project was validated by the Ethical Committee (CEEA) no. 26 and was then granted French government authorizations under number 517-2015042114005883 and 2734-2015111711418501. Animal experiments performed in Finland were done in accordance with the Finnish Act on Animal Experimentation (animal license number ESAVI/12558/2021 and ESAVI/6253/2024). Mice were obtained from Charles River France and Germany, housed and bred at the Gustave Roussy animal core facility (accreditation number E-94-076-11) and at TCDM (Turku Center for Disease Modelling). Animals were humanely euthanized according to endpoints that were validated by the Ethical Committee, the French government (Ministère de l'Enseignement Supérieur, de la Recherche et de l'Innovation) and the Finnish government.

Three human colorectal tumors (9C corresponding to LRB-0009C, 12P corresponding to IGR-0012P and 14P corresponding to IGR-014P) from the CReMEC tumor collection were maintained in NSG mice (strain: NOD.Cg-*Prkdc*^{scid} *Il2rg*^{tm1Wjl}/SzJ) as described in Canet-Jourdan et al., 2022 and in Julien et al. 2012. Briefly, small tumor fragments were subcutaneously engrafted on both flanks of anesthetized mice (2.5% isoflurane). Tumor growth was measured once to twice a week. When the combined tumor burden reached 1700 mm^3, mice were sacrificed, tumors were used for *ex vivo* experiments and 50 mm^3 fragments engrafted on the flanks of new mice.

6.1.1.2 Generation of tumor spheres

Organoids were prepared according to Sato and Clevers 2013 and adapted for muco-secreting tumors as follows. The 9C, 12P or 14P tumors between 1200 and 1700 mm^3 were retrieved from the mice, minced into small fragments using a sterile scalpel and were incubated for 1 h at 37°C in a final volume of 5 to 10 ml of culture medium (Dulbecco's modified Eagle's medium; DMEM) without fetal bovine serum (FBS) and with 2 mg/ml collagenase (Sigma, C2139). The samples were then mixed with 20 ml of DMEM and filtered on 100 µm mesh size cell strainers (Greiner, EASYstrainer, 542000) and centrifuged 10 min at 277 g. Clusters were isolated from the remaining mucin and single cells by washing in 10 ml of DMEM and pulse centrifugating at 277 g five times. The clusters, now free of mucin and single cells, were maintained for 3 days in ultra-low attachment plates (Corning, CLS3471) in culture medium. Then, organoids were pelleted at 277 g and used for further experiments.

6.1.1.3 Collagen embedding and culture of tumor spheres

Collagen-I (Corning, 354236) was neutralized with 1.0 M NaOH and 10× MEM (Life Technologies, 21430-02) according to the ratio: 1.0:0.032:0.1 (v/v/v). The concentration was then adjusted to 2 mg/ml with 1x DMEM, and the collagen-I was incubated on ice for 1h. The organoids, after spending 3 days in suspension as described previously, were then embedded in neutralized collagen-I and were added on top of pre-coated (using 7µl of the collagen mix per well) wells of an µ-Slide 8 Well ibiTreat slide (Ibidi, 80826) at a concentration of 30–50 organoids/5 µl. The gel was allowed to polymerize for 1h at 37°C. Organoids were then cultured in culture medium supplemented with FBS 10% for up to 6 days (3 days for PDX#3). The drugs were diluted in the medium as follows: AIIB2 (DSHB, AB528306, 1 µg/ml), Heregulin-β1 (Peprotech, 100-03-10UG, 20 ng/ml), Trastuzumab (Herceptin, Roche, 10 µg/ml), Pertuzumab (Perjeta, Genentech, 10 µg/ml), Saracatinib (Selleckchem, S1006, 1 µM), EHT-1864 (R&D Systems, 3872, 5 µM), P1E6 (DSHB, AB2619597, 10 µg/ml), FAK14 (Tocris, 3414, 10 µM).

6.1.1.4 Generation of a 14P-derived PDO line

The clusters obtained from the PDX as described previously were pulsed centrifuged at 277 g and resuspended in Matrigel (Corning, 354230) and plated in 10 x 15 µl droplets in the bottom of a 6-well plate (Greiner, 657160). Cells were then incubated at 37°C for 15 minutes to let the basement membrane extract polymerize, then culture medium was added as described in Fujii et al 2018, without any human R-spondin1, A83-01 and Afamin-Wnt-3A serum-free condition medium. During the first two days, the organoid expansion medium was supplemented with Y-27632 (Calbiochem, 688000, 10 µM). This medium was renewed every two days and PDOs were passaged every 7 to 14 days as described in Cartry et al 2023.

6.1.1.5 Culture of LS513 and generation of TSIPs

LS513 cells were obtained from ATCC (#CRL-2134) and cultured in RPMI-1640 medium supplemented with 10% FBS. LS513 were cultured in 10 cm cell culture dish. To generate TSIPs from the LS513 monolayer, the medium was changed every two days until the monolayer reached confluence. After waiting 5 days, the medium was collected and pulse centrifuged at 277g to collect the LS513 TSIPs. These were left for 3 days in suspension in ultra-low attachment plates (Corning, CLS3471), and embedded in collagen as described earlier (using the LS513 medium). For passaging, the monolayer was digested with 1x trypsin when 70% confluence was reached.

6.1.2 hiPSCs (IV)

6.1.2.1 Culture of naïve and primed stem cells

Primed hiPSCs HEL24.3 were a kind gift from Timo Otonkoski (University of Helsinki). They were cultured in Matrigel-precoated plates (354277, Corning) and in Essential 8 Medium (A1517001, ThermoFisher) at +37°C and 5% CO2. For passaging, 50 mM EDTA in PBS was used until detachment of the edges of the colonies as described in Närvä et al., 2017. The medium was changed daily.

To culture naïve hiPSCs, a monolayer of feeder cells was prepared. For this, inactivated mouse embryonic fibroblasts (iMEFs, A24903, Life Technologies) were cultures on 0.1% gelatin-precoated (07903, StemCell Technologies) dishes in DMEM/F12 (11320033, Gibco) supplemented with 10% FBS at 37°C, 5% CO2.

Naïve hiPSCs were obtained after reversion of the primed HEL24.3 using the NaïveCult Induction Kit (05580, StemCell Technologies). They were then cultured on the feeder cell monolayer after washing it twice with PBS and cultured in NaïveCult Expansion Medium (StemCell Technologies). The medium was changed daily. The cells were cultured at 37°C, 5%CO2 and 5% O2. For passaging, cells were dissociated with TrypLE Express (12604-21, Gibco), and re-plated on a feeder-cell monolayer in culture medium - supplemented with 10 μM ROCK inhibitor Y-27632 (72302, StemCell Technologies) during the first 24 hours. In cells cultured with Mab13 (in-house, 10 μM), the antibody was added 24h after passaging and introduced in the freshly changed medium every day.

6.1.2.2 Capacitation

For the capacitation process, naïve hiPSCs were first plated on a Matrigel-precoated plates (354277, Corning) supplemented with 10 μM Y-27632 (72302, Stemcell Technologies). After two days, the NaïveCult medium was changed to capacitation medium, called N2B27, as described in Rostovskaya et al., 2019 (DMEM/F12 [1:2; 11320033, Gibco], Neurobasal medium [1:2; 21103049, Gibco], N2 supplement [in house], 1 mM l-glutamine [Sigma-Aldrich] and 0,1 mM β-mercaptoethanol [M3148, Sigma-Aldrich]) medium supplemented with 2 μM XAV-939 (Tocris Bio-Techne, 3748) at +37˚C, 5 % CO2 (Guo et al. 2017). N2 was prepared by supplementing DMEM/F12 with 0.4 mg/ml insulin (I9278, Sigma-Aldrich), 10 mg/ml apo-transferrin (3188-AT-001G, R&D systems), 3 μM sodium selenite (S5261, Sigma-Aldrich), 1.6 mg/ml putrescine (P5780-5G, Sigma-Alrich) and 2 μg/ml progesterone (P8783, Sigma-Aldrich). Depending on the experiment, the cells were capacitated for 2 to 5 days. The capacitation process was followed with an Incucyte S3 live-cell analysis instrument (Sartorius).

6.1.2.3 Colony formation assay

Similarly to what is described in Rostovskaya et al., 2019, previously capacitated cells were passaged according to that of the Naïve cell passaging protocol into Matrigel-precoated 12 well plates at a density of $4x10^3$ cells/well. Depending on the conditions, cells were cultured in NaïveCult Medium (reversion) or E8 medium (control), supplemented with 10 μM Y-27632 for the first 24 hours. After 7 days, colonies were fixed and stained with Crystal Violet. Pictures of the whole plate were taken and analyzed using the ImageJ Colony Area plugin (Guzmán et al., 2014).

6.2 Protein and gene expressions

6.2.1 Western blotting (II)

Spheres embedded in collagen were first released from the matrix by incubation of DMEM without serum supplemented with 2 mg/ml collagenase (Sigma, C2139) for 45 minutes. After pulse centrifugating at 277g, spheres were washed with PBS and pulse centrifugated at 277 g twice. Spheres were then lysed in TXLB buffer [50 mM Hepes, 1% Triton X-100, 0.5% sodium deoxycholate, 0.1% SDS, 0.5 mM EDTA, 50 mM NaF, 10 mM Na_3VO_4, and protease inhibitor cocktail (cOmplete Mini, EDTA-free, Roche)]. Cells cultured in 2D were washed twice with PBS and directly lysed with TXLB. Separation was performed by gel electrophoresis (Mini-PROTEAN TGX Precast Gels 4-20%, Bio-Rad, 4561096), before transferring onto a nitrocellulose membrane (Trans-Blot Turbo Transfer System, Bio-Rad) and blocking with AdvanBlock-Fluor (Advansta, R-03729-E10). Primary antibodies in AdvanBlock-Fluor were incubated overnight at 4°C with the dilutions mentioned in Table 2. Membranes were washed thrice between primary and secondary antibody treatments with Tris-buffered saline with 0.1% Tween 20 (TBST). IRDye secondary antibodies (see Table 2) were incubated for at least 1 hour at RT, before detection on an Odyssey fluorescence imager CLx (LI-COR). Densitometry analysis was performed in Fiji by normalizing the signal to GAPDH, which was used as a loading control.

6.2.2 PNGase digestion of lysates (II)

For PNGase digestion, cell lysates were prepared in a SDS-free buffer [50 mM Hepes, 1%NP-40, 0.5% sodium deoxycholate, 0.5 mM EDTA, 50 mM NaF, 10 mM Na_3VO_4, and protease inhibitor cocktail (cOmplete Mini, EDTA-free, Roche)]. 9 μl of lysate was mixed to 1 μl of Glycoprotein Denaturing Buffer 10X) (NEB, B1704S). The lysate was denatured at 100°C for 10 minutes, then chilled on ice. 2 μl GlycoBuffer 2 (10X) (NEB, B3704S), 2 μl 10% NP-40 (NEB, B2704S), 5 μl H_2O and 1 μl PNGase F (NEB, P0704S) were then added to the lysate, and mixed gently. The lysate was then incubated at 37°C for 1h. From there, the samples were prepared and run as described before.

6.2.3 Mass cytometry (II)

Spheroids in collagen for 3/6 days underwent collagen digestion by incubation of DMEM without serum supplemented with 2 mg/ml collagenase (Sigma, C2139) for 45 minutes. After resuspending in DMEM + 10% FBS and pulse centrifugating at 277g, they were collected. Spheroids cultured in suspension, clusters obtained from PDX digestion or spheroids released from collagen as described previously were washed with PBS thrice and pulsed centrifuged at 277 g thrice in order to keep the clusters/spheroids and get rid of any single cells and secreted mucins. The spheres were then digested in Cell Dissociation Buffer Enzyme-Free PBS-based (gibco, 13151-014) supplemented with 2 mg/ml collagenase (Sigma, C2139) and incubated for 1h at 37°C with occasional mechanical dissociation by pipetting. After addition of DMEM+10% FBS to quench the collagenase, cells were centrifuged at 200 g for 3 minutes and washed thrice with PBS. They were then resuspended in 1 ml cold PBS and filtered through a 5 ml polystyrene round bottom tube with Cell-Strainer cap (Falcon, 352235), and kept on ice until analysis. The sample was then run through a Helios™ Mass Cytometer and the data analyzed with Cytobank and clustered through SPADE and viSNE analysis.

6.2.4 Whole exome sequencing (II)

DNA was extracted using the DNeasy ikit (Qiagen, Cat. No. 69504) from organoids either after 3 days in suspension (wash one time in PBS supplemented with Ca^{2+} and Mg^{2+} as mentioned above). Whole exome analysis was performed by Integragen SA (France), comparing the three samples (9C, 12P and 14P) to a PON (panel of normal) and analyzed with MERCURY™.

6.2.5 Analysis of SORLA and ITGB1 gene expression in human tumors (II)

Preprocessed TCGA colon adenocarcinoma cohort RNAseq data and raw RSEM-counts were downloaded from https://gdc.cancer.gov/node/905/ and https://gdac.broadinstitute.org/runs/stddata__2016_01_28/data/, respectively. CMSCaller (Eide et al., 2017) was used to infer consensus molecular subtypes (CMS) from RSEM-counts, excluding calls with FDR > 0.05. The samples were categorized as mucinous and control cases based on previously conducted characterization (Nguyen et al., 2021). Associations between SORLA and ITGB1 gene expression were assessed with the preprocessed normalized log2 mRNA expression data by computing linear regression within each CMS group.

6.2.6 Single cell RNA sequencing (scRNAseq) (IV)

Naïve hiPSCs were seeded on Matrigel-coated 6 well plates at a density of 10^4 cells/well (354277, Corning), with or without Mab13 (inhouse, 10 μM) in naïve conditions as previously described. After two days of culture, selected plates were put in normoxia in capacitation medium as detailed earlier, for 2 days. Similary, HEL24.3 cells were cultured on Matrigel-coated 6 well plates at a density of 10^4 cells/well, with or withour Mab13, in primed conditions for 4 days.

After the 4 full days, cells were detached with EDTA (for primed hiPSCs) or TryPLE express (for naïve hiPSCs) as previously described. For each condition, 3 wells were used. Cells were washed thrice with PBS and resuspended in 15 µl 0.04% BSA in PBS. The sequencing and analysis were carried by the Single-Cell Omics facility at the University of Turku.

6.3 Quantification of cell-matrix interactions

6.3.1 Generation of fluorescent collagen (II & III)

To fluorescently label rat tail type I collagen (~4.24 mg/mL, 354236, Corning), 1.65 mL was mixed with 450 µL of Milli- Q water and 500 µL of neutralizing buffer (20 mM NaH_2PO_4, 112 mM $Na_2HPO_4 \cdot 2H_2O$, 0.4 M NaCl, and 46 mM NaOH) and incubated at 37 °C for 30 min. The polymerized collagen was then washed thrice with PBS for 10 min. Then, 3 mL of Milli-Q water and 1 mL of bicarbonate buffer [1 M $NaHCO_3$ (pH 8), raised dropwise to pH 8.3 using 1.17 M Na_2CO_3 (pH 11)] were added to the collagen gel before addition of the Alexa Fluor™ 647 NHS Ester (Succinimidyl Ester) dye (A20006, Invitrogen) in 100 µL of PBS. After incubating the collagen mix overnight at 4 °C, the dye was then removed, and the collagen was washed with PBS with rotation at room temperature for 30 min, changing the PBS five times. Stained collagen was then depolymerized through the addition of 2 mL HCl (20 mM) and gentle rotation at 4 °C overnight. The collagen was finally centrifuged at 20,000 g for 10 min, collecting the labeled collagen from the supernatant. The fluorescent collagen was then used at a 1:1000 concentration in the previously described neutralized collagen gel.

6.3.2 Generation of CNA35 and cloning (II)

Molecular cloning and recombinant protein purification. To generate the CNA35-mScarlet construct, pET28a-CNA35-EGFP (A kind gift from Maarten Merkx (Eindhoven University of Technology, MB Eindhoven, The Netherlands), Addgene plasmid #61603) was digested with NheI/EcoRI and ligated with a NheI/EcoRI digested mScarlet gene fragment (IDT) to generate pET28a-mScarlet-CNA35. This was validated by analytical digestion and sequencing. Recombinant protein purification for CNA35-mScarlet was performed as described in James R. W. Conway et al., 2023.

6.3.3 Peritoneum *ex vivo* assay (II)

Peritoneum samples were collected from mice and decellularized by incubating them in a 1M NH_4OH solution for 1h at RT. After washing thrice with PBS for 15 minutes, peritoneum samples were left to incubate with PBS and penicillin-streptomycin (1:100) at 4°C overnight. After washing thrice with PBS for 15 minutes, the peritoneum was sectioned in 1cmx1cm pieces and adhered (using Tissue Adhesive, 3M, 1469SB) to the bottom of plastic transwell inserts (Greiner, Thincerts, 8 um pore size, 662638) after removing the filter with a scalpel. 100 tumor spheres were resuspended in 100 ml of DMEM+10%FBS and placed in the well with AIIB2 (DSHB, AB528306, 1 μg/ml), Y27632 (Calbiochem, 688000, 25 μM), Heregulin-β1 (Peprotech, 100-03-10UG, 20 ng/ml), Trastuzumab (Herceptin, Roche, 10 μg/ml), Pertuzumab (Perjeta, Genentech, 10 μg/ml) for 6 days. The fixing and IF staining was performed as described previously. Peritoneum bits were placed upside-down on a glass bottom dishes (Cellvis, D35-14-1-N), and imaged as described previously, using the x20 objective.

6.3.4 Collagen orientation analysis (II)

Type I collagen gels with 14P and 12P spheroids were prepared on glass bottom dishes (Cellvis, D35-14-1-N). 80 μl of PureCol EZ Gel (Advanced BioMatrix, 5074) was spread on

the glass bottom using a micropipette tip and allowed to polymerize at +37 °C for 1 h. Next, 14P or 12P spheroids were pulse centrifuged at 277 g to remove the mucin and single cells. Approximately 100 spheroids were mixed with 80 µl of PureCol EZ Gel and pipetted on top of the previously polymerized collagen layer, after which the mixture was allowed to polymerize at +37 °C for 1 h. Spheres were treated with AIIB2 (DSHB, AB528306, 1 µg/ml), Y27632 (Calbiochem, 688000, 25 µM), Heregulin-β1 (Peprotech, 100-03-10UG, 20 ng/ml), Trastuzumab (Herceptin, Roche, 10 µg/ml), Pertuzumab (Perjeta, Genentech, 10 µg/ml). One day before the samples were imaged, the cultures were supplemented with 1:1000 SiR-actin (Sprichrome, SC001) and ~40 µg/ml of mScarlet-conjugated collagen probe CNA35 (Aper et al 2014).

The spheroids were imaged live using a Marianas spinning disk confocal microscope, 20x objective, Orca Flash4 sCMOS camera, and 2x2 binning (see Microscopy for details). 60-80 µm stacks were acquired around the center (z) of each spheroid. In order to analyze collagen fiber orientation around the spheroids, ca. 4 µm substacks were acquired near the center of each spheroid and used for creating maximum intensity projections. Next, 200x200 µm regions of interest depicting CNA35 directly proximal to each spheroid, but excluding any dense collagen aggregates on the spheroid surface, were selected from the projections for analysis. If the matrix surrounding the spheroid was obviously heterogeneous, the region was selected to maximize the local alignment.

The selected regions were analyzed with ImageJ plugin OrientationJ, using cubic spline gradient and a local window size of 4 pixels. In the color survey, hue represented orientation and saturation represented coherency. All the local orientations were exported and analyzed using a custom R script to yield fiber orientation indices (Ferdman et al 1993, Taufalele et al 2019). Briefly, the orientations (-90°...+90°) representing each region were normalized, i.e., their distribution was centered around zero based on the peak of the histogram. Next, orientation indices (*S*) were calculated such that

$$S = 2 < cos^2\alpha > -1$$

where α is the angle between an individual (fiber) orientation and the average orientation of the entire region, and $<cos^2\alpha>$ is the averaged square cosine of all α per analyzed

region. And index of 0 represents a random distribution, and an index of 1 represents a perfectly aligned distribution.

6.3.5 Collagen displacement fields (II)

In order to measure transient displacements exerted on the collagen matrix by the 14P and 12P spheroids, the spheroids were prepared and embedded in type I collagen, as described above. The spheroids were grown in the gels for 6 days and supplemented with 1:1000 SiR-actin and ~40 µg/ml mScarlet-CNA35 one day before the imaging. 60-80 µm stacks were acquired around/near the center of each spheroid, before and after the cells and matrix were relaxed by adding 10 µM latrunculin B and incubating for ca. 20 minutes. Marianas spinning disk confocal microscope, 20x objective, Orca Flash4 sCMOS camera, and 2x2 binning were used for the imaging (see Microscopy for details).

3D displacement fields were calculated using TFMLAB (Barrasa-Fano et al 2021a, Sanz-Herrera et al 2021, Barrasa-Fano et al 2021b), a traction force microscopy toolbox implemented in MATLAB R2022a (MathWorks). The spheroids were segmented using actin images, variable threshold adjustment and a minimum object size of 10^4 voxels. Rigid image registration was done using the default phase correlation-based algorithm. The displacements were calculated from CNA35 images using 10x10x10 µm grid spacing, default registration metric and optimizer (normalized correlation coefficient, adaptive stochastic gradient descent) and post-shift correction. The results were visualized using ParaView v5.11.0 (Ahrens et al 2005).

6.4 Infections and polarity/trafficking analysis (II)

6.4.1 SorLA silencing using shRNA lentiviral transduction

During passaging of the 14P-generated PDO line as described previously, 10^5 cells were resuspended in 36 μl of organoid expansion medium were infected with 4M TU [62 μl of the virus (Origene, TL309181V)], 1 μl polybrene (Merck, TR-1003-G, stock solution at 1 mg/ml) and 1 μl Y-27362 (Calbiochem, 688000, 10 μM, stock solution 1 mM), in a U-bottom 96-well plate (Falcon, 351177) for 6 hours at 37°C. 1 ml of DMEM+10%FBS was added, and cells were centrifugated at 200 g for 3 minutes. Cells were then resuspended in 60 μl Matrigel (Corning, 354230) and 4x15 μl droplets were poured in a 24 well cell culture plate (Cellstar, 662 160) and left at 37°C degrees to polymerize for 15 minutes. 1 ml organoid expansion medium (supplemented with 10 μM Y-27362 for the first two days). The medium was changed every two days and organoids left to grow for 7 days. For polarity assays, the well was first washed thrice with PBS, before adding 1 ml of Cell Recovery Solution (Corning 354253). Cells were then left to incubate at 4°C for 20 minutes; Mechanical dissociation was then applied with a p1000 pipette until Matrigel was completely dissolved. 4 ml of PBS was added and spheroids were pulse centrifuged at 277 g. The spheres, now free of Matrigel, were maintained for 3 days in ultra-low attachment plates (Corning, CLS3471) in PDX culture medium. Then, organoids were pelleted at 277 g and used for further experiments.

6.4.2 SorLA KO using siRNA transient transfection

LS513 were plated in a 6 well plate at 80% confluency. Transient siRNA transfections were performed using Lipofectamine RNAiMAX reagent (Invitrogen, 56532) according to the

manufacturer's instructions. SORLA-targeting siRNAs were ON-TARGETplus obtained from Dharmacon—siSORLA #1 (J-004722-08), siSORLA #2 (J-004722-06). For controls, Allstars negative control (Qiagen, Cat. No. 1027281) was used. siRNA concentrations used were all 20 nM and cells were transfected with siRNAs 72 h prior to experiments.

6.4.3 Integrin recycling assay

Surface biotinylation-based integrin trafficking assays in SorLA-silenced LS513 cells were performed based on previously published methods (Farage et al., 2021; Arjonen et al. 2012), with some modifications. Nunc MaxiSorb 96-well plates (Thermo Fischer, 44-2404-21) Enzyme-linked immunosorbent assay (ELISA) plates were coating with anti-β1-integrin antibody mix (5 µg/ml of AIIB2 (in-house) and anti-CD29 (BD Bioscience #610468)) in TBS (50 µl per well) overnight at +4 °C. The wells were blocked with 5% BSA in TBS for 2 h at 37 °C, (100 µl per well). LS513 cells were silenced three days before the experiment as described earlier. 2 hours prior to the experiment, the medium was changed to prewarmed RPMI with 10% FBS to induce receptor traffic. The cells were placed on ice and washed once with cold PBS. Cell surface proteins were labelled with 0.13 mg/ml EZ-link cleavable sulfo-NHS-SS-biotin (Thermo Scientific, 21331) in serum-free RPMI medium for 30 min at +4 °C. Any unbound biotin was removed by washing with cold medium and pre-warmed RPMI+10% FBS with or without 100 µM primaquine (Sigma, 160393) was added to the cells. The biotin-labelled surface proteins were allowed to traffic at +37 °C for 15 or 30 minutes. Cells were placed on ice, washed once with cold PBS and cold cell surface reduction buffer (50 mm Tris–HCl, pH 8.6 and 100 mm NaCl). Cell surface biotin was cleaved with non-membrane permeant reducing reagent MesNa (30 mg/ml, sodium 2-mercaptoethanesulfonate; Fluka, 63705) in cell surface reduction buffer 20 min at 4 °C, followed by quenching with 100 mM iodoacetamide (Sigma, I3750) for 15 min on ice. For the 0 min internalization, cells were maintained on ice in serum-free RPMI until cell surface reduction with MesNA. The cells were lysed by scraping in lysis buffer (1.5% octylglucoside, 1% NP-40, 0.5% BSA, 1 mM EDTA, and protease and phosphatase inhibitors) and incubation at +4 °C for 20 min with rotation and cleared by centrifugation (16,000*g*, 10 min, 4 °C). To detect the biotinylated

integrins, 50 µl volumes of the cell lysates were incubated in duplicate wells at +4 °C overnight, washed extensively with TBST, incubated for 2 h at 4 °C with 1:1,000 horseradish peroxidase-coupled streptavidin (Fisher, 21130), washed and detected with antibody for ELISA detection.

6.5 Stainings and microscopy (II)

6.5.1 Immunofluorescence staining

After incubation for 3 days in suspension or for 3 to 6 days in collagen, the apicobasolateral polarity of organoids was quantified. Cells were washed thrice with PBSCM (PBS supplemented with $CaCl_2$ (0.1 mM) and $MgCl_2$ (1 mM)), fixed with 4% paraformaldehyde (PFA) for 5 minutes (for spheres in suspension) or 45 minutes (for spheres in collagen) at RT. Spheres fixed in suspension were then embedded in collagen for imaging as previously described. Permeabilization was then performed in PBSCM supplemented with 0.5% Triton X-100 for 45 minutes. Spheres were incubated with primary antibodies overnight at 4°C with the dilutions mentioned in Table 2 in PBSCM supplemented with 10% FBS and 0.1% Triton X-100. After washing thrice with PBSCM supplemented with 0.05% Tween, spheres were incubated with secondary antibodies and phalloidin for 2h at RT with the dilutions mentioned in Table 2, as well as with DAPI (1 µg/ml). Spheres were then washed thrice with PBSCM supplemented with 0.05% Tween. The gel was then immerged in PBS before imaging.

6.5.2 Confocal imaging

Images were acquired either using a SpinningDisk CSU-W1 microscope (Yokogawa) with a ZylasCMOC camera piloted with an Olympus X83, or with a 3i CSU-W1 spinning disk confocal microscope with Hamamatsu CMOS (x40 water immersion objective). Images were processed using ImageJ.

6.5.3 Immunohistochemistry staining

Histology CRC and peritoneum specimens obtained after surgical resection were formalin fixed and paraffin embedded according to routine protocols. Sections (3 µm) of formalin-fixed and paraffin-embedded samples were deparaffinized, unmasked (pH 8) and rehydrated before HES or Alcian Blue (pH 2.5) staining, immunohistochemistry or immunofluorescence. Immunohistochemistry Sections were immunostained for SORLA, HER2, HER3 or with anti-CK20 mouse monoclonal antibody (see Table 2). Slides were imaged using Axioscan Z1, Zeiss (x20) and analysed using QuPath.

6.6 Statistical analysis and polarity quantification

6.6.1 Statistical analysis (II, III & IV)

All statistical comparisons were performed using Prism 7 (GraphPad software), as indicated in the figure legends, repeating all experiments at least three times independently.

6.6.2 Polarity score (II)

To quantify polarity, a polarity score was established by computing three parameters:

→ the absence/presence of a lumen (1 if one ore more lumen, 0 if none).

→ The quantification of protrusions through the measure of corrected circularity (1-circularity) using the phalloidin signal (varying from 0 if no protrusions, to 1)

→ The quantification of the ezrin fluorescence signal ratio R ($R = \frac{F_{luminal}}{F_{cortical}+F_{luminal}}$ varying from 0 if cortical signal only, 1 if luminal signal only). If there is no lumen but a strongly polarized ezrin signal, this is set to 0.

By adding these parameters, we get a score varying from 0 (apical-out) to 3 (apical-in). If there is no lumen and no polarized ezrin signal, the score is set to 1.5.

6.7 Annexes

Table 1-Antibodies

Protein	Company	Catalog Number	Application	Concentration
Ezrin	DHSB	AB-210031	IF	1 : 400
SorLA	C.M. Petersen (Aarhus U)		IF	1:200
RAB11FIP1 (RCP)	ThermoFischer	PA5-55276	IF/WB	1 :400 / 1 :1000
HER2	ThermoFischer	MA5-14057	IF/WB/IHC	1 :400/1 :1000/1 :400
HER3	Cell Signaling	12708S	IF/WB	1 :1000/1 :100
P5D2 (Total integrin-β1)	Abcam	Ab193592	IF	1 :500
12G10 (Active integrin-β1)	Abcam	Ab202641	IF	1 :500
WGA-lectin	GeneTex	GTX01502	IF	1 :500
CNA-35	In-house		IF	40 ug/ml
Phalloidin 488	Invitrogen	A12379	IF	1 :1000
Phalloidin 647	Sigma	65906	IF	1 :1000
Phalloidin 750	Sigma	07373	IF	1 :1000
SorLA	BD Biosciences	624084	WB	1 :500
Anti-ms 568	Invitrogen	A10037	IF	1 :500
Anti-ms 488	Invitrogen	A21202	IF	1 :500
Anti-rbt 488	Invitrogen	A21206	IF	1 :500
Anti-rbt 561	Invitrogen	A10042	IF	1 :500
GAPDH	HyTest	5G4MAB6C5	WB	1 :2000
Integrin-β1	Abcam	Ab52971	WB	1 :500
Erk	Cell Signaling	4696S	WB	1 :500
p-Erk	Cell Signaling	4370S	WB	1 :500
Src	Cell Signaling	2108S	WB	1 :500
p-Src (active)	Cell Signaling	2101S	WB	1 :500
Ms sec 650	Azure Biosystems	AC2166	WB	1 :1000
Ms sec 800	Azure Biosystems	AC2135	WB	1 :1000

Rbt sec 650	Azure Biosystems	AC2165	WB	1 :1000
Rbt sec 800	Azure Biosystems	AC2134	WB	1 :1000
HER3	Dako	DAK-H3-IC	IHC	1 :50
SorLA	Atlas	HPA031321	IHC	1 :400
Pan-CK	Invitrogen	MA5-13203	IHC	1 :400
P1E6 (Integrin-α2)	DSHB	AB2619597	FB	10 μg/ml
AIIB2 (Integrin-β1)	DHSB	AB528306	FB	1 μg/ml
AIIB2 (Integrin-β1)	In-house		ELISA	5 μg/ml
CD29	BD Bioscience	610468	ELISA	5 μg/ml
^{89}Y-Integrin-αIIb	AH Diagnostics	3089004B	MC	1 :100
^{141}Pr-EpCAM	AH Diagnostics	3141006B	MC	1 :100
^{142}Nd-PETA-3	AH Diagnostics	3142011B	MC	1 :100
^{143}Nd-N-Cadherin	AH Diagnostics	3143016B	MC	1 :100
^{145}Nd-Syndecan-1	AH Diagnostics	3145003B	MC	1 :100
^{146}Nd-Integrin-β3	AH Diagnostics	3145011B	MC	1 :100
^{148}Nd-HER2	AH Diagnostics	3148011A	MC	1 :100
^{149}Sm-CD34	AH Diagnostics	3149013B	MC	1 :100
^{150}Nd-Integrin-αvβ3	AH Diagnostics	3150026B	MC	1 :100
^{151}Eu-ICAM-2	AH Diagnostics	3151015B	MC	1 :100
^{156}Gd-Integrin-β1	AH Diagnostics	3156007B	MC	1 :100
^{158}Gd-E-cadherin	AH Diagnostics	3158018B	MC	1 :100
^{159}Tb-CD98	AH Diagnostics	3159022B	MC	1 :100
^{160}Gd-Integrin-α5	AH Diagnostics	3160015B	MC	1 :100
^{161}Dy-Integrin-α2	AH Diagnostics	3161012B	MC	1 :100
^{162}Dy-Integrin-β7	AH Diagnostics	3162026B	MC	1 :100
^{163}Dy-Integrin-α1	AH Diagnostics	3163015B	MC	1 :100
^{164}Dy-Integrin-α6	AH Diagnostics	3164006B	MC	1 :100
^{165}Ho-Notch2	AH Diagnostics	3165026B	MC	1 :100

^{166}Er-CD44	AH Diagnostics	3166001B	MC	1 :100
^{168}Er-Integrin-α9β1	AH Diagnostics	3168013B	MC	1 :100
^{169}Tm-CD24	AH Diagnostics	3169004B	MC	1 :100
^{170}Er-ICAM-1	AH Diagnostics	3170014B	MC	1 :100
^{171}Yb-CD9	AH Diagnostics	3171009B	MC	1 :400
^{173}Yb-Integrin-β4	AH Diagnostics	3173008B	MC	1 :100
^{174}Yb-Integrin-α4	AH Diagnostics	3174018B	MC	1 :100
^{176}Yb-NCAM	AH Diagnostics	3176001B	MC	1 :100
^{209}Bi-CD47	AH Diagnostics	3209004B	MC	1 :100
^{112}Cd-EGFR	Biolegend	352902	MC	1 :50
^{114}Cd-Integrin-αV	R&D Systems	MAB1219	MC	1 :50
^{111}Cd-Integrin-α3	Sigma	MAB1952Z	MC	1 :50
^{166}Cd-HER4	R&D Systems	MAB11311	MC	1 :50
^{110}Cd-HER3	R&D Systems	MAB3481	MC	1 :50
^{106}Cd-Integrin-α11	R&D Systems	MAB4235	MC	1 :50
^{144}Nd-Syndecan-4	R&D Systems	MAB29181	MC	1 :50
^{152}Sm-Integrin-αvβ5	R&D Systems	MAB2528	MC	1 :50
^{155}Gd-Integrin-α8	R&D Systems	MAB6194	MC	1 :50
^{175}Lu-Integrin-β8	R&D Systems	MAB4775	MC	1 :50
^{153}Eu-Integrin-β6	R&D Systems	MAB4155	MC	1 :50
^{147}Sm-CD166	Biolegend	343902	MC	1 :200
^{154}Sm-Notch-1	Biolegend	352102	MC	1 :50
^{167}Er-Notch-3	Biolegend	345407	MC	1 :50
^{172}Yb-Neuropilin-1	Biolegend	354502	MC	1 :50
^{113}Cd-CD10	Biolegend	312223	MC	1 :50

Table 2-siRNA and shRNA

Reagent	Catalog number	Company
siSORL1 #1	J-004722-08	Dharmacon
siSORL1 #2	J-004722-06	Dharmacon
AllStar	1027281	Qiagen
shSCR	TL309181V	Origene
shSORLA #A	TL309181V	Origene

7 Results

7.1 Implication of Integrin-β1 trafficking in the apicobasal polarity orientation of CRC metastasis (II)

This project was the main project during my PhD work; therefore, the results will be detailed thoroughly in the following sections.

7.1.1 MUC CRC polarity is regulated by ECM interactions and the Focal Adhesion Pathway

Inverted polarity in cancer has been reported multiple times before (Onuma and Inoue, 2022; Zajac et al., 2018) with the occurrences of TSIPs for instance. However, the mechanisms of polarity orientation of TSIPs once embedded in a matrix is unclear. Being able to decipher this process is clinically relevant, since it had been shown that a higher burden of apical-out structures is associated with a poorer prognosis (Canet-Jourdan et al., 2022). By using MUC-CRC PDXs from the CreMEC bank (Julien et al., 2012), we were able to use clinically relevant models to further investigate the polarity orientation process, in two primary tumor models (12P and 14P) and one PC model (9C). Through generation of tumoroids from these three PDXs and culturing them in suspension or in a collagen-I matrix, we were able to observe two polarity phenotypes. While all these tumoroids are apical-out in suspension, 14P tumoroids revert to an apical-in polarity once embedded in collagen (II, Fig. 1A). 12P and 9C tumoroids remain apical-out in the matrix. All these IF observations (through actin and ezrin staining) were backed up with the computation of a polarity score (described in **6.6.2** and II, Fig.S1A), and by the staining of mucin, which secretion also happens to be polarized (II, Fig. S1B). This polarity score is based on the quantification of protrusions (through the measure of the circularity of

the tumoroid), the presence or absence of a lumen, and the ezrin fluorescence ratio between the cortical and the luminal membranes. By computing these parameters, we establish a polarity score varying from 0 (perfect apical-out) to 3 (perfect apical-in). While all models in suspension and collagen (except the 14P in collagen) presented a polarity score (PS) lower than 0.75, the 14P in collagen harbored a PS of almost 2, showing a unique polarity shift solely in the 14P upon contact with the collagen matrix (II, Fig. 1B). Live imaging of 14P in collagen allowed to see lumen-like structures and beginnings of protrusions as early as 5 hours after embedding (II, Fig. 1B).

Since previously performed transcriptome analysis (GSE152299) on these three models reported an upregulation of the KEGG Focal Adhesion pathway in the collagen-embedded 14P tumoroids, we decided to investigate this pathway deeper. To illustrate this, we plotted the 45 most upregulated genes in 14P in collagen compared to the other conditions (II, Fig.S1C and S1D). Inhibition of key regulators of this pathway, namely Rac, FAK and Src all prevented the polarity reversion of 14P (II, Fig.1D and 1E). Concordantly, we observed a Src phosphorylation in 14P upon embedding in collagen (II, Fig. S1E and S1F).

7.1.2 Collagen-binding integrins regulate polarity establishment in MUC CRC

Because the $\alpha 2\beta 1$ integrin heterodimer, which is the best documented collagen-interactor, is upstream of the FA pathway, we investigated the relative levels and localization of this integrin in our PDXs. IF staining with P5D2 and 12G10 antibodies has shown that the localization of both total and active Integrin-$\beta 1$ receptors changed upon collagen embedding in the 14P. While integrins are mostly intercellular in suspension, they strongly localize on the cortex, at the cell/ECM interface in collagen in 14P (II, Fig. 2A). Through single-cell mass cytometry (CyTOF) of our models, we were able to see that the surface expressions of $\beta 1$ and $\alpha 2$ were higher in the 14P PDX than in the other PDXs (II, Fig. 2B and S2A, S2B and S2C). When generating tumoroids from these PDXs, we noticed that embedding 14P in collagen showed an increase in the surface expression of

these two subunits (II, Fig. 2C and S2D). Upon blocking them with AIIB2 (anti-β1-integrin) and P1E6 (anti-α2-integrin) blocking antibodies, we significantly inhibited the polarity reversion of 14P tumoroids (II, Fig.2D and 2E). It was also possible to observe this through live imaging (II, Fig. S2E and S2F).

7.1.3 Inverted polarity is linked to altered expression of integrin trafficking regulators

Motivated by the observation that the polarity status was correlated to a differential surface expression of integrins and was functionally dependent on integrin-ECM interaction, we decided to investigate this more precisely. Cell surface levels of integrins are largely controlled by the balance of constant integrin endocytosis and recycling (Bridgewater et al., 2012; Caswell and Norman, 2006; Moreno-Layseca et al., 2019) as explained in **4.1**. By screening through well-documented integrin traffic regulators, we were able to identify two interesting targets that were respectively down- and up-regulated in the collagen-embedded 14P: RAB11FIP1 (or RCP) and SORL1 (II, Fig. 3A and 3B). RAB11FIP1 encodes for a Rab associated protein which has been shown to be a positive regulator of β1-integrin recycling in different cancer cell types (Caswell et al., 2008; Eva et al., 2010; Machesky, 2019). SORL1 encodes for the SorLA protein which has been implicated in the rapid recycling of β1-integrins in breast cancer (Pietilä et al., 2019). Western-blots and IF stainings of these two proteins showed a downregulation of RCP in all three models upon embedding in collagen, while SorLA was upregulated upon collagen embedding, but only in 14P (II, Fig. 3C, 3E, 3G and S3B). Interestingly, this was accompanied by an elevated Erk phosphorylation in 14P tumoroids in collagen, which was sensitive to Integrin-β1 blocking through function blocking antibodies (II, Fig 3H, 3I, S3C and S3D). These data suggested the possibility that in 14P, integrin recycling might undergo a switch from a Rab11fip1-mediated Rab11-dependent long recycling loop to a SorLA-driven rapid recycling loop, contributing to increased cell surface integrin levels compared to that of the other models.

To explore this in more detail, we blotted for Integrin-β1. Although the total level of integrins does not significantly change in the different tumoroids between the suspension and collagen conditions, we observe an increase in the mature, heavier glycoform of Integrin-β1 in 14P in collagen (II, Fig. 4A). We were able to validate this result by digesting the used lysates with PNGase (an enzyme cocktail removing N-glycosylations from the extracellular domain of integrins, as seen in II, Fig.S4A). The ratio of mature/immature integrin-β1 has previously been linked to alterations in integrin traffic with a higher ratio of the mature form being correlated to increased β1-integrin recycling (Böttcher et al., 2012). Studying integrin-β1 trafficking in tumoroids has proven technically challenging, and we therefore had to find a relevant alternative. Our choice was LS513 cells, a mucinous CRC cell line which generates TSIPs in the medium upon confluency when cultured in 2D. These LS513 TSIPs replicate the 14P polarity phenotype well, with a polarity reversion and a SorLA upregulation when embedded in collagen (II, Fig. S4B, S4C and S4D). Previous studies have shown that impaired recycling of β1-integrin can lead to its accumulation inside of the cell (Sahgal et al., 2019). Through SorLA silencing of LS513 and performing a cell-surface biotinylation-based integrin uptake assay, we were able to determine that SorLA silencing increases the intracellular levels of cell surface-derived endocytosed β1-integrin, indicative of defective recycling in CRCs (II, Fig.4C). We then aimed at reproducing these results in 14P. Because efficient silencing SorLA in 14P tumoroids turned out to be technically challenging, we generated a PDO line from the 14P PDXs. Passaging these PDOs transiently goes through a single-cell stage which facilitated the efficacy of shSORLA lentiviral infection. This approach enabled us to generate SorLA-silenced organoids of 14P, which showed a clearly reduced polarity reversion in comparison to the control (II, Fig. 4D and 4E), further demonstrating that SorLA is necessary for polarity reversion in CRC spheroid response to collagen.

7.1.4 The SorLA-dependent integrin trafficking loop is induced by HER2 and HER3

Human epidermal growth factor receptor 2 and 3 (HER2 and HER3) are two transmembrane receptor tyrosine kinase (RTKs) which have been shown to interact with SorLA. By doing so, SorLA stabilizes the HER2/HER3 heterodimer, increasing protein levels of the two receptors, and supports its rapid recycling in breast and gastric cancer (Al-Akhrass et al., 2021). Through IF staining and Western-Blotting, we have found that only the 14P model showed a simultaneous increase in HER2 and HER3 upon collagen embedding (II, Fig. 5A, 5B, 5C and S5A). Similar to the collagen-induced SorLA expression, HER2 and HER3 upregulation were also integrin-dependent in 14P tumoroids in collagen (II, Fig. 5D, 5E and S5B). As it was shown in Al-Akhrass et al., 2021, the HER2/HER3 signaling via the Erk pathway induces a transcriptional regulation of SorLA. In return, SorLA regulates HER3 at a post-transcriptional level, as it was shown that the expression of ERBB3 is unchanged upon SorLA overexpression or silencing in breast cancer.

We have performed HER2/HER3 signaling inhibition using a Pertuzumab/Trastuzumab cocktail (which prevents respectively HER2/HER3 heterodimerization and HER2/HER2 homodimerization) and are both clinically in use in breast cancer (Swain et al., 2015). Upon inhibition, we prevented the 14P tumoroid polarity reversion in collagen, which shows an important functional role of HER2/HER3 signaling in the polarity reversion process (II, Fig. 5F and 5G). Conversely, activating this signalization through Heregulin-β1 (the main HER3 ligand) treatment of 12P (which was thus far blind to the matrix and stays apical-out in a collagen matrix) initiates a polarity-reversion process, turning them apical-in (II, Fig.5H and 5I). Upon HER3 stimulation with Heregulin-β1, SorLA was also found to be upregulated in 12P (II, Fig. 5J and S5E). The 9C model however does not respond to Heregulin-β1 stimulation (II, Fig. S5C and S5D) which correlates well with its aforementioned low HER3 expression level. These results show the validity of the HER2/HER3/SorLA feed-forward loop, as the stimulation with Heregulin-β1 in 12P leads to a SorLA upregulation which, in returns, regulates HER3 at a post-transcriptional level (Al-Akhrass et al., 2021). The upregulation of SorLA consequently leads to an activation

of the SorLA-dependent Integrin-β1 recycling loop, therefore allowing 12P to sense the matrix and orient its polarity accordingly.

7.1.5 The apicobasal polarity orientation allows proper interaction with the matrix

The HER2/HER3/SorLA complex seems to play a cornerstone role in the apicobasal polarity orientation in our MUC CRC tumoroids. It was possible to correlate it to their interaction with the matrix. Through Traction Force Microscopy (TFM) and collagen-labelling, we were able to visualize the collagen fibers orientation as well as their displacement. Embedding 14P in a collagen matrix causes marked fiber displacement compared to 12P, showing a higher matrix interaction which goes hand in hand with an apical-in polarity and a basal localization of integrins (II, Fig. 6C, 6D, 6E and S6C). Upon blocking Integrin-β1 or blocking HER2/HER3 signaling, we were able to see a decrease in collagen-fiber orientation, once more indicating a reduced tumoroid/ECM interaction which correlates with the decrease in polarity reversion. Conversely, activating HER2/HER3 signaling in 12P results in a higher alignment in collagen fibers proximal to the tumoroid (II, Fig.6A, 6B, S6A and S6B). To better visualize this interaction with the matrix and the stroma, we performed *ex vivo* invasion assays of 12P and 14P tumoroids on decellularized peritoneum. We observed a efficient spreading of 14P tumoroids, which goes well with a basal localization of integrins. Blocking Integrin-β1 or HER2/HER3 reduces this spreading. Conversely, activating HER2/HER3 in 12P increases the spreading area on the peritoneum (II, Fig. 6F, 6G and 6H).

7.1.6 Higher HER2/HER3/SorLA expression correlates with apical-in polarity

We eventually wanted a more clinical readout of HER2/HER3/SorLA expression. By using previously characterized MUC CRC cohort (Canet-Jourdan et al., 2022), we stained

Formalin-fixed paraffin-embedded (FFPE) tumor sections for HER2, HER3 and SorLA. We observed a higher expression of HER2 in apical-in structures than in apical-out structures, corresponding well with our in vitro observations (II, Fig. 7A, 7C and S7B). This correlates well with the relative HER2 expression in 14P vs. 12P. in the PDX FFPEs (II, Fig. S7A). In all structures, a positive correlation between HER2 and HER3, as well as between HER2 and SorLA, was seen (II, Fig. 7B). Interestingly, by analysing a CRC cohort (Nguyen et al., 2021) and dividing them into two groups (mucinous and non-mucinous), we were able to see a positive correlation between ITGB1 and SORLA expression both in CMS1 and CMS3 solely for mucinous CRCs, which was not the case for the non-mucinous (II, Fig.7D and S7C).

Cumulatively, using cell- and mechanobiology methods to interrogate CRC PDX tumors ex-vivo and patient samples we report a novel polarity determination (see Figure 9) mechanism whereby HER2/HER3/SORLA-controlled β1-integrin traffic control tumor-ECM interactions, ECM rearrangements and invasion into the peritoneum.

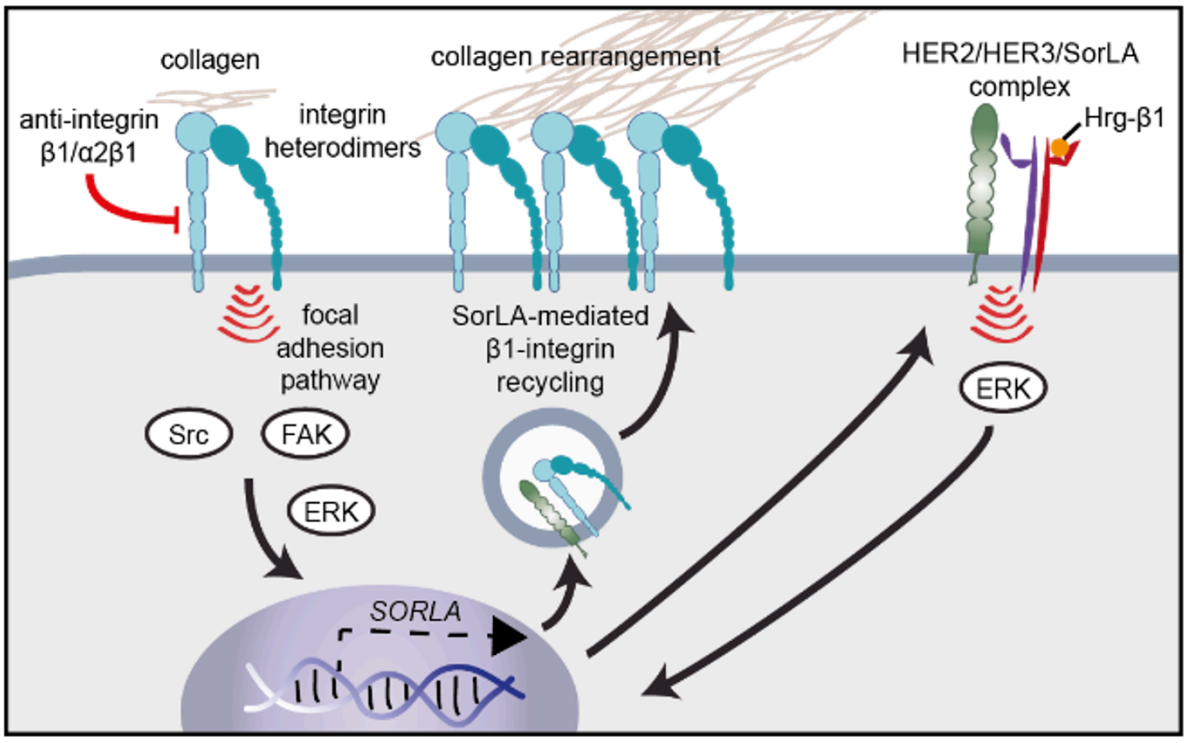

Figure 9 - HER2/HER3/SorLA-dependent Integrin-β1 recycling (from II)

7.2 Uncoupling stiffness and matrix composition to determine ideal conditions for integrin-dependent cancer cell spreading (III)

This project was a side project during my PhD work; therefore an emphasis will be put on my contribution to this work (see Figure 10).

Cell spreading is one of the mechanisms by which cancer cells invade their direct environment (Augoff et al., 2020). While different models show differential spreading depending on the ECM composition (equivalent to a healthy or a diseased ECM state), the coupling of such results with physical properties of the matrix, such as stiffness, is still unclear. To unravel this, we established a high-throughput ECM array with different compositions and stiffnesses. This aimed at better understanding the invasiveness and spreading of cancer cells, taking into account both chemical and physical parameters.

To answer this question, different ECM compositions were printed on polyacrylamide (PA) gels with two different stiffnesses: 0.5 kPa (soft) and 50 kPa (stiff). This was made possible by finding that all these components adhere on PA with no cratering or defaults after printing, using fluorescent collagen (III, Fig. S1, reported here in Figure 10). Chosen concentrations for further experiments were 400 μg/ml.

Through the analysis of cell spreading, it was possible to find matrix compositions that uncoupled stiffness and ligand repertoire, and enhanced U2OS and TIF spreading even on soft substrates: Collagen and Laminin (Coll/Lam), as well as Laminin and Tenascin C (Lam/TNC) (III, Fig.1 and Fig.2). This can be explained by an increase of molecular clutches at the cell surface. Indeed, TIFs on soft Coll/Lam substrates present more zyxin- and vinculin-positive foci, which can explain a better adhesion to the substrate (III, Fig.3). Additionally, because TIFs and U2OS present both collagen-binding ($\alpha2\beta1$ and $\alpha11\beta1$) and laminin-binding ($\alpha3\beta1$, $\alpha6\beta1$, $\alpha6\beta4$) integrins at their surface, they are able to engage a broader integrin repertoire for ECM interaction in a Coll/Lam matrix than on collagen or

laminin alone (III, Fig.3). This goes hand in hand with an increase in integrin signaling (III, Fig.4).

It was thus possible to find matrix compositions that engaged a higher diversity of integrins, and therefore initiate a higher number of molecular clutches on the cancer cell surface, therefore creating stiffness-independent conditions for cancer cell spreading and invasion.

Figure 10- Fig. S1 from III (see next page).

(A) Schematic of the microcontact printing technique applied to print the ECM mixtures as spots on hydrogels of different stiffness. (B) Schematic of the ECM spot array following microcontact printing on the different polyacrylamide hydrogels. (C) Representative images (left) and quantification (right) from initial FN test spots on 50 kPa stiffness gels (n=4 biological replicates; 4 spots/mixture/replicate; equal protein concentrations printed by making each mixture up to 400 µg/ml total protein with BSA; scale bars, 50 µm). (D to F) Representative images (D; whole spots imaged with half presented from each channel) and quantification of Collagen-I-647 (ColI-647) signal (E) or Lam staining (F) after spotting stiffness gels (0.5 and 50 kPa) with different dilutions of ColI-647, Lam or ColI-647/Lam (n=4 5 biological replicates; 2 spots/mixture/replicate; equal protein concentrations printed by making each mixture up to 400 µg/ml total protein with BSA; scale bars, 50 µm; XZ maximum projections given below representative XY images).

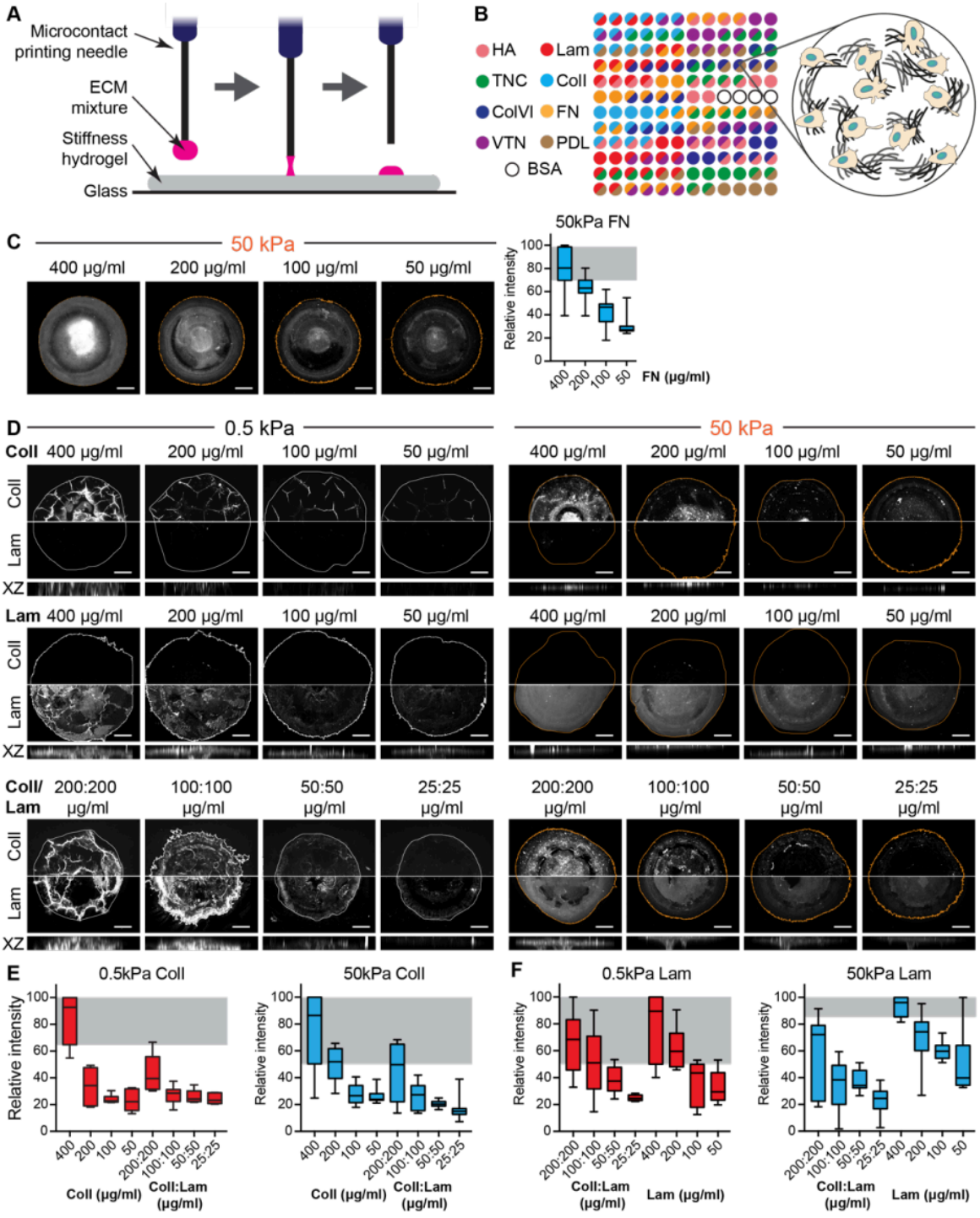
A
Microcontact printing needle
ECM mixture
Stiffness hydrogel
Glass
B
HA
Lam
TNC
Coll
ColVI
FN
VTN
PDL
BSA
C
50 kPa
400 µg/ml
200 µg/ml
100 µg/ml
50 µg/ml
50kPa FN
Relative intensity
FN (µg/ml)
D
0.5 kPa
50 kPa
Coll
Lam
XZ
Coll/ Lam
200:200 µg/ml
100:100 µg/ml
50:50 µg/ml
25:25 µg/ml
E
0.5kPa Coll
50kPa Coll
Coll (µg/ml)
Coll:Lam (µg/ml)
F
0.5kPa Lam
50kPa Lam
Coll:Lam (µg/ml)
Lam (µg/ml)

7.3 Integrin-β1: a cornerstone in hiPSC capacitation (IV)

This project was a side project during my PhD work; therefore an emphasis will be put on my contribution to this work (see IV, Figures 4 and 6).

7.3.1 Blocking Integrin-β1 delays the capacitation process

The action of Integrin-β1 on the blastocyst implantation and on the priming process which enables primed hiPSCs to evolve from naïve hiPSCs is still poorly understood, which is what has been the core of our research here.

While capacitation has already been molecularly characterized (Rostovskaya et al., 2019), the impact of Integrin-β1 on this process has not been studied. After growing naïve hiPSC colonies in NaïveCult for 48h with or without Mab13 (an integrin-β1-blocking antibody), the medium was changed to capacitation medium (N2B27 + 2μM XAV-939) and the growth was monitored with an IncuCyte. Colonies both adopt naïve-like features with a dome rounded shape in NaïveCult. After 48h in capacitation medium, colonies cultured without Mab13 lose their naïve-specific architecture and spread on the plastic, while the colonies cultured with Mab13 maintained a very similar phenotype to that of naïve hiPSCs. After 120 hours of capacitation, both conditions present a similar primed-like phenotype, lose their dome-shaped architecture and spread (IV, Fig.4A).

To further investigate the capacitation, we performed a colony count assay similar to the one described in Rostovskaya et al., 2019. Naïve hiPSCs were either capacitized for 48h (2d) or 120h (5d), both with or without Mab13. Cells were then passaged on a Matrigel-coated plate and cultured in either NaïveCult (to revert them to a naïve state) or E8 (to maintain them in a primed state) for 7 days (IV, Fig.4B). Colonies were then fixed and stained with CrystalViolet, and the colony area ratio between the NaïveCult and the E8 conditions was assessed from brightfield microscopy pictures. For both conditions, with or without Mab13, we normalized this area ratio to the area of non-capacitized colonies

(IV, Fig.4C). Without Mab13, we noticed a significant decrease in the colony area ratio in naïve hiPSCs capacitated for 5 days as opposed to the ones capacitated for 2 days, indicating that during the 5 days of capacitation, the cells have exited their naïve state and are no longer able to grow in NaïveCult. However, when cultured in presence of Mab13, the area ratio remains unaltered despite the capacitation duration, indicating that Mab13 attenuated exit from the naïve state, such that after 5 days the cells remain capable of growing and renewing in NaïveCult.

Taken together, these data suggest that blocking Integrin-β1 using Mab13 delays the capacitation process both on a phenotypical and molecular level. In this sense, integrin-β1 is essential for the capacitation process.

7.3.2 Integrin-β1 is central to a fully primed feature acquisition during capacitation

To further understand the genetic changes cause by capacitation, we performed single cell RNA sequencing (scRNAseq) using 6 different conditions: naïve hiPSCs cultured with (d0_Mab13) or without (d0) Mab13, previously capacitized (for 48h) naïve hiPSCs with (d2_Mab13) or without (d2) Mab13, and primed hiPSCS cultured with (HEL24.3_Mab13) or without (HEL24.3) Mab13. The U-map of these 6 groups shows that clustering patterns of naïve cells cultured without Mab13 is similar to that of capacitated cells cultured without Mab13, while the d0_Mab13 and d2_Mab13 groups also cluster alike. Primed HEL24.3 cells clustering is identical whether with or without Mab13 (IV, Fig. 6A). The overlayed SFRP2 expression (IV, Fig. 6B) shows a consistent pattern considering the capacitation process: as a primed marker, it is increasingly expressed with the capacitation stage and maximal in primed cells.

To better understand the effect of Mab13 on the capacitation process, we plotted the top up- and down-regulated genes in the d2 condition compared to the d0 condition (IV, Fig. 6C). From this geneset, we identified three populations: genes that remained downregulated in d2_Mab13 compared to d0_Mab13 (written in blue), genes that remained upregulated in d2_Mab13 compared to d0_Mab13 (written in red), and genes

that were differentially regulated in the absence of Mab13 but not in d2_Mab13 compared to d0_Mab13 (written in green). DPPA3 and L1TD1, two well characterized naïve markers (Palangi et al., 2017; Rostovskaya et al., 2019; Zhao et al., 2019) and therefore logically downregulated during capacitation seemed to be impacted by Integrin-β1 function blocking. Indeed, upon addition of Mab13, their expression stays unchanged upon capacitation. The case of Mab13-sensitive upregulation of MT1G and MT1H upon capacitation is interesting, as these metallothioneins have been reported to be upregulated during the differentiation process of cardiomyocytes (Branco et al., 2019) but also as part of naïve genesets in other studies (Liu et al., 2020; Molè et al., 2021) (IV, Fig.6D). Interestingly, CGA which is involved in the embryo attachment to the endometrium (Idelevich and Vilella, 2020) and therefore upregulated upon capacitation (IV, Fig.6D), was slightly downregulated after integrin-β1 blocking, once more underlining the strong inhibitory effect of Mab13 on the capacitation process.

Taken together, these data show the impact of Integrin-β1 function blocking on the capacitation with Mab13-treatment inhibiting capacitated cells to fully display a primed-like expression profile.

8 Discussion

8.1 Understanding inverted polarity in health and disease (I)

Inverted apicobasal polarity plays crucial roles in developmental processes, ranging from embryo implantation to immune surveillance. Conversely to the EMT paradigm, inverted polarity can also be a hallmark of invasive cancer progression. The significance of polarity inversion in the pathophysiology and molecular origins of these diseases is therefore becoming evident.

Our research compiles observations from cancer subtypes and genetic diseases to explain the development of inverted apicobasal polarity. It focuses on cellular responses to polarizing ECM cues, actomyosin contractility, and changes in membrane trafficking. Many of these molecular mechanisms have been identified through in vitro studies on cellular spheroids within standardized 3D matrices. However, to identify key molecular targets more precisely, more complex systems involving co-culture with stromal cells are necessary.

Recent advancements in manipulating cell polarity orientation, such as those reported by Watson et al., 2023, are needed to bridge the knowledge gap required for therapeutic interventions in diseases characterized by inverted polarity. These advancements will greatly help in developing targeted treatments to either restore normal cell polarity or induce polarity inversion as needed, enhancing our ability to modulate immune detection, drug responsiveness or cell migration. Overall, understanding and manipulating cell polarity dynamics hold significant promises for improving outcomes in a range of diseases, and especially cancer treatment.

8.2 A HER2/HER3/SorLA-dependent integrin-β1 recycling loop as a polarity regulator in CRC metastasis (II)

A prevailing view has been that the normal apicobasal polarity of epithelial tissues is progressively lost during carcinogenesis via the EMT process. However, this idea has increasingly been challenged with the occurrence of well polarized cancer structures (Diepenbruck and Christofori, 2016). Our study reveals an new mechanism through which CRC metastasis orient their polarity. We show a new interaction network involving integrins, HER-family RTKs and SorLA, explaining the efficient trafficking of Integrin-β1 in a collagen matrix and explaining the consequent apicobasal polarity orientation of MUC CRC metastasis. In this polarity regulation pathway, HER2/HER3/SorLA-regulated Integrin-β1 trafficking influences the interaction between tumor tissues and the ECM, as well as the ECM rearrangement and the peritoneal invasion of PC. We also show a correlation between the polarity phenotype and HER2, as well as an expression correlation between HER2, HER3 and SorLA in a MUC CRC cohort.

SorLA is a known sorting protein that regulates membrane traffic of amyloid precursor protein (APP) in neurons, insulin receptor in adipocytes and HER2/HER3 in HER2-positive breast cancer. Silencing SorLA has also been previously correlated with a lower Integrin-β1 recycling in breast cancer (Al-Akhrass et al., 2021; Andersen et al., 2006, 2005; Klinger et al., 2011; Pietilä et al., 2019; Schmidt et al., 2016; Spoelgen et al., 2009; Whittle et al., 2015). However, SorLA has not been previously shown as being implicated in CRC polarity regulation. Our findings indicate that SorLA is crucial for polarity orientation in MUC CRC tumoroids. SorLA levels are low in TSIPs cultured in suspension but increase in TSIPs showing a high surface-integrin expression. These TSIPs can form initial contacts with collagen and adopt an apical-in polarity once embedded in the matrix. ECM contact triggers two feed-forward loops:

→ the increased integrin-β1 recycling maintains an apical-in polarity phenotype.

→ the increased HER2/HER3 signaling induces SorLA expression.

We have found that inhibiting integrin-β1 or HER2/HER3 signaling, as well as silencing SorLA, prevents a normal apicobasal polarity orientation of MUC CRC TSIPs. These findings enhance our understanding of MUC CRC TSIP behavior during metastatic invasion and their functional consequences. Indeed, inverted polarity has been correlated with a shift in the cell migration mode (from collective mesenchymal to collective amoeboid as explained in Pagès et al., 2022) and in anti-cancer drug sensitivity (Ashley et al., 2019).

As we have extensively described in **4.1**, integrins constantly traffic between the PM and endosomes, both in normal and cancer cells. Most of these integrins are recycled back to the membrane (Moreno-Layseca et al., 2019; Paul et al., 2015). This integrin trafficking is central to cancer invasion, as it promotes metastasis in many carcinomas such as breast and pancreas. The role of Rab11fip1 in this process has also been described as it promotes integrin-β1 recycling and consequent cancer cell motility (Caswell et al., 2008; Caswell and Norman, 2006; Jacquemet et al., 2013; Machesky, 2019; Muller et al., 2009; Rainero et al., 2012). Interestingly, in our MUC CRC system, collagen interaction effectively reduces Rab11fip1 expression. We hypothesize that this is followed by a downregulation of the Rab11-dependent long loop of integrin recycling. The CRC-ECM contact upregulates SorLA, which implies that integrin-β1 trafficking switches to a short SorLA-dependent loop. This loop, supported by HER2/HER3 signaling, allows a proper localization of Integrin-β1 at the PM which signals for a normal polarity orientation.

CRCs show altered integrin expression compared to that of normal cells. Indeed, the laminin-binding α6β4 heterodimer is overexpressed in cancer (Beaulieu, 2020). We have efficiently shown that both the α1β1 and α2β1-collagen binding heterodimers were expressed in our CRCs, which we have decided to investigate. While the α1β1 dimer has been shown to be upregulated in 65% of CRC cases (Boudjadi et al., 2016), the role of α2β1 in CRC invasion has not been extensively studied. Normally polarized CRC tissues harbor a higher surface expression of both α2 and β1-integrins than apical-out CRC tissues. Conversely, blocking α2 and β1 integrins prevents the polarity reversion. α2

blocking alone is enough for a normal polarity orientation, showing that a1β1-collagen interaction does not support polarity reversion.

While HER2-targeting therapy is extensively used in HER2 amplified breast cancer with substantial clinical benefit, there is no such clinically validated therapy for CRC (Nowak, 2020; Ye et al., 2022). Interestingly, HER2 amplified CRC as well as high levels of Heregulin-β1 are correlated with a resistance to anti-EGFR therapy (Martin et al., 2013; Yonesaka et al., 2011). Because polarity effectively changes the way cancer cells react to anti-cancer drugs (Ashley et al., 2019), and inverted polarity has been correlated with a poorer prognosis (Canet-Jourdan et al., 2022), the way the HER2/HER3/SorLA signaling pathway and subsequent integrin-trafficking loop functions requires further investigation in order to decipher the clinical implications of polarity orientation in MUC CRCs. Further studies may for example facilitate patient stratification for targeted therapy.

8.3 Ligand availability and integrin engagement determine cell behavior and stiffness-independent spreading (III)

While it is now known that cancer cells remodel the substrate by changing the ECM stiffness and composition, few studies have aimed at uncoupling these parameters to further understand the underlying causes of cancer cell invasion (Najafi et al., 2019). Indeed, the adhesion maturation caused by talin unfolding and vinculin recruitment explains adhesions on rigid substrates, but it does not explain cell migration on compliant matrixes (Atherton et al., 2015; Friedland et al., 2009). Here, we developed a composite ECM spot array system to analyze cellular responses to matrix composition and its mechanical properties. We uncovered two ECM compositions promoting stiff-like behavior on compliant substrates. These findings align with observations that cells in soft tissues migrate without rigid support, mostly depending on ligand density and the affinity of specific integrin heterodimers to specific ligands (Su et al., 2016). For instance, the expression of integrin heterodimers with varied affinities to fibrillar and non-fibrillar

collagen (Lerche et al., 2020; Tiger et al., 2001; Tulla et al., 2001) shows the implication of a varied integrin repertoire within the same ligand-binding family. The nature of the expressed integrin families explains why some of the matrix combinations we found promoted cancer cells spreading on compliant substrates when others did not.

A computational motor-clutch model was applied to simulate cell spreading on soft substrates as a function of ECM ligand availability and motor activity, showing that a higher number of molecular clutches could compensate for the lack of mechanical support, promoting cell spreading. Experimental verification confirmed that cell spreading on soft ECM depends on the balance between available clutches and motor activity. However, mechanical adhesion reinforcement is less likely on soft substrates, which suggests that ligand density and integrin affinities play a larger role in cell adhesion on compliant matrixes (Elosegui-Artola et al., 2016; Su et al., 2016).

The current platform focuses on a limited set of ECM proteins and mechanical properties. To address these limitations, future research should aim to refine the model and validate findings in more complex 3D systems. This will enhance our understanding of ECM dynamics and improve the relevance of drug screening platforms, ultimately leading to better therapeutic strategies for diseases such as cancer, where the ECM plays a critical role in tumor progression and treatment response. Indeed, matrix compliance has been shown to be implicated in treatment resistance in breast cancer (Drain et al., 2021).

8.4 Integrin-β1 blocking promotes naïve-like features and prevents effective capacitation of hiPSCs (IV)

Although the establishment of naïve hiPSCs, their chemical reversion and their capacitation into a primed state has been documented (Hassani et al., 2019; Rostovskaya et al., 2019; Taei et al., 2020), the influence of Integrin-β1 in this process has been widely overlooked. In this study, we show that inhibition of Integrin-β1 supports naïve-like features and architecture in hiPSC cells and reproduces well the maintenance state of the early blastocyst ICM cells.

Across this publication, we have shown that integrin-β1 inhibition downregulates Angiomotin-Like 2 (AMOTL2) in primed hiPSCs. AMOTL2 is known as a negative regulator of YAP and YAP inhibition is crucial for the differentiation process of PSCs. Therefore, we suggest the importance of Integrin-β1 signaling into the priming and differentiation process of stem cells, although some more information on its action and that of AMOTL2 on the establishment of primed hiPSC colony architecture and morphology is needed (Pagliari et al., 2021; Wang et al., 2011; Zhao et al., 2011). Upon Integrin-β1 blocking in naïve hiPSCs, we have shown an upregulation of actin regulators such as Phosphatase Actin Regulator-1 (PHACTR-1) and Filamin A-Binding Protein (FILIP1) which regulate actomyosin assembly, lamellipodium formation and cell migration (Allain et al., 2012; Jarray et al., 2011; Nagano et al., 2002; Wiezlak et al., 2012), but deeper studies should be done to further grasp their impact on the maintenance of naïve-like features.

We also show that Integrin-β1 is crucial for the capacitation of hiPSCs, ie. the transition from the naïve to primed state. Blocking integrin-β1 seems to effectively delay capacitation, support a naïve-like morphology and induce a higher growth ability in naïve condition. Capacitation is accompanied by the upregulation of primed markers, such as secreted frizzled related protein 2 (SFRP2) and by the downregulation of naïve markers, namely DPPA3 and L1TD1 (Messmer et al., 2019; Rostovskaya et al., 2019; Yilmaz and Benvenisty, 2019). However, blocking Integrin-β1 prevents the shift towards a fully

primed signature, with equal levels of these two markers in Mab13-treated capacitated cells to that of naïve cells. Furthermore, integrin-β1 inhibition prevents the upregulation of metallothioneins (MT1G and MT1H) upon capacitation. This is an interesting lead to follow in the future as altered metallothionein expression have been linked to cell state transitions.

Altogether, we show a crucial role of Integrin-β1 in the exit from naïve cell. Integrin-β1 inhibition delays and a full capacitation of hiPSCs and supports a naïve-like phenotype. This moves the understanding of cell state transition one step forward and puts Integrin-β1 as a key regulator in the early embryonic development.

9 Conclusion

The aim of this thesis was to understand the role of integrins, and especially integrin-β1 in different cell processes, namely apicobasal polarity orientation, stiffness-independent cancer cell invasion on different substrates and capacitation of hiPSCs. While these projects had very different outcomes and readouts, they allowed to identify Integrin-β1 as a cornerstone in the establishment of cell states and morphology. Through this study, we uncovered a previously unknown HER2/HER3/SorLA-dependent Integrin-β1 recycling loop, matrix compositions allowing a stiffness-independent spreading of cancer cells and further uncovered the role of Integrin-β1 in the early phases of development.

9.1 Original Publication I

Here we explain the role of inverted polarity in health and disease, studying different examples. Inverted polarity can be considered as a relatively newly described hallmark of cancer, and effectively impacts cancer invasion and growth, treatment resistance and its immune escape. Inverted polarity is also seen in genetic diseases and immune response to pathogen defense. Because inverted polarity is not necessarily pathological, we have also focused on the blastocyst polarity, which shows a perfect example of apicobasal inverted polarity at the pre-implantation stage.

Altogether this work allows to further understand the current knowledge on inverted apicobasal polarity, its molecular mechanisms and its pathological implications.

9.2 Original Publication II

We discovered here a Focal Adhesion pathway-dependent mechanism by which MUC CRC metastasis orient their apicobasal polarity. Indeed, we show that upon embedding tumoroids in collagen, a Rab11-dependent long Integrin-β1 recycling loops is

downregulated and replaced by a SorLA-dependent short loop. This loop is induced by HER2 and HER3 signaling, which initiates positive feedback as the upregulation of SorLA further stabilizes HER2 and HER3 at the membrane. This newly described Integrin-β1 recycling loop is responsible for the proper localization of integrin heterodimers at the membrane of MUC CRC metastasis, allowing interactions with the matrix and proper orientation of the apicobasal polarity. These data show relevance clinically, since the polarity status correlates with HER2 expression *in vivo* and HER2, HER3 and SorLA levels show a positive correlation in MUC CRC tissues. Because the polarity status of such tumors has been correlated with survival, this unlocks interesting opportunities for further polarity-oriented anti-cancer targets.

9.3 Original Publication III

Here we explained how osteosarcoma cells and fibroblasts spread in a stiffness-independent fashion on the substrate, and we explain it by the increase in the number of molecular clutches to form interactions with the matrix. By expressing a specific repertoire of specific-ligand binding integrins, cancer cells invaded compliant substrates in a stiff-like fashion. We identified two matrix compositions which supported this: Collagen and Laminin (Coll/Lam), as well as Laminin and Tenascin C (Lam/TNC). Because ECM physical and chemical properties can influence anti-cancer treatment response and resistance, this study impacts in a relevant way by further explaining stiff-like spreading of cancer cells on soft substrates.

9.4 Original Publication IV

Here we unravel how integrin-β1 acts in the capacitation process of hiPSCs. Integrin-β1 blocking supports naïve-like features in primed hiPSCs related to their architecture and gene expression patterns. It also maintains a naïve-like state in naïve hiPSCs through the enhancement of cell clustering. Integrin-β1 blocking effectively delays and weakens the capacitation process and promotes cell growth once back in naïve medium. By changing

the expression profile of naïve and primed markers, we show that Integrin-β1 is a key regulator of capacitation, and therefore a cornerstone in the early development.

10 References

Adams, S.A., Smith, M.E.F., Cowley, G.P., Carr, L.A., 2004. Reversal of glandular polarity in the lymphovascular compartment of breast cancer. J. Clin. Pathol. 57, 1114–1117. https://doi.org/10.1136/jcp.2004.016980

Al-Akhrass, H., Conway, J.R.W., Poulsen, A.S.A., Paatero, I., Kaivola, J., Padzik, A., Andersen, O.M., Ivaska, J., 2021. A feed-forward loop between SorLA and HER3 determines heregulin response and neratinib resistance. Oncogene 40, 1300–1317. https://doi.org/10.1038/s41388-020-01604-5

Alanko, J., Mai, A., Jacquemet, G., Schauer, K., Kaukonen, R., Saari, M., Goud, B., Ivaska, J., 2015. Integrin endosomal signalling suppresses anoikis. Nat. Cell Biol. 17, 1412–1421. https://doi.org/10.1038/ncb3250

Allain, B., Jarray, R., Borriello, L., Leforban, B., Dufour, S., Liu, W., Pamonsinlapatham, P., Bianco, S., Larghero, J., Hadj-Slimane, R., Garbay, C., Raynaud, F., Lepelletier, Y., 2012. Neuropilin-1 regulates a new VEGF-induced gene, *Phactr-1*, which controls tubulogenesis and modulates lamellipodial dynamics in human endothelial cells. Cell. Signal. 24, 214–223. https://doi.org/10.1016/j.cellsig.2011.09.003

Al-Obaidy, K.I., Eble, J.N., Cheng, L., Williamson, S.R., Sakr, W.A., Gupta, N., Idrees, M.T., Grignon, D.J., 2019. Papillary Renal Neoplasm With Reverse Polarity: A Morphologic, Immunohistochemical, and Molecular Study. Am. J. Surg. Pathol. 43, 1099. https://doi.org/10.1097/PAS.0000000000001288

Al-Obaidy, K.I., Eble, J.N., Nassiri, M., Cheng, L., Eldomery, M.K., Williamson, S.R., Sakr, W.A., Gupta, N., Hassan, O., Idrees, M.T., Grignon, D.J., 2020. Recurrent KRAS mutations in papillary renal neoplasm with reverse polarity. Mod. Pathol. 33, 1157–1164. https://doi.org/10.1038/s41379-019-0362-1

Amornphimoltham, P., Rechache, K., Thompson, J., Masedunskas, A., Leelahavanichkul, K., Patel, V., Molinolo, A., Gutkind, J.S., Weigert, R., n.d. Rab25 Regulates Invasion and Metastasis in Head and Neck Cancer. Clin. Cancer Res.

Anastasiadis, P.Z., Moon, S.Y., Thoreson, M.A., Mariner, D.J., Crawford, H.C., Zheng, Y., Reynolds, A.B., 2000. Inhibition of RhoA by p120 catenin. Nat. Cell Biol. 2, 637–644. https://doi.org/10.1038/35023588

Andersen, O.M., Reiche, J., Schmidt, V., Gotthardt, M., Spoelgen, R., Behlke, J., von Arnim, C.A.F., Breiderhoff, T., Jansen, P., Wu, X., Bales, K.R., Cappai, R., Masters, C.L., Gliemann, J., Mufson, E.J., Hyman, B.T., Paul, S.M., Nykjær, A., Willnow, T.E., 2005. Neuronal sorting protein-related receptor sorLA/LR11 regulates processing of the amyloid precursor protein. Proc. Natl. Acad. Sci. 102, 13461–13466. https://doi.org/10.1073/pnas.0503689102

Andersen, O.M., Schmidt, V., Spoelgen, R., Gliemann, J., Behlke, J., Galatis, D., McKinstry, W.J., Parker, M.W., Masters, C.L., Hyman, B.T., Cappai, R., Willnow, T.E., 2006. Molecular Dissection of the Interaction between Amyloid Precursor Protein and Its Neuronal Trafficking Receptor SorLA/LR11. Biochemistry 45, 2618–2628.

https://doi.org/10.1021/bi052120v

Anthis, N.J., Wegener, K.L., Ye, F., Kim, C., Goult, B.T., Lowe, E.D., Vakonakis, I., Bate, N., Critchley, D.R., Ginsberg, M.H., Campbell, I.D., 2009. The structure of an integrin/talin complex reveals the basis of inside-out signal transduction. EMBO J. 28, 3623–3632. https://doi.org/10.1038/emboj.2009.287

Aoyagi, T., Terracina, K.P., Raza, A., Takabe, K., 2014. Current treatment options for colon cancer peritoneal carcinomatosis. World J. Gastroenterol. WJG 20, 12493–12500. https://doi.org/10.3748/wjg.v20.i35.12493

Apodaca, G., Gallo, L.I., Bryant, D.M., 2012. Role of membrane traffic in the generation of epithelial cell asymmetry. Nat. Cell Biol. 14, 1235–1243. https://doi.org/10.1038/ncb2635

Arias-Salgado, E.G., Lizano, S., Sarkar, S., Brugge, J.S., Ginsberg, M.H., Shattil, S.J., 2003. Src kinase activation by direct interaction with the integrin β cytoplasmic domain. Proc. Natl. Acad. Sci. 100, 13298–13302. https://doi.org/10.1073/pnas.2336149100

Arjonen, A., Alanko, J., Veltel, S., Ivaska, J., 2012. Distinct Recycling of Active and Inactive β1 Integrins. Traffic 13, 610–625. https://doi.org/10.1111/j.1600-0854.2012.01327.x

Arnaout, M.A., Mahalingam, B., Xiong, J.-P., 2005. INTEGRIN STRUCTURE, ALLOSTERY, AND BIDIRECTIONAL SIGNALING. Annu. Rev. Cell Dev. Biol. 21, 381–410. https://doi.org/10.1146/annurev.cellbio.21.090704.151217

Ashley, N., Ouaret, D., Bodmer, W.F., 2019. Cellular polarity modulates drug resistance in primary colorectal cancers via orientation of the multidrug resistance protein ABCB1. J. Pathol. 247, 293–304. https://doi.org/10.1002/path.5179

Asioli, S., Erickson, L.A., Righi, A., Lloyd, R.V., 2013. Papillary thyroid carcinoma with hobnail features: histopathologic criteria to predict aggressive behavior. Hum. Pathol. 44, 320–328. https://doi.org/10.1016/j.humpath.2012.06.003

Atherton, P., Stutchbury, B., Wang, D.-Y., Jethwa, D., Tsang, R., Meiler-Rodriguez, E., Wang, P., Bate, N., Zent, R., Barsukov, I.L., Goult, B.T., Critchley, D.R., Ballestrem, C., 2015. Vinculin controls talin engagement with the actomyosin machinery. Nat. Commun. 6, 10038. https://doi.org/10.1038/ncomms10038

Augoff, K., Hryniewicz-Jankowska, A., Tabola, R., 2020. Invadopodia: clearing the way for cancer cell invasion. Ann. Transl. Med. 8, 902. https://doi.org/10.21037/atm.2020.02.157

Bachmann, M., Kukkurainen, S., Hytönen, V.P., Wehrle-Haller, B., 2019. Cell Adhesion by Integrins. Physiol. Rev. 99, 1655–1699. https://doi.org/10.1152/physrev.00036.2018

Bagante, F., Spolverato, G., Beal, E., Merath, K., Chen, Q., Akgül, O., Anders, R.A., Pawlik, T.M., 2018. Impact of histological subtype on the prognosis of patients undergoing surgery for colon cancer. J. Surg. Oncol. 117, 1355–1363. https://doi.org/10.1002/jso.25044

Bangasser, B.L., Rosenfeld, S.S., Odde, D.J., 2013. Determinants of Maximal Force Transmission in a Motor-Clutch Model of Cell Traction in a Compliant Microenvironment. Biophys. J. 105, 581–592. https://doi.org/10.1016/j.bpj.2013.06.027

Banno, A., Goult, B.T., Lee, H., Bate, N., Critchley, D.R., Ginsberg, M.H., 2012.

Subcellular Localization of Talin Is Regulated by Inter-domain Interactions *. J. Biol. Chem. 287, 13799–13812. https://doi.org/10.1074/jbc.M112.341214

Barker, N., van Es, J.H., Kuipers, J., Kujala, P., van den Born, M., Cozijnsen, M., Haegebarth, A., Korving, J., Begthel, H., Peters, P.J., Clevers, H., 2007. Identification of stem cells in small intestine and colon by marker gene Lgr5. Nature 449, 1003–1007. https://doi.org/10.1038/nature06196

Barnes, J.M., Kaushik, S., Bainer, R.O., Sa, J.K., Woods, E.C., Kai, F., Przybyla, L., Lee, M., Lee, H.W., Tung, J.C., Maller, O., Barrett, A.S., Lu, K.V., Lakins, J.N., Hansen, K.C., Obernier, K., Alvarez-Buylla, A., Bergers, G., Phillips, J.J., Nam, D.-H., Bertozzi, C.R., Weaver, V.M., 2018. A tension-mediated glycocalyx–integrin feedback loop promotes mesenchymal-like glioblastoma. Nat. Cell Biol. 20, 1203–1214. https://doi.org/10.1038/s41556-018-0183-3

Barresi, V., Branca, G., Vitarelli, E., Tuccari, G., 2014. Micropapillary Pattern and Poorly Differentiated Clusters Represent the Same Biological Phenomenon in Colorectal Cancer: A Proposal for a Change in Terminology. Am. J. Clin. Pathol. 142, 375–383. https://doi.org/10.1309/AJCPFEA7KA0SBBNA

Barret, C., Roy, C., Montcourrier, P., Mangeat, P., Niggli, V., 2000. Mutagenesis of the Phosphatidylinositol 4,5-Bisphosphate (Pip2) Binding Site in the Nh2-Terminal Domain of Ezrin Correlates with Its Altered Cellular Distribution. J. Cell Biol. 151, 1067–1080. https://doi.org/10.1083/jcb.151.5.1067

Bass, M.D., Roach, K.A., Morgan, M.R., Mostafavi-Pour, Z., Schoen, T., Muramatsu, T., Mayer, U., Ballestrem, C., Spatz, J.P., Humphries, M.J., 2007. Syndecan-4–dependent Rac1 regulation determines directional migration in response to the extracellular matrix. J. Cell Biol. 177, 527–538. https://doi.org/10.1083/jcb.200610076

Bateman, J.F., Boot-Handford, R.P., Lamandé, S.R., 2009. Genetic diseases of connective tissues: cellular and extracellular effects of ECM mutations. Nat. Rev. Genet. 10, 173–183. https://doi.org/10.1038/nrg2520

Baumann, H., Schwingel, M., Sestu, M., Burcza, A., Marg, S., Ziegler, W., Taubenberger, A.V., Muller, D.J., Bastmeyer, M., Franz, C.M., 2023. Biphasic reinforcement of nascent adhesions by vinculin. J. Mol. Recognit. 36, e3012. https://doi.org/10.1002/jmr.3012

Beaulieu, J.-F., 2020. Integrin α6β4 in Colorectal Cancer: Expression, Regulation, Functional Alterations and Use as a Biomarker. Cancers 12, 41. https://doi.org/10.3390/cancers12010041

Bedzhov, I., Zernicka-Goetz, M., 2014. Self-Organizing Properties of Mouse Pluripotent Cells Initiate Morphogenesis upon Implantation. Cell 156, 1032–1044. https://doi.org/10.1016/j.cell.2014.01.023

Bellis, S.L., 2004. Variant glycosylation: an underappreciated regulatory mechanism for β1 integrins. Biochim. Biophys. Acta BBA - Biomembr. 1663, 52–60. https://doi.org/10.1016/j.bbamem.2004.03.012

Bernick, P.E., Klimstra, D.S., Shia, J., Minsky, B., Saltz, L., Shi, W., Thaler, H., Guillem, J., Paty, P., Cohen, A.M., Wong, W.D., 2004. Neuroendocrine Carcinomas of the Colon and Rectum. Dis. Colon Rectum 47, 163–169. https://doi.org/10.1007/s10350-003-0038-1

Bertotti, A., Comoglio, P.M., Trusolino, L., 2006. Beta4 integrin activates a Shp2-Src signaling pathway that sustains HGF-induced anchorage-independent growth. J. Cell Biol. 175, 993–1003. https://doi.org/10.1083/jcb.200605114

Bertotti, A., Comoglio, P.M., Trusolino, L., 2005. Beta4 integrin is a transforming molecule that unleashes Met tyrosine kinase tumorigenesis. Cancer Res. 65, 10674–10679. https://doi.org/10.1158/0008-5472.CAN-05-2827

Bevins, C.L., Salzman, N.H., 2011. Paneth cells, antimicrobial peptides and maintenance of intestinal homeostasis. Nat. Rev. Microbiol. 9, 356–368. https://doi.org/10.1038/nrmicro2546

Bigorgne, A.E., Farin, H.F., Lemoine, R., Mahlaoui, N., Lambert, N., Gil, M., Schulz, A., Philippet, P., Schlesser, P., Abrahamsen, T.G., Oymar, K., Davies, E.G., Ellingsen, C.L., Leteurtre, E., Moreau-Massart, B., Berrebi, D., Bole-Feysot, C., Nischke, P., Brousse, N., Fischer, A., Clevers, H., Basile, G. de S., 2014. *TTC7A* mutations disrupt intestinal epithelial apicobasal polarity. J. Clin. Invest. 124, 328–337. https://doi.org/10.1172/JCI71471

Bilder, D., Perrimon, N., 2000. Localization of apical epithelial determinants by the basolateral PDZ protein Scribble. Nature 403, 676–680. https://doi.org/10.1038/35001108

Birchenough, G.M.H., Johansson, M.E., Gustafsson, J.K., Bergström, J.H., Hansson, G.C., 2015. New developments in goblet cell mucus secretion and function. Mucosal Immunol. 8, 712–719. https://doi.org/10.1038/mi.2015.32

Blomme, A., Van Simaeys, G., Doumont, G., Costanza, B., Bellier, J., Otaka, Y., Sherer, F., Lovinfosse, P., Boutry, S., Palacios, A.P., De Pauw, E., Hirano, T., Yokobori, T., Hustinx, R., Bellahcène, A., Delvenne, P., Detry, O., Goldman, S., Nishiyama, M., Castronovo, V., Turtoi, A., 2018. Murine stroma adopts a human-like metabolic phenotype in the PDX model of colorectal cancer and liver metastases. Oncogene 37, 1237–1250. https://doi.org/10.1038/s41388-017-0018-x

Bonifacino, J.S., 2014. Adaptor proteins involved in polarized sorting. J. Cell Biol. 204, 7–17. https://doi.org/10.1083/jcb.201310021

Bonnans, C., Chou, J., Werb, Z., 2014. Remodelling the extracellular matrix in development and disease. Nat. Rev. Mol. Cell Biol. 15, 786–801. https://doi.org/10.1038/nrm3904

Borghi, N., Lowndes, M., Maruthamuthu, V., Gardel, M.L., Nelson, W.J., 2010. Regulation of cell motile behavior by crosstalk between cadherin- and integrin-mediated adhesions. Proc. Natl. Acad. Sci. 107, 13324–13329. https://doi.org/10.1073/pnas.1002662107

Bos, J.L., Rehmann, H., Wittinghofer, A., 2007. GEFs and GAPs: critical elements in the control of small G proteins. Cell 129, 865–877. https://doi.org/10.1016/j.cell.2007.05.018

Böttcher, R.T., Stremmel, C., Meves, A., Meyer, H., Widmaier, M., Tseng, H.-Y., Fässler, R., 2012. Sorting nexin 17 prevents lysosomal degradation of β1 integrins by binding to the β1-integrin tail. Nat. Cell Biol. 14, 584–592. https://doi.org/10.1038/ncb2501

Boudjadi, S., Carrier, J.C., Groulx, J.-F., Beaulieu, J.-F., 2016. Integrin α1β1 expression is controlled by c-MYC in colorectal cancer cells. Oncogene 35, 1671–1678.

https://doi.org/10.1038/onc.2015.231

Boulter, E., Garcia-Mata, R., 2012. Analysis of the Role of RhoGDI1 and Isoprenylation in the Degradation of RhoGTPases, in: Rivero, F. (Ed.), Rho GTPases: Methods and Protocols. Springer, New York, NY, pp. 97–105. https://doi.org/10.1007/978-1-61779-442-1_7

Branco, M.A., Cotovio, J.P., Rodrigues, C.A.V., Vaz, S.H., Fernandes, T.G., Moreira, L.M., Cabral, J.M.S., Diogo, M.M., 2019. Transcriptomic analysis of 3D Cardiac Differentiation of Human Induced Pluripotent Stem Cells Reveals Faster Cardiomyocyte Maturation Compared to 2D Culture. Sci. Rep. 9, 9229. https://doi.org/10.1038/s41598-019-45047-9

Bridgewater, R.E., Norman, J.C., Caswell, P.T., 2012. Integrin trafficking at a glance. J. Cell Sci. 125, 3695–3701. https://doi.org/10.1242/jcs.095810

Brown, F.D., Rozelle, A.L., Yin, H.L., Balla, T., Donaldson, J.G., 2001. Phosphatidylinositol 4,5-bisphosphate and Arf6-regulated membrane traffic. J. Cell Biol. 154, 1007–1018. https://doi.org/10.1083/jcb.200103107

Bryant, D.M., Datta, A., Rodríguez-Fraticelli, A.E., Peränen, J., Martín-Belmonte, F., Mostov, K.E., 2010. A molecular network for de novo generation of the apical surface and lumen. Nat. Cell Biol. 12, 1035–1045. https://doi.org/10.1038/ncb2106

Bryant, D.M., Mostov, K.E., 2008. From cells to organs: building polarized tissue. Nat. Rev. Mol. Cell Biol. 9, 887–901. https://doi.org/10.1038/nrm2523

Bryant, D.M., Roignot, J., Datta, A., Overeem, A.W., Kim, M., Yu, W., Peng, X., Eastburn, D.J., Ewald, A.J., Werb, Z., Mostov, K.E., 2014. A Molecular Switch for the Orientation of Epithelial Cell Polarization. Dev. Cell 31, 171–187. https://doi.org/10.1016/j.devcel.2014.08.027

Buckley, C.E., St Johnston, D., 2022. Apical–basal polarity and the control of epithelial form and function. Nat. Rev. Mol. Cell Biol. 23, 559–577. https://doi.org/10.1038/s41580-022-00465-y

Burridge, K., 2005. Foot in mouth: do focal adhesions disassemble by endocytosis? Nat. Cell Biol. 7, 545–547. https://doi.org/10.1038/ncb0505-545

Byron, A., Askari, J.A., Humphries, J.D., Jacquemet, G., Koper, E.J., Warwood, S., Choi, C.K., Stroud, M.J., Chen, C.S., Knight, D., Humphries, M.J., 2015. A proteomic approach reveals integrin activation state-dependent control of microtubule cortical targeting. Nat. Commun. 6, 6135. https://doi.org/10.1038/ncomms7135

Calderwood, D.A., Yan, B., De Pereda, J.M., Alvarez, B.G., Fujioka, Y., Liddington, R.C., Ginsberg, M.H., 2002. The Phosphotyrosine Binding-like Domain of Talin Activates Integrins. J. Biol. Chem. 277, 21749–21758. https://doi.org/10.1074/jbc.M111996200

Campbell, I.D., Humphries, M.J., 2011. Integrin Structure, Activation, and Interactions. Cold Spring Harb. Perspect. Biol. 3, a004994. https://doi.org/10.1101/cshperspect.a004994

Canel, M., Serrels, A., Frame, M.C., Brunton, V.G., 2013. E-cadherin–integrin crosstalk in cancer invasion and metastasis. J. Cell Sci. 126, 393–401. https://doi.org/10.1242/jcs.100115

Canet-Jourdan, C., Pagès, D.-L., Nguyen-Vigouroux, C., Cartry, J., Zajac, O., Desterke, C., Lopez, J.-B., Gutierrez-Mateyron, E., Signolle, N., Adam, J., Raingeaud, J., Polrot, M., Gonin, P., Mathieu, J.R.R., Souquere, S., Pierron, G., Gelli, M., Dartigues, P., Ducreux, M., Barresi, V., Jaulin, F., 2022. Patient-derived organoids identify an apico-basolateral polarity switch associated with survival in colorectal cancer. J. Cell Sci. 135, jcs259256. https://doi.org/10.1242/jcs.259256

Cartry, J., Bedja, S., Boilève, A., Mathieu, J.R.R., Gontran, E., Annereau, M., Job, B., Mouawia, A., Mathias, P., De Baère, T., Italiano, A., Besse, B., Sourrouille, I., Gelli, M., Bani, M.-A., Dartigues, P., Hollebecque, A., Smolenschi, C., Ducreux, M., Malka, D., Jaulin, F., 2023. Implementing patient derived organoids in functional precision medicine for patients with advanced colorectal cancer. J. Exp. Clin. Cancer Res. 42, 281. https://doi.org/10.1186/s13046-023-02853-4

Case, L.B., Baird, M.A., Shtengel, G., Campbell, S.L., Hess, H.F., Davidson, M.W., Waterman, C.M., 2015. Molecular mechanism of vinculin activation and nanoscale spatial organization in focal adhesions. Nat. Cell Biol. 17, 880–892. https://doi.org/10.1038/ncb3180

Case, L.B., De Pasquale, M., Henry, L., Rosen, M.K., 2022. Synergistic phase separation of two pathways promotes integrin clustering and nascent adhesion formation. eLife 11, e72588. https://doi.org/10.7554/eLife.72588

Caswell, P.T., Chan, M., Lindsay, A.J., McCaffrey, M.W., Boettiger, D., Norman, J.C., 2008. Rab-coupling protein coordinates recycling of α5β1 integrin and EGFR1 to promote cell migration in 3D microenvironments. J. Cell Biol. 183, 143–155. https://doi.org/10.1083/jcb.200804140

Caswell, P.T., Norman, J.C., 2006. Integrin Trafficking and the Control of Cell Migration. Traffic 7, 14–21. https://doi.org/10.1111/j.1600-0854.2005.00362.x

Caswell, P.T., Spence, H.J., Parsons, M., White, D.P., Clark, K., Cheng, K.W., Mills, G.B., Humphries, M.J., Messent, A.J., Anderson, K.I., McCaffrey, M.W., Ozanne, B.W., Norman, J.C., 2007. Rab25 Associates with α5β1 Integrin to Promote Invasive Migration in 3D Microenvironments. Dev. Cell 13, 496–510. https://doi.org/10.1016/j.devcel.2007.08.012

Cesare, E., Urciuolo, A., Stuart, H.T., Torchio, E., Gesualdo, A., Laterza, C., Gagliano, O., Martewicz, S., Cui, M., Manfredi, A., Di Filippo, L., Sabatelli, P., Squarzoni, S., Zorzan, I., Betto, R.M., Martello, G., Cacchiarelli, D., Luni, C., Elvassore, N., 2022. 3D ECM-rich environment sustains the identity of naive human iPSCs. Cell Stem Cell 29, 1703-1717.e7. https://doi.org/10.1016/j.stem.2022.11.011

Chan, C.E., Odde, D.J., 2008. Traction Dynamics of Filopodia on Compliant Substrates. Science 322, 1687–1691. https://doi.org/10.1126/science.1163595

Charras, G., Sahai, E., 2014. Physical influences of the extracellular environment on cell migration. Nat. Rev. Mol. Cell Biol. 15, 813–824. https://doi.org/10.1038/nrm3897

Chastney, M.R., Conway, J.R.W., Ivaska, J., 2021. Integrin adhesion complexes. Curr. Biol. 31, R536–R542. https://doi.org/10.1016/j.cub.2021.01.038

Chastney, M.R., Lawless, C., Humphries, J.D., Warwood, S., Jones, M.C., Knight, D., Jorgensen, C., Humphries, M.J., 2020. Topological features of integrin adhesion complexes

revealed by multiplexed proximity biotinylation. J. Cell Biol. 219, e202003038. https://doi.org/10.1083/jcb.202003038

Cheng, K.W., Lahad, J.P., Kuo, W., Lapuk, A., Yamada, K., Auersperg, N., Liu, J., Smith-McCune, K., Lu, K.H., Fishman, D., Gray, J.W., Mills, G.B., 2004. The RAB25 small GTPase determines aggressiveness of ovarian and breast cancers. Nat. Med. 10, 1251–1256. https://doi.org/10.1038/nm1125

Chiang, S., Weigelt, B., Wen, H.-C., Pareja, F., Raghavendra, A., Martelotto, L.G., Burke, K.A., Basili, T., Li, A., Geyer, F.C., Piscuoglio, S., Ng, C.K.Y., Jungbluth, A.A., Balss, J., Pusch, S., Baker, G.M., Cole, K.S., von Deimling, A., Batten, J.M., Marotti, J.D., Soh, H.-C., McCalip, B.L., Serrano, J., Lim, R.S., Siziopikou, K.P., Lu, S., Liu, X., Hammour, T., Brogi, E., Snuderl, M., Iafrate, A.J., Reis-Filho, J.S., Schnitt, S.J., 2016. IDH2 Mutations Define a Unique Subtype of Breast Cancer with Altered Nuclear Polarity. Cancer Res. 76, 7118–7129. https://doi.org/10.1158/0008-5472.CAN-16-0298

Cho, S., Irianto, J., Discher, D.E., 2017. Mechanosensing by the nucleus: From pathways to scaling relationships. J. Cell Biol. 216, 305–315. https://doi.org/10.1083/jcb.201610042

Christoforides, C., Rainero, E., Brown, K.K., Norman, J.C., Toker, A., 2012. PKD Controls αvβ3 Integrin Recycling and Tumor Cell Invasive Migration through Its Substrate Rabaptin-5. Dev. Cell 23, 560–572. https://doi.org/10.1016/j.devcel.2012.08.008

Collier, A.J., Bendall, A., Fabian, C., Malcolm, A.A., Tilgner, K., Semprich, C.I., Wojdyla, K., Nisi, P.S., Kishore, K., Roamio Franklin, V.N., Mirshekar-Syahkal, B., D'Santos, C., Plath, K., Yusa, K., Rugg-Gunn, P.J., 2022. Genome-wide screening identifies Polycomb repressive complex 1.3 as an essential regulator of human naïve pluripotent cell reprogramming. Sci. Adv. 8, eabk0013. https://doi.org/10.1126/sciadv.abk0013

Comprehensive molecular characterization of human colon and rectal cancer, 2012. . Nature 487, 330–337. https://doi.org/10.1038/nature11252

Conner, S.D., Schmid, S.L., 2003. Regulated portals of entry into the cell. Nature 422, 37–44. https://doi.org/10.1038/nature01451

Conway, James R. W., Dinç, D.D., Follain, G., Paavolainen, O., Kaivola, J., Boström, P., Hartiala, P., Peuhu, E., Ivaska, J., 2023. IGFBP2 secretion by mammary adipocytes limits breast cancer invasion. Sci. Adv. 9, eadg1840. https://doi.org/10.1126/sciadv.adg1840

Conway, James R. W., Isomursu, A., Follain, G., Härmä, V., Jou-Ollé, E., Pasquier, N., Välimäki, E.P.O., Rantala, J.K., Ivaska, J., 2023. Defined extracellular matrix compositions support stiffness-insensitive cell spreading and adhesion signaling. Proc. Natl. Acad. Sci. 120, e2304288120. https://doi.org/10.1073/pnas.2304288120

Conway, J.R.W., Jacquemet, G., 2019. Cell matrix adhesion in cell migration. Essays Biochem. 63, 535–551. https://doi.org/10.1042/EBC20190012

Coucouvanis, E., Martin, G.R., 1995. Signals for death and survival: A two-step mechanism for cavitation in the vertebrate embryo. Cell 83, 279–287. https://doi.org/10.1016/0092-8674(95)90169-8

Coureuil, M., Mikaty, G., Miller, F., Lécuyer, H., Bernard, C., Bourdoulous, S., Duménil, G., Mège, R.-M., Weksler, B.B., Romero, I.A., Couraud, P.-O., Nassif, X., 2009. Meningococcal

Type IV Pili Recruit the Polarity Complex to Cross the Brain Endothelium. Science 325, 83–87. https://doi.org/10.1126/science.1173196

Cox, T.R., Bird, D., Baker, A.-M., Barker, H.E., Ho, M.W.-Y., Lang, G., Erler, J.T., 2013. LOX-Mediated Collagen Crosslinking Is Responsible for Fibrosis-Enhanced Metastasis. Cancer Res. 73, 1721–1732. https://doi.org/10.1158/0008-5472.CAN-12-2233

Date, S., Sato, T., 2015. Mini-Gut Organoids: Reconstitution of the Stem Cell Niche. Annu. Rev. Cell Dev. Biol. 31, 269–289. https://doi.org/10.1146/annurev-cellbio-100814-125218

de Boer, M., van Dijck, J.A.A.M., Bult, P., Borm, G.F., Tjan-Heijnen, V.C.G., 2010. Breast Cancer Prognosis and Occult Lymph Node Metastases, Isolated Tumor Cells, and Micrometastases. JNCI J. Natl. Cancer Inst. 102, 410–425. https://doi.org/10.1093/jnci/djq008

De Franceschi, N., Arjonen, A., Elkhatib, N., Denessiouk, K., Wrobel, A.G., Wilson, T.A., Pouwels, J., Montagnac, G., Owen, D.J., Ivaska, J., 2016. Selective integrin endocytosis is driven by interactions between the integrin α-chain and AP2. Nat. Struct. Mol. Biol. 23, 172–179. https://doi.org/10.1038/nsmb.3161

Dekker, E., Tanis, P.J., Vleugels, J.L.A., Kasi, P.M., Wallace, M.B., 2019. Colorectal cancer. The Lancet 394, 1467–1480. https://doi.org/10.1016/S0140-6736(19)32319-0

Desgrosellier, J.S., Barnes, L.A., Shields, D.J., Huang, M., Lau, S.K., Prévost, N., Tarin, D., Shattil, S.J., Cheresh, D.A., 2009. An integrin αvβ3–c-Src oncogenic unit promotes anchorage-independence and tumor progression. Nat. Med. 15, 1163–1169. https://doi.org/10.1038/nm.2009

Di Paolo, G., De Camilli, P., 2006. Phosphoinositides in cell regulation and membrane dynamics. Nature 443, 651–657. https://doi.org/10.1038/nature05185

Di Paolo, G., Pellegrini, L., Letinic, K., Cestra, G., Zoncu, R., Voronov, S., Chang, S., Guo, J., Wenk, M.R., De Camilli, P., 2002. Recruitment and regulation of phosphatidylinositol phosphate kinase type 1γ by the FERM domain of talin. Nature 420, 85–89. https://doi.org/10.1038/nature01147

Dieckmann, N.M.G., Frazer, G.L., Asano, Y., Stinchcombe, J.C., Griffiths, G.M., 2016. The cytotoxic T lymphocyte immune synapse at a glance. J. Cell Sci. 129, 2881–2886. https://doi.org/10.1242/jcs.186205

Diepenbruck, M., Christofori, G., 2016. Epithelial–mesenchymal transition (EMT) and metastasis: yes, no, maybe? Curr. Opin. Cell Biol., Differentiation and disease 43, 7–13. https://doi.org/10.1016/j.ceb.2016.06.002

Drain, A.P., Zahir, N., Northey, J.J., Zhang, H., Huang, P.-J., Maller, O., Lakins, J.N., Yu, X., Leight, J.L., Alston-Mills, B.P., Hwang, E.S., Chen, Y.-Y., Park, C.C., Weaver, V.M., 2021. Matrix compliance permits NF-κB activation to drive therapy resistance in breast cancer. J. Exp. Med. 218, e20191360. https://doi.org/10.1084/jem.20191360

D'Souza-Schorey, C., Chavrier, P., 2006. ARF proteins: roles in membrane traffic and beyond. Nat. Rev. Mol. Cell Biol. 7, 347–358. https://doi.org/10.1038/nrm1910

Ducibella, T., Ukena, T., Karnovsky, M., Anderson, E., 1977. Changes in cell surface and cortical cytoplasmic organization during early embryogenesis in the preimplantation mouse embryo. J. Cell Biol. 74, 153–167. https://doi.org/10.1083/jcb.74.1.153

Dumortier, J.G., Le Verge-Serandour, M., Tortorelli, A.F., Mielke, A., de Plater, L., Turlier, H., Maître, J.-L., 2019. Hydraulic fracturing and active coarsening position the lumen of the mouse blastocyst. Science 365, 465–468. https://doi.org/10.1126/science.aaw7709

Dumortier, J.G., Maître, J.-L., 2017. Early embryos kept in check. Nature 552, 178–179. https://doi.org/10.1038/d41586-017-07436-w

Ebnet, K. (Ed.), 2015. Cell Polarity 1: Biological Role and Basic Mechanisms. Springer International Publishing, Cham. https://doi.org/10.1007/978-3-319-14463-4

Eddy, R.J., Weidmann, M.D., Sharma, V.P., Condeelis, J.S., 2017. Tumor Cell Invadopodia: Invasive Protrusions that Orchestrate Metastasis. Trends Cell Biol. 27, 595–607. https://doi.org/10.1016/j.tcb.2017.03.003

Ehrlich, J.S., Hansen, M.D.H., Nelson, W.J., 2002. Spatio-Temporal Regulation of Rac1 Localization and Lamellipodia Dynamics during Epithelial Cell-Cell Adhesion. Dev. Cell 3, 259–270. https://doi.org/10.1016/S1534-5807(02)00216-2

Elbediwy, A., Zihni, C., Terry, S.J., Clark, P., Matter, K., Balda, M.S., 2012. Epithelial junction formation requires confinement of Cdc42 activity by a novel SH3BP1 complex. J. Cell Biol. 198, 677–693. https://doi.org/10.1083/jcb.201202094

Elosegui-Artola, A., Oria, R., Chen, Y., Kosmalska, A., Pérez-González, C., Castro, N., Zhu, C., Trepat, X., Roca-Cusachs, P., 2016. Mechanical regulation of a molecular clutch defines force transmission and transduction in response to matrix rigidity. Nat. Cell Biol. 18, 540–548. https://doi.org/10.1038/ncb3336

Emsley, J., Knight, C.G., Farndale, R.W., Barnes, M.J., Liddington, R.C., 2000. Structural Basis of Collagen Recognition by Integrin α2β1. Cell 101, 47–56. https://doi.org/10.1016/S0092-8674(00)80622-4

Etienne-Manneville, S., Hall, A., 2002. Rho GTPases in cell biology. Nature 420, 629–635. https://doi.org/10.1038/nature01148

Eva, R., Dassie, E., Caswell, P.T., Dick, G., ffrench-Constant, C., Norman, J.C., Fawcett, J.W., 2010. Rab11 and Its Effector Rab Coupling Protein Contribute to the Trafficking of β1 Integrins during Axon Growth in Adult Dorsal Root Ganglion Neurons and PC12 Cells. J. Neurosci. 30, 11654–11669. https://doi.org/10.1523/JNEUROSCI.2425-10.2010

Ezratty, E.J., Bertaux, C., Marcantonio, E.E., Gundersen, G.G., 2009. Clathrin mediates integrin endocytosis for focal adhesion disassembly in migrating cells. J. Cell Biol. 187, 733–747. https://doi.org/10.1083/jcb.200904054

Ezratty, E.J., Partridge, M.A., Gundersen, G.G., 2005. Microtubule-induced focal adhesion disassembly is mediated by dynamin and focal adhesion kinase. Nat. Cell Biol. 7, 581–590. https://doi.org/10.1038/ncb1262

Fabbri, M., Di Meglio, S., Gagliani, M.C., Consonni, E., Molteni, R., Bender, J.R., Tacchetti, C., Pardi, R., 2005. Dynamic Partitioning into Lipid Rafts Controls the Endo-Exocytic

Cycle of the αL/β2 Integrin, LFA-1, during Leukocyte Chemotaxis. Mol. Biol. Cell 16, 5793–5803. https://doi.org/10.1091/mbc.e05-05-0413

Fang, Z., Takizawa, N., Wilson, K.A., Smith, T.C., Delprato, A., Davidson, M.W., Lambright, D.G., Luna, E.J., 2010. The Membrane-Associated Protein, Supervillin, Accelerates F-Actin-Dependent Rapid Integrin Recycling and Cell Motility. Traffic 11, 782–799. https://doi.org/10.1111/j.1600-0854.2010.01062.x

Fehon, R.G., McClatchey, A.I., Bretscher, A., 2010. Organizing the cell cortex: the role of ERM proteins. Nat. Rev. Mol. Cell Biol. 11, 276–287. https://doi.org/10.1038/nrm2866

Fernandez-Garcia, B., Eiró, N., Marín, L., González-Reyes, S., González, L.O., Lamelas, M.L., Vizoso, F.J., 2014. Expression and prognostic significance of fibronectin and matrix metalloproteases in breast cancer metastasis. Histopathology 64, 512–522. https://doi.org/10.1111/his.12300

Fessler, E., Medema, J.P., 2016. Colorectal Cancer Subtypes: Developmental Origin and Microenvironmental Regulation. Trends Cancer 2, 505–518. https://doi.org/10.1016/j.trecan.2016.07.008

Flier, L.G. van der, Clevers, H., 2009. Stem Cells, Self-Renewal, and Differentiation in the Intestinal Epithelium. Annu. Rev. Physiol. 71, 241–260. https://doi.org/10.1146/annurev.physiol.010908.163145

Fortin, S., Le Mercier, M., Camby, I., Spiegl-Kreinecker, S., Berger, W., Lefranc, F., Kiss, R., 2010. Galectin-1 Is Implicated in the Protein Kinase C ε/Vimentin-Controlled Trafficking of Integrin-β1 in Glioblastoma Cells. Brain Pathol. 20, 39–49. https://doi.org/10.1111/j.1750-3639.2008.00227.x

Friedland, J.C., Lee, M.H., Boettiger, D., 2009. Mechanically Activated Integrin Switch Controls α5β1 Function. Science 323, 642–644. https://doi.org/10.1126/science.1168441

Fu, R., Zhang, Y.-W., Li, H.-M., Lv, W.-C., Zhao, L., Guo, Q.-L., Lu, T., Weiss, S.J., Li, Z.-Y., Wu, Z.-Q., 2018. LW106, a novel indoleamine 2,3-dioxygenase 1 inhibitor, suppresses tumour progression by limiting stroma-immune crosstalk and cancer stem cell enrichment in tumour micro-environment. Br. J. Pharmacol. 175, 3034–3049. https://doi.org/10.1111/bph.14351

Fukuyama, T., Ogita, H., Kawakatsu, T., Inagaki, M., Takai, Y., 2006. Activation of Rac by cadherin through the c-Src–Rap1–phosphatidylinositol 3-kinase–Vav2 pathway. Oncogene 25, 8–19. https://doi.org/10.1038/sj.onc.1209010

Furtak, V., Hatcher, F., Ochieng, J., 2001. Galectin-3 Mediates the Endocytosis of β-1 Integrins by Breast Carcinoma Cells. Biochem. Biophys. Res. Commun. 289, 845–850. https://doi.org/10.1006/bbrc.2001.6064

Gahmberg, C.G., Fagerholm, S.C., Nurmi, S.M., Chavakis, T., Marchesan, S., Grönholm, M., 2009. Regulation of integrin activity and signalling. Biochim. Biophys. Acta BBA - Gen. Subj. 1790, 431–444. https://doi.org/10.1016/j.bbagen.2009.03.007

Gan, Y., McGraw, T.E., Rodriguez-Boulan, E., 2002. The epithelial-specific adaptor AP1B mediates post-endocytic recycling to the basolateral membrane. Nat. Cell Biol. 4, 605–609. https://doi.org/10.1038/ncb827

Gao, J., Bao, Y., Ge, S., Sun, P., Sun, J., Liu, J., Chen, F., Han, L., Cao, Z., Qin, J., White, G.C., Xu, Z., Ma, Y.-Q., 2019. Sharpin suppresses β1-integrin activation by complexing with the β1 tail and kindlin-1. Cell Commun. Signal. CCS 17, 101. https://doi.org/10.1186/s12964-019-0407-6

Gassama-Diagne, A., Yu, W., ter Beest, M., Martin-Belmonte, F., Kierbel, A., Engel, J., Mostov, K., 2006. Phosphatidylinositol-3,4,5-trisphosphate regulates the formation of the basolateral plasma membrane in epithelial cells. Nat. Cell Biol. 8, 963–970. https://doi.org/10.1038/ncb1461

Georgiadou, M., Lilja, J., Jacquemet, G., Guzmán, C., Rafaeva, M., Alibert, C., Yan, Y., Sahgal, P., Lerche, M., Manneville, J.-B., Mäkelä, T.P., Ivaska, J., 2017. AMPK negatively regulates tensin-dependent integrin activity. J. Cell Biol. 216, 1107–1121. https://doi.org/10.1083/jcb.201609066

Gerke, V., Creutz, C.E., Moss, S.E., 2005. Annexins: linking Ca2+ signalling to membrane dynamics. Nat. Rev. Mol. Cell Biol. 6, 449–461. https://doi.org/10.1038/nrm1661

Gerri, C., Menchero, S., Mahadevaiah, S.K., Turner, J.M.A., Niakan, K.K., 2020. Human Embryogenesis: A Comparative Perspective. Annu. Rev. Cell Dev. Biol. 36, 411–440. https://doi.org/10.1146/annurev-cellbio-022020-024900

Gingras, A.R., Ziegler, W.H., Bobkov, A.A., Joyce, M.G., Fasci, D., Himmel, M., Rothemund, S., Ritter, A., Grossmann, J.G., Patel, B., Bate, N., Goult, B.T., Emsley, J., Barsukov, I.L., Roberts, G.C.K., Liddington, R.C., Ginsberg, M.H., Critchley, D.R., 2009. Structural Determinants of Integrin Binding to the Talin Rod *. J. Biol. Chem. 284, 8866–8876. https://doi.org/10.1074/jbc.M805937200

Gomez, G.A., McLachlan, R.W., Yap, A.S., 2011. Productive tension: force-sensing and homeostasis of cell–cell junctions. Trends Cell Biol. 21, 499–505. https://doi.org/10.1016/j.tcb.2011.05.006

Gribble, F.M., Reimann, F., 2016. Enteroendocrine Cells: Chemosensors in the Intestinal Epithelium. Annu. Rev. Physiol. 78, 277–299. https://doi.org/10.1146/annurev-physiol-021115-105439

Grillet, F., Bayet, E., Villeronce, O., Zappia, L., Lagerqvist, E.L., Lunke, S., Charafe-Jauffret, E., Pham, K., Molck, C., Rolland, N., Bourgaux, J.F., Prudhomme, M., Philippe, C., Bravo, S., Boyer, J.C., Canterel-Thouennon, L., Taylor, G.R., Hsu, A., Pascussi, J.M., Hollande, F., Pannequin, J., 2017. Circulating tumour cells from patients with colorectal cancer have cancer stem cell hallmarks in ex vivo culture. Gut 66, 1802–1810. https://doi.org/10.1136/gutjnl-2016-311447

Guo, X., Fan, Y., Lang, R., Gu, F., Chen, L., Cui, L., Pringle, G.A., Zhang, X., Fu, L., 2008. Tumor infiltrating lymphocytes differ in invasive micropapillary carcinoma and medullary carcinoma of breast. Mod. Pathol. 21, 1101–1107. https://doi.org/10.1038/modpathol.2008.72

Guzmán, C., Bagga, M., Kaur, A., Westermarck, J., Abankwa, D., 2014. ColonyArea: An ImageJ Plugin to Automatically Quantify Colony Formation in Clonogenic Assays. PLOS ONE 9, e92444. https://doi.org/10.1371/journal.pone.0092444

Hamidi, H., Ivaska, J., 2018. Every step of the way: integrins in cancer progression and metastasis. Nat. Rev. Cancer 18, 533–548. https://doi.org/10.1038/s41568-018-0038-z

Han, S.J., Azarova, E.V., Whitewood, A.J., Bachir, A., Guttierrez, E., Groisman, A., Horwitz, A.R., Goult, B.T., Dean, K.M., Danuser, G., 2021. Pre-complexation of talin and vinculin without tension is required for efficient nascent adhesion maturation. eLife 10, e66151. https://doi.org/10.7554/eLife.66151

Han, S.J., Oak, Y., Groisman, A., Danuser, G., 2015. Traction microscopy to identify force modulation in subresolution adhesions. Nat. Methods 12, 653–656. https://doi.org/10.1038/nmeth.3430

Hang, Q., Isaji, T., Hou, S., Wang, Y., Fukuda, T., Gu, J., 2017. A Key Regulator of Cell Adhesion: Identification and Characterization of Important N-Glycosylation Sites on Integrin α5 for Cell Migration. Mol. Cell. Biol. 37, e00558-16. https://doi.org/10.1128/MCB.00558-16

Harburger, D.S., Bouaouina, M., Calderwood, D.A., 2009. Kindlin-1 and -2 Directly Bind the C-terminal Region of β Integrin Cytoplasmic Tails and Exert Integrin-specific Activation Effects*. J. Biol. Chem. 284, 11485–11497. https://doi.org/10.1074/jbc.M809233200

Hassani, S.-N., Moradi, S., Taleahmad, S., Braun, T., Baharvand, H., 2019. Transition of inner cell mass to embryonic stem cells: mechanisms, facts, and hypotheses. Cell. Mol. Life Sci. 76, 873–892. https://doi.org/10.1007/s00018-018-2965-y

Hershberg, R.M., Cho, D.H., Youakim, A., Bradley, M.B., Lee, J.S., Framson, P.E., Nepom, G.T., 1998. Highly polarized HLA class II antigen processing and presentation by human intestinal epithelial cells. J. Clin. Invest. 102, 792–803. https://doi.org/10.1172/JCI3201

Himmel, M., Ritter, A., Rothemund, S., Pauling, B.V., Rottner, K., Gingras, A.R., Ziegler, W.H., 2009. Control of High Affinity Interactions in the Talin C Terminus: HOW TALIN DOMAINS COORDINATE PROTEIN DYNAMICS IN CELL ADHESIONS*. J. Biol. Chem. 284, 13832–13842. https://doi.org/10.1074/jbc.M900266200

Hirakawa, T., Goto, M., Takahashi, K., Iwasawa, T., Fujishima, A., Makino, K., Shirasawa, H., Sato, W., Sato, T., Kumazawa, Y., Terada, Y., 2022. Na+/K+ ATPase α1 and β3 subunits are localized to the basolateral membrane of trophectoderm cells in human blastocysts. Hum. Reprod. 37, 1423–1430. https://doi.org/10.1093/humrep/deac124

Hirate, Y., Hirahara, S., Inoue, K., Suzuki, A., Alarcon, V.B., Akimoto, K., Hirai, T., Hara, T., Adachi, M., Chida, K., Ohno, S., Marikawa, Y., Nakao, K., Shimono, A., Sasaki, H., 2013. Polarity-Dependent Distribution of Angiomotin Localizes Hippo Signaling in Preimplantation Embryos. Curr. Biol. 23, 1181–1194. https://doi.org/10.1016/j.cub.2013.05.014

Höfer, D., Püschel, B., Drenckhahn, D., 1996. Taste receptor-like cells in the rat gut identified by expression of alpha-gustducin. Proc. Natl. Acad. Sci. 93, 6631–6634. https://doi.org/10.1073/pnas.93.13.6631

Hordijk, P.L., ten Klooster, J.P., van der Kammen, R.A., Michiels, F., Oomen, L.C.J.M., Collard, J.G., 1997. Inhibition of Invasion of Epithelial Cells by Tiam1-Rac Signaling. Science 278, 1464–1466. https://doi.org/10.1126/science.278.5342.1464

Horton, E.R., Byron, A., Askari, J.A., Ng, D.H.J., Millon-Frémillon, A., Robertson, J.,

Koper, E.J., Paul, N.R., Warwood, S., Knight, D., Humphries, J.D., Humphries, M.J., 2015. Definition of a consensus integrin adhesome and its dynamics during adhesion complex assembly and disassembly. Nat. Cell Biol. 17, 1577–1587. https://doi.org/10.1038/ncb3257

Horton, E.R., Humphries, J.D., James, J., Jones, M.C., Askari, J.A., Humphries, M.J., 2016. The integrin adhesome network at a glance. J. Cell Sci. jcs.192054. https://doi.org/10.1242/jcs.192054

Hugen, N., Brown, G., Glynne-Jones, R., de Wilt, J.H.W., Nagtegaal, I.D., 2016. Advances in the care of patients with mucinous colorectal cancer. Nat. Rev. Clin. Oncol. 13, 361–369. https://doi.org/10.1038/nrclinonc.2015.140

Hugen, N., Verhoeven, R.H., Lemmens, V.E., van Aart, C.J., Elferink, M.A., Radema, S.A., Nagtegaal, I.D., de Wilt, J.H., 2015. Colorectal signet-ring cell carcinoma: benefit from adjuvant chemotherapy but a poor prognostic factor. Int. J. Cancer 136, 333–339. https://doi.org/10.1002/ijc.28981

Humphries, J.D., Byron, A., Bass, M.D., Craig, S.E., Pinney, J.W., Knight, D., Humphries, M.J., 2009. Proteomic Analysis of Integrin-Associated Complexes Identifies RCC2 as a Dual Regulator of Rac1 and Arf6. Sci. Signal. 2. https://doi.org/10.1126/scisignal.2000396

Humphries, J.D., Byron, A., Humphries, M.J., 2006. Integrin ligands at a glance. J. Cell Sci. 119, 3901–3903. https://doi.org/10.1242/jcs.03098

Humphries, J.D., Chastney, M.R., Askari, J.A., Humphries, M.J., 2019. Signal transduction via integrin adhesion complexes. Curr. Opin. Cell Biol., Cell Architecture 56, 14–21. https://doi.org/10.1016/j.ceb.2018.08.004

Humphries, M., 2000. *Integrin Structure. Biochem. Soc. Trans. 28, 311–39. https://doi.org/10.1042/0300-5127:0280311

Hurd, T.W., Gao, L., Roh, M.H., Macara, I.G., Margolis, B., 2003. Direct interaction of two polarity complexes implicated in epithelial tight junction assembly. Nat. Cell Biol. 5, 137–142. https://doi.org/10.1038/ncb923

Hynes, R.O., 2002. Integrins: Bidirectional, Allosteric Signaling Machines. Cell 110, 673–687. https://doi.org/10.1016/S0092-8674(02)00971-6

Hynes, R.O., 1987. Integrins: A family of cell surface receptors. Cell 48, 549–554. https://doi.org/10.1016/0092-8674(87)90233-9

Idelevich, A., Vilella, F., 2020. Mother and Embryo Cross-Communication. Genes 11, 376. https://doi.org/10.3390/genes11040376

Isaji, T., Gu, J., Nishiuchi, R., Zhao, Y., Takahashi, M., Miyoshi, E., Honke, K., Sekiguchi, K., Taniguchi, N., 2004. Introduction of Bisecting GlcNAc into Integrin α5β1 Reduces Ligand Binding and Down-regulates Cell Adhesion and Cell Migration *. J. Biol. Chem. 279, 19747–19754. https://doi.org/10.1074/jbc.M311627200

Isaji, T., Sato, Y., Fukuda, T., Gu, J., 2009. N-Glycosylation of the I-like Domain of β1 Integrin Is Essential for β1 Integrin Expression and Biological Function. J. Biol. Chem. 284, 12207–12216. https://doi.org/10.1074/jbc.M807920200

Ishihara, A., Yoshida, T., Tamaki, H., Sakakura, T., 1995. Tenascin expression in cancer cells and stroma of human breast cancer and its prognostic significance. Clin. Cancer Res. 1, 1035–1041.

Islami, F., Goding Sauer, A., Miller, K.D., Siegel, R.L., Fedewa, S.A., Jacobs, E.J., McCullough, M.L., Patel, A.V., Ma, J., Soerjomataram, I., Flanders, W.D., Brawley, O.W., Gapstur, S.M., Jemal, A., 2018. Proportion and number of cancer cases and deaths attributable to potentially modifiable risk factors in the United States. CA. Cancer J. Clin. 68, 31–54. https://doi.org/10.3322/caac.21440

Isomursu, A., Park, K.-Y., Hou, J., Cheng, B., Mathieu, M., Shamsan, G., Fuller, B., Kasim, J., Mohsen Mahmoodi, M., Lu, T.J., Genin, G.M., Xu, F., Lin, M., Distefano, M., Ivaska, J., Odde, D.J., 2022. Negative durotaxis: cell movement toward softer environments. Nat. Mater. 21, 1081–1090. https://doi.org/10.1038/s41563-022-01294-2

Itoh, M., Sasaki, H., Furuse, M., Ozaki, H., Kita, T., Tsukita, S., 2001. Junctional adhesion molecule (JAM) binds to PAR-3 : a possible mechanism for the recruitment of PAR-3 to tight junctions. J. Cell Biol. 154, 491–498. https://doi.org/10.1083/jcb.200103047

Izumi, G., Sakisaka, T., Baba, T., Tanaka, S., Morimoto, K., Takai, Y., 2004. Endocytosis of E-cadherin regulated by Rac and Cdc42 small G proteins through IQGAP1 and actin filaments. J. Cell Biol. 166, 237–248. https://doi.org/10.1083/jcb.200401078

Jacquemet, G., Morgan, M.R., Byron, A., Humphries, J.D., Choi, C.K., Chen, C.S., Caswell, P.T., Humphries, M.J., 2013. Rac1 is deactivated at integrin activation sites via an IQGAP1/filamin-A/RacGAP1 pathway. J. Cell Sci. jcs.121988. https://doi.org/10.1242/jcs.121988

Jacquemet, G., Stubb, A., Saup, R., Miihkinen, M., Kremneva, E., Hamidi, H., Ivaska, J., 2019. Filopodome Mapping Identifies p130Cas as a Mechanosensitive Regulator of Filopodia Stability. Curr. Biol. 29, 202-216.e7. https://doi.org/10.1016/j.cub.2018.11.053

Jaffe, A.B., Kaji, N., Durgan, J., Hall, A., 2008. Cdc42 controls spindle orientation to position the apical surface during epithelial morphogenesis. J. Cell Biol. 183, 625–633. https://doi.org/10.1083/jcb.200807121

Janik, M.E., Lityńska, A., Vereecken, P., 2010. Cell migration—The role of integrin glycosylation. Biochim. Biophys. Acta BBA - Gen. Subj. 1800, 545–555. https://doi.org/10.1016/j.bbagen.2010.03.013

Jäntti, N.Z., Moreno-Layseca, P., Chastney, M.R., Dibus, M., Conway, J.R.W., Leppänen, V.-M., Hamidi, H., Eylmann, K., Oliveira-Ferrer, L., Veltel, S., Ivaska, J., 2024. EPLINα controls integrin recycling from Rab21 endosomes to drive breast cancer cell migration. https://doi.org/10.1101/2024.06.27.600789

Jarray, R., Allain, B., Borriello, L., Biard, D., Loukaci, A., Larghero, J., Hadj-Slimane, R., Garbay, C., Lepelletier, Y., Raynaud, F., 2011. Depletion of the novel protein PHACTR-1 from human endothelial cells abolishes tube formation and induces cell death receptor apoptosis. Biochimie 93, 1668–1675. https://doi.org/10.1016/j.biochi.2011.07.010

Jensen, J., Pedersen, E.E., Galante, P., Hald, J., Heller, R.S., Ishibashi, M., Kageyama, R., Guillemot, F., Serup, P., Madsen, O.D., 2000. Control of endodermal endocrine development

by Hes-1. Nat. Genet. 24, 36–44. https://doi.org/10.1038/71657

Jin, H., Tang, Y., Yang, L., Peng, X., Li, B., Fan, Q., Wei, S., Yang, S., Li, X., Wu, B., Huang, M., Tang, S., Liu, J., Li, H., 2021. Rab GTPases: Central Coordinators of Membrane Trafficking in Cancer. Front. Cell Dev. Biol. 9. https://doi.org/10.3389/fcell.2021.648384

Joberty, G., Petersen, C., Gao, L., Macara, I.G., 2000. The cell-polarity protein Par6 links Par3 and atypical protein kinase C to Cdc42. Nat. Cell Biol. 2, 531–539. https://doi.org/10.1038/35019573

Jones, J.C.R., Kam, C.Y., Harmon, R.M., Woychek, A.V., Hopkinson, S.B., Green, K.J., 2017. Intermediate Filaments and the Plasma Membrane. Cold Spring Harb. Perspect. Biol. 9, a025866. https://doi.org/10.1101/cshperspect.a025866

Jones, M.C., Caswell, P.T., Norman, J.C., 2006. Endocytic recycling pathways: emerging regulators of cell migration. Curr. Opin. Cell Biol., Cell-to-cell contact and extracellular matrix 18, 549–557. https://doi.org/10.1016/j.ceb.2006.08.003

Julien, S., Merino-Trigo, A., Lacroix, L., Pocard, M., Goéré, D., Mariani, P., Landron, S., Bigot, L., Nemati, F., Dartigues, P., Weiswald, L.-B., Lantuas, D., Morgand, L., Pham, E., Gonin, P., Dangles-Marie, V., Job, B., Dessen, P., Bruno, A., Pierré, A., De Thé, H., Soliman, H., Nunes, M., Lardier, G., Calvet, L., Demers, B., Prévost, G., Vrignaud, P., Roman-Roman, S., Duchamp, O., Berthet, C., 2012. Characterization of a Large Panel of Patient-Derived Tumor Xenografts Representing the Clinical Heterogeneity of Human Colorectal Cancer. Clin. Cancer Res. 18, 5314–5328. https://doi.org/10.1158/1078-0432.CCR-12-0372

Kanchanawong, P., Shtengel, G., Pasapera, A.M., Ramko, E.B., Davidson, M.W., Hess, H.F., Waterman, C.M., 2010. Nanoscale architecture of integrin-based cell adhesions. Nature 468, 580–584. https://doi.org/10.1038/nature09621

Karaköse, E., Schiller, H.B., Fässler, R., 2010. The kindlins at a glance. J. Cell Sci. 123, 2353–2356. https://doi.org/10.1242/jcs.064600

Katara, G.K., Kulshrestha, A., Mao, L., Wang, X., Sahoo, M., Ibrahim, S., Pamarthy, S., Suzue, K., Shekhawat, G.S., Gilman-Sachs, A., Beaman, K.D., 2018. Mammary epithelium-specific inactivation of V-ATPase reduces stiffness of extracellular matrix and enhances metastasis of breast cancer. Mol. Oncol. 12, 208–223. https://doi.org/10.1002/1878-0261.12159

Kechagia, J.Z., Ivaska, J., Roca-Cusachs, P., 2019. Integrins as biomechanical sensors of the microenvironment. Nat. Rev. Mol. Cell Biol. 20, 457–473. https://doi.org/10.1038/s41580-019-0134-2

Kemphues, K.J., Priess, J.R., Morton, D.G., Cheng, N., 1988. Identification of genes required for cytoplasmic localization in early C. elegans embryos. Cell 52, 311–320. https://doi.org/10.1016/S0092-8674(88)80024-2

Kierbel, A., Gassama-Diagne, A., Rocha, C., Radoshevich, L., Olson, J., Mostov, K., Engel, J., 2007. Pseudomonas aeruginosa exploits a PIP3-dependent pathway to transform apical into basolateral membrane. J. Cell Biol. 177, 21–27. https://doi.org/10.1083/jcb.200605142

Klinger, S.C., Glerup, S., Raarup, M.K., Mari, M.C., Nyegaard, M., Koster, G., Prabakaran, T., Nilsson, S.K., Kjaergaard, M.M., Bakke, O., Nykjær, A., Olivecrona, G.,

Petersen, C.M., Nielsen, M.S., 2011. SorLA regulates the activity of lipoprotein lipase by intracellular trafficking. J. Cell Sci. 124, 1095–1105. https://doi.org/10.1242/jcs.072538

Krasna, M.J., Flancbaum, L., Cody, R.P., Shneibaum, S., Ari, G.B., 1988. Vascular and neural invasion in colorectal carcinoma. Incidence and prognostic significance. Cancer 61, 1018–1023. https://doi.org/10.1002/1097-0142(19880301)61:5<1018::AID-CNCR2820610527>3.0.CO;2-H

Kumari, R., Ven, K., Chastney, M., Kokate, S.B., Peränen, J., Aaron, J., Kogan, K., Almeida-Souza, L., Kremneva, E., Poincloux, R., Chew, T.-L., Gunning, P.W., Ivaska, J., Lappalainen, P., 2024. Focal adhesions contain three specialized actin nanoscale layers. Nat. Commun. 15, 2547. https://doi.org/10.1038/s41467-024-46868-7

Kuroda, H., Sakamoto, G., Ohnisi, K., Itoyama, S., 2004. Clinical and pathologic features of invasive micropapillary carcinoma. Breast Cancer 11, 169–174. https://doi.org/10.1007/BF02968297

Labernadie, A., Kato, T., Brugués, A., Serra-Picamal, X., Derzsi, S., Arwert, E., Weston, A., González-Tarragó, V., Elosegui-Artola, A., Albertazzi, L., Alcaraz, J., Roca-Cusachs, P., Sahai, E., Trepat, X., 2017. A mechanically active heterotypic E-cadherin/N-cadherin adhesion enables fibroblasts to drive cancer cell invasion. Nat. Cell Biol. 19, 224–237. https://doi.org/10.1038/ncb3478

Laiho, P., Kokko, A., Vanharanta, S., Salovaara, R., Sammalkorpi, H., Järvinen, H., Mecklin, J.-P., Karttunen, T.J., Tuppurainen, K., Davalos, V., Schwartz, S., Arango, D., Mäkinen, M.J., Aaltonen, L.A., 2007. Serrated carcinomas form a subclass of colorectal cancer with distinct molecular basis. Oncogene 26, 312–320. https://doi.org/10.1038/sj.onc.1209778

Lakshminarayan, R., Wunder, C., Becken, U., Howes, M.T., Benzing, C., Arumugam, S., Sales, S., Ariotti, N., Chambon, V., Lamaze, C., Loew, D., Shevchenko, A., Gaus, K., Parton, R.G., Johannes, L., 2014. Galectin-3 drives glycosphingolipid-dependent biogenesis of clathrin-independent carriers. Nat. Cell Biol. 16, 592–603. https://doi.org/10.1038/ncb2970

Laprise, P., Viel, A., Rivard, N., 2004. Human Homolog of Disc-large Is Required for Adherens Junction Assembly and Differentiation of Human Intestinal Epithelial Cells *. J. Biol. Chem. 279, 10157–10166. https://doi.org/10.1074/jbc.M309843200

Larocque, G., Royle, S.J., 2022. Integrating intracellular nanovesicles into integrin trafficking pathways and beyond. Cell. Mol. Life Sci. 79, 335. https://doi.org/10.1007/s00018-022-04371-6

Latorre, R., Sternini, C., De Giorgio, R., Greenwood-Van Meerveld, B., 2016. Enteroendocrine cells: a review of their role in brain–gut communication. Neurogastroenterol. Motil. 28, 620–630. https://doi.org/10.1111/nmo.12754

Law, D.A., DeGuzman, F.R., Heiser, P., Ministri-Madrid, K., Killeen, N., Phillips, D.R., 1999. Integrin cytoplasmic tyrosine motif is required for outside-in ⎵IIb␣3 signalling and platelet function 401.

Lawson et al., 2014. The on-off relationship of Rho and Rac during integrin-mediated adhesion and cell migration [WWW Document]. https://doi.org/10.4161/sgtp.27958

Lee, J.-O., Bankston, L.A., Robert C Liddington, M.A.A.A., 1995. Two conformations of the integrin A-domain (I-domain): a pathway for activation? Structure 3, 1333–1340. https://doi.org/10.1016/S0969-2126(01)00271-4

Lee, M., Vasioukhin, V., 2008. Cell polarity and cancer – cell and tissue polarity as a non-canonical tumor suppressor. J. Cell Sci. 121, 1141–1150. https://doi.org/10.1242/jcs.016634

Lehtonen, E., Badley, R.A., 1980. Localization of cytoskeletal proteins in preimplantation mouse embryos. Development 55, 211–225. https://doi.org/10.1242/dev.55.1.211

Lemmers, C., Michel, D., Lane-Guermonprez, L., Delgrossi, M.-H., Médina, E., Arsanto, J.-P., Le Bivic, A., 2004. CRB3 Binds Directly to Par6 and Regulates the Morphogenesis of the Tight Junctions in Mammalian Epithelial Cells. Mol. Biol. Cell 15, 1324–1333. https://doi.org/10.1091/mbc.e03-04-0235

Lemoine, L., Sugarbaker, P., Van der Speeten, K., 2016. Pathophysiology of colorectal peritoneal carcinomatosis: Role of the peritoneum. World J. Gastroenterol. 22, 7692–7707. https://doi.org/10.3748/wjg.v22.i34.7692

Lerche, M., Elosegui-Artola, A., Kechagia, J.Z., Guzmán, C., Georgiadou, M., Andreu, I., Gullberg, D., Roca-Cusachs, P., Peuhu, E., Ivaska, J., 2020. Integrin Binding Dynamics Modulate Ligand-Specific Mechanosensing in Mammary Gland Fibroblasts. iScience 23. https://doi.org/10.1016/j.isci.2020.100907

Li, C., Zheng, H., Jia, H., Huang, D., Gu, W., Cai, S., Zhu, J., 2019. Prognosis of three histological subtypes of colorectal adenocarcinoma: A retrospective analysis of 8005 Chinese patients. Cancer Med. 8, 3411–3419. https://doi.org/10.1002/cam4.2234

Li, H., Findlay, I.A., Sheppard, D.N., 2004. The relationship between cell proliferation, Cl− secretion, and renal cyst growth: A study using CFTR inhibitors. Kidney Int. 66, 1926–1938. https://doi.org/10.1111/j.1523-1755.2004.00967.x

Li, J., Jo, M.H., Yan, J., Hall, T., Lee, J., López-Sánchez, U., Yan, S., Ha, T., Springer, T.A., 2024. Ligand binding initiates single-molecule integrin conformational activation. Cell 0. https://doi.org/10.1016/j.cell.2024.04.049

Li, S.R., Gulieva, R.E., Helms, L., Cruz, N.M., Vincent, T., Fu, H., Himmelfarb, J., Freedman, B.S., 2022. Glucose absorption drives cystogenesis in a human organoid-on-chip model of polycystic kidney disease. Nat. Commun. 13, 7918. https://doi.org/10.1038/s41467-022-35537-2

Liao, H.-Y., Da, C.-M., Liao, B., Zhang, H.-H., 2021. Roles of matrix metalloproteinase-7 (MMP-7) in cancer. Clin. Biochem. 92, 9–18. https://doi.org/10.1016/j.clinbiochem.2021.03.003

Libanje, F., Raingeaud, J., Luan, R., Thomas, Z., Zajac, O., Veiga, J., Marisa, L., Adam, J., Boige, V., Malka, D., Goéré, D., Hall, A., Soazec, J.-Y., Prall, F., Gelli, M., Dartigues, P., Jaulin, F., 2019. ROCK2 inhibition triggers the collective invasion of colorectal adenocarcinomas. EMBO J. 38, e99299. https://doi.org/10.15252/embj.201899299

Liebig, C., Ayala, G., Wilks, J., Verstovsek, G., Liu, H., Agarwal, N., Berger, D.H., Albo,

D., 2009. Perineural Invasion Is an Independent Predictor of Outcome in Colorectal Cancer. J. Clin. Oncol. 27, 5131–5137. https://doi.org/10.1200/JCO.2009.22.4949

Lin, D., Edwards, A.S., Fawcett, J.P., Mbamalu, G., Scott, J.D., Pawson, T., 2000. A mammalian PAR-3–PAR-6 complex implicated in Cdc42/Rac1 and aPKC signalling and cell polarity. Nat. Cell Biol. 2, 540–547. https://doi.org/10.1038/35019582

Liu, J., Wang, Y., Goh, W.I., Goh, H., Baird, M.A., Ruehland, S., Teo, S., Bate, N., Critchley, D.R., Davidson, M.W., Kanchanawong, P., 2015. Talin determines the nanoscale architecture of focal adhesions. Proc. Natl. Acad. Sci. 112. https://doi.org/10.1073/pnas.1512025112

Liu, X., Ouyang, J.F., Rossello, F.J., Tan, J.P., Davidson, K.C., Valdes, D.S., Schröder, J., Sun, Y.B.Y., Chen, J., Knaupp, A.S., Sun, G., Chy, H.S., Huang, Z., Pflueger, J., Firas, J., Tano, V., Buckberry, S., Paynter, J.M., Larcombe, M.R., Poppe, D., Choo, X.Y., O'Brien, C.M., Pastor, W.A., Chen, D., Leichter, A.L., Naeem, H., Tripathi, P., Das, P.P., Grubman, A., Powell, D.R., Laslett, A.L., David, L., Nilsson, S.K., Clark, A.T., Lister, R., Nefzger, C.M., Martelotto, L.G., Rackham, O.J.L., Polo, J.M., 2020. Reprogramming roadmap reveals route to human induced trophoblast stem cells. Nature 586, 101–107. https://doi.org/10.1038/s41586-020-2734-6

Lopez, J.-B.R., 2022. Mécanismes moléculaires et cellulaires de la formation des TSIP : médiateurs de la dissémination des cancers colorectaux (phdthesis). Université Paris-Saclay.

Luciano, L., Reale, E., 1990. Brush cells of the mouse gallbladder. Cell Tissue Res. 262, 339–349. https://doi.org/10.1007/BF00309889

Luna-Moré, S., Gonzalez, B., Acedo, C., Rodrigo, I., Luna, C., 1994. Invasive micropapillary carcinoma of the breast*. Pathol. - Res. Pract. 190, 668–674. https://doi.org/10.1016/S0344-0338(11)80745-4

Lynch, H.T., Lynch, J.F., Lynch, P.M., Attard, T., 2008. Hereditary colorectal cancer syndromes: molecular genetics, genetic counseling, diagnosis and management. Fam. Cancer 7, 27–39. https://doi.org/10.1007/s10689-007-9165-5

Macara, I.G., McCaffrey, L., 2013. Cell polarity in morphogenesis and metastasis. Philos. Trans. R. Soc. B Biol. Sci. 368, 20130012. https://doi.org/10.1098/rstb.2013.0012

Macedo, J.K.A., Fox, J.W., Castro, M. de S., n.d. Disintegrins from Snake Venoms and their Applications in Cancer Research and Therapy. Curr. Protein Pept. Sci. 16, 532–548. https://doi.org/10.2174/1389203716666150515125002

Machesky, L.M., 2019. Rab11FIP proteins link endocytic recycling vesicles for cytoskeletal transport and tethering. Biosci. Rep. 39, BSR20182219. https://doi.org/10.1042/BSR20182219

Mack, N.A., Georgiou, M., 2014. The interdependence of the Rho GTPases and apicobasal cell polarity. Small GTPases 5, e973768. https://doi.org/10.4161/21541248.2014.973768

Maître, J.-L., 2017. Mechanics of blastocyst morphogenesis. Biol. Cell 109, 323–338. https://doi.org/10.1111/boc.201700029

Maître, J.-L., Turlier, H., Illukkumbura, R., Eismann, B., Niwayama, R., Nédélec, F.,

Hiiragi, T., 2016. Asymmetric division of contractile domains couples cell positioning and fate specification. Nature 536, 344–348.

Malliri, A., Es, S. van, Huveneers, S., Collard, J.G., 2004. The Rac Exchange Factor Tiam1 Is Required for the Establishment and Maintenance of Cadherin-based Adhesions *. J. Biol. Chem. 279, 30092–30098. https://doi.org/10.1074/jbc.M401192200

Mao, J.-R., Bristow, J., 2001. The Ehlers-Danlos syndrome: on beyond collagens. J. Clin. Invest. 107, 1063–1069. https://doi.org/10.1172/JCI12881

Maqbool, A., 2013. Colon: Structure, Function, and Disorders, in: Encyclopedia of Human Nutrition. Elsevier, pp. 378–396. https://doi.org/10.1016/B978-0-12-375083-9.00059-3

Margadant, C., Monsuur, H.N., Norman, J.C., Sonnenberg, A., 2011. Mechanisms of integrin activation and trafficking. Curr. Opin. Cell Biol. 23, 607–614. https://doi.org/10.1016/j.ceb.2011.08.005

Martel, V., Vignoud, L., Dupé, S., Frachet, P., Block, M.R., Albigès-Rizo, C., 2000. Talin controls the exit of the integrin α5β1 from an early compartment of the secretory pathway. J. Cell Sci. 113, 1951–1961. https://doi.org/10.1242/jcs.113.11.1951

Martin, V., Landi, L., Molinari, F., Fountzilas, G., Geva, R., Riva, A., Saletti, P., De Dosso, S., Spitale, A., Tejpar, S., Kalogeras, K.T., Mazzucchelli, L., Frattini, M., Cappuzzo, F., 2013. HER2 gene copy number status may influence clinical efficacy to anti-EGFR monoclonal antibodies in metastatic colorectal cancer patients. Br. J. Cancer 108, 668–675. https://doi.org/10.1038/bjc.2013.4

Martin-Belmonte, F., Gassama, A., Datta, A., Yu, W., Rescher, U., Gerke, V., Mostov, K., 2007. PTEN-Mediated Apical Segregation of Phosphoinositides Controls Epithelial Morphogenesis through Cdc42. Cell 128, 383–397. https://doi.org/10.1016/j.cell.2006.11.051

Martin-Belmonte, F., Mostov, K., 2007. Phosphoinositides Control Epithelial Development. Cell Cycle 6, 1957–1961. https://doi.org/10.4161/cc.6.16.4583

Matsumine, A., Ogai, A., Senda, T., Okumura, N., Satoh, K., Baeg, G.-H., Kawahara, T., Kobayashi, S., Okada, M., Toyoshima, K., Akiyama, T., 1996. Binding of APC to the Human Homolog of the Drosophila Discs Large Tumor Suppressor Protein. Science 272, 1020–1023. https://doi.org/10.1126/science.272.5264.1020

Maury, J., Nicoletti, C., Guzzo-Chambraud, L., Maroux, S., 1995. The Filamentous Brush Border Glycocalyx, a Mucin-like Marker of Enterocyte Hyper-Polarization. Eur. J. Biochem. 228, 323–331. https://doi.org/10.1111/j.1432-1033.1995.0323n.x

Mekenkamp, L.J.M., Heesterbeek, K.J., Koopman, M., Tol, J., Teerenstra, S., Venderbosch, S., Punt, C.J.A., Nagtegaal, I.D., 2012. Mucinous adenocarcinomas: Poor prognosis in metastatic colorectal cancer. Eur. J. Cancer 48, 501–509. https://doi.org/10.1016/j.ejca.2011.12.004

Menezes, L.F., Germino, G.G., 2019. The pathobiology of polycystic kidney disease from a metabolic viewpoint. Nat. Rev. Nephrol. 15, 735–749. https://doi.org/10.1038/s41581-019-0183-y

Messmer, T., Meyenn, F. von, Savino, A., Santos, F., Mohammed, H., Lun, A.T.L., Marioni, J.C., Reik, W., 2019. Transcriptional Heterogeneity in Naive and Primed Human Pluripotent Stem Cells at Single-Cell Resolution. Cell Rep. 26, 815-824.e4. https://doi.org/10.1016/j.celrep.2018.12.099

Michel, D., Arsanto, J.-P., Massey-Harroche, D., Béclin, C., Wijnholds, J., Le Bivic, A., 2005. PATJ connects and stabilizes apical and lateral components of tight junctions in human intestinal cells. J. Cell Sci. 118, 4049–4057. https://doi.org/10.1242/jcs.02528

Mizuno, K., Suzuki, A., Hirose, T., Kitamura, K., Kutsuzawa, K., Futaki, M., Amano, Y., Ohno, S., 2003. Self-association of PAR-3-mediated by the Conserved N-terminal Domain Contributes to the Development of Epithelial Tight Junctions *. J. Biol. Chem. 278, 31240–31250. https://doi.org/10.1074/jbc.M303593200

Mohammed, S.I., Torres-Luquis, O., Walls, E., Lloyd, F., 2019. Lymph-circulating tumor cells show distinct properties to blood-circulating tumor cells and are efficient metastatic precursors. Mol. Oncol. 13, 1400–1418. https://doi.org/10.1002/1878-0261.12494

Mohrmann, Karin, Sluijs, P. van der, 1999. Regulation of membrane transport through the endocytic pathway by rabGTPases. Mol. Membr. Biol. 16, 81–87. https://doi.org/10.1080/096876899294797

Molè, M.A., Coorens, T.H.H., Shahbazi, M.N., Weberling, A., Weatherbee, B.A.T., Gantner, C.W., Sancho-Serra, C., Richardson, L., Drinkwater, A., Syed, N., Engley, S., Snell, P., Christie, L., Elder, K., Campbell, A., Fishel, S., Behjati, S., Vento-Tormo, R., Zernicka-Goetz, M., 2021. A single cell characterisation of human embryogenesis identifies pluripotency transitions and putative anterior hypoblast centre. Nat. Commun. 12, 3679. https://doi.org/10.1038/s41467-021-23758-w

Moreno-Layseca, P., Icha, J., Hamidi, H., Ivaska, J., 2019. Integrin trafficking in cells and tissues. Nat. Cell Biol. 21, 122–132. https://doi.org/10.1038/s41556-018-0223-z

Moser, M., Nieswandt, B., Ussar, S., Pozgajova, M., Fässler, R., 2008. Kindlin-3 is essential for integrin activation and platelet aggregation. Nat. Med. 14, 325–330. https://doi.org/10.1038/nm1722

Mu÷sch, A., Cohen, D., Yeaman, C., Nelson, W.J., Rodriguez-Boulan, E., Brennwald, P.J., 2002. Mammalian Homolog of Drosophila Tumor Suppressor Lethal (2) Giant Larvae Interacts with Basolateral Exocytic Machinery in Madin-Darby Canine Kidney Cells. Mol. Biol. Cell 13, 158–168. https://doi.org/10.1091/mbc.01-10-0496

Muller, P.A.J., Caswell, P.T., Doyle, B., Iwanicki, M.P., Tan, E.H., Karim, S., Lukashchuk, N., Gillespie, D.A., Ludwig, R.L., Gosselin, P., Cromer, A., Brugge, J.S., Sansom, O.J., Norman, J.C., Vousden, K.H., 2009. Mutant p53 Drives Invasion by Promoting Integrin Recycling. Cell 139, 1327–1341. https://doi.org/10.1016/j.cell.2009.11.026

Nacke, M., Sandilands, E., Nikolatou, K., Román-Fernández, Á., Mason, S., Patel, R., Lilla, S., Yelland, T., Galbraith, L.C.A., Freckmann, E.C., McGarry, L., Morton, J.P., Shanks, E., Leung, H.Y., Markert, E., Ismail, S., Zanivan, S., Blyth, K., Bryant, D.M., 2021. An ARF GTPase module promoting invasion and metastasis through regulating phosphoinositide metabolism. Nat. Commun. 12, 1623. https://doi.org/10.1038/s41467-021-21847-4

Nader, G.P.F., Ezratty, E.J., Gundersen, G.G., 2016. FAK, talin and PIPKIγ regulate endocytosed integrin activation to polarize focal adhesion assembly. Nat. Cell Biol. 18, 491–503. https://doi.org/10.1038/ncb3333

Nagano, T., Yoneda, T., Hatanaka, Y., Kubota, C., Murakami, F., Sato, M., 2002. Filamin A-interacting protein (FILIP) regulates cortical cell migration out of the ventricular zone. Nat. Cell Biol. 4, 495–501. https://doi.org/10.1038/ncb808

Nagtegaal, I.D., Hugen, N., 2015. The Increasing Relevance of Tumour Histology in Determining Oncological Outcomes in Colorectal Cancer. Curr. Colorectal Cancer Rep. 11, 259–266. https://doi.org/10.1007/s11888-015-0280-7

Nagtegaal, I.D., Odze, R.D., Klimstra, D., Paradis, V., Rugge, M., Schirmacher, P., Washington, K.M., Carneiro, F., Cree, I.A., 2020. The 2019 WHO classification of tumours of the digestive system. Histopathology 76, 182–188. https://doi.org/10.1111/his.13975

Najafi, M., Farhood, B., Mortezaee, K., 2019. Extracellular matrix (ECM) stiffness and degradation as cancer drivers. J. Cell. Biochem. 120, 2782–2790. https://doi.org/10.1002/jcb.27681

Nardone, G., Oliver-De La Cruz, J., Vrbsky, J., Martini, C., Pribyl, J., Skládal, P., Pešl, M., Caluori, G., Pagliari, S., Martino, F., Maceckova, Z., Hajduch, M., Sanz-Garcia, A., Pugno, N.M., Stokin, G.B., Forte, G., 2017. YAP regulates cell mechanics by controlling focal adhesion assembly. Nat. Commun. 8, 15321. https://doi.org/10.1038/ncomms15321

Närvä, E., Stubb, A., Guzmán, C., Blomqvist, M., Balboa, D., Lerche, M., Saari, M., Otonkoski, T., Ivaska, J., 2017. A Strong Contractile Actin Fence and Large Adhesions Direct Human Pluripotent Colony Morphology and Adhesion. Stem Cell Rep. 9, 67–76. https://doi.org/10.1016/j.stemcr.2017.05.021

Nassar, H., Pansare, V., Zhang, H., Che, M., Sakr, W., Ali-Fehmi, R., Grignon, D., Sarkar, F., Cheng, J., Adsay, V., 2004. Pathogenesis of invasive micropapillary carcinoma: role of MUC1 glycoprotein. Mod. Pathol. 17, 1045–1050. https://doi.org/10.1038/modpathol.3800166

Nelson, W.J., 2003. Adaptation of core mechanisms to generate cell polarity. Nature 422, 766–774. https://doi.org/10.1038/nature01602

Ngok, S.P., Lin, W.-H., Anastasiadis, P.Z., 2014. Establishment of epithelial polarity – GEF who's minding the GAP? J. Cell Sci. 127, 3205–3215. https://doi.org/10.1242/jcs.153197

Nikas, G., Ao, A., Winston, R.M.L., Handyside, A.H., 1996. Compaction and Surface Polarity in the Human Embryo in Vitro. Biol. Reprod. 55, 32–37. https://doi.org/10.1095/biolreprod55.1.32

Nikolatou, K., Sandilands, E., Román-Fernández, A., Cumming, E.M., Freckmann, E., Lilla, S., Buetow, L., McGarry, L., Neilson, M., Shaw, R., Strachan, D., Miller, C., Huang, D.T., McNeish, I.A., Norman, J.C., Zanivan, S., Bryant, D.M., 2023. PTEN deficiency exposes a requirement for an ARF GTPase module for integrin-dependent invasion in ovarian cancer. EMBO J. 42, e113987. https://doi.org/10.15252/embj.2023113987

Nobis, M., McGhee, E.J., Morton, J.P., Schwarz, J.P., Karim, S.A., Quinn, J., Edward, M., Campbell, A.D., McGarry, L.C., Evans, T.R.J., Brunton, V.G., Frame, M.C., Carragher, N.O., Wang, Y., Sansom, O.J., Timpson, P., Anderson, K.I., 2013. Intravital FLIM-FRET Imaging

Reveals Dasatinib-Induced Spatial Control of Src in Pancreatic Cancer. Cancer Res. 73, 4674–4686. https://doi.org/10.1158/0008-5472.CAN-12-4545

Nowak, J.A., 2020. HER2 in Colorectal Carcinoma. Surg. Pathol. Clin. 13, 485–502. https://doi.org/10.1016/j.path.2020.05.007

O'Brien, L.E., Jou, T.-S., Pollack, A.L., Zhang, Q., Hansen, S.H., Yurchenco, P., Mostov, K.E., 2001. Rac1 orientates epithelial apical polarity through effects on basolateral laminin assembly. Nat. Cell Biol. 3, 831–838. https://doi.org/10.1038/ncb0901-831

Ohta, Y., Hartwig, J.H., Stossel, T.P., 2006. FilGAP, a Rho- and ROCK-regulated GAP for Rac binds filamin A to control actin remodelling. Nat. Cell Biol. 8, 803–814. https://doi.org/10.1038/ncb1437

Okuyama, H., Kondo, J., Sato, Y., Endo, H., Nakajima, A., Piulats, J.M., Tomita, Y., Fujiwara, T., Itoh, Y., Mizoguchi, A., Ohue, M., Inoue, M., 2016. Dynamic Change of Polarity in Primary Cultured Spheroids of Human Colorectal Adenocarcinoma and Its Role in Metastasis. Am. J. Pathol. 186, 899–911. https://doi.org/10.1016/j.ajpath.2015.12.011

Onuma, K., Inoue, M., 2022. Abnormality of apico–basal polarity in adenocarcinoma. Cancer Sci. 113, 3657–3663. https://doi.org/10.1111/cas.15549

Onuma, K., Sato, Y., Okuyama, H., Uematsu, H., Homma, K., Ohue, M., Kondo, J., Inoue, M., 2021. Aberrant activation of Rho/ROCK signaling in impaired polarity switching of colorectal micropapillary carcinoma. J. Pathol. 255, 84–94. https://doi.org/10.1002/path.5748

Pagès, D.-L., Dornier, E., de Seze, J., Gontran, E., Maitra, A., Maciejewski, A., Wang, L., Luan, R., Cartry, J., Canet-Jourdan, C., Raingeaud, J., Lemahieu, G., Lebel, M., Ducreux, M., Gelli, M., Scoazec, J.-Y., Coppey, M., Voituriez, R., Piel, M., Jaulin, F., 2022. Cell clusters adopt a collective amoeboid mode of migration in confined nonadhesive environments. Sci. Adv. 8, eabp8416. https://doi.org/10.1126/sciadv.abp8416

Pagliari, S., Vinarsky, V., Martino, F., Perestrelo, A.R., Oliver De La Cruz, J., Caluori, G., Vrbsky, J., Mozetic, P., Pompeiano, A., Zancla, A., Ranjani, S.G., Skladal, P., Kytyr, D., Zdráhal, Z., Grassi, G., Sampaolesi, M., Rainer, A., Forte, G., 2021. YAP–TEAD1 control of cytoskeleton dynamics and intracellular tension guides human pluripotent stem cell mesoderm specification. Cell Death Differ. 28, 1193–1207. https://doi.org/10.1038/s41418-020-00643-5

Palangi, F., Samuel, S.M., Thompson, I.R., Triggle, C.R., Emara, M.M., 2017. Effects of oxidative and thermal stresses on stress granule formation in human induced pluripotent stem cells. PLOS ONE 12, e0182059. https://doi.org/10.1371/journal.pone.0182059

Pappenheimer, J.R., 2001. Intestinal Absorption of Hexoses and Amino Acids: From Apical Cytosol to Villus Capillaries 184, 233–239. https://doi.org/10.1007/s00232-001-0094-1

Parsons, M., Keppler, M.D., Kline, A., Messent, A., Humphries, M.J., Gilchrist, R., Hart, I.R., Quittau-Prevostel, C., Hughes, W.E., Parker, P.J., Ng, T., 2002. Site-Directed Perturbation of Protein Kinase C- Integrin Interaction Blocks Carcinoma Cell Chemotaxis. Mol. Cell. Biol. 22, 5897–5911. https://doi.org/10.1128/MCB.22.16.5897-5911.2002

Pasquier, N., Jaulin, F., Peglion, F., 2024. Inverted apicobasal polarity in health and disease. J. Cell Sci. 137, jcs261659. https://doi.org/10.1242/jcs.261659

Passaniti, A., Hart, G.W., 1988. Cell surface sialylation and tumor metastasis. Metastatic potential of B16 melanoma variants correlates with their relative numbers of specific penultimate oligosaccharide structures. J. Biol. Chem. 263, 7591–7603. https://doi.org/10.1016/S0021-9258(18)68540-0

Paszek, M.J., Boettiger, D., Weaver, V.M., Hammer, D.A., 2009. Integrin Clustering Is Driven by Mechanical Resistance from the Glycocalyx and the Substrate. PLoS Comput. Biol. 5, e1000604. https://doi.org/10.1371/journal.pcbi.1000604

Paszek, M.J., DuFort, C.C., Rossier, O., Bainer, R., Mouw, J.K., Godula, K., Hudak, J.E., Lakins, J.N., Wijekoon, A.C., Cassereau, L., Rubashkin, M.G., Magbanua, M.J., Thorn, K.S., Davidson, M.W., Rugo, H.S., Park, J.W., Hammer, D.A., Giannone, G., Bertozzi, C.R., Weaver, V.M., 2014. The cancer glycocalyx mechanically primes integrin-mediated growth and survival. Nature 511, 319–325. https://doi.org/10.1038/nature13535

Paul, N.R., Jacquemet, G., Caswell, P.T., 2015. Endocytic Trafficking of Integrins in Cell Migration. Curr. Biol. 25, R1092–R1105. https://doi.org/10.1016/j.cub.2015.09.049

Peglion, F., Etienne-Manneville, S., 2023. Cell polarity changes in cancer initiation and progression. J. Cell Biol. 223, e202308069. https://doi.org/10.1083/jcb.202308069

Pellinen, T., Arjonen, A., Vuoriluoto, K., Kallio, K., Fransen, J.A.M., Ivaska, J., 2006. Small GTPase Rab21 regulates cell adhesion and controls endosomal traffic of β1-integrins. J. Cell Biol. 173, 767–780. https://doi.org/10.1083/jcb.200509019

Pellinen, T., Ivaska, J., 2006. Integrin traffic. J. Cell Sci. 119, 3723–3731. https://doi.org/10.1242/jcs.03216

Pietilä, M., Sahgal, P., Peuhu, E., Jäntti, N.Z., Paatero, I., Närvä, E., Al-Akhrass, H., Lilja, J., Georgiadou, M., Andersen, O.M., Padzik, A., Sihto, H., Joensuu, H., Blomqvist, M., Saarinen, I., Boström, P.J., Taimen, P., Ivaska, J., 2019. SORLA regulates endosomal trafficking and oncogenic fitness of HER2. Nat. Commun. 10, 2340. https://doi.org/10.1038/s41467-019-10275-0

Plow, E.F., Haas, T.A., Zhang, L., Loftus, J., Smith, J.W., 2000. Ligand Binding to Integrins. J. Biol. Chem. 275, 21785–21788. https://doi.org/10.1074/jbc.R000003200

Plusa, B., Frankenberg, S., Chalmers, A., Hadjantonakis, A.-K., Moore, C.A., Papalopulu, N., Papaioannou, V.E., Glover, D.M., Zernicka-Goetz, M., 2005. Downregulation of Par3 and aPKC function directs cells towards the ICM in the preimplantation mouse embryo. J. Cell Sci. 118, 505–515. https://doi.org/10.1242/jcs.01666

Pluskota, E., Dowling, J.J., Gordon, N., Golden, J.A., Szpak, D., West, X.Z., Nestor, C., Ma, Y.-Q., Bialkowska, K., Byzova, T., Plow, E.F., 2011. The integrin coactivator Kindlin-2 plays a critical role in angiogenesis in mice and zebrafish. Blood 117, 4978–4987. https://doi.org/10.1182/blood-2010-11-321182

Pocard, T., Le Bivic, A., Galli, T., Zurzolo, C., 2007. Distinct v-SNAREs regulate direct and indirect apical delivery in polarized epithelial cells. J. Cell Sci. 120, 3309–3320. https://doi.org/10.1242/jcs.007948

Powelka, A.M., Sun, J., Li, J., Gao, M., Shaw, L.M., Sonnenberg, A., Hsu, V.W., 2004. Stimulation-Dependent Recycling of Integrin β1 Regulated by ARF6 and Rab11. Traffic 5, 20–

36. https://doi.org/10.1111/j.1600-0854.2004.00150.x

Pretzsch, E., Bösch, F., Neumann, J., Ganschow, P., Bazhin, A., Guba, M., Werner, J., Angele, M., 2019. Mechanisms of Metastasis in Colorectal Cancer and Metastatic Organotropism: Hematogenous versus Peritoneal Spread. J. Oncol. 2019, 7407190. https://doi.org/10.1155/2019/7407190

Puthenveedu, M.A., Lauffer, B., Temkin, P., Vistein, R., Carlton, P., Thorn, K., Taunton, J., Weiner, O.D., Parton, R.G., Zastrow, M. von, 2010. Sequence-Dependent Sorting of Recycling Proteins by Actin-Stabilized Endosomal Microdomains. Cell 143, 761–773. https://doi.org/10.1016/j.cell.2010.10.003

Quinn, K.E., Matson, B.C., Wetendorf, M., Caron, K.M., 2020. Pinopodes: Recent advancements, current perspectives, and future directions. Mol. Cell. Endocrinol. 501, 110644. https://doi.org/10.1016/j.mce.2019.110644

Rainero, E., Caswell, P.T., Muller, P.A.J., Grindlay, J., McCaffrey, M.W., Zhang, Q., Wakelam, M.J.O., Vousden, K.H., Graziani, A., Norman, J.C., 2012. Diacylglycerol kinase α controls RCP-dependent integrin trafficking to promote invasive migration. J. Cell Biol. 196, 277–295. https://doi.org/10.1083/jcb.201109112

Rainero, E., Howe, J.D., Caswell, P.T., Jamieson, N.B., Anderson, K., Critchley, D.R., Machesky, L., Norman, J.C., 2015. Ligand-Occupied Integrin Internalization Links Nutrient Signaling to Invasive Migration. Cell Rep. 10, 398–413. https://doi.org/10.1016/j.celrep.2014.12.037

Ramovs, V., Te Molder, L., Sonnenberg, A., 2017. The opposing roles of laminin-binding integrins in cancer. Matrix Biol. J. Int. Soc. Matrix Biol. 57–58, 213–243. https://doi.org/10.1016/j.matbio.2016.08.007

Ramsay, A.G., Keppler, M.D., Jazayeri, M., Thomas, G.J., Parsons, M., Violette, S., Weinreb, P., Hart, I.R., Marshall, J.F., 2007. HS1-Associated Protein X-1 Regulates Carcinoma Cell Migration and Invasion via Clathrin-Mediated Endocytosis of Integrin αvβ6. Cancer Res. 67, 5275–5284. https://doi.org/10.1158/0008-5472.CAN-07-0318

Ratheesh, A., Gomez, G.A., Priya, R., Verma, S., Kovacs, E.M., Jiang, K., Brown, N.H., Akhmanova, A., Stehbens, S.J., Yap, A.S., 2012. Centralspindlin and α-catenin regulate Rho signalling at the epithelial zonula adherens. Nat. Cell Biol. 14, 818–828. https://doi.org/10.1038/ncb2532

Reddy, B.V.V.G., Kalraiya, R.D., 2006. Sialilated β1,6 branched N-oligosaccharides modulate adhesion, chemotaxis and motility of melanoma cells: Effect on invasion and spontaneous metastasis properties. Biochim. Biophys. Acta BBA - Gen. Subj. 1760, 1393–1402. https://doi.org/10.1016/j.bbagen.2006.05.003

Reeve, W.J.D., Ziomek, C.A., 1981. Distribution of microvilli on dissociated blastomeres from mouse embryos: evidence for surface polarization at compaction. Development 62, 339–350. https://doi.org/10.1242/dev.62.1.339

Reglero-Real, N., Álvarez-Varela, A., Cernuda-Morollón, E., Feito, J., Marcos-Ramiro, B., Fernández-Martín, L., Gómez-Lechón, M.J., Muntané, J., Sandoval, P., Majano, P.L., Correas, I., Alonso, M.A., Millán, J., 2014. Apicobasal Polarity Controls Lymphocyte Adhesion

to Hepatic Epithelial Cells. Cell Rep. 8, 1879–1893. https://doi.org/10.1016/j.celrep.2014.08.007

Ridley, A.J., Hall, A., 1992. Distinct Patterns of Actin Organization Regulated by the Small GTP-binding Proteins Rac and Rho. Cold Spring Harb. Symp. Quant. Biol. 57, 661–671. https://doi.org/10.1101/SQB.1992.057.01.072

Ritch, S.J., Telleria, C.M., 2022. The Transcoelomic Ecosystem and Epithelial Ovarian Cancer Dissemination. Front. Endocrinol. 13. https://doi.org/10.3389/fendo.2022.886533

Rizzo, G., Bertotti, A., Leto, S.M., Vetrano, S., 2021. Patient-derived tumor models: a more suitable tool for pre-clinical studies in colorectal cancer. J. Exp. Clin. Cancer Res. 40, 178. https://doi.org/10.1186/s13046-021-01970-2

Roberts, M., Barry, S., Woods, A., Norman, J., n.d. PDGF-regulated rab4-dependent recycling of ⎵v␋3 integrin from early endosomes is necessary for cell adhesion and spreading.

Robertson, J., Jacquemet, G., Byron, A., Jones, M.C., Warwood, S., Selley, J.N., Knight, D., Humphries, J.D., Humphries, M.J., 2015. Defining the phospho-adhesome through the phosphoproteomic analysis of integrin signalling. Nat. Commun. 6, 6265. https://doi.org/10.1038/ncomms7265

Roca-Cusachs, P., del Rio, A., Puklin-Faucher, E., Gauthier, N.C., Biais, N., Sheetz, M.P., 2013. Integrin-dependent force transmission to the extracellular matrix by α-actinin triggers adhesion maturation. Proc. Natl. Acad. Sci. 110, E1361–E1370. https://doi.org/10.1073/pnas.1220723110

Rodriguez-Boulan, E., Macara, I.G., 2014. Organization and execution of the epithelial polarity programme. Nat. Rev. Mol. Cell Biol. 15, 225–242. https://doi.org/10.1038/nrm3775

Roh, M.H., Margolis, B., 2003. Composition and function of PDZ protein complexes during cell polarization. Am. J. Physiol.-Ren. Physiol. 285, F377–F387. https://doi.org/10.1152/ajprenal.00086.2003

Rossier, O., Octeau, V., Sibarita, J.-B., Leduc, C., Tessier, B., Nair, D., Gatterdam, V., Destaing, O., Albigès-Rizo, C., Tampé, R., Cognet, L., Choquet, D., Lounis, B., Giannone, G., 2012. Integrins β1 and β3 exhibit distinct dynamic nanoscale organizations inside focal adhesions. Nat. Cell Biol. 14, 1057–1067. https://doi.org/10.1038/ncb2588

Rostovskaya, M., Stirparo, G.G., Smith, A., 2019. Capacitation of human naïve pluripotent stem cells for multi-lineage differentiation. Development 146, dev172916. https://doi.org/10.1242/dev.172916

Rubashkin, M.G., Cassereau, L., Bainer, R., DuFort, C.C., Yui, Y., Ou, G., Paszek, M.J., Davidson, M.W., Chen, Y.-Y., Weaver, V.M., 2014. Force engages vinculin and promotes tumor progression by enhancing PI3K activation of phosphatidylinositol (3,4,5)-triphosphate. Cancer Res. 74, 4597–4611. https://doi.org/10.1158/0008-5472.CAN-13-3698

Sahgal, P., Alanko, J., Icha, J., Paatero, I., Hamidi, H., Arjonen, A., Pietilä, M., Rokka, A., Ivaska, J., 2019. GGA2 and RAB13 promote activity-dependent β1-integrin recycling. J. Cell Sci. 132, jcs233387. https://doi.org/10.1242/jcs.233387

Salat-Canela, C., Pérez, P., Ayté, J., Hidalgo, E., 2023. Stress-induced cell depolarization

through the MAP kinase–Cdc42 axis. Trends Cell Biol. 33, 124–137. https://doi.org/10.1016/j.tcb.2022.06.004

Saotome, I., Curto, M., McClatchey, A.I., 2004. Ezrin Is Essential for Epithelial Organization and Villus Morphogenesis in the Developing Intestine. Dev. Cell 6, 855–864. https://doi.org/10.1016/j.devcel.2004.05.007

Sasaki, A.T., Chun, C., Takeda, K., Firtel, R.A., 2004. Localized Ras signaling at the leading edge regulates PI3K, cell polarity, and directional cell movement. J. Cell Biol. 167, 505–518. https://doi.org/10.1083/jcb.200406177

Schiller, H.B., Hermann, M.-R., Polleux, J., Vignaud, T., Zanivan, S., Friedel, C.C., Sun, Z., Raducanu, A., Gottschalk, K.-E., Théry, M., Mann, M., Fässler, R., 2013. β1- and αv-class integrins cooperate to regulate myosin II during rigidity sensing of fibronectin-based microenvironments. Nat. Cell Biol. 15, 625–636. https://doi.org/10.1038/ncb2747

Schlüter, M.A., Pfarr, C.S., Pieczynski, J., Whiteman, E.L., Hurd, T.W., Fan, S., Liu, C.-J., Margolis, B., 2009. Trafficking of Crumbs3 during Cytokinesis Is Crucial for Lumen Formation. Mol. Biol. Cell 20, 4652–4663. https://doi.org/10.1091/mbc.e09-02-0137

Schmidt, V., Schulz, N., Yan, X., Schürmann, A., Kempa, S., Kern, M., Blüher, M., Poy, M.N., Olivecrona, G., Willnow, T.E., 2016. SORLA facilitates insulin receptor signaling in adipocytes and exacerbates obesity. J. Clin. Invest. 126, 2706–2720. https://doi.org/10.1172/JCI84708

Schneeberger, K., Vogel, G.F., Teunissen, H., van Ommen, D.D., Begthel, H., El Bouazzaoui, L., van Vugt, A.H.M., Beekman, J.M., Klumperman, J., Müller, T., Janecke, A., Gerner, P., Huber, L.A., Hess, M.W., Clevers, H., van Es, J.H., Nieuwenhuis, E.E.S., Middendorp, S., 2015. An inducible mouse model for microvillus inclusion disease reveals a role for myosin Vb in apical and basolateral trafficking. Proc. Natl. Acad. Sci. 112, 12408–12413. https://doi.org/10.1073/pnas.1516672112

Schuck, S., Simons, K., 2004. Polarized sorting in epithelial cells: raft clustering and the biogenesis of the apical membrane. J. Cell Sci. 117, 5955–5964. https://doi.org/10.1242/jcs.01596

Semel, A.C., Seales, E.C., Singhal, A., Eklund, E.A., Colley, K.J., Bellis, S.L., 2002. Hyposialylation of Integrins Stimulates the Activity of Myeloid Fibronectin Receptors*. J. Biol. Chem. 277, 32830–32836. https://doi.org/10.1074/jbc.M202493200

Shafaq-Zadah, M., Dransart, E., Wunder, C., Chambon, V., Valades-Cruz, C.A., Leconte, L., Sarangi, N.K., Robinson, J., Bai, S.-K., Regmi, R., Cicco, A.D., Hovasse, A., Bartels, R., Nilsson, U.J., Cianférani-Sanglier, S., Leffler, H., Keyes, T.E., Lévy, D., Raunser, S., Roderer, D., Johannes, L., 2023. Spatial N-glycan rearrangement on α5β1 integrin nucleates galectin-3 oligomers to determine endocytic fate. https://doi.org/10.1101/2023.10.27.564026

Shafaq-Zadah, M., Gomes-Santos, C.S., Bardin, S., Maiuri, P., Maurin, M., Iranzo, J., Gautreau, A., Lamaze, C., Caswell, P., Goud, B., Johannes, L., 2016. Persistent cell migration and adhesion rely on retrograde transport of β1 integrin. Nat. Cell Biol. 18, 54–64. https://doi.org/10.1038/ncb3287

Shin, H.-W., Hayashi, M., Christoforidis, S., Lacas-Gervais, S., Hoepfner, S., Wenk, M.R.,

Modregger, J., Uttenweiler-Joseph, S., Wilm, M., Nystuen, A., Frankel, W.N., Solimena, M., De Camilli, P., Zerial, M., 2005. An enzymatic cascade of Rab5 effectors regulates phosphoinositide turnover in the endocytic pathway. J. Cell Biol. 170, 607–618. https://doi.org/10.1083/jcb.200505128

Shin, K., Straight, S., Margolis, B., 2005. PATJ regulates tight junction formation and polarity in mammalian epithelial cells. J. Cell Biol. 168, 705–711. https://doi.org/10.1083/jcb.200408064

Shroyer, N.F., Wallis, D., Venken, K.J.T., Bellen, H.J., Zoghbi, H.Y., 2005. Gfi1 functions downstream of Math1 to control intestinal secretory cell subtype allocation and differentiation. Genes Dev. 19, 2412–2417. https://doi.org/10.1101/gad.1353905

Siegel, R.L., Wagle, N.S., Cercek, A., Smith, R.A., Jemal, A., 2023. Colorectal cancer statistics, 2023. CA. Cancer J. Clin. 73, 233–254. https://doi.org/10.3322/caac.21772

Simpson, J.C., Jones, A.T., 2005. Early endocytic Rabs: functional prediction to functional characterization. Biochem. Soc. Symp. 72, 99–108. https://doi.org/10.1042/bss0720099

Siriaunkgul, S., Tavassoli, F.A., 1993. Invasive micropapillary carcinoma of the breast. Mod. Pathol. 6, 660–662.

Slováková, J., Sikora, M., Arslan, F.N., Caballero-Mancebo, S., Krens, S.F.G., Kaufmann, W.A., Merrin, J., Heisenberg, C.-P., 2022. Tension-dependent stabilization of E-cadherin limits cell–cell contact expansion in zebrafish germ-layer progenitor cells. Proc. Natl. Acad. Sci. 119, e2122030119. https://doi.org/10.1073/pnas.2122030119

Speiser, D.E., Chijioke, O., Schaeuble, K., Münz, C., 2023. CD4+ T cells in cancer. Nat. Cancer 4, 317–329. https://doi.org/10.1038/s43018-023-00521-2

Spoelgen, R., Adams, K.W., Koker, M., Thomas, A.V., Andersen, O.M., Hallett, P.J., Bercury, K.K., Joyner, D.F., Deng, M., Stoothoff, W.H., Strickland, D.K., Willnow, T.E., Hyman, B.T., 2009. Interaction of the apolipoprotein E receptors low density lipoprotein receptor-related protein and sorLA/LR11. Neuroscience 158, 1460–1468. https://doi.org/10.1016/j.neuroscience.2008.10.061

Stachowiak, J.C., Schmid, E.M., Ryan, C.J., Ann, H.S., Sasaki, D.Y., Sherman, M.B., Geissler, P.L., Fletcher, D.A., Hayden, C.C., 2012. Membrane bending by protein–protein crowding. Nat. Cell Biol. 14, 944–949. https://doi.org/10.1038/ncb2561

Stanifer, M.L., Mukenhirn, M., Muenchau, S., Pervolaraki, K., Kanaya, T., Albrecht, D., Odendall, C., Hielscher, T., Haucke, V., Kagan, J.C., Bartfeld, S., Ohno, H., Boulant, S., 2020. Asymmetric distribution of TLR3 leads to a polarized immune response in human intestinal epithelial cells. Nat. Microbiol. 5, 181–191. https://doi.org/10.1038/s41564-019-0594-3

Steinberg, F., Heesom, K.J., Bass, M.D., Cullen, P.J., 2012. SNX17 protects integrins from degradation by sorting between lysosomal and recycling pathways. J. Cell Biol. 197, 219–230. https://doi.org/10.1083/jcb.201111121

Stewart, C.J.R., Koay, M.H.E., Leslie, C., Acott, N., Leung, Y.C., 2018. Cervical carcinomas with a micropapillary component: a clinicopathological study of eight cases. Histopathology 72, 626–633. https://doi.org/10.1111/his.13419

Straight, S.W., Shin, K., Fogg, V.C., Fan, S., Liu, C.-J., Roh, M., Margolis, B., 2004. Loss of PALS1 Expression Leads to Tight Junction and Polarity Defects. Mol. Biol. Cell 15, 1981–1990. https://doi.org/10.1091/mbc.e03-08-0620

Stubb, A., Guzmán, C., Närvä, E., Aaron, J., Chew, T.-L., Saari, M., Miihkinen, M., Jacquemet, G., Ivaska, J., 2019. Superresolution architecture of cornerstone focal adhesions in human pluripotent stem cells. Nat. Commun. 10, 4756. https://doi.org/10.1038/s41467-019-12611-w

Su, Y., Xia, W., Li, J., Walz, T., Humphries, M.J., Vestweber, D., Cabañas, C., Lu, C., Springer, T.A., 2016. Relating conformation to function in integrin α5β1. Proc. Natl. Acad. Sci. 113, E3872–E3881. https://doi.org/10.1073/pnas.1605074113

Suardet, L., Gaide, A.-C., Calmès, J.-M., Sordat, B., Givel, J.-C., Eliason, J.F., Odartchenko, N., 1992. Responsiveness of Three Newly Established Human Colorectal Cancer Cell Lines to Transforming Growth Factors β1 and β21. Cancer Res. 52, 3705–3712.

Sun, P., Zhong, Z., Lu, Q., Li, M., Chao, X., Chen, D., Hu, W., Luo, R., He, J., 2020. Mucinous carcinoma with micropapillary features is morphologically, clinically and genetically distinct from pure mucinous carcinoma of breast. Mod. Pathol. 33, 1945–1960. https://doi.org/10.1038/s41379-020-0554-8

Sutherland, A.E., Calarco, P.G., Damsky, C.H., 1993. Developmental regulation of integrin expression at the time of implantation in the mouse embryo. Development 119, 1175–1186. https://doi.org/10.1242/dev.119.4.1175

Suwińska, A., Czołowska, R., Ożdżeński, W., Tarkowski, A.K., 2008. Blastomeres of the mouse embryo lose totipotency after the fifth cleavage division: Expression of *Cdx2* and *Oct4* and developmental potential of inner and outer blastomeres of 16- and 32-cell embryos. Dev. Biol. 322, 133–144. https://doi.org/10.1016/j.ydbio.2008.07.019

Suzuki, A., Yamanaka, T., Hirose, T., Manabe, N., Mizuno, K., Shimizu, M., Akimoto, K., Izumi, Y., Ohnishi, T., Ohno, S., 2001. Atypical Protein Kinase C Is Involved in the Evolutionarily Conserved Par Protein Complex and Plays a Critical Role in Establishing Epithelia-Specific Junctional Structures. J. Cell Biol. 152, 1183–1196. https://doi.org/10.1083/jcb.152.6.1183

Sveen, A., Bruun, J., Eide, P.W., Eilertsen, I.A., Ramirez, L., Murumägi, A., Arjama, M., Danielsen, S.A., Kryeziu, K., Elez, E., Tabernero, J., Guinney, J., Palmer, H.G., Nesbakken, A., Kallioniemi, O., Dienstmann, R., Lothe, R.A., 2018. Colorectal Cancer Consensus Molecular Subtypes Translated to Preclinical Models Uncover Potentially Targetable Cancer Cell Dependencies. Clin. Cancer Res. 24, 794–806. https://doi.org/10.1158/1078-0432.CCR-17-1234

Swain, S.M., Baselga, J., Kim, S.-B., Ro, J., Semiglazov, V., Campone, M., Ciruelos, E., Ferrero, J.-M., Schneeweiss, A., Heeson, S., Clark, E., Ross, G., Benyunes, M.C., Cortés, J., 2015. Pertuzumab, Trastuzumab, and Docetaxel in HER2-Positive Metastatic Breast Cancer. N. Engl. J. Med. 372, 724–734. https://doi.org/10.1056/NEJMoa1413513

Taei, A., Rasooli, P., Braun, T., Hassani, S.-N., Baharvand, H., 2020. Signal regulators of human naïve pluripotency. Exp. Cell Res. 389, 111924. https://doi.org/10.1016/j.yexcr.2020.111924

Takada, Y., Ye, X., Simon, S., 2007. The integrins. Genome Biol. 8, 215. https://doi.org/10.1186/gb-2007-8-5-215

Takahashi, K., Tanabe, K., Ohnuki, M., Narita, M., Ichisaka, T., Tomoda, K., Yamanaka, S., 2007. Induction of Pluripotent Stem Cells from Adult Human Fibroblasts by Defined Factors. Cell 131, 861–872. https://doi.org/10.1016/j.cell.2007.11.019

Takahashi, K., Yamanaka, S., 2006. Induction of Pluripotent Stem Cells from Mouse Embryonic and Adult Fibroblast Cultures by Defined Factors. Cell 126, 663–676. https://doi.org/10.1016/j.cell.2006.07.024

Tepass, U., Theres, C., Knust, E., 1990. crumbs encodes an EGF-like protein expressed on apical membranes of Drosophila epithelial cells and required for organization of epithelia. Cell 61, 787–799. https://doi.org/10.1016/0092-8674(90)90189-L

Tiger, C.-F., Fougerousse, F., Grundström, G., Velling, T., Gullberg, D., 2001. α11β1 Integrin Is a Receptor for Interstitial Collagens Involved in Cell Migration and Collagen Reorganization on Mesenchymal Nonmuscle Cells. Dev. Biol. 237, 116–129. https://doi.org/10.1006/dbio.2001.0363

Tiwari, S., Askari, J.A., Humphries, M.J., Bulleid, N.J., 2011. Divalent cations regulate the folding and activation status of integrins during their intracellular trafficking. J. Cell Sci. 124, 1672–1680. https://doi.org/10.1242/jcs.084483

Toolan, H.W., 1953. Growth of Human Tumors in Cortisone-treated Laboratory Animals: The Possibility of Obtaining Permanently Transplantable Human Tumors* †. Cancer Res. 13, 389–394.

Tran, C.S., Eran, Y., Ruch, T.R., Bryant, D.M., Datta, A., Brakeman, P., Kierbel, A., Wittmann, T., Metzger, R.J., Mostov, K.E., Engel, J.N., 2014. Host Cell Polarity Proteins Participate in Innate Immunity to *Pseudomonas aeruginosa* Infection. Cell Host Microbe 15, 636–643. https://doi.org/10.1016/j.chom.2014.04.007

Tsunoyama, T.A., Watanabe, Y., Goto, J., Naito, K., Kasai, R.S., Suzuki, K.G.N., Fujiwara, T.K., Kusumi, A., 2018. Super-long single-molecule tracking reveals dynamic-anchorage-induced integrin function 14, 497–506. https://doi.org/10.1038/s41589-018-0032-5

Tulla, M., Pentikäinen, O.T., Viitasalo, T., Käpylä, J., Impola, U., Nykvist, P., Nissinen, L., Johnson, M.S., Heino, J., 2001. Selective Binding of Collagen Subtypes by Integrin α1I, α2I, and α10I Domains *. J. Biol. Chem. 276, 48206–48212. https://doi.org/10.1074/jbc.M104058200

U Kroneld, R.J., 1998. Expression of the mucosal lymphocyte integrin aEß7 and its ligand E-cadherin in salivary glands of patients with Sjögren's syndrome. Scand. J. Rheumatol. https://doi.org/10.1080/030097498440831

Veillat, V., Spuul, P., Daubon, T., Egaña, I., Kramer, Ij., Génot, E., 2015. Podosomes: Multipurpose organelles? Int. J. Biochem. Cell Biol. 65, 52–60. https://doi.org/10.1016/j.biocel.2015.05.020

Verdú, M., Román, R., Calvo, M., Rodón, N., García, B., González, M., Vidal, A., Puig, X., 2011. Clinicopathological and molecular characterization of colorectal micropapillary carcinoma. Mod. Pathol. 24, 729–738. https://doi.org/10.1038/modpathol.2011.1

Verras, G.-I., Tchabashvili, L., Mulita, F., Grypari, I.M., Sourouni, S., Panagodimou, E., Argentou, M.-I., 2023. Micropapillary Breast Carcinoma: From Molecular Pathogenesis to Prognosis. Breast Cancer Targets Ther. 14, 41–61. https://doi.org/10.2147/BCTT.S346301

Wang, Q., Chen, X.-W., Margolis, B., 2007. PALS1 Regulates E-Cadherin Trafficking in Mammalian Epithelial Cells. Mol. Biol. Cell 18, 874–885. https://doi.org/10.1091/mbc.e06-07-0651

Wang, W., Huang, J., Chen, J., 2011. Angiomotin-like Proteins Associate with and Negatively Regulate YAP1 *. J. Biol. Chem. 286, 4364–4370. https://doi.org/10.1074/jbc.C110.205401

Wang, X., Xiang, Y., Yu, Y., Wang, R., Zhang, Y., Xu, Q., Sun, H., Zhao, Z.-A., Jiang, X., Wang, Xiaoqing, Lu, X., Qin, D., Quan, Y., Zhang, J., Shyh-Chang, N., Wang, H., Jing, N., Xie, W., Li, L., 2021. Formative pluripotent stem cells show features of epiblast cells poised for gastrulation. Cell Res. 31, 526–541. https://doi.org/10.1038/s41422-021-00477-x

Wang, Y., Arjonen, A., Pouwels, J., Ta, H., Pausch, P., Bange, G., Engel, U., Pan, X., Fackler, O.T., Ivaska, J., Grosse, R., 2015. Formin-like 2 Promotes β1-Integrin Trafficking and Invasive Motility Downstream of PKCα. Dev. Cell 34, 475–483. https://doi.org/10.1016/j.devcel.2015.06.015

Wang, Y., Zhang, C., Yang, W., Shao, S., Xu, X., Sun, Y., Li, P., Liang, L., Wu, C., 2021. LIMD1 phase separation contributes to cellular mechanics and durotaxis by regulating focal adhesion dynamics in response to force. Dev. Cell 56, 1313-1325.e7. https://doi.org/10.1016/j.devcel.2021.04.002

Watanabe, N., Bodin, L., Pandey, M., Krause, M., Coughlin, S., Boussiotis, V.A., Ginsberg, M.H., Shattil, S.J., 2008. Mechanisms and consequences of agonist-induced talin recruitment to platelet integrin αIIbβ3. J. Cell Biol. 181, 1211–1222. https://doi.org/10.1083/jcb.200803094

Wegener, K.L., Partridge, A.W., Han, J., Pickford, A.R., Liddington, R.C., Ginsberg, M.H., Campbell, I.D., 2007. Structural Basis of Integrin Activation by Talin. Cell 128, 171–182. https://doi.org/10.1016/j.cell.2006.10.048

Whitby, S., Zhou, W., Dimitriadis, E., 2020. Alterations in Epithelial Cell Polarity During Endometrial Receptivity: A Systematic Review. Front. Endocrinol. 11. https://doi.org/10.3389/fendo.2020.596324

Whittaker, C.A., Hynes, R.O., 2002. Distribution and Evolution of von Willebrand/Integrin A Domains: Widely Dispersed Domains with Roles in Cell Adhesion and Elsewhere. Mol. Biol. Cell 13, 3369–3387. https://doi.org/10.1091/mbc.E02-05-0259

Whittle, A.J., Jiang, M., Peirce, V., Relat, J., Virtue, S., Ebinuma, H., Fukamachi, I., Yamaguchi, T., Takahashi, M., Murano, T., Tatsuno, I., Takeuchi, M., Nakaseko, C., Jin, W., Jin, Z., Campbell, M., Schneider, W.J., Vidal-Puig, A., Bujo, H., 2015. Soluble LR11/SorLA represses thermogenesis in adipose tissue and correlates with BMI in humans. Nat. Commun. 6, 8951. https://doi.org/10.1038/ncomms9951

Wick, M.R., Vitsky, J.L., Ritter, J.H., Swanson, P.E., Mills, S.E., 2005. Sporadic Medullary Carcinoma of the Colon: A Clinicopathologic Comparison With Nonhereditary Poorly

Differentiated Enteric-Type Adenocarcinoma and Neuroendocrine Colorectal Carcinoma. Am. J. Clin. Pathol. 123, 56–65. https://doi.org/10.1309/1VFJ1C3LP52A4FP8

Wiezlak, M., Diring, J., Abella, J., Mouilleron, S., Way, M., McDonald, N.Q., Treisman, R., 2012. G-actin regulates the shuttling and PP1 binding of the RPEL protein Phactr1 to control actomyosin assembly. J. Cell Sci. 125, 5860–5872. https://doi.org/10.1242/jcs.112078

Wilhelmsen, K., Litjens, S.H.M., Kuikman, I., Margadant, C., van Rheenen, J., Sonnenberg, A., 2007. Serine Phosphorylation of the Integrin β4 Subunit Is Necessary for Epidermal Growth Factor Receptor–induced Hemidesmosome Disruption. Mol. Biol. Cell 18, 3512–3522. https://doi.org/10.1091/mbc.e07-04-0306

Wilson Patricia D., 2004. Polycystic Kidney Disease. N. Engl. J. Med. 350, 151–164. https://doi.org/10.1056/NEJMra022161

Winklbauer, R., 2015. Cell adhesion strength from cortical tension – an integration of concepts. J. Cell Sci. 128, 3687–3693. https://doi.org/10.1242/jcs.174623

Winograd-Katz, S.E., Fässler, R., Geiger, B., Legate, K.R., 2014. The integrin adhesome: from genes and proteins to human disease. Nat. Rev. Mol. Cell Biol. 15, 273–288. https://doi.org/10.1038/nrm3769

Wishart, A.L., Conner, S.J., Guarin, J.R., Fatherree, J.P., Peng, Y., McGinn, R.A., Crews, R., Naber, S.P., Hunter, M., Greenberg, A.S., Oudin, M.J., 2020. Decellularized extracellular matrix scaffolds identify full-length collagen VI as a driver of breast cancer cell invasion in obesity and metastasis. Sci. Adv. 6, eabc3175. https://doi.org/10.1126/sciadv.abc3175

Wodarz, A., Näthke, I., 2007. Cell polarity in development and cancer. Nat. Cell Biol. 9, 1016–1024. https://doi.org/10.1038/ncb433

Woods, A.J., White, D.P., Caswell, P.T., Norman, J.C., 2004. PKD1/PKCμ promotes αvβ3 integrin recycling and delivery to nascent focal adhesions. EMBO J. 23, 2531–2543. https://doi.org/10.1038/sj.emboj.7600267

Wosen, J.E., Mukhopadhyay, D., Macaubas, C., Mellins, E.D., 2018. Epithelial MHC Class II Expression and Its Role in Antigen Presentation in the Gastrointestinal and Respiratory Tracts. Front. Immunol. 9. https://doi.org/10.3389/fimmu.2018.02144

Xia, S., Yim, E.K.F., Kanchanawong, P., 2019. Molecular Organization of Integrin-Based Adhesion Complexes in Mouse Embryonic Stem Cells. ACS Biomater. Sci. Eng. 5, 3828–3842. https://doi.org/10.1021/acsbiomaterials.8b01124

Yamada, S., Nelson, W.J., 2007. Localized zones of Rho and Rac activities drive initiation and expansion of epithelial cell–cell adhesion. J. Cell Biol. 178, 517–527. https://doi.org/10.1083/jcb.200701058

Yamazaki, D., Oikawa, T., Takenawa, T., 2007. Rac-WAVE-mediated actin reorganization is required for organization and maintenance of cell-cell adhesion. J. Cell Sci. 120, 86–100. https://doi.org/10.1242/jcs.03311

Yang, S., Yu, M., 2021. Role of Goblet Cells in Intestinal Barrier and Mucosal Immunity. J. Inflamm. Res. 14, 3171–3183. https://doi.org/10.2147/JIR.S318327

Ye, P., Wang, Y., Li, R., Chen, W., Wan, L., Cai, P., 2022. The HER family as therapeutic targets in colorectal cancer. Crit. Rev. Oncol. Hematol. 174, 103681. https://doi.org/10.1016/j.critrevonc.2022.103681

Yilmaz, A., Benvenisty, N., 2019. Defining Human Pluripotency. Cell Stem Cell 25, 9–22. https://doi.org/10.1016/j.stem.2019.06.010

Yin, H.L., Janmey, P.A., 2003. Phosphoinositide Regulation of the Actin Cytoskeleton. Annu. Rev. Physiol. 65, 761–789. https://doi.org/10.1146/annurev.physiol.65.092101.142517

Yonesaka, K., Zejnullahu, K., Okamoto, I., Satoh, T., Cappuzzo, F., Souglakos, J., Ercan, D., Rogers, A., Roncalli, M., Takeda, M., Fujisaka, Y., Philips, J., Shimizu, T., Maenishi, O., Cho, Y., Sun, J., Destro, A., Taira, K., Takeda, K., Okabe, T., Swanson, J., Itoh, H., Takada, M., Lifshits, E., Okuno, K., Engelman, J.A., Shivdasani, R.A., Nishio, K., Fukuoka, M., Varella-Garcia, M., Nakagawa, K., Jänne, P.A., 2011. Activation of ERBB2 Signaling Causes Resistance to the EGFR-Directed Therapeutic Antibody Cetuximab. Sci. Transl. Med. 3, 99ra86-99ra86. https://doi.org/10.1126/scitranslmed.3002442

Yu, W., Datta, A., Leroy, P., O'Brien, L.E., Mak, G., Jou, T.-S., Matlin, K.S., Mostov, K.E., Zegers, M.M.P., 2004. β1-Integrin Orients Epithelial Polarity via Rac1 and Laminin. Mol. Biol. Cell 16, 433–445. https://doi.org/10.1091/mbc.e04-05-0435

Yu, W., Shewan, A.M., Brakeman, P., Eastburn, D.J., Datta, A., Bryant, D.M., Fan, Q., Weiss, W.A., Zegers, M.M.P., Mostov, K.E., 2008. Involvement of RhoA, ROCK I and myosin II in inverted orientation of epithelial polarity. EMBO Rep. 9, 923–929. https://doi.org/10.1038/embor.2008.135

Zaidel-Bar, R., Ballestrem, C., Kam, Z., Geiger, B., 2003. Early molecular events in the assembly of matrix adhesions at the leading edge of migrating cells. J. Cell Sci. 116, 4605–4613. https://doi.org/10.1242/jcs.00792

Zaidel-Bar, R., Cohen, M., Addadi, L., Geiger, B., 2004. Hierarchical assembly of cell–matrix adhesion complexes. Biochem. Soc. Trans. 32, 416–420. https://doi.org/10.1042/bst0320416

Zaidel-Bar, R., Milo, R., Kam, Z., Geiger, B., 2007. A paxillin tyrosine phosphorylation switch regulates the assembly and form of cell-matrix adhesions. J. Cell Sci. 120, 137–148. https://doi.org/10.1242/jcs.03314

Zajac, O., Raingeaud, J., Libanje, F., Lefebvre, C., Sabino, D., Martins, I., Roy, P., Benatar, C., Canet-Jourdan, C., Azorin, P., Polrot, M., Gonin, P., Benbarche, S., Souquere, S., Pierron, G., Nowak, D., Bigot, L., Ducreux, M., Malka, D., Lobry, C., Scoazec, J.-Y., Eveno, C., Pocard, M., Perfettini, J.-L., Elias, D., Dartigues, P., Goéré, D., Jaulin, F., 2018. Tumour spheres with inverted polarity drive the formation of peritoneal metastases in patients with hypermethylated colorectal carcinomas. Nat. Cell Biol. 20, 296–306. https://doi.org/10.1038/s41556-017-0027-6

Zerial, M., McBride, H., 2001. Rab proteins as membrane organizers. Nat. Rev. Mol. Cell Biol. 2, 107–117. https://doi.org/10.1038/35052055

Zhang, K., Chen, J., 2012. The regulation of integrin function by divalent cations. Cell Adhes. Migr. 6, 20–29. https://doi.org/10.4161/cam.18702

Zhang, N., Zhang, H., Khan, L.A., Jafari, G., Eun, Y., Membreno, E., Gobel, V., 2023. The biosynthetic-secretory pathway, supplemented by recycling routes, determines epithelial membrane polarity. Sci. Adv. 9, eade4620. https://doi.org/10.1126/sciadv.ade4620

Zhao, B., Li, L., Lu, Q., Wang, L.H., Liu, C.-Y., Lei, Q., Guan, K.-L., 2011. Angiomotin is a novel Hippo pathway component that inhibits YAP oncoprotein. Genes Dev. 25, 51–63. https://doi.org/10.1101/gad.2000111

Zhao, S., Xu, J., Liu, S., Cui, K., Li, Z., Liu, N., 2019. Dppa3 in pluripotency maintenance of ES cells and early embryogenesis. J. Cell. Biochem. 120, 4794–4799. https://doi.org/10.1002/jcb.28063

Zhao, Y., Sato, Y., Isaji, T., Fukuda, T., Matsumoto, A., Miyoshi, E., Gu, J., Taniguchi, N., 2008. Branched N-glycans regulate the biological functions of integrins and cadherins. FEBS J. 275, 1939–1948. https://doi.org/10.1111/j.1742-4658.2008.06346.x

11 Original Publications

I- **Pasquier, N.**, Jaulin, F., & Peglion, F. (2024). **Inverted apicobasal polarity in health and disease.** *Journal of Cell Science*, *137*(5).

I- **Pasquier N**.*, Jaulin F., Péglion F. (2024). **Inverted apicobasal polarity in health and disease**. *Journal of Cell Science*, 137(5).

© 2024. Published by The Company of Biologists Ltd | Journal of Cell Science (2024) 137, jcs261659. doi:10.1242/jcs.261659

REVIEW

SPECIAL ISSUE: CELL AND TISSUE POLARITY

Inverted apicobasal polarity in health and disease

Nicolas Pasquier[1,2], Fanny Jaulin[1] and Florent Peglion[1,*]

ABSTRACT

Apicobasal epithelial polarity controls the functional properties of most organs. Thus, there has been extensive research on the molecular intricacies governing the establishment and maintenance of cell polarity. Whereas loss of apicobasal polarity is a well-documented phenomenon associated with multiple diseases, less is known regarding another type of apicobasal polarity alteration – the inversion of polarity. In this Review, we provide a unifying definition of inverted polarity and discuss multiple scenarios in mammalian systems and human health and disease in which apical and basolateral membrane domains are interchanged. This includes mammalian embryo implantation, monogenic diseases and dissemination of cancer cell clusters. For each example, the functional consequences of polarity inversion are assessed, revealing shared outcomes, including modifications in immune surveillance, altered drug sensitivity and changes in adhesions to neighboring cells. Finally, we highlight the molecular alterations associated with inverted apicobasal polarity and provide a molecular framework to connect these changes with the core cell polarity machinery and to explain roles of polarity inversion in health and disease. Based on the current state of the field, failure to respond to extracellular matrix (ECM) cues, increased cellular contractility and membrane trafficking defects are likely to account for most cases of inverted apicobasal polarity.

KEY WORDS: Apicobasal polarity, Extracellular matrix sensing, Membrane trafficking, Micropapillary cancer, Monogenic diseases, Embryo implantation

Introduction

Cell polarity orchestrates key biological processes such as cell division, cell migration and cell differentiation to ensure tissue morphogenesis and homeostasis, immune defense and wound healing. As such it is a hallmark of all living systems. Cell polarity refers to the asymmetric distribution of molecules and subcellular structures into two opposite poles; this asymmetry typically underlies specialized cellular functions (Nelson, 2003). In human development, the first polarized cells are observed at the 8-to-16-cell blastocyst stage (Gerri et al., 2020a; Nikas et al., 1996). Later, embryos develop to form organs and vasculature composed of a wide range of epithelial and endothelial cell types, all of which share a robust apicobasal polarity. These cells feature an apical pole, which contacts the external milieu or body cavities, and a basal pole, which interacts with the basement membrane and adjacent cells. Through regulation of cell–cell contact positioning, individual cells give rise to the tissue-scale polarity necessary for the barrier and exchange functions of epithelia.

The establishment and maintenance of epithelial apicobasal polarity involves dynamic spatiotemporal regulation of a core molecular machinery consisting of protein complexes that are highly conserved across the animal kingdom: the so-called polarity complexes (Fig. 1A) (Buckley and St Johnston, 2022; Peglion and Goehring, 2019; Rodriguez-Boulan and Macara, 2014). In brief, the PAR [Par6, atypical protein kinase C (aPKC) and Cdc42] and CRUMBS [Crumbs, Pals1 and Patj] complexes specify the apical domain, whereas the Scribble complex [Scrib, Lethal giant larvae (LgL) and Discs large (Dlg)] defines the basolateral domain, which is localized below Par3 (also known as PARD3)-enriched cell–cell junctions (Bilder and Perrimon, 2000; Hutterer et al., 2004; Kemphues et al., 1988; Plant et al., 2003; Tanentzapf and Tepass, 2003; Wodarz et al., 1995, 2000). The core polarity machinery, the proteins of which come in multiple forms in mammals, also includes unpolarized cytoplasmic polarity proteins, such as liver kinase B1 (LKB1, also known as STK11; PAR-4 in *Caenorhabditis elegans*) and 14.3.3ζ (encoded by *YWHAZ*; PAR-5 in *C. elegans*) (Baas et al., 2004; Hurd et al., 2003; Winter et al., 2012). Altogether, this hub of protein complexes is able to both read and integrate external polarizing cues to induce self-polarization (Lang and Munro, 2017) and to maintain membrane domain identities by excluding apical complexes from the basolateral plasma membrane and vice versa. For more details on the molecular interaction of the polarity complexes required to build and maintain apicobasal polarity, we refer the reader to several excellent reviews (Buckley and St Johnston, 2022; Martin et al., 2021; Riga et al., 2020; St Johnston, 2018; Stephens et al., 2018). Once activated and in place, the polarity machinery functionally polarizes the entire cell by controlling the spatial organization of the cytoskeleton networks, the asymmetric lipid composition of the plasma membrane and the orientation of membrane traffic, which further reinforces the initial cell asymmetry (Buckley and St Johnston, 2022).

The alteration of apicobasal polarity is associated with numerous pathological conditions, including cancer, autosomal dominant polycystic kidney disease, cystic fibrosis, asthma and viral infections (Tilston-Lunel and Varelas, 2023; Wilson, 1997). Apicobasal polarity perturbations classically include the partial or complete loss of polarity, the extent of which usually correlates with the progression of the disease (Halaoui et al., 2017). In some instances, the polarity alteration might also arise from the inversion of the apical and basolateral domains in cells that maintain an otherwise perfectly polarized state (Box 1). Whereas extensive literature has reviewed how loss of apicobasal polarity contributes to disease progression (Ebnet, 2015), very little is known about the impact of inverted polarity. Orientation of apicobasal polarity relies on the interaction between the core polarity machinery and both the cell–extracellular matrix (ECM) and cell–cell contacts. Changes affecting the biochemical and biomechanical nature of cues from

[1]Collective Invasion Team, Inserm U-1279, Gustave Roussy, Villejuif F-94805, France. [2]Cell Adhesion and Cancer lab, University of Turku, FI-20520 Turku, Finland.

*Author for correspondence (florent.peglion@gustaveroussy.fr)

F.J., 0000-0002-5110-1800; F.P., 0000-0002-9364-9444

Journal of Cell Science (2024) 137, jcs261659. doi:10.1242/jcs.261659

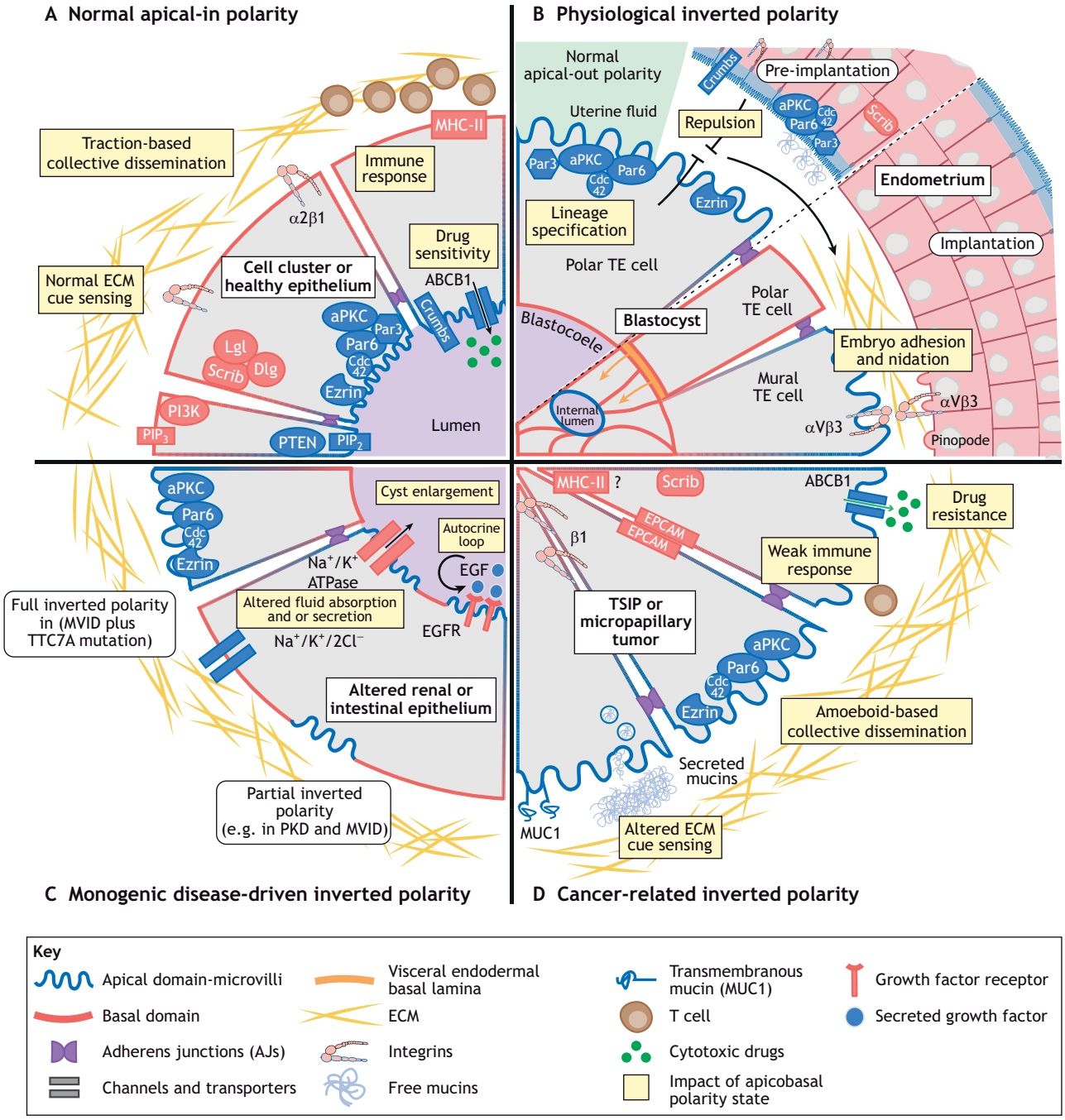

Fig. 1. Hallmarks and consequences of inverted apicobasal polarity in health and disease. (A) Normal epithelial polarity is regulated by the asymmetric localization of mutually antagonistic complexes. The Par and the Crumbs complexes define the apical pole which is enriched in PIP_2, PTEN and ezrin (proteins marked in blue). Below AJs, the Scribble complex defines the basolateral domain, which is enriched in PIP_3 and PI3K (proteins marked in red). ECM sensing through integrins controls the orientation of apicobasal polarity and ensures traction-based collective migration. Basal localization of MHC-II is thought to promote immune clearance of damaged cells by permitting T cell recruitment. Apical localization of the multidrug resistance transporter ABCB1 allows drugs to persist in lumens of epithelia. PIP_3, phosphatidylinositol 3,4,5-phosphate. (B) The pre-implantation blastula displays apical-out polarity, which prevents adhesion to the uterine wall due to apical–apical repulsion. During the menstrual cycle, to permit successful embryo nidation, apical determinants in the endometrium disappear from the lumen-facing membranes while integrins and pinopodes appear. In parallel, polar trophectoderm (TE) cells invert their polarity in response to emergence of the endodermal basal lamina and mural TE cells express integrins at the periphery of the blastula to promote implantation. (C) MVID enterocytes show partial inverted polarity of microvilli structures. MVID with an additional mutation in *TTC7A* results in fully inverted polarity in these cells. In PKD renal tubules, inverted polarity of ion channels and EGFR contribute to the growth of cysts via altered fluid absorption and secretion. (D) TSIPs arise from micropapillary and mucinous carcinoma. The absence of integrins and presence of mucins at the TSIP periphery prevent cell–ECM interactions resulting in tissue invasion via the collective amoeboid mode of migration. The inverted polarity of ABCB1 enhances cytotoxic drug resistance whereas basolateral localization of MHC-II could limit T cell infiltration and increase immune escape.

Journal of Cell Science (2024) 137, jcs261659. doi:10.1242/jcs.261659

Table 1. Examples of inverted apicobasal polarity in disease

Polarity inversion	Case	Cause of inversion	Molecular markers	Impact	
Full	Cancer structures with inverted polarity and tumor spheres with inverted polarity (TSIPs)	Mutations in IDH2 and PI3KCA in breast solid papillary carcinoma Mutations in SMAD and altered TGFβ signaling in mucinous colorectal TSIPs.	Tumor glands with an apical-out inverted polarity from individuals with cancer Apical glycoprotein MUC1 on the outside of the gland, and basolateral determinant EPCAM on the inside of the gland Apical localization of nuclei and Golgi markers TSIPs embedded in collagen matrices marked by the presence of microvilli, Par complex proteins, ezrin and occludin on the outside of and Scrib, EPCAM and α-catenin on the inside	Increased resistance to treatment Increased metastatic progression Invasion via a collective amoeboid mode of migration Enhanced immune escape potentially via decreased infiltration by cytotoxic T cells (seen in micropapillary tumors with inverted polarity)	Chiang et al., 2016, Canet-Jourdan et al., 2022, Verras et al., 2022, Al-Obaidy et al., 2019; Kim et al., 2020., Ashley et al., 2019, Zajac et al., 2018, Pagès et al., 2022, Guo et al., 2008
Full	MVID+*TTC7A* mutation	Mutations in *MYO5B* and *TTC7A*	Fully inverted apicobasal polarity in patient established intestinal epithelia Apical markers (microvilli, CDC42, PAR6, aPKCι and ezrin) at ECM-abutting membrane Disappearance of apical markers from the lumen-facing membranes	Unknown	Michaux et al., 2016
Partial	MVID	Mutations in *MYO5B*, *STX3*, *STXBP2*	Disappearance of apical proteins (Cdc42, Par6, aPKCi and ezrin) from lumen-facing membrane *in vivo* Apical localization of the basolateral Na^+/K^+-ATPase ion channel in enterocytes *in vivo* in MYO5B-knockout mouse model Apical-out inverted polarity in Myo5b-depleted CaCo2 cell clusters embedded in collagen. Basolateral targeting of apical cargos in STXBP2 mutant epithelial cells	Altered fluid absorption through intestinal epithelium and gradual loss of apical microvilli	Müller et al., 2008; Vogel et al., 2017; Wiegerinck et al., 2014; Michaux et al., 2016; Schneeberger et al., 2015; Riento et al., 2000; Cutz et al., 1989
Partial	PKD (Polycystic Kidney Disease)	Mutations in *PKD1* and *PKD2*	Apical localization of EGFR Apical localization of Na^+/K^+-ATPase and basolateral localization of $Na^+/K^+/2Cl^-$ symporter *In vitro* PKD cysts embedded in collagen with inverted apical-out polarity as marked by the presence primary cilia of ZO-1 on the ECM-abutting membrane	Cystic enlargement of renal tubules leading to increased fluid secretion and renal failure Inverted localization of EGFR and normally polarized secretion of EGF generate an autocrine loop that fuels cell proliferation and cyst enlargement	Wilson, 2004; Du and Wilson, 1995; Wilson et al., 1991; Li et al., 2022; Wilson, 2011
Partial	MIA-CID	Mutations in *TTC7A*	ROCK-dependent full apical-out inverted polarity of patient-derived gut organoids embedded in collagen	Alterations in epithelial gut barrier with pseudostratified cell structures High level of apoptosis Low number of apical villi Altered lymphocyte homeostasis	Bigorgne et al., 2014
Partial	Dent's disease	Mutations in *CLCN5*	Basolateral redistribution of the apical H^+-ATPase	Low-molecular-mass proteinuria, hypercalciuria, nephrolithiasis, nephrocalcinosis, leading to renal failure	Moulin et al., 2003

Continued

Journal of Cell Science

Table 1. Continued

Polarity inversion	Case	Cause of inversion	Molecular markers	Impact	
Partial	Turku's mutation-associated familial hypercholesterolemia	LDLR mutation G823D	Inverted LDLR localization to the apical surface of hepatocytes	Failure of hepatocytes to access and internalize LDL leading to an increased concentration of LDL in the blood	Koivisto et al., 2001
Partial	Polarity inversion as an immune system trigger	Chronic liver diseases	Basolateral enrichment of ICAM-1	Inverted polarity of ICAM-1 causes increased recruitment and adhesion of T-lymphocytes to hepatocytes to enhance immune clearance of damaged cells	Reglero-Real et al., 2014
Partial	Pathogen-triggered polarity inversion	*P. aeruginosa* infection	Local apical polarity inversion at host-pathogen contact sites Formation of actin-rich protrusions enriched in basolateral markers [PI3K and its lipid product PIP_3, β1-integrin, E-cadherin, β-catenin, p58 and the Na^+/K^+-ATPase)	Formation of a basolateral niche at host-pathogen contact sites that favors *P. aeruginosa* entry Colocalization of apical Par complex with PI3K and PiP3 triggers the formation of Rac1-dependent actin-rich protrusions to activate a local NFκB-dependent immune response	Kierbel et al., 2007; Tran et al., 2014
Partial	Pathogen-triggered polarity inversion	*Neisseria meningitidis*	Local apical polarity inversion at host-pathogen contact sites Formation of filopodia-like membrane extensions enriched in basolateral AJ components and apical Par proteins	Destabilization of the endothelium via intercellular gaps caused by weakened adherens junctions. Increased pathogen crossing of the endothelial barrier	Coureuil et al., 2009

these elements and alteration of the systems that respond to these cues can both lead to abnormal orientation of the apicobasal axis. In this Review, we present a uniform definition of inverted apicobasal polarity based on multiple examples found in physiological and pathological situations, explore its impact on cell and tissue functions and examine the potential origins of inverted polarity from general cell-autonomous or non-cell-autonomous molecular pathways.

Inverted polarity in cancer

Apicobasal polarity dictates the polarized functioning of epithelial cells, and loss of apicobasal polarity has long been associated with tumor initiation and invasive progression of carcinoma (cancer deriving from epithelial tissues; Macara and McCaffrey, 2013; Wodarz and Näthke, 2007). Many studies have highlighted that unpolarized epithelia are more prone to carcinoma induction and invasion compared to fully polarized epithelia (reviewed by Lee and Vasioukhin, 2008; Peglion and Etienne-Manneville, 2024). However, histological analysis of tumor specimens has revealed that invasive cancers like colorectal adenocarcinomas display clearly differentiated morphologies with intact polarized epithelial structures that delineate internal luminal cavities within the neoplastic glands (Libanje et al., 2019). Whether the presence of inverted apicobasal polarity in such structures bears consequences for carcinoma pathophysiology is an increasingly explored hypothesis (Peglion and Etienne-Manneville, 2024).

Neoplastic epithelial glands in a subset of highly invasive cancers called micropapillary carcinoma exhibit fully inverted apicobasal polarity (Verras et al., 2022). This type of cancer is diagnosed upon detection of an apical-out polarity pattern. In these tumors, the apical transmembrane glycoprotein MUC1 [also known as epithelial membrane antigen (EMA)] is found at the tumor periphery, and the basolateral protein epithelial cell adhesion molecule (EPCAM) is found on the inward-facing membranes (Fig. 1D; Table 1). In addition to being well-described in breast and lung carcinomas (Adams et al., 2004; Hirakawa et al., 2022; Luna-Moré et al., 1994; Nassar et al., 2004; Siriaunkgul and Tavassoli, 1993), these inverted structures are also found in colorectal (Verdú et al., 2011), cervical (Stewart et al., 2018) and thyroid carcinomas (Asioli et al., 2013). Furthermore, epithelial structures with inversely polarized nuclei are typically seen in the breast solid papillary carcinoma with reverse polarity (SPCRP) tumor subtype (Chiang et al., 2016). Apically localized nuclei in single-layered eosinophilic cells is a feature also used to diagnose papillary renal neoplasm with reverse polarity (PRNRP), a type of kidney cancer with typically good prognoses (Al-Obaidy et al., 2019; Al-Obaidy et al., 2020; Kim et al., 2020).

In addition, cancer clusters with apical-out polarity are often found in non-adhesive tissue interfaces (Box 1). Examples include clusters in suspension in peritoneal or pleural effusions (Ritch and Telleria, 2022; Zajac et al., 2018), in the lumen of lymphatic vessels, in lymph nodes (Mohammed et al., 2019; de Boer et al., 2010) and in pools of mucins (Sun et al., 2020). These clusters were originally called tumor spheres with inverted polarity (TSIP), even though apical-out polarity is typically a normal feature of cell clusters in suspension. For some individuals with cancer, however, clusters retrieved from

Journal of Cell Science (2024) 137, jcs261659. doi:10.1242/jcs.261659

Box 1. Definitions of inverted polarity

Normal polarity

Normal polarity in established epithelial tissues is defined by an apical domain facing the lumen and a basolateral domain contacting the neighboring cells and the basal membrane (bottom left of figure). In cell clusters, polarity is influenced by the extracellular environment. Cell clusters embedded in physiological matrices normally polarize with the apical membranes facing the interior lumen and the outward-facing membrane abutting the ECM (apical-in, top left of figure) (Debnath and Brugge, 2005; Mostov et al., 2003), whereas cell clusters found in extracellular fluid or interstitial spaces normally establish an apical domain on the outward-facing membranes with the basolateral domains facing the interior (apical-out, top center of figure).

Inverted polarity

Inverted polarity occurs when some or all components of the apical and basolateral domains are reversed while the overall polarity axis remains intact. This applies to both established epithelial tissues and cell clusters. The term 'reverse polarity' is also used by clinicians. Inverted polarity is almost always pathological and the only physiological example is found during mammalian embryo implantation (Sutherland et al., 1993; Whitby et al., 2018).

Fully inverted polarity

Full inversion of apicobasal polarity can occur when polarity cues or the response of the cell to the cues are disrupted. In epithelial cells, this means the outward-facing ECM-adjacent membranes are depleted of basolateral proteins and enriched in apical markers such as microvilli and apical polarity proteins (bottom right of figure). This is observed in cancerous aggregates called TSIP (Canet-Jourdan et al., 2022; Zajac et al., 2018), and in established epithelia of individuals with MVID with additional *TTC7A* gene alteration (Michaux et al., 2016). When embedded in physiological matrices, organoids derived from individuals affected by several monogenic diseases also show fully inverted polarity (top right of figure) (Bigorgne et al., 2014; Li et al., 2022; Michaux et al., 2016). Depending on the epithelial cell identity, cavities can sometimes be found within inverted spheroids (not shown here).

Partially inverted polarity

In partially inverted polarity, only a subset of apical or basolateral molecules are mispolarized to the opposing domain, whereas the core structural and molecular features of each domain remain intact (bottom center of figure).

Polarity inversion

The process by which apicobasal polarity becomes inverted.

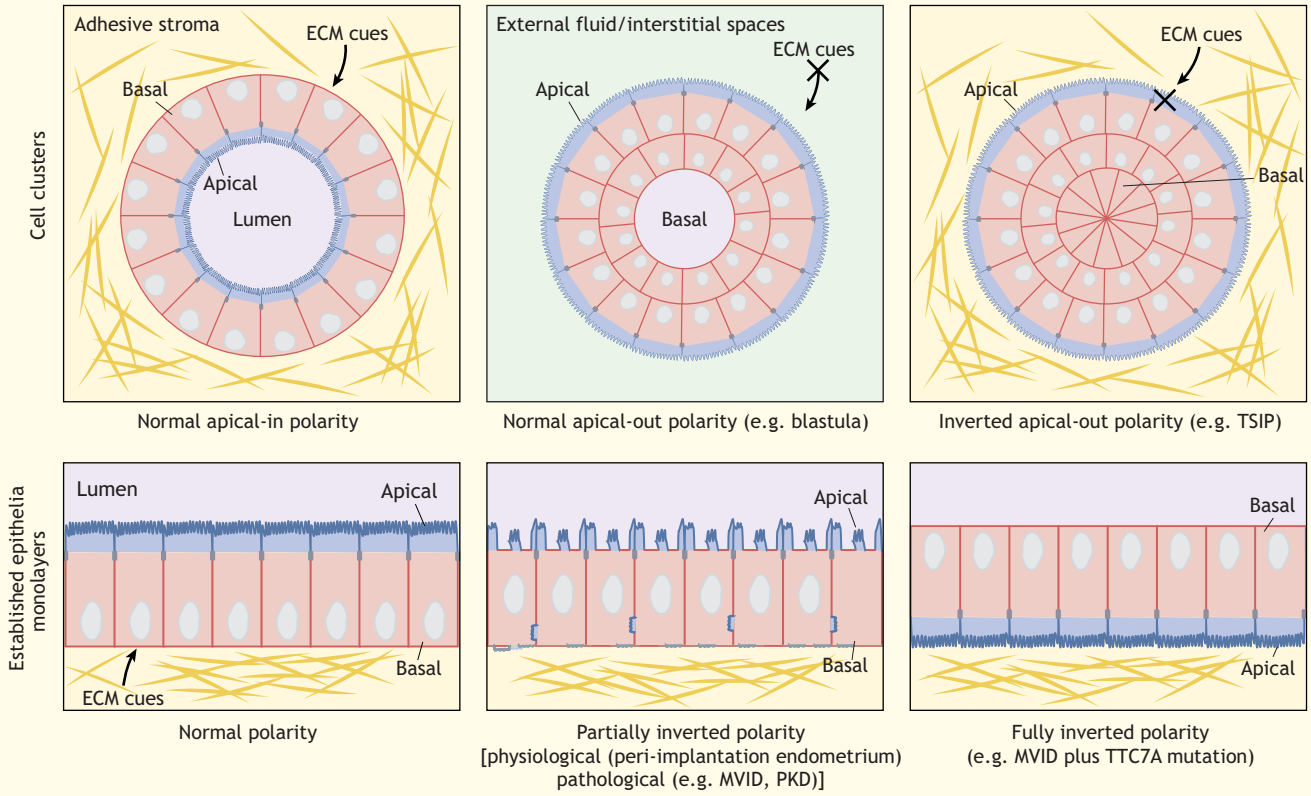

non-adhesive substrates maintain their apical-out polarity even when placed in 3D physiological matrices, suggesting a genuine inverted apicobasal polarity phenotype (Canet-Jourdan et al., 2022; Okuyama et al., 2016; Onuma et al., 2021; Zajac et al., 2018).

The exact role played by apicobasal polarity inversion in cancer initiation and progression is still poorly understood. Functional studies have revealed that variants in *IDH2* and *PIK3CA* oncogenes in the breast SPCRP tumor subtype are sufficient to elicit the inverted polarity phenotype in healthy breast organoids (Chiang et al., 2016). These data suggest apicobasal polarity inversion could directly contribute to cancer initiation and progression.

Roles in cancer invasion

Polarity-inverted micropapillary carcinomas are highly infiltrative cancers with a high incidence of lymph node metastasis (Kuroda et al., 2004). More recently, our laboratory has identified TSIPs as the malignant intermediates in the metastatic spread of micropapillary and mucinous colorectal cancers (Zajac et al., 2018).

That study demonstrated that TSIPs are migratory neoplastic structures on their way to colonizing secondary organs. Identified in the peritoneal fluids of individuals with highly metastatic disease, TSIPs are defined by having an apical-out topology along the entire course of their metastatic spread in fluids and tissues, as seen during peritoneal invasion *ex vivo* and in a mouse colorectal liver metastasis model (Zajac et al., 2018). They are unable to sense and strongly adhere to the ECM due to the absence of integrins on their outward-facing membranes, and TSIPs do not generate actin-based protrusions. This raises the question of how TSIPs collectively migrate and disseminate if they cannot perform traction-based migration (Fig. 1A,D). TSIPs were found to propagate by self-generating smaller cell clusters that bud out from the mother TSIP (Zajac et al., 2018). Most interestingly, a recent study suggests that TSIPs can actively invade the matrix using a collective amoeboid mode of migration (Pagès et al., 2022). Using non-adhesive microchannels, Pagès et al. revealed that the entire TSIP propels itself in a confined environment in a similar fashion to single immune cells and amoeba. Collective amoeboid migration relies both on friction forces generated by the fluctuating deformation (‘jiggling’) of the peripheral cells and the polarized enrichment of a contractile supracellular cortical actomyosin cap spanning multiple cells at the rear of the cluster (Pagès et al., 2022). The ability of TSIPs, and more globally of tumor clusters, which both lack the specific adhesion receptors required to interact with the surrounding ECM, to keep migrating in this atypical fashion likely fuels tumor invasion. Even partial apicobasal polarity inversion following β1-integrin depletion is sufficient to trigger long-term invasion of Madin–Darby canine kidney (MDCK) spheroids into Matrigel® in a collective amoeboid fashion (Bryant et al., 2014), reinforcing that the absence of ECM sensing does not prevent cell clusters from invading tissues. Whether the hypothesis that pro-metastatic ‘all-terrain’ collective amoeboid migration holds true *in vivo* remains to be addressed.

Cancer growth and treatment resistance

Inverted apicobasal polarity also affects tumor growth and treatment resistance. Primary colorectal cancer organoids with an inverted apical-out phenotype better survive chemotherapeutic treatment compared to normally polarized apical-in organoids (Canet-Jourdan et al., 2022). This could be due to a reduced proliferation rate in TSIPs compared to apical-in organoids, making them less susceptible to anti-mitotic drugs (Canet-Jourdan et al., 2022). Another explanation could be that TSIPs are better protected structurally against cytotoxic drugs. Normally polarized apical-in cancer clusters display apically located multidrug resistance transporters, such as the efflux transporter ATP binding cassette subfamily B member 1 (ABCB1), on the lumen-facing membranes. ABCB1 drug substrates thus accumulate in the cluster lumen, which might prolong their cytotoxic effects (Ashley et al., 2019) (Fig. 1A). In TSIPs, ABCB1 is expressed on the outward-facing membranes, and drug substrates are therefore excluded more easily (Ashley et al., 2019) (Fig. 1D).

Cancer immune escape

Epithelial cells act as non-professional antigen-presenting cells and participate in immune surveillance and response (Wosen et al., 2018). Antigen-presenting membrane receptors, such as the major histocompatibility complex class II (MHC-II) receptors, display a polarized location in intestinal and lung epithelial cells. Multiple *in vitro* and *in vivo* human studies have revealed that MHC-II proteins such as HLA-DR and HLA-DM are restricted to the basolateral surfaces of intestinal epithelial cells (Hirata et al., 1986; Sarles et al., 1987; Wosen et al., 2019). Their polarized localization enables activation, modulation or maintenance of CD4+ T cells (Hershberg et al., 1998), whose role in anti-tumor immunity is increasingly being recognized (Speiser et al., 2023). Alteration of MHC-II signaling plays a central role in immune evasion during cancer development and is regarded to be a causal factor for immunotherapy failure (Axelrod et al., 2019). Owing to their inverted apical-out, basal-in polarized state, mucinous and micropapillary carcinomas are expected to be depleted of MHC-II molecules on their outward-facing membranes, thus reducing accessibility for resident T-cells. Whether the altered presentation of MHC-II proteins contributes to immune escape in mucinous and micropapillary carcinoma remains a hypothesis worth addressing. Interestingly, invasive micropapillary breast carcinomas are less infiltrated by cytotoxic T cells compared to normally polarized medullary breast carcinomas (Guo et al., 2008) (Fig. 1D).

Toll-like receptors (TLRs) are another family of antigen recognition receptors involved in triggering immune responses, mostly during pathogen infection. TLRs also impact cancer progression, either positively or negatively depending on the identity of the TLR. For example, TLR-3 stimulation triggers apoptosis and directly kills human cancer cells (Salaun et al., 2006). In human intestinal epithelial cells, TLR-3 localization is restricted to the basolateral domain, enabling an asymmetric immune response in which apical commensal bacteria are tolerated while crossing of the epithelium and basolateral intrusion of pathogens is actively guarded against (Stanifer et al., 2020). A tempting untested hypothesis is that the absence of TLR-3 on the outward-facing apical membrane of TSIPs in intestinal tumors could alter the anti-tumoral activity of TLR-3 and enhance tumor immune escape.

Apicobasal polarity inversion is thus a multifaceted feature of invasive cancers. Although to what extent inverted polarity plays a role in tumor initiation remains unknown, accumulating evidence suggests it is involved in cancer progression by promoting all-terrain migration, treatment resistance and immune escape. Further work is needed to confirm untested hypotheses and reveal the molecular processes explaining how inverted polarity drives aggressive cancers.

Inverted polarity in genetic diseases

Inverted polarity structures also occur in epithelial tissues of many organs impacted by monogenic diseases. One of the clearest examples is the microvillus inclusion disease (MVID), a genetic disorder affecting intestinal absorption, which often causes fatal watery diarrhea. MVID is characterized by a gradual loss of apical microvilli and the formation of microvilli inclusions inside enterocytes (Cutz et al., 1989). In 90% of cases, MVID is caused by gene variants of Myosin Vb (*MYO5B*), with variants of syntaxin-3 (*STX3*) and its binding partner syntaxin binding protein 2 (*STXBP2*) are responsible for the remaining 10% of cases (Müller et al., 2008; Vogel et al., 2017; Wiegerinck et al., 2014). Depletion of Myo5B in an MVID mouse model causes a partially inverted polarity phenotype with total loss of apical microvilli, an inverted apical localization of the Na^+-K^+ pump (Na^+/K^+-ATPase) and basolateral presence of E-cadherin in enterocytes (Schneeberger et al., 2015) (Fig. 1C, Table 1). Interestingly, two individuals with MVID that have an additional mutation in the tetratricopeptide repeat domain 7A (*TTC7A*) gene of unknown function display complete inversion of apical polarity determinants, such as microvilli, Cdc42, Par6, aPKCι and ezrin in the intestinal epithelium (Michaux et al., 2016) (Fig. 1C, Table 1).

A rare bowel obstruction disease called multiple intestinal atresia associated with combined immunodeficiency (MIA-CID) is linked to variants in the same *TTC7A* gene. Studies on intestinal organoids derived from cells from individuals with MIA-CID have revealed that TTC7A deficiency causes a Rho-associated protein kinase (ROCK; herein referring to both ROCK1 and ROCK2)-dependent full inversion of apicobasal polarity (Bigorgne et al., 2014). Whether the inversion of polarity is involved in the defects in cell growth, intestinal epithelial differentiation and immune cell homeostasis remains to be investigated.

Partially inverted apicobasal polarity is also observed in the ciliated kidney epithelium of individuals with polycystic kidney disease (PKD). In PKD, normal renal tubules are replaced by fluid-filled cysts which dissociate from the nephron, expand and proliferate, leading to end-stage renal disease (Menezes and Germino, 2019; Simons and Walz, 2006). PKD is mainly caused by autosomal dominant (AD) mutations in one of the two genes, *PKD1* and *PKD2*, encoding for ubiquitously expressed polycystin-1 (PC1), a transmembrane protein, and polycystin-2 (PC2), an ion channel (Wilson, 2004). How these mutations initiate the polycystic phenotype remains unresolved (Ong, 2017). Nevertheless, a consensus exists on the crucial role played by the inversion of apicobasal polarity in tubular renal epithelial cells. Many basolateral proteins, such as the epidermal growth factor receptors (EGFRs), are enriched at the apical luminal pole in epithelial cells that line PKD cysts (Wilson, 2011). The presence of EGFR together with its ligand EGF, which is normally secreted from the apical luminal pole, generates an autocrine loop that fuels cell proliferation and cyst enlargement (Du and Wilson, 1995). In PKD cysts, Na^+/K^+-ATPase and the $Na^+/K^+/2Cl^-$ symporter switch their polarity, which is thought to lead to increased fluid secretion into the cyst lumen and enlargement of the cysts (Wilson et al., 1991). Recently, analysis of results from a PKD-kidney-on-chip model, in which cysts that detached from peripheral tubular epithelium embedded in collagen present a fully inverted apical-out phenotype, has suggested an alternative mechanism (Li et al., 2022). The authors propose that the inverted polarity fuels absorption of glucose and fluids from the cyst periphery, leading to increased internal pressure, epithelium stretching and cyst expansion (Fig. 1C). Evidence suggests that a partial apicobasal polarity inversion involving a restricted number of polarized proteins could also lead to pathological conditions in several other monogenic disease (see Table 1).

Inverted polarity in immune response and pathogen defense

Specific instances of inversion of apicobasal cell polarity are required in mammalian organisms to regulate epithelial homeostasis and respond to pathogen infection. Next, we will discuss several examples of inverted polarity found to be involved in inflammation and the immune responses to pathogens.

The partial polarity inversion of damaged and dysfunctional epithelia can act as a signal for unhealthy cells to be cleared by the immune system. Healthy hepatocytes segregate intracellular adhesion molecule 1 (ICAM-1) at the apical pole, which faces the bile caniculi lumen (Reglero-Real et al., 2014). Individuals with chronic liver disease often display inverted ICAM-1 localization in basally located microvilli-like structures, a phenotype that has been reproduced experimentally by treatment with pro-inflammatory tumor necrosis factor α (TNFα; also known as TNF). In this study, the inverted polarity of ICAM-1 increased the recruitment and adhesion of T-lymphocytes to hepatocytes (Reglero-Real et al., 2014). Here, the apicobasal polarity inversion is thus harnessed to favor adhesion of leukocytes and promote faster clearance of the damaged cells displaying inverted polarity.

Changes in apicobasal intestinal epithelial and endothelial polarity are also observed during early stages of pathogen infection (Tapia et al., 2017). In some instances, the plasma membrane that makes direct contact with bacterial aggregates loses its apical identity and expresses basolateral markers. The most striking example of such polarity inversion has been observed during often-lethal infection by *Pseudomonas aeruginosa* bacteria. Using polarized monolayers of MDCK cells, Kierbel et al. found *de novo* formation of cell protrusions around bacterial clusters at the apical pole of the cells. These protrusions are devoid of the apical sialomucin gp135 (also known as podocalyxin) and enriched in basolateral determinants, including phosphoinositide 3-kinase (PI3K) and its lipid product phosphatidylinositol (3,4,5)-trisphosphate (PIP_3), β1-integrin, E-cadherin, β-catenin and p58 (also known as the Na^+/K^+ ATPase transporting subunit β, ATP1B1) Na^+/K^+-ATPase (Kierbel et al., 2007). *P. aeruginosa* exploits the ability of PIP_3 to convert apical membranes to a basolateral identity in order to create a more favorable nesting microenvironment by activating PI3K (Gassama-Diagne et al., 2006; Kierbel et al., 2005). Intriguingly, the Par3–Par6–aPKC apical polarity complex remains present in the actin-rich protrusions surrounding bacterial aggregates. The presence of this complex is thought to locally activate Rac1, which, together with PI3K, induces NF-κB activity and downstream immune response signaling (Tran et al., 2014). Although this spatially restricted inversion of polarity at the host–pathogen contact site enables entry of *P. aeruginosa* into host cells, it could also thus act as a 'danger signal' for the host organism to hasten detection of the infected epithelial cell.

Local inversions of polarity are also sometimes used by pathogens to alter endothelial barrier integrity and fuel aggressive infection. Aggregates of *Neisseria meningitidis* bacteria, the causative agent of cerebrospinal meningitis, induce plasma membrane remodeling at host–pathogen contact sites. Newly formed filopodia-like membrane extensions are enriched in both basolateral adherens junction (AJ) components and apical Par proteins (Coureuil et al., 2009). Here, unlike what occurs upon infection with *P. aeruginosa*, the presence of ectopic basolateral cell–cell adhesions at the apical pole destabilizes the endothelium, opens intercellular gaps and promotes crossing of the endothelial barrier by *N. meningitidis* (Coureuil et al., 2009). Thus, inverted polarity plays a role in tissue homeostasis and integrity, but this feature can also be maliciously hijacked to initiate and/or fuel disease progression.

Inverted polarity in development

Outside the context of disease, inversion of apicobasal cell polarity is a biological process used at key moments of mammalian development. Early embryonic development and nidation (implantation of the embryo into the uterine wall) are some of the clearest examples of physiologically relevant inversion of apicobasal polarity (see Box 2 and Box 3). From the eight-cell stage in mice and humans, the blastomeres of the embryo start to compact and develop an apical-out polarity marked by the asymmetrical localization of microvilli, actin, actin-binding proteins and the Par3–Par6–aPKC complex on the outward-facing membranes of the blastocyst (Ducibella et al., 1977; Lehtonen and Badley, 1980; Nikas et al., 1996; Plusa et al., 2005; Reeve and Ziomek, 1981; Vinot et al., 2005), and the localization of basolateral proteins Scrib and Llg1 at cell–cell contacts (Hirate et al., 2013). The polarized blastomeres (or polar cells) retain this apical pole during successive divisions and later differentiate to form the trophectoderm (TE), the first apicobasally polarized sheet

Journal of Cell Science (2024) 137, jcs261659. doi:10.1242/jcs.261659

Box 2. Apicobasal polarity in the mammalian embryo

Specification of polar and apolar cells within the embryo is key to defining and maintaining the overall polarity axis. Cell localization depends on differences in cortical tension, cell signaling and modes of cell division. During embryo compaction, cells exhibiting higher cortical tension are pushed inwards and will not polarize, whereas cells with lower cortical tension develop the apical domain on the outside of the embryo (Maître et al., 2016; Samarage et al., 2015). Asymmetric division leading to differential inheritance of the apical domain increases the pool of apolar cells and directs their positioning inside the embryo, while maintaining polar cells on the outside (Maître et al., 2016). Symmetric division is also crucial to extending the apical domain at the embryo periphery as the blastocyst grows (Niwayama et al., 2019). Emergence of an aPKC-rich apical domain facing the external milieu is suggested to be key to controlling early lineage specification by orchestrating cell positioning, cell contractility and the orientation of cell division (Gerri et al., 2020b; Zhang and Hiiragi, 2018). The crosstalk between the Par complex and the Hippo pathway is crucial for coupling the structural and functional polarization of the embryo. The core Hippo pathway is a kinase cascade leading to the cytoplasmic sequestration of the YAP/TAZ transcription factors to control cell proliferation, organ size and pluripotency of embryonic stem cells (Badouel and McNeill, 2011). In polar cells, Par6b and aPKC suppress Hippo signaling thereby enhancing the expression of the YAP downstream target gene *Cdx2,* a marker of trophectoderm (TE) cells, which acts as an inhibitor of Nanog and Oct4 (also known as POU5F1), two stemness markers. This molecular cascade explains how cell polarity restricts the activation of stemness markers in the apolar cells of the inner cell mass (ICM) (Anani et al., 2014; Hirate et al., 2013; Mo et al., 2014). Further into blastocyst development, some internal ICM cells mature, start expressing polarity genes, self-organize on the periphery of the ICM and later form the primitive endoderm. The remaining non-polarized cells become the epiblast or embryo per se (Zhu and Zernicka-Goetz, 2020).

of cells, which will become the placenta (Box 2) (Johnson and Ziomek, 1981; Suwińska et al., 2008). During the pre-implantation period, the embryo is in contact with the external milieu and the presence of an apical domain on its outer surface reflects a normal apical-out polarity state (see Box 1). During implantation, the apical-out polarized TE cells need to adhere to the luminal epithelial cells of the endometrium for successful nidation of the embryo (Thie et al., 1996). As implantation proceeds, both the embryo and the endometrium modify their polarity to prevent polar repulsion caused by apical–apical sensing (Fig. 1B). On one side of the embryo, a pool of polar TE cells inverts their apicobasal polarity at a tissue-scale level. This transition is caused by rapid cell proliferation and expansion of the visceral endodermal basal lamina, whose polarizing cues trigger the generation of an internal apical domain within the embryo and the disappearance of apical markers from the outward-facing TE cell membranes (Ozguldez et al., 2023) (Fig. 1B). On the opposite side of the embryo, the mural trophoblast cells directly contacting the uterine wall maintain their apical domain on the outward-facing surface but express and display an inverted localization of αVβ3 integrins, which engage with laminin ligands upregulated in the uterine environment, to promote trophoblast attachment (Sutherland et al., 1993) (Fig. 1B). In parallel, the receptivity of the endometrium is controlled by hormone-dependent changes in apicobasal polarity of the luminal epithelium (Whitby et al., 2020). Apical enrichment of Par proteins, Crumbs and mucins, and basolateral enrichment of Scrib progressively disappear during the menstrual cycle (Whitby et al., 2018). Furthermore, instead of forming microvilli, the apical membrane of endometrial cells reorganizes into smooth bulbous projections called pinopodes, the abundance of which peaks at the end of the secretory phase, when the endometrium is receptive to implantation (Quinn et al., 2020). Concomitantly, together with the apical secretion of the αVβ3 integrin ligand osteopontin, which is crucial for blastocyst implantation (Illera et al., 2000), basolateral adhesive molecules, such as αVβ3 integrin itself, switch their polarized localization and become enriched in the lumen-facing apical domain (Aplin et al., 1996; Lessey, 2002) (Fig. 1B). Here, hormone-dependent partial inversion of polarity is used to transiently adapt the adhesive needs of both the uterine wall and the embryo for successful nidation and pregnancy. Taken together, the examples above can be seen as physiologically relevant instances of polarity inversion at play during successful development.

Box 3. The intriguing case of the first lumen generated during mammalian embryonic development

Early embryonic development includes an extreme case of polarity inversion whereby both apical and basolateral domains face extracellular fluids. At the blastocyst stage, trophectoderm (TE) cells envelop a fluid-filled lumen called the blastocoele cavity which bathes the apolar inner cell mass (ICM) cells. At the onset of blastocoel formation, fluids and osmolytes are transported and secreted asymmetrically to the basolateral compartment of internal cells as a result of basolateral enrichment of fluid pumps like the Na^+/K^+-ATPase (Hirata et al., 1986; Schliffka and Maître, 2019). The increasing fluid pressure breaks basolateral cell–cell bonds, creating small cavities which coalesce into a single blastocoele lumen at the TE–ICM interface. This process is controlled by anisotropies in cell contractility and cell adhesion. Because the ICM is more contractile than the TE, extracellular fluid is thought to be directed towards the softer tissue to generate the single blastocoele cavity (Dumortier et al., 2019). As such, the first lumen-facing membrane during development has a basolateral identity, revealing an interesting case of inverted apicobasal polarity in which both the apical and the basolateral domains face a fluid external milieu.

Molecular determinants of apicobasal polarity inversion

The molecular mechanisms underlying establishment and maintenance of apicobasal polarity are now well documented (Buckley and St Johnston, 2022). In contrast, the regulation of the orientation of the polarity axis is less well understood. Lumen-forming epithelia and cell clusters generally polarize in a basal-to-apical fashion by integrating dominant polarizing cues from the ECM (Martin-Belmonte and Mostov, 2008) (Fig. 2). We will next explore the molecular drivers of apicobasal polarity inversion in the aforementioned pathological conditions to unveil the critical pathways controlling epithelial polarity orientation.

Failure to read and integrate polarizing ECM cues drives basal-to-apical polarity inversion

Seminal work from the Nelson laboratory has revealed the importance of the ECM in dictating the orientation of the apicobasal polarity axis. Aggregates of MDCK cells in suspension switch from an apical-out to an apical-in polarity phenotype upon inclusion in collagen gels, providing an excellent model to study the spatiotemporal events responsible for normal emergence of apicobasal polarity (Wang et al., 1990a,b). These studies have implicated β1-integrin signaling in translating ECM cues via activation of Rac1 GTPase (Ojakian and Schwimmer, 1994; Yu et al., 2005). Follow-up studies highlight the importance of downregulating the activity of RhoA and ROCK, and hence actomyosin contractility, upon integrin engagement to successfully drive cell cluster polarization, independently of Rac1 activity (Ferrari et al., 2008). In brief, ECM ligands sensed by β1-integrin activate focal adhesion kinase (FAK; also known as PTK2) at focal adhesions, which recruits p190RhoGAP (also known as p190A

Journal of Cell Science (2024) 137, jcs261659. doi:10.1242/jcs.261659

or ARHGAP35) to locally inhibit RhoA at the ECM-abutting membrane (Bryant et al., 2014). Decreased activity of RhoA and ROCK destabilizes the anti-adhesive apical sialomucin gp135 (also known as podocalyxin; Pdxl), which, along with the Par6–aPKC–Par3 complex, is internalized and transcytosed in a Rab11–Cdc42–exocyst complex-dependent fashion to the opposite membrane to initiate formation of a lumen (Bryant et al., 2010, 2014; Martin-Belmonte et al., 2007) (Fig. 2). Delivery of the apical membrane components to the newly formed lumen-abutting domain also relies on Rab35, either via its capacity to tether gp135-positive vesicles (Klinkert et al., 2016) or via its regulation of the small GTPase Arf6 (Mrozowska and Fukuda, 2016). Intestinal organoids derived from individuals with MIA-CID with inhibitory variants in *TTC7A* show an inverted apical-out polarity phenotype when embedded in 3D matrices (Bigorgne et al., 2014). Interestingly, inhibiting ROCK-dependent actomyosin contractility is sufficient to restore normal apical-in polarity, reinforcing the key role of RhoA–ROCK activity in controlling apicobasal polarity orientation (Bigorgne et al., 2014). Alternatively, to achieve the apical-out to apical-in polarity inversion upon 3D matrix inclusion, clusters of mammary gland epithelial cells

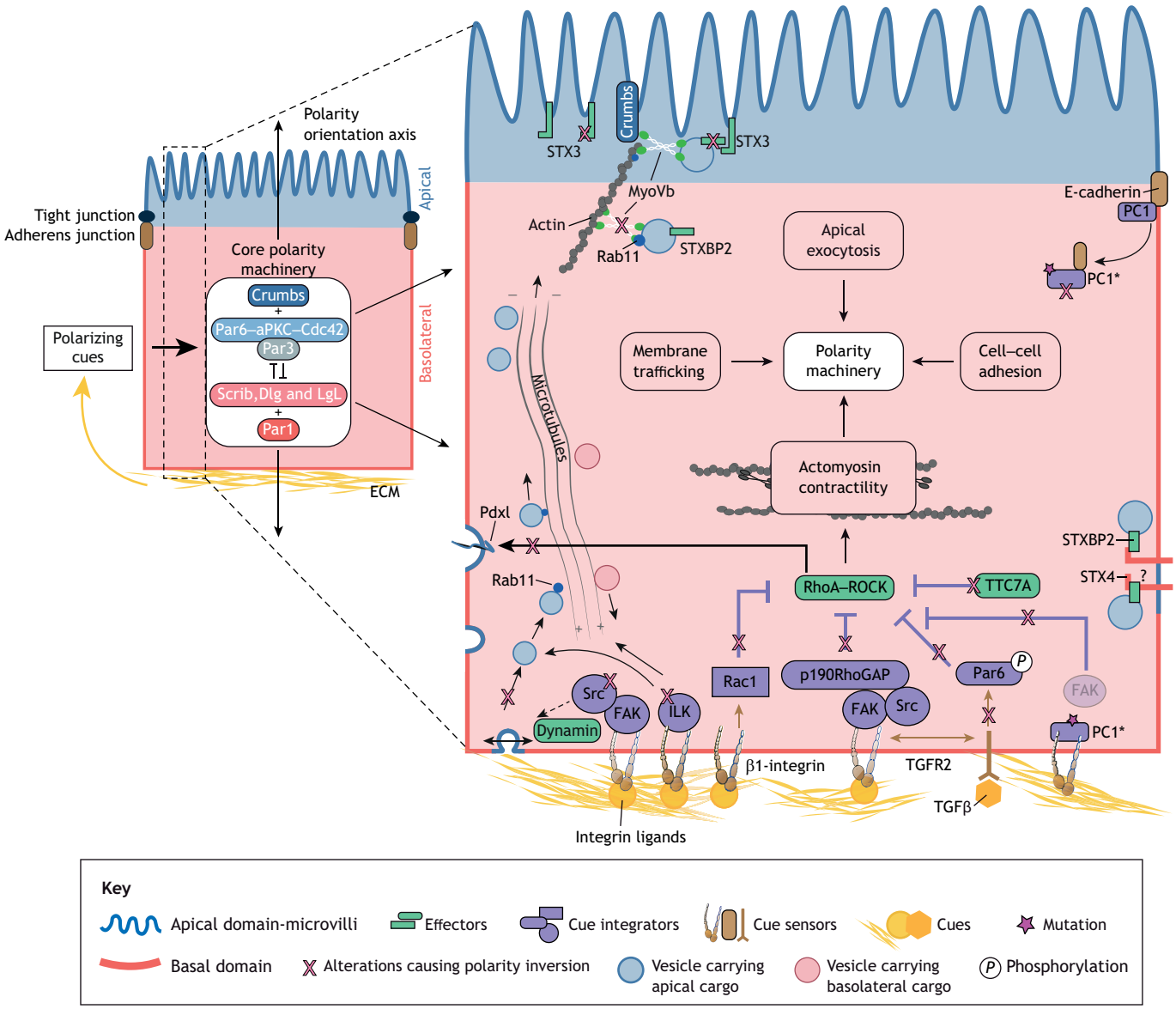

Fig. 2. Molecular pathways controlling apicobasal polarity inversion. Polarizing cue sensing and integration by epithelial cells controls how the apicobasal polarity machinery establish and maintain the appropriate polarity state. The enlarged view of the cell on the right shows how basolateral integrins and growth factor receptors sense ECM adhesive cues and growth factors (orange). Multiple cue-integration pathways (purple) trigger local activation of effectors (green), which control the orientation of the polarity machinery. Integrin engagement activates FAK and Src kinases, which downregulate RhoA activity to reduce actomyosin contractility. Decreased RhoA activity directly promotes the endocytosis and Rab11–Cdc42-dependent transcytosis of apical determinants, such as Pdxl (blue vesicles). Integrin engagement also activates ILK, which repolarizes the microtubule network to favor endocytosis and trafficking of apical determinants. TGFβ signaling via TGFR2 downregulates RhoA activity through phosphorylation of Par6. Impairments in these pathways (pink Xs) cause various degrees of apicobasal polarity inversion. In MVID, mutations in STX3, STXBP2 and Myo5B are thought to cause inverted trafficking of apical cargo towards the basolateral domain. The binding of apical vesicles to STX4, a close homolog of STX3 located basolaterally, could contribute to inverted polarity associated with STX3 mutations. In PKD, PC1 mutations prevent FAK from associating with activated integrins in focal adhesions. Alternatively, mutant PC1 is known to sequester E-cadherin in the cytoplasm, preventing the sensing of polarizing cues from adherens junctions.

require β1-integrin-dependent activation of the integrin-linked kinase (ILK) and microtubule polarity inversion (Akhtar and Streuli, 2013). Activation of ILK stabilizes microtubule plus-ends at the outward-facing surface, which enhances endocytosis and removal of apical determinants from the cluster periphery. Furthermore, by re-orienting microtubule minus-ends away from the outward-facing surface, the β1-integrin–ILK–microtubule network promotes repositioning of the Golgi and membrane trafficking of apical components from the periphery to the newly forming lumen-facing membrane (Akhtar and Streuli, 2013) (Fig. 2). For more details on the role played by microtubules and associated molecular motors in controlling polarity inversion, we refer readers to the excellent review by Kreitzer and Myat (2018). The diversity of signaling pathways that are involved in polarity inversion downstream of β1-integrin likely reflects the different experimental settings, including the nature of ECM molecules (collagen versus Matrigel) and differing epithelial cell types (kidney versus mammary) used in the experiments.

The study of organoids derived from individuals with colorectal cancer (CRC) has unveiled several other key molecular alterations leading to polarity inversion. Among them, the lack of active canonical and non-canonical transforming growth factor β (TGFβ) signaling is key to explaining the inverted apical-out polarity orientation of 3D matrix-embedded CRC clusters both *in vitro* and in host tissue following mouse xenografting (Canet-Jourdan et al., 2022; Zajac et al., 2018). This likely results from several downstream mechanisms including an altered positive-feedback loop between TGFβ and integrin expression levels (Munger and Sheppard, 2011). Downstream of integrin engagement, actomyosin contractility plays a crucial role in controlling the apicobasal polarity state of CRC clusters in 3D matrices. Downregulation of RhoA activity is sufficient to restore normal apical-in polarity in CRC clusters in 3D matrices, whereas increased contractility in initially normal apical-in polarized clusters drives polarity inversion (Canet-Jourdan et al., 2022; Onuma et al., 2021; Zajac et al., 2018). An interesting candidate which might bridge the TGFβ signaling module with inhibition of the RhoA–ROCK effector module is the polarity protein Par6. It was previously reported in mammary gland epithelial cells that upon binding with its ligand, the TGFβ receptor complex phosphorylates Par6, which increases the interaction of Par6 with the E3 ubiquitin ligase Smurf1 and causes the local degradation of RhoA (Ozdamar et al., 2005). Zajac et al. found that Par6 depletion partially blocks TGFβ-treated CRC clusters from establishing a normal apical-in polarity in collagen matrices (Zajac et al., 2018), suggesting that a similar molecular cascade could be at play to control apicobasal polarity orientation in cell clusters (Fig. 2). Alterations in other growth-factor-dependent signaling pathways might also be involved, as EGF and insulin growth factor-1 (IGF-1) have been shown to control lumen formation upon inclusion of CRC organoids in 3D matrices (Ashley et al., 2019). Finally, pharmacological inhibition of FAK and microtubule dynamics do not significantly prevent lumen formation and apical-in polarity of CRC clusters embedded in collagen, in contrast to what is seen for MDCK cells and mammary acini, suggesting additional pathways are involved in polarity inversion in colorectal cancer (Okuyama et al., 2016). Treating CRC clusters with the Src inhibitor Dasatinib or inactivating dynamin through addition of Dynasore and MitMAB strongly block the restoration of an apical-in polarity state, suggesting that Src kinase and dynamin play a role in controlling polarity inversion downstream of β1-integrin engagement with ECM molecules (Okuyama et al., 2016) (Fig. 2). Src kinase can directly activate the GTPase activity of dynamin2 (Dyn2; also known as DNM2) (Weller et al., 2010). In addition to its role in promoting cell membrane endocytosis, Dyn2 regulates Rac1 activity by stabilizing its guanine nucleotide exchange factor (GEF) Vav1 (Razidlo et al., 2013). Whether Src and dynamin act together downstream of β1-integrin to enhance Rac-1 mediated inversion of polarity remains to be tested.

Apical-out inverted polarity in tumor clusters could also be fueled by the altered tumoral microenvironment. For example, colorectal TSIPs secrete mucus at their periphery, which isolates the tumor cluster from polarizing ECM cues, further stabilizing the apical-out polarity (N.P., Jacques Mathieu, Johanna Ivaska, F.J., unpublished). In other cases, increased stiffness of the stroma (the noncancerous tissue which surrounds and supports a tumor), which is often associated with carcinoma progression, could foster TSIP formation. Augmenting matrix stiffness triggers the partial inversion of apicobasal polarity in mammary epithelial cell clusters via increased integrin-dependent focal adhesion signaling, which enhances growth factor-dependent extracellular signal-regulated kinases 1 and 2 (ERK1/2) activation and downstream RhoA activity (Paszek et al., 2005). Decreasing actomyosin contractility rescues the polarity defects in malignant and non-malignant mammary epithelial cell clusters caused by high matrix stiffness (Paszek et al., 2005). These two examples highlight the role played by the tumor environment in potentiating the cell-autonomous molecular alterations that cause the inverted polarity phenotype.

Altogether, these studies on matrix-embedded cell clusters have revealed key molecular cascades at play during apicobasal polarity inversion. Alterations in cue-sensing via integrins and the TGFβ receptor, in integration of ECM cues via Src, FAK, ILK, Par6 or Rac, and in effector modules, such as actomyosin contractility and membrane trafficking, might all contribute to failure to establish and maintain a normal apicobasal polarity orientation (Fig. 2). Whether these mechanisms also control the orientation of apicobasal polarity in established epithelia requires further investigation. Early studies in partially inverted renal epithelia in individuals with PKD suggest that ECM cue-sensing via integrins and cue integration via FAK could potentially be involved. In normal renal tubules, the polycystin protein PC1 (also known as PKD1) interacts with α2β1 integrins at focal adhesions (Wilson et al., 1999). In cells individuals with PKD with *PC1* gene variants, FAK is absent from the focal adhesion macromolecular complex, suggesting transmission of polarizing ECM cues is flawed due to dysfunctional focal adhesions (Wilson, 2011).

Alteration of apical membrane trafficking primes epithelia for partial apical-to-basal polarity inversion

In a vast majority of cases, the epithelia affected by partial or full apicobasal polarity inversion suffer from defects in membrane trafficking and vesicle recycling. For example, *P. aeruginosa* infection triggers PI3K-dependent transcytosis of basolateral markers, such as E-cadherin, integrin and PIP_3, towards the lumen-facing pole, as well as displacement of the apical marker gp153 (Kierbel et al., 2007; Tran et al., 2014). The exact molecular mechanisms responsible for this inverted targeting of apical and basal membrane determinants remain poorly understood. Next, we discuss findings that have begun to point toward these elusive mechanisms.

One scenario involves defective apical endosome recycling (Schneeberger et al., 2018). MYO5B, variants in which cause MVID and inverse apical and basolateral protein targeting, tethers endosomal vesicles along actin filaments and stabilizes them at the apical pole by interacting with the apical determinant Crumbs

(Pocha et al., 2011). By also interacting with the small GTPase Rab11a, MYO5B controls apical trafficking and activation of Cdc42 and ezrin (Bryant et al., 2014; Dhekne et al., 2014; Roland et al., 2011). In enterocytes from individuals with MVID and in Myo5b-mutant CaCo-2 cells, Rab11a-enriched recycling endosomes no longer reach the apical pole, which likely explains the absence of apical determinants at the apical pole (Dhekne et al., 2014; Knowles et al., 2014) (Table 1). Efficient apical protein targeting requires not only trafficking and docking to the apical pole, but also fusion of the vesicles to the plasma membrane. This is achieved by interaction between soluble N-ethylmaleimide-sensitive factor attachment receptors (SNAREs) on both the vesicle (v-SNARE) and the targeted membrane (t-SNARE). In mammals, STX3 is a t-SNARE that is enriched at the apical pole (Delgrossi et al., 1997) and interacts with the v-SNARE SLP4A (also known as SYTL4) via STXBP2. MVID caused by variants in *STX3* or *STXBP2* might thus result from alterations in the apical membrane fusion machinery (Fig. 2). Whereas the molecular factors causing apical protein mislocalization are now beginning to be understood, why some of them are redirected to the basal compartment, thus leading to partial apicobasal polarity inversion, is unknown. A putative explanation is that because apical recycling endosomes are prevented from binding and fusing to the apical membrane, they instead interact with the basolateral STX4, which is highly similar to STX3 (ter Beest et al., 2005) and exclusively found in the basolateral compartments (Low et al., 1996) (Fig. 2).

Another scenario explaining partial epithelial polarity inversion involves the perturbation of cadherin-based AJ. E-cadherin engagement is an early event in epithelial cell polarization (Wang et al., 1990a). In renal epithelia of individuals with PKD, variants in the polycystins PC1 and PC2 (also known as PKD2) are thought to drive apicobasal polarity inversion by impairing E-cadherin sorting to the epithelial zonula adherens, a cell–cell junction belt ensuring mechanical anchoring of neighboring cells (Charron et al., 2000). By interacting with E-cadherin (Huan and van Adelsberg, 1999), mutant PC1 might sequester E-cadherin in the cytoplasm or destabilize it from cell–cell contacts (Fig. 2). The mislocalization of the exocyst complex proteins Sec6 and Sec8 in cells derived from individuals with PKD affects basolateral membrane trafficking and could also be responsible for failure of E-cadherin to reach the membrane (Charron et al., 2000). These data reveal that PKD-associated mutations weaken cell–cell adhesions and sustain polarity inversion. However, why AJ alteration in PKD epithelia leads to partially inverted polarity and not complete loss of the polarity axis is still unclear.

Similarly, the local inversion of polarity at bacteria–host cell contacts upon *N. meningitidis* infection involves the mistrafficking of AJ proteins to the apical pole (Coureuil et al., 2009). In response to infection, cells activate Cdc42, which recruits p120 catenin (p120ctn; also known as δ-catenin 1 or CTNND1), potentially via their shared interactor N-WASP (also known as WASL) (Rajput et al., 2013; Rohatgi et al., 2000). p120ctn repositioning at the apical pole causes relocalization of the remaining AJ proteins, leading to weakening of cell–cell junctions and increased bacterial invasion through the endothelial barrier (Coureuil et al., 2009). Here, a pathogen-driven interaction of a basolateral protein (p120ctn) with an apical determinant (Cdc42) is sufficient to drive local inversion of membrane polarity.

Altogether the scenarios presented above provide partial explanations of how mutations in genes affecting membrane trafficking, cell–cell junction remodeling and endosomal recycling might lead to inverted apicobasal polarity. Additional studies are required to better understand why in some cases polarity inversion only affects a subset of molecular determinants despite global alterations in membrane trafficking. The requirement for genetically modified animal models or samples derived from individuals with diseases for such studies has been a practical challenge for research into determinants of polarity orientation in whole epithelia compared to studies using *in vitro* cell cluster assays. Recent improvement and wider use of 3D human organoid culture will hopefully help fill this knowledge gap (Tran et al., 2022).

Concluding remarks

Transient reversal of apicobasal polarity serves vital roles in development processes from embryo implantation to immune surveillance. Furthermore, scenarios such as host–pathogen interactions demonstrate how polarity inversion can be both a defense mechanism and a mechanism driving vulnerability to infection. Beyond these physiological roles, inverted polarity is a distinct feature of invasive cancer progression and numerous monogenic diseases. The importance of polarity inversion in the pathophysiology and molecular origin of these diseases is increasingly being demonstrated. A better understanding of the integrated pathways controlling this process is still needed in order to develop methods to restore normal polarity or artificially induce polarity inversion on demand to influence drug sensitivity, immune detection and modes of cell migration, or to improve fertility. By gathering observations made in subtypes of cancers and genetic diseases, we have provided a molecular framework to explain the development of inverted apicobasal polarity centered on the cellular response to polarizing ECM cues, actomyosin contractility and alterations in membrane trafficking. Because most of these molecular mechanisms have been uncovered from *in vitro* studies on cellular spheroids in stereotypical 3D matrices, more complex biomimetic systems involving co-culture with stromal cells are now required to further narrow down key molecular targets. Finally, recent advances in manipulation of the orientation of cell polarity (Watson et al., 2023) will greatly help bridge the knowledge gap required for therapeutic intervention in diseases featuring inverted polarity.

Acknowledgements

We would like to thank the members of the Jaulin lab for their insightful input on the manuscript.

Competing interests

F.J. is the CEO of a Gustave Roussy spin-off (Orakl).

Funding

Our work in this area was supported by Agence Nationale de la Recherche (ANR) grant ANR-20-CE13-0031-01, Institut National du Cancer (INCa) grant 2020-1-PLBIO-04-IGR-1, fundraising against colorectal cancer and the Mars Bleu campaign from the Gustave Roussy foundation. The Review was written with financial support from Institut National de la Santé et de la Recherche Médicale (INSERM) Cancer (3R program 20CR046-00). This work has benefited from a government grant managed by the National Research Agency (ANR) under the 5th PIA, integrated into France 2030 with the reference ANR-21-RHUS-0003. N.P. is financed by a fellowship from Fondation Philantropia. Open Access funding provided by INSERM (U1279, Tumor Cell Dynamics). Deposited in PMC for immediate release.

References

Adams, S. A., Smith, M. E. F., Cowley, G. P. and Carr, L. A. (2004). Reversal of glandular polarity in the lymphovascular compartment of breast cancer. *J. Clin. Pathol.* **57**, 1114-1117. doi:10.1136/jcp.2004.016980

Akhtar, N. and Streuli, C. H. (2013). An integrin-ILK-microtubule network orients cell polarity and lumen formation in glandular epithelium. *Nat. Cell Biol.* **15**, 17-27. doi:10.1038/ncb2646

Al-Obaidy, K. I., Eble, J. N., Cheng, L., Williamson, S. R., Sakr, W. A., Gupta, N., Idrees, M. T. and Grignon, D. J. (2019). Papillary renal neoplasm with reverse polarity: a morphologic, immunohistochemical, and molecular study. *Am. J. Surg. Pathol.* **43**, 1099-1111. doi:10.1097/PAS.0000000000001288

Al-Obaidy, K. I., Eble, J. N., Nassiri, M., Cheng, L., Eldomery, M. K., Williamson, S. R., Sakr, W. A., Gupta, N., Hassan, O., Idrees, M. T. et al. (2020). Recurrent KRAS mutations in papillary renal neoplasm with reverse polarity. *Mod. Pathol.* **33**, 1157-1164. doi:10.1038/s41379-019-0362-1

Anani, S., Bhat, S., Honma-Yamanaka, N., Krawchuk, D. and Yamanaka, Y. (2014). Initiation of Hippo signaling is linked to polarity rather than to cell position in the pre-implantation mouse embryo. *Development* **141**, 2813-2824. doi:10.1242/dev.107276

Aplin, J. D., Spanswick, C., Behzad, F., Kimber, S. J. and Vićovac, L. (1996). Integrins β 5, β 3 and alpha v are apically distributed in endometrial epithelium. *Mol. Hum. Reprod.* **2**, 527-534. doi:10.1093/molehr/2.7.527

Ashley, N., Ouaret, D. and Bodmer, W. F. (2019). Cellular polarity modulates drug resistance in primary colorectal cancers via orientation of the multidrug resistance protein ABCB1. *J. Pathol.* **247**, 293-304. doi:10.1002/path.5179

Asioli, S., Erickson, L. A., Righi, A. and Lloyd, R. V. (2013). Papillary thyroid carcinoma with hobnail features: histopathologic criteria to predict aggressive behavior. *Hum. Pathol.* **44**, 320-328. doi:10.1016/j.humpath.2012.06.003

Axelrod, M. L., Cook, R. S., Johnson, D. B. and Balko, J. M. (2019). Biological consequences of MHC-II expression by tumor cells in cancer. *Clin. Cancer Res.* **25**, 2392-2402. doi:10.1158/1078-0432.CCR-18-3200

Baas, A. F., Kuipers, J., van der Wel, N. N., Batlle, E., Koerten, H. K., Peters, P. J. and Clevers, H. C. (2004). Complete polarization of single intestinal epithelial cells upon activation of LKB1 by STRAD. *Cell* **116**, 457-466. doi:10.1016/S0092-8674(04)00114-X

Badouel, C. and McNeill, H. (2011). SnapShot: the hippo signaling pathway. *Cell* **145**, 484-484.e1. doi:10.1016/j.cell.2011.04.009

Bigorgne, A. E., Farin, H. F., Lemoine, R., Mahlaoui, N., Lambert, N., Gil, M., Schulz, A., Philippet, P., Schlesser, P., Abrahamsen, T. G. et al. (2014). TTC7A mutations disrupt intestinal epithelial apicobasal polarity. *J. Clin. Invest.* **124**, 328-337. doi:10.1172/JCI71471

Bilder, D. and Perrimon, N. (2000). Localization of apical epithelial determinants by the basolateral PDZ protein Scribble. *Nature* **403**, 676-680. doi:10.1038/35001108

Bryant, D. M., Datta, A., Rodríguez-Fraticelli, A. E., Peränen, J., Martín-Belmonte, F. and Mostov, K. E. (2010). A molecular network for de novo generation of the apical surface and lumen. *Nat. Cell Biol.* **12**, 1035-1045. doi:10.1038/ncb2106

Bryant, D. M., Roignot, J., Datta, A., Overeem, A. W., Kim, M., Yu, W., Peng, X., Eastburn, D. J., Ewald, A. J., Werb, Z. et al. (2014). A molecular switch for the orientation of epithelial cell polarization. *Dev. Cell* **31**, 171-187. doi:10.1016/j.devcel.2014.08.027

Buckley, C. E. and St Johnston, D. (2022). Apical-basal polarity and the control of epithelial form and function. *Nat. Rev. Mol. Cell Biol.* **23**, 559-577. doi:10.1038/s41580-022-00465-y

Canet-Jourdan, C., Pagès, D.-L., Nguyen-Vigouroux, C., Cartry, J., Zajac, O., Desterke, C., Lopez, J.-B., Gutierrez-Mateyron, E., Signolle, N., Adam, J. et al. (2022). Patient-derived organoids identify an apico-basolateral polarity switch associated with survival in colorectal cancer. *J. Cell Sci.* **135**, jcs259256. doi:10.1242/jcs.259256

Charron, A. J., Nakamura, S., Bacallao, R. and Wandinger-Ness, A. (2000). Compromised cytoarchitecture and polarized trafficking in autosomal dominant polycystic kidney disease cells. *J. Cell Biol.* **149**, 111-124. doi:10.1083/jcb.149.1.111

Chiang, S., Weigelt, B., Wen, H.-C., Pareja, F., Raghavendra, A., Martelotto, L. G., Burke, K. A., Basili, T., Li, A., Geyer, F. C. et al. (2016). IDH2 mutations define a unique subtype of breast cancer with altered nuclear polarity. *Cancer Res.* **76**, 7118-7129. doi:10.1158/0008-5472.CAN-16-0298

Coureuil, M., Mikaty, G., Miller, F., Lécuyer, H., Bernard, C., Bourdoulous, S., Duménil, G., Mège, R.-M., Weksler, B. B., Romero, I. A. et al. (2009). Meningococcal type IV pili recruit the polarity complex to cross the brain endothelium. *Science* **325**, 83-87. doi:10.1126/science.1173196

Cutz, E., Rhoads, J. M., Drumm, B., Sherman, P. M., Durie, P. R. and Forstner, G. G. (1989). Microvillus inclusion disease: an inherited defect of brush-border assembly and differentiation. *N. Engl. J. Med.* **320**, 646-651. doi:10.1056/NEJM198903093201006

de Boer, M., van Dijck, J. A. A. M., Bult, P., Borm, G. F. and Tjan-Heijnen, V. C. G. (2010). Breast cancer prognosis and occult lymph node metastases, isolated tumor cells, and micrometastases. *J. Natl. Cancer Inst.* **102**, 410-425. doi:10.1093/jnci/djq008

Debnath, J. and Brugge, J. S. (2005). Modelling glandular epithelial cancers in three-dimensional cultures. *Nat. Rev. Cancer* **5**, 675-688. doi:10.1038/nrc1695

Delgrossi, M. H., Breuza, L., Mirre, C., Chavrier, P. and Le Bivic, A. (1997). Human syntaxin 3 is localized apically in human intestinal cells. *J. Cell Sci.* **110**, 2207-2214. doi:10.1242/jcs.110.18.2207

Dhekne, H. S., Hsiao, N.-H., Roelofs, P., Kumari, M., Slim, C. L., Rings, E. H. H. M. and van Ijzendoorn, S. C. D. (2014). Myosin Vb and Rab11a regulate phosphorylation of ezrin in enterocytes. *J. Cell Sci.* **127**, 1007-1017. doi:10.1242/jcs.137273

Du, J. and Wilson, P. D. (1995). Abnormal polarization of EGF receptors and autocrine stimulation of cyst epithelial growth in human ADPKD. *Am. J. Physiol.* **269**, C487-C495. doi:10.1152/ajpcell.1995.269.2.C487

Ducibella, T., Ukena, T., Karnovsky, M. and Anderson, E. (1977). Changes in cell surface and cortical cytoplasmic organization during early embryogenesis in the preimplantation mouse embryo. *J. Cell Biol.* **74**, 153-167. doi:10.1083/jcb.74.1.153

Dumortier, J. G., Le Verge-Serandour, M., Tortorelli, A. F., Mielke, A., de Plater, L., Turlier, H. and Maître, J.-L. (2019). Hydraulic fracturing and active coarsening position the lumen of the mouse blastocyst. *Science* **365**, 465-468. doi:10.1126/science.aaw7709

Ebnet, K. (2015). *Cell Polarity 2: Role in Development and Disease*, 1st edn. Springer Cham.

Ferrari, A., Veligodskiy, A., Berge, U., Lucas, M. S. and Kroschewski, R. (2008). ROCK-mediated contractility, tight junctions and channels contribute to the conversion of a preapical patch into apical surface during isochoric lumen initiation. *J. Cell Sci.* **121**, 3649-3663. doi:10.1242/jcs.018648

Gassama-Diagne, A., Yu, W., ter Beest, M., Martin-Belmonte, F., Kierbel, A., Engel, J. and Mostov, K. (2006). Phosphatidylinositol-3,4,5-trisphosphate regulates the formation of the basolateral plasma membrane in epithelial cells. *Nat. Cell Biol.* **8**, 963-970. doi:10.1038/ncb1461

Gerri, C., Menchero, S., Mahadevaiah, S. K., Turner, J. M. A. and Niakan, K. K. (2020a). Human embryogenesis: a comparative perspective. *Annu. Rev. Cell Dev. Biol.* **36**, 411-440. doi:10.1146/annurev-cellbio-022020-024900

Gerri, C., McCarthy, A., Alanis-Lobato, G., Demtschenko, A., Bruneau, A., Loubersac, S., Fogarty, N. M. E., Hampshire, D., Elder, K., Snell, P. et al. (2020b). Initiation of a conserved trophectoderm program in human, cow and mouse embryos. *Nature* **587**, 443-447. doi:10.1038/s41586-020-2759-x

Guo, X., Fan, Y., Lang, R., Gu, F., Chen, L., Cui, L., Pringle, G. A., Zhang, X. and Fu, L. (2008). Tumor infiltrating lymphocytes differ in invasive micropapillary carcinoma and medullary carcinoma of breast. *Mod. Pathol.* **21**, 1101-1107. doi:10.1038/modpathol.2008.72

Halaoui, R., Rejon, C., Chatterjee, S. J., Szymborski, J., Meterissian, S., Muller, W. J., Omeroglu, A. and McCaffrey, L. (2017). Progressive polarity loss and luminal collapse disrupt tissue organization in carcinoma. *Genes Dev.* **31**, 1573-1587. doi:10.1101/gad.300566.117

Hershberg, R. M., Cho, D. H., Youakim, A., Bradley, M. B., Lee, J. S., Framson, P. E. and Nepom, G. T. (1998). Highly polarized HLA class II antigen processing and presentation by human intestinal epithelial cells. *J. Clin. Invest.* **102**, 792-803. doi:10.1172/JCI3201

Hirakawa, T., Goto, M., Takahashi, K., Iwasawa, T., Fujishima, A., Makino, K., Shirasawa, H., Sato, W., Sato, T., Kumazawa, Y. et al. (2022). Na+/K+ ATPase α1 and β3 subunits are localized to the basolateral membrane of trophectoderm cells in human blastocysts. *Hum. Reprod.* **37**, 1423-1430. doi:10.1093/humrep/deac124

Hirata, I., Austin, L. L., Blackwell, W. H., Weber, J. R. and Dobbins, W. O. (1986). Immunoelectron microscopic localization of HLA-DR antigen in control small intestine and colon and in inflammatory bowel disease. *Dig. Dis. Sci.* **31**, 1317-1330. doi:10.1007/BF01299810

Hirate, Y., Hirahara, S., Inoue, K.-I., Suzuki, A., Alarcon, V. B., Akimoto, K., Hirai, T., Hara, T., Adachi, M., Chida, K. et al. (2013). Polarity-dependent distribution of angiomotin localizes Hippo signaling in preimplantation embryos. *Curr. Biol.* **23**, 1181-1194. doi:10.1016/j.cub.2013.05.014

Huan, Y. and van Adelsberg, J. (1999). Polycystin-1, the PKD1 gene product, is in a complex containing E-cadherin and the catenins. *J. Clin. Invest.* **104**, 1459-1468. doi:10.1172/JCI5111

Hurd, T. W., Fan, S., Liu, C. J., Kweon, H. K., Hakansson, K. and Margolis, B. (2003). Phosphorylation-dependent binding of 14-3-3 to the polarity protein Par3 regulates cell polarity in mammalian epithelia. *Curr. Biol.* **13**, 2082-2090. doi:10.1016/j.cub.2003.11.020

Hutterer, A., Betschinger, J., Petronczki, M. and Knoblich, J. A. (2004). Sequential roles of Cdc42, Par-6, aPKC, and Lgl in the establishment of epithelial polarity during Drosophila embryogenesis. *Dev. Cell* **6**, 845-854. doi:10.1016/j.devcel.2004.05.003

Illera, M. J., Cullinan, E., Gui, Y., Yuan, L., Beyler, S. A. and Lessey, B. A. (2000). Blockade of the alpha(v)beta(3) integrin adversely affects implantation in the mouse. *Biol. Reprod.* **62**, 1285-1290. doi:10.1095/biolreprod62.5.1285

Johnson, M. H. and Ziomek, C. A. (1981). The foundation of two distinct cell lineages within the mouse morula. *Cell* **24**, 71-80. doi:10.1016/0092-8674(81)90502-X

Kemphues, K. J., Priess, J. R., Morton, D. G. and Cheng, N. S. (1988). Identification of genes required for cytoplasmic localization in early C. elegans embryos. *Cell* **52**, 311-320. doi:10.1016/S0092-8674(88)80024-2

Kierbel, A., Gassama-Diagne, A., Mostov, K. and Engel, J. N. (2005). The phosphoinositol-3-kinase-protein kinase B/Akt pathway is critical for Pseudomonas aeruginosa strain PAK internalization. *Mol. Biol. Cell* **16**, 2577-2585. doi:10.1091/mbc.e04-08-0717

Kierbel, A., Gassama-Diagne, A., Rocha, C., Radoshevich, L., Olson, J., Mostov, K. and Engel, J. (2007). Pseudomonas aeruginosa exploits a PIP3-

dependent pathway to transform apical into basolateral membrane. *J. Cell Biol.* **177**, 21-27. doi:10.1083/jcb.200605142

Kim, S. S., Cho, Y. M., Kim, G. H., Kee, K. H., Kim, H.-S., Kim, K. M., Kim, J.-H. and Choi, C. (2020). Recurrent KRAS mutations identified in papillary renal neoplasm with reverse polarity-a comparative study with papillary renal cell carcinoma. *Mod. Pathol.* **33**, 690-699. doi:10.1038/s41379-019-0420-8

Klinkert, K., Rocancourt, M., Houdusse, A. and Echard, A. (2016). Rab35 GTPase couples cell division with initiation of epithelial apico-basal polarity and lumen opening. *Nat. Commun.* **7**, 11166. doi:10.1038/ncomms11166

Knowles, B. C., Roland, J. T., Krishnan, M., Tyska, M. J., Lapierre, L. A., Dickman, P. S., Goldenring, J. R. and Shub, M. D. (2014). Myosin Vb uncoupling from RAB8A and RAB11A elicits microvillus inclusion disease. *J. Clin. Invest.* **124**, 2947-2962. doi:10.1172/JCI71651

Koivisto, U. M., Hubbard, A. L. and Mellman, I. (2001). A novel cellular phenotype for familial hypercholesterolemia due to a defect in polarized targeting of LDL receptor. *Cell* **105**, 575-585. doi:10.1016/S0092-8674(01)00371-3

Kreitzer, G. and Myat, M. M. (2018). Microtubule Motors in Establishment of Epithelial Cell Polarity. *Cold Spring Harb. Perspect. Biol.* **10**, a027896. doi:10.1101/cshperspect.a027896

Kuroda, H., Sakamoto, G., Ohnisi, K. and Itoyama, S. (2004). Clinical and pathologic features of invasive micropapillary carcinoma. *Breast Cancer* **11**, 169-174. doi:10.1007/BF02968297

Lang, C. F. and Munro, E. (2017). The PAR proteins: from molecular circuits to dynamic self-stabilizing cell polarity. *Development* **144**, 3405-3416. doi:10.1242/dev.139063

Lee, M. and Vasioukhin, V. (2008). Cell polarity and cancer–cell and tissue polarity as a non-canonical tumor suppressor. *J. Cell Sci.* **121**, 1141-1150. doi:10.1242/jcs.016634

Lehtonen, E. and Badley, R. A. (1980). Localization of cytoskeletal proteins in preimplantation mouse embryos. *J. Embryol. Exp. Morphol.* **55**, 211-225.

Lessey, B. A. (2002). Adhesion molecules and implantation. *J. Reprod. Immunol.* **55**, 101-112. doi:10.1016/S0165-0378(01)00139-5

Li, S. R., Gulieva, R. E., Helms, L., Cruz, N. M., Vincent, T., Fu, H., Himmelfarb, J. and Freedman, B. S. (2022). Glucose absorption drives cystogenesis in a human organoid-on-chip model of polycystic kidney disease. *Nat. Commun.* **13**, 7918. doi:10.1038/s41467-022-35537-2

Libanje, F., Raingeaud, J., Luan, R., Thomas, Z., Zajac, O., Veiga, J., Marisa, L., Adam, J., Boige, V., Malka, D. et al. (2019). ROCK2 inhibition triggers the collective invasion of colorectal adenocarcinomas. *EMBO J.* **38**, e99299. doi:10.15252/embj.201899299

Low, S. H., Chapin, S. J., Weimbs, T., Kömüves, L. G., Bennett, M. K. and Mostov, K. E. (1996). Differential localization of syntaxin isoforms in polarized Madin-Darby canine kidney cells. *Mol. Biol. Cell* **7**, 2007-2018. doi:10.1091/mbc.7.12.2007

Luna-Moré, S., Gonzalez, B., Acedo, C., Rodrigo, I. and Luna, C. (1994). Invasive micropapillary carcinoma of the breast. A new special type of invasive mammary carcinoma. *Pathol. Res. Pract.* **190**, 668-674. doi:10.1016/S0344-0338(11)80745-4

Macara, I. G. and McCaffrey, L. (2013). Cell polarity in morphogenesis and metastasis. *Philos. Trans. R. Soc. Lond. B. Biol. Sci.* **368**, 20130012. doi:10.1098/rstb.2013.0012

Maître, J.-L., Turlier, H., Illukkumbura, R., Eismann, B., Niwayama, R., Nédélec, F. and Hiiragi, T. (2016). Asymmetric division of contractile domains couples cell positioning and fate specification. *Nature* **536**, 344-348. doi:10.1038/nature18958

Martin, E., Girardello, R., Dittmar, G. and Ludwig, A. (2021). New insights into the organization and regulation of the apical polarity network in mammalian epithelial cells. *FEBS J.* **288**, 7073-7095. doi:10.1111/febs.15710

Martin-Belmonte, F. and Mostov, K. (2008). Regulation of cell polarity during epithelial morphogenesis. *Curr. Opin. Cell Biol.* **20**, 227-234. doi:10.1016/j.ceb.2008.01.001

Martin-Belmonte, F., Gassama, A., Datta, A., Yu, W., Rescher, U., Gerke, V. and Mostov, K. (2007). PTEN-mediated apical segregation of phosphoinositides controls epithelial morphogenesis through Cdc42. *Cell* **128**, 383-397. doi:10.1016/j.cell.2006.11.051

Menezes, L. F. and Germino, G. G. (2019). The pathobiology of polycystic kidney disease from a metabolic viewpoint. *Nat. Rev. Nephrol.* **15**, 735-749. doi:10.1038/s41581-019-0183-y

Michaux, G., Massey-Harroche, D., Nicolle, O., Rabant, M., Brousse, N., Goulet, O., Le Bivic, A. and Ruemmele, F. M. (2016). The localisation of the apical Par/Cdc42 polarity module is specifically affected in microvillus inclusion disease. *Biol. Cell* **108**, 19-28. doi:10.1111/boc.201500034

Mo, J.-S., Park, H. W. and Guan, K.-L. (2014). The Hippo signaling pathway in stem cell biology and cancer. *EMBO Rep.* **15**, 642-656. doi:10.15252/embr.201438638

Mohammed, S. I., Torres-Luquis, O., Walls, E. and Lloyd, F. (2019). Lymph-circulating tumor cells show distinct properties to blood-circulating tumor cells and are efficient metastatic precursors. *Mol. Oncol.* **13**, 1400-1418. doi:10.1002/1878-0261.12494

Mostov, K., Su, T. and ter Beest, M. (2003). Polarized epithelial membrane traffic: conservation and plasticity. *Nat. Cell Biol.* **5**, 287-293. doi:10.1038/ncb0403-287

Moulin, P., Igarashi, T., Van der Smissen, P., Cosyns, J.-P., Verroust, P., Thakker, R. V., Scheinman, S. J., Courtoy, P. J. and Devuyst, O. (2003). Altered polarity and expression of H+-ATPase without ultrastructural changes in kidneys of Dent's disease patients. *Kidney Int.* **63**, 1285-1295. doi:10.1046/j.1523-1755.2003.00851.x

Mrozowska, P. S. and Fukuda, M. (2016). Regulation of podocalyxin trafficking by Rab small GTPases in 2D and 3D epithelial cell cultures. *J. Cell Biol.* **213**, 355-369. doi:10.1083/jcb.201512024

Müller, T., Hess, M. W., Schiefermeier, N., Pfaller, K., Ebner, H. L., Heinz-Erian, P., Ponstingl, H., Partsch, J., Röllinghoff, B., Köhler, H. et al. (2008). MYO5B mutations cause microvillus inclusion disease and disrupt epithelial cell polarity. *Nat. Genet.* **40**, 1163-1165. doi:10.1038/ng.225

Munger, J. S. and Sheppard, D. (2011). Cross talk among TGF-β signaling pathways, integrins, and the extracellular matrix. *Cold Spring Harb. Perspect. Biol.* **3**, a005017. doi:10.1101/cshperspect.a005017

Nassar, H., Pansare, V., Zhang, H., Che, M., Sakr, W., Ali-Fehmi, R., Grignon, D., Sarkar, F., Cheng, J. and Adsay, V. (2004). Pathogenesis of invasive micropapillary carcinoma: role of MUC1 glycoprotein. *Mod. Pathol.* **17**, 1045-1050. doi:10.1038/modpathol.3800166

Nelson, W. J. (2003). Adaptation of core mechanisms to generate cell polarity. *Nature* **422**, 766-774. doi:10.1038/nature01602

Nikas, G., Ao, A., Winston, R. M. and Handyside, A. H. (1996). Compaction and surface polarity in the human embryo in vitro. *Biol. Reprod.* **55**, 32-37. doi:10.1095/biolreprod55.1.32

Niwayama, R., Moghe, P., Liu, Y.-J., Fabrèges, D., Buchholz, F., Piel, M. and Hiiragi, T. (2019). A tug-of-war between cell shape and polarity controls division orientation to ensure robust patterning in the mouse blastocyst. *Dev. Cell* **51**, 564-574.e6. doi:10.1016/j.devcel.2019.10.012

Ojakian, G. K. and Schwimmer, R. (1994). Regulation of epithelial cell surface polarity reversal by beta 1 integrins. *J. Cell Sci.* **107**, 561-576. doi:10.1242/jcs.107.3.561

Okuyama, H., Kondo, J., Sato, Y., Endo, H., Nakajima, A., Piulats, J. M., Tomita, Y., Fujiwara, T., Itoh, Y., Mizoguchi, A. et al. (2016). Dynamic change of polarity in primary cultured spheroids of human colorectal adenocarcinoma and its role in metastasis. *Am. J. Pathol.* **186**, 899-911. doi:10.1016/j.ajpath.2015.12.011

Ong, A. C. M. (2017). Making sense of polycystic kidney disease. *Lancet* **389**, 1780-1782. doi:10.1016/S0140-6736(17)30928-5

Onuma, K., Sato, Y., Okuyama, H., Uematsu, H., Homma, K., Ohue, M., Kondo, J. and Inoue, M. (2021). Aberrant activation of Rho/ROCK signaling in impaired polarity switching of colorectal micropapillary carcinoma. *J. Pathol.* **255**, 84-94. doi:10.1002/path.5748

Ozdamar, B., Bose, R., Barrios-Rodiles, M., Wang, H.-R., Zhang, Y. and Wrana, J. L. (2005). Regulation of the polarity protein Par6 by TGFbeta receptors controls epithelial cell plasticity. *Science* **307**, 1603-1609. doi:10.1126/science.1105718

Ozguldez, H. O., Govindasamy, N., Fan, R., Long, H., Mildner, K., Zeuschner, D., Trappmann, B., Ranga, A. and Bedzhov, I. (2023). Polarity inversion reorganizes the stem cell compartment of the trophoblast lineage. *Cell Rep.* **42**, 112313. doi:10.1016/j.celrep.2023.112313

Pagès, D.-L., Dornier, E., de Seze, J., Gontran, E., Maitra, A., Maciejewski, A., Wang, L., Luan, R., Cartry, J., Canet-Jourdan, C. et al. (2022). Cell clusters adopt a collective amoeboid mode of migration in confined nonadhesive environments. *Sci. Adv.* **8**, eabp8416. doi:10.1126/sciadv.abp8416

Paszek, M. J., Zahir, N., Johnson, K. R., Lakins, J. N., Rozenberg, G. I., Gefen, A., Reinhart-King, C. A., Margulies, S. S., Dembo, M., Boettiger, D. et al. (2005). Tensional homeostasis and the malignant phenotype. *Cancer Cell* **8**, 241-254. doi:10.1016/j.ccr.2005.08.010

Peglion, F. and Etienne-Manneville, S. (2024). Cell polarity changes in cancer initiation and progression. *J. Cell Biol.* **223**, e202308069. doi:10.1083/jcb.202308069

Peglion, F. and Goehring, N. W. (2019). Switching states: dynamic remodelling of polarity complexes as a toolkit for cell polarization. *Curr. Opin. Cell Biol.* **60**, 121-130. doi:10.1016/j.ceb.2019.05.002

Plant, P. J., Fawcett, J. P., Lin, D. C. C., Holdorf, A. D., Binns, K., Kulkarni, S. and Pawson, T. (2003). A polarity complex of mPar-6 and atypical PKC binds, phosphorylates and regulates mammalian Lgl. *Nat. Cell Biol.* **5**, 301-308. doi:10.1038/ncb948

Plusa, B., Frankenberg, S., Chalmers, A., Hadjantonakis, A.-K., Moore, C. A., Papalopulu, N., Papaioannou, V. E., Glover, D. M. and Zernicka-Goetz, M. (2005). Downregulation of Par3 and aPKC function directs cells towards the ICM in the preimplantation mouse embryo. *J. Cell Sci.* **118**, 505-515. doi:10.1242/jcs.01666

Pocha, S. M., Shevchenko, A. and Knust, E. (2011). Crumbs regulates rhodopsin transport by interacting with and stabilizing myosin V. *J. Cell Biol.* **195**, 827-838. doi:10.1083/jcb.201105144

Quinn, K. E., Matson, B. C., Wetendorf, M. and Caron, K. M. (2020). Pinopodes: recent advancements, current perspectives, and future directions. *Mol. Cell. Endocrinol.* **501**, 110644. doi:10.1016/j.mce.2019.110644

Rajput, C., Kini, V., Smith, M., Yazbeck, P., Chavez, A., Schmidt, T., Zhang, W., Knezevic, N., Komarova, Y. and Mehta, D. (2013). Neural Wiskott-Aldrich syndrome protein (N-WASP)-mediated p120-catenin interaction with Arp2-Actin

complex stabilizes endothelial adherens junctions. *J. Biol. Chem.* **288**, 4241-4250. doi:10.1074/jbc.M112.440396
Razidlo, G. L., Wang, Y., Chen, J., Krueger, E. W., Billadeau, D. D. and McNiven, M. A. (2013). Dynamin 2 potentiates invasive migration of pancreatic tumor cells through stabilization of the Rac1 GEF Vav1. *Dev. Cell* **24**, 573-585. doi:10.1016/j.devcel.2013.02.010
Reeve, W. J. and Ziomek, C. A. (1981). Distribution of microvilli on dissociated blastomeres from mouse embryos: evidence for surface polarization at compaction. *J. Embryol. Exp. Morphol.* **62**, 339-350.
Reglero-Real, N., Álvarez-Varela, A., Cernuda-Morollón, E., Feito, J., Marcos-Ramiro, B., Fernández-Martín, L., Gómez-Lechón, M. J., Muntané, J., Sandoval, P., Majano, P. L. et al. (2014). Apicobasal polarity controls lymphocyte adhesion to hepatic epithelial cells. *Cell Rep.* **8**, 1879-1893. doi:10.1016/j.celrep.2014.08.007
Riento, K., Kauppi, M., Keranen, S. and Olkkonen, V. M. (2000). Munc18-2, a functional partner of syntaxin 3, controls apical membrane trafficking in epithelial cells. *J. Biol. Chem.* **275**, 13476-13483. doi:10.1074/jbc.275.18.13476
Riga, A., Castiglioni, V. G. and Boxem, M. (2020). New insights into apical-basal polarization in epithelia. *Curr. Opin. Cell Biol.* **62**, 1-8. doi:10.1016/j.ceb.2019.07.017
Ritch, S. J. and Telleria, C. M. (2022). The Transcoelomic Ecosystem and Epithelial Ovarian Cancer Dissemination. *Front. Endocrinol.* **13**, 886533. doi:10.3389/fendo.2022.886533
Rodriguez-Boulan, E. and Macara, I. G. (2014). Organization and execution of the epithelial polarity programme. *Nat. Rev. Mol. Cell Biol.* **15**, 225-242. doi:10.1038/nrm3775
Rohatgi, R., Ho, H. Y. and Kirschner, M. W. (2000). Mechanism of N-WASP activation by CDC42 and phosphatidylinositol 4, 5-bisphosphate. *J. Cell Biol.* **150**, 1299-1310. doi:10.1083/jcb.150.6.1299
Roland, J. T., Bryant, D. M., Datta, A., Itzen, A., Mostov, K. E. and Goldenring, J. R. (2011). Rab GTPase-Myo5B complexes control membrane recycling and epithelial polarization. *Proc. Natl. Acad. Sci. USA* **108**, 2789-2794. doi:10.1073/pnas.1010754108
Salaun, B., Coste, I., Rissoan, M.-C., Lebecque, S. J. and Renno, T. (2006). TLR3 can directly trigger apoptosis in human cancer cells. *J. Immunol.* **176**, 4894-4901. doi:10.4049/jimmunol.176.8.4894
Samarage, C. R., White, M. D., Álvarez, Y. D., Fierro-González, J. C., Henon, Y., Jesudason, E. C., Bissiere, S., Fouras, A. and Plachta, N. (2015). Cortical tension allocates the first inner cells of the mammalian embryo. *Dev. Cell* **34**, 435-447. doi:10.1016/j.devcel.2015.07.004
Sarles, J., Gorvel, J. P., Olive, D., Maroux, S., Mawas, C. and Giraud, F. (1987). Subcellular localization of class I (A,B,C) and class II (DR and DQ) MHC antigens in jejunal epithelium of children with coeliac disease. *J. Pediatr. Gastroenterol. Nutr.* **6**, 51-56. doi:10.1097/00005176-198701000-00010
Schliffka, M. F. and Maître, J.-L. (2019). Stay hydrated: basolateral fluids shaping tissues. *Curr. Opin. Genet. Dev.* **57**, 70-77. doi:10.1016/j.gde.2019.06.015
Schneeberger, K., Vogel, G. F., Teunissen, H., van Ommen, D. D., Begthel, H., El Bouazzaoui, L., van Vugt, A. H. M., Beekman, J. M., Klumperman, J., Müller, T. et al. (2015). An inducible mouse model for microvillus inclusion disease reveals a role for myosin Vb in apical and basolateral trafficking. *Proc. Natl. Acad. Sci. USA* **112**, 12408-12413. doi:10.1073/pnas.1516672112
Schneeberger, K., Roth, S., Nieuwenhuis, E. E. S. and Middendorp, S. (2018). Intestinal epithelial cell polarity defects in disease: lessons from microvillus inclusion disease. *Dis. Model. Mech.* **11**, dmm031088. doi:10.1242/dmm.031088
Simons, M. and Walz, G. (2006). Polycystic kidney disease: cell division without a c(l)ue? *Kidney Int.* **70**, 854-864. doi:10.1038/sj.ki.5001534
Siriaunkgul, S. and Tavassoli, F. A. (1993). Invasive micropapillary carcinoma of the breast. *Mod. Pathol.* **6**, 660-662.
Speiser, D. E., Chijioke, O., Schaeuble, K. and Münz, C. (2023). CD4+ T cells in cancer. *Nat. Cancer* **4**, 317-329. doi:10.1038/s43018-023-00521-2
St Johnston, D. (2018). Establishing and transducing cell polarity: common themes and variations. *Curr. Opin. Cell Biol.* **51**, 33-41. doi:10.1016/j.ceb.2017.10.007
Stanifer, M. L., Mukenhirn, M., Muenchau, S., Pervolaraki, K., Kanaya, T., Albrecht, D., Odendall, C., Hielscher, T., Haucke, V., Kagan, J. C. et al. (2020). Asymmetric distribution of TLR3 leads to a polarized immune response in human intestinal epithelial cells. *Nat. Microbiol.* **5**, 181-191. doi:10.1038/s41564-019-0594-3
Stephens, R., Lim, K., Portela, M., Kvansakul, M., Humbert, P. O. and Richardson, H. E. (2018). The scribble cell polarity module in the regulation of cell signaling in tissue development and tumorigenesis. *J. Mol. Biol.* **430**, 3585-3612. doi:10.1016/j.jmb.2018.01.011
Stewart, C. J. R., Koay, M. H. E., Leslie, C., Acott, N. and Leung, Y. C. (2018). Cervical carcinomas with a micropapillary component: a clinicopathological study of eight cases. *Histopathology* **72**, 626-633. doi:10.1111/his.13419
Sun, P., Zhong, Z., Lu, Q., Li, M., Chao, X., Chen, D., Hu, W., Luo, R. and He, J. (2020). Mucinous carcinoma with micropapillary features is morphologically, clinically and genetically distinct from pure mucinous carcinoma of breast. *Mod. Pathol.* **33**, 1945-1960. doi:10.1038/s41379-020-0554-8
Sutherland, A. E., Calarco, P. G. and Damsky, C. H. (1993). Developmental regulation of integrin expression at the time of implantation in the mouse embryo. *Development* **119**, 1175-1186. doi:10.1242/dev.119.4.1175
Suwińska, A., Czołowska, R., Ozdzeński, W. and Tarkowski, A. K. (2008). Blastomeres of the mouse embryo lose totipotency after the fifth cleavage division: expression of Cdx2 and Oct4 and developmental potential of inner and outer blastomeres of 16- and 32-cell embryos. *Dev. Biol.* **322**, 133-144. doi:10.1016/j.ydbio.2008.07.019
Tanentzapf, G. and Tepass, U. (2003). Interactions between the crumbs, lethal giant larvae and bazooka pathways in epithelial polarization. *Nat. Cell Biol.* **5**, 46-52. doi:10.1038/ncb896
Tapia, R., Kralicek, S. E. and Hecht, G. A. (2017). Modulation of epithelial cell polarity by bacterial pathogens. *Ann. N. Y. Acad. Sci.* **1405**, 16-24. doi:10.1111/nyas.13388
ter Beest, M. B. A., Chapin, S. J., Avrahami, D. and Mostov, K. E. (2005). The role of syntaxins in the specificity of vesicle targeting in polarized epithelial cells. *Mol. Biol. Cell* **16**, 5784-5792. doi:10.1091/mbc.e05-07-0661
Thie, M., Fuchs, P. and Denker, H. W. (1996). Epithelial cell polarity and embryo implantation in mammals. *Int. J. Dev. Biol.* **40**, 389-393.
Tilston-Lunel, A. M. and Varelas, X. (2023). Polarity in respiratory development, homeostasis and disease. *Curr. Top. Dev. Biol.* **154**, 285-315. doi:10.1016/bs.ctdb.2023.02.004
Tran, C. S., Eran, Y., Ruch, T. R., Bryant, D. M., Datta, A., Brakeman, P., Kierbel, A., Wittmann, T., Metzger, R. J., Mostov, K. E. et al. (2014). Host cell polarity proteins participate in innate immunity to Pseudomonas aeruginosa infection. *Cell Host Microbe* **15**, 636-643. doi:10.1016/j.chom.2014.04.007
Tran, T., Song, C. J., Nguyen, T., Cheng, S.-Y., McMahon, J. A., Yang, R., Guo, Q., Der, B., Lindström, N. O., Lin, D. C.-H. et al. (2022). A scalable organoid model of human autosomal dominant polycystic kidney disease for disease mechanism and drug discovery. *Cell Stem Cell* **29**, 1083-1101.e7. doi:10.1016/j.stem.2022.06.005
Verdú, M., Román, R., Calvo, M., Rodón, N., García, B., González, M., Vidal, A. and Puig, X. (2011). Clinicopathological and molecular characterization of colorectal micropapillary carcinoma. *Mod. Pathol.* **24**, 729-738. doi:10.1038/modpathol.2011.1
Verras, G.-I., Tchabashvili, L., Mulita, F., Grypari, I. M., Sourouni, S., Panagodimou, E. and Argentou, M.-I. (2022). Micropapillary breast carcinoma: from molecular pathogenesis to prognosis. *Breast Cancer Dove Med. Press* **14**, 41-61. doi:10.2147/BCTT.S346301
Vinot, S., Le, T., Ohno, S., Pawson, T., Maro, B. and Louvet-Vallée, S. (2005). Asymmetric distribution of PAR proteins in the mouse embryo begins at the 8-cell stage during compaction. *Dev. Biol.* **282**, 307-319. doi:10.1016/j.ydbio.2005.03.001
Vogel, G. F., van Rijn, J. M., Krainer, I. M., Janecke, A. R., Posovszky, C., Cohen, M., Searle, C., Jantchou, P., Escher, J. C., Patey, N. et al. (2017). Disrupted apical exocytosis of cargo vesicles causes enteropathy in FHL5 patients with Munc18-2 mutations. *JCI Insight* **2**, e94564. doi:10.1172/jci.insight.94564
Wang, A. Z., Ojakian, G. K. and Nelson, W. J. (1990a). Steps in the morphogenesis of a polarized epithelium. I. Uncoupling the roles of cell-cell and cell-substratum contact in establishing plasma membrane polarity in multicellular epithelial (MDCK) cysts. *J. Cell Sci.* **95**, 137-151. doi:10.1242/jcs.95.1.137
Wang, A. Z., Ojakian, G. K. and Nelson, W. J. (1990b). Steps in the morphogenesis of a polarized epithelium. II. Disassembly and assembly of plasma membrane domains during reversal of epithelial cell polarity in multicellular epithelial (MDCK) cysts. *J. Cell Sci.* **95**, 153-165. doi:10.1242/jcs.95.1.153
Watson, J. L., Krüger, L. K., Ben-Sasson, A. J., Bittleston, A., Shahbazi, M. N., Planelles-Herrero, V. J., Chambers, J. E., Manton, J. D., Baker, D. and Derivery, E. (2023). Synthetic Par polarity induces cytoskeleton asymmetry in unpolarized mammalian cells. *Cell* **186**, 4710-4727.e35. doi:10.1016/j.cell.2023.08.034
Weller, S. G., Capitani, M., Cao, H., Micaroni, M., Luini, A., Sallese, M. and McNiven, M. A. (2010). Src kinase regulates the integrity and function of the Golgi apparatus via activation of dynamin 2. *Proc. Natl. Acad. Sci. USA* **107**, 5863-5868. doi:10.1073/pnas.0915123107
Whitby, S., Salamonsen, L. A. and Evans, J. (2018). The endometrial polarity paradox: differential regulation of polarity within secretory-phase human endometrium. *Endocrinology* **159**, 506-518. doi:10.1210/en.2016-1877
Whitby, S., Zhou, W. and Dimitriadis, E. (2020). Alterations in epithelial cell polarity during endometrial receptivity: a systematic review. *Front. Endocrinol.* **11**, 596324. doi:10.3389/fendo.2020.596324
Wiegerinck, C. L., Janecke, A. R., Schneeberger, K., Vogel, G. F., van Haaften-Visser, D. Y., Escher, J. C., Adam, R., Thöni, C. E., Pfaller, K., Jordan, A. J. et al. (2014). Loss of syntaxin 3 causes variant microvillus inclusion disease. *Gastroenterology* **147**, 65-68.e10. doi:10.1053/j.gastro.2014.04.002
Wilson, P. D. (1997). Epithelial cell polarity and disease. *Am. J. Physiol.* **272**, F434-F442. doi:10.1152/ajprenal.1997.272.4.F434
Wilson, P. D. (2004). Polycystic kidney disease. *N. Engl. J. Med.* **350**, 151-164. doi:10.1056/NEJMra022161
Wilson, P. D. (2011). Apico-basal polarity in polycystic kidney disease epithelia. *Biochim. Biophys. Acta* **1812**, 1239-1248. doi:10.1016/j.bbadis.2011.05.008

Wilson, P. D., Sherwood, A. C., Palla, K., Du, J., Watson, R. and Norman, J. T. (1991). Reversed polarity of Na(+) -K(+) -ATPase: mislocation to apical plasma membranes in polycystic kidney disease epithelia. *Am. J. Physiol.* **260**, F420-F430. doi:10.1152/ajpcell.1991.260.2.C355

Wilson, P. D., Geng, L., Li, X. and Burrow, C. R. (1999). The PKD1 gene product, "polycystin-1," is a tyrosine-phosphorylated protein that colocalizes with alpha2beta1-integrin in focal clusters in adherent renal epithelia. *Lab. Invest.* **79**, 1311-1323.

Winter, J. F., Höpfner, S., Korn, K., Farnung, B. O., Bradshaw, C. R., Marsico, G., Volkmer, M., Habermann, B. and Zerial, M. (2012). Caenorhabditis elegans screen reveals role of PAR-5 in RAB-11-recycling endosome positioning and apicobasal cell polarity. *Nat. Cell Biol.* **14**, 666-676. doi:10.1038/ncb2508

Wodarz, A. and Näthke, I. (2007). Cell polarity in development and cancer. *Nat. Cell Biol.* **9**, 1016-1024. doi:10.1038/ncb433

Wodarz, A., Hinz, U., Engelbert, M. and Knust, E. (1995). Expression of crumbs confers apical character on plasma membrane domains of ectodermal epithelia of Drosophila. *Cell* **82**, 67-76. doi:10.1016/0092-8674(95)90053-5

Wodarz, A., Ramrath, A., Grimm, A. and Knust, E. (2000). Drosophila atypical protein kinase C associates with Bazooka and controls polarity of epithelia and neuroblasts. *J. Cell Biol.* **150**, 1361-1374. doi:10.1083/jcb.150.6.1361

Wosen, J. E., Mukhopadhyay, D., Macaubas, C. and Mellins, E. D. (2018). Epithelial MHC class II expression and its role in antigen presentation in the gastrointestinal and respiratory tracts. *Front. Immunol.* **9**, 2144. doi:10.3389/fimmu.2018.02144

Wosen, J. E., Ilstad-Minnihan, A., Co, J. Y., Jiang, W., Mukhopadhyay, D., Fernandez-Becker, N. Q., Kuo, C. J., Amieva, M. R. and Mellins, E. D. (2019). Human intestinal enteroids model MHC-II in the gut epithelium. *Front. Immunol.* **10**, 1970. doi:10.3389/fimmu.2019.01970

Yu, W., Datta, A., Leroy, P., O'Brien, L. E., Mak, G., Jou, T.-S., Matlin, K. S., Mostov, K. E. and Zegers, M. M. P. (2005). Beta1-integrin orients epithelial polarity via Rac1 and laminin. *Mol. Biol. Cell* **16**, 433-445. doi:10.1091/mbc.e04-05-0435

Zajac, O., Raingeaud, J., Libanje, F., Lefebvre, C., Sabino, D., Martins, I., Roy, P., Benatar, C., Canet-Jourdan, C., Azorin, P. et al. (2018). Tumour spheres with inverted polarity drive the formation of peritoneal metastases in patients with hypermethylated colorectal carcinomas. *Nat. Cell Biol.* **20**, 296-306. doi:10.1038/s41556-017-0027-6

Zhang, H. T. and Hiiragi, T. (2018). Symmetry breaking in the mammalian embryo. *Annu. Rev. Cell Dev. Biol.* **34**, 405-426. doi:10.1146/annurev-cellbio-100617-062616

Zhu, M. and Zernicka-Goetz, M. (2020). Principles of self-organization of the mammalian embryo. *Cell* **183**, 1467-1478. doi:10.1016/j.cell.2020.11.003

II- **Pasquier N.**, Isomursu A., Mathieu J., Hamidi H., Härkönen J., Follain G., Desterke C., Barresi V., Fusilier Z., Jaulin F. & Ivaska J., **Signaling downstream of tumor-stroma interactions regulates mucinous CRC apicobasal polarity**, *manuscript submitted*

Signaling downstream of tumor-stroma interaction regulates mucinous colorectal carcinoma apicobasal polarity

Nicolas Pasquier[1,2], Aleksi Isomursu[1], Jacques R.R. Mathieu[2], Hellyeh Hamidi[1], Jouni Härkönen[1], Gautier Follain[1], Christophe Desterke[3], Zoé Fusilier[4,5], Valeria Barresi[6], Fanny Jaulin*[2] & Johanna Ivaska*[1,7-10]

[1]Turku Bioscience Centre, University of Turku and Åbo Akademi University, Turku, Finland
[2]INSERM-U1279, Gustave Roussy, Université Paris-Saclay, Villejuif F-94805, France
[3]INSERM UMR-S-MD A9, Hôpital Paul Brousse, Villejuif F-94805, France
[4]INSERM-U932, Immunity and Cancer, Institut Curie, Paris-Cité University, Paris, France
[5]INSERM-U932, Immunity and Cancer, Institut Curie, PSL University, Paris, France
[6]Department of Diagnostics and Public Health, University of Verona, Verona 37129, Italy
[7]Department of Life Technologies, University of Turku, Turku, Finland
[8]InFLAMES Research Flagship Center, University of Turku, Turku, Finland
[9]Foundation for the Finnish Cancer Institute, Helsinki, Finland
[10]Western Finnish Cancer Center, University of Turku, Turku FI-20520, Finland
*Correspondence: johanna.ivaska@utu.fi and fanny.jaulin@gustaveroussy.fr

Abstract

Mucinous colorectal carcinoma (MUC CRC) dissemination into the tumor stroma and metastasis to multiple organs, including the peritoneum, is associated with poor prognosis. Disseminating MUC CRCs exhibit either a conventional 'apical-in' or an inverted 'apical-out' polarity phenotype that determine patient outcome. Identifying the mechanisms controlling MUC CRC polarity is critical to understand disease progression. Here, we analyze patient-derived MUC CRC xenografts, with apical-in or apical-out polarity, ex vivo or within collagen gels to mimic the peritumoral stroma. Single-cell analyses reveal $\alpha 2\beta 1$-integrin as a key collagen-binding receptor in these models. Collagen–$\alpha 2\beta 1$-integrin interaction activates Src and ERK/MAPK signaling and upregulates the expression of SorLA, an endosomal sorting receptor. SorLA supports apical-in polarity by promoting integrin recycling to the plasma membrane and HER2/HER3 expression through a positive feedback mechanism. Accordingly, we observe positive correlation between HER2, HER3 and SorLA in patient samples with the highest expression in apical-in-presenting tissues. Treatment of tumor spheres with clinically relevant HER2/HER3-targeting antibodies reverts sphere polarity and impedes collagen remodeling and adhesion to mouse peritoneum. This SorLA—integrin—HER2/HER3 signaling axis may represent a basis for MUC CRC-patient stratification and shed light on other carcinomas with similar apical-out phenotypes.

Introduction

Apicobasal polarity is a critical cellular process essential for normal tissue function. Its disruption is implicated in various pathological conditions including cancer (Macara and McCaffrey, 2013; Wodarz; Onuma Inoue 2022 and Näthke, 2007). While the loss of polarity has been extensively studied, the phenomenon of inverted polarity (also referred to as Apical-Out), where the apical and basolateral domains are reversed, is less understood.

Apical-out topology, characterized by the mislocalization of apical and basolateral markers (Lee and Vasioukhin, 2008; Peglion et al., 2023, Pasquier et al., 2024, Verdú et al., 2011) and aggressive tumor behavior (Jakubowska et al., 2016), is a hallmark of several aggressive cancer subtypes, including micropapillary carcinomas and mucinous colorectal adenocarcinomas (MUC CRC). Micropapillary carcinoma exhibit a fully inverted apicobasal polarity (Verras et al., 2022). This type of cancer is diagnosed upon detection of an apical-out polarity pattern. MUC CRC represents a distinct subtype of colorectal carcinoma (CRC), characterized by abundant mucinous components constituting at least 50% of the tumor volume. CRC is the third most common cancer globally and the second leading cause of cancer-related deaths (Siegel et al., 2023). MUC CRC comprises 10-15% of CRC cases, predominantly affecting young women and the right colon. It carries a poor prognosis, particularly in metastatic disease, with a high incidence of peritoneal metastasis (Mekenkamp et al., 2012; Luo et al., 2019; Bettington et al., 2013; Yamane et al., 2014; Libanje et al., 2019; Hugen et al., 2014). Therefore, there is an urgent need to better understand the mechanisms contributing to acquisition of inverted polarity in cancer.

Histological analyses have revealed that MUC CRCs disseminate not as individual cells but rather as clusters of hundreds of cells called tumor spheres with inverted polarity (TSIPs) (Zajac et al., 2018). These structures, first identified in patients' peritoneal effusions, act as tumor intermediates arising from the primary tumor and invading tissues to form metastasis in the peritoneum, facilitating cancer motility and dissemination (Pagès et al., 2022).
While these TSIPs maintain an inverted (apical-out) polarity in suspension, they display distinct responses within tumor stroma. Once in contact with the extracellular matrix (ECM), TSIPs either revert to a normal (apical-in polarity) or remain inverted (apical-out). The mechanisms underpinning the differential polarity response to the tumor stroma environment are not fully understood, although the TGF-β pathway has been implicated (Okuyama et al., 2016, Onuma et al., 2021, Canet-Jourdan et al., 2022). Regardless, the functional implications of this behavior are becoming obvious as apical-out polarity is supportive of a collective amoeboid mode of migration enhancing tumor invasion efficiency (Pagès et al., 2022), and significantly impacts tumor sensitivity to anti-cancer drugs (Ashley et al, 2019).
Here, using patient-derived MUC CRC tumor spheres, we uncovered a novel mechanism of TSIP polarity orientation. Tumor sphere contact with stromal collagen, via $\alpha 2\beta 1$-integrin

signaling to Src and ERK/MAPK, upregulates a HER2/HER3/SorLA complex and increases SorLA-dependent β1-integrin recycling to the plasma membrane. This maintains tumor–stroma adhesion to support apical-in polarity. Increased ligand-induced HER3 signaling is sufficient to trigger apical-in topology in inherently apical-out tumors. Conversely, clinically used HER2/HER3 targeting antibodies inhibit apical-in phenotype. Accordingly, in clinical specimens, SorLA/HER2/HER3 levels positively correlate and are highest in apical-in tumors. Our study demonstrates the central role of SorLA in the regulation of integrin and HER-family receptor function in CRC, significantly contributing to our understanding of polarity regulation in this aggressive cancer type and paving the way for further investigations into the relevance of this signaling axis in MUC CRC disease progression and patient outcome. Moreover, as inverted polarity is a characteristic of a number of aggressive cancers, these findings have broader implications beyond MUC CRC.

Results

Mucinous CRC polarity is regulated by ECM interaction and mucins.

To investigate the molecular mechanisms of ECM-regulated MUC CRC polarity we used previously described patient-derived xenograft (PDX) models. We focused on three PDXs issued from the CReMEC bank (Julien et al. 2012) representing mucinous histotypes of CRCs (Canet-Jourdan et al. 2022) derived either from a peritoneal metastasis (PDX#1, 9C) or from the primary tumor (PDX#2, 12P; PDX#3, 14P) (see Table 1). We cultured the MUC CRC PDX-derived cell clusters (here on referred to as tumoroids) either in suspension (three days) or in suspension (three days) followed by embedding in collagen-I gels, a surrogate for the cancer stroma (Wolf and Friedl, 2011). These two setups mimic the *in vivo* relevant scenarios of MUC CRC progression as peritoneal effusions or as cell clusters in tissue, respectively. In order to quantitatively score polarity phenotypes, we computed a polarity score according to three parameters: presence/absence of a lumen, protrusions, ezrin fluorescence ratio between the cortical and luminal sides (Fig. S1A). Confocal microscopy imaging of the apical marker ezrin and quantifications revealed that two of the three PDX tumoroids (9C and 12P) maintain apical-out polarity in both suspension and collagen, whereas 14P tumoroids partially revert to an apical-in polarity in collagen, forming ezrin-positive lumens (Fig. 1A,B). These data are concordant with previous studies indicating that 66% of patient-derived TSIPs retain their apico-basolateral polarity in suspension and in collagen (Zajac et al 2018, Canet-Jourdan et al 2022). Characteristically, MUC CRCs secrete high levels of free mucin. Upon staining with WGA-lectin, we were able to visualize mucin secretions by the tumoroids. In the non-ECM responsive 9C and 12P, mucin surrounded the spheres, indicative inverted polarity while in 14P the mucin was concentrated within the lumen confirming the polarity reversion–from Apical-Out to Apical-In–in this model (Fig. S1B). To investigate the collagen-induced polarity reversal in detail, we embedded the 14P tumoroids into collagen gels containing fluorescently labelled collagen and performed live-imaging using a filamentous actin live-cell dye (SiR-Actin). We observed dynamic contact between tumoroid cells and the ECM and the clear

formation of lumen-like structures and protrusions as early as 5 hours post embedding (Fig. 1C + video in the supplementary). Together, these data imply that only the 14P tumoroids are able to respond to their ECM environment.

Models	**CReMEC ID**	**Origin**	**Profiling**
PDX#1 (**9C**)	LRB-009C	Metastatic (peritoneum)	MSS, BRAF WT, $KRAS^{G12V}$
PDX#2 (**12P**)	IGR-012P	Primary	MSS, BRAF WT, $KRAS^{G13D}$
PDX#3 (**14P**)	IGR-014P	Primary	MSS, BRAF WT, $KRAS^{G12D}$

Table 1-MUC CRC PDX Models implemented in this study.

Focal adhesion pathway signaling regulates collagen-induced polarity reversion.

To understand the differential response of the three tumoroid models to collagen embedding, we performed pathway analysis on available transcriptome data (GSE152299) for the three PDX models (suspension versus collagen-embedded tumoroids) (Canet-Jourdan et al., 2022). These analyses revealed the Focal Adhesion Pathway as a top upregulated pathway in the matrix-responsive 14P tumoroids following embedding in collagen. Upon plotting the 45 top differentially regulated genes in the KEGG Focal Adhesion Pathway, we noticed a clear distinction between 14P gene expression in collagen compared to the 9C and 12P tumoroids (Fig. S1C). The corresponding GSEA enrichment plot (Canet-Jourdan et al. 2022) as well as the Principal Component Analysis (PCA) based on the KEGG FA geneset confirmed a clear shift in the transcriptome signature of 14P tumoroids upon collagen embedding (Fig. S1D). These data prompted us to test the functional relevance of the key focal adhesion pathway signaling components on the collagen-induced polarity reversal. We inhibited the small GTPase Rac and the tyrosine kinases, focal adhesion kinase (FAK) and Src with established inhibitors (Onesto et al 2008, Hochwald et al 2009, Kawata et al 2022). Each of these inhibitors dampened the polarity shift of 14P in collagen, reducing protrusions, the number of lumens and the luminal/cortical ezrin signal ratio (Fig 1D-E). Concordantly, Src phosphorylation was induced in 14P upon embedding in collagen (Fig S1E-F), indicating that ECM interaction triggers focal adhesion pathway signaling, contributing to 14P polarity reversal in collagen.

Collagen binding integrins are upstream of the polarity establishment signaling pathway

Integrins, in particular β1-integrin-containing heterodimers, are the principal receptors for the ECM upstream of the focal adhesion pathway and represent established polarity markers in epithelia (Manninen 2015, Zajac et al 2018). We visualized β1-integrin localization and activity in the tumoroids (suspension and collagen). In 14P tumoroids, the localization of β1-integrins, total and active receptors (detected with the P5D2 and 12G10 antibodies, respectively),

shifted from lateral (cell-cell) to basal (cell-ECM). In contrast, β1-integrin localization shows substantially more modest alterations with low expression levels in 9C and 12P tumoroids in the same conditions.(Fig. 2A).

To assess which b1-integrin heterodimers are involved, we applied high-dimensional mass cytometry analysis, focusing on cell-surface integrin receptor expression at the single cell resolution in the PDX models under different conditions. We designed an extensive antibody panel including all the human ECM-binding integrins (see materials and methods for details). We then analyzed freshly isolated and processed samples directly from mice, digesting the resulting PDX tumoroids into a single cell suspension. Using mass cytometry and downstream analyses ,we generated a heatmap of the median surface expression of all the integrin subunits in our panel for each PDX model. Among these integrins, the surface expression of β1- and α2-integrin subunits (α2β1 is the main collagen I–binding integrin heterodimer)(Moreno-Layseca et al 2019 and Chastney et al 2021) was the highest in the 14P model (Fig. S2A). To visualize the overall integrin cell-surface profile, we applied the t-Distributed Stochastic Neighbor Embedding (tSNE; Amir et al 2013) dimensionality reduction approach. By plotting a principal component analysis and applying a FlowSOM clustering (Quintelier et al 2021), it was first possible to distinguish three populations depending on the expression of all the integrins in our panel (Fig. S2B). Overall, the 14P model has a higher integrin expression level of all subunits considered. By overlaying the signal intensity to every event in the PCA, we were able visualize the surface expression of β1-integrin and α2-integrin (Fig. S2C).

We extracted the normalized surface expression of β1- and α2-integrin signal values for all independent events. The histograms further demonstrate a significant distribution of the cell surface integrin intensity across the individual cells in the PDX tumors and demonstrates how 14P is distinguished by a higher surface β1- and α2-integrin expression (Fig. 2B).

To further characterize the impact of the *ex vivo* culture on integrin surface expression, we performed a similar mass cytometry analysis, on tumoroids cultured three days in suspension or three days in collagen. These data recapitulated the integrin expression profiles of the cells directly extracted from the PDX tumors mentioned above (Fig. S2D). When plotting the corresponding histograms (Fig. 2C), we observed that collagen embedding of the 14P tumoroids clearly shifted the intensities of surface β1- and α2-integrin in the cell population in line with their ability to revert polarity in collagen. This prompted us to test the outcome of integrin inhibition on 14P tumoroid polarity following embedding in collagen. Blocking both α2- and β1-integrins using established function-blocking antibodies (AIIB2 for β1-integrin and P1E6 for α2-integrin; Yu et al 2008, Berdichevsky et al 1992) prevented the polarity reversion of 14P in collagen (Fig. 2D-E). Furthermore, the outcome of integrin inhibition was evident in abolished tumoroid–collagen interactions and a round tumoroid morphology in live-imaging experiments (Fig. S2E-F). Taken together these data indicate that α2β1-integrin-mediated cell

interaction with collagen-I and the ensuing downstream signaling are required for the phenotypic polarity reversion in the 14P model (Fig. 2F).

Polarity reversion is linked to altered expression of integrin traffic regulators

Whole exome sequencing revealed no mutations in ITGB1 and ITGA2 genes across the three PDXs (Fig. S2G), excluding a loss of protein function in 9C/12P as a potential explanation for the observed differences between the models. Cell-surface integrin levels are influenced not only by gene transcription but also by the dynamic process of integrin traffic, the continuous endocytosis of integrins from the plasma membrane and their return (recycling) (Caswell and Norman 2006, Bridgewater et al 2012, Moreno-Layseca et al 2019). To investigate the potential role of integrin trafficking in our models, we generated a list of 22 genes known to regulate this process and examined their expression in the same transcriptome data set (GSE152299) (Fig. 3A). PCA representation of this data (Fig. S3A) demonstrates a larger effect of matrix conditions on 14P compared to 9C and 12P. The Volcano plot representation of this gene set (Fig. 3B) identified two interesting targets for further investigation: *RAB11FIP1* and *SORL1*. *RAB11FIP1* encodes the Rab coupling protein (RCP; also called Rab11fip1, Rab11 family-interacting protein 1) which has been implicated in numerous studies as an important positive regulator of β1-integrin recycling, cancer cell invasion and metastasis (Caswell et al 2008, Eva et al 2011, Machesky 2019). *SORL1* encodes the SorLA protein, a cell-surface sorting receptor implicated in trafficking of APP (Amyloid precursor protein) in neurons and rapid recycling of β1-integrins in breast cancer (Eggert et al 2018, Pietilä et al 2019). To validate the transcriptome data, we analyzed *RCP* and SorLA protein levels in the PDX tumoroids in suspension and collagen. RCP was downregulated upon collagen embedding on the protein level in all of the tumoroids and on the mRNA level in 9C and 14P (Fig. 3C-D). In contrast, *SORL1*/SorLA mRNA and protein expression were significantly upregulated only in collagen-embedded 14P tumoroids (Fig. 3E-G and Fig. S3B). In breast cancer cells, integrin-ECM engagement activates the MAPK/ERK signaling pathway and ERK activity positively regulates *SORL1* transcription (Al-Akhrass et al 2021, Al-Akhrass et al 2022), which could also be a possible mechanism for collagen-induced upregulation of *SORL1*/SorLA in mucinous CRC. Indeed, we detected significantly elevated ERK phosphorylation in 14P tumoroids in collagen (Fig. 3H and S3C) and collagen-induced SorLA upregulation was sensitive to integrin function-blocking antibodies (Fig. 3I and S3D). These data suggest the possibility that the 14P tumoroids in collagen switch from RCP-mediated long-loop integrin recycling to a SorLA-driven rapid recycling pathway in a manner that is dependent on initial matrix-induced integrin signaling.

Apical-in polarity in collagen is established through a SorLA-dependent β1-integrin recycling.

To explore SorLA-mediated β1-integrin recycling, we first investigated the impact of collagen-embedding on β1-integrin mRNA and total protein levels (Fig. 4A-B). Western blot analysis of β1-integrin typically reveals two bands, a slower-migrating band representing the mature, fully-glycosylated protein, and a faster-migrating band, indicating the immature, ER-resident protein. The relative abundance of these two protein forms has been linked to alterations in integrin traffic, with a higher ratio of the slower-migrating band corresponding to increased β1-integrin recycling (Böttcher et al., 2012). Interestingly, overall β1-integrin levels were not affected in any of the three PDX tumoroids in response to collagen-I. However, quantification of the ratio of the mature versus immature protein form revealed a significant increase in integrin maturation in the 14P model in response to collagen-I. The identity of the slower migrating band as mature β1-integrin was further confirmed with digestion of the lysates with PNGase (Fig. S4A).

To formally assess the role of SorLA in integrin recycling within MUC CRCs, we sought to establish a more tractable cell-based model, given the technical challenges associated with PDX models. As with other cell lines (Lubarsky et al., 2003), the MUC CRC cell line LS513 generates buds from confluent cultures and secretes TSIPs in the medium (). We observed that these cells phenocopied all the key features of the 14P tumoroids. Once embedded in collagen, the LS513-generated TSIPs formed lumens, shifted significantly towards an apical-in polarity (Fig. S4B-C) and upregulated SorLA levels (Fig. S4D). We concluded that these cells are a good surrogate to study β1-integrin traffic. Previous work has shown that β1-integrins recycle to the plasma membrane with a turnover rate of 10–15 min (Argenzio et al., 2014; Diggins et al., 2018; Dozynkiewicz et al., 2012). Impaired recycling can lead to the gradual intracellular accumulation of β1-integrin (Sahgal et al 2019). We silenced *SORL1* in LS513 with two independent siRNA oligos (Fig. S4E) and used the gold-standard cell-surface biotinylation-based integrin uptake assay to monitor endocytosed β1-integrin levels (Arjonen et al 2012, Farage et al 2021). *SORL1* silencing significantly elevated intracellular β1-integrin levels within 15 minutes, mirroring the effects of the recycling inhibitor primaquine (Fig. 4C). This data indicates that loss of SorLA, similar to our previous findings in breast cancer (Pietilä et al 2019), primarily increases intracellular β1-integrin levels by inhibition recycling (Pietilä et al 2019).

To functionally test the role of SorLA in collagen-induced polarity reversion, we established a patient-derived organoid line (PDO line; as described in Cartry et al 2023) from the 14P tumor (14P PDO line) and silenced *SORL1* using lentiviral shRNA. We obtained more than 50% silencing (Fig. S4F) and observed a significant reduction in 14P polarity reversion in collagen-I, with clusters retaining a mostly apical-out polarity (Fig. 4D-E).

Taken together the data thus far are supportive of a feed-forward loop (Fig. 4F) whereby α2β1-integrin adhesion initiates signaling from collagen through Src, FAK and ERK, upregulating SorLA expression. This induces rapid integrin recycling, giving rise to higher integrin cell-surface localization that supports enhanced cell–collagen interaction and apical-in polarity.

SorLA-dependent Integrin-β1 trafficking is induced by HER2/HER3 signaling.

The human epidermal growth factor receptor 2 (HER2) is a transmembrane receptor tyrosine kinase (RTK) implicated in breast and gastroesophageal cancers, where targeted therapies against this RTK have already been developed for clinical use (Bartley et al 2022). HER2 is also an emerging biomarker in CRC (Ivanova et al 2022). We have shown that SorLA interacts with HER2 homo- and HER2/HER3 heterodimers supporting rapid HER2/HER3 recycling and protein stability and oncogenic signaling in breast and gastric cancers (Pietilä et al 2019, Al-Akhrass et al 2021). Furthermore, Heregulin-β1-induced HER2/HER3 signaling to ERK increases SorLA transcription (Al-Akhrass et al 2021). To explore whether RTK signaling is implicated in MUC CRC polarity, we analyzed HER2 and HER3 expression in 9C, 12P and 14P tumoroids in suspension and collagen. Although HER2 is upregulated in both 12P and 14P, only the collagen-responsive 14P upregulated both HER2 and HER3 protein expression simultaneously when embedded in collagen (Fig. 5A-B). Immunofluorescence staining further validated these results with clear simultaneous HER2 and HER3 signal detected only in 14P in collagen, where HER2 mostly localized at the basal pole (Fig. 5C and Fig. S5A). Similar to the collagen-induced SorLA expression, HER2 and HER3 upregulation were also integrin dependent in 14P in collagen (Fig. 5D-E and Fig. S5B).

To assess the impact of HER2 and HER3 signalling on tumoroid polarity we used two monoclonal antibodies: trastuzumab (prevents HER2 homodimerization and autophosphorylation) and pertuzumab (prevents HER2 and HER3 heterodimerization), both of which are in clinical use for breast cancer treatment (Swain et al 2015). In our set up, trastuzumab alone had no significant effect on 14P polarity. However, pertuzumab alone or in combination with trastuzumab significantly shifted 14P tumoroids toward an apical-out polarity (Fig. 5F-G), indicating a functional role for HER2/HER3 signaling, but not HER2/HER2 homodimers, in 14P polarity reversion in response to collagen. Conversely, HER2/HER3 activation with the HER3 ligand Heregulin-β1 was sufficient to trigger collagen-induced polarity reversion in the thus far matrix agnostic 12P tumoroids (Fig. 5H-I). Upon HER3 stimulation with Heregulin-β1, SorLA was also found to be upregulated in 12P (Fig. 5J and S5E). The 9C tumoroids, did not respond, presumably due to their lack of HER3 expression (Fig. S5C-D). Additionally, Whole exome sequencing (Fig. S5E) indicated that there are no mutations in the aforementioned genes, RAB11FIP1, SORL1, HER2 and HER3, except for a missense mutation in HER2 in 12P, which SIFT and PolyPhen scores suggest is benign on its structure and function (Flanagan et al 2010, Adzhubei et al 2013).

Apical-in CRC polarity is associated with enhanced collagen remodeling.

Since the reversion of 14P tumoroid polarity in collagen was dependent on direct integrin-mediated cell-ECM interactions, we wanted to investigate whether this would also lead to concomitant remodeling of the ECM itself. To further investigate the mechanics of the SorLA/HER2/HER3-dependent polarity reversion, we visualized collagen fiber rearrangements using a fluorescent probe specific for fibrillar collagen (mScarlet-conjugated ©35; Aper et al.

2014). The 14P tumoroids remodeled the collagen matrix resulting in increased fiber alignment in the tumoroid-proximal ECM (Fig. 6A-B and Fig. S6A), whereas integrin inhibition with AIIB2 antibody or dual inhibition of HER2/HER3, with the combination of pertuzumab and trastuzumab, significantly decreased matrix alignment (Fig. 6A-B and Fig. S6A). Conversely, treating 12P tumoroids with Heregulin-β1 increased collagen fiber orientation, indicating elevated collagen remodeling (Fig. 6A-B and Fig. S6B).

To interrogate biophysical interaction between cells and their extracellular matrix, we imaged collagen-embedded 14P and 12P tumoroids before and after Latrunculin B treatment, which disrupts the actin cytoskeletons, releasing cellular tension and causing matrix displacement (Fig. 6C-D and Fig. S6C). Comparing the images before and after treatment allowed us to compute the displacement of collagen fibers in each condition. Using a previously described MATLAB pipeline (Barrasa-Fano et al 2021a), we observed significantly higher reversible collagen displacements proximal to the 14P tumoroids compared to 12P (Fig. 6C-E). This suggests that the collagen fibers are under constant mechanical tension, and such traction forces are higher in the collagen-embedded 14P tumoroids.

CRC often metastasizes to the peritoneum and successful metastasis depends on the cancer cells' ability to adhere to and invade this tissue (Glentis et al., 2017). To study peritoneal invasion with high granularity and in response to various treatments, we set up an in vitro model that recapitulates CRC clusters adhering to and invading the surface of the peritoneum. We isolated and de-cellularized the mouse peritoneum, a techniques previously applied to the mouse mesentery, which was shown to recapitulate the organization and characteristics of the in vivo basement membrane (Schoumacher et al., 2010, 2013). We plated the PDX tumoroids on the de-cellularized peritoneum (Fig. 6F) and tested the outcome of different treatments (AIIB2 or Trastuzumab+Pertuzumab for 14P, Heregulin-β1 for 12P) on the ability of the tumoroids to adhere and spread on the tissue. Despite the appearance of a low adhesion rate, we observed colonization of the peritoneum by tumor spheres through actin staining (Fig. 6G) and quantified the circularity of three randomly chosen spheres in each experiment. The 14P tumoroids, which revert their polarity to apical-in when embedded in collagen, spread extensively on the peritoneum with individual cells dissociating from the clusters. Integrin and HER2/HER3 inhibiting antibodies significantly blocked this (Fig. 6G). In contrast, the untreated 12P tumoroids did not display extensive spreading on the peritoneum. However, stimulation with the HER3 ligand Heregulin-β1 enhanced spreading and reduced spheroid circularity (Fig. 6G-I).

Taken together, these data are concordant with a model where HER2 and HER3 regulate integrin-collagen interactions in MUC CRC tumoroids, and increased integrin cell surface availability and signaling are associated with both apical-in polarity and altered tumoroid-proximal ECM architecture.

High HER2/HER3/SORLA expression correlates with apical-in polarity of CRC tumors and with peritoneum invasion ex-vivo

To determine if the ex-vivo findings on SorLA, HER2, and HER3 were applicable in vivo, we investigated their correlation within PDX tumours. We observed high SORLA/HER2/HER3 staining and predominantly apical-in polarity in the 14P tumors. Conversely, the staining intensities were low in the predominantly apical-out 12P tumor (Fig. S7A). Encouraged by the concordant results between in vivo and ex-vivo, we stained a cohort of 25 human MUC CRC patient samples (Barresi et al., 2015) for these three proteins. The staining revealed a strong positive signal for HER2/SorLA and HER2/HER3 in the epithelium of apical-in CRC clusters whereas in apical-out structures the staining intensities of SorLA and HER2 were lower (Fig. 7A and Fig. S7B). It should be noted that these panels have been made from two different slides that were cut at different depths of the tumor which explains the slight change in structure between the pictures. The quantifications revealed interesting findings: first, there is a positive correlation between HER2 and HER3, as well as between HER2 and SorLA, both in apical-in and apical-out structures (Fig. 7B). Second, there is a correlation between the polarity status and HER2 expression (higher in apical-in than in apical-out). Although similar tendencies were seen for HER3 and SorLA, the statistical robustness did not allow us to draw any strong conclusions (Fig. 7C), most likely due to the limited number of patients within the cohort.

Interestingly, by analyzing a CRC cohort (Nguyen et al., 2021) and dividing them into two groups (mucinous and non-mucinous) (Fig. S7C), we were able to see a positive correlation between ITGB1 and SORLA mRNA expression both in CMS1 and CMS3 (Consensus Molecular Subtype 1 and 3) solely for MUC CRCs (CMS2 being mostly non-represented in the mucinous CRCs), which was not the case for the non-mucinous CRCs (Fig. 7D-E).

Cumulatively, using cell- and mechanobiology methods to interrogate MUC CRC PDX tumors ex-vivo and patient samples we report a novel polarity determination mechanism whereby HER2/HER3/SorLA-controlled -β1-integrin traffic controls tumor-ECM interactions, ECM rearrangements and invasion into the peritoneum (Fig. 7F).

Discussion

Epithelial polarity is often considered a feature of normal tissue, maintained by cell-cell and cell-basement membrane interactions, and which is progressively lost in cancer in conjunction with increased invasion and metastasis. Our study uncovers a dynamic crosstalk network of integrins, HER-family receptor tyrosine kinases and receptor membrane traffic orchestrated by SorLA in determining MUC CRC polarity. Cumulatively, using cell- and mechanobiology methods to interrogate CRC PDX tumors ex-vivo and patient samples we report a novel polarity determination mechanism whereby HER2/HER3/SorLA-controlled β1-integrin traffic

control tumor-ECM interactions, ECM rearrangements and invasion on the peritoneum. Furthermore, expression of these receptors shows significant positive correlation in clinical patient specimens (Fig 7B).

SorLA is a well-established sorting protein regulating membrane traffic of APP in neurons, insulin receptor in adipocytes and HER2/HER3 receptors specifically in HER2-dependent breast cancer (Al-Akhrass et al., 2021; Pietilä et al., 2019; Andersen et al., 2005, 2006; Klinger et al., 2011; Spoelgen et al., 2009; Schmidt et al., 2016; Whittle et al., 2015). To the best of our knowledge, SorLA has not been previously implicated in CRC or in the regulation of cell polarity. We find that SorLA is a central nexus in polarity determination in MUC CRC TSIPs. SorLA levels are low in TSIPs is suspension but become rapidly upregulated in integrin-high TSIPs capable of forming initial contacts with collagen and adopting apical-in topology. ECM contact triggers two feed-forward regulatory loops: increased integrin recycling supportive on polarity maintenance and enhanced HER2/HER3 protein levels inducing SorLA-expression. Conversely, inhibition of integrins, HER2/HER3 receptors or silencing of SorLA impair ECM-induced polarity reversion of TSIPs. These data increase significantly our comprehension of MUC CRC cluster behavior during cancer progression and are likely to have important functional implications as previous work has implicated that non-reverted CRC clusters are capable of long-distance collective ameboid migration and are more resistant to chemotherapy (Pagès et al., 2022; Ashley et al., 2019).

In normal and cancer cells, integrins are constantly trafficked from the plasma membrane to endosomes and recycled back to facilitate dynamic cell adhesion (Moreno-Layseca et al., 2019; Paul et al., 2015). Increased integrin traffic facilitates invasion and metastasis in many cancer types, including breast and pancreatic cancer (Caswell et al., 2006; De Franceschi et al., 2015) and in particular increased integrin recycling via Rab11FIP1 (rab-coupling protein RCP) has been linked to β1-integrin recycling in complex with EGFR to drive cancer cell motility in 3D matrix (Machesky, 2019; Caswell et al., 2008; Rainero et al., 2012; Jacquemet et al., 2013; Muller et al., 2009). Here we find that MUC CRC tumor spheres, interacting with collagen, significantly downregulate Rab11FIP1 expression and upregulate SORLA. This implies that in reverted polarity TSIPs integrin recycling is switched to a polarity-maintaining receptor traffic program supportive of HER2/HER3 signaling.

Integrin expression is frequently altered in CRC with laminin-binding α6β4-integrin being frequently overexpressed and perhaps the most broadly studied (Beaulieu et al., 2020). Of the collagen-binding integrins, α1β1-integrin is normally restricted to the crypt epithelium but is upregulated in 65% of CRC where its expression is driven by MYC (Boudjadi et al., 2013, 2016). Surprisingly, the main fibrillar-collagen binding integrin-α2β1, has not been intensively investigated in CRC. We find here that both α1β1- and α2β1-integrins are expressed in the PDX-tumors and tumor spheres, with α2β1-having the highest expression in the apical-in polarity PDX. Inhibitory antibodies for α2-integrin are sufficient to block collagen-induced polarity reversion, implying that α1β1-collagen interaction is not supportive of polarity

reversion. This is an interesting distinction which could be linked to the pro-tumorigenic role of $\alpha 1\beta 1$-integrin in CRC and warrants further investigation in the future.

In the treatment of colon cancer, anti-EGFR therapy is in clinical use whereas trials for targeted therapies against HER2 have not resulted in approval of anti-HER2 therapy in CRC (Ye et al., 2022; Nowak et al., 2020). Interestingly, HER2 amplifications and elevated levels of the ligand of HER3, Heregulin-$\beta 1$, are linked to resistance of CRC to anti-EGFR therapeutic antibody cetuximab (Martin et al., 2013; Yonesaka et al., 2011). As expected, distinct CRC subtypes show differential responses to cancer therapeutics owing to their different biology. Our discovery of polarity regulation of MUC CRC by HER2/HER3/SorLA signaling ex-vivo and in patient samples, suggests a functionally important role for the pathway in this CRC subtype and might be a valuable consideration deserving further attention in the field of CRC therapy.

Acknowledgements

We thank P. Laasola and J. Siivonen for technical assistance and the Ivaska lab and Jaulin lab for scientific discussions. For services, we thank the Cytometry Core of the University of Turku, as well as the Turku Center for Disease modelling (TCDM). This work was supported by the Finnish Cancer Institute (K. Albin Johansson Professorship to J.I.); a Research Council of Finland research project (grant no. 325464 to J.I.) and Centre of Excellence program (grant no. 346131 to J.I.); the Cancer Foundation Finland (to J.I.); the Sigrid Juselius Foundation (to J.I.); and the Research Council of Finland InFLAMES Flagship program (grant no. 337530 and 357910). This work also received support from the Institut National du Cancer (INCa) (grant 2020-1-PLBIO-04-IGR-1), fundraising against CRC and Mars Bleu from the Gustave Roussy foundation. This work has also benefited from a government grant managed by the National Research Agency under the 5th PIA, integrated into France 2030 with the reference ANR-21-RHUS-0003. N.P. was supported by the "PhD in Oncology" program of the Fondation Philantropia, as well as the Pentti and Tyyni Ekbom Fund. A.I. was supported by the Finnish Cultural Foundation (00210428), the Orion Research Foundation, and the K. Albin Johansson's Foundation.

Author contributions

N.P, A.I and Z.F. performed the experiments. N.P, A.I, J.H, G.F and C.D. undertook the data analysis. V.B. provided resources. A.I. provided methodology. J.M, H.H. reviewed and edited the manuscript. N.P. and J.I. wrote the original draft of the manuscript. F.J. and J.I. supervised the project. F.J. and J.I. obtained research funding.

Material and methods

Culture and passaging of patient-derived xenografts

Animal experiments: Animal experiments performed in France were compliant with French legislation and EU Directive 2010/63. The project was validated by the Ethical Committee (CEEA) no. 26 and was then granted French government authorizations under number 517-2015042114005883 and 2734-2015111711418501. Animal experiments performed in Finland were done in accordance with the Finnish Act on Animal Experimentation (animal license number ESAVI/12558/2021). Mice were obtained from Charles River France and Germany, housed and bred at the Gustave Roussy animal core facility (accreditation number E-94-076-11) and at TCDM (Turku Center for Disease Modelling). Animals were euthanized according to endpoints that were validated by the Ethical Committee, the French government (Ministère de l'Enseignement Supérieur, de la Recherche et de l'Innovation) and the Finnish government.

Three human colorectal tumors (PDX#1 (9C) corresponding to LRB-0009C, PDX#2 (12P) corresponding to IGR-0012P and PDX#3 (14P) corresponding to IGR-014P)) from the CReMEC tumor collection were maintained in NSG mice (strain: NOD.Cg-*Prkdc*^{scid} *Il2rg*^{tm1Wjl}/SzJ, female, 6-8 weeks old at grafting) as described in Canet-Jourdan et al. 2022 and in Julien et al. 2012. Briefly, small tumor fragments were subcutaneously engrafted on both flanks of anesthetized mice (2.5% isoflurane). Tumor growth was measured once to twice a week. When the combined tumor burden reached 1700 mm^3, mice were sacrificed, tumors were used for *ex vivo* experiments and 50 mm^3 fragments engrafted on the flanks of new mice in order to maintain the biological material source.

Generation of tumoroids: Tumoroids were prepared according to Sato et al., 2011 and adapted for muco-secreting tumors as follows. The 9C, 12P or 14P tumors of 1200-1700 mm^3 were retrieved from the mice, minced into small fragments using a sterile scalpel and were incubated for 1 h at 37°C in a final volume of 5 to 10 ml of culture medium (Dulbecco's modified Eagle's medium; DMEM) without fetal bovine serum (FBS) and with 2 mg/ml collagenase (Sigma, C2139). The samples were then mixed with 20 ml of DMEM and filtered on 100 µm mesh size cell strainers (Greiner, EASYstrainer, 542000) and centrifuged 10 min at 277 g. Clusters were isolated from the remaining mucin and single cells by washing in 10 ml of DMEM and pulse centrifugating at 277 g five times. The clusters, now free of mucin and single cells, were maintained for 3 days in ultra-low attachment plates (Corning, CLS3471) in culture medium. Then, organoids were pelleted at 277 g and used for further experiments.

Collagen embedding and culture of tumoroids: Collagen-I (Corning, 354236) was neutralized with 1.0 M NaOH and 10× MEM (Life Technologies, 21430-02) according to the ratio: 1.0:0.032:0.1 (v/v/v). The concentration was then adjusted to 2 mg/ml with 1x DMEM, and the collagen-I was incubated on ice for 1h. The organoids, after spending 3 days in suspension as described previously, were then embedded in neutralized collagen-I and were added on top of pre-coated (using 7µl of the collagen mix per well) wells of a µ-Slide 8 Well ibiTreat slide

(Ibidi, 80826) at a concentration of 30–50 organoids/5 µl. The gel was allowed to polymerize for 1h at 37°C. Organoids were then cultured in culture medium supplemented with FBS 10% for up to 6 days (3 days for PDX#3). The drugs were diluted in the medium as follows: AIIB2 (DSHB, AB528306, 1 µg/ml), Heregulin-β1 (Peprotech, 100-03-10UG, 20 ng/ml), Trastuzumab (Herceptin, Roche, 10 µg/ml), Pertuzumab (Perjeta, Genentech, 10 µg/ml), Saracatinib (Selleckchem, S1006, 1 µM), EHT-1864 (R&D Systems, 3872, 5 µM), P1E6 (DSHB, AB2619597, 10 µg/ml), FAK14 (Tocris, 3414, 10 µM).

Generation of a Patient-Derived Organoid line: The clusters obtained from the PDX as described previously were pulsed centrifuged at 277 g and resuspended in Matrigel (Corning, 354230) and plated in 10 x 15 µl droplets in the bottom of a 6-well plate (Greiner, 657160). Cells were then incubated at 37°C for 15 minutes to let the basement membrane extract polymerize, then culture medium was added as described in Fujii et al 2018, without any human R-spondin1, A83-01 and Afamin-Wnt-3A serum-free condition medium. During the first two days, the organoid expansion medium was supplemented with Y-27632 (Calbiochem, 688000, 10 µM). This medium was renewed every two days and PDOs were passaged every 7 to 14 days as described in Cartry et al 2023.

LS513 culture and LS513 TSIPs formation : LS513 cells were obtained from ATCC (#CRL-2134) and cultured in RPMI-1640 medium supplemented with 10% FBS. LS513 were cultured in 10 cm cell culture dish. To generate TSIPs from the LS513 monolayer, the medium was changed every two days until the monolayer reached confluence. After waiting 5 days, the medium was collected and pulse centrifuged at 277g to collect the LS513 TSIPs. These were left for 3 days in suspension in ultra-low attachment plates (Corning, CLS3471), and embedded in collagen as described earlier (using the LS513 medium). For passaging, the monolayer was digested with 1x trypsin when 70% confluence was reached.

Immunofluorescence staining

After incubation for 3 days in suspension or for 3 to 6 days in collagen, the apico-basolateral polarity of organoids was quantified. Cells were washed thrice with PBSCM (PBS supplemented with $CaCl_2$ (0.1 mM) and $MgCl_2$ (1 mM)), fixed with 4% paraformaldehyde (PFA) for 5 minutes (for spheres in suspension) or 45 minutes (for spheres in collagen) at RT. Spheres fixed in suspension were then embedded in collagen for imaging as previously described. Permeabilization was then performed in PBSCM supplemented with 0.5% Triton X-100 for 45 minutes. Spheres were incubated with primary antibodies overnight at 4°C with the dilutions mentioned in Table 2 in PBSCM supplemented with 10% FBS and 0.1% Triton X-100. After washing thrice with PBSCM supplemented with 0.05% Tween, spheres were incubated with secondary antibodies and phalloidin for 2h at RT with the dilutions mentioned in Table 2, as

well as with DAPI (1 μg/ml). Spheres were then washed thrice with PBSCM supplemented with 0.05% Tween. The gel was then immerged in PBS before imaging.

Confocal imaging

Images were acquired either using a SpinningDisk CSU-W1 microscope (Yokogawa) with a ZylasCMOC camera piloted with an Olympus X83, or with a 3i CSU-W1 spinning disk confocal microscope with Hamamatsu CMOS (x40 water immersion objective). Basic image processing including look up table optimization, channels overlay, projections, etc.. were performed using Fiji software (citation). More specific quantifications are detailed in the following sections.

Western blotting

Spheres embedded in collagen were first released from the matrix by incubation of DMEM without serum supplemented with 2 mg/ml collagenase (Sigma, C2139) for 45 minutes. After pulse centrifugating at 277g, spheres were washed with PBS and pulse centrifugated at 277 g twice. Spheres were then lysed in TXLB buffer [50 mM Hepes, 1% Triton X-100, 0.5% sodium deoxycholate, 0.1% SDS, 0.5 mM EDTA, 50 mM NaF, 10 mM Na_3VO_4, and protease inhibitor cocktail (cOmplete Mini, EDTA-free, Roche)]. Cells cultured in 2D were washed twice with PBS and directly lysed with TXLB. Separation was performed by gel electrophoresis (Mini-PROTEAN TGX Precast Gels 4-20%, Bio-Rad, 4561096), before transferring onto a nitrocellulose membrane (Trans-Blot Turbo Transfer System, Bio-Rad) and blocking with AdvanBlock-Fluor (Advansta, R-03729-E10). Primary antibodies in AdvanBlock-Fluor were incubated overnight at 4°C with the dilutions mentioned in Table 2. Membranes were washed thrice between primary and secondary antibody treatments with Tris-buffered saline with 0.1% Tween 20 (TBST). IRDye secondary antibodies (see Table 2) were incubated for at least 1 hour at RT, before detection on an Odyssey fluorescence imager CLx (LI-COR). Densitometry analysis was performed in Fiji by normalizing the signal to GAPDH, which was used as a loading control.

PNGase digestion of lysates For PNGase digestion, cell lysates were prepared in a SDS-free buffer [50 mM Hepes, 1%NP-40, 0.5% sodium deoxycholate, 0.5 mM EDTA, 50 mM NaF, 10 mM Na_3VO_4, and protease inhibitor cocktail (cOmplete Mini, EDTA-free, Roche)]. 9 μl of lysate was mixed to 1 μl of Glycoprotein Denaturing Buffer 10X) (NEB, B1704S). The lysate was denatured at 100°C for 10 minutes, then chilled on ice. 2 μl GlycoBuffer 2 (10X) (NEB, B3704S), 2 μl 10% NP-40 (NEB, B2704S), 5 μl H_2O and 1 μl PNGase F (NEB, P0704S) were then added to the lysate, and mixed gently. The lysate was then incubated at 37°C for 1h. From there, the samples were prepared and run as described before.

SorLA silencing using shRNA lentiviral transduction During passaging of the 14P-generated PDO line as described previously, 10^5 cells were resuspended in 36 µl of organoid expansion medium and infected with 4M TU [62 µl of each virus (Origene, TL309181V)], 1 µl polybrene (Merck, TR-1003-G, stock solution at 1 mg/ml) and 1 µl Y-27362 (Calbiochem, 688000, 10 µM, stock solution 1 mM), in a U-bottom 96-well plate (Falcon, 351177) for 6 hours at 37°C. The content of the wells were then collected in a 1.5 mL Eppendorf tube, 1 ml of DMEM+10%FBS was added, and cells were centrifugated at 200 g for 3 minutes. Cells were then resuspended in 60 µl Matrigel (Corning, 354230) and 4x15 µl droplets were poured in a 24 well cell culture plate (Cellstar, 662 160) and left at 37°C degrees to polymerize for 15 minutes. 1 ml organoid expansion medium (supplemented with 10 uM Y-27362 for the first two days). The medium was changed every two days and organoids left to grow for 7 days. For polarity assays, the well was first washed thrice with PBS, before adding 1 ml of Cell Recovery Solution (Corning 354253). Cells were then left to incubate at 4°C for 20 minutes; Mechanical dissociation was then applied with a p1000 pipette until Matrigel was completely dissolved. 4 ml of PBS was added and spheroids were pulse centrifuged at 277 g. The spheres, now free of Matrigel, were maintained for 3 days in ultra-low attachment plates (Corning, CLS3471) in PDX culture medium. Then, organoids were pelleted at 277 g and used for further experiments.

SORLA KO using siRNA transient transfection LS513 were plated in a 6 well plate at 80% confluency. Transient siRNA transfections were performed using Lipofectamine RNAiMAX reagent (Invitrogen, 56532) according to the manufacturer's instructions. SORLA-targeting siRNAs were ON-TARGETplus obtained from Dharmacon—siSORLA #1 (J-004722-08), siSORLA #2 (J-004722-06), siSORLA #3 (J-004722-07), siSORLA #4 (J-004722-05). For controls, Allstars negative control (Qiagen, Cat. No. 1027281) was used. siRNA concentrations used were all 20 nM and cells were transfected with siRNAs 72 h prior to experiments.

Integrins recycling assay Surface biotinylation-based integrin trafficking assays in SorLA-silenced LS513 cells were performed based on previously published methods (Farage et al., 2021; Arjonen et al. 2012), with some modifications. Nunc MaxiSorb 96-well plates (Thermo Fischer, 44-2404-21) Enzyme-linked immunosorbent assay (ELISA) plates were coating with anti-b1-integrin antibody mix (5 µg/ml of AIIB2 (in-house) and anti-CD29 (BD Bioscience #610468)) in TBS (50 µl per well) overnight at +4 °C. The wells were blocked with 5% BSA in TBS for 2 h at 37 °C, (100 µl per well). LS513 cells were silenced three days before the experiment as described earlier. 2 hours prior to the experiment, the medium was changed to prewarmed RPMI with 10% FBS to induce receptor traffic. The cells were placed on ice and washed once with cold PBS. Cell surface proteins were labelled with 0.13 mg/ml EZ-link cleavable sulfo-NHS-SS-biotin (Thermo Scientific, 21331) in serum-free RPMI medium for 30 min at +4 °C. Any unbound biotin was removed by washing with cold medium and pre-warmed RPMI+10% FBS with or without 100 µM primaquine (Sigma, 160393) was added to

the cells. The biotin-labelled surface proteins were allowed to traffic at +37 °C for 15 or 30 minutes. Cells were placed on ice, washed once with cold PBS and cold cell surface reduction buffer (50 mm Tris–HCl, pH 8.6 and 100 mm NaCl). Cell surface biotin was cleaved with non-membrane permeant reducing reagent MesNa (30 mg/ml, sodium 2-mercaptoethanesulfonate; Fluka, 63705) in cell surface reduction buffer 20 min at 4 °C, followed by quenching with 100 mM iodoacetamide (Sigma, I3750) for 15 min on ice. For the 0 min internalization, cells were maintained on ice in serum-free RPMI until cell surface reduction with MesNA. The cells were lysed by scraping in lysis buffer (1.5% octylglucoside, 1% NP-40, 0.5% BSA, 1 mM EDTA, and protease and phosphatase inhibitors) and incubation at +4 °C for 20 min with rotation and cleared by centrifugation (16,000*g*, 10 min, 4 °C). To detect the biotinylated integrins, 50 µl volumes of the cell lysates were incubated in duplicate wells at +4 °C overnight, washed extensively with TBST, incubated for 2 h at 4 °C with 1:1,000 horseradish peroxidase-coupled streptavidin (Fisher, 21130), washed and detected with antibody for ELISA detection.

Immunohistochemistry Histology CRC and peritoneum specimens obtained after surgical resection were formalin fixed and paraffin embedded according to routine protocols. Sections (3 µm) of formalin-fixed and paraffin-embedded samples were deparaffinized, unmasked (pH 8) and rehydrated before HES or Alcian Blue (pH 2.5) staining, immunohistochemistry or immunofluorescence. Immunohistochemistry Sections were immunostained for SORLA, HER2, HER3 or with anti-CK20 mouse monoclonal antibody (see Table 2). Slides were imaged using Axioscan Z1, Zeiss (x20) and analysed using QuPath.

Mass cytometry Spheroids in collagen for 3/6 days underwent collagen digestion by incubation of DMEM without serum supplemented with 2 mg/ml collagenase (Sigma, C2139) for 45 minutes. After resuspending in DMEM + 10% FBS and pulse centrifugating at 277g, they were collected. Spheroids cultured in suspension, clusters obtained from PDX digestion or spheroids released from collagen as described previously were washed with PBS thrice and pulsed centrifuged at 277 g thrice in order to keep the clusters/spheroids and get rid of any single cells and secreted mucins. The spheres were then digested in Cell Dissociation Buffer Enzyme-Free PBS-based (gibco, 13151-014) supplemented with 2 mg/ml collagenase (Sigma, C2139) and incubated for 1h at 37°C with occasional mechanical dissociation by pipetting. After addition of DMEM+10% FBS to quench the collagenase, cells were centrifuged at 200 g for 3 minutes and washed thrice with PBS. They were then resuspended in 1 ml cold PBS and filtered through a 5 ml polystyrene round bottom tube with Cell-Strainer cap (Falcon, 352235), and kept on ice until staining, which was done according to the Fluidigm Maxpar Cell Surface Staining with Fresh Fix protocol. The sample was then run through a Helios™ Mass Cytometer and the data analyzed with Cytobank and clustered through SPADE and viSNE analysis.

Statistical analysis All statistical comparisons were performed using Prism 7 (GraphPad software), as indicated in the figure legends, repeating all experiments at least three times independently.

Generation of fluorescent collagen To fluorescently label rat tail type I collagen (~4.24 mg/mL, 354236, Corning), 1.65 mL was mixed with 450 µL of Milli- Q water and 500 µL of neutralizing buffer (20 mM NaH2PO4, 112 mM Na2HPO4·2H2O, 0.4 M NaCl, and 46 mM NaOH) and incubated at 37 °C for 30 min. The polymerized collagen was then washed thrice with PBS for 10 min. Then, 3 mL of Milli- Q water and 1 mL of bicarbonate buffer [1 M NaHCO3 (pH 8), raised dropwise to pH 8.3 using 1.17 M Na2CO3 (pH 11)] were added to the collagen gel before addition of the Alexa Fluor™ 647 NHS Ester (Succinimidyl Ester) dye (A20006, Invitrogen) in 100 µL of PBS. After incubating the collagen mix overnight at 4 °C, the dye was then removed, and the collagen was washed with PBS with rotation at room temperature for 30 min, changing the PBS five times. Stained collagen was then depolymerized through the addition of 2 mL HCl (20 mM) and gentle rotation at 4 °C overnight. The collagen was finally centrifuged at 20,000 g for 10 min, collecting the labeled collagen from the supernatant. The fluorescent collagen was then used at a 1:1000 concentration in the previously described neutralized collagen gel.

Generation ©CNA35 and cloning Molecular cloning and recombinant protein purification. To generat©he CNA35-mScarlet construct©ET28a-CNA35-EGFP (A kind gift from Maarten Merkx (Eindhoven University of Technology, MB Eindhoven, The Netherlands), Addgene plasmid #61603) was digested with NheI/EcoRI and ligated with a NheI/EcoRI digested mScarlet gene fragment (IDT) to generate pET2©mScarlet-CNA35 (Addgene plasmid #X). This was validated by analytical digestion and sequencing. Recombinant protein pu©ication for CNA35-mScarlet was performed as described previously.

Peritoneum ex vivo assay Peritoneum samples were collected from mice and decellularized by incubating them in a 1M NH_4OH solution for 1h at RT. After washing thrice with PBS for 15 minutes, peritoneum samples were left to incubate with PBS and penicillin-streptomycin (1:100) at 4°C overnight. After washing thrice with PBS for 15 minutes, the peritoneum was sectioned in 1cmx1cm pieces and adhered (using Tissue Adhesive, 3M, 1469SB) to the bottom of plastic transwell inserts (Greiner, Thincerts, 8 um pore size, 662638) after removing the filter with a scalpel. 100 tumor spheres were resuspended in 100 ml of DMEM+10%FBS and placed in the well with AIIB2 (DSHB, AB528306, 1 µg/ml), Y27632 (Calbiochem, 688000, 25 µM), Heregulin-β1 (Peprotech, 100-03-10UG, 20 ng/ml), Trastuzumab (Herceptin, Roche, 10

μg/ml), Pertuzumab (Perjeta, Genentech, 10 μg/ml) for 6 days. The fixing and IF staining was performed as described previously. Peritoneum bits were placed upside-down on a glass bottom dishes (Cellvis, D35-14-1-N), and imaged as described previously, using the x20 objective.

Whole Exome Sequencing DNA was extracted using the DNeasy ikit (Qiagen, Cat. No. 69504) from organoids either after 3 days in suspension (wash one time in PBS supplemented with Ca^{2+} and Mg^{2+} as mentioned above). Whole exome analysis was performed by Integragen SA (France), comparing the three samples (9C, 12P and 14P) to a PON (panel of normal) and analyzed with MERCURY™.

Collagen orientation analysis Type I collagen gels with 14P and 12P spheroids were prepared on glass bottom dishes (Cellvis, D35-14-1-N). 80 μl of PureCol EZ Gel (Advanced BioMatrix, 5074) was spread on the glass bottom using a micropipette tip and allowed to polymerize at +37 °C for 1 h. Next, 14P or 12P spheroids were pulse centrifuged at 277 g to remove the mucin and single cells. Approximately 100 spheroids were mixed with 80 μl of PureCol EZ Gel and pipetted on top of the previously polymerized collagen layer, after which the mixture was allowed to polymerize at +37 °C for 1 h. Spheres were treated with AIIB2 (DSHB, AB528306, 1 μg/ml), Y27632 (Calbiochem, 688000, 25 μM), Heregulin-β1 (Peprotech, 100-03-10UG, 20 ng/ml), Trastuzumab (Herceptin, Roche, 10 μg/ml), Pertuzumab (Perjeta, Genentech, 10 μg/ml). One day before the samples were imaged, the cultures were supplemented with 1:1000 SiR-actin (Sprichrome, SC001) and ~40 μg/ml of mScarlet-conjugat©collagen probe CNA35 (Aper et al 2014).

The spheroids were imaged live using a Marianas spinning disk confocal microscope, 20x objective, Orca Flash4 sCMOS camera, and 2x2 binning (see Microscopy for details). 60-80 μm stacks were acquired around the center (z) of each spheroid. In order to analyze collagen fiber orientation around the spheroids, ca. 4 μm substacks were acquired near the center of each spheroid and used for creating maximum intensity projections. Next, 200x200 μm regions o©nterest depicting CNA35 directly proximal to each spheroid, but excluding any dense collagen aggregates on the spheroid surface, were selected from the projections for analysis. If the matrix surrounding the spheroid was obviously heterogeneous, the region was selected to maximize the local alignment.

The selected regions were analyzed with ImageJ plugin OrientationJ, using cubic spline gradient and a local window size of 4 pixels. In the color survey, hue represented orientation and saturation represented coherency. All the local orientations were exported and analyzed using a custom R script to yield fiber orientation indices (Ferdman et al 1993, Taufalele et al 2019). Briefly, the orientations (-90°…+90°) representing each region were normalized, i.e.,

their distribution was centered around zero based on the peak of the histogram. Next, orientation indices (S) were calculated such that

$$S = 2 < cos^2\alpha > -1 \quad (1)$$

where α is the angle between an individual (fiber) orientation and the average orientation of the entire region, and $<cos^2\alpha>$ is the averaged square cosine of all α per analyzed region. And index of 0 represents a random distribution, and an index of 1 represents a perfectly aligned distribution.

Collagen displacement fields In order to measure transient displacements exerted on the collagen matrix by the 14P and 12P spheroids, the spheroids were prepared and embedded in type I collagen, as described above. The spheroids were grown in the gels for 6 days and supplemented with 1:1000 SiR-actin©d ~40 µg/ml mScarlet-CNA35 one day before the imaging. 60-80 µm stacks were acquired around/near the center of each spheroid, before and after the cells and matrix were relaxed by adding 10 µM latrunculin B and incubating for ca. 20 minutes. Marianas spinning disk confocal microscope, 20x objective, Orca Flash4 sCMOS camera, and 2x2 binning were used for the imaging (see Microscopy for details).

3D displacement fields were calculated using TFMLAB (Barrasa-Fano et al 2021a, Sanz-Herrera et al 2021, Barrasa-Fano et al 2021b), a traction force microscopy toolbox implemented in MATLAB R2022a (MathWorks). The spheroids were segmented using actin images, variable threshold adjustment and a minimum object size of 10^4 voxels. Rigid image registration was done using the default phase correlation-based algorithm. The displace©ts were calculated from CNA35 images using 10x10x10 µm grid spacing, default registration metric and optimizer (normalized correlation coefficient, adaptive stochastic gradient descent) and post-shift correction. The results were visualized using ParaView v5.11.0 (Ahrens et al 2005).

Analysis of SORLA and ITGB1 gene expression in human tumors Preprocessed TCGA colon adenocarcinoma cohort RNAseq data and raw RSEM-counts were downloaded from https://gdc.cancer.gov/node/905/ and https://gdac.broadinstitute.org/runs/stddata__2016_01_28/data/, respectively. CMSCaller (Eide et al., 2017) was used to infer consensus molecular subtypes (CMS) from RSEM-counts, excluding calls with FDR > 0.05. The samples were categorized as mucinous and control cases based on previously conducted characterization (Nguyen et al., 2021). Associations between SORLA and ITGB1 gene expression were assessed with the preprocessed normalized log2 mRNA expression data by computing linear regression within each CMS group.

Protein	Company	Catalog Number	Application	Concentrat on

Ezrin	DHSB	AB-210031	IF	1 : 400
SorLA	C.M. Petersen (Aarhus U)		IF	1:200
RAB11FIP1 (RCP)	T ermoFisc er	PA5-55276	IF/WB	1 :400 / 1 :1000
HER2	Therm Fische	MA5-14 57	IF/WB/IHC	1 :400/1 :1000/1 :400
HER3 Cell Si naling	12708S	IF/WB	1 :1000/1 :100	
P5D2 (Total in egrin-β1)	Abcam	Ab193592	IF	1 :500
12G10 (Active in egrin-β1)	Abcam	Ab202641	IF	1 :500
WG -lectin	GeneTex	GTX01502	IF	1 :500
CNA-35	In-house		IF	40 ug/ml
Phalloi in 488	Invitrogen	A12379	IF	1 :1000
P alloidin 647	Sigma	65906	IF	1 :1000
P alloidin 750	Sigma	07373	IF	1 :1000
So LA	BD Biosciences	624084	WB	1 :500
Anti ms 568	Invitrogen	A10037	IF	1 :500
Anti ms 488	Invitrogen	A21202	IF	1 :500
Anti- bt 488	Invitrogen	A21206	IF	1 :500
Anti- bt 561	Invitrogen	A10042	IF	1 :50
GAPDH	HyTest	5G4MAB6C5	WB	1 :2000
Erk	Cell Signaling	4696S	WB	1 :500
Src	Cell Signaling	2108S	WB	1 :500
p-Src (act ve)	Cell Signaling	2101S	WB	1 :500
Ms sec 65	Azure Biosystems	AC2166	WB	1 :1000
Ms sec 80	Azure Biosystems	AC2135	WB	1 :1000
Rbt sec 65	Azure Biosystems	AC2165	WB	1 :1000
Rbt sec 80	Azure Biosystems	AC2134	WB	1 :1 00
HER3	Dako	DAK-H3-IC	IHC	1 :5
SorLA	Atlas	HPA031321	IHC	1 :400
Pan CK	Invitrogen	MA5-13203	IHC	1 :400
P1E6 (Integrin-α2)	DSHB	AB2619597	FB	10 μg/ml
AIIB2 (Integrin-β1)	DHSB	AB528306	FB	1 μg/ml
AIIB2 (Integrin-β1)	In-house		ELISA	5 μg/ml
CD29	BD Bioscience	610468	eLISA	5 μg/ml
^{89}Y-Integrin-αII	AH Diagnostics	3089004B	MC	1 :100
^{141}Pr-EpCA	AH Diagnostics	3141006B	MC	1 :100

^{142}Nd-PETA-	AH Diagnostics	3142011B	MC	1 :100
^{143}Nd-N-Cadheri	AH Diagnostics	3143016B	MC	1 :100
^{145}Nd-Syndecan-	AH Diagnostics	3145003B	MC	1 :100
^{146}Nd-Integrin-β	AH Diagnostics	3145011B	MC	1 :100
^{148}Nd-HER	AH Diagnostics	3148011A	MC	1 :100
^{149}Sm-CD3	AH Diagnostics	3149013B	MC	1 :100
^{150}Nd-Integrin-αvβ	AH Diagnostics	3150026B	MC	1 :100
^{151}Eu-ICAM-	AH Diagnostics	3151015B	MC	1 :100
^{156}Gd-Integrin-β	AH Diagnostics	3156007B	MC	1 :100
^{158}Gd-E-cadheri	AH Diagnostics	3158018B	MC	1 :100
^{159}Tb-CD9	AH Diagnostics	3159022B	MC	1 :100
^{160}Gd-Integrin-α	AH Diagnostics	3160015B	MC	1 :100
^{161}Dy-Integrin-α	AH Diagnostics	3161012B	MC	1 :100
^{162}Dy-Integrin-β	AH Diagnostics	3162026B	MC	1 :100
^{163}Dy-Integrin-α	AH Diagnostics	3163015B	MC	1 :100
^{164}Dy-Integrin-α	AH Diagnostics	3164006B	MC	1 :100
^{165}Ho-Notch	AH Diagnostics	3165026B	MC	1 :100
^{166}Er-CD4	AH Diagnostics	3166001B	MC	1 :100
^{168}Er-Integrin-α9β	AH Diagnostics	3168013B	MC	1 :100
^{169}Tm-CD2	AH Diagnostics	3169004B	MC	1 :100
^{170}Er-ICAM-	AH Diagnostics	3170014B	MC	1 :100
^{171}Yb-CD	AH Diagnostics	3171009B	MC	1 :400
^{173}Yb-Integrin-β	AH Diagnostics	3173008B	MC	1 :100
^{174}Yb-Integrin-α	AH Diagnostics	3174018B	MC	1 :100
^{176}Yb-NCA	AH Diagnostics	3176001B	MC	1 :100
^{209}Bi-CD4	AH Diagnostics	3209004B	MC	1 :100
^{11} Cd-EGFR	Biolegend	352902	MC	1 :50
^{114}Cd-Integr n-αV	R&D Systems	MAB1219	MC	1 :50
^{111}Cd-I tegrin-α3	Sigma	MAB1952Z	MC	1 :50
^{166}Cd- ER4	R&D Systems	MAB11311	MC	1 :50

^{110}Cd HER3	R&D Systems	MAB3481	MC	1 :50
^{106}Cd-Integri -α11	R&D Systems	MAB4235	MC	1 :50
^{144}Nd-Syndec n-4	R&D Systems	MAB29181	MC	1 :50
^{152}Sm-Integrin αvβ5	R&D Systems	MAB2528	MC	1 :50
^{155}Gd-Integr n-α8	R&D Systems	MAB6194	MC	1 :50
^{175}Lu-Integr n-β8	R&D Systems	MAB4775	MC	1 :50
^{153}Eu-Integr n-β6	R&D Systems	MAB4155	MC	1 :50
^{147} m-CD166	Biolegend	343902	MC	1 :200
^{154}Sm Notch-1	Biolegend	352102	MC	1 :50
^{167}Er Notch-3	Biolegend	345407	MC	1 :50
^{172}Yb-Neur pilin-1	Biolegend	354502	MC	1 :50
^{11} Cd-CD10	Biolegend	312223	MC	1 :50

Table 2- Antibodies and Reagents (WB=Western Blot; IF=Immunofluorescence; IHC=Immunohistochemistry; FB=Function blocking; MC=Mass cytometry, ELISA=enzyme-linked immunosorbent assay)

References

Adzhubei, I., Jordan, D. M., & Sunyaev, S. R. (2013). Predicting functional effect of human missense mutations using PolyPhen-2. *Current protocols in human genetics*, *76*(1), 7-20.

Al-Akhrass, H., Conway, J. R., Poulsen, A. S. A., Paatero,©, Kaivola, J., Padzik, A., ... & Ivaska, J. (2021). A feed-forward loop between SorLA and HER3 determines heregulin response and neratinib resistance. *Oncogene*, *40*(7), 1300-1317.

Al-Akhrass, H., Pietilä, M., Lilja, J., Vesilahti, E. M., Anttila, J. M., Haikala, H. M., ... & Ivaska, J. (2022). Sortilin-related receptor is a druggable therapeutic target in breast cancer. *Molecular oncology*, *16*(1), 116-129.

Amir, E. A. D., Davis, K. L., Tadmor, M. D., Simonds, E. F.©ev'ne, J. H., Bendall, S. C., ... & Pe'er, D. (2013). viSNE enables visualization of high dimensional single-cell data and reveals phenotypic heterogeneity of leukemia. *Nature biotechnology*, *31*(6), 545-552.

Andersen, O. M. et al. Molecular dissection of the interaction between amyloid precursor protein and its neuronal trafficking receptor SorLA/LR11. *Biochemistry* 45, 2618–2628 (2006).

Andersen, O. M. et al. Neuron24aracrting protein-related receptor sorLA/LR11 regulates processing of the amyloid precursor protein. *Proc. Natl. Acad. Sci. USA* 102, 13461–13466 (2005).

Aper, S. J., van Spreeuwel, A. C., van Turnhout, M. C., van der Linden, A. J., Pieters, P. A., van der Zon, N. L., ... & Merkx, M. (2014). Colorful protein-based fluorescent probes for collagen imaging. *PloS one*, *9*(12), e114983.

Argenzio, E., Margadant, C., Leyton-Puig, D., Janssen, H., Jalink, K., Sonnenberg, A., & Moolenaar, W. H. (2014). CLIC4 regulates cell adhesion and β1 integrin trafficking. *Journal of cell science*, *127*(24), 5189-5203.

Arjonen, A., Alanko, J., Veltel, S. & Ivaska, J. Distinct recycling of active and inactive β1 integrins. *Traffic* 13, 610–625 (2012)

Ashley, Neil, Dj“mila Ouaret, and Walter F. Bodmer. "Cellular polarity modulates drug resistance in primary colorectal cancers via orientation of the”multidrug resistance protein ABCB1." *The Journal of Pathology* 247.3 (2019): 293-304.

Barrasa-Fano, J., Shapeti, A., de Jong, J., Ranga, A., Sanz-Herrera, J. A., & Van Oosterwyck, H. (2021b). Advanced in silico validation framework for three-dimensional Traction Force Microscopy and application to an in vitro model of sprouting angiogenesis. Acta Biomaterialia, 126, 326-338.

Barrasa-Fano, J., Shapeti, A., Jorge-Penas, A., Barzegari, M., Sanz-Herrera, J. A., & Van Oosterwyck, H. (2021a). TFMLAB: A MATLAB toolbox for 4D traction force microscopy. *SoftwareX*, *1“*, 100723.

Barresi, Valeria, et al. "Prognostic significance of grading based on the counting of poorly differentiated clusters in”colorectal mucinous adenocarcinoma." *Human Pathology* 46.11 (2015): 1722-1729.

Bartley, A. N., Washington, M. K., Ventura, C. B., Ismaila, N.©olasacco, C., Benson III, A. B., ... & Ajani, J. A. (2016). HER2 testing and clinical decision making in gastroesophageal adenocarcinoma: guideline from the College of American Pathologists, American Society for Clinical Pathology, and American Society of Clinical Oncology. *American journal of clinical pathology*, *146*(6), 647-669.

Beaulieu J-F. Integrin α6β4 in Colorectal Cancer: Expression, Regulation, Functional Alterations and Use as a Biomarker. *Cancers*. 2020; 12(1):41. https://doi.org/10.3390/cancers12010041

Berdichevsky, F., Gilbert, C., Shearer, M., & Taylor-Papadimitriou, J. (1992). Collagen-induced rapid morphogenesis of human mammary epithelial cells: The role of the α 2 β 1 integrin. *Journal of Cell Science*, *102*(3), 437-446.

Bettington, M., Walker, N., Clouston, A., Brown, I., Leggett, B., & Whitehall, V. (2013). The serrated pathway to colorectal carcinoma: current concepts and challenges. *Histopathology*, *62*“3), 367-386.

Bettington, Mark, et al. "The serrated pathway to colorectal carc”noma: current concepts and challenges." *Histopathology* 62.3 (2013): 367-386.

Bosman, F. T., Carneiro, F., Hruban, R. H., & Theise, N. D. (2010). *WHO classification of tumours of the digestive system* (No. Ed. 4). World Health Organization.

Boudjadi S., Carrier J.C., Beaulieu J.F. Integrin alpha1 subunit is up-regulated in colorectal cancer. *Biomark. Res.* 2013;1:16.

Boudjadi S., Carrier J.C., Groulx J.F., Beaulieu J.F. Integrin alpha1beta1 expression is controlled by c-myc in colorectal cancer cells. *Oncogene.* 2016;35:1671–1678.

Bridgewater, R. E., Norman, J. C., & Caswell, P. T. (2012). Integrin trafficking at a glance. *Journal of cell science*, *125*(16), 3695-3701.

Böttcher, R. T., Stremmel, C., Meves, A., Meyer, H., Widmaier, M., Tseng, H. Y., & Fässler, R. (2012). Sorting nexin 17 prevents lysosomal degradation of β1 integrins by binding to the β1-integrin tail. *Nature cell biology*, *14*(6), 584“592.

Canet-Jourdan, Charlotte, et al. "Patient-derived organoids identify an apico-basolateral polarity switch associa”ed with survival in colorectal cancer." *Journal of Cell Science* 135.14 (2022): jcs259256.

Cartry, J., Bedja, S., Boilève, A., Math©, J. R., Gontran, E., Annereau, M., ... & Jaulin, F. (2023). Implementing patient derived organoids in functional precision medicine for patients with advanced colorectal cancer. *Journal of Experimental & Clinical Cancer Research*, *42*(1), 1-17.

Caswell P.T., Chan M., Lindsay A.J., McCaffrey M.W., Boettiger D. and Norman J.C. (2008) Rab-coupling protein coordinates recycling of alpha5beta1 integrin and EGFR1 to promote cell migration in 3D microenvironments. J. Cell Biol. 183, 143–155

Caswell, P. T., & Norman, J. C. (2006). Integrin trafficking and the control of cell migration. *Traffic*, *7*(1), 14-21.

Chastney, M. R., Conway, J. R., & Ivaska, J. (2021). Integrin adhesion complexes. *Current Biology*, *31*(10), R“36-R542.

De Sousa E Melo, Felipe, et al. "Poor-prognosis colon cancer is defined by a molecularly distinct subtype and”develops from serrated precursor lesions." *Nature medicine* 19.5 (2013): 614-618.

Diggins, N. L., Kang, H., Weaver, A., & Webb, D. J. (2018). α5β1 integrin trafficking and Rac activation are regulated by APPL1 in a Rab5-dependent manner to inhibit cell migration. *Journal of cell science*, *131*(5), jcs207019.

Dozynkiewicz, M. A., Jamieson, N. B., MacPherson, I., Grindlay,©, van den Berghe, P. V., von Thun, A., ... & Norman, J. C. (2012). Rab25 and CLIC3 collaborate to promote integrin recycling from late endosomes/lysosomes and drive cancer progression. *Developmental cell*, *22*(1), 131-145.

Eide, P. W., Bruun, J., Lothe, R. A., & Sveen, A. (2017). CMScaller: an R package for consensus molecular subtyping of colorectal cancer pre-clinical models. *Scientific reports*, *7*(1), 16618.

Eggert, S., Thomas, C., Kins, S., & Hermey, G. (2018). Trafficking in Alzheimer's disease: modulation of APP transport and processing by the transmembrane proteins LRP1, SorLA, SorCS1c, sortilin, and calsyntenin. *Molecular neurobiology*, *55*, 5809-5829.

Eva, R., Dassie, E., Caswell, P. T., Dick, G., Norman, J. C., & Fawcett, J. W. (2010). Rab11 and its effector Rab coupling protein contribute to the trafficking of β1 integrins during axon growth in adult dorsal root ganglion neurons and PC12 cells. *Journal of Neuroscience*, *30*(35), 11654-11669.

Farage, E. & Caswell, P. T. Quantitative analysis of integrin trafficking. *Methods Mol. Biol.* 2217, 251–263 (2021).

Ferdman et al. 1993. Scattering of light from histologic sections: a new method for the analysis of connective tissue. J Invest Dermatol.

Fujii, M., Matano, M., Toshimitsu, K., Takano, A., Mikami, Y., Nishikori, S., ... & Sato, T. (2018). Human intestinal organoids maintain self-renewal capacity and cellular diversity in niche-inspired culture condition. *Cell stem cell*, *23*(6), 787-793.

Hochwald, S. N., Nyberg, C., Zhe© M., Zheng, D., Wood, C., Massoll, N. A., ... & Golubovskaya, V. M. (2009). A novel small molecule inhibitor of FAK decreases growth of human pancreatic cancer. *Cell cycle*, *8*(15), 2435-2443.

Hugen, N., Van de Velde, C. J. H., De Wilt, J. H. W., & Nagtegaal, I. D. (2014). Metastatic pattern in colorectal cancer is strongly influenced by histological subtype. *Annals of oncology*, *25*(3), 651-657.

Ivanova, M., Venetis, K., Guerini-Rocco, E., Bot©lieri, L., Mastropasqua, M. G., Garrone, O., ... & Ghidini, M. (2022). HER2 in metastatic colorectal cancer: pathology, somatic alterations, and perspectives for novel therapeutic schemes. *Life*, *12*(9), 1403.

Jacquemet, G., Green, D. M., Bridgewater, R. E., von Kriegsheim, A., Humphries, M. J., Norman, J. C., & Caswell, P. T. (2013). RCP-driven α5β1 recycling suppresses Rac and promotes RhoA activity via the RacGAP1–IQGAP1 complex. *Journal of Cell Biology*, *202*(6), 917-935.

Jakubowska, Katarzyna, K“tarzyna Guzińska-Ustymowicz, and Anna Pryc27araca "Invasive micropapillary component and its clinico-histopathologic”l significance in patients with colorectal cancer." *Oncology Letters* 12.2 (2016): 1154-1158.

James Ahrens, Berk Geveci, and Charles Law. “ParaView: An End-User Tool for Large Data Visualization.” In Visualization Handbook. Elesvier, 2005. ISBN 978-0123875822.

Julien, S., Merino-Trigo, A.©acroix, L., Pocard, M., Goéré, D., Mariani, P., ... & Berthet, C. (2012). Characterization of a large panel of patient-derived tumor xenografts representing the clinical heterogeneity of human colorectal cancer. *Clinical Cancer Research*, *18*(19), 5314-5328.

Kawata, M., Kon© J., Onuma, K., Ito, Y., Yokoi, T., Hamanishi, J., ... & Inoue, M. (2022). Polarity switching of ovarian cancer cell clusters via SRC family kinase is involved in the peritoneal dissemination. *Cancer Science*, *113*(10), 3437-3448.

Klinger, S. C. et al. SorLA regulates the activity of lipoprotein lipase by intracellular trafficking. *J. Cell. Sci.* 12“, 1095–1105 (2011).

Lee, Minhui, and Valeri Vasioukhin. "Cell polarity and cancer–cell”and tissue polarity as a non-canonical tumor suppressor." *Journal of cell “cience* 121.8 (2008): 1141-1150.

Libanje, Fotine, et al. "ROCK 2 inhibition trigge”s the collective invasion of colorectal adenocarcinomas." *The EMBO journal* 38.14 (2019): e99299.

Lubarsky, B., & Krasnow, M. A. (2003). Tube morphogenesis: making and shaping biological tubes. *Cell*, *112*(1), 19-28.

Luo, C., Cen, S., Ding, G., & Wu, W. (2019). Mucinous colorectal adenocarcinoma: clinical pathology and treatment options. *Cancer commu“ications*, *39*, 1-13.

Macara, Ian G., and Luke M”Caffrey. "Cell polarity in morphogenesis and metastasis." *Philosophical Transactions of the Royal Society B: Biological Sciences* 368.1629 (2013): 20130012.

Machesky, L. M. (2019). Rab11FIP proteins link endocytic recycling vesicles for cytoskeletal transport and tethering. *Bioscience reports*, *39*(1), BSR20182219.

Manninen, A. (2015). Epithelial polarity–generating and integrating signals from the ECM with integrins. *Experimental cell research*, *334*(2), 337-349.

Martin, V., Land©L., Molinari, F., Fountzilas, G., Geva, R., Riva, A., ... & Cappuzzo, F. (2013). HER2 gene copy number status may influence clinical efficacy to anti-EGFR monoclonal antibodies in metastatic colorectal cancer patients. *British journal of cancer*, *108*(3), 668-675.

Mekenkamp, L. J., Heesterbeek, K.©, Koopman, M., Tol, J., Teerenstra, S., Venderbosch, S., ... & Nagtegaal, I. D. (2012). Mucinous adenocarcinomas: poor prognosis in metastatic colorectal cancer. *European journal of cancer*, *48*(4), 501-509.

Moreno-Layseca, P., Icha, J., Hamidi, H., & Ivaska, J. (2019). Integrin trafficking in cells and tissues. *Nature cell biology*, *21*(2), 122-132.

Muller, P. A., Casw©, P. T., Doyle, B., Iwanicki, M. P., Tan, E. H., Karim, S., ... & Vousden, K. H. (2009). Mutant p53 drives invasion by promoting integrin recycling. *Cell*, *139*(7), 1327-1341.

Nguyen, B., Sanchez-Vega, F., Fong, C. J., Chatila, W. K., Boroujeni, A. M., Pareja, F., ... & Schultz, N. (2021). The genomic landscape of carcinomas with mucinous differentiation. *Scientific reports*, *11*(1), 9478.

Nowak, J. A. (2020). HER2 in colorectal carcinoma: ’re we there yet?. *Surgical Pathology Clinics“ 13*(3), 485-502.

O'Brien, Michael J., Qing Zhao, ”nd Shi Yang. "Colorectal serrated pathway cancers and precurs“rs." *Histopathology* 66.1 (2015): 49-65.

Okuyama, Hiroaki, et al. "Dynamic change of polarity in primary cultured sphero”ds of human colorectal adenocarcinoma and its role in metastasis." *The American Journal of Pathology* 186.4 (2016): 899-911.

Onesto, C., Shutes, A., Picard, V., Schweighoffer, F., & Der, C. J. (2008). Characterization of EHT 1864, a novel small molecule inhibitor of Rac family small GTPases. *Methods i“ enzymology*, *439*, 111-129.

Onuma, Kunishige, and Masah”ro Inoue. "Abnormality of apico–basal polarity in adenocarcinoma." *“ancer Science* 113.11 (2022): 3657-3663.

Onuma, Kunishige, et al. "Aberrant activation of Rho/ROCK signaling in i”paired polarity switching of colorectal micropapillary carcinoma." *The Jou“nal of Pathology* 255.1 (2021): 84-94.

Pagès, Diane-Laure, et al. "Cell clusters adopt a collectiv” amoeboid mode of migration in confined nonadhesive environments." *“cience Advances* 8.39 (2022): eabp8416.

Pasquier, Ni”olas, et al. "Inverted apicobasal polarity in health and disease." *Journal of Cell “cience* (2024)

Peglion, Florent, and Sandrine Etienne-Mannev”lle. "Cell polarity changes in cancer initiation and progression." *Journal of Cell Biology* 223.1 (2023): e202308069.

Pietilä, © Sahgal, P., Peuhu, E., Jäntti, N. Z., Paatero, I., Närvä, E., ... & Ivaska, J. (2019). SORLA regulates endosomal trafficking and oncogenic fitness of HER2. *Nature Communications*, *10*(1), 2340.

Quintelier, K., Couckuyt, A., Emmaneel, A., Aerts, J., Saeys, Y., & Van Gassen, S. (2021). Analyzing high-dimensional cytometry data using FlowSOM. *Nature protocols*, *16*(8), 3775-3801.

Rainero, E., Caswe© P. T., Muller, P. A., Grindlay, J., McCaffrey, M. W., Zhang, Q., ... & Norman, J. C. (2012). Diacylglycerol kinase α controls RCP-dependent integrin trafficking to promote invasive migration. *Journal of Cell Biology*, *196*(2), 277-295.

Rogaeva, E. et al. The neuronal sortilin-related receptor SORL1 is genetically associated with Alzheimer disease. *Nat. Genet.* 39, 168–177 (2007).

Sahgal, P., Alanko, J., Icha, J., Paatero, I., Hamidi, H., Arjonen, A., ... & Ivaska, J. (2019). GGA2 and RAB13 promote activity-dependent β1-integrin recycling. *Journal of cell science*, *132*(11), jcs233387.

Sanz-Herrera, J. A., Barrasa-Fano, J., Cóndor, M., & Van Oosterwyck,29aracatinib29Inverse method based on 3D nonlinear physically constrained minimisation in the framework of traction force microscopy. Soft Matter.

Sato, T., & Clevers, H. (2013). Growing self-organizing mini-guts from a single intestinal stem cell: mechanism and applications. *Science*, *340*(6137), 1190-1194.

Schmidt, V. et al. SORLA facilitates insulin receptor signaling in adipocytes and exacerbates obes“ty. *J. Clin. Invest.* 126, 2706–2720”(2016).

Siegel, Rebecca L., et al. "Colorectal cancer statistics, 2023." *CA: a cancer journal for clinicians* 73.3 (2023): 233-254.

Spoelgen, R. et al. Interaction of the apolipop29aracn E receptors low density lipoprotein receptor-related protein and sorLA/LR11. *Neuroscience* 158, 1460–1468 (2009).

Swai©S. M., Baselga, J., Kim, S. B., Ro, J., Semiglazov, V., Campone, M., ... & Cortés, J. (2015). Pertuzumab, trastuzumab, and docetaxel in HER2-positive metastatic breast cancer. *New England journal of medicine*, *372*(8), 724-734.

Taufalele et al. 2019. Fiber alignment drives changes in architectural and “echanical features in collagen matrices. PLoS One.

Tsai, Jia-”uei, et al. "Traditional Serrated Pathway–associated Colorectal Carcinoma." *The American j“urnal of surgical pathology* 43.8 (2019): 1042-1051.

Verdu, Montse, et al. "Clinicopatholog”cal and molecular characterization of colorectal micropapillary carcinoma." *Modern Pathology* 24.5 (2011): 729-738.

Whittle, A. J. et al. Soluble LR11/SorLA represses thermogenesis in adipose tissue and correlates with BMI“in humans. *Nat. Commun.* 6, 8951 (2015).

”odarz, Andreas, and Inke Näthke. "Cell polarity in development and cancer." *Nature cell biology* 9.9 (2007): 1016-1024.

Wolf, K., & Friedl, P. (2011). Extracellular matrix determinants of proteolytic and non-proteolytic cell m“gration. *Trends in cell biology*, *21*(12), 736-7”4.

Yamane, Letícia, et al. "Serrated pathway in colorectal carcinogenesis." *World journal of gastroenterology: WJG* 20.10 (2014): 2634.

Ye, P., Wang, Y., Li, R., Chen, W., Wan, L., & Cai, P. (2022). The HER family as therapeutic targets in colorectal cancer. *Critical Reviews in Oncology/Hematology*, *174*, 103681.

Yonesaka©., Zejnullahu, K., Okamoto, I., Satoh, T., Cappuzzo, F., Souglakos, J., ... & Jänne, P. A. (2011). Activation of ERBB2 signaling causes resistance to the EGFR-directed therapeutic antibody cetuximab. *Science translational medicine*, *3*(99), 99ra86-99ra86.

Yu©., Shewan, A. M., Brakeman, P., Eastburn, D. J., Datta, A., Bryant, D. M., ... & Mostov, K. E. (2008). Involvement of RhoA, ROCK I and myosin II in inverted orienta“ion of epithelial polarity. *EMBO reports*, *9*(9), 923-929.

Zajac, Olivier, et al. "Tumour spheres with inverted polarity drive the formation”of peritoneal metastases in patients with hypermethylated colorectal carcinomas." *Nature cell biology* 20.3 (2018): 296-306.

Zou, M., Baitei, E. Y., Alzahrani, A. S., Parhar, R. S., Al-Mohanna, F. A., Meyer, B. F., & Shi, Y. (2011). Mutation prediction by PolyPhen or functional assay, a detailed comparison of CYP27B1 missense mutations. *Endocrine*, *40*, 14-20.

Figures & Legends

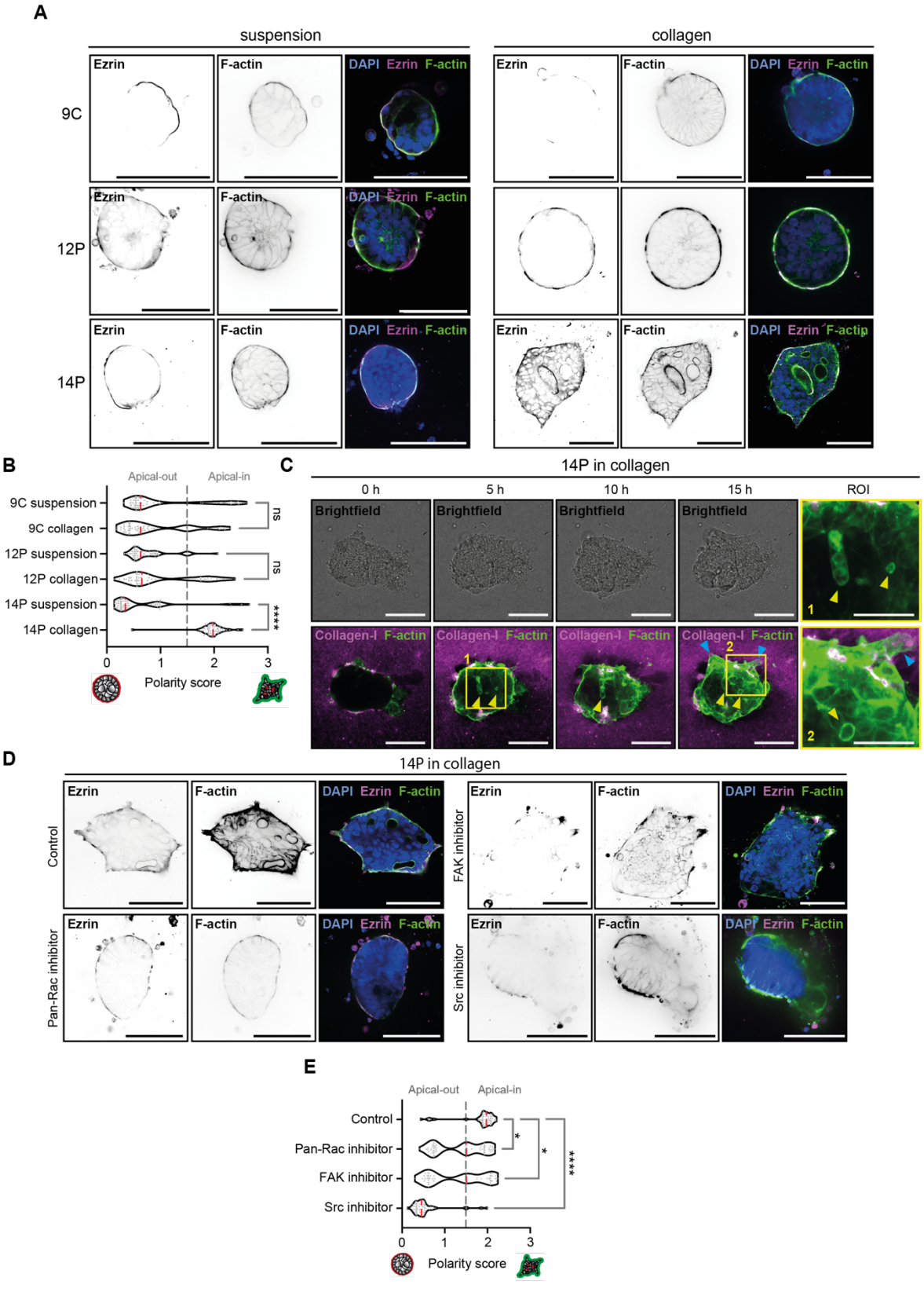
A
suspension
collagen
9C
12P
14P
Ezrin
F-actin
DAPI Ezrin F-actin
B
Apical-out
Apical-in
9C suspension
9C collagen
12P suspension
12P collagen
14P suspension
14P collagen
ns
ns
****
0
1
2
3
Polarity score
C
14P in collagen
0 h
5 h
10 h
15 h
ROI
Brightfield
Collagen-I F-actin
1
2
D
14P in collagen
Control
FAK inhibitor
Pan-Rac inhibitor
Src inhibitor
E
Apical-out
Apical-in
Control
Pan-Rac inhibitor
FAK inhibitor
Src inhibitor
*
*
****
0
1
2
3
Polarity score

FIG1. Apicobasal polarity of mucinous CRC PDXs is controlled by the FA signaling pathway.

(A, B) Representative immunofluorescence images of 9C-, 12P- and 14P-generated tumoroids, fixed in suspension or when embedded in collagen and stained for Ezrin (polarity marker), F-actin and DAPI (A). Comparison of polarity scores amongst the models is shown (B) [n_{9C} = 51 (suspension), 49 (collagen); n_{12P} = 43 (suspension), 51 (collagen); n_{14P} = 51 (suspension), 52 (collagen); Kruskal-Wallis test with Dunn's multiple comparison tests, p_{9C}>0.9999, p_{12P}>0.9999, p_{14P}<0.0001]. (C) Representative snapshots of live-imaging of 14P tumoroid polarity reversion following collagen embedding (time point 0) over 15 h. Tumoroids were stained with F-actin for visualization. Yellow arrows indicate lumen-like structures, blue arrows indicate protrusion-like structures. (D, E) Representative immunofluorescence images of 14P tumoroids in collagen treated with either a Pan-Rac inhibitor (EHT-1864, 5 μM), a FAK inhibitor (FAK14, 10 μM) or a Src inhibitor (Saracatinib, 1 μM) and ©ined for Ezrin (D). Analysis of polarity score afte33aracatinibtments is shown (E) [n = 45 (control); 53 (EHT-1864); 36 (FAK14) and 35 (saracatinib) 14P tumoroids; Kruskal-Wallis test with33aracatinibtiple comparison; p-value = 0.0224 (EHT-1864), 0.0204 (FAK14), < 0.0001 (saracatinib)]. Scale bars, 100 μm (main), 50 μm (insets).

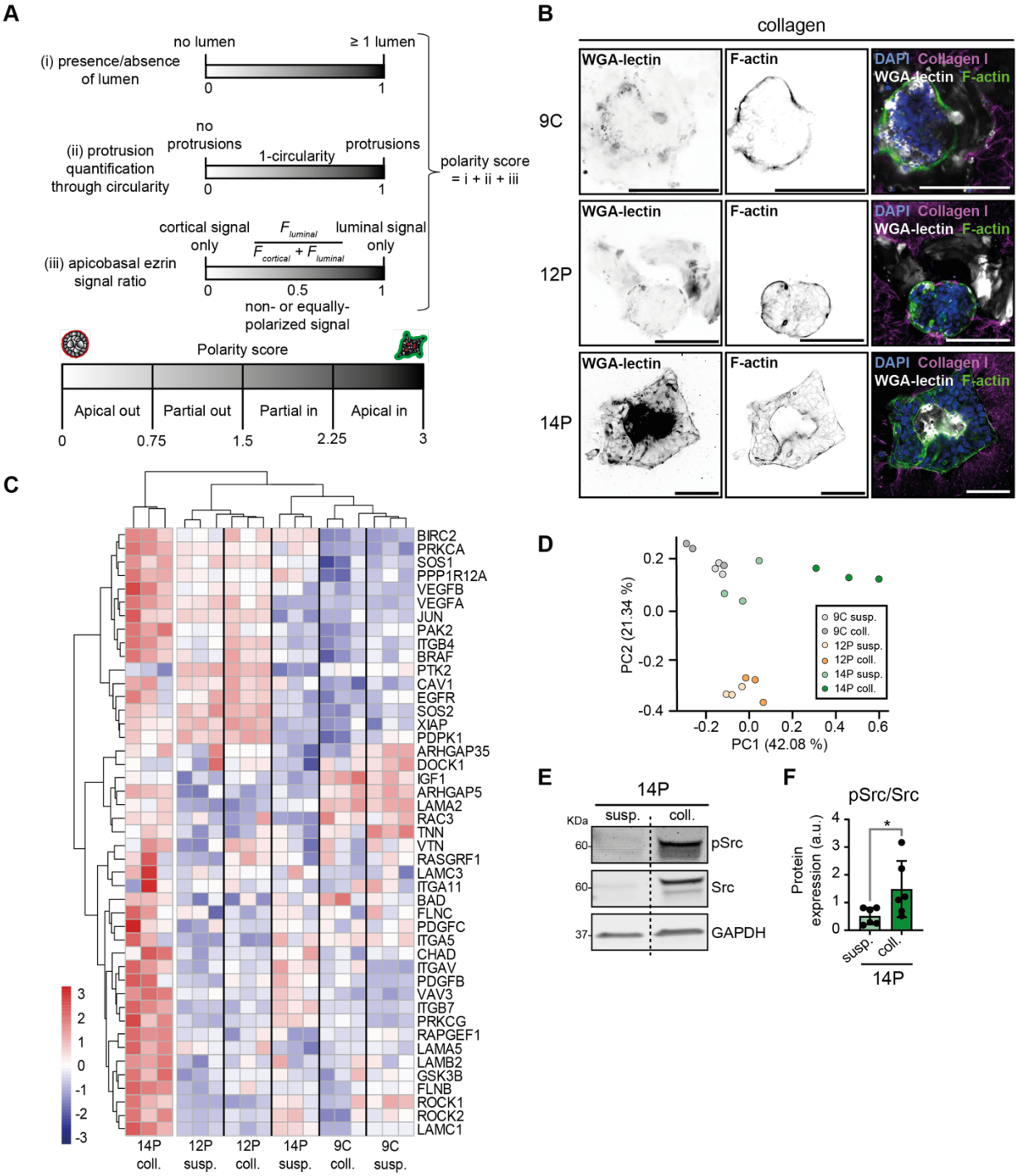
A
no lumen
≥ 1 lumen
(i) presence/absence of lumen
0
1
no protrusions
protrusions
1-circularity
(ii) protrusion quantification through circularity
0
1
cortical signal only
luminal signal only
(iii) apicobasal ezrin signal ratio
0
0.5
1
non- or equally-polarized signal
polarity score = i + ii + iii
Polarity score
Apical out
Partial out
Partial in
Apical in
0
0.75
1.5
2.25
3
B
collagen
WGA-lectin
F-actin
DAPI Collagen I
WGA-lectin F-actin
9C
12P
14P
C
BIRC2
PRKCA
SOS1
PPP1R12A
VEGFB
VEGFA
JUN
PAK2
ITGB4
BRAF
PTK2
CAV1
EGFR
SOS2
XIAP
PDPK1
ARHGAP35
DOCK1
IGF1
ARHGAP5
LAMA2
RAC3
TNN
VTN
RASGRF1
LAMC3
ITGA11
BAD
FLNC
PDGFC
ITGA5
CHAD
ITGAV
PDGFB
VAV3
ITGB7
PRKCG
RAPGEF1
LAMA5
LAMB2
GSK3B
FLNB
ROCK1
ROCK2
LAMC1
3
2
1
0
-1
-2
-3
14P coll.
12P susp.
12P coll.
14P susp.
9C coll.
9C susp.
D
PC2 (21.34 %)
PC1 (42.08 %)
0.2
0.0
-0.2
-0.4
-0.2
0.0
0.2
0.4
0.6
9C susp.
9C coll.
12P susp.
12P coll.
14P susp.
14P coll.
E
14P
susp.
coll.
KDa
60
60
37
pSrc
Src
GAPDH
F
pSrc/Src
Protein expression (a.u.)
4
3
2
1
0
*
susp.
coll.
14P

FIGS1. Characterization of apicobasal polarity of mucinous CRC PDX models

(A) (A) Outline of polarity score calculation used for all experiments. The score (from 0: apical-out to 3: apical-in) is a sum of three parameters, i) the presence of a lumen, ii) circularity, and iii) ratio of luminal/cortical ezrin fluorescence. (B) Representative immunofluorescence images of 9C-, 12P- and 14P-generated tumoroids in collagen, stained with F-actin and WGA-lectin to show mucin secretion. (C)) Heatmap of the 45 top differentially regulated genes in the KEGG Focal Adhesion Pathway in 14P collagen vs. suspension. (D) Associated Principal Component Analysis on the same geneset for 9C, 12P and 14P models in suspension and collagen. (E, F) Western blot analysis of pSrc and Src levels in 14P tumoroids in suspension or collagen and associated quantifications n = 6, Paired t-test, p=0.0361).

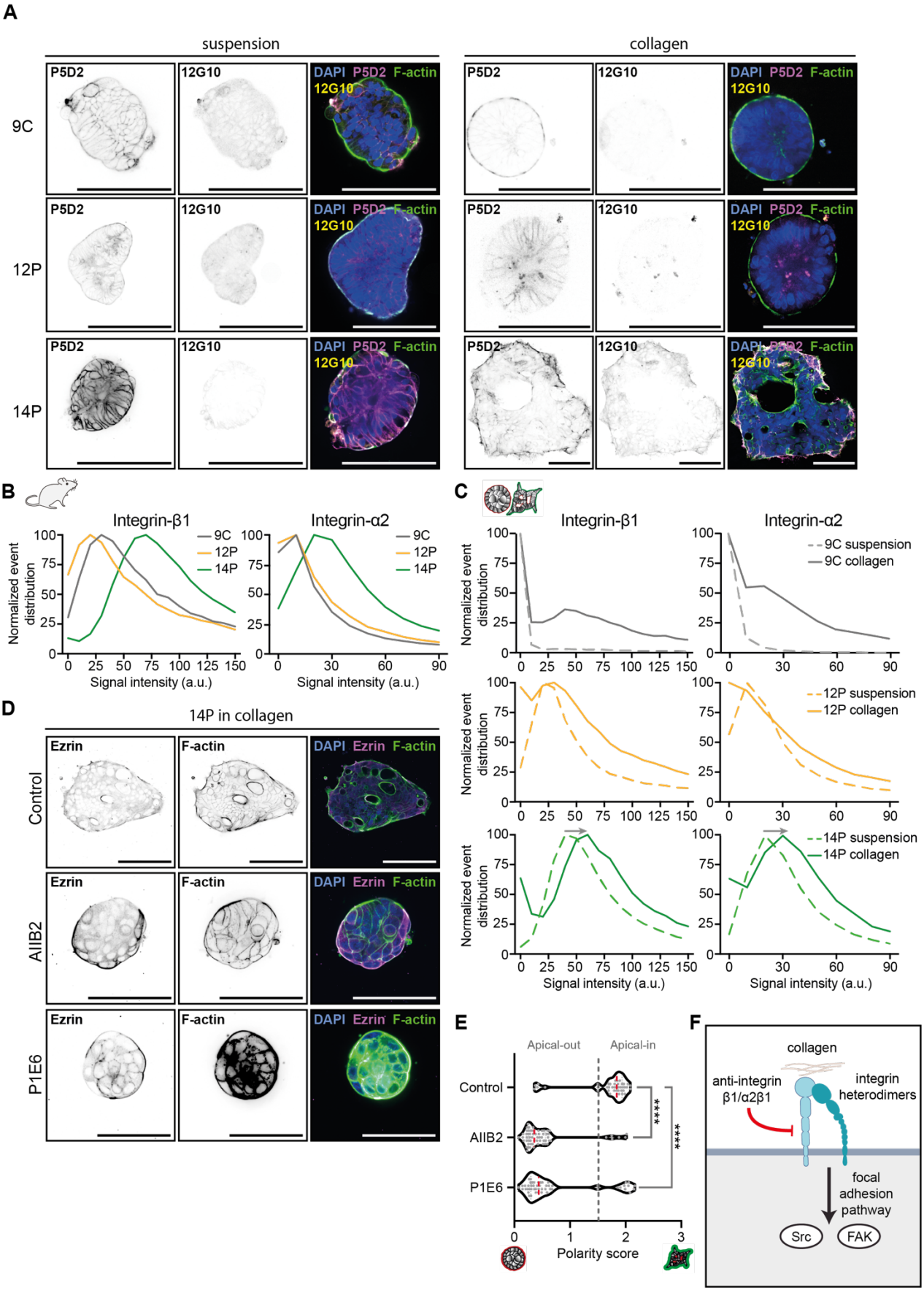
A
suspension
collagen
9C
12P
14P
P5D2
12G10
DAPI P5D2 F-actin
12G10
B
Integrin-β1
Integrin-α2
9C
12P
14P
Normalized event distribution
Signal intensity (a.u.)
C
Integrin-β1
Integrin-α2
9C suspension
9C collagen
12P suspension
12P collagen
14P suspension
14P collagen
Normalized event distribution
Signal intensity (a.u.)
D
14P in collagen
Control
AIIB2
P1E6
Ezrin
F-actin
DAPI Ezrin F-actin
E
Apical-out
Apical-in
Control
AIIB2
P1E6
****
****
Polarity score
F
collagen
anti-integrin β1/α2β1
integrin heterodimers
focal adhesion pathway
Src
FAK

FIG2. Surface expression of integrin heterodimer $\alpha_2\beta_1$ varies amongst PDX models and matrix conditions.

(A) Representative immunofluorescence images of 9C-, 12P- and 14P-generated tumoroids in suspension and in collagen, stained for total integrin-β1 (P5D2), active integrin-β1 (12G10), F-actin and DAPI. (B)) Distribution of the integrin-β1 and integrin-a2 surface expression signal intensity in 9C, 12P and 14P tumors out of mice (N > 36000). (C) Distribution of Integrin-β1 and Integrin-α2 surface expression signal intensity in 9C-, 12P- and 14P-generated tumoroids in suspension and in collagen (N > 7000). (D) Representative immunofluorescence images of 9C-, 12P- and 14P-generated tumoroids in suspension and in collagen treated with an integrin-β1 blocking antibody (AIIB2, 1 μg/ml) or with an integrin-α2 blocking antibody (P1E6, 10 μg/ml) and stained for ezrin, F-actin and DAPI. (E) Comparison of polarity scores of 14P in collagen after integrin-β1 and integrin-α2 blocking [(n = 40 (Control); 61 (AIIB2); 51 (P1E6); Kruskal-Wallis test with Dunn's multiple comparison; p-value <0.0001 (AIIB2 and for P1E6)]. (F)) Proposed mechanism of collagen-induced signaling and activation of Src and FAK pathways in MUC CRCs.

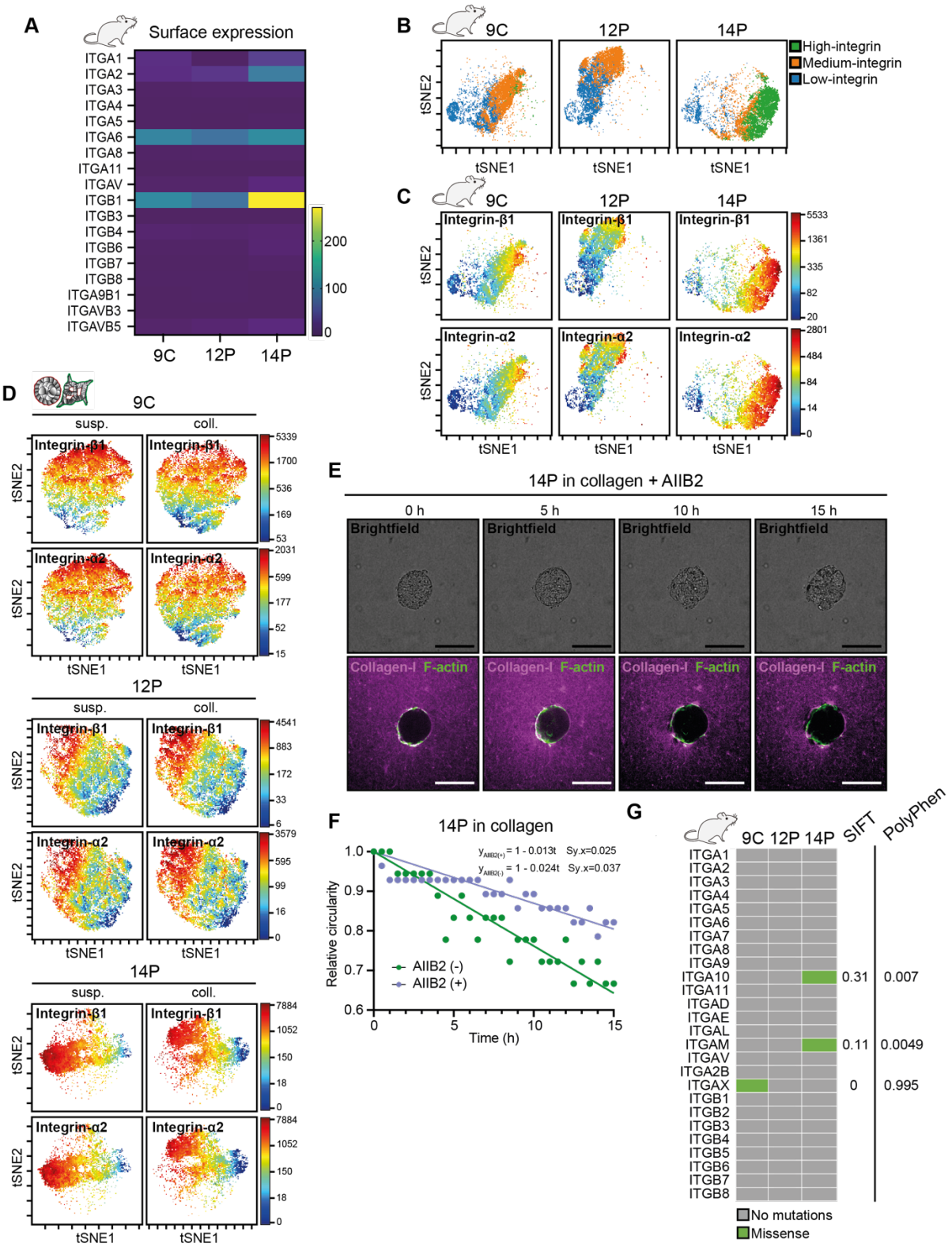
A
Surface expression
ITGA1
ITGA2
ITGA3
ITGA4
ITGA5
ITGA6
ITGA8
ITGA11
ITGAV
ITGB1
ITGB3
ITGB4
ITGB6
ITGB7
ITGB8
ITGA9B1
ITGAVB3
ITGAVB5
200
100
0
9C
12P
14P
B
9C
12P
14P
High-integrin
Medium-integrin
Low-integrin
tSNE2
tSNE1
C
Integrin-β1
Integrin-α2
5533
1361
335
82
20
2801
484
84
14
0
D
9C
susp.
coll.
5339
1700
536
169
53
2031
599
177
52
15
12P
4541
883
172
33
6
3579
595
99
16
0
14P
7884
1052
150
18
0
E
14P in collagen + AIIB2
0 h
5 h
10 h
15 h
Brightfield
Collagen-I F-actin
F
14P in collagen
$y_{AIIB2(+)}$ = 1 - 0.013t Sy.x=0.025
$y_{AIIB2(-)}$ = 1 - 0.024t Sy.x=0.037
Relative circularity
AIIB2 (-)
AIIB2 (+)
Time (h)
G
9C 12P 14P
SIFT
PolyPhen
0.31
0.007
0.11
0.0049
0
0.995
No mutations
Missense

FIGS2. Integrin surface expressions in 9C, 12P and 14P tumors and generated tumoroids

(A) Heatmaps representing mean cell-surface expression of the indicated integrins in 9C, 12P and 14P tumors out of mouse. (B) FlowSOM clustering of integrins following a viSNE analysis of single-cell mass cytometry data obtained from 9C, 12P and 14P tumors out of mice shows three distinct cell clusters based on integrin surface expression levels. (C) viSNE analysis of single-cell mass cytometry data obtained from 9C, 12P and 14P tumors out of mice on the whole panel of surface receptors (see Material and Methods, table 2), overlayed with the intensity of Integrin-α2 and Integrin-β1 signal intensity. (D) viSNE analysis of 9C-, 12P- and 14P-generated tumoroids in suspension and collagen on the whole panel of surface receptors, overlayed with the intensity of Integrin-α2 and Integrin-β1 signal intensities. (E)) Snapshots of a live polarity reversion of 14P in 15 hours, with AIIB2 (1 μg/ml), from the embedding in collagen timepoint (Control in Fig. 1C). (F) Quantification of the sphere circularity of **Videos 1** and **2**, showing different evolutions when the spheres are cultured with or without AIIB2. (G) Whole-Exome Sequencing data, showing mutation profiles in 9C, 12P and 14P in different integrin subunits.

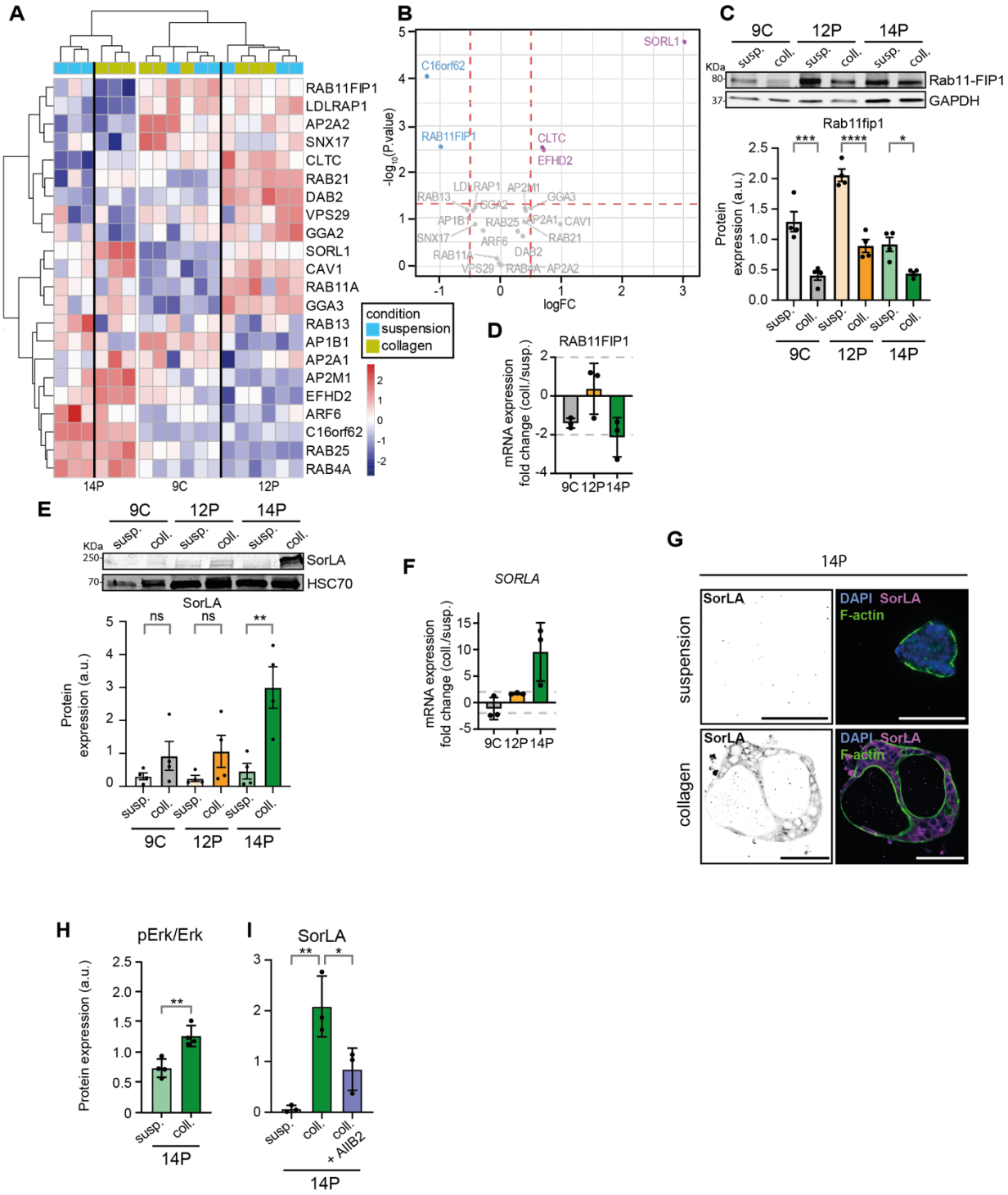
A
RAB11FIP1
LDLRAP1
AP2A2
SNX17
CLTC
RAB21
DAB2
VPS29
GGA2
SORL1
CAV1
RAB11A
GGA3
RAB13
AP1B1
AP2A1
AP2M1
EFHD2
ARF6
C16orf62
RAB25
RAB4A
14P
9C
12P
condition
suspension
collagen
B
SORL1
C16orf62
RAB11FIP1
CLTC
EFHD2
-log10(P.value)
logFC
C
9C
12P
14P
susp.
coll.
KDa
80
37
Rab11-FIP1
GAPDH
Rab11fip1
Protein expression (a.u.)
D
RAB11FIP1
mRNA expression fold change (coll./susp.)
E
SorLA
HSC70
250
70
SorLA
Protein expression (a.u.)
ns
**
F
SORLA
mRNA expression fold change (coll./susp.)
G
14P
SorLA
DAPI SorLA
F-actin
suspension
collagen
H
pErk/Erk
Protein expression (a.u.)
I
SorLA
+ AllB2

FIG3. Key Integrin-β1 trafficking regulators are differentially expressed amongst PDX models and matrix conditions.

(A) Relative expression of key regulators in Integrin-β1 trafficking, generated from an RNA microarray analysis of 9C-, 12P- and 14P-generated tumoroids in suspension and in collagen. (B) Volcano plot generated for the same geneset comparing 14P-generated tumoroids in collagen vs. suspension. Significantly upregulated genes in collagen are in purple, downregulated genes are in blue. (C) Western-blot and corresponding quantifications of Rab11FIP1 in 9C-, 12P- and 14P-generated tumoroids in suspension and in collagen and corresponding quantifications (N=4, One-way ANOVA with Tukey's multiple comparison tests, p-value$_{9C\ coll\ vs.\ susp}$=0.0002, p-value$_{12Pcoll\ vs.\ susp}$<0.0001, p-value$_{14P\ coll\ vs.\ susp}$=0.0492). (D) RAB11FIP1 mRNA expression fold change in collagen vs. suspension generated from an RNA microarray analysis of 9C-, 12P- and 14P-generated tumoroids. (E)) Western-blot and corresponding quantifications of SorLA in 9C-, 12P- and 14P-generated tumoroids in suspension and in collagen and corresponding quantifications (N=4, One-way ANOVA with Tukey's multiple comparison tests, p-value$_{9C\ coll\ vs.\ susp}$=0.8651, p-value$_{12P\ coll\ vs.\ susp}$=0.6725, p-value$_{14P\ coll\ vs.\ susp}$=0.0024). (F) SORL1 mRNA expression fold change in collagen vs. suspension generated from an RNA microarray analysis of 9C-, 12P- and 14P-generated tumoroids. (G) Immunofluorescence of 14P-generated tumoroids in suspension and in collagen, showing SorLA. (H) Western-Blot quantifications of Erk phosphorylation ratio in 14P in suspension and collagen (N=4, t-test, p-value=0.0036). (I) Western-Blot quantifications of SorLA expression in 14P in suspension, collagen, and collagen treated with AIIB2 (N=3, One-way ANOVA with Tukey's multiple comparison tests, p-value$_{coll.\ vs.\ susp.}$=0.0027, p-value$_{coll.+AIIB2\ vs.\ coll.}$=0.0271).

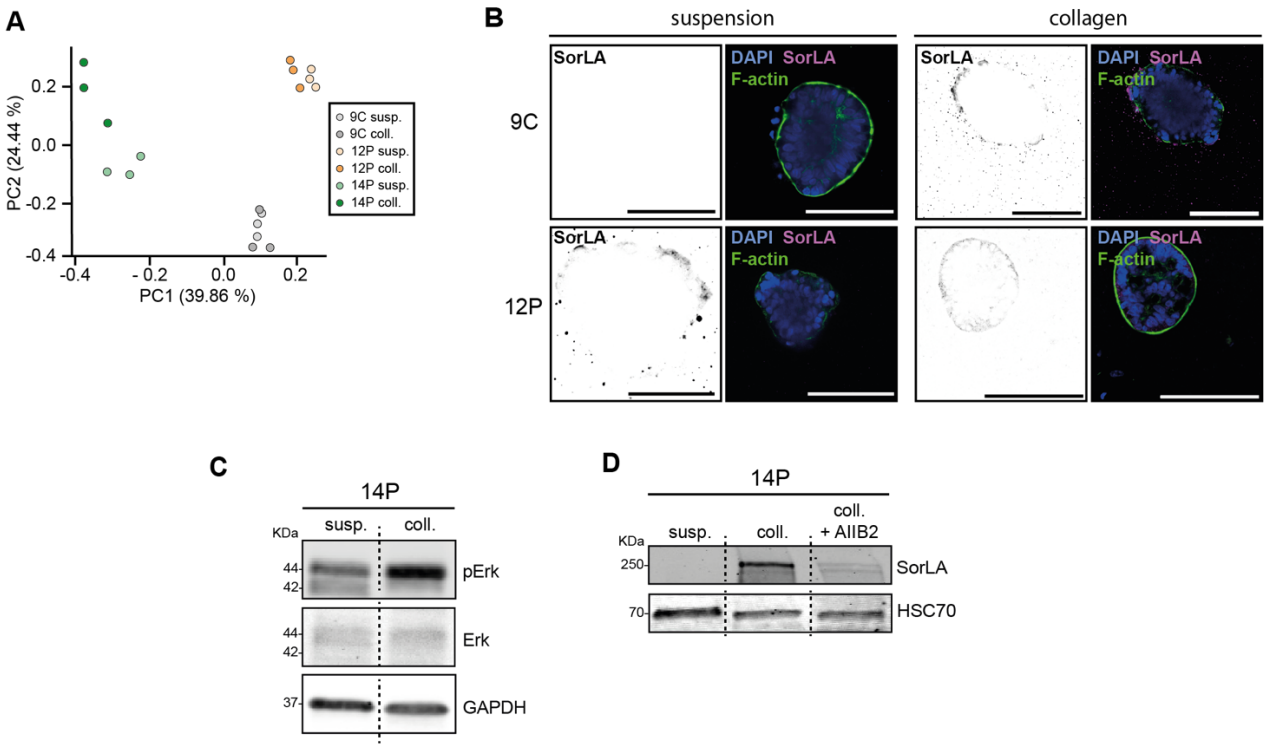

FIGS3. RCP and SorLA signaling regulates polarity in MUC CRCs

(A) PCA associated to the relative expression of key regulators in Integrin-β1 trafficking, generated from an RNA microarray analysis of 9C-, 12P- and 14P-generated tumoroids in suspension and in collagen. (B) Immunofluorescence of 9C- and 12P-generated tumoroids in suspension and in collagen, showing SorLA staining. (C) Western-Blot showing pErk and Erk expression in 14P-generated tumoroids in suspension and collagen. (D) Western-Blot showing SorLA expression in 14P-generated tumoroids in suspension, collagen, and collagen + AIIB2 (1 μg/ml).

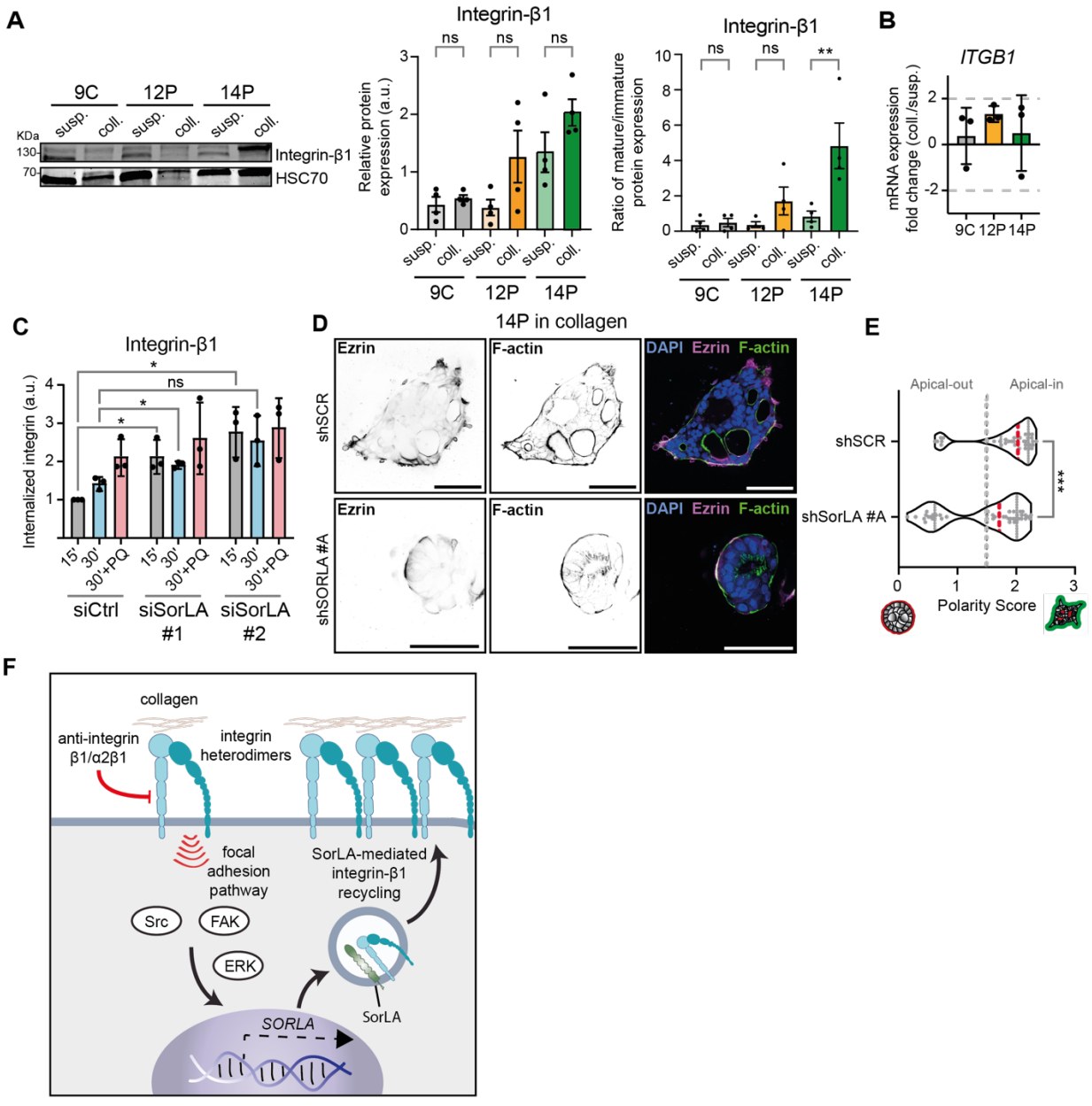
A
9C
12P
14P
susp.
coll.
KDa
130-
70-
Integrin-β1
HSC70
Integrin-β1
Relative protein expression (a.u.)
ns
Integrin-β1
Ratio of mature/immature protein expression
**
B
ITGB1
mRNA expression fold change (coll./susp.)
C
Integrin-β1
Internalized integrin (a.u.)
15'
30'
30'+PQ
siCtrl
siSorLA #1
siSorLA #2
D
14P in collagen
shSCR
shSORLA #A
Ezrin
F-actin
DAPI Ezrin F-actin
E
Apical-out
Apical-in
shSCR
shSorLA #A
***
Polarity Score
F
collagen
anti-integrin β1/α2β1
integrin heterodimers
focal adhesion pathway
SorLA-mediated integrin-β1 recycling
Src
FAK
ERK
SORLA
SorLA

FIG4. Integrin-β1 trafficking impairment is correlated with an inverted polarity in collagen.

(A) Western-blot and corresponding quantifications and maturation ratios of Integrin-β1 in 9C-, 12P- and 14P-generated tumoroids in suspension and in collagen and corresponding quantifications (for total expression: N=4, One-way ANOVA with Tukey's multiple comparison tests, p-value$_{9C\ coll\ vs.\ susp}$=0.9996, p-value$_{12P\ coll\ vs.\ susp}$=0.2173, p-value$_{14P\ coll\ vs.\ susp}$=0.4623; for maturation ratio: N=4, One-way ANOVA with Tukey's multiple comparison tests, p-value$_{9C\ coll\ vs.\ susp}$>0.9999, p-value$_{12P\ coll\ vs.\ susp}$=0.6903, p-value$_{14P\ coll\ vs.\ susp}$=0.0043). (B) ITGB1 mRNA expression fold change in collagen vs. suspension generated from an RNA microarray analysis of 9C-, 12P- and 14P-generated tumoroids. (C) Integrin-β1recycling assay in 2D-plated LS513 after siRNA-induced KO of SorLA. Timepoints are 15', 30', and the endocytosis inhibitor used is primaquine (PQ) (N=3, independent Welch's t-tests, p-value$_{15'\ si\#1\ vs.\ siCtrl}$=0.0432, p-value$_{15'\ si\#2\ vs.\ siCtrl}$=0.0406, p-value$_{30'\ si\#1\ vs.\ siCtrl}$=0.0172, p-value$_{30'\ si\#2\ vs.\ siCtrl}$=0.0877). (D) Immunofluorescence of 9C-, 12P- and 14P-generated tumoroids in suspension and in collagen, showing their polarity status through Ezrin staining after KD of SorLA through LV shRNA. (E) Comparison of polarity scores of 14P in collagen after SorLA silencing. (N_{shSCR}=38, $N_{shSORLA\ \#A}$=44, Mann-Whitney test, p-value$_{shSORLA\ \#A\ vs.\ shSCR}$=0.0007). (F) Proposed mechanism of collagen-induced Erk, FAK and Src activation and SorLA expression, leading to Integrin-β1 recycling.

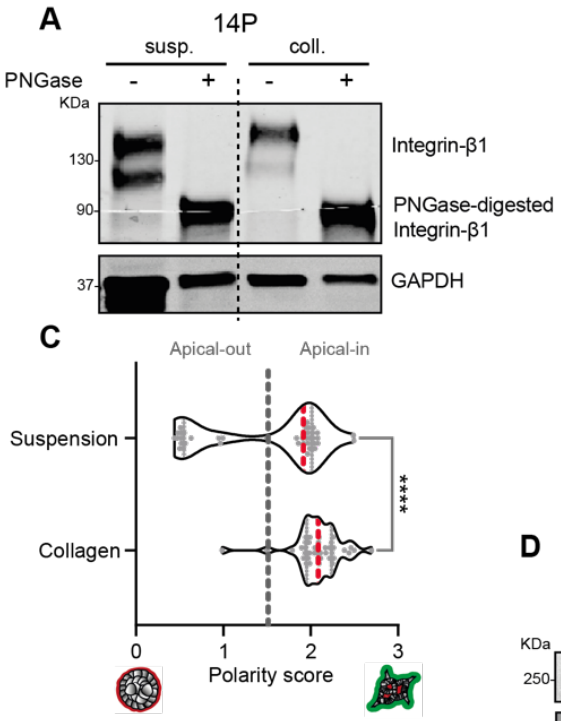
A
14P
susp.
coll.
PNGase
-
+
-
+
KDa
130
90
37
Integrin-β1
PNGase-digested
Integrin-β1
GAPDH
C
Apical-out
Apical-in
Suspension
Collagen
****
0
1
2
3
Polarity score

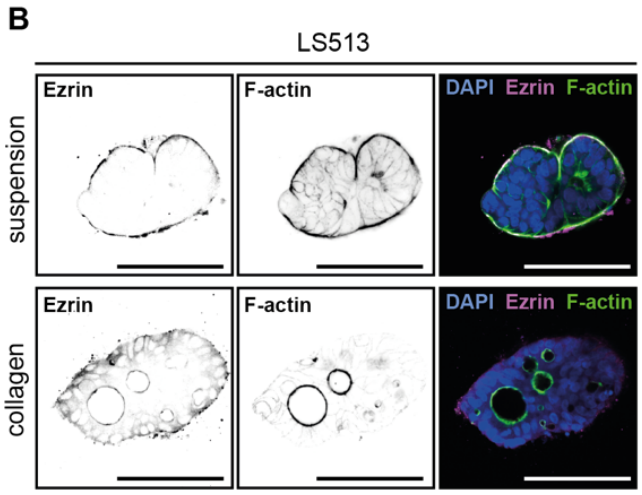
B
LS513
suspension
collagen
Ezrin
F-actin
DAPI Ezrin F-actin

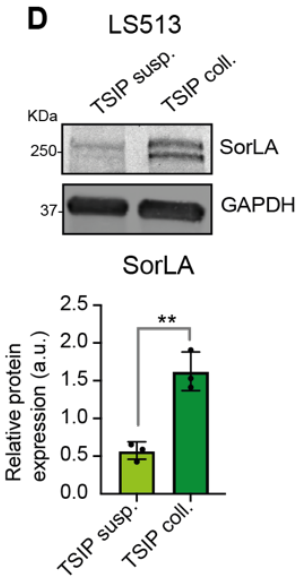
D
LS513
TSIP susp.
TSIP coll.
KDa
250
37
SorLA
GAPDH
SorLA
Relative protein expression (a.u.)
**
TSIP susp.
TSIP coll.

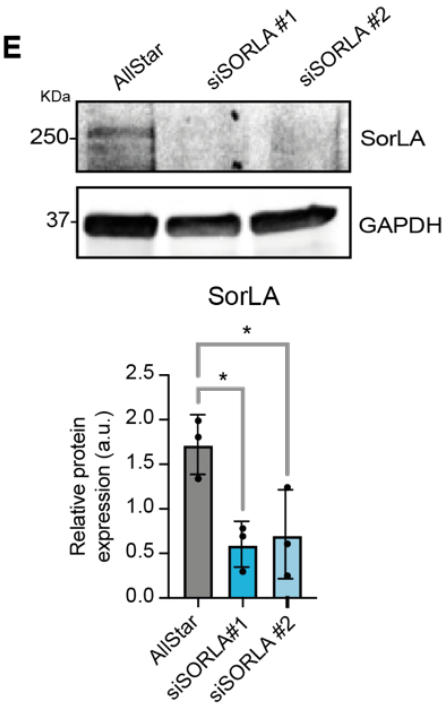
E
AllStar
siSORLA #1
siSORLA #2
KDa
250
37
SorLA
GAPDH
SorLA
Relative protein expression (a.u.)
*
*
AllStar
siSORLA#1
siSORLA #2

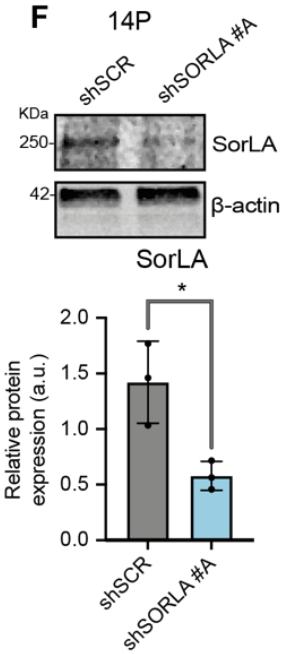
F
14P
shSCR
shSORLA #A
KDa
250
42
SorLA
β-actin
SorLA
Relative protein expression (a.u.)
*
shSCR
shSORLA #A

FIGS4. Existence of a SorLA-dependent Integrin-β1 recycling loop in 14P.

(A) Western-Blot of Integrin-β1 in 14P-generated tumoroids in suspension and collagen, before and after PNGase digestion of lysates. (B) Immunofluorescence of LS513 TSIPs in suspension and in collagen, showing their polarity status through Ezrin staining. (C) Comparison of polarity scores amongst models in collagen ($N_{suspension}$=42, $N_{collagen}$=40, Mann-Whitney test, p-value<0.0001). (D) Western-Blot of SorLA in LS513 TSIPs in suspension and collagen (N=3, t-test, p-value=0.0029). (E) Western-Blot of SorLA in LS513 transfected with SORLA-targetting siRNA (N=3, ANOVA, $p\text{-value}_{\#1}$=0.0259, $p\text{-value}_{\#1}$=0.0393). (F) Western-Blot of SorLA in 14P-generated organoids infected with SORLA-targetting shRNA (N=3, t-test, p-value=0.0203).

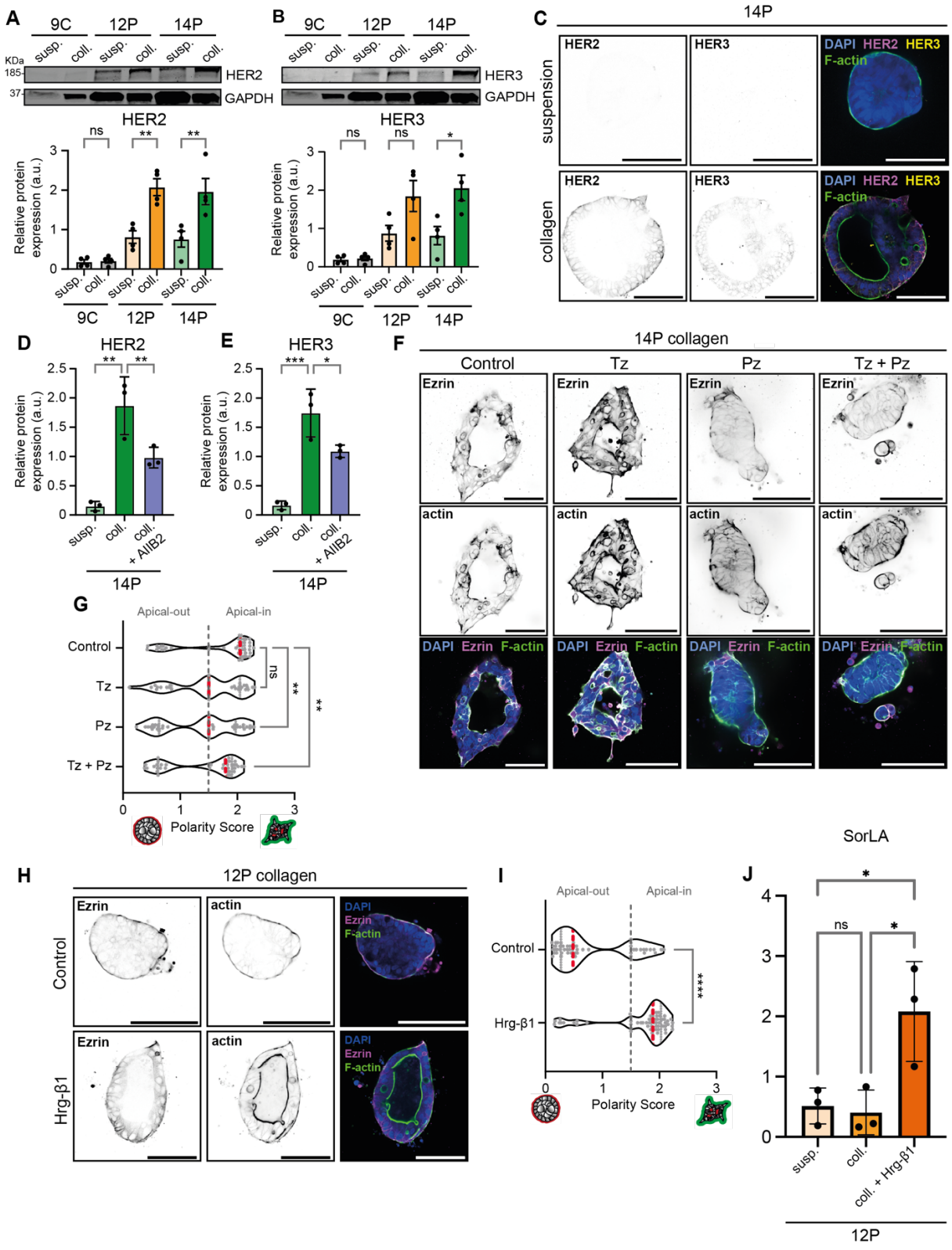
A
9C
12P
14P
susp.
coll.
KDa
185-
37-
HER2
GAPDH
HER2
Relative protein expression (a.u.)
ns
**
**
B
HER3
GAPDH
HER3
ns
ns
*
C
14P
suspension
collagen
HER2
HER3
DAPI HER2 HER3
F-actin
D
HER2
**
**
coll. + AIIB2
14P
E
HER3
***
*
F
14P collagen
Control
Tz
Pz
Tz + Pz
Ezrin
actin
DAPI Ezrin F-actin
G
Apical-out
Apical-in
ns
**
**
Polarity Score
H
12P collagen
Hrg-β1
I
****
J
SorLA
coll. + Hrg-β1
12P

FIG5. HER2 and HER3 control apicobasal polarity orientation.

(A) Western-blot and corresponding quantifications of HER2 in 9C-, 12P- and 14P-generated tumoroids in suspension and in collagen and corresponding quantifications (for total expression: N=4, One-way ANOVA with Tukey's multiple comparison tests, p-value$_{9C\ coll\ vs.\ susp}$>0.9999, p-value$_{12P\ coll\ vs.\ susp}$=0.0027, p-value$_{14P\ coll\ vs.\ susp}$=0.0042). (B) Western-blot and corresponding quantifications of HER3 in 9C-, 12P- and 14P-generated tumoroids in suspension and in collagen and corresponding quantifications (for total expression: N=4, One-way ANOVA with Tukey's multiple comparison tests, p-value$_{9C\ coll\ vs.\ susp}$>0.9999, p-value$_{12P\ coll\ vs.\ susp}$=0.1165, p-value$_{14P\ coll\ vs.\ susp}$=0.0264). (C) Immunofluorescence of 14P-generated tumoroids in suspension and in collagen, showing HER2 and HER3. (D) Western-Blot quantifications of HER2 expression in 14P in suspension, collagen, and collagen treated with AIIB2 (N=3, One-way ANOVA with Tukey's multiple comparison tests, p-value$_{coll.\ vs.\ susp.}$=0.0011, p-value$_{coll.+AIIB2\ vs.\ coll.}$=0.0282). (E) Western-Blot quantifications of HER3 expression in 14P in suspension, collagen, and collagen treated with AIIB2 (N=3, One-way ANOVA with Tukey's multiple comparison tests, p-value$_{coll.\ vs.\ susp.}$=0.0006, p-value$_{coll.+AIIB2\ vs.\ coll.}$=0.0403). (F) Immunofluorescence of 14P-generated tumoroids in suspension, collagen, and collagen treated with a HER2/HER2 homodimerization blocking antibody (Trastuzumab, Tz, 10 μg/ml), a HER2/HER3 heterodimerization blocking antibody (Pertuzumab, Pz, 10 μg/ml) and a combination of both (Tz+Pz), showing HER2 and HER3, showing their polarity status through Ezrin staining. (G) Comparison of polarity scores in 14P in collagen with Erbb-blocking antibodies (N_{Ctrl}=44, N_{Tz}=39, N_{Pz}=47, N_{Tz+Pz}=38, One-way ANOVA, p-value$_{Tz\ vs.\ Ctrl}$=0.2086, p-value$_{Pz\ vs.\ Ctrl}$=0.0063, p-value$_{Pz+Tz\ vs.\ Ctrl}$=0.0042). (H) Immunofluorescence of 12P-generated tumoroids in suspension, collagen, and collagen treated with a HER3 ligand (Heregulin-β1, Hrg-β1, 20 ng/ml), showing their polarity status through Ezrin staining. (I) Comparison of polarity scores in 14P in collagen with Erbb-blocking antibodies (N_{Ctrl}=56, $N_{Hrg\text{-}\beta1}$=62, Mann-Whitney test, p-value<0.0001). (J) Western-Blot quantifications of SorLA expression in 12P in suspension, collagen, and collagen treated with Heregulin-β1 (N=3, One-way ANOVA with Tukey's multiple comparison tests, p-value$_{susp.\ vs.\ coll+\ Hrg\text{-}\beta1\ =}$0.0305, p-value$_{coll.+Hrg\text{-}\beta1\ vs.\ coll.}$=0.0231).

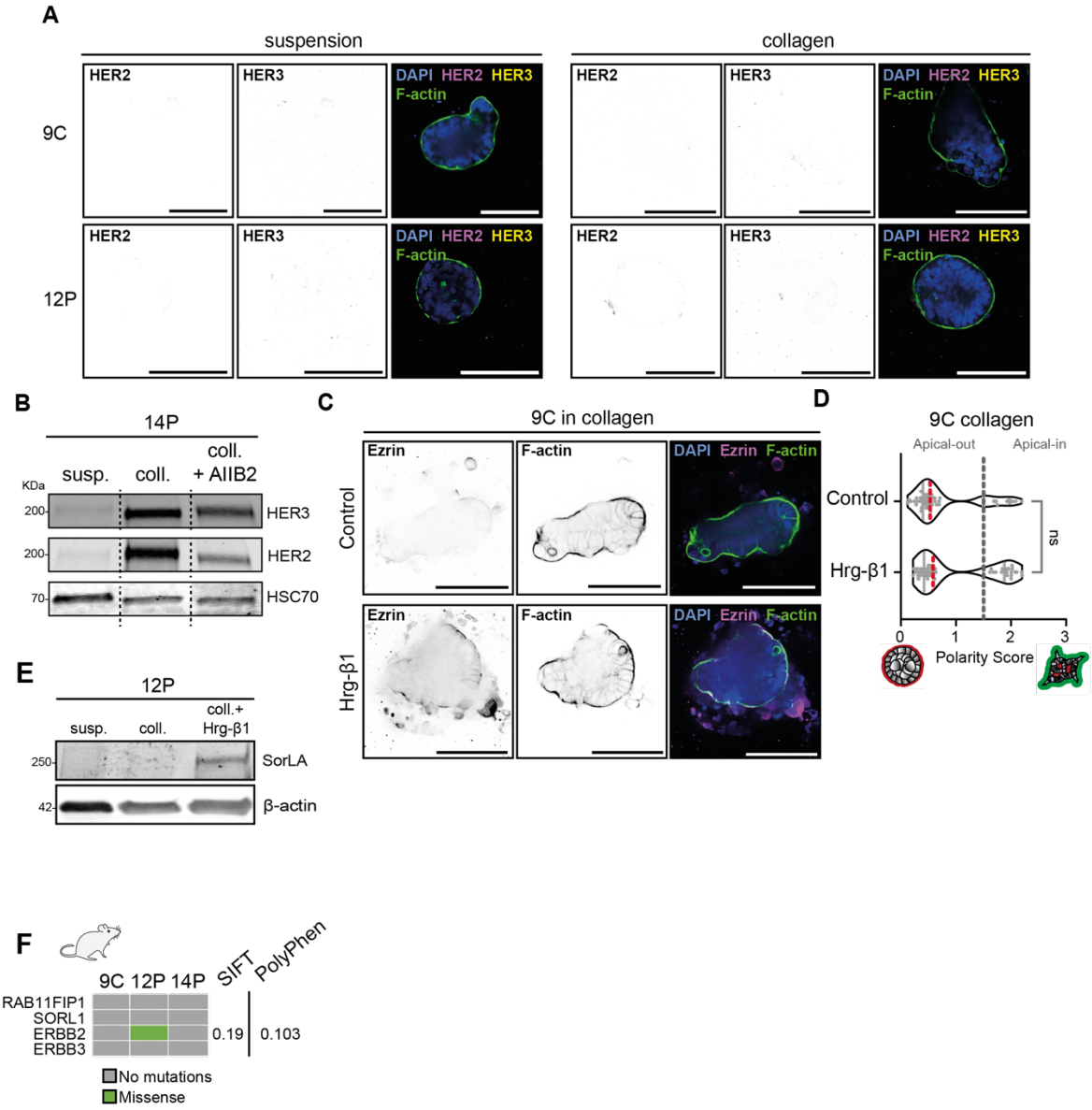

FIGS5. HER2 and HER3 characterization in MUC CRC PDXs.

(A) Immunofluorescence of 9C- and 12P-generated tumoroids in suspension and in collagen, showing the localization of HER2 and HER3. (B) Western-Blot showing HER2 and HER3 expression in 14P-generated tumoroids in suspension, collagen, and collagen + AIIB2 (1 μg/ml). (C) Immunofluorescence of 9C-generated tumoroids in collagen, showing their polarity status through Ezrin staining after Hrg-β1 treatment (20 ng/ml). (D) Comparison of polarity scores in 9C in collagen after Hrg-β1 treatment (20 ng/ml). (N_{Ctrl}=59, $N_{Hrg\text{-}\beta1}$ =55), Mann-Whitney test, p=0.2359). (E) Western-Blot showing SorLA expression in 12P-generated tumoroids in suspension, collagen and collagen+Heregulin-β1. (F) Whole-Exome Sequencing data, showing mutation profiles in 9C, 12P and 14P in RAB11FIP1, SORL1, ERBB2 and ERBB3.

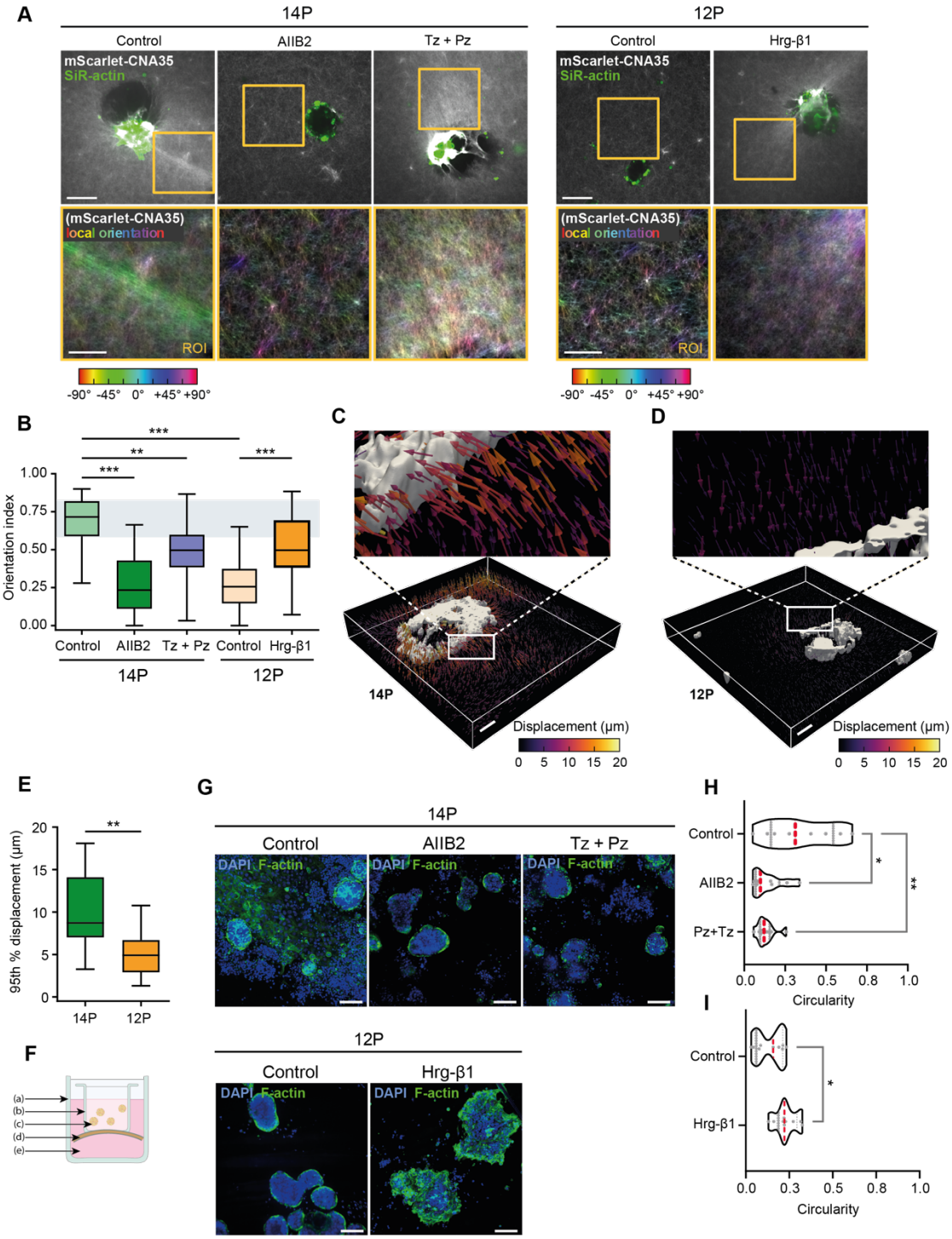
A
14P
12P
Control
AIIB2
Tz + Pz
Control
Hrg-β1
mScarlet-CNA35
SiR-actin
(mScarlet-CNA35)
local orientation
ROI
-90° -45° 0° +45° +90°
B
Orientation index
1.00
0.75
0.50
0.25
0.00
***
**
***
***
Control
AIIB2
Tz + Pz
Control
Hrg-β1
14P
12P
C
D
14P
12P
Displacement (μm)
0 5 10 15 20
E
95th % displacement (μm)
20
15
10
5
0
**
14P
12P
F
(a)
(b)
(c)
(d)
(e)
G
14P
Control
AIIB2
Tz + Pz
DAPI F-actin
12P
Control
Hrg-β1
H
Control
AIIB2
Pz+Tz
*
**
0.0 0.3 0.5 0.8 1.0
Circularity
I
Control
Hrg-β1
*
0.0 0.3 0.5 0.8 1.0
Circularity

FIG6. Collagen fiber displacements is correlated with apicobasal polarity status in collagen

Visualization of collagen fiber orientations in 12P and 14P with Integrin-β1-blocking antibody (AIIB2), HER2/HER3-blocking antibodies (Pz+Tz) and HER3 ligand (Hrg-β1). Collagen fibers are marked with an mScarlet-CNA35 probe, and fibers are color-coded depending on their orientation. (B) Collagen fibers orientation index in 12P and 14P with Integrin-β1-blocking antibody (AIIB2), HER2/HER3-blocking antibodies (Pz+Tz) and HER3 ligand (Hrg-β1) ($N_{14P\ Ctrl}$=28, $N_{14P\ AIIB2}$=28, $N_{14P\ Pz+Tz}$=21, $N_{12P\ Ctrl}$=29, $N_{Hrg\text{-}\beta1}$=23, One way ANOVA with Šidák's multiple comparison tests, $p\text{-value}_{14PAIIB2\ vs.\ Ctrl}$<0.0001, $p\text{-value}14P_{Pz+Tz\ vs.\ Ctrl}$=0.0008, p-value $12P_{Hrg\text{-}\beta1\ vs.\ Ctrl}$<0.0001, $p\text{-value}_{14P\ vs.\ 12P}$<0.0001). (C) Representation of the matrix displacement in 14P. (D) Representation of the matrix displacement in 12P. (E) Quantification of the matrix displacement in 14P and 12P (N_{14P}=27, N_{12P}=29, p-value=0.0032). (F) Set-up for the peritoneum invasion assay: (a): well of a 12-well cell culture plate, (b) Transwell cell invasion insert, which membrane has been removed, (c) tumoroids, (d) decellularized peritoneum, (e) medium. (G) Fluorescence imaging of 12P- and 14P-generated tumoroids after 6 days of invasion on decellularized peritoneum, after treatment with AIIB2 (1 μg/ml), Pertuzumab+Trastuzumab (Tz+Pz, 10 μg/ml, 10 μg/ml) or Heregulin-β1 (Hrg-β1, 20 ng/ml). (H) Comparison of polarity scores in 14P in collagen after treatment with AIIB2 (1 μg/ml) or Pertuzumab+Trastuzumab (Tz+Pz, 10 μg/ml, 10 μg/ml) on 9 spheres selected randomly (Mann-Whitney test, $p_{Ctrl.\ Vs.\ Pz+Tz}$=0.0073, $p_{Ctrl.\ Vs.\ AIIB2}$=0.0121). (I) Comparison of polarity scores in 12P in collagen after treatment with Heregulin-β1 (Hrg-β1, 20 ng/ml) on 9 spheres selected randomly (Mann-Whitney test, $p\text{-value}_{Hrg\text{-}\beta1\ vs.\ Ctrl}$=0.0142).

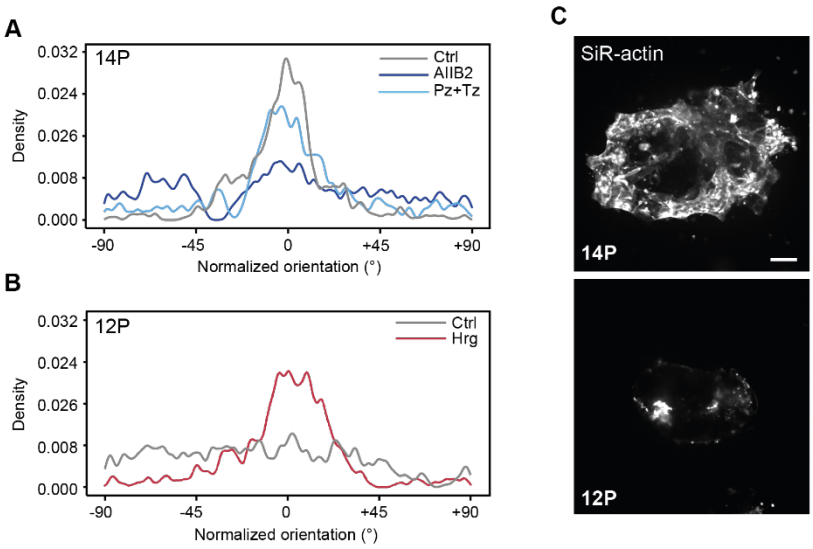

FIGS6. HER2 and HER3 characterization in MUC CRC PDXs.

(A) Normalized orientation of collagen fibers in 14P-generated tumoroids after 6 days in collagen, with AIIB2 treatment (1 μg/ml) or Trastuzumab+Pertuzumab treatment (Pz+Tz, 10 μg/ml, 10 μg/ml (B) Normalized orientation of collagen fibers in 12P-generated tumoroids after 6 days in collagen with Hrg-β1 treatment (20 ng/ml). (C) Immunofluorescence of 12P- and 14P-generated tumoroids in collagen, showing the Sir-actin staining used for the TFM calculations.

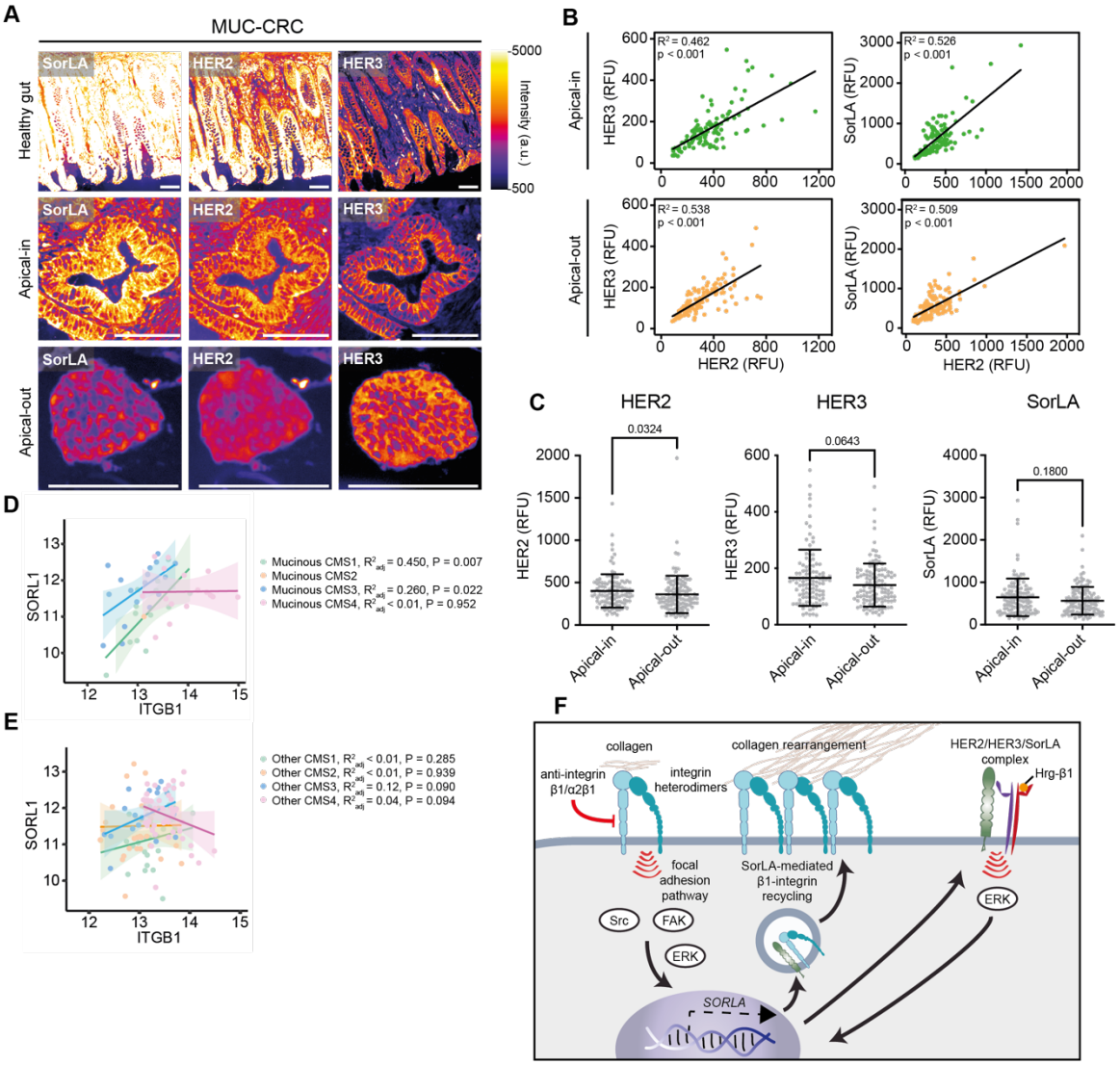

FIG7. HER2, HER3 and SorLA expressions are correlated *in vivo*

(A) Immunohistochemistry of healthy gut tissue, apical-in and apical-out cancer structures stained for HER2, HER3 and SorLA. (B) Correlation plots for HER2, HER3 and SorLA in a cohort of 25 patients (5 apical-in and 5 apical out structures chosen by patient) in apical-in and apical-out cancer structures. (C). Expression of HER2, HER3 and SorLA in a cohort of 25 patients (5 apical-in and 5 apical out structures chosen by patient) both in apical-in and apical-out structures. (D) Correlation between ITGB1 and SorLA expression in mucinous CRCs of CMS1-4, (E) Correlation between ITGB1 and SorLA expression in non-mucinous CRCs of CMS1-4, (F) Proposed mechanism of collagen-induced Erk, FAK and Src activation and SorLA expression, leading to Integrin-β1 recycling. This mechanism is supported by a HER2/HER3/SorLA feed-forward loop and results in efficient matrix-sensing and collagen rearrangement.

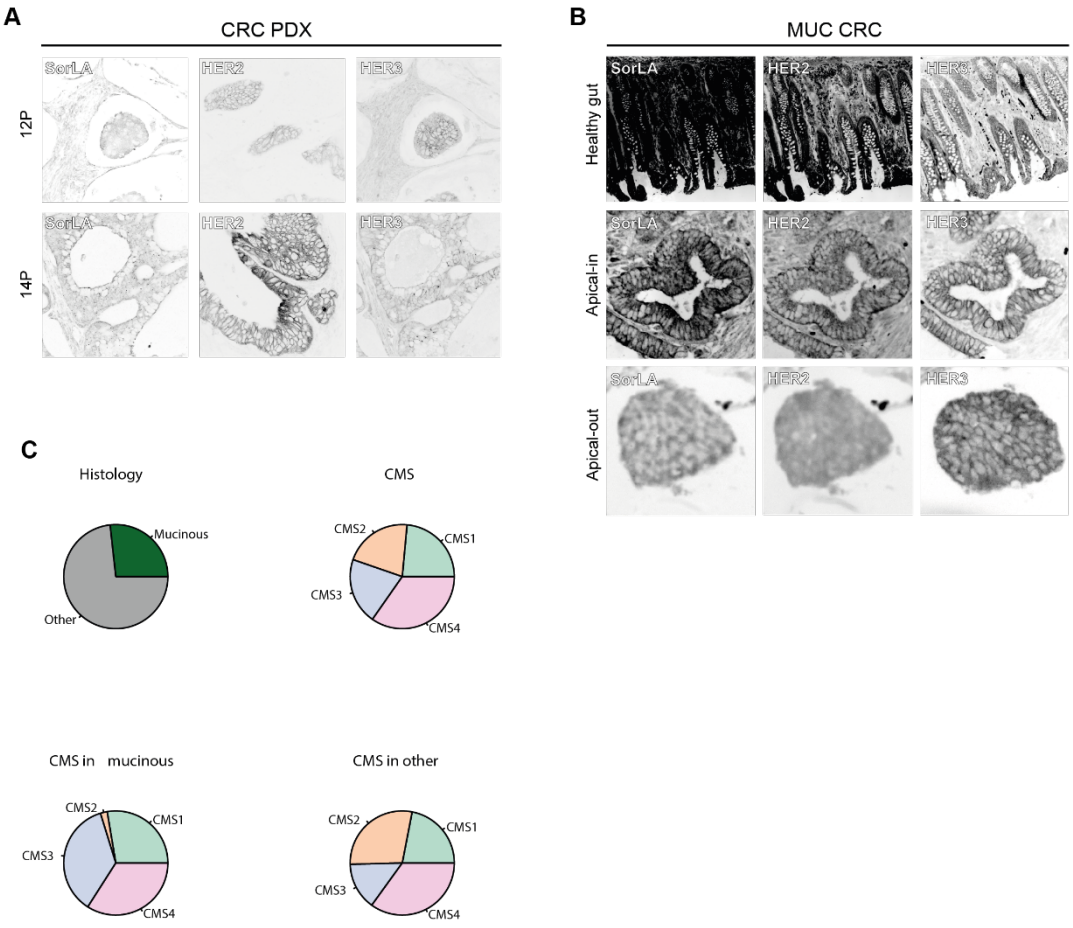

FIGS7. HER2, HER3 and SorLA expressions are correlated *in vivo*

(A) Immunohistochemistry of 12P and 14P tumors stained for HER2 and SorLA, and HER2 and HER3. (B) Immunohistochemistry of healthy gut tissue, apical-in and apical-out cancer structures stained for HER2, HER3 and SorLA. (C) Classification of the histotypes of the cohort used for FIG7D-E, amongst mucinous and non-mucinous CRCs.

III- Conway, J. R., Isomursu, A., Follain, G., Härmä, V., Jou-Ollé, E., **Pasquier, N.**, Välimäki E., Rantala J. & Ivaska, J. (2023). **Defined extracellular matrix compositions support stiffness-insensitive cell spreading and adhesion signaling**. *Proceedings of the National Academy of Sciences*, *120*(43)

PNAS RESEARCH ARTICLE | CELL BIOLOGY OPEN ACCESS

Defined extracellular matrix compositions support stiffness-insensitive cell spreading and adhesion signaling

James R. W. Conway[a,1], Aleksi Isomursu[a], Gautier Follain[a], Ville Härmä[b,c], Eva Jou-Ollé[a], Nicolas Pasquier[a], Eetu P. O. Välimäki[b], Juha K. Rantala[b,c], and Johanna Ivaska[a,d,e,f,g,1]

Edited by Joan Brugge, Harvard Medical School, Boston, MA; received March 15, 2023; accepted September 15, 2023

Integrin-dependent adhesion to the extracellular matrix (ECM) mediates mechanosensing and signaling in response to altered microenvironmental conditions. In order to provide tissue- and organ-specific cues, the ECM is composed of many different proteins that temper the mechanical properties and provide the necessary structural diversity. Despite most human tissues being soft, the prevailing view from predominantly in vitro studies is that increased stiffness triggers effective cell spreading and activation of mechanosensitive signaling pathways. To address the functional coupling of ECM composition and matrix rigidity on compliant substrates, we developed a matrix spot array system to screen cell phenotypes against different ECM mixtures on defined substrate stiffnesses at high resolution. We applied this system to both cancer and normal cells and surprisingly identified ECM mixtures that support stiffness-insensitive cell spreading on soft substrates. Employing the motor-clutch model to simulate cell adhesion on biochemically distinct soft substrates, with varying numbers of available ECM–integrin–cytoskeleton (clutch) connections, we identified conditions in which spreading would be supported on soft matrices. Combining simulations and experiments, we show that cell spreading on soft is supported by increased clutch engagement on specific ECM mixtures and even augmented by the partial inhibition of actomyosin contractility. Thus, "stiff-like" spreading on soft is determined by a balance of a cell's contractile and adhesive machinery. This provides a fundamental perspective for in vitro mechanobiology studies, identifying a mechanism through which cells spread, function, and signal effectively on soft substrates.

integrins | substrate stiffness | microcontact printing | extracellular matrix | molecular clutch

Significance

The ECM (extracellular matrix) provides an essential structural scaffold for tissue and organ functionality. Its composition and physical properties must be carefully controlled to give rise to the myriad forms taken by multicellular life. However, the mechanisms by which cells recognize distinct ECM landscapes and integrate these mechano-chemical signals remain unclear. Here, we demonstrate that ECM ligand availability and the integrin repertoire engaged jointly determine cell behavior in response to matrix rigidity. Through computational simulations and experimental validation, we propose a model whereby increasing the number of cell-matrix connections, "clutches", by providing cells with defined ECM combinations can fully support cell spreading on compliant matrices, offering insight into the mechanisms of cell behavior in soft tissues.

Multicellular organisms depend upon a complex network of extracellular matrix (ECM) components to provide a supportive scaffold for the function of organs and tissues. This network is deposited and remodeled predominantly by resident stromal cells and in turn guides stromal and epithelial cells as they respond to precise ECM compositions, modifications, stiffnesses, and architectures. The detection of different ECMs, and the ensuing downstream signaling in cells, occurs primarily through integrin adhesion receptors that coordinate cellular responses to different ligand combinations and can support both healthy and disease states (1–3). Indeed integrin–ECM adhesion signaling drives specific transcriptional responses (4, 5), and the functional significance of the ECM for tissues is exemplified by the severity of connective tissue disorders resulting from point mutations in collagens, laminin (Lam) isoforms, and fibrillin (6, 7). Similarly, many matrix components have been linked to a poorer prognosis in different cancer subtypes, including collagen VI (ColVI) (8), tenascin C (TNC) (9), and fibronectin (FN) (10). In order to assess the role of particular matrix components on cellular responses, matrix spot arrays have been developed to screen for the relative effects of different ECM combinations on stem cell differentiation (11, 12), stellate cells during liver fibrosis (13), and niche formation by metastatic cancer cells (14). Such an array format provides equal opportunity for the cells seeded to land preferentially on any spot, effectively negating the bias that can occur in a multiwell format, while providing a high-throughput platform for screening applications (14, 15).

Further to the diversity of the ECM, the architecture and mechanical properties of the tissue are increasingly recognized as essential for function (16). In the body, the ECM composition and rigidity are highly variable between tissues, ranging from >1 MPa for bone and cartilage, to 10 to 100 kPa for skin and lung tissues, down to 0.1 to 10 kPa for brain and adipose tissue (16). Notably, during fibrosis or cancer progression, the normal deposition and density of matrix components is disrupted, leading to a stiffer microenvironment and a corresponding loss in tissue functionality, strongly correlating with the likelihood and severity of disease (5, 17–21). While many models include an ECM composition equivalent to that of the normal or disease state, few overlay this information

Author contributions: J.R.W.C., A.I., J.K.R., and J.I. designed research; J.R.W.C., A.I., G.F., V.H., E.J.-O., and E.P.O.V. performed research; N.P. and J.K.R. contributed new reagents/analytic tools; J.R.W.C., A.I., G.F., and E.J.-O. analyzed data; A.I. and G.F. edited the paper; and J.R.W.C. and J.I. wrote the paper.

The authors declare no competing interest.

This article is a PNAS Direct Submission.

[1]To whom correspondence may be addressed. Email: jdconw@utu.fi or joivaska@utu.fi.

This article contains supporting information online at https://www.pnas.org/lookup/suppl/doi:10.1073/pnas.2304288120/-/DCSupplemental.

Published October 16, 2023.

with a corresponding mechanical state representative of the modeled tissue, typically applying tissue culture plastics with a stiffness higher than that of bone. Thus, to address the mechanochemical signaling outcomes triggered by distinct ECM composition and matrix rigidity, we developed a high-throughput ECM printing approach on soft (0.5 kPa) and stiff (50 kPa) polyacrylamide hydrogels and monitored cell behavior in response to different matrix compositions and defined stiffnesses. Using this approach, we identified ECM compositions that uncouple cell spreading from matrix rigidity and support spreading on a soft substrate. Through computational modeling and experimental validation, we link this to an increase in cell-matrix connections and adhesion signaling on specific ECMs. Thus, we demonstrate contexts in which specific ECM compositions can dictate cellular mechanoresponses and dissociate the widely studied linear relationship of cell spreading and force with increasing substrate stiffness.

Results

Preferential Spreading of Different Cell Types on ECM Components at Defined Stiffnesses. Given the increasing evidence for the role of substrate stiffness in cellular responses, we printed a composite ECM protein microarray onto polyacrylamide gels of different stiffnesses (*SI Appendix*, Fig. S1*A*). These arrays were composed of seven ECM components [i.e., collagen I (ColI), Lam, ColVI, TNC, FN, hyaluronic acid (HA), vitronectin (VTN)], and poly-D-lysine (PDL), a substrate that supports cell adhesion and spreading via electrostatic interactions, either printed alone or in a 1:1 ratio with one of the other eight components (*SI Appendix*, Fig. S1*B*). The different components were found to adhere to both soft (0.5 kPa) and stiff (50 kPa) composite arrays, at titratable concentrations, with no visible cratering after ECM printing on either substrate (*SI Appendix*, Fig. S1 *C–F*).

Initial experiments with telomerase immortalized fibroblast (TIF; Fig. 1*A*) and U2OS osteosarcoma cells (Fig. 1*B*) seeded on soft and stiff arrays led us to the observation that cells on ECM mixtures spread better on soft substrates than those on a single ECM ligand (Fig. 1 *A* and *B*). To explore this further, we seeded TIF, MDA-MB-231 (MM231, breast cancer), and U2OS cells on soft and stiff composite ECM arrays (*SI Appendix*, Fig. S2). Furthermore, to assess the signaling in response to the different ECM ligands, we engineered cell lines to stably express a reporter for ERK activity (22), a key component of adhesion signaling cascades (1, 23, 24). Upon phosphorylation, the kinase-translocation reporter (KTR) applied herein is transported out of the nucleus, allowing monitoring of kinase activity within intact cells (*SI Appendix*, validation of KTR sensitivity to mitogen-activated protein kinase kinase (MEK)/ERK inhibitor in live cells shown in Movie S1 and *SI Appendix*, Fig. S3*A*, quantified in *SI Appendix*, Fig. S3*B*).

Altogether, we assessed 10 distinct cellular parameters on the soft and stiff ECM arrays: cell density, KTR ratio (nuclear vs. cytoplasmic); nuclear area and roundness (based on nuclear labeling); cell area and roundness (based on actin cytoskeleton labeling); integrin adhesion complex (IAC) number, area, shape (Feret) and size [detected as paxillin foci between 0.1 and 15 μm^2; *SI Appendix*, Fig. S4 (TIFs), *SI Appendix*, Fig. S5 (U2OS) and *SI Appendix*, Fig. S6 (MM231s)]. These parameters were then used as active variables for a principal component analysis (PCA) that was applied to plot the mean of each parameter on soft and stiff spots for each cell line and ECM mixture, finding that 62.1% of the variance was explained by the first two principal components (Fig. 1*C*). These allowed us to plot the relative contributions of each parameter to their respective components (Fig. 1*D*). From these data, we observed that cell size opposed the nuclear and cell shape (i.e., roundness) parameters, indicating that spread cells also tended to be more asymmetric, and that IAC count was less connected with IAC size, Feret and area than the three parameters were with one another. Interestingly, the variables of cell density and KTR ratio were poorly represented by these principal components, suggesting that they were less powerful for explaining the differences between conditions than the other parameters. When plotting the PCA, we observed higher cos2 values further from the center of the plot (Fig. 1*E*), indicating that those spots were better represented. In addition, the distribution of spots allowed effective visual separation of the different cell lines (Fig. 1*F*) and substrate stiffnesses (Fig. 1*G*). Notably, the MM231 cells remained largely unaffected by different ECM mixtures on a soft substrate, consistently displaying poor cell spreading, few adhesions, and a rounded morphology [Fig. 1*G*, MM231 cells on soft (0.5 kPa) are highlighted with a circle]. In contrast, on several ECM mixtures on a soft substrate, TIF and U2OS cells showed a "stiff-like" set of parameters (Fig. 1*G*, stiff-like spots labeled with their respective details), indicating that for these cell types, specific ECM compositions are supportive of a stiff-like phenotype on soft substrates.

Spreading on ColI/Lam and Lam/TNC Is Uncoupled from YAP (Yes-Associated Protein) Nuclear Translocation. To further explore the effects of the matrix compositions supporting stiff-like phenotypes, we next seeded TIFs on these ECM mixtures (Fig. 2). In accordance with the ECM array data, the mixtures of ColI/Lam and Lam/TNC supported cell spreading equally well on soft and stiff hydrogels (Fig. 2*A*, quantified in Fig. 2*B*). This was consistent in the U2OS cells for the ColI/Lam, but not the Lam/TNC mixture (*SI Appendix*, Fig. S7*A*, quantified in *SI Appendix*, Fig. S7*B*). In contrast, all of the individual ECM molecules, and many of the ECM combinations, showed the expected significant increase in cell spreading on the stiffer hydrogels compared to the soft [Fig. 2 *A* and *B*, compare soft (blue) and stiff (red)], indicating that the ECM mixtures of ColI/Lam, and in some cell lines Lam/TNC, have a specific ability to support stiff-like spreading of cells on soft matrices.

The transcriptional coactivator YAP is a key mechanotransducer that regulates proliferation and cell fate, and its nuclear translocation is supported by higher substrate rigidities, as well as cell spreading and stress fiber formation (25–27). Hence, to assess the molecular mechanoresponses associated with the different ECM compositions, we evaluated the nuclear localization of YAP on soft and stiff hydrogels (Fig. 2*C*, quantified in Fig. 2*D*; *SI Appendix*, Fig. S7*C*, quantified in *SI Appendix*, Fig. S7*D*). As expected, the levels of nuclear YAP were significantly higher on stiff than on soft substrates, consistent with the role of YAP in sensing the increased stiffness of the substrate. However, the increased spreading of cells on the mixtures ColI/Lam and Lam/TNC did not trigger an increase in YAP nuclear localization, suggesting that spreading alone is not sufficient to induce nuclear translocation in these cells on soft. This could be linked to the lack of obvious stress fibers on soft ColI/Lam and Lam/TNC and the reported ability of focal complexes to exert sufficient force to maintain a lamella and support cell spreading, even before maturation into a larger focal adhesion (FA) (28). Indeed, YAP nuclear translocation has been reported to require adhesion reinforcement, FA maturation, and sufficient formation of stress fibers (29, 30). Interestingly, two-dimensional nuclear cross-sectional area corresponded closely to cell area but not YAP nuclear localization, contrary to previous reports (29), implying a more nuanced relationship between cell spreading, nuclear stress and strain, and YAP activation on the different ECM mixtures (Fig. 2*C*, quantified in Fig. 2*E*; *SI Appendix*, Fig. S7*C*, quantified in *SI Appendix*, Fig. S7*E*).

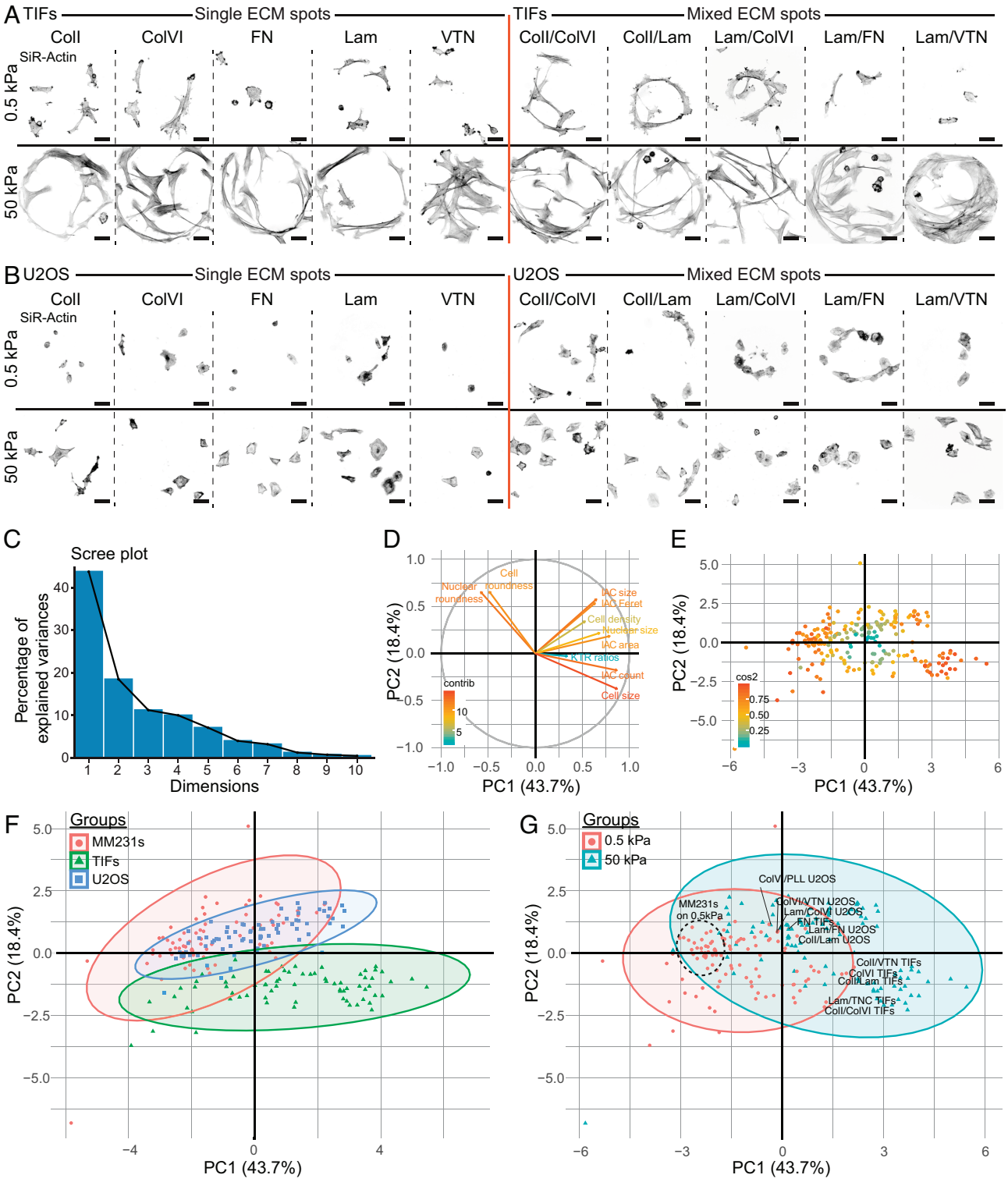

Fig. 1. ECM spot arrays on soft versus stiff hydrogels. (*A* and *B*) Representative images from TIF (*A*) and U2OS (*B*) cells seeded on 0.5 kPa or 50 kPa stiffness hydrogels with different ECM spots [n = 3 biological replicates, 4 spots/replicate/ECM mixture/stiffness; (Scale bar, 50 μm)]. (*C* and *D*) Scree plot of eigenvalues (*C*) and weighting the different parameters (*D*) from the PCA. (*E*) Factor map indicating the quality of representation by the principal components, where a high cos2 indicates a high degree of representation within the variable range from the PCA. (*F* and *G*) PCA using the median from each parameter on each ECM spot for both stiff and soft substrates (n = 3 biological replicates, 4 spots/replicate/ECM mixture/stiffness). Data are highlighted according to the cell line (*F*) or the substrate stiffness (*G*), where supportive mixtures on soft substrates are labeled. The complete ECM array datasets are included in *SI Appendix*, Figs. S4–S6).

Cells employ small GTPases to regulate their cytoskeleton, with the coordination of Rac1 and RhoA GTP-bound activities governing protrusion and retraction initiation and reinforcement (31–33). This careful balance in activity is essential for efficient cell migration and spreading (34, 35) and is often regulated by integrin-mediated signaling (36). This prompted us to explore whether changes in RhoA activity were associated with the increased cell spreading on supportive ECM mixtures on soft substrates. To this end, we employed a Förster resonance energy transfer (FRET) reporter [RhoA-2G, (37)], and fluorescence lifetime

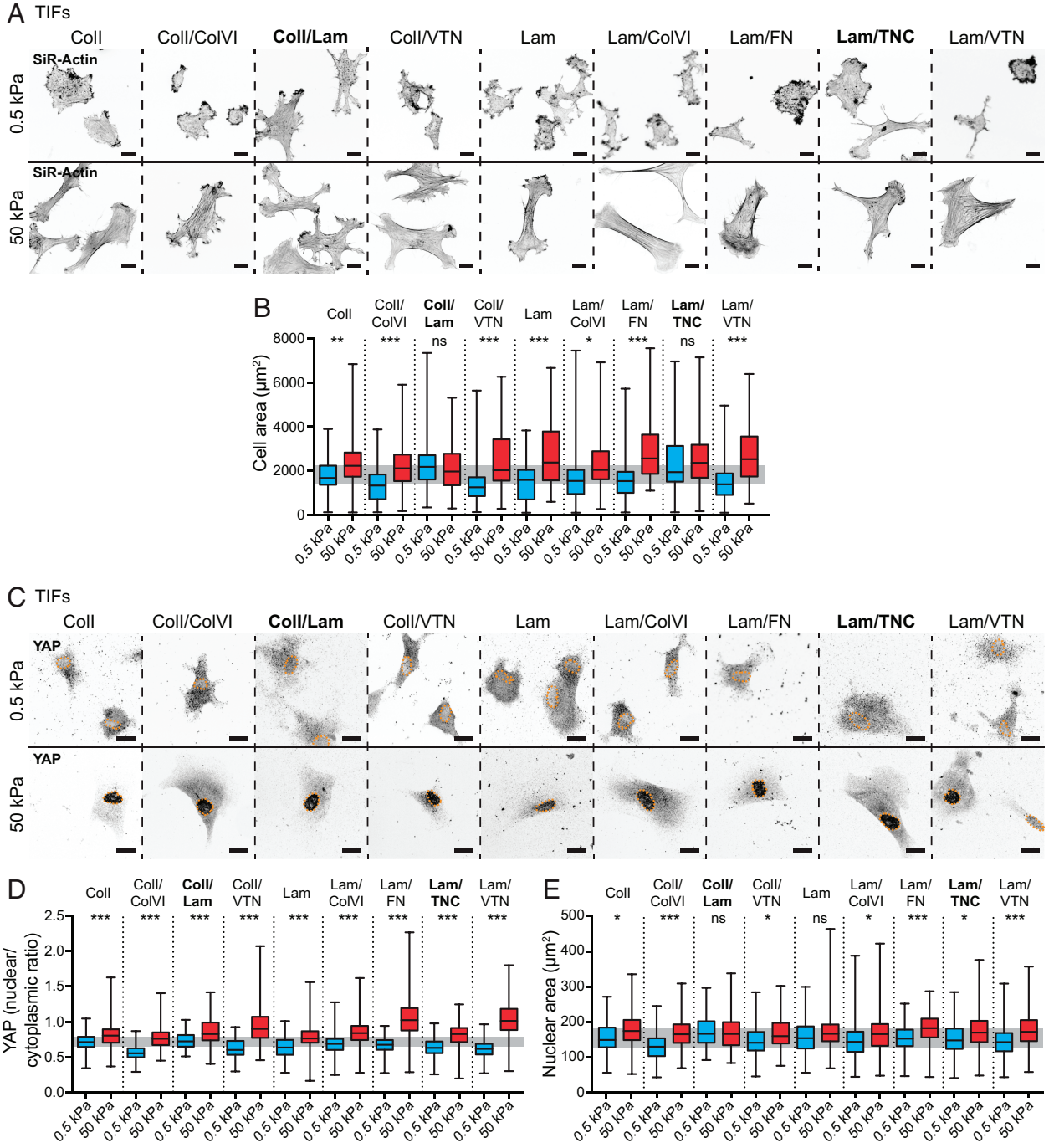

Fig. 2. Validation of ECM mixtures that support cell spreading on soft substrates. (*A* and *B*) Representative images (*A*) and quantification of cell area (*B*) after TIFs were seeded for 2 h on soft (0.5 kPa) and stiff (50 kPa) gels coated with different ECM mixtures, as indicated [n = 3 biological replicates, 13 to 59 cells/condition/replicate; (Scale bars, 20 μm); *P*-values from a one-way ANOVA with a Šidák correction for multiple comparisons; **P* < 0.05, ***P* < 0.01, ****P* < 0.001, and ns—not significant]. (*C*–*E*) Representative images (*C*) and quantification of YAP nuclear/cytoplasmic staining (*D*) and nuclear area (*E*) of TIFs seeded for 2 h on soft (0.5 kPa) and stiff (50 kPa) gels coated with different ECM mixtures, as indicated [n = 3 biological replicates, 13 to 59 cells/condition/replicate; (Scale bars, 20 μm); *P*-values from a one-way ANOVA with a Šidák correction for multiple comparisons; **P* < 0.05, ***P* < 0.01, ****P* < 0.001, ns—not significant]. Gray bars are drawn to mark the interquartile range of the control ColI 0.5 kPa condition in boxplots. Nuclei are marked with orange dashed lines (*A* and *C*).

imaging microscopy (FLIM)-FRET to read out relative changes in RhoA activation state in U2OS cells (*SI Appendix*, Fig. S8*A*). Concordant with previous reports for different cell types (36), all of the ECMs demonstrated an increased RhoA activation state on the stiffer 50 kPa substrates (*SI Appendix*, Fig. S8*B*, quantified in *SI Appendix*, Fig. S8*C*). While established RhoA activators, RhoA guanine nucleotide exchange factor, GEF-H1 (*SI Appendix*, Fig. S8*D*), and treatment with calpeptin increased RhoA activity (*SI Appendix*, Fig. S8*E*), we observed no consistent differences in RhoA activity between cells adhering to ColI/Lam mixture and the Lam and ColI alone on the softer 0.5 kPa gels (*SI Appendix*, Fig. S8 *B* and *C*). Together, these results suggest that altered balance in small GTPase activity is not likely to explain the increased spreading on ColI/Lam on the soft substrates.

Increased Clutch Numbers Can Explain the Increased Spreading of Cells on Soft ECM Mixtures. In order to test the role of integrins in the increased spreading of cells on specific ECM mixtures on soft, we treated TIFs on ColI/Lam with integrin β1 function-blocking antibodies (AIIB2 and mAb13), which block integrin-mediated

adhesion to ColI and Lam (Fig. 3*A*, quantified in Fig. 3 *B* and *C*). These antibodies severely compromised cell spreading on stiff and soft substrates, indicating a key role for integrins in the increased spreading on ColI/Lam and Lam/TNC on soft. These data also suggest that while mature FAs might be absent on soft substrates, the formation of IACs remains an important factor for cellular function. To further characterize TIF IACs on different ECM compositions, we investigated their subcellular distribution, comparing cells on single ECMs and the ColI/Lam mixture. The centripetal movement of IACs is often linked to their maturation from nascent to FAs, and can be indicative of cytoskeletal forces being exerted on these complexes. However, we observed minimal differences in IAC localization in TIFs seeded on ColI, Lam or the mixture of ColI/Lam (*SI Appendix*, Fig. S9). Next, in order to study the compositional heterogeneity of these IACs, we stained for zyxin and vinculin (*SI Appendix*, Fig. S10 *A* and *B*). Zyxin is an adhesion component with a particularly fast turnover (38, 39). Like vinculin, zyxin's recruitment to IACs has been linked

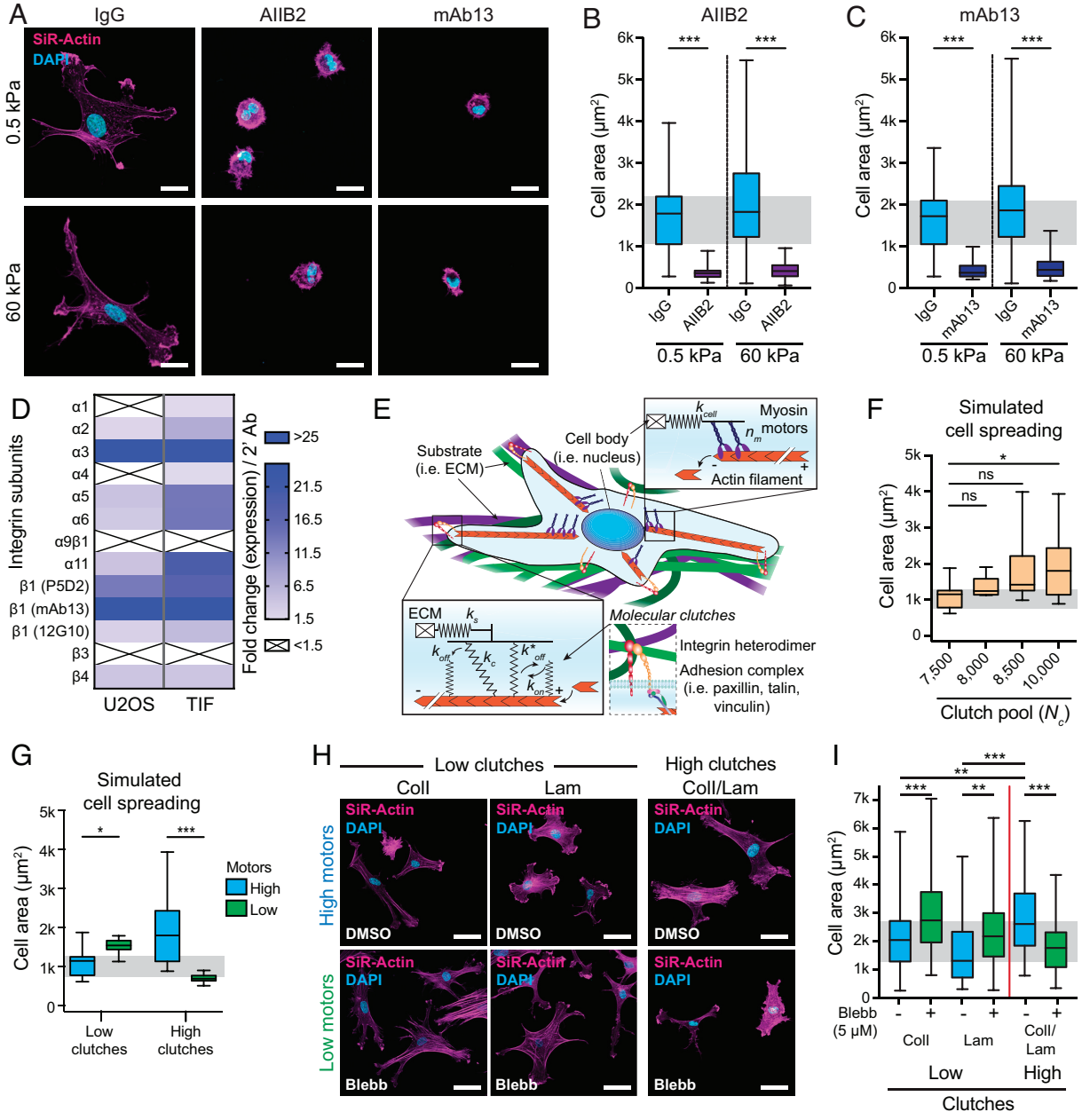

Fig. 3. Improved cell spreading on soft substrates can be explained by an increase in the number of molecular clutches. (*A*–*C*) Representative images (*A*) and quantification (*B* and *C*) of TIFs seeded for 2 h on 0.5 or 60 kPa hydrogels coated with ColI/Lam, treated with AIIB2 (*B*, 10 μg/mL) or mAb13 [*C*, 10 μg/mL; (Scale bars, 20 μm); n = 3 biological replicates, 12 to 25 cells/condition/replicate; *P*-values from a one-way ANOVA with a Tukey correction for multiple comparisons; ***$P < 0.001$]. (*D*) Flow cytometry to assess the relative surface expression of different integrin isoforms and heterodimers on TIF and U2OS cells (n = 5 biological replicates). (*E*) Schematic of the motor-clutch model used to simulate spreading of cells with different numbers of molecular clutches or motors. See *Methods* and *SI Appendix*, Table S1 for more details. (*F*) Simulation of cell spreading with an increasing number of available clutches (N_c) on a soft substrate (k_s = 0.5 pN/nm). The gray band indicates the interquartile range from the control (N_c = 7,500) condition (n = 6 to 12 simulated cells/condition; Kruskal–Wallis test with a Dunn's correction for multiple comparisons; *$P < 0.05$). (*G*) Simulation of cell spreading on a soft substrate with high or low number of clutches and motors (k_s = 0.5 pN/nm; high N_c/N_m ~ 10,000; low N_c/N_m ~ 7,500; 9 to 12 simulations/condition; *P*-values from a Kruskal–Wallis test with a Dunn's correction for multiple comparisons; *$P < 0.05$, ***$P < 0.001$). The gray band indicates the interquartile range from the control (low clutches/high motors) condition. (*H* and *I*) Representative images (*H*) and quantification (*I*) of TIFs seeded for 2 h on 0.5 kPa hydrogels coated with ColI, Lam, or ColI/Lam, treated with Blebbistatin (Blebb; 5 μM) or DMSO control. [(Scale bars, 50 μm); n = 3 biological replicates, 16 to 41 cells/condition/replicate; *P*-values from a one-way ANOVA with a Tukey correction; **$P < 0.01$ and ***$P < 0.001$].

to external and internal forces and is supported by vinculin tension, irrespective of adhesion maturation or stress fiber linkage (40–43). The number of zyxin- and vinculin-positive foci correlated with cell spreading in the different conditions with more zyxin and vinculin-positive foci detected in cells spreading on the ECM mixture on soft, suggesting improved cell-matrix interaction on soft substrates coated with ColI/Lam mixture compared to the single ECMs (*SI Appendix*, Fig. S10 *C–E*). Taken together, these results suggest that TIFs on soft ColI/Lam substrates present with more IACs than cells on ColI or Lam alone, but do not support the idea that this would correlate with increased IAC maturation, or the forces exerted on individual adhesions.

As the integrin β1 subunit is shared by the majority of ECM-binding integrins, we assessed the surface expression of different integrin heterodimers on TIF and U2OS cells (Fig. 3*D* and *SI Appendix*, Fig. S11). Both cell types expressed the main ColI-binding integrins, α2β1 and α11β1, as well as the primary Lam-binding integrins α3β1, α6β1, and α6β4, demonstrating that on a ColI/Lam mixture these cells are able to employ a broader repertoire of adhesion receptors than on either matrix alone.

This, together with the increased number of IACs on soft ColI/Lam substrates, prompted us to hypothesize that increased ligand diversity was resulting in increased integrin engagement, by the virtue of a larger number of potential cell-ECM binding sites being available to the cell. To investigate the effects of an increased propensity for integrin-ECM engagement on a soft substrate with a mixed ECM, we employed a motor-clutch model developed to explain stiffness-dependent cell migration, and more recently durotaxis (44–46). The model describes a ligand-binding unit (clutch) composed of an adhesion receptor (i.e., an integrin heterodimer) and the adaptors linking it to the actin cytoskeleton (Fig. 3*E*, the clutch assembly is represented in the model by a single bond). The "motor" unit represents the actomyosin contractile force that is transmitted to the substrate through clutches to enable cell spreading and motility [for more details on the model, see *SI Appendix, Extended Methods* and (45–48)]. Previous work has shown that altering the ratio of clutches to motors, that is, the amount of cell adhesion molecules relative to intracellular contractility, can drastically affect cell behavior, including the capacity to exert traction or migrate on a given substrate stiffness (46, 47). Using this model, we altered the total number of molecular clutches (N_c; i.e., potential integrin-ECM connections, available to each cell), while maintaining substrate rigidity (spring constant) at 0.5 pN/nm to mimic our soft hydrogels (*SI Appendix*, Table S1). Through these simulations, we found that an incremental increase in the number of clutches, relative to motors, results in a steady increase in the average cell area, indicative of cell spreading on a soft substrate (Fig. 3*F* and Movie S2). We next simulated the outcome of tuning cell contractility (increasing or decreasing motor number) relative to the clutch number. These simulations predicted that in cells with a low clutch number, a decreased motor number increases cell area; whereas in cells with a higher number of clutches, lowering the motor number decreases cell spreading (Fig. 3*G*). To test these predictions, we then treated TIFs plated on ColI, Lam or ColI/Lam mixture with low doses of the myosin II inhibitor Blebbistatin. In concordance with the model, decreasing motor number using Blebbistatin increased cell spreading on single ECM molecules by ≥50% and reverted the stiff-like increased cell spreading on soft ColI/Lam to a similar degree as that observed with DMSO-treated cells on single ECMs (Fig. 3*H*, quantified in Fig. 3*I*). These data further suggest that cell spreading on soft is a delicate balance between cell adhesion and cell contraction dynamics and is favored by a slightly higher clutch:motor ratio; a scenario potentially supported by a more complex ECM environment. However, the synergistic effect on cell spreading on soft was not observed with all ECM combinations (Figs. 1 and 2), indicating that the repertoire of integrins engaged and downstream signaling to the cytoskeleton are also essential in determining the outcome of cell adhesion to complex ECM mixtures as a function of substrate rigidity.

Increased Spreading on Soft Substrates with Mixed ECMs Corresponds with a Concomitant Increase in Adhesion Signaling. To assess the biological outcome of increased cell spreading on specific ECM mixtures, we returned to the ECM array ERK activation data (ERK KTR signal; Fig. 4*A* and *SI Appendix*, Fig. S4*B*). Notably, there was a significant increase in ERK activation in TIFs on ColI/Lam, compared to ColI or Lam alone on soft substrates (Fig. 4*B*, quantified in Fig. 4*C*). As the MAPK pathway is activated by IACs (2, 23, 24), we then revisited the simulations and investigated the relationship between the available pool of clutches and the number of clutches engaged by the ECM at any given time. The motor-clutch computational modeling predicts that increasing the pool of available clutches by 25% significantly increases mean clutch engagement in cells on a soft substrate (Fig. 4*D*). To investigate this experimentally, we assessed the activation state of integrins on single and mixed ECMs on a soft substrate. As active, ligand-engaged integrin β1 adopts an extended-open conformation (2, 49), we applied an antibody specific to ligand-engaged integrin β1 [12G10; (50)] to assess the relative integrin β1—ECM engagement between conditions. In concordance with the predictions of the model, we observed lower levels of active integrin β1 heterodimers in the soft Lam and ColI conditions, compared to the significantly higher integrin activity on the ColI/Lam mixed ECM on soft substrates (Fig. 4*E*, quantified in Fig. 4*F*). In line with the increased ERK activity observed with the KTR (Fig. 4 *B* and *C*), and the increased level of active integrin β1, phosphorylated FA kinase (pFAK) was also significantly higher on the mixed ECM (Fig. 4*E*, quantified in Fig. 4*G*). On collagen, where adhesion is mediated by α1β1, α2β1, and α11β1 (Fig. 3), activated integrin β1 and pFAK showed a high degree of colocalization (*SI Appendix*, Fig. S12), as expected. Interestingly, this colocalization between the active integrin β1 and pFAK signals was lower on Lam than ColI and intermediate on the ColI/Lam mixture. This suggests that in ECM conditions with Lam present, the Lam-specific α6β4 integrin, not recognized by 12G10, may be synergizing with the Lam-binding α3β1 and α6β1 integrins in mediating adhesion and downstream signaling to FAK (*SI Appendix*, Fig. S12). Activation of FAK through autophosphorylation is one of the first steps in integrin signaling and occurs already in nascent adhesions, in addition to mature FAs (2, 38). Therefore, the supportive ECM mixture on soft not only facilitates stiff-like spreading but also triggers key integrin-proximal signaling pathways on soft matrices by engaging multiple integrin subtypes. Cumulatively, we see that the mixed ECMs can provide an efficient signaling response, as cells are able to apply a larger number of integrin receptors to interact effectively with softer substrates (Fig. 4*H*). This supports the observation that specialized cell types in multicellular organisms can function effectively in very soft environments and provides a springboard for future work into the diversity of ECM combinations, organizations, and modifications that permit such multifaceted cellular activities.

Discussion

Here, we have developed a composite ECM spot array system that combines the assessment of cellular responses with that of matrix composition and the mechanical properties of the adhered

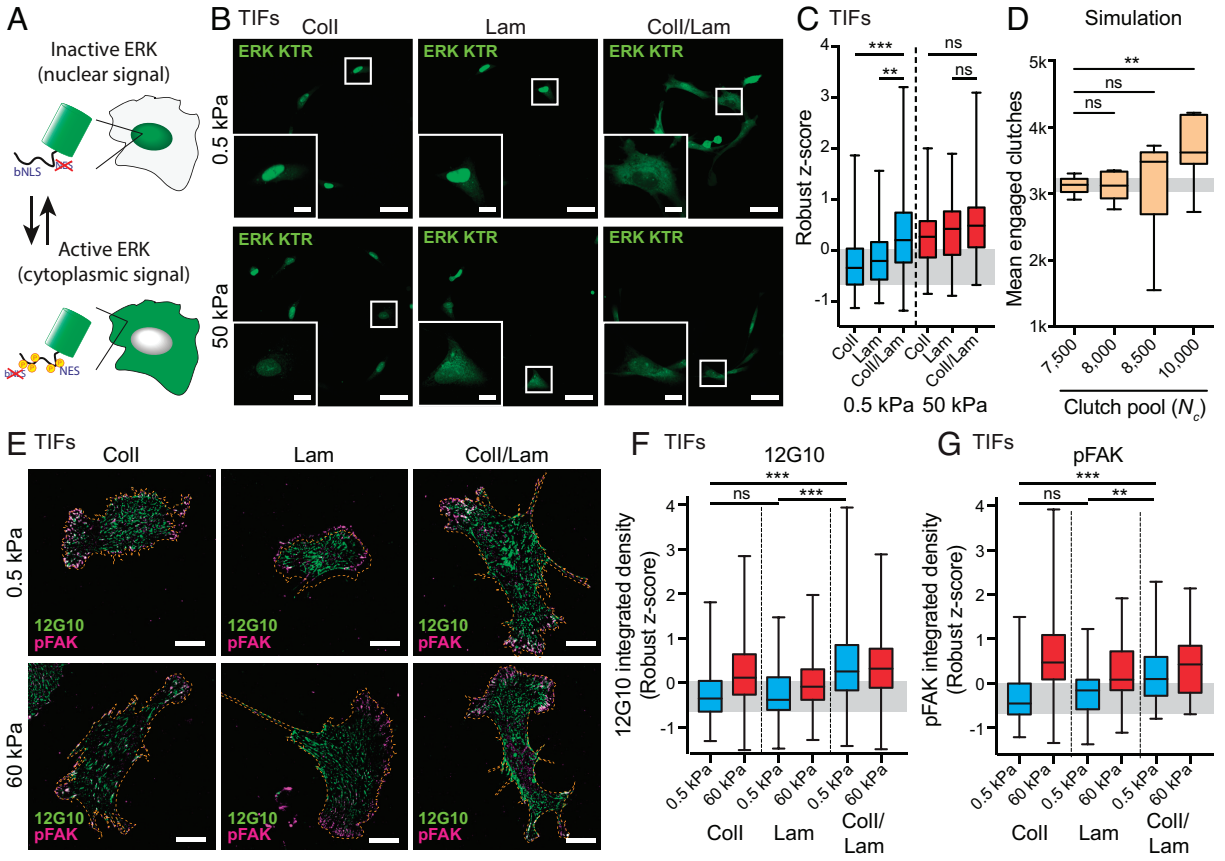

Fig. 4. Increased spreading occurs in conjunction with a concomitant increase in integrin signaling. (*A*) Schematic of the ERK KTR activity reporter, where high ERK activity leads to an increase in phosphorylation and inactivation of the bNLS and shuttling out of the nucleus. (*B* and *C*) Representative images (*B*) and quantification (*C*) of the ERK KTR reporter expressed in TIF cells seeded on ECM array spots [scale bars, 50 μm (main), 10 μm (*Insets*); n = 3 biological replicates, 4 spots/ECM mixture/substrate/replicate; *P*-values from a one-way ANOVA with a Šidák correction for multiple comparisons; $^{**}P < 0.01$, $^{***}P < 0.001$, and ns—not significant]. (*D*) Mean number of engaged clutches in simulated cells with an increasing number of total available clutches (N_c), on a soft substrate (k_s = 0.5 pN/nm). The gray band indicates the interquartile range from the control (7,500 N_c) condition (n = 6 to 12 simulated cells/condition; Kruskal–Wallis test with a Dunn's correction for multiple comparisons; $^{**}P < 0.01$). (*E–G*) Representative images (*E*) and quantification (*F* and *G*) of TIFs seeded for 2 h on 0.5 or 60 kPa stiffness gels coated with Coll, Lam or Coll/Lam and stained for 12G10 (*F*, n = 5 biological replicates) and pFAK [*G*, n = 3 biological replicates; 12 to 25 cells/condition/replicate; (Scale bars, 20 μm); *P*-values from a one-way ANOVA with a Tukey correction for multiple comparisons; $^{*}P < 0.05$, $^{***}P < 0.001$, and ns—not significant]. Gray bars are drawn to mark the interquartile range of the control Coll 0.5 kPa condition in boxplots (*C*, *F*, and *G*).

substrate. Through this screening platform, we uncovered ECM compositions that uncouple cell spreading from stiffness and promote stiff-like cell behavior on more compliant substrates. This unexpected in vitro observation is in line with the fact that cells in soft tissues are similarly capable of functioning without a rigid support. In line with this finding, we applied a computational motor-clutch model to simulate cell spreading on soft substrates as a function of ECM ligand availability and demonstrated that a higher number of molecular clutches (i.e., available integrin-ECM bonds) could compensate for the lack of mechanical support provided by the substrate, effectively promoting spreading. We then verified experimentally the fundamental predictions of the model: that cell spreading on soft ECM depends on the balance between available clutches and motor activity, and that the number of functional integrin-ECM bonds scales with the overall availability of integrin-ECM binding sites. Collectively, the high-throughput screening, modeling, and experimental validation uncover a mechanosensing paradigm, where cell spreading and integrin downstream signaling are equivalently activated on soft and stiff substrates under specific matrix conditions.

Several studies have looked at the force-mediated activation of integrins, where affinity is increased with loading, giving rise to talin unfolding and vinculin recruitment, which enables adhesion reinforcement by preventing talin refolding and subsequently facilitating adhesion maturation (40, 41). On soft substrates, however, mechanical adhesion reinforcement is less likely to occur, which has led to the notion that cells have a compromised ability to transmit ECM-induced signals (48). This suggests that factors such as ligand density and the varied affinities of integrins to different ligands may play a larger role in effective cell adhesion on softer substrates (49). To exemplify the varied application of integrin heterodimers, cells adhering to FN commonly apply integrin β3 heterodimers for the formation of small nascent adhesions, while larger adhesions are stabilized with integrin β1 heterodimers (51). Similarly, the affinity of different integrin β1 heterodimers has been linked to conformational changes that radically modulate the on and off rates for ligand binding (52). Furthermore, the expression of different collagen-binding integrins, with distinct binding affinities to fibrillar or nonfibrillar collagens (53–55), or to defined Lam subtypes (56), highlights the varied application of integrin heterodimers even within the same ligand-binding family. These studies, and the data presented herein, place a spotlight on the biological complexity of cell-ECM interactions, extending beyond the role of any factor in isolation. They are also likely to explain why only some of the ECM mixtures present in our compliant substrate arrays supported stiff-like phenotypic changes, while others did not.

A shift in drug discovery strategies away from target-based approaches and toward image-based phenotypic screening highlights the challenge of efficacious targeting of disease states and

the power of modern microscopy to overcome such challenges (57). Recent studies assessing the efficacy of treatment responses between 2D plastic and 3D systems in ECM gels have helped to explain the high attrition rates of compounds in clinical trials, where the mechanical and compositional properties of the ECM in vivo have a significant effect on drug efficacy at later stages of the drug discovery pipeline (58). This is particularly evident in relation to cancer therapy, where solid tumors with a higher stiffness show increased radio- and chemoresistance (17, 59), which changes upon therapeutic intervention to a softer matrix and altered responses to therapies (60, 61). In line with the importance of the ECM, the progression of several cancer subtypes can be more robustly predicted using gene signatures from the stromal compartment, than from the cancer cells themselves (62–65). The convoluted relationship between the tumor and associated stroma/ECM is further illustrated by the suppressive role of healthy stroma on cancer cell growth (4), while the cancer-associated stroma is linked to both disease containment and prosurvival niche formation (66). Our data, and the many studies showing distinct cell behaviors on substrates of differing stiffnesses, imply that screening platforms encompassing matrix rigidities and ECM compositions tailored to align with the in vivo situation of the given tumor type would be expected to be significantly more relevant.

Here, we present a platform for assessing matrix composition in the context of different rigidities to screen for mixtures supportive of spreading and intracellular signaling responses. Aligning computational modeling and experimental validation, we uncovered 'stiff-like' cell spreading and signaling on soft matrices as being dependent on increased engagement of a more diverse range of integrin heterodimers on a mixed matrix. Thus, this work demonstrates the importance of considering the vast array of ECM combinations, modifications, stiffnesses, as well as the interacting cell types, that occur in tissues and are essential to our understanding of both healthy and disease states.

Methods

Polyacrylamide Hydrogels with Defined Stiffnesses. Commercial [Softview Easy Coat hydrogels, 35 mm dish with 10 mm glass bottom, SV3510-EC-0.5-EA (0.5 kPa) or SV3510-EC-50-EA (50 kPa)] or in-house stiffness gels were used as indicated. In-house gels were prepared using glass-bottom dishes (D35-14-1N, Cellvis). The dishes were treated with bind silane solution [71.4 μL Bind Silane ([3-(Methacryloyloxy)propyl]trimethoxysilane; Sigma, M6514), Glacial Acetic Acid (71.4 μL; Sigma, 33209) up to 1 mL in Ethanol (96%)] for 30 min at room temperature and then wash twice with ethanol (96%). 12 μL of gel mixture [0.5 kPa: 63 μL 40% Acrylamide Solution (Sigma, A4058), 10 μL 2% bis-acrylamide solution (Sigma, M1533), 399 μL PBS, 2.5 μL 20% ammonium persulfate (APS; Sigma, A3678, diluted in Milli-Q water) and 1 μL TEMED (Sigma, T9281); 60 kPa: 225 μL 40% Acrylamide Solution, 100 μL 2% bis-acrylamide solution, 175 μL PBS, 2.5 μL 20% APS and 1 μL TEMED] was applied to dry, bind silane treated dish(es) and overlaid gently by placing 13 mm glass coverslips on top of the gel mixture, allowing it to set for 1 h at room temperature, as described previously (67). A sufficient amount of PBS was then added to cover the coverslip completely before carefully removing the coverslip. Surface activation was performed with Sulfo-Sanpah (sulfosuccinimidyl 6-(4′-azido-2′-nitrophenylamino)hexanoate; 0.2 mg/mL in 50 mM HEPES; Thermo Fisher Scientific, 22589) and EDC (N-Ethyl-N′-(3-dimethylaminopropyl) carbodiimide hydrochloride; 2 mg/mL in 50 mM HEPES; Sigma, 03450), applied to the surface for 30 min at room temperature with gentle agitation. Gels were then incubated in a UV oven (UVO-cleaner 342 to 220, Jelight Company) at 5 cm distance for 10 min before washing thrice with PBS. Commercial or in-house hydrogel coating was performed with saturating concentrations of all ECM mixtures at 20 μg/mL final ECM concentration (*SI Appendix*, Fig. S13).

Cell Lines. Human dermal fibroblasts, TIFs [a kind gift from J.C. Norman (Beatson Institute, Glasgow, Scotland, UK)], MM231 (HTB-26, ATCC), HEK293FT (R70007, ThermoFisher), and U2OS (HTB-96, ATCC) cells were maintained in Dulbecco's modified Eagle's medium (Sigma, D5796) supplemented with 10% serum (FBS; Biowest, S181T), L-glutamine (100 mM, Sigma, G7513), HEPES (10 mM, Sigma, H0887), and sodium pyruvate (1 mM, Sigma, S8636).

Composite ECM Spot Arrays. ECM mixtures at 400 μg/mL were prepared in printing buffer (RPMI, 20 mM HEPES, 17 mM EDTA, 0.6 M sucrose) using PDL (A-0030E, Sigma), FN (Millipore, 341631), ColI (Millipore, 08 to 115), TNC (Merck, CC065), HA (HyStem Cell Culture Scaffold Kit, HYS010-1KT, Sigma-Aldrich), Lam EHS (Sigma-Aldrich, L2020), ColVI (Abcam, ab7538), and VTN-N (purified as in ref. 68). Arrays were printed on commercial stiffness gels (Softwell 24-well plate Easy coat, SW24-EC-0.5-EA, SW24-EC-50-EA, Matrigen) using an OmniGrid (Gene Machines) microarray printer with 200 μm solid tip pins (PTLS200, 401774, PointTechnologies). Printed arrays were then blocked with 1% bovine serum albumin (BSA; A8022, Sigma) in phosphate-buffered saline (PBS; Biowest, L0615) overnight at +4 °C. 2×10^5 TIF, MM231, and U2OS cells were blocked in 1% BSA and then seeded on 0.5 and 50 kPa spot arrays in 24-well wells for 2 h prior to fixation for 10 min at 37 °C in 4% PFA in PEM buffer [EGTA (10 mM; VWR Chemicals, 0732), $MgSO_4$ (1 mM; Fluka Analytical, 00627), PIPES (pH 6.9; 100 mM; Sigma, P6757), sucrose (75 mM; Sigma, S9378), and Triton X-100 (0.2%; Sigma, T8787) in H_2O].

Collagen Labeling. To fluorescently label rat tail type I collagen (~4.24 mg/mL, 354236, Corning), 1.65 mL was mixed with 450 μL of Milli-Q water and 500 μL of neutralizing buffer (20 mM NaH_2PO_4, 112 mM $Na_2HPO_4 \cdot 2H_2O$, 0.4 M NaCl, and 46 mM NaOH) and incubated at 37 °C for 30 min. The polymerized collagen was then washed thrice with PBS for 10 min. Then, 3 mL of Milli-Q water and 1 mL of bicarbonate buffer [1 M $NaHCO_3$ (pH 8), raised dropwise to pH 8.3 using 1.17 M Na_2CO_3 (pH 11)] were added to the collagen gel before addition of the Alexa Fluor™ 647 NHS Ester (Succinimidyl Ester) dye (A20006, Invitrogen) in 100 μL of PBS. After incubating the collagen mix overnight at 4 °C, the dye was then removed, and the collagen was washed with PBS with rotation at room temperature for 30 min, changing the PBS five times. Stained collagen was then depolymerized through the addition of 2 mL HCl (20 mM) and gentle rotation at 4 °C overnight. The collagen was finally centrifuged at 20,000 g for 10 min, collecting the labeled collagen from the supernatant.

Flow Cytometry of Surface Integrin Isoforms. Cells from 2D culture plates were trypsinized and then fixed with 2% PFA for 10 min at 37 °C before washing twice with PBS. A total of 200,000 cells were incubated with primary antibodies (1:100 dilution in Tyrode's buffer [ITGA1 (MAB1973, Millipore), ITGA2 (MCA2025, Bio-Rad), ITGA3 (ab228485, Abcam), ITGA4 (MAB16983, Millipore), ITGA5 (ab78614, Abcam), ITGA6 (MCA699, Serotec), ITGA11 (MAB4235, R&D Systems), α9β1 (sc-59969, Santa Cruz), ITGB3 (ab179473, Abcam), ITGB4 (ab29042, Abcam), active β1 (clone 12G10, in-house production from Developmental Studies Hybridoma Bank (DSHB) hybridoma), β1 (clone P5D2, in-house production from DSHB hybridoma), and inactive β1 (clone mAb13, in-house production from DSHB hybridoma)]) for 1 h at 4° C with gentle agitation before washing twice with PBS and incubating with secondary antibodies (Alexa-488 conjugated Anti-Mouse/Anti-Rat Invitrogen; 1:300 dilution in Tyrode's buffer) for a further hour at 4 °C with gentle agitation. Cells were then washed again with PBS before being resuspended in 200 μL of PBS and loading into a 96-well plate. Cytometry was then performed on an LSRFortessa cell analyzer using the High-Throughput Sampler (BD Biosciences). Up to 10,000 single-cell events were collected per condition. Gating and statistical analysis of the cell population were performed in FlowJo (BD Biosciences).

Frequency-Domain FLIM-FRET. All FLIM experiments were performed on a LIFA fast frequency-domain FLIM system (Lambert Instruments) attached to an inverted microscope (Zeiss AXIO Observer.D1) with sinusoidally modulated (40 MHz) epi-illumination (1 W) at 406 nm from a temperature-stabilized multi-LED system (Lambert Instruments) and a 63×/1.15 objective (Zeiss, Objective LD C-Apochromat 63×/1.15 W Corr M27). Atto425 (Sigma, 56759) in PBS at 1 μM, pH 7.4, was used as a lifetime reference standard. An appropriate filter set for mTFP1 was used (No excitation filter; beam splitter, FT 455; emission, BP 475/20) in order to measure per cell, the phase and modulation fluorescence lifetimes per pixel from images acquired at 12 phase settings, using the manufacturer's software. The apparent FRET efficiency (E_{app}) was calculated using the measured lifetimes of each donor–acceptor pair (τ_{DA}) and the average lifetime of the donor-only (τ_D) samples. For all experiments, the donor-only samples were parental U2OS cells that had been

transfected with pEF.DEST51-mTFP1(cp227) overnight using Lipofectamine 3000 (ThermoFisher, L3000015), as per the manufacturer's protocol.

$$E_{app} = (1 - \tau_{DA} / \tau_{D}) \times 100.$$

For the 30-min calpeptin (50 μM; Selleckchem, S7396) treatments, U2OS cells stably expressing the RhoA-2G FRET reporter were seeded overnight in glass-bottom 24-well wells (Cellvis, P24-1.5H-N) with DMSO as a control. Similarly, for the transfections with pEF.DEST51-mScarlet and pDEST-mCherry-ARHGEF2, U2OS cells stably expressing the RhoA-2G FRET reporter were seeded overnight in glass-bottom 24-well wells, transfecting after 6 h seeding using Lipofectamine 3000, as per the manufacturer's protocol. Experiments on stiffness gels were performed on 0.5 kPa or 50 kPa gels in 24-well wells after first coating with different ECM components and blocking with 2% BSA. These coated gels were then seeded with BSA-blocked RhoA-2G-expressing U2OS cells for 2 h at 37 °C. All experiments were fixed for 10 min at 37 °C in 4% PFA before washing with PBS and 1M glycine and imaging as above.

Immunofluorescence. Prior to seeding with TIF or U2OS cells, in-house (details above) or commercial stiffness gels were coated with ECM mixtures in PBS at 37 °C for 1 h and then blocked with sterile 2% BSA for a further hour at 37 °C. Cells were also blocked in 2% BSA before seeding for 2 h on coated gels, prior to fixation for 10 min at 37 °C in 4% PFA in PEM buffer. Treatment with Blebbistatin (5 μM; STEMCELL Technologies, 74202), or Integrin function-blocking antibodies against integrin β1 (clones mAb13 and AIIB2, in-house production using hybridomas from DSHB) or IgG [Rat IgGa, kappa monoclonal (RTK2758)–Isotype control; Abcam, ab18450] occurred during cell seeding where indicated. Fixed samples were then blocked in blocking buffer (2% BSA and Glycine (1 M; PanReac AppliChem, A1067) in PBS) overnight at 4 °C. Cell nuclei were stained with Hoechst 33342 (1:1,000, ThermoFisher, 62249), SiR-Actin (1 μM, Spirochrome, sc001) in parallel with primary antibodies against paxillin [(Y113); 1:100, Abcam, ab32084], zyxin (EPR4302; 1:100, Abcam, ab109316), vinculin (1:100, Sigma, V9131), active β1 (1:25 from 0.25 mg/mL stock (in-house production); clone 12G10), ColI (1:200, Abcam, ab34710), FN (1:100, Sigma, F3648), Lam (1:100, Sigma, L9393), p-FAK(Y397) (1:100, Cell Signaling, 8556), and/or YAP (63.7; 1:100, Santa Cruz, sc-101199) in PBS overnight at 4 °C. Samples were then washed twice with PBS before staining with appropriate secondary antibodies for 1 h at room temperature and a further two washes with PBS. Imaging was performed on a Zeiss 3i CSU-W1 spinning disk confocal microscope using SlideBook 6 acquisition software and a 40×/1.1 Zeiss LD C-Apochromat or 63×/0.75 Zeiss LD Plan-NEOFLUAR objectives with water immersion. Analysis of microscopy data was performed in Fiji (NIH), assessing colocalization using Pearson's coefficients from the Coloc2 plugin.

Lentiviral Transduction. Lentivirus transduction was used to generate cell lines (TIF, MM231, and U2OS) stably expressing the ERK KTR, or RhoA-"G FRET reporters. The lentiviruses were produced in HEK293FT cells by cotransfecting with a third-generation lentiviral packaging system composed of pMDLg/pRRE (Addgene plasmid #12251), pRSV-Rev (Addgene plasmid #12253), pMD2.G (Addgene plasmid #12259), along with the pLentiPGK Puro DEST ERKKTRClover [a kind gift from Markus Covert; Addgene plasmid #90227 (22)], pLenti-RhoA-2G [a gift from Olivier Pertz; Addgene plasmid #40179 (37)] transfer plasmids, using Lipofectamine 3000 (ThermoFisher) in OptiMEM (Gibco, 21985070), as per the manufacturer's protocol. After 24 h, the media were changed for complete growth medium and incubated for a further 24 h, at which point the media were collected and filtered through a 0.45 μm syringe filter. Cells were then transduced with lentivirus for 48 h in the presence of polybrene (8 μg/mL; Sigma, TR-1003-G) before washing and selection of stable positive cells using puromycin (2 μg/mL). Cells were then sorted by fluorescence-activated cell sorting to isolate a population within a similar fluorescence range.

Live imaging of KTR Cells. A total of 2,000 KTR-expressing TIF cells were seeded in 8-well dishes (Ibidi, 80827) and incubated overnight prior to imaging with SiR-DNA (1 μM; Spirochrome, sc007) to mark the nuclei. Imaging was performed using a Zeiss 3i CSU-W1 spinning disk confocal microscope with SlideBook 6 acquisition software and a Zeiss 20x Plan-Apochromat 0.8 NA air objective. Live imaging conditions were achieved with an Okolab bold line heating system at 37 °C, 20% O_2, and 5% CO_2, acquiring images every 3 min for 75 min, treating with DMSO or trametinib (GSK1120212; 1 μM; Selleckchem, S2673) after first imaging for 15 min.

Molecular Cloning. To generate the pENTR221-mTFP1(cp227) construct, mTFP1(cp227) was PCR amplified from the pLenti-Rac1-2G plasmid [a gift from Olivier Pertz; Addgene plasmid #66111 (69)] to add flanking attB1/attB2 sites using the mTFP1_attB1_F: 5′-TAGAACAAGTTTGTACAAAAAAGCAGGCTCAGCCACC ATGGCACACCATCACCACCATCACG-3′ and mTFP1_attB2_R: 5′-TAGGGACCACTTTGT ACAAGAAAGCTGGGTAGCGTCCGGAGTTGCGGGCCAC-3′ primers. This PCR fragment was then BP subcloned with pDONR221 (ThermoFisher, 12536-017) using BP clonase II (ThermoFisher, 11789), as per the manufacturer's instructions, to yield pENTR221-mTFP1(cp227). The mScarlet (70) fragment was ordered as a gBlock gene fragment from IDT with flanking XhoI/BamHI sites to allow ligation into the pENTR2b (A10463, ThermoFisher) vector to generate pENTR2b-mScarlet (Addgene plasmid #207961), after both were digested with XhoI (ThermoFisher, FD0694) and BamHI (ThermoFisher, FD0054). These vectors then facilitated LR subcloning with pEF.DEST51 (ThermoFisher, 12285-011) using LR clonase II (ThermoFisher, 11791), as per the manufacturer's instructions, to generate pEF.DEST51-mTFP1(cp227) and pEF.DEST51-mScarlet (Addgene plasmid #207960). Similarly, pENTR221-ARHGEF2 was LR subcloned with pDEST-N-term_mCherry (a kind gift from Maria Vartiainen, University of Helsinki, Helsinki, Finland) to generate pDEST-mCherry-ARHGEF2 (Addgene plasmid #207959).

Statistical Analysis. All statistical comparisons were performed using Prism 7 (GraphPad software), as indicated in the figure legends, repeating all experiments at least three times independently. PCA was performed in RStudio using the factoextra package, while robust z-scores were calculated using the stats package.

Stochastic Computational Model of Cell Spreading. The spreading of cells on soft elastic substrates was modeled using a previously described MATLAB implementation of the 2D whole-cell model for spreading and motility (cell migration simulator; CMS) developed by Odde and colleagues (44). The method uses Gillespie Stochastic Simulation Algorithm (71) to model an entire cell by connecting several molecular motor-clutch modules to a central cell body and balancing the resulting forces at the center. The detailed algorithms and equations governing the base CMS have been reported in full previously (44). Here, we added a previously described maximum limit of 100 s^{-1} on the effective clutch off-rate $k_{off,i}$ to increase the simulation efficiency (46). See *SI Appendix*, *Extended Methods* and *SI Appendix*, Table S1 for more information on the model and its parameters.

Individual cells were simulated for 60 min (in-simulation) to allow the system to reach a dynamic steady state, after which the simulation was continued for 4 h and the results were recorded. The average surface areas covered by each cell and the average numbers of engaged clutches during the course of the simulation were calculated and reported.

The CMS was run using MATLAB R2021a with the following toolboxes: Optimization, Mapping, Image Processing, Curve Fitting, and Parallel Computing. Simulation results were visualized using a custom MATLAB script, based on the definition of cell mask in the original CMS.

Data, Materials, and Software Availability. All study data are included in the article and supporting information. The CMS code is available online on the Odde lab website (https://oddelab.umn.edu/) (44), while the custom MATLAB script for visualizing CMS output is available via GitHub (https://github.com/Ivaska-Lab-UTU/CellMigrationSimulator) (72).

ACKNOWLEDGMENTS. We thank P. Laasola and J. Siivonen for technical assistance and the Ivaska lab for scientific discussion and feedback on the manuscript. For critical reading and editing, we thank Dr. Hellyeh Hamidi. For services, instrumentation, and expertise at Turku Bioscience (University of Turku, Turku, Finland), we would like to thank the Cell Imaging and Cytometry Core and the Genome Editing core, which are supported by Biocenter Finland. The clone pENTR221-ARHGEF2 was from the ORFeome library at the Genome Biology Unit core facility, supported by HiLIFE and the Faculty of Medicine, University of Helsinki, and Biocenter Finland. This work was supported by the Finnish Cancer Institute (K. Albin Johansson Professorship to J.I.); a Research Council of Finland research project (grant no. 325464 to J.I.) and Centre of Excellence program (grant no. 346131 to J.I.); the Cancer Foundation Finland (to J.I.); the Sigrid Juselius Foundation (to J.I.); and the Research Council of Finland InFLAMES Flagship program (grant no. 337530 and 357910). J.R.W.C. was supported by the European Union's Horizon 2020 research and innovation program under the Marie Sklodowska-Curie grant agreement (841973) and a Research Council of

Finland postdoctoral research grant (338585). G.F. was supported by a Research Council of Finland postdoctoral research grant (332402). A.I. was supported by the Finnish Cultural Foundation (00210428), the Orion Research Foundation, and the K. Albin Johansson's Foundation. N.P. was supported by the "PhD in Oncology" program of the Philantropia Foundation.

Author affiliations: [a]Turku Bioscience Centre, University of Turku and Åbo Akademi University, Turku FI-20520, Finland; [b]Misvik Biology Oy, Turku FI-20520, Finland; [c]Department of Oncology and Metabolism, University of Sheffield, Sheffield S10 2TN, United Kingdom; [d]Department of Life Technologies, University of Turku, Turku FI-20520, Finland; [e]InFLAMES Research Flagship, University of Turku, Turku FI-20520, Finland; [f]Western Finnish Cancer Center, University of Turku, Turku FI-20520, Finland; and [g]Foundation for the Finnish Cancer Institute, Helsinki FI-00014, Finland

1. H. Hamidi, J. Ivaska, Every step of the way: Integrins in cancer progression and metastasis. *Nat. Rev. Cancer* **18**, 533–548 (2018), 10.1038/s41568-018-0038-z.
2. J. R. W. Conway, G. Jacquemet, Cell matrix adhesion in cell migration. *Essays Biochem.* **63**, 535–551 (2019).
3. S. McFarlane, C. McFarlane, N. Montgomery, A. Hill, D. J. Waugh, CD44-mediated activation of alpha5beta1-integrin, cortactin and paxillin signaling underpins adhesion of basal-like breast cancer cells to endothelium and fibronectin-enriched matrices. *Oncotarget* **6**, 36762–36773 (2015).
4. R. Kaukonen *et al.*, Normal stroma suppresses cancer cell proliferation via mechanosensitive regulation of JMJD1a-mediated transcription. *Nat. Commun.* **7**, 12237 (2016).
5. V. Izzi *et al.*, Pan-cancer analysis of the expression and regulation of matrisome genes across 32 tumor types. *Matrix Biol. Plus* **1**, 100004 (2019).
6. J. R. Mao, J. Bristow, The Ehlers-Danlos syndrome: On beyond collagens. *J. Clin. Invest.* **107**, 1063–1069 (2001).
7. J. F. Bateman, R. P. Boot-Handford, S. R. Lamande, Genetic diseases of connective tissues: Cellular and extracellular effects of ECM mutations. *Nat. Rev. Genet.* **10**, 173–183 (2009).
8. A. L. Wishart *et al.*, Decellularized extracellular matrix scaffolds identify full-length collagen VI as a driver of breast cancer cell invasion in obesity and metastasis. *Sci. Adv.* **6**, eabc3175 (2020).
9. A. Ishihara, T. Yoshida, H. Tamaki, T. Sakakura, Tenascin expression in cancer cells and stroma of human breast cancer and its prognostic significance. *Clin. Cancer Res.* **1**, 1035–1041 (1995).
10. B. Fernandez-Garcia *et al.*, Expression and prognostic significance of fibronectin and matrix metalloproteases in breast cancer metastasis. *Histopathology* **64**, 512–522 (2014).
11. C. J. Flaim, S. Chien, S. N. Bhatia, An extracellular matrix microarray for probing cellular differentiation. *Nat. Methods* **2**, 119–125 (2005).
12. M. Ahmed *et al.*, Combinatorial ECM arrays identify cooperative roles for matricellular proteins in enhancing the generation of TH+ neurons from human pluripotent cells. *Front. Cell Dev. Biol.* **9**, 755406 (2021).
13. A. Brougham-Cook *et al.*, High throughput interrogation of human liver stellate cells reveals microenvironmental regulation of phenotype. *Acta Biomater.* **138**, 240–253 (2022).
14. N. E. Reticker-Flynn *et al.*, A combinatorial extracellular matrix platform identifies cell-extracellular matrix interactions that correlate with metastasis. *Nat. Commun.* **3**, 1122 (2012).
15. T. Pellinen *et al.*, A functional genetic screen reveals new regulators of beta1-integrin activity. *J. Cell Sci.* **125**, 649–661 (2012).
16. C. F. Guimarães, L. Gasperini, A. P. Marques, R. L. Reis, The stiffness of living tissues and its implications for tissue engineering. *Nat. Rev. Mater.* **5**, 351–370 (2020).
17. I. Acerbi *et al.*, Human breast cancer invasion and aggression correlates with ECM stiffening and immune cell infiltration. *Integr. Biol. (Camb)* **7**, 1120–1134 (2015).
18. B. Piersma, M. K. Hayward, V. M. Weaver, Fibrosis and cancer: A strained relationship. *Biochim. Biophys. Acta Rev. Cancer* **1873**, 188356 (2020).
19. A. E. Mayorca-Guiliani *et al.*, ISDoT: In situ decellularization of tissues for high-resolution imaging and proteomic analysis of native extracellular matrix. *Nat. Med.* **23**, 890–898 (2017).
20. S. J. Heo *et al.*, Aberrant chromatin reorganization in cells from diseased fibrous connective tissue in response to altered chemomechanical cues. *Nat. Biomed. Eng.* **7**, 177–191 (2022), 10.1038/s41551-022-00910-5.
21. M. Papanicolaou *et al.*, Temporal profiling of the breast tumour microenvironment reveals collagen XII as a driver of metastasis. *Nat. Commun.* **13**, 4587 (2022).
22. T. Kudo *et al.*, Live-cell measurements of kinase activity in single cells using translocation reporters. *Nat. Protocols* **13**, 155 (2017).
23. K. L. Yee, V. M. Weaver, D. A. Hammer, Integrin-mediated signalling through the MAP-kinase pathway. *IET Syst. Biol.* **2**, 8–15 (2008).
24. A. E. Aplin, S. A. Stewart, R. K. Assoian, R. L. Juliano, Integrin-mediated adhesion regulates ERK nuclear translocation and phosphorylation of Elk-1. *J. Cell Biol.* **153**, 273–282 (2001).
25. M. Aragona *et al.*, A mechanical checkpoint controls multicellular growth through YAP/TAZ regulation by actin-processing factors. *Cell* **154**, 1047–1059 (2013).
26. T. Panciera, L. Azzolin, M. Cordenonsi, S. Piccolo, Mechanobiology of YAP and TAZ in physiology and disease. *Nat. Rev. Mol. Cell Biol.* **18**, 758–770 (2017).
27. S. Dupont *et al.*, Role of YAP/TAZ in mechanotransduction. *Nature* **474**, 179–183 (2011).
28. C. G. Galbraith, K. M. Yamada, M. P. Sheetz, The relationship between force and focal complex development. *J. Cell Biol.* **159**, 695–705 (2002).
29. A. Elosegui-Artola *et al.*, Force triggers YAP nuclear entry by regulating transport across nuclear pores. *Cell* **171**, 1397–1410.e14 (2017).
30. A. Elosegui-Artola *et al.*, Rigidity sensing and adaptation through regulation of integrin types. *Nat. Mater.* **13**, 631–637 (2014).
31. C. D. Lawson, K. Burridge, The on-off relationship of Rho and Rac during integrin-mediated adhesion and cell migration. *Small GTPases* **5**, e27958 (2014).
32. R. G. Hodge, A. J. Ridley, Regulating Rho GTPases and their regulators. *Nat. Rev. Mol. Cell Biol.* **17**, 496–510 (2016).
33. J. Hu, X. Gong, S. Stromblad, Local temporal Rac1-GTP nadirs and peaks restrict cell protrusions and retractions. *Sci. Adv.* **8**, eabl3667 (2022).
34. H. Warner, B. J. Wilson, P. T. Caswell, Control of adhesion and protrusion in cell migration by Rho GTPases. *Curr. Opin. Cell Biol.* **56**, 64–70 (2019).
35. M. Machacek *et al.*, Coordination of Rho GTPase activities during cell protrusion. *Nature* **461**, 99–103 (2009).
36. S. Seetharaman *et al.*, Microtubules tune mechanosensitive cell responses. *Nat. Mater.* **21**, 366–377 (2022).
37. R. D. Fritz *et al.*, A versatile toolkit to produce sensitive FRET biosensors to visualize signaling in time and space. *Sci. Signal.* **6**, rs12 (2013).
38. A. Tao *et al.*, Identifying constitutive and context-specific molecular-tension-sensitive protein recruitment within focal adhesions. *Dev. Cell* **58**, 522–534.e7 (2023).
39. K. Legerstee, B. Geverts, J. A. Slotman, A. B. Houtsmuller, Dynamics and distribution of paxillin, vinculin, zyxin and VASP depend on focal adhesion location and orientation. *Sci. Rep.* **9**, 10460 (2019).
40. J. C. Friedland, M. H. Lee, D. Boettiger, Mechanically activated integrin switch controls alpha5beta1 function. *Science* **323**, 642–644 (2009).
41. P. Atherton *et al.*, Vinculin controls talin engagement with the actomyosin machinery. *Nat. Commun.* **6**, 10038 (2015).
42. J. S. Cheah *et al.*, Spatial proximity of proteins surrounding zyxin under force-bearing conditions. *Mol. Biol. Cell* **32**, 1221–1228 (2021).
43. M. S. Schmitt *et al.*, Zyxin is all you need: Machine learning adherent cell mechanics. ArXiv [Preprint] (2023). https://doi.org/10.48550/arXiv.2303.00176 (Accessed 1 March 2023).
44. B. L. Bangasser *et al.*, Shifting the optimal stiffness for cell migration. *Nat. Commun.* **8**, 15313 (2017).
45. C. E. Chan, D. J. Odde, Traction dynamics of filopodia on compliant substrates. *Science* **322**, 1687–1691 (2008).
46. A. Isomursu *et al.*, Directed cell migration towards softer environments. *Nat. Mater.* **21**, 1081–1090 (2022), 10.1038/s41563-022-01294-2.
47. B. L. Bangasser, S. S. Rosenfeld, D. J. Odde, Determinants of maximal force transmission in a motor-clutch model of cell traction in a compliant microenvironment. *Biophys. J.* **105**, 581–592 (2013).
48. A. Elosegui-Artola *et al.*, Mechanical regulation of a molecular clutch defines force transmission and transduction in response to matrix rigidity. *Nat. Cell Biol.* **18**, 540–548 (2016).
49. Y. Su *et al.*, Relating conformation to function in integrin alpha5beta1. *Proc. Natl. Acad. Sci. U.S.A.* **113**, E3872–E3881 (2016).
50. A. Byron *et al.*, Anti-integrin monoclonal antibodies. *J. Cell Sci.* **122**, 4009–4011 (2009).
51. H. B. Schiller *et al.*, beta1- and alphav-class integrins cooperate to regulate myosin II during rigidity sensing of fibronectin-based microenvironments. *Nat. Cell Biol.* **15**, 625–636 (2013).
52. J. Li, J. Yan, T. A. Springer, Low-affinity integrin states have faster ligand-binding kinetics than the high-affinity state. *Elife* **10**, e73359 (2021).
53. M. Tulla *et al.*, Selective binding of collagen subtypes by integrin alpha 1I, alpha 2I, and alpha 10I domains. *J. Biol. Chem.* **276**, 48206–48212 (2001).
54. C. F. Tiger, F. Fougerousse, G. Grundstrom, T. Velling, D. Gullberg, Alpha11beta1 integrin is a receptor for interstitial collagens involved in cell migration and collagen reorganization on mesenchymal nonmuscle cells. *Dev. Biol.* **237**, 116–129 (2001).
55. M. Lerche *et al.*, Integrin binding dynamics modulate ligand-specific mechanosensing in mammary gland fibroblasts. *iScience* **23**, 100907 (2020).
56. M. Yamada, K. Sekiguchi, Molecular basis of laminin-integrin interactions. *Curr. Top Membr.* **76**, 197–229 (2015).
57. J. R. W. Conway, N. O. Carragher, P. Timpson, Developments in preclinical cancer imaging: Innovating the discovery of therapeutics. *Nat. Rev. Cancer* **14**, 314–328 (2014).
58. R. Straussman *et al.*, Tumour micro-environment elicits innate resistance to RAF inhibitors through HGF secretion. *Nature* **487**, 500–504 (2012).
59. K. R. Levental *et al.*, Matrix crosslinking forces tumor progression by enhancing integrin signaling. *Cell* **139**, 891–906 (2009).
60. K. J. Murphy *et al.*, Intravital imaging technology guides FAK-mediated priming in pancreatic cancer precision medicine according to Merlin status. *Sci. Adv.* **7**, eabh0363 (2021).
61. A. P. Drain *et al.*, Matrix compliance permits NF-kappaB activation to drive therapy resistance in breast cancer. *J. Exp. Med.* **218**, e20191360 (2021).
62. G. Bianchini *et al.*, Molecular anatomy of breast cancer stroma and its prognostic value in estrogen receptor-positive and -negative cancers. *J. Clin. Oncol.* **28**, 4316–4323 (2010).
63. H. Y. Chang *et al.*, Robustness, scalability, and integration of a wound-response gene expression signature in predicting breast cancer survival. *Proc. Natl. Acad. Sci. U.S.A.* **102**, 3738–3743 (2005).
64. A. Planche *et al.*, Identification of prognostic molecular features in the reactive stroma of human breast and prostate cancer. *PLoS One* **6**, e18640 (2011).
65. G. Finak *et al.*, Stromal gene expression predicts clinical outcome in breast cancer. *Nat. Med.* **14**, 518–527 (2008).
66. J. J. Lee *et al.*, Stromal response to Hedgehog signaling restrains pancreatic cancer progression. *Proc. Natl. Acad. Sci. U.S.A.* **111**, E3091–E3100 (2014).
67. N. Barber-Perez *et al.*, Mechano-responsiveness of fibrillar adhesions on stiffness-gradient gels. *J. Cell Sci.* **133**, jcs242909 (2020).
68. G. Chen *et al.*, Chemically defined conditions for human iPSC derivation and culture. *Nat. Methods* **8**, 424–429 (2011).
69. R. D. Fritz *et al.*, SrGAP2-dependent integration of membrane geometry and slit-robo-repulsive cues regulates fibroblast contact inhibition of locomotion. *Dev. Cell* **35**, 78–92 (2015).
70. D. S. Bindels *et al.*, mScarlet: A bright monomeric red fluorescent protein for cellular imaging. *Nat. Methods* **14**, 53–56 (2017).
71. D. T. Gillespie, Exact stochastic simulation of coupled chemical reactions. *J. Phys. Chem.* **81**, 2340–2361 (1977).
72. J. R. W. Conway *et al.*, Ivaska-Lab-UTU/CellMigrationSimulator. GitHub. https://github.com/Ivaska-Lab-UTU/CellMigrationSimulator. Deposited 9 February 2023.

PNAS

Supporting Information for

Defined extracellular matrix compositions support stiffness-insensitive cell spreading and adhesion signaling

James R.W. Conway[a,1], Aleksi Isomursu[a], Gautier Follain[a], Ville Härmä[b,c], Eva Jou-Ollé[a], Nicolas Pasquier[a], Eetu P.O. Välimäki[b], Juha K. Rantala[b,c] and Johanna Ivaska[a,d,e,f,g,1]

[a]Turku Bioscience Centre, University of Turku and Åbo Akademi University, FI-20520 Turku, Finland
[b]Misvik Biology Oy, FI-20520 Turku, Finland
[c]Department of Oncology and Metabolism, University of Sheffield, Sheffield, United Kingdom
[d]Department of Life Technologies, University of Turku, FI-20520 Turku, Finland
[e]InFLAMES Research Flagship Center, University of Turku, Turku, Finland
[f]Western Finnish Cancer Center (FICAN West), University of Turku, FI-20520 Turku, Finland
[g]Foundation for the Finnish Cancer Institute, Tukholmankatu 8, FI-00014 Helsinki, Finland

[1]James R.W. Conway and Johanna Ivaska
Email: jdconw@utu.fi and joivaska@utu.fi

This PDF file includes:

Extended Methods
Figures S1 to S13
Table S1
Legends for Movies S1 to S2
SI References

Other supporting materials for this manuscript include the following:

Movies S1 to S2

Extended Methods

Detailed description of the computational model. In order to investigate cell spreading on soft substrates with different ligand densities, a MATLAB implementation of the Odde lab Cell Migration Simulator (1) was used. The model represents an individual cell on a 2D substrate, and comprises multiple motor-clutch modules that mimic cellular protrusions (Fig. 3*E*). Each module contains a set number of clutches (i.e., possible cell-matrix connections employing integrins and their related adaptor molecules) that restrict motor (i.e., myosin)-induced retrograde flow of actin by linking the cytoskeleton to the underlying substrate. Cell motion, including spreading and migration, is determined by a force balance between the modules and a central cell body. New modules are nucleated stochastically, module length increases over time due to actin polymerization that is simultaneously counteracted by the retrograde flow, and modules are removed when they become too short. Total actin and the number of clutches and motors are kept constant in accordance with the conservation of mass.

In each module, clutches bind elastic substrate springs with a constant rate of k_{on}. When they connect the actin cytoskeleton to the substrate, resulting in a direct mechanical link between the components, the clutches themselves are exposed to actomyosin-mediated forces. The unbinding rate of a connected clutch i, $k_{off,i}$, varies with force F_i according to the Bell model (2):

$$k_{off,i} = k_{off}^{*}\, exp(F_i/F_b) \qquad \text{(eq. S1)}$$

where k_{off}^{*} is the unloaded clutch unbinding rate, F_b is the characteristic clutch rupture force, and F_i is the force on the i^{th}clutch. The clutches are modeled as Hookean springs, and consequently the force on any individual clutch is given by

$$F_i = k_c x_i \qquad \text{(eq. S2)}$$

where x_i is the elongation of the spring representing the i^{th} connected clutch, and k_c is the clutch spring constant. Myosin motors in each module j drive actin retrograde flow at an effective rate

$$v_{m,j} = v_m^{*}\left(1 - \frac{F_j}{n_{m,j}F_m}\right) \qquad \text{(eq. S3)}$$

where v_m^{*} is the unloaded flow rate, $n_{m,j}$ is the number of motors in the module, F_m is the stall force of an individual myosin motor, and F_j is the total traction force exerted on the module. F_j can be defined as

$$F_j = \sum_{i=1}^{n_{c,on}} F_i \qquad \text{(eq. S4)}$$

where $n_{c,on}$ is the total number of connected clutches in the module, and F_i is the force on the i^{th} connected clutch. The central node has additional clutches to capture the drag caused by the cell body, and the forces associated with these are resolved similar to the individual modules (eq. S4). Finally, the sum of all forces acting on the cell must be zero:

$$F_{cell} + \sum_{j=1}^{n_{mod}} F_j = 0 \qquad \text{(eq. S5)}$$

New actin monomers are added to the barbed (+) ends of actin filaments in the modules at a polymerization rate v_p, constrained by the total actin pool A_{tot} in the cell:

$$v_p = v_p^*\left(A_{free}/A_{tot}\right) \qquad \text{(eq. S6)}$$

where A_{free} is the amount of free G-actin and v_p^* is the maximum polymerization rate. Net module elongation/retraction results from this polymerization and the actin retrograde flow (v_m). Filaments can also be capped and polymerization arrested at a capping rate k_{cap}, whereas actin is depolymerized back into monomers and added to the total G-actin pool when it passes the position of the myosin motors. Finally, actin filaments, and the corresponding modules, are removed from the simulation when their length falls below l_{min}. New motor-clutch modules are created at a nucleation rate

$$k_{mod} = k_{mod}^*\left(A_{free}/A_{tot}\right)^4 \qquad \text{(eq. S7)}$$

where k_{mod}^* is the maximum module nucleation rate. Upon nucleation, the new modules are assigned motors and clutches, each from their respective pools, according to

$$n_m = n_m^*\left(N_{m,free}/N_m\right) \qquad \text{(eq. S8)}$$

$$n_c = n_c^*\left(N_{c,free}/N_c\right) \qquad \text{(eq. S9)}$$

where $n_{m/c}^*$ is the maximum number of motors/clutches per module, $N_{m/c,free}$ is the total amount of free motors/clutches, and $N_{m/c}$ is the total pool of motors/clutches available to the cell. The direction of the new module is assigned randomly.

The model is implemented using a direct Gillespie Stochastic Simulation Algorithm (3). For each iteration of the simulation, two random numbers are generated. Together with the various event rates, including k_{on}, $k_{off,i}$, k_{mod}, and k_{cap}, these random numbers are used to determine 1) the time increment to the next event and 2) the event that occurred. Here, we added an additional maximum cap (100 s^{-1}) on $k_{off,i}$ to increase simulation efficiency, as described in (4).

Figures S1 to S13

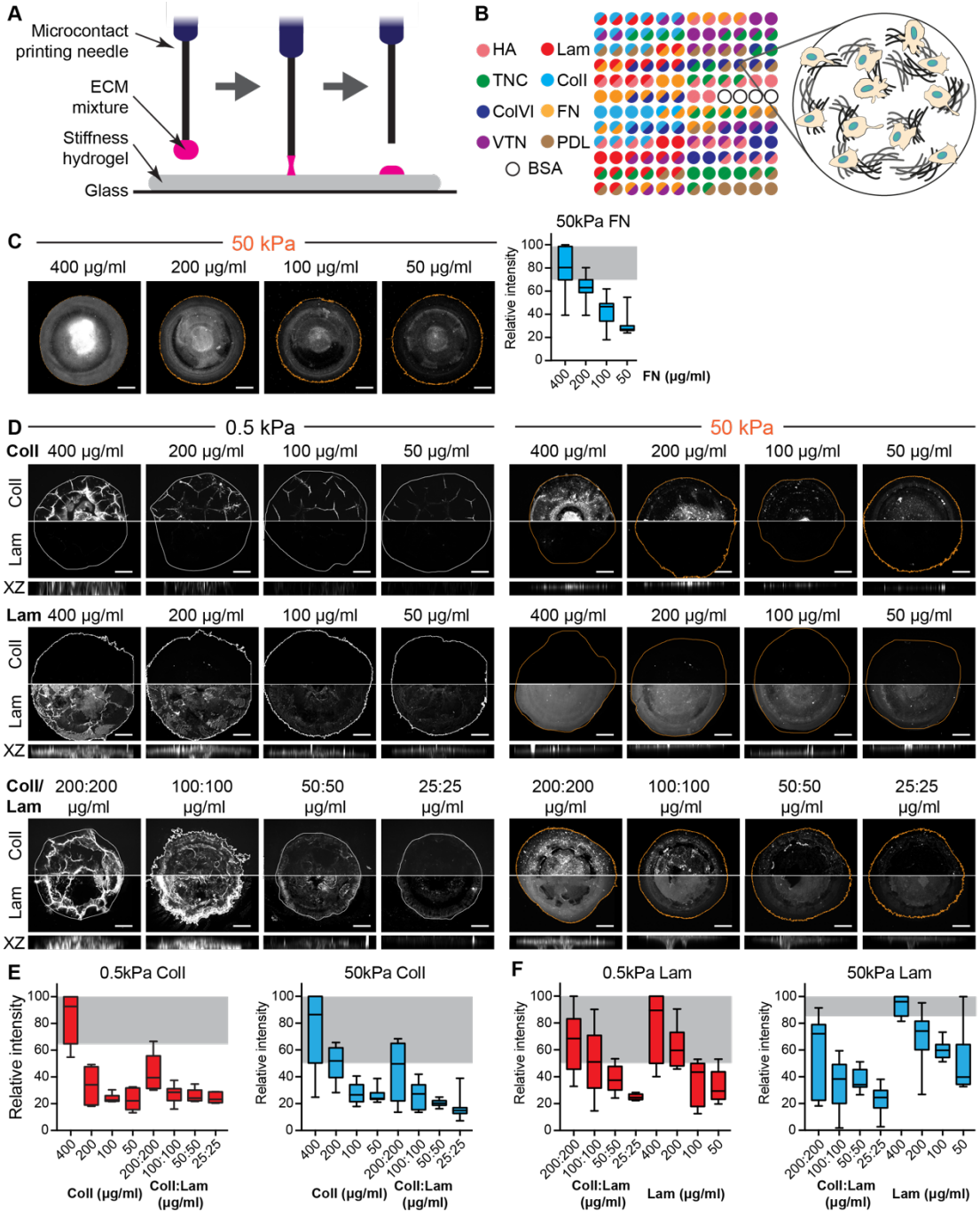

Fig. S1. Microcontact printing quality control spots for ColI/Lam. (*A*) Schematic of the microcontact printing technique applied to print the ECM mixtures as spots on hydrogels of different stiffness. (*B*) Schematic of the ECM spot array following microcontact printing on the different polyacrylamide hydrogels. (C) Representative images (left) and quantification (right) from initial FN test spots on 50 kPa stiffness gels (n=4 biological replicates; 4 spots/mixture/replicate; equal protein concentrations printed by making each mixture up to 400 µg/ml total protein with BSA; scale bars, 50 µm). (*D* to *F*) Representative images (D; whole spots imaged with half presented from each channel) and quantification of Collagen-I-647 (ColI-647) signal (E) or Lam staining (F) after spotting stiffness gels (0.5 and 50 kPa) with different dilutions of ColI-647, Lam or ColI-647/Lam (n=4

biological replicates; 2 spots/mixture/replicate; equal protein concentrations printed by making each mixture up to 400 μg/ml total protein with BSA; scale bars, 50 μm; XZ maximum projections given below representative XY images).

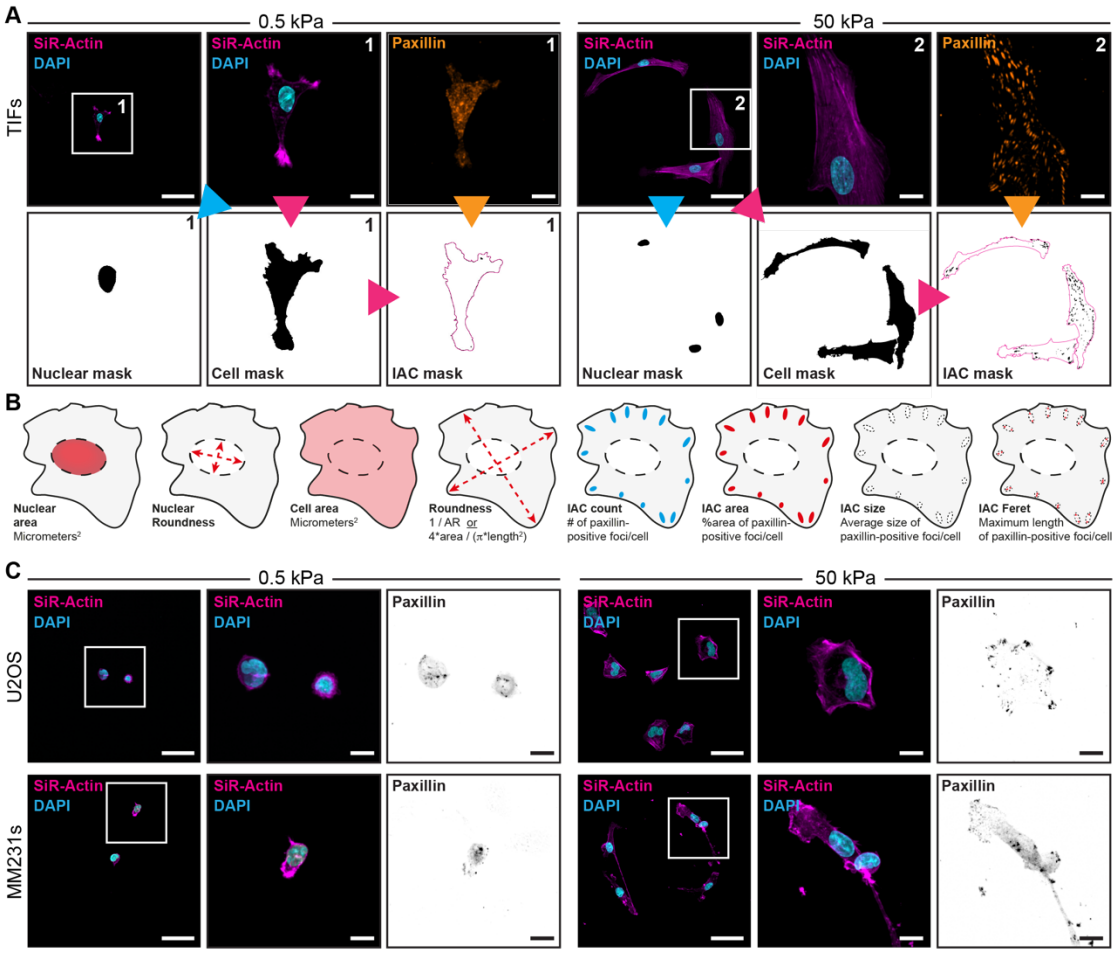

Fig. S2. Representative imaging metrics from the spot array analysis. (*A*) Representative images from TIF cells seeded on FN spots on 0.5 kPa (inset 1) or 50 kPa (inset 2) stiffness hydrogels, demonstrating the Fiji image analysis pipelines that provided the various cell metrics (n=3 biological replicates, 4 spots/replicate/ECM mixture/stiffness; scale bars, 50 μm (main), 10 μm (inset)). (*B*) Schematics of the different individual cell metrics assessed for each cell on the ECM spot arrays on 0.5 kPa or 50 kPa substrates. (*C*) Representative images from U2OS and MM231 cells seeded on FN spots on 0.5 kPa or 50 kPa stiffness hydrogels (n=3 biological replicates, 4 spots/replicate/ECM mixture/stiffness; scale bars, 50 μm (main), 10 μm (inset)).

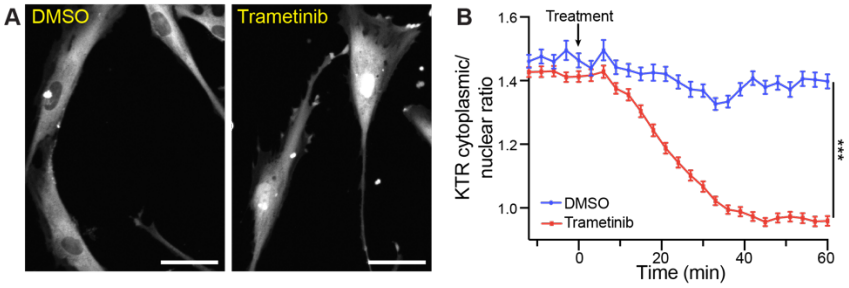

Fig. S3. Validation of ERK KTR functionality. (*A* and *B*) Representative images (A) and quantification (B) of TIFs stably expressing the ERK KTR after 60 minutes with DMSO or trametinib (1 μM; MEK inhibitor; scale bar, 50 μm; n=3 biological replicates, 33-65 cells/condition/replicate; p-value from an unpaired Student's t test with a Welch's correction; ***p<0.001).

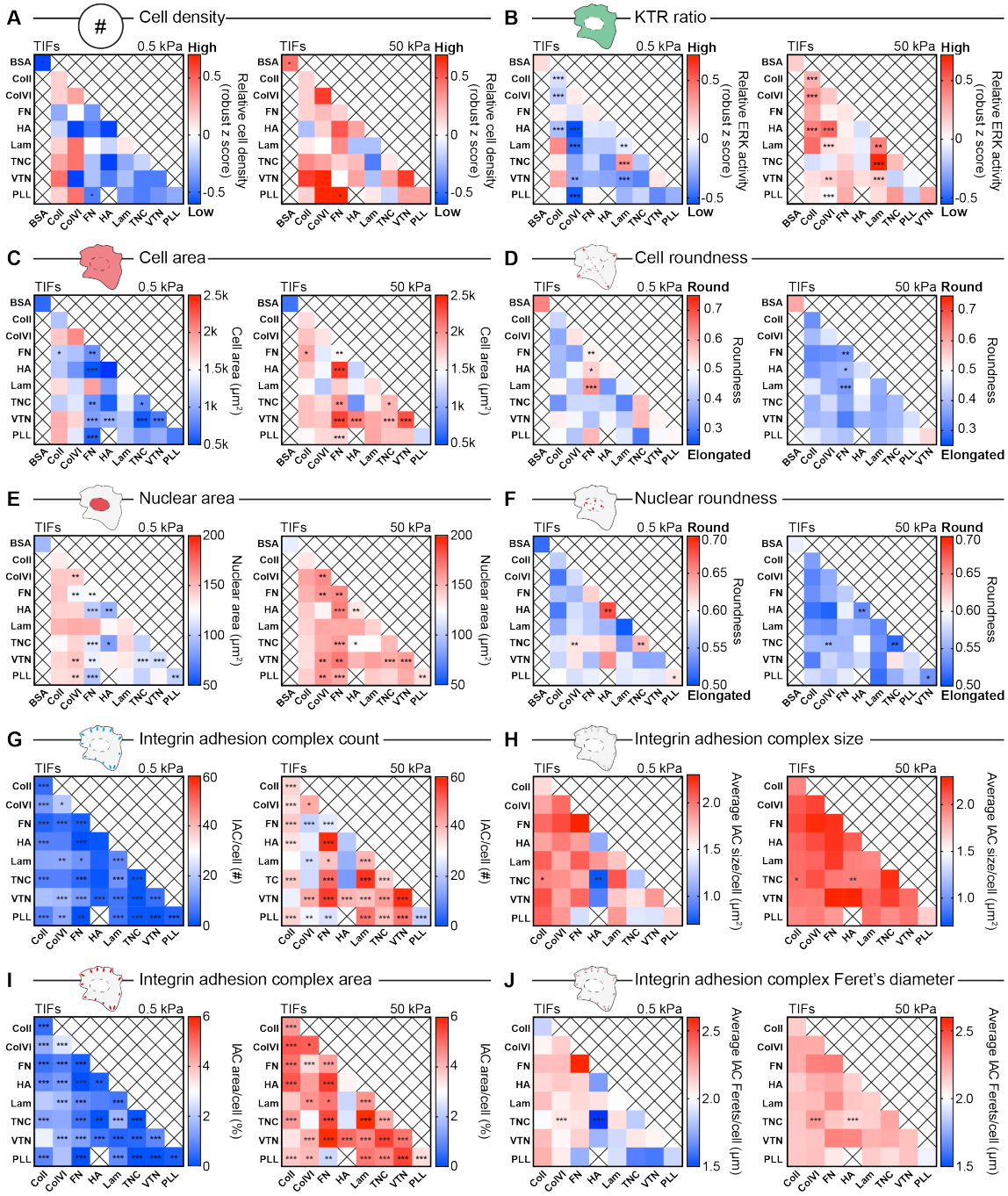

Fig. S4. TIF cells seeded on ECM arrays with different substrate stiffnesses. (*A* to *I*) Heatmaps representing the median for ten cellular parameters describe the response of TIFs to soft (0.5 kPa) and stiff (50 kPa) substrates on 36 different ECM mixtures (n=3 biological replicates, 4 spots/ECM mixture/substrate/replicate; p-values are from a one-way ANOVA with a Šidák correction for multiple comparisons, comparing the differences in individual parameters on each ECM mixture, on soft vs. stiff substrates; *p<0.05, **p<0.01, ***p<0.001. The absence of stars in a box indicates no significant difference, i.e. the cell parameters measured were statistically equivalent on that particular matrix mixture between soft and stiff substrates. The parameters described include relative cell density (A) and ERK activity (B) from Robust z-scores (calculated with the combined 0.5 and 50 kPa datasets for a given metric), cell area (C) and roundness (D), nuclear area (E) and roundness (F), as well as IAC count (G), size (H), area (I) and Feret's (J).

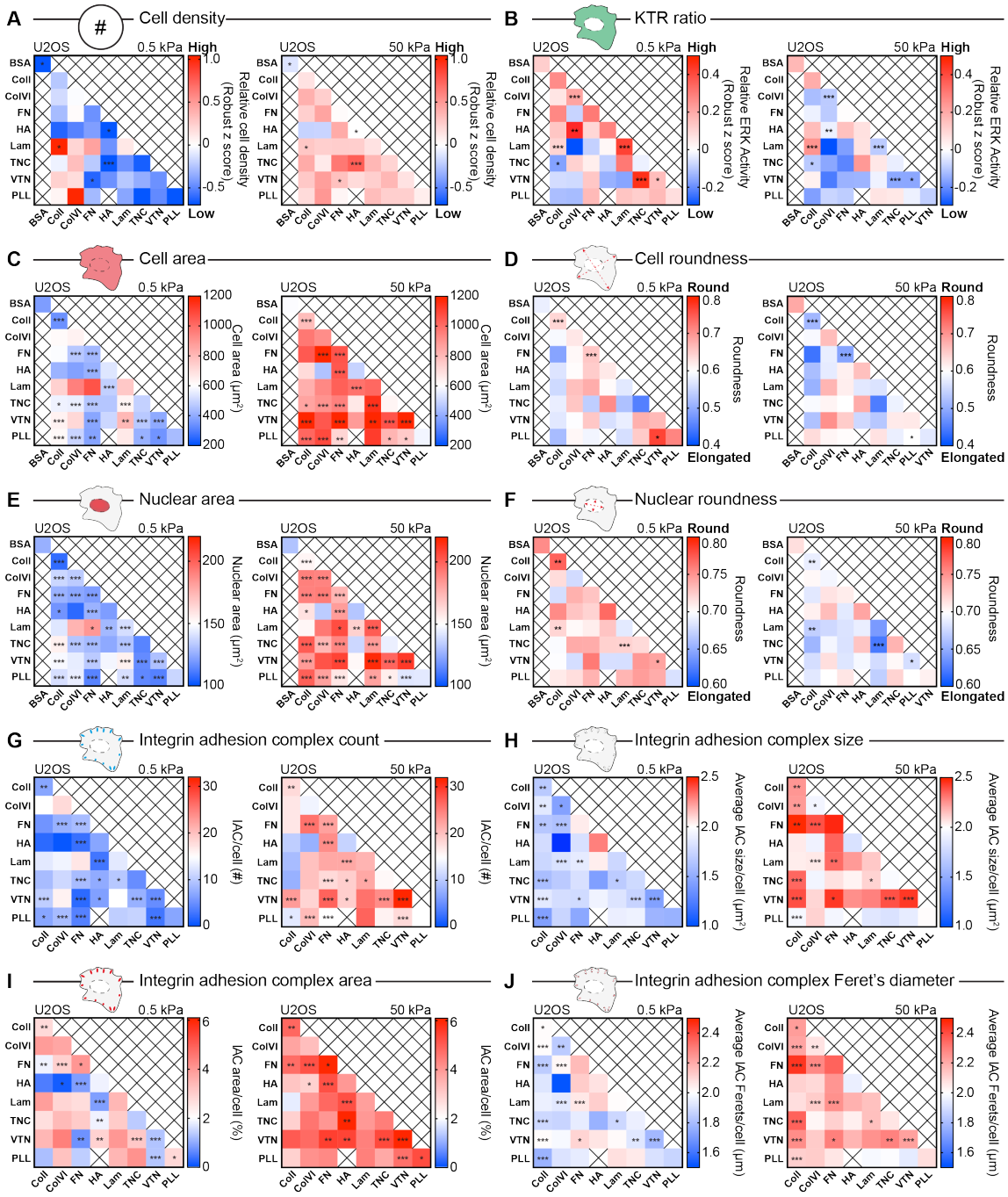

Fig. S5. U2OS cells seeded on ECM arrays with different substrate stiffnesses. (*A* to *I*) Heatmaps representing the median for ten cellular parameters describe the response of U2OS cells to soft (0.5 kPa) and stiff (50 kPa) substrates on 36 different ECM mixtures (n=3 biological replicates, 4 spots/ECM mixture/substrate/replicate; p-values are from a one-way ANOVA with a Šidák correction for multiple comparisons, comparing the differences in individual parameters on each ECM mixture, on soft vs. stiff substrates; *p<0.05, **p<0.01, ***p<0.001. The absence of stars in a box indicates no significant difference, i.e. the cell parameters measured were statistically equivalent on that particular matrix mixture between soft and stiff substrates. The parameters described include relative cell density (A) and ERK activity (B) from Robust z-scores (calculated with the combined 0.5 and 50 kPa datasets for a given metric), cell area (C) and roundness (D), nuclear area (E) and roundness (F), as well as IAC count (G), size (H), area (I) and Feret's (J).

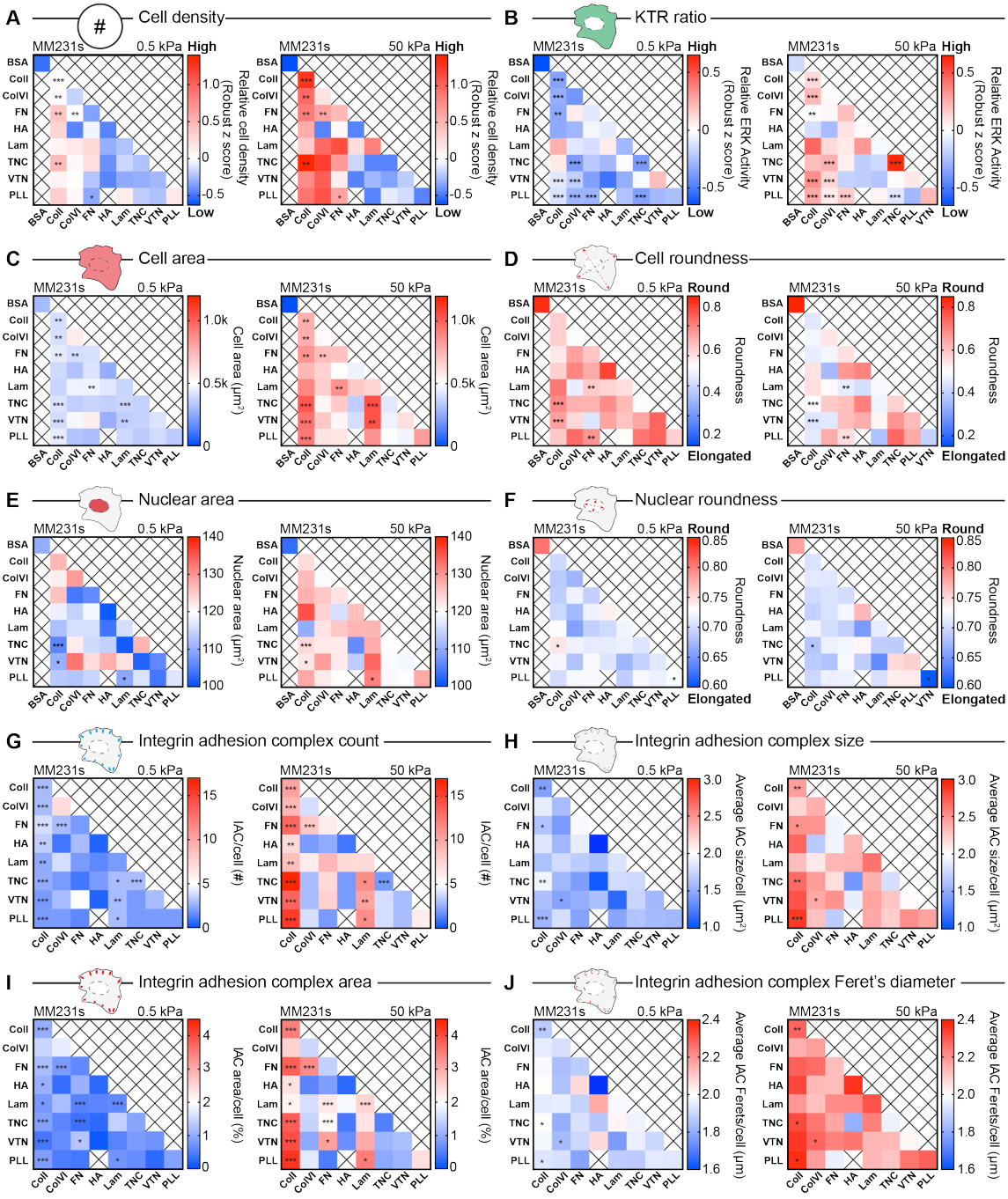

Fig. S6. MM231 cells seeded on ECM arrays with different substrate stiffnesses. (*A* to *I*) Heatmaps representing the median for ten cellular parameters describe the response of MM231 cells to soft (0.5 kPa) and stiff (50 kPa) substrates on 36 different ECM mixtures (n=3 biological replicates, 4 spots/ECM mixture/substrate/replicate; p-values are from a one-way ANOVA with a Šidák correction for multiple comparisons, comparing the differences in individual parameters on each ECM mixture, on soft vs. stiff substrates; *p<0.05, **p<0.01, ***p<0.001. The absence of stars in a box indicates no significant difference, i.e. the cell parameters measured were statistically equivalent on that particular matrix mixture between soft and stiff substrates. The parameters described include relative cell density (A) and ERK activity (B) from Robust z-scores (calculated with the combined 0.5 and 50 kPa datasets for a given metric), cell area (C) and roundness (D), nuclear area (E) and roundness (F), as well as IAC count (G), size (H), area (I) and Feret's (J).

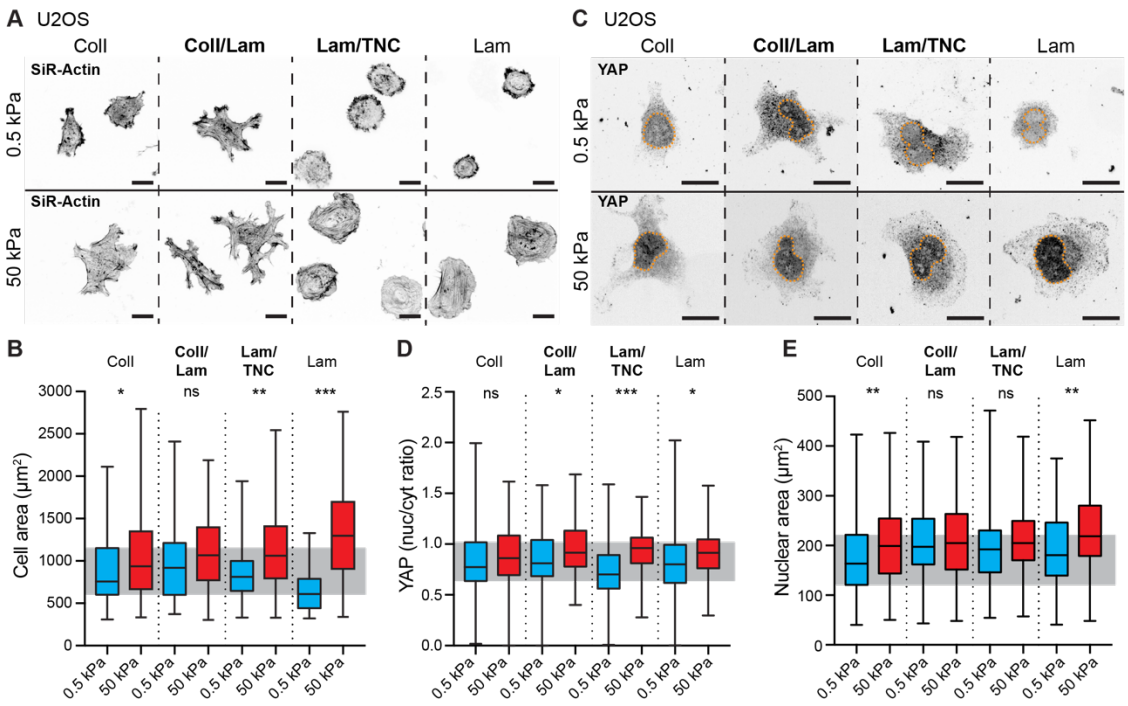

Fig. S7. Validation of supportive ECM mixtures on soft substrates. (*A* and *B*) Representative images (A) and quantification of cell area (B) after U2OS cells were seeded for 2 h on soft (0.5 kPa) and stiff (50 kPa) gels coated with different ECM mixtures, as indicated (n=3 biological replicates, 17-58 cells/condition/replicate; scale bars, 20 µm; p-values from a one-way ANOVA with a Šidák correction; *p<0.05, **p<0.01, ***p<0.001, ns – not significant). (*C* to *E*) Representative images (C) and quantification of (D) YAP nuclear/cytoplasmic staining and (E) nuclear area of U2OS cells seeded for 2 h on soft (0.5 kPa) and stiff (50 kPa) gels coated with different ECM mixtures, as indicated (n=3 biological replicates, 17-58 cells/condition/replicate; scale bars, 20 µm; p-values from a one-way ANOVA with a Šidák correction; *p<0.05, **p<0.01, ***p<0.001, ns – not significant). Grey bars are drawn to mark the interquartile range of the control Coll 0.5 kPa condition in boxplots. Nuclei are marked with orange dashed lines (C).

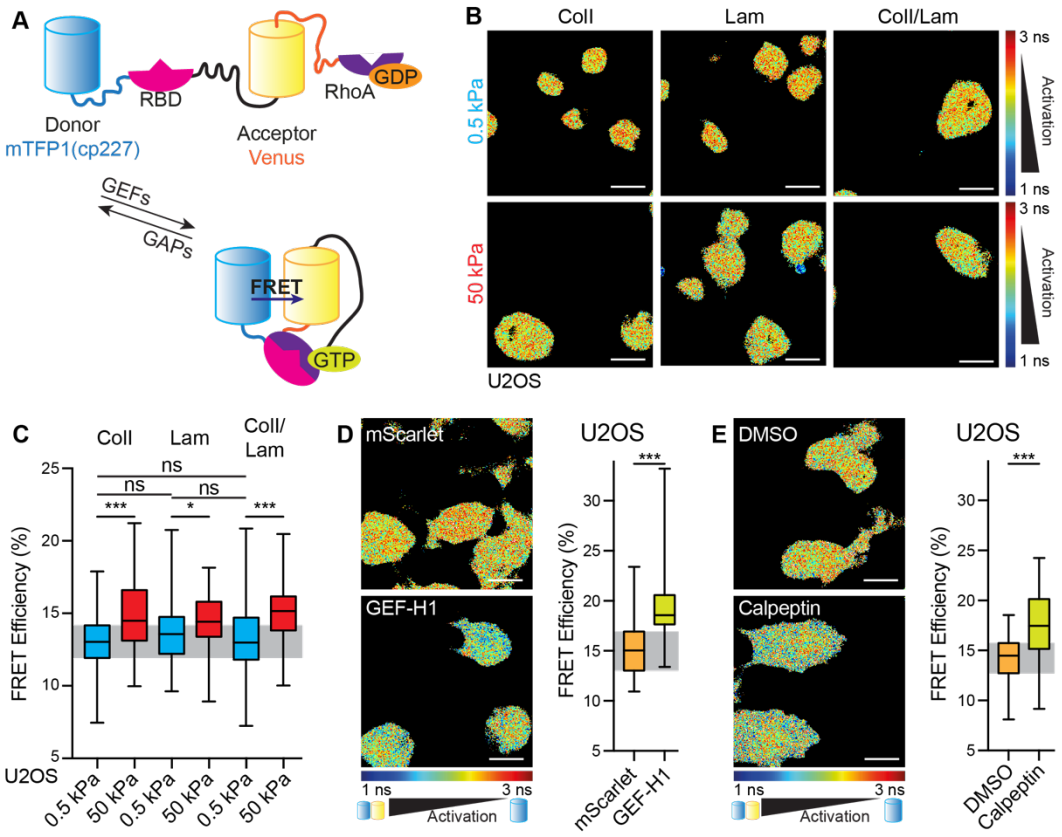

Fig. S8. RhoA activation state is not significantly different on specific spreading-supportive soft substrates. (*A*) Schematic of the RhoA-2G FRET reporter. (*B* and *C*) Representative images (B) and quantification of the phase lifetime (C) of U2OS cells stably expressing the RhoA-2G FRET reporter and seeded for 2 hours on soft (0.5 kPa) and stiff (50 kPa) gels coated with either ColI, Lam or ColI/Lam (n=4 biological replicates, 26-35 cells/condition/replicate; scale bars, 20 μm; p-values from a one-way ANOVA with a Tukey correction; *p<0.05, ***p<0.001). (D) Representative images (left) and quantification of the phase lifetime (right) of U2OS cells stably expressing the RhoA-2G FRET reporter, transfected with mScarlet alone or mCherry-GEF-H1 (n=4 biological replicates, 24-36 cells/condition/replicate; scale bars, 20 μm; p-value from an unpaired Student's t test with a Welch's correction; ***p<0.001). (*E*) Representative images (left) and quantification of the phase lifetime (right) of U2OS cells stably expressing the RhoA-2G FRET reporter, treated with Calpeptin (50 μM) or DMSO control for 30 minutes (n=4 biological replicates, 27-33 cells/condition/replicate; scale bars, 20 μm; p-value from an unpaired Student's t test with a Welch's correction; ***p<0.001). Grey bars are drawn to mark the interquartile ranges of the control conditions [i.e. (C) ColI 0.5kPa, (D) mScarlet or (E) DMSO] in boxplots.

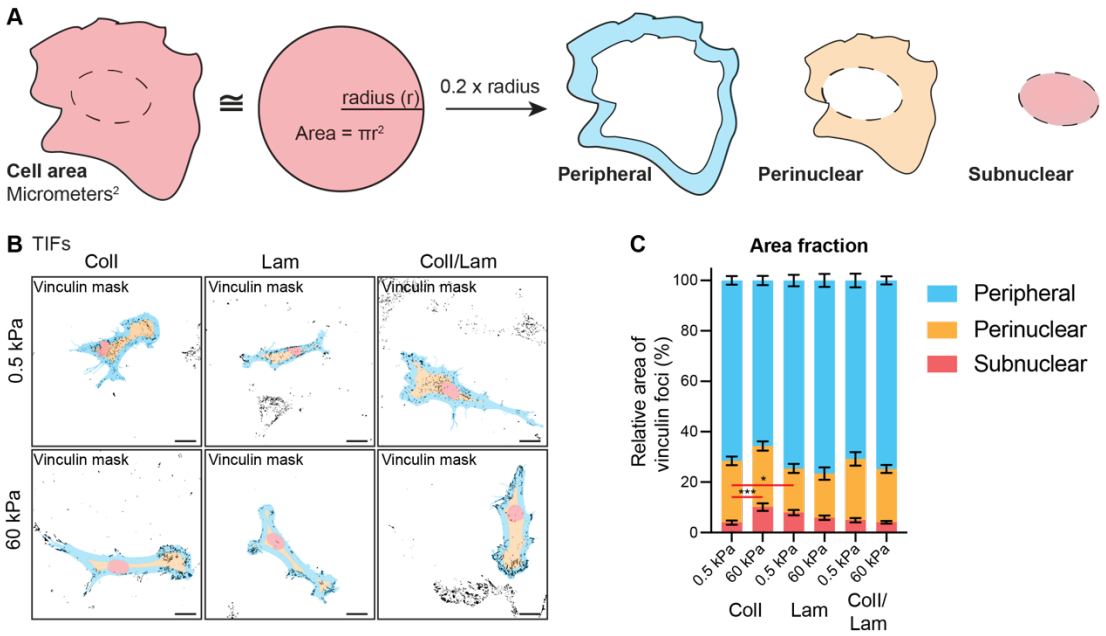

Fig. S9. The different ECM mixtures on soft versus stiff substrates show only subtle differences in IAC subcellular distribution. (*A*) Scheme of the analysis approach that equated cell area with the area of a circle to find the cell "radius", which was then used to scale the peripheral region adjacent to the cell membrane from the actin masked area. The subnuclear region was then taken from the DAPI masked area and the remaining actin masked area was then deemed perinuclear to indicate the cytoplasm adjacent to the nucleus. (*B*) Representative images of TIFs seeded for 2 hours on 0.5 and 60 kPa hydrogels coated with Lam, Coll and Coll/Lam, and stained with vinculin to mark IACs, masking these based on size cut-offs between 0.1 and 15 μm^2. The peripheral (blue), perinuclear (yellow) and subnuclear (red) regions from the actin and DAPI masks are then indicated for each cell as a colored overlay. Scale bars, 20 μm. (C) Quantification of the relative area of vinculin foci from the percentage area in each region, as fractions of the total area/cell (n=4 biological replicates, 8-27 cells/condition/replicate; p-values from a one-way ANOVA with a Tukey correction; *p<0.05, ***p<0.001).

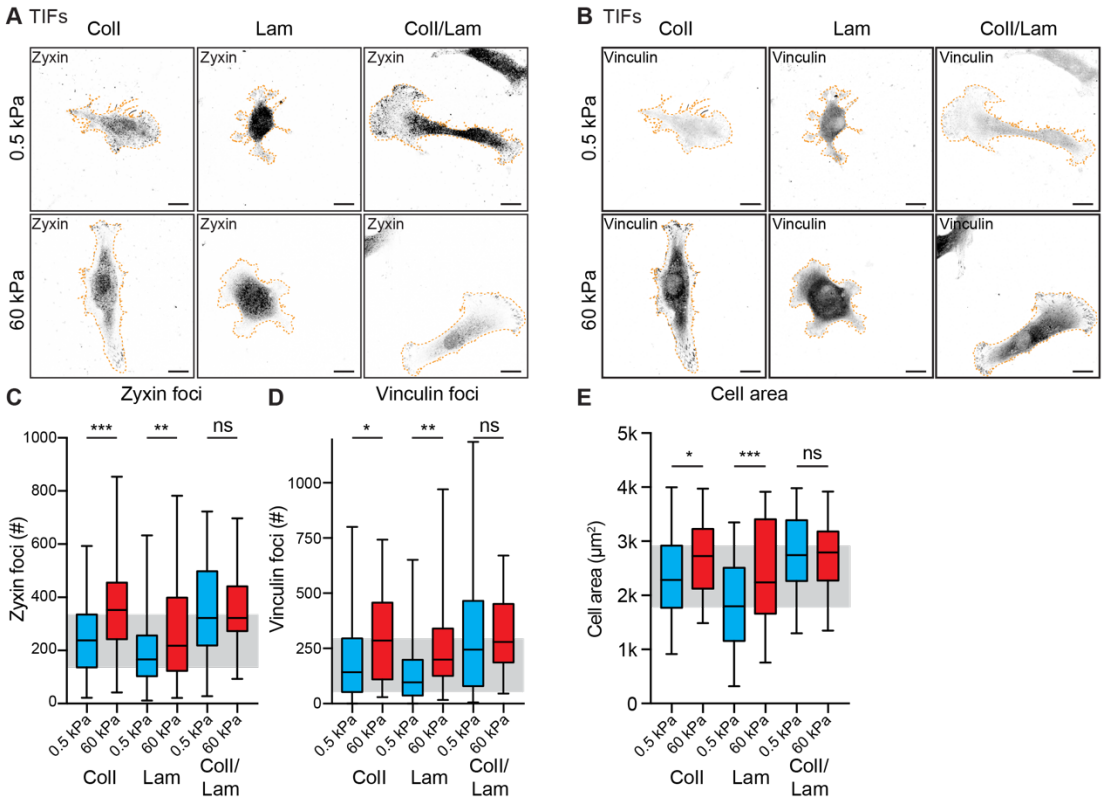

Fig. S10. Zyxin and vinculin staining of TIFs on different ECM mixtures and substrate stiffnesses. (*A* and *B*) Representative images of TIFs seeded for 2 hours on 0.5 and 60 kPa hydrogels coated with Lam, Coll and Coll/Lam, and stained for zyxin (A) or vinculin (B). Scale bars, 20 µm. (*C* and *D*) Quantification of zyxin (C) and vinculin (D) foci number (n=4 biological replicates, 8-27 cells/condition/replicate; p-values from a one-way ANOVA with a Šidák correction; *p<0.05, **p<0.01, ***p<0.001, ns – not significant). (*E*) Assessment of cell area for TIFs seeded on 0.5 and 60 kPa hydrogels coated with Lam, Coll and Coll/Lam for 2 hours (n=4 biological replicates, 8-27 cells/condition/replicate; p-values from a one-way ANOVA with a Tukey correction; *p<0.05, ***p<0.001, ns – not significant). Grey bars are drawn to mark the interquartile range of the control Coll 0.5 kPa condition in boxplots.

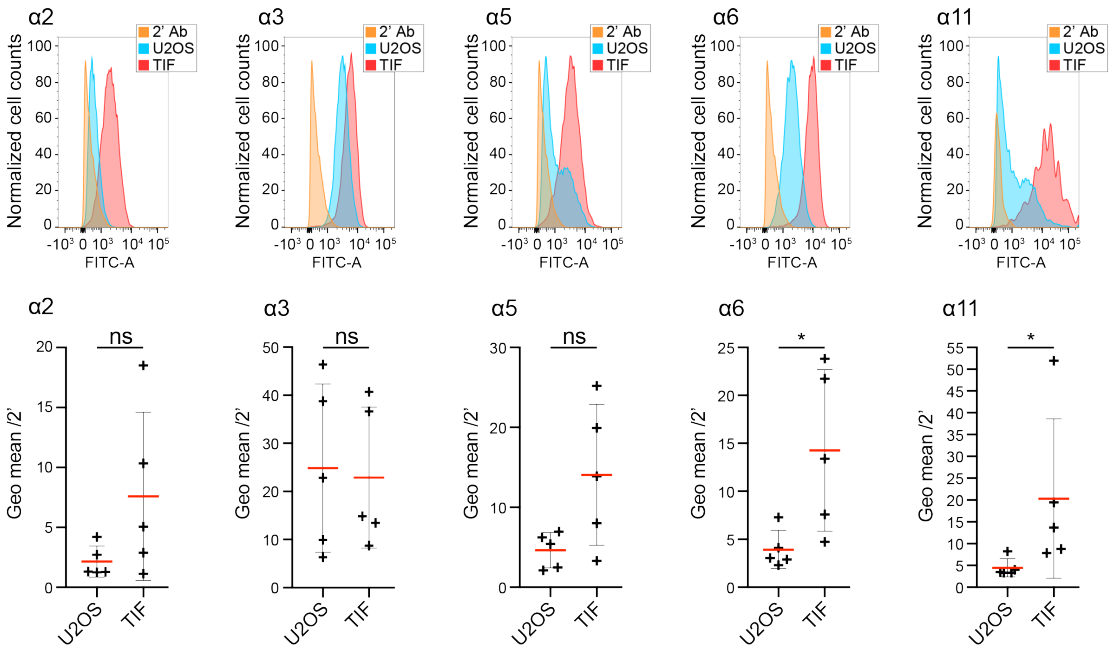

Fig. S11. Representative histograms and statistical analysis for the flow cytometry data presented in Fig. 3D (n=5 biological replicates; Mann-Whitney test; *p<0.05, ns – not significant). All channels in the histograms were scaled according to the mode, as a percentage of the maximum count.

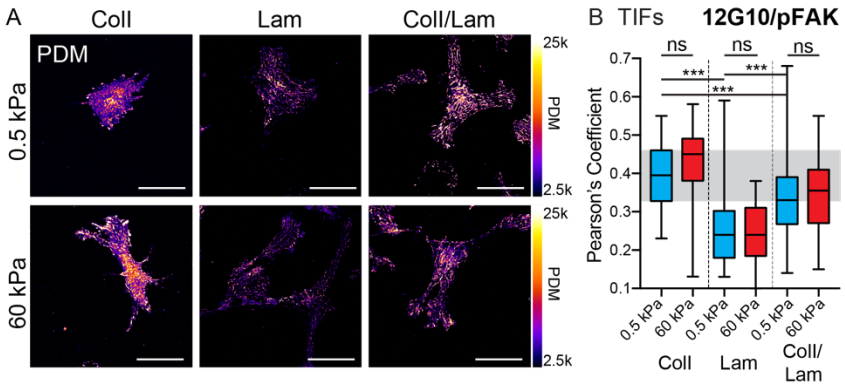

Fig. S12. Colocalization analysis of 12G10 and pFAK. (*A*) Representative images of the product of the difference of the mean (PDM) to highlight colocalization of the 12G10 and pFAK signals in the different ECM and stiffness conditions (scale bars, 50 µm; n=2 biological replicates). (*B*) Analysis of the colocalization using Pearson's correlation coefficients for each signal in individual cells (n=2 biological replicates, 10-28 cells/condition/replicate; one-way ANOVA with a Tukey correction for multiple comparisons; ***p<0.001, ns – not significant). Grey bars are drawn to mark the interquartile range of the control ColI 0.5 kPa condition in boxplots.

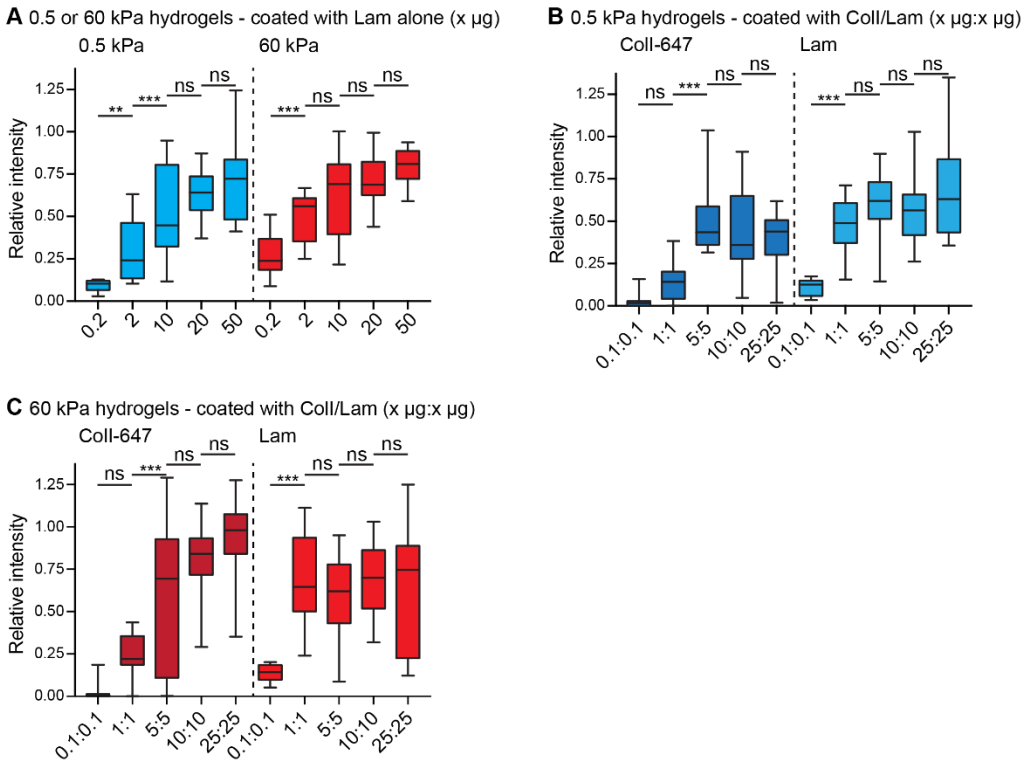

Fig. S13. Assessment of coating efficiency of Lam and Coll on 0.5 and 60 kPa polyacrylamide hydrogels. (*A*) Quantification of staining from Lam coating of 0.5 and 60 kPa hydrogels (n=3 biological replicates, 8 regions/condition/replicate; scale bars, 50 µm; p-values from a one-way ANOVA with a Tukey correction; **p<0.01, ***p<0.001, ns – not significant). (*B* and *C*) Quantification of staining from Coll/Lam coating of 0.5 kPa (B) and 60 kPa (C) hydrogels (n=3 biological replicates, 8 regions/condition/replicate; scale bars, 50 µm; p-values from a one-way ANOVA with a Tukey correction; ***p<0.001, ns – not significant).

Table S1. Whole-cell computational model parameters.

Parameter	Symbol	Value	Source
Total number of myosin motors	N_m	7,500–10,000	(1), adjusted
Total number of clutches	N_c	7,500–10,000	(1), adjusted
Maximum total actin length	A_{tot}	300,000 nm	Typical cell dimensions
Maximum actin polymerization rate	v_p^*	200 nm/s	(5)
Maximum module nucleation rate	k_{mod}^*	1 s^{-1}	(1)
Module capping rate	k_{cap}	0.001 s^{-1}	(1, 6)
Initial module length	l_{in}	5 µm	(1)
Minimum module length	l_{min}	0.1 µm	(1)
Cell spring constant	k_{cell}	10,000 pN/nm	(1) (>k_s)
Number of cell body clutches	$n_{c,cell}$	10	(1) (<N_c)
Substrate spring constant	k_s	0.5 pN/nm	Experimental conditions and (7)
Maximum number of module motors	n_m^*	N_m x 0.1	(1)
Myosin motor stall force	F_m	2 pN	(5, 8)
Unloaded actin flow rate	v_m^*	120 nm/s	(5)
Maximum number of module clutches	n_c^*	N_c x 0.1	(1)
Clutch on-rate	k_{on}	1 s^{-1}	(5)
Unloaded clutch off-rate	k_{off}^*	0.1 s^{-1}	(5, 9)
Clutch spring constant	k_c	8 pN/nm	(4); on the order of pN/nm (10)
Characteristic clutch rupture force	F_b	2 pN	(5, 11)

Movie S1 (separate file). Treatment of TIFs stably expressing the ERK KTR with DMSO or trametinib (1 μM) for 60 minutes (scale bar, 50 μm).

Movie S2 (separate file). Simulated cells from CMS modelling to compare the spreading dynamics upon variation of the total number of clutches (N_c either 7,500 or 10,000; scale bar, 50 μm).

SI References

1. B. L. Bangasser *et al.*, Shifting the optimal stiffness for cell migration. *Nat Commun* **8**, 15313 (2017).

2. G. I. Bell, Models for the specific adhesion of cells to cells. *Science* **200**, 618-627 (1978).

3. D. T. Gillespie, Exact stochastic simulation of coupled chemical reactions. *The Journal of Physical Chemistry* **81**, 2340-2361 (1977).

4. A. Isomursu *et al.*, Directed cell migration towards softer environments. *Nat Mater* 10.1038/s41563-022-01294-2 (2022).

5. C. E. Chan, D. J. Odde, Traction dynamics of filopodia on compliant substrates. *Science* **322**, 1687-1691 (2008).

6. D. A. Schafer, P. B. Jennings, J. A. Cooper, Dynamics of capping protein and actin assembly in vitro: uncapping barbed ends by polyphosphoinositides. *J Cell Biol* **135**, 169-179 (1996).

7. J. C. Hou *et al.*, Modeling distributed forces within cell adhesions of varying size on continuous substrates. *Cytoskeleton (Hoboken)* **76**, 571-585 (2019).

8. J. E. Molloy, J. E. Burns, J. Kendrick-Jones, R. T. Tregear, D. C. White, Movement and force produced by a single myosin head. *Nature* **378**, 209-212 (1995).

9. T. P. Lele, C. K. Thodeti, J. Pendse, D. E. Ingber, Investigating complexity of protein-protein interactions in focal adhesions. *Biochem Biophys Res Commun* **369**, 929-934 (2008).

10. T. E. Fisher, A. F. Oberhauser, M. Carrion-Vazquez, P. E. Marszalek, J. M. Fernandez, The study of protein mechanics with the atomic force microscope. *Trends Biochem Sci* **24**, 379-384 (1999).

11. G. Jiang, G. Giannone, D. R. Critchley, E. Fukumoto, M. P. Sheetz, Two-piconewton slip bond between fibronectin and the cytoskeleton depends on talin. *Nature* **424**, 334-337 (2003).

IV- Taskinen, M., **Pasquier N.***, Stubb A.*, Joshi S., Rasila P., Vahlman S., Sokka J., Trokovic R., Lönnberg T., Mikkola L. & Ivaska J., **Inhibition of integrin-β1 activity and contractility support naïve-like state in human induced pluripotent stem cells**, *manuscript submitted*

* equal contribution

Inhibition of integrin β1 activity support a naïve-like state in human inducedpluripotent stem cells

Taskinen M.E.[1], Pasquier N.[1,7*], Stubb A.[1*], Joshi S. [1], Rasila P.[1], Vahlman S.[1], Sokka J.[2], Trokovic R.[2] Lönnberg,T. [1], Mikkola L. [1], & Ivaska J.[1,3,4,5,6#]

1. Turku Bioscience Centre, University of Turku and Åbo Akademi University, FI-20520 Turku,Finland
2. Research Programs Unit, Stem cells and Metabolism and Biomedicum Stem Cell Centre,Faculty of Medicine, University of Helsinki, FI-00014 Helsinki, Finland.
3. InFLAMES Research Flagship Center, University of Turku, FI-20520 Turku, Finland.
4. Department of Life Technologies, University of Turku, FI-20520 Turku, Finland
5. Western Finnish Cancer Center (FICAN West), University of Turku, FI-20520 Turku,Finland
6. Foundation for the Finnish Cancer Institute, Tukholmankatu 8, FI-00014 Helsinki, Finland
7. INSERM U-1279, Gustave Roussy, Villejuif F-94805, France

* Equal contribution
#Correspondence: johanna.ivaska@utu.fi

SUMMARY

Cell states are governed by cell-intrinsic properties and external cues that regulate cell shape and signaling via cell-cell junctions or adhesions. Integrin β1-mediated adhesion is dispensable in early mouse embryogenesis at pre-implantation but becomes indispensable post-implantation. This implies distinct roles for β1-integrins in the naïve pre-implantation and primed post-implantation pluripotent stem cells (PSC). These, however, remain poorly understood. We investigated β1-integrin control of naïve-like and primed human induced PSC (hiPSC). We find that integrin β1 is active in naïve and primed hiPSCs and the degree of activity varies *in vitro* on different ECMs. Inhibition of integrin β1 in primed hiPSCs induces naïve-like colony features, reduces actomyosin contraction and ERK activity and alters gene expression, indicative of more naïve-like features. Reverting the primed state of pluripotency to naïve involves dramatic reorganization of colony morphology, actin and adhesions. Importantly, functional and single-cell transcriptomics analyses demonstrated that β1 integrin inhibition impairs cells exiting from naïve pluripotency. These data reveal unprecedented integrin-dependent regulation of PSC states and demonstrate how integrin inhibitors may help to fine-tune hiPSC function and properties *in vitro*.

INTRODUCTION

Integrins are heterodimeric cell-surface receptors that mediate adhesion to the extracellular matrix (ECM) and are connected to the intracellular actin cytoskeleton (Brakebusch and Fässler, 2003; Campbell and Humphries, 2011; Hynes, 2002). Integrin β1 is essential for the survival and development of mouse embryos. Mouse embryos lacking integrin β1 develop normally until the pre-implantation stage but degenerate at implantation (Fässler et al., 1995; Stephens et al., 1995), implying distinct roles for β1-integrins pre- and post-implantation. However, the functional role of integrin signaling during the pre- to post-implantation transition remains poorly understood. More recently, integrin β1 has been shown to regulate the actomyosin organization in mouse embryos upon implantation (Molè et al., 2021)and mediate proper organization of the epiblast and primitive endoderm in late mouse blastocysts (E. J. Y. Kim et al., 2022). However, integrin β1 regulation and role in controlling actomyosin contractility in human embryonic development remain elusive.

Human induced pluripotent stem cells (hiPSC) are reprogrammed from human somatic cells and closely resemble embryonic stem cells (ESC) with their epithelial morphology, gene expression and function (Takahashi et al., 2007; Takahashi and Yamanaka, 2006). Since pluripotent stem cells (PSC) are able to self-renew and differentiate into nearly any adult human cell type, they are powerful tools in disease modeling and treatment (Pera and Rossant, 2021). Naïve and primed states of pluripotency are well established in mice, where naïve PSCs resemble pre-implantation and primed post-implantation epiblast cells (Nichols and Smith, 2009). For human cells, *in vitro* cultured hiPSCs are considered to be in a primed state. They have epithelial-like features and grow in tightly packed colonies delimited by an integrin adhesion-dependent cornerstone adhesions connected to a actin "fence" structure (Närvä et al., 2017; Stubb et al., 2019). The position of hiPSCs in the colony, with respect to the edge, correlates with different aspects of cell polarity (E. J. Y. Kim et al., 2022). Thus, integrin-mediated focal adhesions and the ECM composition are key regulators of primed hiPSCs maintenance *in vitro*. Human naïve-like cells can be generated from hiPSCs using various methods (Collier et al., 2022; Hassani et al., 2019; Taei et al., 2020). The naïve- like cells differ from the primed cells in their gene expression patterns and signaling pathways, (Lynchet al., 2020; Martinez-Val et al., 2021; Nichols et al., 2009; Sim et al., 2017; Takashima et al., 2014; Weinberger et al., 2016) and adopt a dome-like colony morphology. This suggests that integrin-mediated ECM interactions in human naïve-like PSCs are distinct from the previously described cornerstone focal adhesion in primed hiPSCs (ref) and would have biologically distinct functions *in vitro*. This, however, has not been investigated in detail. Furthermore, during development, naïve PSCs must transition to state of primed pluripotency which facilitates formation of germ layers. The role of cell ECM interactions in this crucial step remains unknown. Naïve hiPSCs open a window to early human development and disease modelling, thus further understanding of their regulation by adhesions *in vitro* is needed.

Here, we demonstrate that integrin β1 is active in naïve and primed hiPSCs when cultured *in vitro* on commonly used ECMs, Matrigel, vitronectin and laminin-521. Inhibition of integrin β1 induces naïve-like features in primed hiPSCs, including dome-like colony morphology, naïve-like gene expression patterns, inhibition of ERK activity and reduced actomyosin contraction. Additionally, integrin inhibition impairs exit from pluripotency in naïve cell capacitation assays.

RESULTS

Inhibition of integrin β1 alters colony morphology and actomyosin contractility in primed hiPSCs

We have shown, using super-resolution iPALM microscopy, that primed hiPSC colonies encompass large integrin β1 positive cornerstone focal adhesions and sharp actin fenced edges on different ECM (Stubb et al., 2019). To investigate the functional relevance of integrin β1 activity for maintaining primed hiPSC colony morphology, we used a function-blocking integrin antibody (MAb13; anti-β1). Within 12 h,

integrin inhibition triggered rearrangement of the flat two-dimensional sharp-edge primed hiPSC colonies into tightly packed, more dome-shaped structures, resembling to some degree the morphology of naïve hiPSC colonies (**Figure 1A-F**). Integrin β1 inhibition significantly decreased the colony area (**Figure 1A-B**), induced tighter cell clustering (**Figure 1C-D**), increased the colony height (**Figure 1E-F**) and triggered re-organization of actin with loss of extended stress fibers. These data suggest that integrin β1 is required to mediate primed hiPSC colony spreading. On the other hand, the protein levels of OCT4, a transcription factor essential in the maintenance of primed pluripotency (Weinberger et al., 2016), were not significantly altered (**Supplemental Figure 1A-B)**, indicating that integrin inhibition alone does not alter pluripotency regulator expression under these culture conditions.

Integrin αVβ5 is also highly expressed specifically at the edges of the integrin β1 positive cornerstone focal adhesions of primed hiPSCs (Stubb et al., 2019). To determine the relative contribution of these adhesion receptors to primed hiPSCs' colony morphology and actin organization, we incubated the cells with IgG (control), anti-β1 or anti-αVβ5 antibodies. Inhibition of integrin β1 or αVβ5 had no significant effect on OCT4 protein levels (**Supplemental Figure 1C-D**). However,immunofluorescence staining of F-actin and phosphorylated myosin light chain (pMLC) revealed significant cytoskeletal differences. Integrin β1 inhibition reduced colony area and induced tighter cell clustering whereas αVβ5 inhibition had no significant effect (**Figure 1G-I**). Even though the more tightly packed organization, induced by β1-integrin inhibition, would imply higher contractility in the colonies, pMLC levels were, in fact, significantly decreased (**Figure 1G-I**). In contrast, αVβ5 inhibition did not influence pMLC levels. These results were validated in another primed hiPSC line (**Supplemental Figure 1E-G)**. The staining of contractile cytoskeletal machinery indicate that the active integrin β1 adhesions mediate forces oriented towards pulling the cells towards ECM and maintaining the colony flat in primed state of pluripotency.

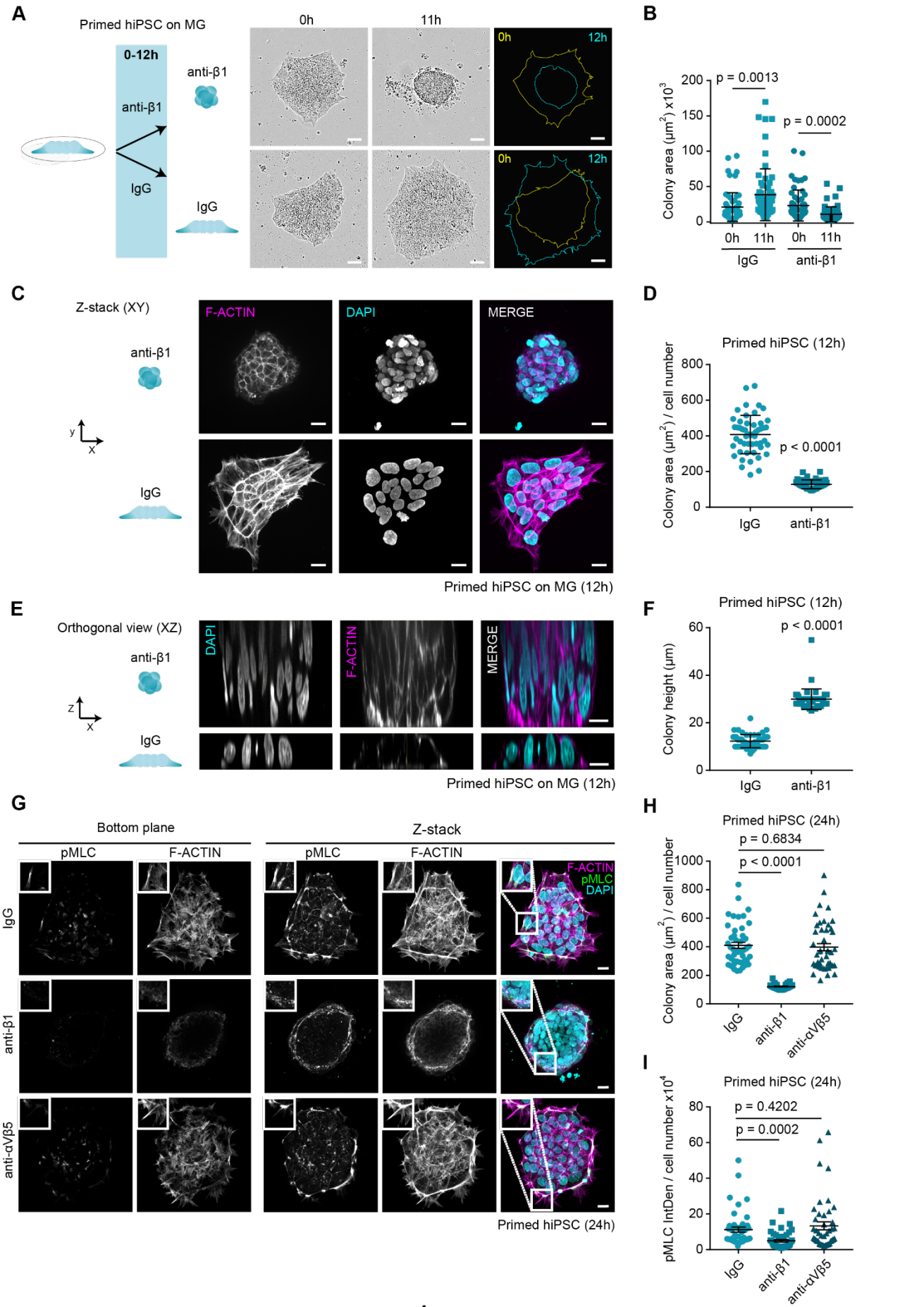
A
Primed hiPSC on MG
0-12h
anti-β1
IgG
0h
11h
12h
B
Colony area (μm²) x10³
p = 0.0013
p = 0.0002
0h
11h
IgG
anti-β1
C
Z-stack (XY)
F-ACTIN
DAPI
MERGE
Primed hiPSC on MG (12h)
D
Primed hiPSC (12h)
Colony area (μm²) / cell number
p < 0.0001
E
Orthogonal view (XZ)
Primed hiPSC on MG (12h)
F
Colony height (μm)
G
Bottom plane
Z-stack
pMLC
Primed hiPSC (24h)
H
p = 0.6834
I
pMLC IntDen / cell number x10⁴
p = 0.4202
p = 0.0002
anti-αVβ5

Figure 1. Integrin β1 inhibition altered primed hiPSCs colony morphology. A-B) Representative bright-field images (A) and colony area quantification (B)of primed hiPSCs on MG after 0 and 12h IgG or MAb13 anti-integrin β1 (anti-β1) treatment. Scale bar 20 µm. Images were acquired on an IncuCyte S3 live-cell analysis instrument (Sartorius). **C-D)** Z-stacks (C; maximum intensity projections) of representative F-Actin and DAPI staining in primed hiPSCs on Matrigel after 12h IgG or anti-β1 treatment, and quantification (D) of cell colony area (based on F-Actin staining) normalized to cell number (n = 3 independent experiments, 45-51 cell colonies in total, unpaired t-test with Welch's correction, mean ± SD). Scale bar 20 µm. Images were acquired on a 3i CSU-W1 spinning disk confocal microscope. **E-F)**Orthogonal view (E; z-axis) of representative F-actin and DAPI staining in primed hiPSCs on Matrigel after 12hIgG or anti-β1 treatment, and quantification of colony height (F). The microscope's working distance limited imaging of the top of the highest colonies. Scale bar 20 µm. Images were acquired on a 3i CSU- W1 spinning disk confocal microscope. **G)** Representative pMLC, F-Actin and DAPI staining of primed hiPSCs plated on Matrigel, andtreated with IgG, anti-β1 or anti-αVβ5 (24 h). Images were acquired on a 3i CSU-W1 spinning disk confocal microscope. **H-I)** Quantification of colony area normalized by cell number (H) and pMLC intensity (I). (n = 3 individual experiments, 44-46 cell colonies in total, unpaired t-test with Welch's correction, mean ± SEM)

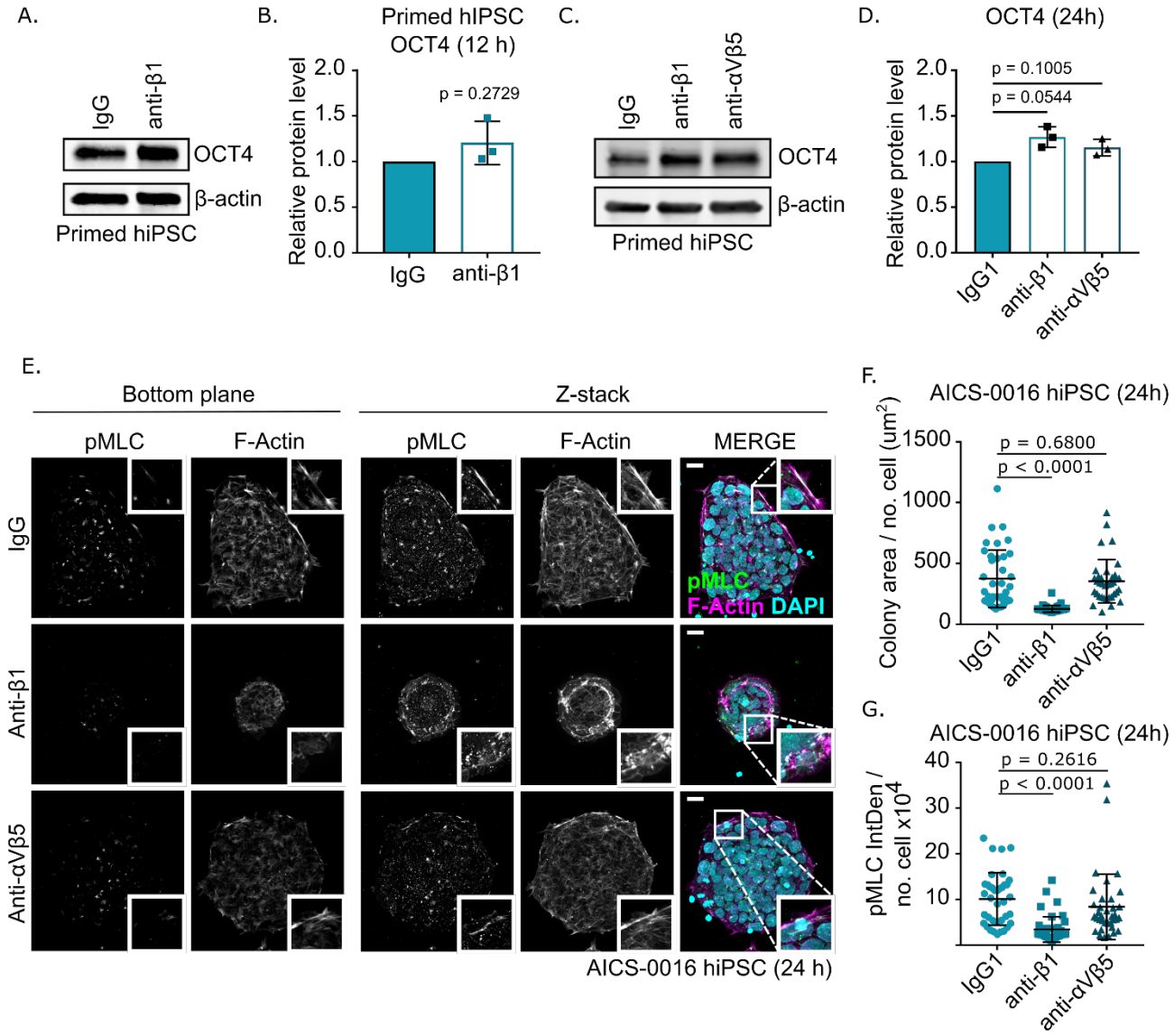

Supplementary Figure 1. Short-term integrin inhibition does not influence OCT4 expression in hiPSCs. A-B) Western blot of OCT4 and β-actin, and quantification of OCT4 protein levels normalized by β-actin in primed hiPSCs treated with control IgG or anti-β1 (MAb13) on Matrigel for 12 h. (n = 3independent experiments, one sample t-test, mean ± SD). **C-D)** Western blot of OCT4 and β-actin, and quantification of OCT4 protein levels normalized by β-actin in primed hiPSCs treated with control IgG or anti-αVβ5 on Matrigel for 42 h. (n = 3 independent experiments, one sample t-test, mean ± SD). **C)** Representative pMLC,F-Actin and DAPI staining of AICS-0016 primed hiPSCs plated on Matrigel, and treated with IgG, anti- β1 or anti-αVβ5 (24 h), acquired on a 3i CSU-W1 spinning disk confocal microscope. Scale bar 20 μm. **D-E)** Quantification of colony area normalized by cell number (D), and pMLC intensity (E). (n = 3 individual experiments, 36-43 cell colonies in total, unpaired t-test with Welch's correction, mean ± SD). **F)** Western blot of Src and pSrc (Y416) normalized by β-actin (n=6 independent experiments, one sample t-test, mean ± SD).

Focal adhesions are lost in KLF17 expressing cells

As integrin β1 inhibition promoted naïve-like compacted colony morphology in primed hiPSCs, we assessed whether integrin β1 inhibition would facilitate the reversion of hiPSCs into a naïve-like state. We reverted primed hiPSCs into a naïve-like state (using an established protocol involving epigenetic reversion (Guo et al., 2017) in the presence or absence of integrin β1 function-blocking antibody (MAb13; anti-β1) (**Figure 2A**). Interestingly, integrin β1 inhibition increased hiPSC proliferation during the reversion process (**Supplemental Figure 2A-B**) while cells in both conditions reached a typical dome-shaped morphology (**Figure 2B**). The mRNA levels of primed markers *ZIC2* and *SFRP2* were decreased and mRNA levels of naïve markers *KLF17* (starting from day 18) and *TBX3* (on day 10 and 48) induced in both of the naïve hiPSC lines during the reversion, as expected (**Figure 2C**; mRNA expression in non-reverted primed hiPSC are included as control for all the time points). There was a slight trend for higher naïve marker expression in the integrin β1 inhibited cells compared to the control naïve cells (**Figure 2C**). In particular the expression of naïve markers seemed higher at the early timepoints of our timeseries. However, these were not statistically significant.

To further investigate the role of integrin β1 in the naïve and primed cell states we investigated their adhesions on different ECM. Primed hiPSCs formed large integrin-mediated focal adhesions at the edge of the cell colonies on vitronectin (**Figure 2D**), as reported earlier (Närvä et al., 2017; Stubb et al., 2019). To study focal adhesions in hiPSCs during chemical reversion to a naïve-like state, we plated cells on Matrigel, vitronectin and laminin-521 at day 10 of the reset protocol, and performed immunofluorescence staining of paxillin, a major component of focal adhesions, and KLF17, a known marker of naïve pluripotency (**Figure 2E, Supplemental Figure 2C-D**). On the 10th day of the reversion, some of the hiPSCs had started to express KLF17. On all of the ECMs investigated, the KLF17-positive cells lacked the clear focal adhesions and prominent actin stress fibers typically detected in the primed-state cells (**Figure 2E, Supplemental Figure 2C-D**). One of the key mediators of integrin signaling in focal adhesions is Src kinase. Interestingly, reversion to a naïve state resulted in strong downregulation of Src activity (detected by Y416 pSrc specific antibody) (**Supplemental Figure 2E**). These data indicate that transition from primed to naïve-like state is accompanied by striking alteration of cell-ECM adhesion.

To further compare our naïve cells with the primed hiPSCs, we studied the protein expression of KLF17 and NANOG (a pluripotency marker) by western blotting. We see KLF17 expression solely in the naïve hiPSCs, while both maintain a similar NANOG expression (**Supplemental Figure 3A**). Furthermore, qPCR data indicate that the primer hiPSCs are negative for the naïve markers (KLF17 and TBX3) and positive for primed markers (ZIC2 and SFRP2). In both cases, the relative mRNA expression of these genes isconcordant with the cell state (**Supplemental Figure 3B**). Immunofluorescence data correlate with these observations as we detect nuclear KLF17 signal only in the naïve cells on different matrixes (Matrigel, vitronectin and laminin-521) than for naïve hiPSCs (**Supplemental Figure 3C**).

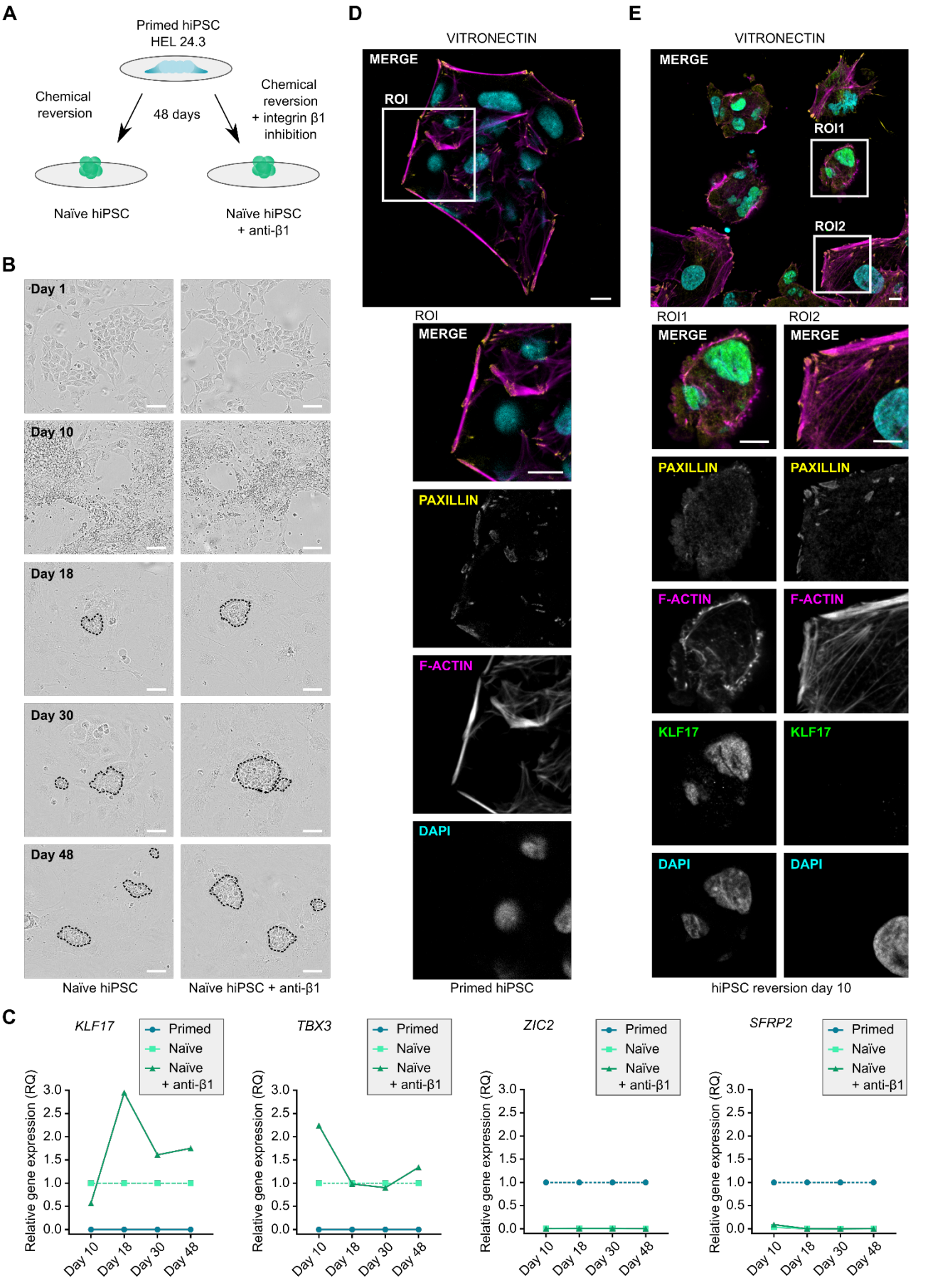
A
Primed hiPSC
HEL 24.3
Chemical reversion
48 days
Chemical reversion + integrin β1 inhibition
Naïve hiPSC
Naïve hiPSC + anti-β1
B
Day 1
Day 10
Day 18
Day 30
Day 48
Naïve hiPSC
Naïve hiPSC + anti-β1
C
KLF17
TBX3
ZIC2
SFRP2
Primed
Naïve
Naïve + anti-β1
Relative gene expression (RQ)
Day 10
Day 18
Day 30
Day 48
D
VITRONECTIN
MERGE
ROI
PAXILLIN
F-ACTIN
DAPI
Primed hiPSC
E
VITRONECTIN
MERGE
ROI1
ROI2
PAXILLIN
F-ACTIN
KLF17
DAPI
hiPSC reversion day 10

Figure 2. Chemical reversion into naïve-like state with integrin β1 inhibition. A) Illustration of experimentaldesign. **B)** Representative images of hiPSCs on feeder cells (iMEFs) during chemical reversion, acquired on an IncyCyte S3 live-cell analysis instrument. The clearly visible naïve-like colonies are marked using dashed line drawn along the colony edge. Scale bar 20 µm. **C)** Relative mRNA levels of *KLF17*, *TBX3, ZIC2* and *SFRP2* in primed (normal culture conditions) and naïve hiPSCs during chemical reversion. Naïve markers *KLF17* and *TBX3*were normalized by naïve hiPSCs' (dashed line), and primed markers *ZIC2* and *SFRP2* were normalized by primed hiPSCs' mRNA expression levels (dashed line). (n = 1) **D)** Representative immunofluorescence stainingof paxillin, F-Actin and DAPI in primed hiPSCs plated on vitronectin. Scale bar 10 µm. **E)** Representative immunofluorescence staining of paxillin, KLF17, F-Actin and DAPI in hiPSCs plated on vitronectin after 10 daysof chemical reversion. Scale bar 10 µm. Images in D-E were acquired on a 3i CSU- W1 spinning disk confocal microscope.

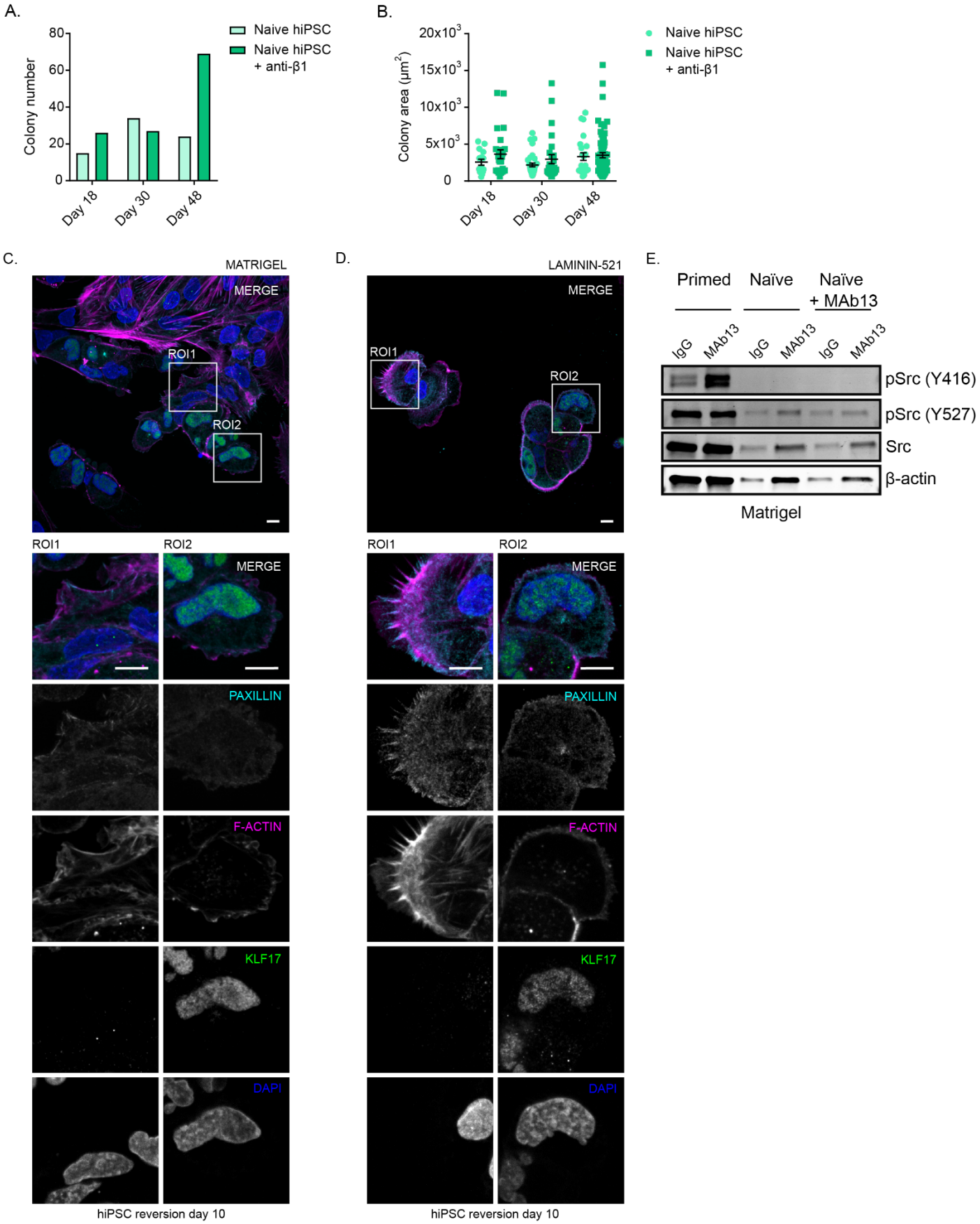
A.
Colony number
80
60
40
20
0
Day 18
Day 30
Day 48
Naive hiPSC
Naive hiPSC
+ anti-β1
B.
Colony area (μm²)
20x10³
15x10³
10x10³
5x10³
0
Day 18
Day 30
Day 48
Naive hiPSC
Naive hiPSC
+ anti-β1
C.
MATRIGEL
MERGE
ROI1
ROI2
ROI1
ROI2
MERGE
PAXILLIN
F-ACTIN
KLF17
DAPI
hiPSC reversion day 10
D.
LAMININ-521
MERGE
ROI1
ROI2
ROI1
ROI2
MERGE
PAXILLIN
F-ACTIN
KLF17
DAPI
hiPSC reversion day 10
E.
Primed
Naïve
Naïve
+ MAb13
IgG
MAb13
IgG
MAb13
IgG
MAb13
pSrc (Y416)
pSrc (Y527)
Src
β-actin
Matrigel

Supplemental Figure 2. A-B) Quantification of hiPSC colony number (A) and area (B) during chemical reversion (related to Figure 1B), acquired on an IncyCyte S3 live-cell analysis instrument (n = 1, 9 images/condition in total). **C-D)** Representative immunofluorescence staining of paxillin, KLF17, F-Actin and DAPI in hiPSCs plated on Matrigel (C) or laminin-521 (D) after 10 days of chemical reversion. Images were acquired on a 3i CSU-W1 spinning disk confocal microscope. Scale bar 10 µm. **E)** Western blot of active pSrc (Y416), pSrc (Y527) and Src in primed and naïve hiPSCS, in naïve hiPSCs cultured with Mab13, in the presenceor absence of Mab13.

Integrin β1 is highly active in naïve and primed hiPSCs when cultured in vitro

Earlier studies have demonstrated that integrin β1 signaling is dispensable for the formation and survival of the pre-implantation mouse embryo inner cell mass (ICM) (Molè et al., 2021; Stephens et al., 1995) but vital in the subsequent steps of development. According to a cell-surface proteomics study, naïve human pluripotent stem cells (hPSC), which resemble the pre-implantation ICM, have less integrin β1 on their cell surface compared to primed hPSCs, which resemble the post-implantation ICM (Wojdyla et al., 2020). These studies, and our data indicative of integrin β1 inhibition inducing a more naïve-like colony morphology, prompted us to investigate whether naïve hPSC would have less active integrin β1 compared to primed hPSCs. We performed immunofluorescence staining of integrin β1 with an antibody specific for the active ligand-engaged conformation of the receptor (12G10; (Byron et al., 2009)) in cells cultured on Matrigel, vitronectin or laminin-521 – ECMs commonly used in hiPSC culture (**Figure 3A-C, Supplemental Figure 3C**). In primed hiPSCs, the intensity of active integrin β1 was highest when cells were cultured on Matrigel and laminin-521. On these ECMs, the primed hiPSCs formed focal adhesions mainly at the edge but also in the middle of the colonies (**Figure 3A-B**). When cultured on vitronectin, the total level of active integrin β1 was lower but the cells formed prominent cornerstone focal adhesions at the colony edges, as reported earlier (Närvä et al., 2017; Stubb et al., 2019).

Surprisingly, we observed significantly higher integrin activity on all matrices in naïve hiPSCs cells. In addition, human embryonic stem cells (hESC) that were reverted to a naïve state using the same protocol, also displayed high levels of active integrin β1 (**Figure 3A-C, Supplemental Figure 3E**). Despite high integrin activity, discernable focal adhesions were lacking in naïve hiPSCs and active integrins were distributed across the entire colony's cell-ECM interface. The naïve hiPSCs cells were strongly positive for nuclear KLF17 on all of the matrixes, with the primed cells showing only low non-nuclear signal (**Supplementary Figure 3C**). However, on laminin-521 the naïve hiPSC colonies were less tightly packed than on vitronectin, where the integrin β1 activity was the lowest (**Figure 3C**). This suggests that high integrin β1 activity is linked to the ECM conditions of the cells impacting the naïve -like colony morphology of hiPSCs without inducing immediate transition from the naïve state.

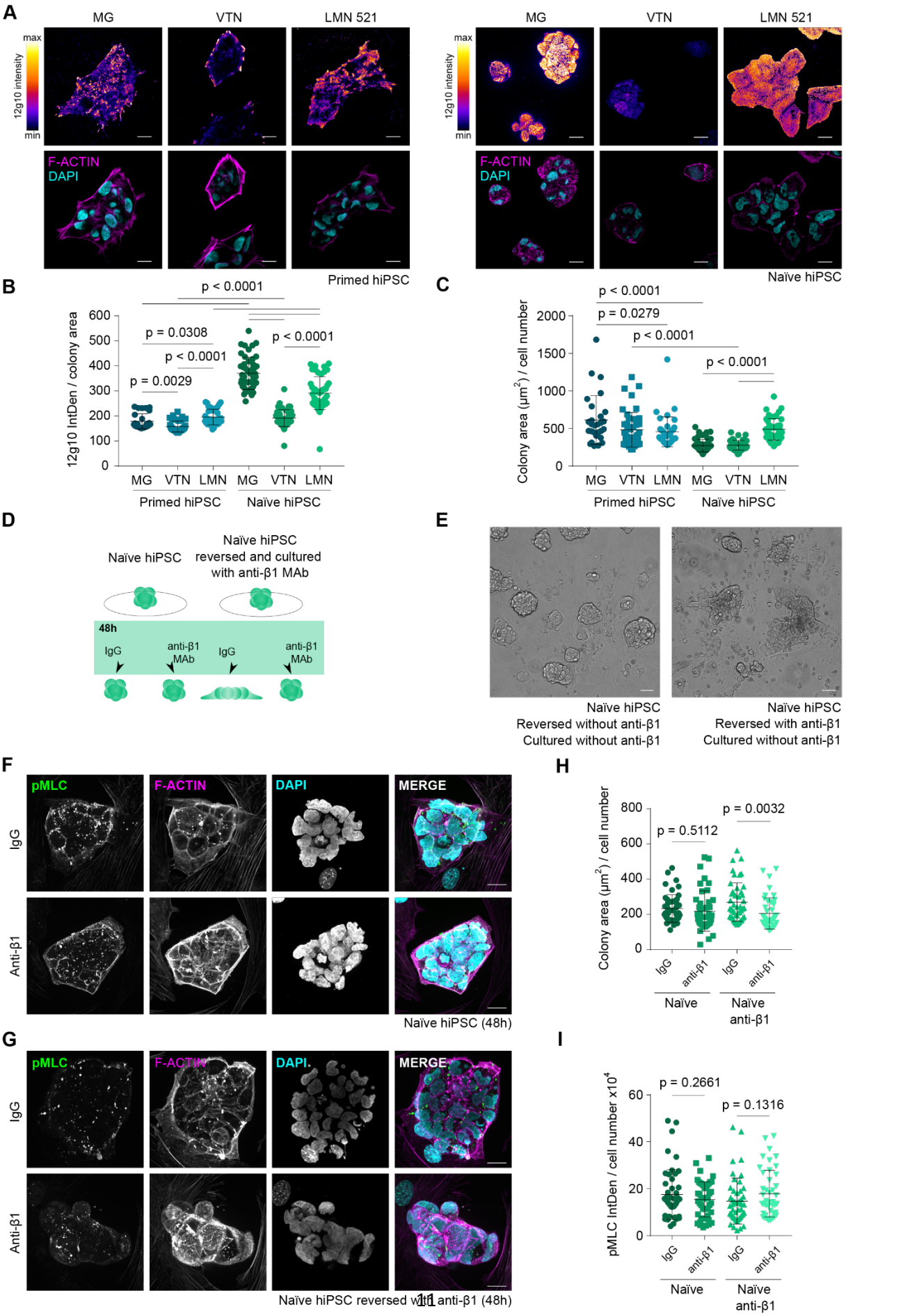
A
MG
VTN
LMN 521
max
12g10 intensity
min
F-ACTIN
DAPI
Primed hiPSC
Naïve hiPSC
B
12g10 IntDen / colony area
p < 0.0001
p = 0.0308
p < 0.0001
p = 0.0029
p < 0.0001
MG VTN LMN MG VTN LMN
Primed hiPSC
Naïve hiPSC
C
Colony area (μm²) / cell number
p < 0.0001
p = 0.0279
p < 0.0001
p < 0.0001
D
Naïve hiPSC
Naïve hiPSC reversed and cultured with anti-β1 MAb
48h
IgG
anti-β1 MAb
E
Naïve hiPSC
Reversed without anti-β1
Cultured without anti-β1
Naïve hiPSC
Reversed with anti-β1
Cultured without anti-β1
F
pMLC
F-ACTIN
DAPI
MERGE
IgG
Anti-β1
Naïve hiPSC (48h)
G
Naïve hiPSC reversed with anti-β1 (48h)
H
Colony area (μm²) / cell number
p = 0.5112
p = 0.0032
IgG anti-β1 IgG anti-β1
Naïve
Naïve anti-β1
I
pMLC IntDen / cell number x10⁴
p = 0.2661
p = 0.1316
IgG anti-β1 IgG anti-β1
Naïve
Naïve anti-β1

Figure 3. Integrin β1 activity is higher in naïve hiPSCs A) Representativeimmunofluorescence staining of active integrin β1 (12G10), F-actin and DAPI on the bottom plane of primed and naïve hiPSCs plated on Matrigel (MG), vitronectin (VTN) or laminin-521 (LMN 521) for 48 h. Scale bar 20µm. Images were acquired on a 3i CSU-W1 spinning disk confocal microscope. **B)** Quantification of 12G10 intensity normalized to the colony area (n = 3 independent experiments, 28-48 cell colonies in total, unpaired t- test with Welch's correction, mean ± SD). **C)** Quantification of cell colony area (based on F-Actin staining) normalized to cell number (n = 3 independent experiments, 28-48 cell colonies in total, unpaired t-test with Welch's correction, mean ± SD).

Supplementary Figure 3

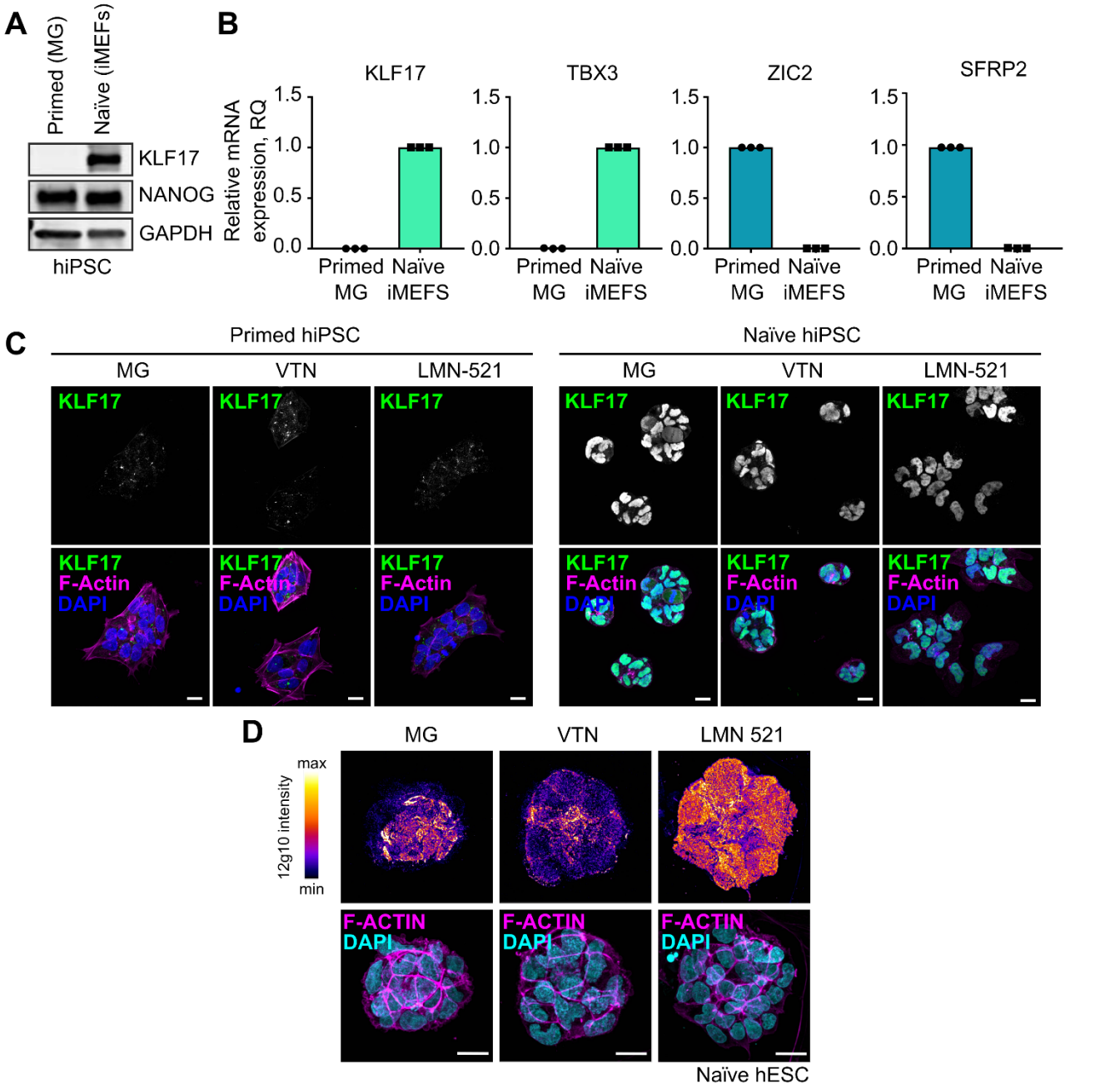

Supplemental Figure 3. Integrin β1 is highly active in primed hiPSCs, naïve hiPSCs and naïve hESCs when cultured *in vitro*. A) Western blot of naïve marker KLF17 and pluripotency marker NANOG in primed hiPSCs cultured on Matrigel, and naïve hiPSCs cultured on iMEFs. **B)** Relative mRNA expression of naïve markers KLF17

and TBX3, and primed markers ZIC2 and SFRP2 in primed hiPSCs cultured on Matrigel, and naïve hiPSCs cultured on iMEFs. **C)** IF staining of KLF17, F-actin and DAPI in primed and naïve hiPSCs plated on Matrigel (MG), vitronectin (VTN) and laminin-521 (LMN-521) on the same colonies as Fig. 1A. **D)** Representative immunofluorescence staining (z-stack) of active integrin β1 (12g10), F-actin and DAPI in naïve hESCs plated on Matrigel (MG), vitronectin (VTN) and laminin-521 (LMN 521), acquired on a 3i CSU-W1 spinning disk confocal microscope. Scale bar 20 μm.

Integrin β1 controls colony morphology and actomyosin contractility in primed and naïvehiPSCs

Next, we investigated the effect of integrin inhibition in the naïve hiPSCs reverted in the presence or absence of integrin β1 inhibitory antibody (anti-β1 naïve and control naïve (with control IgG) from here on). Withdrawal of the anti-β1 antibody from anti-β1 naïve cells resulted in marked flattening and loss of naïve-like colony morphology compared to the control naïve cells cultured in the presence of the control IgG after 48 h (**Figure 3D-E)**. Integrin inhibition had no effect on colony size (F-actin staining) in control naïve cells whereas cell clustering was significantly decreased in the IgG-treated anti-β1 naïve hiPSC colonies (**Figure 3F-H**). pMLC levels were not altered upon integrin β1 inhibition in either naïve population (**Figure 3F, G, I**). These data imply that cells reverted in the presence of integrin β1 inhibition may have adapted to these conditions and depend on continuous integrin β1 inhibition to maintain their state. Furter, this indicates that integrin β1 has different role in mediating forces in naïve pluripotent state. Based on immunofluorescence, β1 mediated cell ECM adhesion do not bear significant forces pulling the cells towards the ECM.

Blocking Integrin β1 delays the capacitation process

Integrin β1 has a well described role in blastocyst cells pre-implantation but become indispensable post-implantation when cells undergo a formative transition exiting the naïve state and gaining competence for lineage induction through a process called capacitation (Rostovskaya et al., 2019). The specific role of integrin β1 in this priming process which enables primed hiPSCs to evolve from naïve hiPSCs has not been explored, prompting us to test the impact of integrin β1 inhibition on capacitation.

Switching naïve hiPSC from naïve culture conditions to N2B27 culture medium supplemented with Wnt inhibition (N2B27 + 2μM XAV-939) triggers capacitation and diminishes the ability of cells to self-renew when returned to naïve conditions in 3 days (Rostovskaya et al., 2019). To test the impact of integrin-β1 on this process we grew naïve hiPSC colonies in NaïveCult for 48h with or without integrin inhibition and then switched the cells to capacitation medium (N2B27 + 2μM XAV-939) and monitored the colonies live with IncuCyte. Concordant with our earlier data, colonies with and without antibody treatment have a dome rounded shape in naïve culture conditions (0 h). After 48h in capacitation medium, colonies cultured without integrin inhibition lose their naïve-specific architecture and spread on the plastic, while the colonies cultured with integrin inhibition maintained a very similar phenotype to naïve hiPSCs. After 120 hours of capacitation, both conditions present a similar primed-like phenotype, lose their dome-shaped architecture and spread (**Figure 4A**).

To further investigate the capacitation, we assessed the ability of the cells to renew in naïve conditions using the established colony assay (Rostovskaya et al., 2019). Naïve hiPSCs were either capacitized for 48h (2d) or 120h (5d), both with or without integrin inhibition after which their ability to give rise to colonies in regular culture medium (E8) or in naïve culture conditions was compared (**Figure 4B)**. Concordant with earlier studies, control naïve hiPSCs grown 5 days in capacitation medium were largely unable to self-renew in naïve conditions compared to E8 (significant reduction in colony grow in naïve conditions; **Figure 4C**), indicating that the cells have exited their naïve state. However, cells capacitated in the presence of integrin inhibition were equally capable of self-renewal in naïve conditions after 2 days and 5 days of capacitation (**Figure 4C)**, indicating that integrin inhibition attenuated exit from the naïve state.

Taken together, these data show that blocking integrin β1 delays the capacitation process both on a colony morphological as well as functional level, indicative of an essential role for integrin-β1 during the formative transition of human naïve cells.

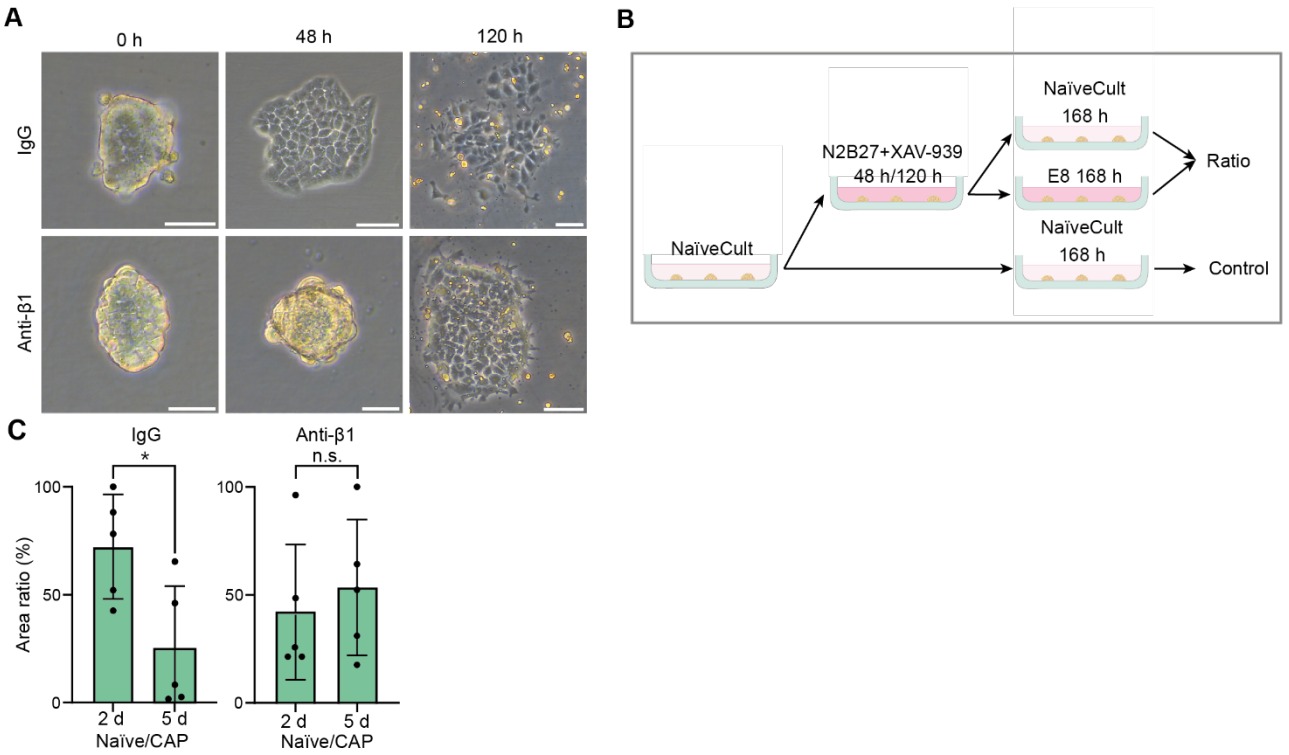

Figure 4. Integrin β1 inhibition delays capacitation of naïve hiPSCs. A) Brightfield imaging of naïve hiPSCs cultured with anti-β1 vs. IgG (control), at different capacitation times (0h, 48h and 120h). Scale bar = 10 µm. B) Explanatory scheme of the capacitation process and the conditions used for the area ratio calculation. C) Quantification of area ratios (n=5, t-test, p-value=0.0246, mean ± SD) The ratios are calculated using the colony area of capacitated cells cultured in NaïveCult and capacitated cells cultured in E8. This ratio is then normalized by the initial area of non-capacitated naïve colonies cultured in NaïveCult with or without Mab13.

Integrin β1 inhibition promotes expression of genes supporting a naïve-like state

Intrigued by the differences in β1 mediated cell-ECM adhesion in naïve and primed states we investigated further how integrin β1 activity affects actin cytoskeleton and pluripotency related gene expression by performing an unbiased genome-wide transcriptome analysis in primed and naïve hiPSCs (**Figure 5**). We found that in primed hiPSCs 10 genes were differentially expressed upon integrin β1 inhibition(12 h) (**Figure 5A, Supplemental Table 1;** false discovery rate (FDR) < 0.05). Nine of the differentially expressed genes were downregulated (**Figure 5A**). Two of the downregulated genes, *PDGFB* and *CCN2*, are involved in the positive regulation of ERK signaling according to gene ontology annotations. In addition, the only upregulated gene, DUSP8, is emerging as a negative regulator of ERK signaling (Ding et al., 2019). Interestingly, inhibition of ERK signaling is reported to support a naïve-like state in mouse embryos and human PSCs (Nichols et al., 2009; Takashima et al., 2014). Consistent with our transcriptome analysis, phosphorylated ERK (pERK) protein levels were also decreased in primed hiPSCs after integrin inhibition (**Figure 5B-C**), implying that integrin β1 inhibition attenuates ERK activity, in line with a more naïve-like phenotype, in primed hiPSCs.

Next we compared the control naïve and the anti-β1 naïve cell populations. 36 genes were differentially expressed, 5 downregulated and 31 upregulated, following continuous integrin β1 inhibition (**Figure 5D**). Interestingly, actin cytoskeleton related genes, *PHACTR-1*, *ACTA2* and *FILIP1* (Allain et al., 2012; Jarray et al., 2011; Nagano et al., 2002; Schildmeyer et al., 2000; Wiezlak et al., 2012), were upregulated in the anti-β1 naïve cells, possibly linking to the differences in colony compaction and actin organization between control and anti-β1 naïve hiPSCs. Furthermore, many of the differentially expressed genes were associated with embryonic development and cell differentiation processes according to gene-annotation analysis (**Figure 5E**). Two of the downregulated genes, *HOXB1* and *GLI2*, are associated with the pattern specification process, and in contrast, two of the upregulated genes, *SIX2* and *PRAME*, are linked to negative regulation of cell differentiation (**Figure 5E**). These results suggest that continuous integrin β1 inhibition may support maintenance of a naïve-like state on the transcriptional level.

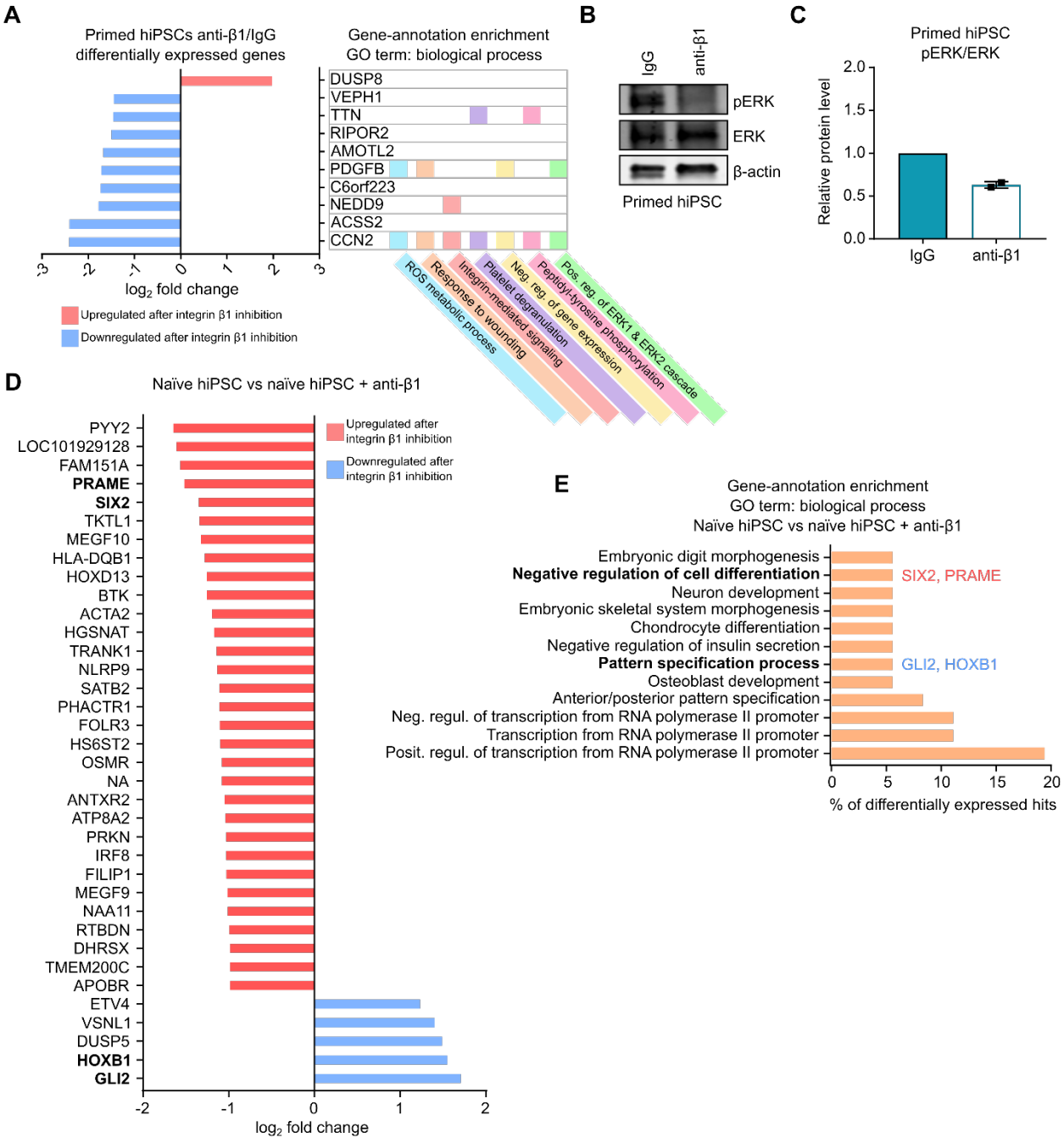
A
Primed hiPSCs anti-β1/IgG
differentially expressed genes
log2 fold change
Upregulated after integrin β1 inhibition
Downregulated after integrin β1 inhibition
Gene-annotation enrichment
GO term: biological process
DUSP8
VEPH1
TTN
RIPOR2
AMOTL2
PDGFB
C6orf223
NEDD9
ACSS2
CCN2
ROS metabolic process
Response to wounding
Integrin-mediated signaling
Platelet degranulation
Neg. reg. of gene expression
Peptidyl-tyrosine phosphorylation
Pos. reg. of ERK1 & ERK2 cascade
B
IgG
anti-β1
pERK
ERK
β-actin
Primed hiPSC
C
Primed hiPSC
pERK/ERK
Relative protein level
IgG
anti-β1
D
Naïve hiPSC vs naïve hiPSC + anti-β1
Upregulated after integrin β1 inhibition
Downregulated after integrin β1 inhibition
PYY2
LOC101929128
FAM151A
PRAME
SIX2
TKTL1
MEGF10
HLA-DQB1
HOXD13
BTK
ACTA2
HGSNAT
TRANK1
NLRP9
SATB2
PHACTR1
FOLR3
HS6ST2
OSMR
NA
ANTXR2
ATP8A2
PRKN
IRF8
FILIP1
MEGF9
NAA11
RTBDN
DHRSX
TMEM200C
APOBR
ETV4
VSNL1
DUSP5
HOXB1
GLI2
log2 fold change
E
Gene-annotation enrichment
GO term: biological process
Naïve hiPSC vs naïve hiPSC + anti-β1
Embryonic digit morphogenesis
Negative regulation of cell differentiation
Neuron development
Embryonic skeletal system morphogenesis
Chondrocyte differentiation
Negative regulation of insulin secretion
Pattern specification process
Osteoblast development
Anterior/posterior pattern specification
Neg. regul. of transcription from RNA polymerase II promoter
Transcription from RNA polymerase II promoter
Posit. regul. of transcription from RNA polymerase II promoter
SIX2, PRAME
GLI2, HOXB1
% of differentially expressed hits

Figure 5. Integrin β1 inhibition promotes expression of naïve-like state supporting genes. A) Differentially expressed genes (false discovery rate, FDR < 0.05) and gene-annotation analysis of anti-β1 vs. IgG (control) treated (12h) primed hiPSCs. **B-C)** Western blot of phosphorylated ERK (pERK), total ERK and β-actin in IgG or anti-β1 treated (12h) primed hiPSCs, and quantification of pERK protein levels normalized by total ERK. (n = 2 individual experiments). **D)** Differentially expressed genes in naïve hiPSCs vs. naïve + anti-β1 hiPSCs (FDR < 0.05). **E)** Gene-annotation enrichment analysis of differentially expressed genes related to Figure 4B.

Single cell characterization reveals that integrin β1 inhibition impairs transition to primed cell state

To further understand the genetic changes cause by capacitation, we performed single cell RNA sequencing (scRNAseq) using 6 different conditions: naïve hiPSCs cultured with (d0_ anti-β1) or without (d0) anti-β1, previously capacitized (for 48h) naïve hiPSCs with (d2_ anti-β1) or without (d2) anti-β1, and primed hiPSCS cultured with (primed hiPSC_ anti-β1) or without (primed hiPSC) anti-β1. The U-map of these 6 groups shows that clustering patterns of naïve cells cultured without anti-β1 is similar to that of capacitated cells cultured without anti-β1, while the d0_ anti-β1 and d2_ anti-β1 groups also cluster alike. Primed HEL24.3 cells clustering is identical whether with or without anti-β1 (**Figure 6A**). SFRP2 is an established marker of primed cell state and the overlayed SFRP2 expression (**Figure 6B**) shows increased expression with the capacitation stage and maximal in primed cells.

To better understand the effect of integrin β1 inhibition on the capacitation process, we plotted the top up- and down- regulated genes in the d2 condition compared to the d0 condition (**Figure 6C**). From this geneset, we identified three populations: genes that remained downregulated in d2_Mab13 compared to d0_Mab13 (written in blue), genes that remained upregulated in d2_Mab13 compared to d0_Mab13 (written in red),and genes that were differentially regulated in the absence of Mab13 but not in d2_Mab13 compared to d0_Mab13 (written in green). DPPA3 and L1TD1, two well markers expressed in naïve cells (Palangi et al., 2017; Rostovskaya et al., 2019; Zhao et al., 2019) and therefore logically downregulated during capacitation seemed to be impacted by Integrin-β1 function blocking. Indeed, upon addition of Mab13, their expression stays unchanged upon capacitation. The case of Mab13-sensitive upregulation of MT1Gand MT1H upon capacitation is interesting, as these metallothioneins have been reported to be upregulated during the differentiation process of cardiomyocytes (Branco et al., 2019) but also as part of naïve gene sets in other studies (Liu et al., 2020; Molè et al., 2021) (**Figure 6D**). Interestingly, CGA which is involved in the embryo attachment to the endometrium (Idelevich and Vilella, 2020) and therefore upregulated uponcapacitation (**Figure 6D**), was slightly downregulated after integrin-β1 blocking, once more underlining the strong inhibitory effect of Mab13 on the capacitation process.

Taken together, these data show the impact of integrin β1 function blocking inhibiting the ability of naïve cells to undergo formal transition to a primed-like gene expression profile and exit their naïve state.

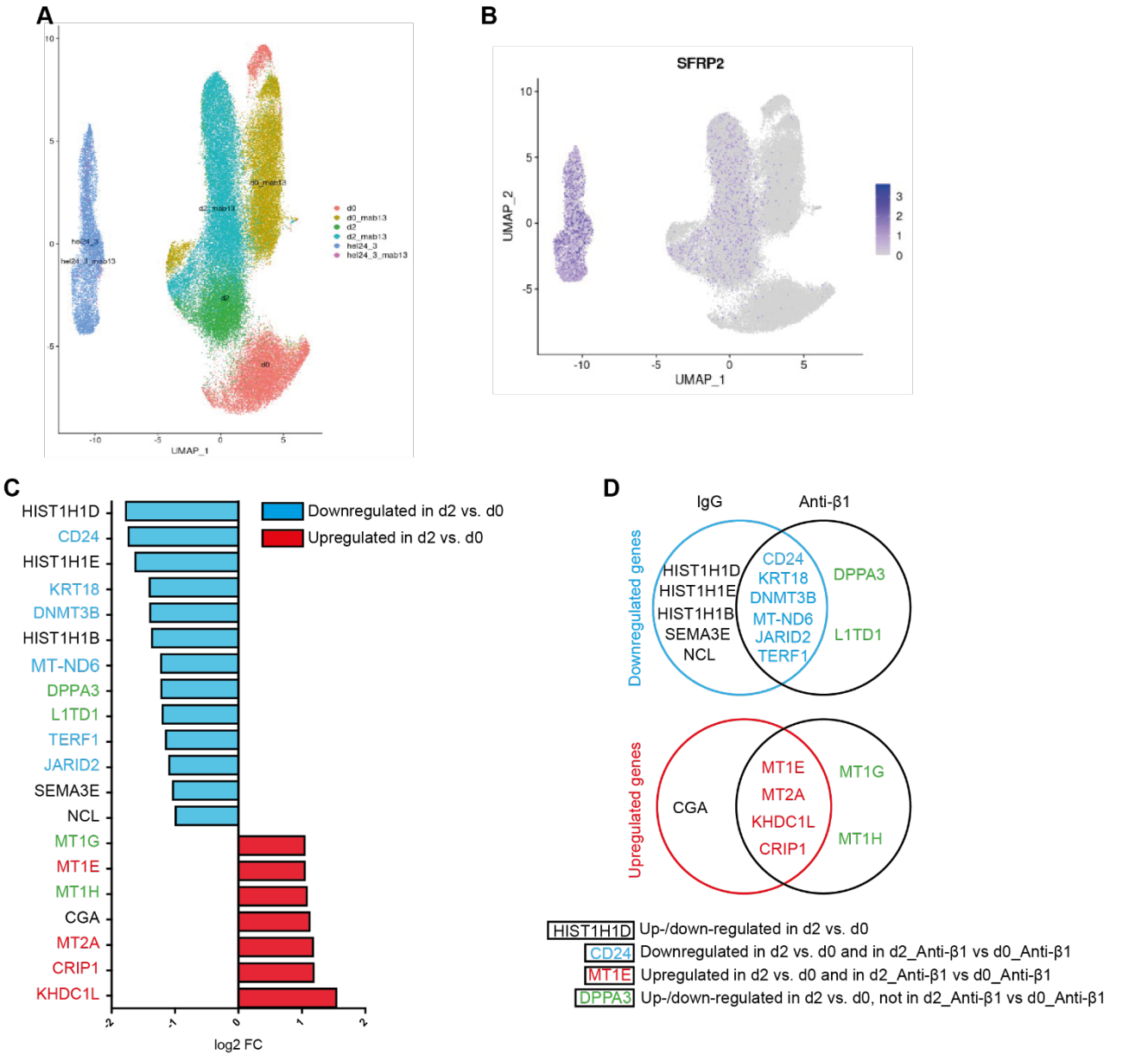
A
d0
d0_mab13
d2
d2_mab13
hel24_3
hel24_3_mab13
UMAP_1
B
SFRP2
UMAP_2
UMAP_1
C
HIST1H1D
CD24
HIST1H1E
KRT18
DNMT3B
HIST1H1B
MT-ND6
DPPA3
L1TD1
TERF1
JARID2
SEMA3E
NCL
MT1G
MT1E
MT1H
CGA
MT2A
CRIP1
KHDC1L
Downregulated in d2 vs. d0
Upregulated in d2 vs. d0
log2 FC
D
IgG
Anti-β1
Downregulated genes
HIST1H1D
HIST1H1E
HIST1H1B
SEMA3E
NCL
CD24
KRT18
DNMT3B
MT-ND6
JARID2
TERF1
DPPA3
L1TD1
Upregulated genes
CGA
MT1E
MT2A
KHDC1L
CRIP1
MT1G
MT1H
HIST1H1D Up-/down-regulated in d2 vs. d0
CD24 Downregulated in d2 vs. d0 and in d2_Anti-β1 vs d0_Anti-β1
MT1E Upregulated in d2 vs. d0 and in d2_Anti-β1 vs d0_Anti-β1
DPPA3 Up-/down-regulated in d2 vs. d0, not in d2_Anti-β1 vs d0_Anti-β1

Figure 6. Integrin β1 inhibition gives rise to distinct single cells transcriptional profiles. A) U-map of the 6 conditions (Naïve d0, d2, d0_anti-β1, d2_ anti-β1, primed, primed_Mab13). **B)** U-map overlayed with SFRP2 expression level. **C)** log2FC of the top up- and down-regulation in d2 vs. d0. The used threshold is (log2FC<-1|log2FC>1). Gene names in blue are also downregulated in d2_Mab13 vs. d0_Mab13. Gene namesin red are also upregulated in d2_Mab13 vs. d0_Mab13. Gene names in green are not up- nor down-regulated in d2_Mab13 vs. d0_Mab13. **D)** Venn diagram representation of the previous list of top up- and down-regulated genes in d2 vs. d0.

DISCUSSION

We describe here unprecedented integrin β1-mediated regulation of human naïve and primed PSC states*in vitro*. We demonstrate that integrin β1 is active in naïve and primed PSCs when cultured on ECMs commonly used in hiPSC cultures (MG LM and VTN) and expressed during early embryo development (LM). Further, we show that the role of integrin β1 differs in naïve and primed states of pluripotency. In primed pluripotency, active β1, seems to facilitate focal adhesion signaling and mediate forces pulling cells flatter towards ECM. In naïve state the active integrin β1 is is high but distributes diffusely and fails to activate Src kinase. Furthermore, in naïve cells integrin β1 does not seem to mediate significant forces pulling colonies flatter towards the ECM. These observations are supported by recent report detecting increased cell-ECM contractility in mouse embryonic stem cells exiting pluripotency (add ref). Importantly, inhibition of β1 supported naïve-like features in primed and naïve hiPSCs regarding colony morphology and gene expression patterns. In primed hiPSCs, acute integrin β1 inhibition reduced actomyosin contraction and ERK signaling, whereas continuous integrin inhibition supported maintenance of naïve-like state through altered gene expression and attenuated exit from the naïve state.

Many protocols for chemical reversion and maintenance of human naïve pluripotency *in vitro* have been developed (Hassani et al., 2019; Taei et al., 2020). However, a clear consensus of how different culture methods affect naïve hiPSC quality and function is lacking. It was recently reported that integrin β1 inhibition supports the mouse ICM cell organization when cultured in Matrigel (E. J. Y. Kim et al., 2022). This is in line with our results of integrin β1 inhibition supporting naïve hiPSC colonycompaction when cultured *in vitro*. Together these findings emphasize the importance of integrin-ECM connections in PSC *in vitro* cultures, and suggest that integrin β1 inhibition supports the maintenance of early blastocyst ICM cells *in vitro*.

Our transcriptome analysis revealed several interesting candidates linked to β1-integrin regulation of cell states. *AMOTL2* was among the downregulated genes following integrin β1 inhibition in primed hiPSCs. Angiomotin-Like 2 (AMOTL2) interacts with and inhibits transcriptional regulator YAP in adult cells (Wang et al., 2011; Zhao et al., 2011). In human PSCs, YAP inhibition is needed for actin cytoskeleton reorganization during differentiation into mesodermal cells (Pagliari et al., 2021). Further, AMOTL2 is enriched on the edge of the human PSC colonies where cells are most prone to differentiation *in vitro* (Y. Kim et al., 2022). The connection of integrin β1 and AMOTL2 in primed hiPSC colony morphology and polarization remains to be studied.

According to our transcriptome analysis, integrin β1 inhibition in naïve hiPSCs initiated upregulation of actin regulators, such as Phosphatase Actin Regulator-1 (*PHACTR-1*), which has been previously shown to bind actin and regulate actomyosin assembly and lamellipodium formation (Allain et al., 2012; Jarray et al., 2011; Wiezlak et al., 2012), Smooth Muscle α-actin (*ACTA2*) which regulates vascular contraction and blood pressure (Schildmeyer et al., 2000), and Filamin A-Binding Protein (*FILIP1*) which regulates cell migration through actin binding protein Filamin-A (Nagano et al., 2002). The role of the aforementioned actin regulators in naïve hiPSC maintenance would need further investigation for better

understanding of actin regulation in naïve pluripotency.

Our capacitation assays further highlight the role of integrin β1 incolony spreading during pluripotency state transitions. Colony spreading due to decreased plasma membrane tension and increased tractional forces have been linked with naïve cells exiting pluripotency in mESCs (add ref). Our data shows that inhibition of β1-integrin has similar effect to colony morphology as reduced cell surface tension. It is tempting to speculate that activation of cell adhesion receptor would be part of the cascade regulating cell surface mechanics during early differentiation. Finally, our scRNA sequencing reveals transcriptional differences between the naïve cells with inactivated β1-integrin. To our surprise integrin inhibition in the naïve cells gave rise to a more marked difference than in the primed cells when compared to the control groups. This indicates unknown mechanism functioning downstream of integrin β1 in naïve pluripotency a notion that is further supported by our immunofluoresence data (Figure 3A). The contradiction between high integrin β1 activity with significant transcriptional consequences and low FA signaling with diffuse distribution outside of FAs in naïve pluripotency suggest to possible association with cortical actin cytoskeleton and role in regulation of mechanical properties of cell surface, however this needs to be investigated in future studies. Lastly, we observed differences in expression of key genes regulating naïve pluripotency when cells were capacitated with or without active β1-integrin. DPPA3 and L1TD1 were significantly decreased only when the cells were capacitated without integrin inhibition. This is in accordance with the observed delay in colony spreading. Ultimately, our results suggest that inhibition of integrin β1 delays the naïve to primed cell transition. Write here something about the scRNAseq data and the capacitation data - @Lea et al?

Taken together, our study reveals that integrin β1 is active in *in vitro* cultured naïve and primed hPSCs, and integrin β1 inhibition induces naïve-like characteristics in primed hiPSCs. These data emphasize the importance of the environment and cell-ECM interaction in maintaining the desired cell state in human PSCs, and uncover a potentially important functional role for integrin inhibitors in fine-tuning transitions in PSC identity..

METHODS

Cell lines and culture

HiPSC line HEL 24.3 was a kind gift from Timo Otonkoski (the University of Helsinki, Finland) and was generated by using Sendai viruses (Mikkola et al., 2013; Trokovic et al., 2015). Cells were cultured on Matrigel (354277, Corning) coated plates in Essential 8™ Medium (A1517001, Thermo Fisher) at +37˚C, 5 % CO_2. 50 mM EDTA in PBS was used for passaging of the cells (Närvä et al. 2017), and Essential 8™ Medium was changed daily.

AICS-0016 (Actin beta, mEGFP; Allen Institute) hiPSCs were cultured on Matrigel (354230, Corning) coated plates in mTeSR™1(85850, Stemcell Technologies) medium at +37˚C, 5 % CO_2. 50 mM EDTAin PBS was used for passaging of the cells (Närvä et al. 2017), and culture medium was changed daily.

Naïve-like hESCs were a kind gift from Timo Otonkoski (the University of Helsinki, Finland).

Mouse (ICR) Inactivated Embryonic Fibroblasts (commercial iMEFs, A24903, Life Technologies) were cultured in DMEM/F12 (11320033, Gibco) supplemented with 10 % FBS (Sigma-Aldrich) at +37˚C, 5 % CO_2, and washed twice with PBS before using as feeder cells for naïve hiPSCs.

The generation of *cpdm* mouse embryonic fibroblasts (MEFs) has been described before (Rantala et al. 2011). The MEFs were cultured in Dulbecco's modified Eagle's medium (DMEM, Sigma-Aldrich) supplemented with 10 % fetal bovine serum (FBS, Sigma-Aldrich), 2 mM l-glutamine (Sigma-Aldrich), 1% sodium pyruvate (Sigma-Aldrich), 1% non-essential amino acid solution (Sigma-Aldrich), 1% penicillin-streptomycin (Sigma-Aldrich) and 0,001% betamercaptoethanol (M3148, Sigma-Aldrich) at +37˚C, 5 % CO_2. Prior to using as feeder cells (in-house iMEFs), the MEFs were plated on 0,1 % gelatin (07903, Stemcell Technologies) coated plates and after reaching full confluency, the proliferation of the MEFs was stopped by treating the cells with Mitomycin C (M4287, Sigma) for 3h at 37˚C, and washed with PBS.

Reversion to naïve-like state

HEL 24.3 hiPS cells were plated on an inactivated mouse embryonic fibroblast (iMEF) monolayer and reverted into a naïve-like state by using NaïveCult™ Induction Kit (05580, Stemcell Technologies) according to manufacturer's instructions. In order to inhibit integrin β1 activity, 5 µg/ml Rat anti-human β1 integrin antibody (mAb13) was included in the culture medium throughout and after the reversion, except during re-plating of the cells. Cells were detached by using StemPro™ Accutase™ Cell Dissociation Reagent (A1110501, Gibco), and re-plated in culture medium supplemented with 10 µM ROCK inhibitor Y-27632 (72302, Stemcell Technologies).

Maintenance of naïve hiPSC

After reversion, the naïve hiPSCs were cultured on commercial or in-house iMEFs in NaïveCult™ Expansion Medium (05590, Stemcell Technologies) or in-house tt2iLGö medium: N2B27 (DMEM/F12 [1:2; 11320033, Gibco], Neurobasal medium [1:2; 21103049, Gibco], N2 supplement [in house], 1 mM l-glutamine [Sigma-Aldrich] and 0,1 mM β-mercaptoethanol [M3148, Sigma-Aldrich]) medium supplemented with 0,3 µM CHIR99021 (SML1046, Sigma-Aldrich), 1 µM PDO325901 (PZ0162, Sigma-Aldrich), 10 ng/ml human LIF (78055.1, Stemcell Technologies) and 2 µM Gö6983 (2285, Tocris Bioscience) at +37˚C, 5 % O_2, 5 % CO_2 (Guo et al. 2017). N2 was prepared by supplementing DMEM/F12 with 0.4 mg/ml insulin (I9278, Sigma-Aldrich), 10 mg/ml apo-transferrin (3188-AT-001G, R&D systems), 3 µM sodium selenite (S5261, Sigma-Aldrich), 1.6 mg/ml putrescine (P5780-5G,

Sigma-Alrich) and 2 µg/ml progesterone (P8783, Sigma-Aldrich). Cells were detached by using StemPro™ Accutase™ Cell Dissociation Reagent (A1110501, Gibco) or TrypLE Express (12604-21, Gibco), and re-plated in culture medium supplemented with 10 µM ROCK inhibitor Y-27632 (72302, Stemcell Technologies).

Immunofluorescence

µ-slide 8 well (Ibidi) chambered coverslips were coated with Matrigel (354277, Corning), 5 µg/ml vitronectin (A14700, Gibco) or 5 µg/ml laminin-521 (A29248, Gibco) at 37˚C for 1h. Cells were platedon coated µ-slide wells and were grown until the indicated time point. Culture medium was changed daily from the cells that were grown more than 24 h. Cells were fixed with 4 % PFA, washed with PSB,incubated with 0,1 M glycine for 10 min at RT, washed with PBS, permeabilized with 0,3 % Triton-X for 10 min at RT, washed again with PBS and incubated with primary antibodies in 1 % BSA in PBS overnight at 4˚C. Cells were washed with PBS and PBST (0,05 % Tween in PBS), and incubated with secondary antibodies, 4',6-Diamidino-2-Phenylindole, Dihydrochloride (DAPI), SiR-Actin (0,5 µM) or Atto-Phalloidin for 1h at RT. Cells were washed with PBS prior to imaging.

Confocal microscopy, live-cell imaging and image analysis

Immunofluorescence stained cells were imaged using 3i CSU-W1 Spinning Disk confocal microscope, sCMOS Orca Flash4.0 (Hamamatsu) camera and 63x Plan-Apochromat (Zeiss) objective. Live-cell imaging was performed using IncyCyte S3 live-cell analysis instrument (Satorius), 10x objective and phase contrast channel. All of the images were analyzed using ImageJ.

Western Blot

Cells were washed with PBS on ice, lysed using TX lysis buffer (TXLB; 50 mM Tris-HCl, pH 7.5, 150 mM NaCl, 0.5% Triton-X, 0.5% glycerol, 1% SDS, Complete protease inhibitor [Sigma-Aldrich], and phos-stop tablet [Sigma-Aldrich]) an collected by scraping. Samples were boiled for 5 min and sonicated. Protein concentrations were measured using DC Protein assay (Bio-Rad) and normalized by adding TXLB. SDS sample buffer was added on the samples, and the samples were boiled for 5 min, and loaded on precast Tris-Glycine-eXtendet SDS-PAGE gels with a 4–20% gradient (Bio-Rad). Afterseparation, the proteins were transferred on nitrocellulose membranes (Bio-Rad) using the Trans-Blot Turbo Transfer System (Bio-Rad), followed by blocking with 5% milk powder in Tris-buffered saline with 0.1% Tween 20 (TBST) for 1h at RT. Membranes were incubated with primary antibodies diluted in AdvanBlock-Fluor blocking solution (Advansta) overnight at +4˚C, washed three times with TBST and incubated with incubated with fluorophore-conjugated Odyssey or Azure secondary antibodies (LI- COR Biosciences) for 1h at RT. Membranes were washed three times with TBST, scanned with Odyssey infrared system (LI-COR Biosciences) or Sapphire Biomolecular RGBNIR Imager (Azure).
Protein band intensities were analyzed using ImageJ

qPCR

Total RNA was extracted using the Nucleospin RNA kit (#740955.250, Macherey-Nagel) according to manufacturers' instructions. Complementary DNA synthesis from RNA was performed using high capacity cDNA Reverse Transcription Kit (Thermo Fisher Scientific). The expression levels of target genes were determined with QuantStudio™ 12K Flex Real-Time PCR System (Thermo Fisher Scientific).

Capacitation

For the capacitation process, naïve hiPSCs were first plated on a Matrigel-precoated plates (354277, Corning) supplemented with 10 μM Y-27632 (72302, Stemcell Technologies). After two days, the NaïveCult medium was changed to capacitation medium, called N2B27, as described in Rostovskaya et al., 2019 (DMEM/F12 [1:2; 11320033, Gibco], Neurobasal medium [1:2; 21103049, Gibco], N2 supplement [in house], 1 mM l-glutamine [Sigma-Aldrich] and 0,1 mM β-mercaptoethanol [M3148, Sigma-Aldrich]) medium supplemented with 2 μM XAV-939 (Tocris Bio-Techne, 3748) at +37˚C, 5 % CO2 (Guo et al. 2017). N2 was prepared by supplementing DMEM/F12 with 0.4 mg/ml insulin (I9278, Sigma-Aldrich), 10 mg/ml apo-transferrin (3188-AT-001G, R&D systems), 3 μM sodium selenite (S5261, Sigma-Aldrich), 1.6 mg/ml putrescine (P5780-5G, Sigma-Alrich) and 2 μg/ml progesterone (P8783, Sigma-Aldrich). Depending on the experiment, the cells were capacitated for 2 to 5 days. The capacitation process was followed with an Incucyte S3 live-cell analysis instrument (Sartorius).

RNA sequencing

RNA was isolated from three biological replicates of IgG or MAb13 treated (12h) primed hiPSCs, naïve hiPSCs and naïve + MAb13 hiPSCs, using NucleoSpin RNA -kit (#740955.250, Macherey-Nagel). The quality of the samples was verified using Agilent Bioanalyzer 2100, and the sample concentrations were measured using Qubit®/Quant-IT® Fluorometric Quantitation (Life Technologies). For the library preparation, 100 ng of RNA was amplified by using Illumina Stranded mRNA Preparation, Ligation kit (Illumina) according to manufacturer's protocol. The quality of the library was verified using Advanced Analytical Fragment Analyzer, and sample concentrations were measured using Qubit®/Quant-IT® Fluorometric Quantitation (Life Technologies). Sequencing was performed using NovaSeq 6000 S4 instrument, v1.5 (Illumina).

The sequencing data read quality was ensured using the FastQ (v.0.11.14, http://www.bioinformatics.babraham.ac.uk/projects/fastqc. Andrews 2019.) and MultiQC (v.1.5) (Ewels et al. 2016) tools. Differentially expressed genes were identified between the IgG or MAb13 treated primed hiPSCs, and between the naïve hiPSCs and naïve + MAb13 hiPSCs. Differential gene expression analysis was performed using Bioconductor R package ROTS (v.1.14.0) (Suomi et al. 2017). Genes with FDR < 0.05 were defined as differentially expressed. Gene-annotation enrichment analysis of differentially expressed genes was done by using The Database for Annotation, Visualization and Integrated Discovery (DAVID) annotation tools (Huang et al. 2009, Huang et al. 2009).

Table 1. Reagents

REAGENT OR RESOURCE	SOURCE	IDENTIFIER
Antibodies		
Rat anti-human β1 integrin (mAb13)	In house	
Mouse anti-human active b1 integrin (12g10; 1:50 for IF)	In house	
Mouse Anti-Integrin αVβ5	Sigma-Aldrich	Cat# MAB1961Z ,RRID: AB_94466
Mouse anti-paxillin (1:150 for IF)	BD Biosciences	Cat# 612405, RRID: AB_647289
Rabbit anti-KLF17 (1:100 for IF, 1:1000 for WB)	Sigma-Aldrich	Cat# HPA024629, RRID: AB_1668927
Rabbit anti-phospho-MLC 2 (Thr18/Ser19; 1:100 for IF)	Cell Signaling Technology	Cat# 3674, RRID: AB_2147464
Rabbit anti OCT3/4 (1:1000 for WB)	Santa Cruz Biotechnology	Cat# sc-9081, RRID :AB_2167703
Goat anti-NANOG (1:400 for WB)	R&D Systems	Cat# AF1997, RRID:AB_355097
Rabbit anti-phospho-ERK (Thr202/Tyr204; 1:1000 forWB)	Cell Signaling Technology	Cat# 4370, RRID:AB_2315112
Mouse anti-ERK (1:1000 for WB)	Cell Signaling Technology	Cat# 4696, RRID:AB_390780
Mouse anti-β-actin (1:1000 for WB)	Sigma-Aldrich	Cat# A1978, RRID:AB_476692
Molecules/labels		
Sir-Actin	Spirochrome AG	Cat# SC001
Phalloidin–Atto 647N (1:200 for IF)	Sigma-Aldrich	Cat# 65906
DAPI(4',6-Diamidino-2-Phenylindole, Dihydrochloride)	Invitrogen™	Cat# D1306
Primers		
TaqMan™ gene expression assay (FAM),Hs00702999_m1, KLF17	Thermo Fisher Scientific	Cat# 4448892
TaqMan™ gene expression assay (FAM),Hs00195612_m1, TBX3	Thermo Fisher Scientific	Cat# 4453320
TaqMan™ gene expression assay (FAM),Hs00600845_m1, ZIC2	Thermo Fisher Scientific	Cat# 4448892

TaqMan™ gene expression assay (FAM),Hs00293258_m1, SFRP2	Thermo Fisher Scientific	Cat# 4453320
TaqMan™ gene expression assay (FAM), GAPDH,Hs02786624_g1, GAPDH	Thermo Fisher Scientific	Cat# 4331182

ACKNOWLEDGEMENTS

We thank J. Siivonen and P. Laasola for technical assistance. The Ivaska laboratory is acknowledged for lively discussions and critical feedback on the manuscript and H. Hamidi for editing the manuscript. We thank Prof. T. Otonkoski for providing cell lines. The Cell Imaging and Cytometry core facility (Turku Bioscience Centre, University of Turku and Åbo Akademi University and Biocenter, Finland); EuroBioimaging node in Turku, and Finnish Functional Genomics Centre (Turku Bioscience Centre, University of Turku and Åbo Akademi University) are acknowledged for services, instrumentation, and expertise. We thank the Medical Bioinformatics Centre of Turku Bioscience Centre for the sequencing data analysis. The Centre is supported by University of Turku, Åbo Akademi University, Biocenter Finland and Elixir-Finland. This study was supported by the Academy of Finland (J.I. 330033; 325464), Academy of Finland CoE in Cell and Tissue Mechanics (J.I.), InFLAMES Flagship Programme of the Academy of Finland (decision number: 337530), the Sigrid Juselius Foundation (J.I.) .E. Taskinen has been supported by the University of Turku Doctoral Program for Molecular Medicine, Finnish Cultural Foundation, K. Albin Johansson Foundation and Magnus Ehrnrooth Foundation.

AUTHOR CONTRIBUTIONS

Conceptualization, M.E.T. and J.I.; Investigation, M.E.T., A.S., P.R., S.V. and J.S.; Formal Analysis, M.E.T.; Writing – Original Draft, M.E.T. and J.I. Writing-editing; M.E.T. and J.I.; Visualization, M.E.T.; Supervision, J.I.; Funding Acquisition, J.I.

DECLARATION OF INTERESTS

The authors declare no competing financial interests.

REFERENCES

Allain, B., Jarray, R., Borriello, L., Leforban, B., Dufour, S., Liu, W., Pamonsinlapatham, P., Bianco, S., Larghero, J., Hadj-Slimane, R., Garbay, C., Raynaud, F., Lepelletier, Y., 2012. Neuropilin-1 regulates a new VEGF-induced gene, Phactr-1, which controls tubulogenesis and modulates lamellipodial dynamics in human endothelial cells. Cell Signal 24, 214–223. https://doi.org/10.1016/j.cellsig.2011.09.003

Brakebusch, C., Fässler, R., 2003. The integrin-actin connection, an eternal love affair. EMBO J 22, 2324–2333. https://doi.org/10.1093/emboj/cdg245

Byron, A., Humphries, J.D., Askari, J.A., Craig, S.E., Mould, A.P., Humphries, M.J., 2009. Anti- integrin monoclonal antibodies. J Cell Sci 122, 4009–4011. https://doi.org/10.1242/jcs.056770

Campbell, I.D., Humphries, M.J., 2011. Integrin Structure, Activation, and Interactions. Cold Spring Harb Perspect Biol 3, a004994. https://doi.org/10.1101/cshperspect.a004994

Collier, A.J., Bendall, A., Fabian, C., Malcolm, A.A., Tilgner, K., Semprich, C.I., Wojdyla, K., Nisi, P.S., Kishore, K., Roamio Franklin, V.N., Mirshekar-Syahkal, B., D'Santos, C., Plath, K., Yusa, K., Rugg-Gunn, P.J., 2022. Genome-wide screening identifies Polycomb repressive complex 1.3 as an essential regulator of human naïve pluripotent cell reprogramming. Sci Adv 8, eabk0013. https://doi.org/10.1126/sciadv.abk0013

Ding, T., Zhou, Y., Long, R., Chen, C., Zhao, J., Cui, P., Guo, M., Liang, G., Xu, L., 2019. DUSP8 phosphatase: structure, functions, expression regulation and the role in human diseases. Cell Biosci 9, 70. https://doi.org/10.1186/s13578-019-0329-4

Fässler, R., Pfaff, M., Murphy, J., Noegel, A.A., Johansson, S., Timpl, R., Albrecht, R., 1995. Lack of beta 1 integrin gene in embryonic stem cells affects morphology, adhesion, and migration but not integration into the inner cell mass of blastocysts. J Cell Biol 128, 979–988. https://doi.org/10.1083/jcb.128.5.979

Guo, G., von Meyenn, F., Rostovskaya, M., Clarke, J., Dietmann, S., Baker, D., Sahakyan, A., Myers, S., Bertone, P., Reik, W., Plath, K., Smith, A., 2017. Epigenetic resetting of human pluripotency. Development 144, 2748–2763. https://doi.org/10.1242/dev.146811

Hassani, S.-N., Moradi, S., Taleahmad, S., Braun, T., Baharvand, H., 2019. Transition of inner cell mass to embryonic stem cells: mechanisms, facts, and hypotheses. Cell Mol Life Sci 76, 873–892. https://doi.org/10.1007/s00018-018-2965-y

Hynes, R.O., 2002. Integrins: bidirectional, allosteric signaling machines. Cell 110, 673–687. https://doi.org/10.1016/s0092-8674(02)00971-6

Jarray, R., Allain, B., Borriello, L., Biard, D., Loukaci, A., Larghero, J., Hadj-Slimane, R., Garbay, C., Lepelletier, Y., Raynaud, F., 2011. Depletion of the novel protein PHACTR-1 from human endothelial cells abolishes tube formation and induces cell death receptor apoptosis. Biochimie 93, 1668–1675. https://doi.org/10.1016/j.biochi.2011.07.010

Kim, E.J.Y., Sorokin, L., Hiiragi, T., 2022. ECM-integrin signalling instructs cellular position sensing to pattern the early mouse embryo. Development 149, dev200140. https://doi.org/10.1242/dev.200140

Kim, Y., Jang, H., Seo, K., Kim, J.H., Lee, B., Cho, H.M., Kim, H.J., Yang, E., Kim, H., Gim, J.-A., Park, Y., Ryu, J.R., Sun, W., 2022. Cell position within human pluripotent stem cell coloniesdetermines apical specialization via an actin cytoskeleton-based mechanism. Stem Cell Reports 17, 68– 81. https://doi.org/10.1016/j.stemcr.2021.11.005

Lynch, C.J., Bernad, R., Martínez-Val, A., Shahbazi, M.N., Nóbrega-Pereira, S., Calvo, I., Blanco-Aparicio, C., Tarantino, C., Garreta, E., Richart-Ginés, L., Alcazar, N., Graña-Castro, O., Gómez- Lopez, G., Aksoy, I., Muñoz-Martín, M., Martinez, S., Ortega, S., Prieto, S., Simboeck, E., Camasses, A., Stephan-Otto Attolini, C., Fernandez, A.F., Sierra, M.I., Fraga, M.F., Pastor, J., Fisher, D., Montserrat, N., Savatier, P., Muñoz, J., Zernicka-Goetz, M., Serrano, M., 2020. Global hyperactivation of enhancers stabilizes human and mouse naive pluripotency through inhibition of CDK8/19 Mediatorkinases. Nat Cell Biol 22, 1223–1238. https://doi.org/10.1038/s41556-020-0573-1

Martinez-Val, A., Lynch, C.J., Calvo, I., Ximénez-Embún, P., Garcia, F., Zarzuela, E., Serrano, M., Munoz, J., 2021. Dissection of two routes to naïve pluripotency using different kinase inhibitors. Nat Commun 12, 1863. https://doi.org/10.1038/s41467-021-22181-5

Molè, M.A., Weberling, A., Fässler, R., Campbell, A., Fishel, S., Zernicka-Goetz, M., 2021. Integrin β1 coordinates survival and morphogenesis of the embryonic lineage upon implantation and pluripotency transition. Cell Rep 34, 108834. https://doi.org/10.1016/j.celrep.2021.108834

Nagano, T., Yoneda, T., Hatanaka, Y., Kubota, C., Murakami, F., Sato, M., 2002. Filamin A-interacting protein (FILIP) regulates cortical cell migration out of the ventricular zone. Nat Cell Biol4, 495–501. https://doi.org/10.1038/ncb808

Närvä, E., Stubb, A., Guzmán, C., Blomqvist, M., Balboa, D., Lerche, M., Saari, M., Otonkoski, T., Ivaska, J., 2017. A Strong Contractile Actin Fence and Large Adhesions Direct Human Pluripotent Colony Morphology and Adhesion. Stem Cell Reports 9, 67–76. https://doi.org/10.1016/j.stemcr.2017.05.021

Nichols, J., Silva, J., Roode, M., Smith, A., 2009. Suppression of Erk signalling promotes ground state pluripotency in the mouse embryo. Development 136, 3215–3222. https://doi.org/10.1242/dev.038893

Nichols, J., Smith, A., 2009. Naive and primed pluripotent states. Cell Stem Cell 4, 487–492. https://doi.org/10.1016/j.stem.2009.05.015

Pagliari, S., Vinarsky, V., Martino, F., Perestrelo, A.R., Oliver De La Cruz, J., Caluori, G., Vrbsky, J., Mozetic, P., Pompeiano, A., Zancla, A., Ranjani, S.G., Skladal, P., Kytyr, D., Zdráhal, Z., Grassi, G., Sampaolesi, M., Rainer, A., Forte, G., 2021. YAP-TEAD1 control of cytoskeleton dynamics and intracellular tension guides human pluripotent stem cell mesoderm specification. Cell Death Differ 28, 1193–1207. https://doi.org/10.1038/s41418-020-00643-5

Pera, M.F., Rossant, J., 2021. The exploration of pluripotency space: Charting cell state transitions in peri-implantation development. Cell Stem Cell 28, 1896–1906. https://doi.org/10.1016/j.stem.2021.10.001

Schildmeyer, L.A., Braun, R., Taffet, G., Debiasi, M., Burns, A.E., Bradley, A., Schwartz, R.J., 2000. Impaired vascular contractility and blood pressure homeostasis in the smooth muscle alpha-actin null mouse. FASEB J 14, 2213–2220. https://doi.org/10.1096/fj.99-0927com

Sim, Y.-J., Kim, M.-S., Nayfeh, A., Yun, Y.-J., Kim, S.-J., Park, K.-T., Kim, C.-H., Kim, K.-S., 2017. 2i Maintains a Naive Ground State in ESCs through Two Distinct Epigenetic Mechanisms. Stem Cell Reports 8, 1312–1328. https://doi.org/10.1016/j.stemcr.2017.04.001

Stephens, L.E., Sutherland, A.E., Klimanskaya, I.V., Andrieux, A., Meneses, J., Pedersen, R.A., Damsky, C.H., 1995. Deletion of beta 1 integrins in mice results in inner cell mass failure and peri- implantation lethality. Genes Dev 9, 1883–1895. https://doi.org/10.1101/gad.9.15.1883

Stubb, A., Guzmán, C., Närvä, E., Aaron, J., Chew, T.-L., Saari, M., Miihkinen, M., Jacquemet, G., Ivaska, J., 2019. Superresolution architecture of cornerstone focal adhesions in human pluripotent stem cells. Nat Commun 10, 4756. https://doi.org/10.1038/s41467-019-12611-w

Taei, A., Rasooli, P., Braun, T., Hassani, S.-N., Baharvand, H., 2020. Signal regulators of humannaïve pluripotency. Exp Cell Res 389, 111924. https://doi.org/10.1016/j.yexcr.2020.111924

Takahashi, K., Tanabe, K., Ohnuki, M., Narita, M., Ichisaka, T., Tomoda, K., Yamanaka, S., 2007. Induction of pluripotent stem cells from adult human fibroblasts by defined factors. Cell 131, 861–872. https://doi.org/10.1016/j.cell.2007.11.019

Takahashi, K., Yamanaka, S., 2006. Induction of pluripotent stem cells from mouse embryonic and adult fibroblast cultures by defined factors. Cell 126, 663–676. https://doi.org/10.1016/j.cell.2006.07.024

Takashima, Y., Guo, G., Loos, R., Nichols, J., Ficz, G., Krueger, F., Oxley, D., Santos, F., Clarke, J., Mansfield, W., Reik, W., Bertone, P., Smith, A., 2014. Resetting transcription factor control circuitry toward ground-state pluripotency in human. Cell 158, 1254–1269. https://doi.org/10.1016/j.cell.2014.08.029

Wang, W., Huang, J., Chen, J., 2011. Angiomotin-like proteins associate with and negatively regulate YAP1. J Biol Chem 286, 4364–4370. https://doi.org/10.1074/jbc.C110.205401

Weinberger, L., Ayyash, M., Novershtern, N., Hanna, J.H., 2016. Dynamic stem cell states: naive to primed pluripotency in rodents and humans. Nat Rev Mol Cell Biol 17, 155–169. https://doi.org/10.1038/nrm.2015.28

Wiezlak, M., Diring, J., Abella, J., Mouilleron, S., Way, M., McDonald, N.Q., Treisman, R., 2012. G-actin regulates the shuttling and PP1 binding of the RPEL protein Phactr1 to control actomyosin assembly. J Cell Sci 125, 5860–5872. https://doi.org/10.1242/jcs.112078

Wojdyla, K., Collier, A.J., Fabian, C., Nisi, P.S., Biggins, L., Oxley, D., Rugg-Gunn, P.J., 2020. Cell-Surface Proteomics Identifies Differences in Signaling and Adhesion Protein Expression between Naive and Primed Human Pluripotent Stem Cells. Stem Cell Reports 14, 972–988. https://doi.org/10.1016/j.stemcr.2020.03.017

Zhao, B., Li, L., Lu, Q., Wang, L.H., Liu, C.-Y., Lei, Q., Guan, K.-L., 2011. Angiomotin is a novel Hippo pathway component that inhibits YAP oncoprotein. Genes Dev 25, 51–63. https://doi.org/10.1101/gad.2000111